Oklahoma Geological Survey
Charles J. Mankin, *Director*

Circular 106
ISSN 0078-4397

Petroleum Systems of Sedimentary Basins in the Southern Midcontinent, 2000 Symposium

KENNETH S. JOHNSON AND DANIEL F. MERRIAM, *Editors*

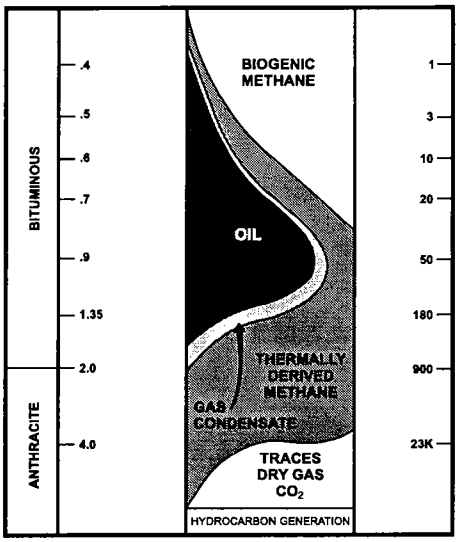

Proceedings of a symposium held March 28–29, 2000, in Oklahoma City, Oklahoma.

Co-sponsored by:

Oklahoma Geological Survey

and

National Petroleum Technology Office,
U.S. Department of Energy

The University of Oklahoma
Norman

2001

OKLAHOMA GEOLOGICAL SURVEY

CHARLES J. MANKIN, *Director*

SURVEY STAFF

JAMES H. ANDERSON, *Manager of Cartography*
RICHARD D. ANDREWS, *Geologist IV*
LARRY T. AUSTIN, *Core and Sample Library Assistant*
BETTY D. BELLIS, *Word-Processing Operator II / Technical Typist*
MITZI G. BLACKMON, *Clerk-Typist I*
DAN T. BOYD, *Geologist III*
JERLENE A. BRIGHT, *Technical Project Specialist*
RAYMON L. BROWN, *Geophysicist III*
RUTH E. BROWN, *Assistant to the Director*
JOCK A. CAMPBELL, *Geologist IV*
BRIAN J. CARDOTT, *Geologist IV*
JAMES R. CHAPLIN, *Geologist IV*
JANISE L. COLEMAN, *Office Assistant IV*
CHRISTIE L. COOPER, *Managing Editor*
TAMMIE K. CREEL-WILLIAMS, *Secretary II*
CHARLES R. DYER III, *Drilling Technician*
WALTER C. ESRY, *Manager, Core and Sample Library*
ROBERT O. FAY, *Geologist IV*
AMIE R. FRIEND, *Research Specialist I*
PATRONALIA M. HANLEY-BROWN, *Chemist*
PRISCILLA A. JOHNSON, *Office Assistant IV*
JAMES W. KING, *Research Specialist II*
JAMES E. LAWSON, JR., *Chief Geophysicist*
LAURIE A. LOLLIS, *Cartographic Technician II*
KENNETH V. LUZA, *Geologist IV*
MICHAEL J. MERCER, *Manager, Log Library*
GALEN W. MILLER, *Research Associate*
RICHARD G. MURRAY, *Copy Center Operator*
SUE M. PALMER, *Office Assistant II*
DAVID O. PENNINGTON, *Operations Assistant II*
CONNIE G. SMITH, *Promotion and Information Specialist*
PAUL E. SMITH, *Supervisor, Offset Press Copy Center*
THOMAS M. STANLEY, *Geologist III*
LLOYD N. START, *Assistant Drilling Technician*
JOYCE A. STIEHLER, *Chief Clerk*
MICHELLE J. SUMMERS, *Technical Project Coordinator*
NEIL H. SUNESON, *Assistant Director, Geological Programs*
JANE L. WEBER, *Publication and Database Coordinator*

Cover Picture

Thermal-maturity diagram showing stages of hydrocarbon generation (modified from Figure 12, p. 68, this volume).

This publication, printed by the Oklahoma Geological Survey, is issued by the Oklahoma Geological Survey as authorized by Title 70, Oklahoma Statutes, 1981, Sections 231–238. 1,050 copies have been prepared for distribution at a cost of $9,996 to the taxpayers of the State of Oklahoma. Copies have been deposited with the Publications Clearinghouse of the Oklahoma Department of Libraries.

PREFACE

The transfer of technical information will aid in the search for, and production of, our oil and gas resources. To facilitate this technology transfer, the Oklahoma Geological Survey (OGS) and the U.S. Department of Energy, National Petroleum Technology Office (DOE–NPTO), in Tulsa, cosponsored a symposium dealing with the search for, and production of, oil and gas resources from sedimentary basins in the southern Midcontinent. The symposium was held on March 28–29, 2000, in Oklahoma City, Oklahoma. This volume contains the proceedings of that symposium.

Research reported upon at the symposium focused on the reservoirs, geologic events, and petroleum in the numerous sedimentary basins of the region. Many clastic and carbonate reservoirs are major sources of oil and gas in the southern Midcontinent, and they have great potential for additional recovery using advanced technologies. The research reports on geology, depositional settings, diagenetic and thermal history, reservoir characterization, geophysical studies, exploration, petroleum production, and enhanced oil recovery. In describing these petroleum systems and reservoirs, the researchers have increased our understanding of how the geologic history of an area can affect reservoir heterogeneity and our ability to efficiently recover the hydrocarbons they contain. We hope that the symposium and these proceedings will bring such research to the attention of the geoscience and energy-research community, and will help foster exchange of information and increased research interest by industry, university, and government workers.

Eighteen talks and posters presented at the symposium are printed here as full papers or extended abstracts. An additional eight talks and posters are presented as abstracts at the end of the volume. About 150 persons attended the symposium. Stratigraphic nomenclature and age determinations used by the various authors in this volume do not necessarily agree with those of the OGS.

This is the thirteenth symposium in as many years dealing with topics of major interest to geologists and others involved in petroleum-resource development in Oklahoma and adjacent states. These symposia are intended to foster the exchange of information that will improve our ability to find and recover our nation's oil and gas resources. Earlier symposia covered: Anadarko Basin (published as OGS Circular 90); Late Cambrian–Ordovician Geology of the Southern Midcontinent (OGS Circular 92); Source Rocks in the Southern Midcontinent (OGS Circular 93); Petroleum-Reservoir Geology in the Southern Midcontinent (OGS Circular 95); Structural Styles in the Southern Midcontinent (OGS Circular 97); Fluvial-Dominated Deltaic Reservoirs in the Southern Midcontinent (OGS Circular 98); Simpson and Viola Groups in the Southern Midcontinent (OGS Circular 99); Ames Structure in Northwest Oklahoma and Similar Features—Origin and Petroleum Production (OGS Circular 100); Platform Carbonates in the Southern Midcontinent (OGS Circular 101); Marine Clastics in the Southern Midcontinent (OGS Circular 103); Pennsylvanian and Permian Geology and Petroleum in the Southern Midcontinent (OGS Circular 104); and Silurian, Devonian, and Mississippian Geology and Petroleum in the Southern Midcontinent (OGS Circular 105).

Persons involved in the organization and planning of this symposium include: Kenneth Johnson and Charles Mankin of the OGS; Daniel Merriam of the Kansas Geological Survey; and Bill Lawson and Herb Tiedemann of DOE–NPTO. Other personnel who contributed include Michelle Summers and Tammie Creel, registration co-chairs; LeRoy Hemish, poster-session chair; Connie Smith, publicity chair; and Michelle Summers, exhibits coordinator. Technical editing of this volume was done by Thomas W. Henry, Westminster, Colorado; layout and production was done by Sandra Rush, Denver, Colorado. Appreciation is expressed to each of them and to the many authors who worked toward a highly successful symposium.

KENNETH S. JOHNSON AND
DANIEL F. MERRIAM
General Chairmen

CONTENTS

Petroleum Systems of Sedimentary Basins in Oklahoma

Jock A. Campbell
Oklahoma Geological Survey
Norman, Oklahoma

Robert A. Northcutt
Independent Geologist
Oklahoma City, Oklahoma

ABSTRACT.—A petroleum system includes elements of petroleum source, maturity, migration, entrapment, and timing. The types of petroleum-source materials are crucial in determining whether significant quantities of petroleum are generated during burial and maturation of the source rocks. As defined by Magoon (1988), these are Type I (algal-amorphous), Type II (sapropelic), and Type III (humic-woody). In Oklahoma, Types II and III are the most prolific producers of oil and gas. The types of petroleum systems in the five Oklahoma petroleum basins are briefly discussed. These are the Anadarko, Ardmore-Marietta, Hollis-Hardeman, and Arkoma basins, and the highly deformed Ouachita basin.

INTRODUCTION

The Petroleum System is one of the newest concepts in petroleum geology, although it is in truth simply a synthesis of the earlier concepts of petroleum source, maturity, migration, entrapment, and timing. In this sense, the petroleum system has become a paradigm of the science. However, the model has been applied specifically to relatively few sedimentary basins.

The petroleum system includes all of the geological elements and processes that are essential for an oil and gas deposit to occur in nature. The basic elements include a petroleum-source rock, migration path, reservoir rock, trap, and seal, and the geologic processes that create each of these basic elements. All these elements must be correctly placed in time and space so that the organic matter in the source rock can be converted into a petroleum deposit (Magoon, 1988).

Petroleum systems are commonly named for major source strata, and are ideally based on geochemical correlation of petroleum and source rocks. The scientific/technological knowledge of specific petroleum systems is variable; thus, the levels of certainty must be defined. Magoon (1988) has developed a system of definitions, and symbols for abbreviated representation of those definitions that are used in this paper (Table 1).

The type of source material is also critical to whether or not petroleum liquids are generated in large quantities during burial and maturation of the source rocks. They are, in general: Type I (algal-amorphous), which yields high-paraffin oils and subsequently gas; Type II (sapropelic), which yields both napthenic and paraffinic oils and gas; and Type III (humic-woody), which yields mainly gas and few liquids. Identified source rocks in Oklahoma are mainly Types II and III. The most prolific, and the most studied petroleum-source rocks in Oklahoma, are the Woodford and the equivalent Chattanooga Shales (Upper Devonian). An excellent synthesis of the geochemistry of those formations is provided by Comer (1992).

OKLAHOMA SEDIMENTARY BASINS

Five sedimentary basins occur in Oklahoma: Anadarko, Ardmore-Marietta, Hollis-Hardeman, Arkoma, and the highly deformed Ouachita basin. The Cherokee platform is also an oil and gas province, but can be considered as the stable shelf of the Arkoma basin for the present purpose. As they are presently recognized (Fig. 1), the basins began to form in the latest Mississippian to earliest Pennsylvanian. Prior to that time, most of Oklahoma was a broad, shallow marine shelf (Fig. 2). The exception to that generalization is the southern Oklahoma aulacogen, a northwest-trending, fault-bounded trough in which a much thicker sequence of pre-Carboniferous sediments was deposited. The only strata that are known to be buried to sufficient depth to generate hydrocarbons at that time were in the aulacogen. The Ouachita basin is unique, because Cambrian through middle-to-late Mississippian strata were deposited well south of their present geographic position (Fig. 2) and were subsequently thrusted northward into Oklahoma (Fig. 1). Each of the Oklahoma basins contains more than one petroleum system, and there

Campbell, J. A.; and Northcutt, R. A., 2001, Petroleum systems of sedimentary basins in Oklahoma, *in* Johnson, K. S.; and Merriam, D. F. (eds.), Petroleum systems of sedimentary basins in the southern Midcontinent, 2000 symposium: Oklahoma Geological Survey Circular 106, p. 1–5.

TABLE 1. — Definitions for Levels of Certainty in Petroleum Systems

Level of certainty	Criteria	Symbol
Known	Oil/source-rock correlation; or gas reservoired in documented gas source rock	(!)
Hypothetical	No oil/source-rock correlation; oil or gas reservoired near postulated source rock	(.)
Speculative	Geological and geophysical evidence	(?)

From Magoon (1988).

are commonly multiple plays within each petroleum system.

The Anadarko basin (including the Anadarko shelf) in western Oklahoma extends into northwestern Texas and parts of Kansas, Colorado, and Nebraska. Gas and oil are produced from strata from Cambro–Ordovician to Permian ages (Fig. 3). At least three petroleum systems are present in the basin (see Table 1): (1) the Simpson-Viola (!), the Woodford-Paleozoic (!), and the Pennsylvanian-Late Paleozoic (.).

The Ardmore and Marietta basins in south-central Oklahoma are separated by a long, narrow, complexly faulted uplift, the Criner Hills (see Cooper, 1995). The stratigraphic columns of the two basins are so similar that they can be considered to be a single basin for the present purpose. Oil and gas are produced in the basin from strata of Cambrian through Permian ages (Fig. 4). The petroleum systems are the same as those for the Anadarko basin; however, vertical migration and mixing of oils from separate sources have been more common as the result of faults associated with large structures.

The Hollis-Hardeman basin in southwestern Oklahoma produces oil and little gas from reservoirs of Mississippian, Pennsylvanian, and Permian ages (Fig. 5). The identifiable petroleum system is the Carboniferous (.), because strata of Middle Ordovician through Devonian are thin or are not represented in the basin.

The Arkoma basin in eastern Oklahoma and adjacent Arkansas produces mainly gas from Cambro–Ordovician, Siluro–Devonian, and Pennsylvanian strata (Fig. 6). Although source rocks are both oil and gas prone, we believe that liquids generated earlier in the burial history of the basin were driven northward onto the Cherokee platform by the subsequently generated gas. There are at least three petroleum systems in the Arkoma basin: the Simpson-Viola (!), Woodford/Chattanooga-Paleozoic (!), and Pennsylvanian (.).

An additional petroleum system may be present in the Anadarko, Ardmore-Marietta, Hollis-Hardeman, and Arkoma basins. Its existence rests on resolution of the controversial question of whether or not the Arbuckle Group is self-sourcing. This question is particularly significant for southern Oklahoma, where the Arbuckle Group reached a depositional thickness of at least 12,000 ft in the southern Oklahoma aulacogen (Fig. 2).

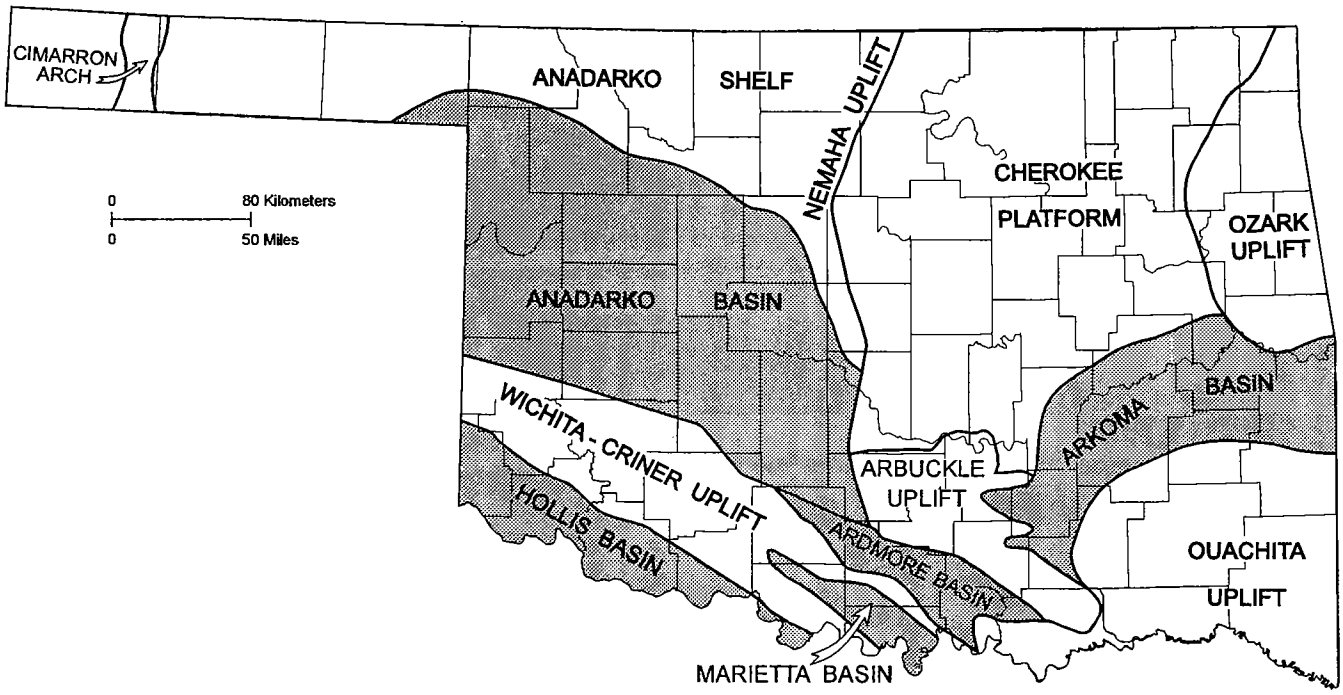

Figure 1. Sedimentary basins (shaded) in Oklahoma. The greater Anadarko basin includes the Anadarko shelf, which extends westward and northwestward into parts of Texas, Kansas, Colorado, and Nebraska (after Northcutt and Campbell, 1996).

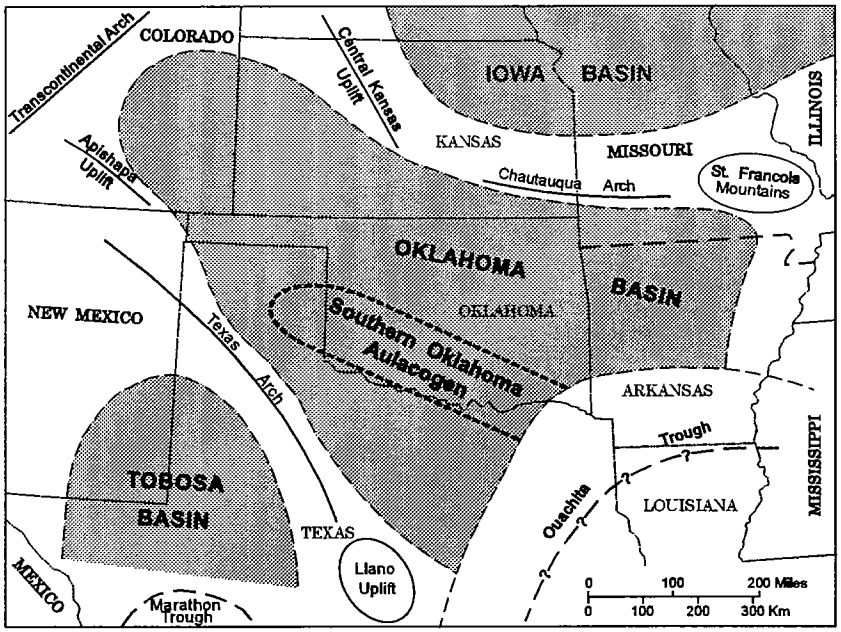

Figure 2. Paleogeography of the southern Midcontinent, showing approximate boundaries of the Oklahoma basin, the southern Oklahoma aulacogen, and other major features that existed during the early and middle Paleozoic (Johnson and others, 1989).

HYDROCARBON - PRODUCING UNITS
ANADARKO BASIN

Ma	SYSTEM	SERIES	PRODUCING UNIT
300	PERMIAN	LOWER	CHASE / COUNCIL GROVE ☼
	PENN.	VIRGILIAN	VIRGIL ● ☼
		MISSOURIAN	MISSOURI GROUPS ● ☼
		DESMOINESIAN	MARMATON / CHEROKEE ● ☼
		ATOKAN	ATOKA ☼
		MORROWAN	MORROW ● ☼
			"SPRINGER" ☼
350	MISS.	CHESTERIAN	CHESTER ● ☼
		MERAMECIAN	MERAMEC ●
		OSAGEAN	MISSISSIPPI LIME ●
		KINDERHOOKIAN	
400	DEVONIAN	UPPER	WOODFORD SHALE ●
		MIDDLE	
		LOWER	HUNTON GROUP ● ☼
	SILURIAN	UPPER	
		LOWER	
450	ORDOVICIAN	UPPER	SYLVAN SHALE ●
			VIOLA GROUP ● ☼
		MIDDLE	SIMPSON GROUP ● ☼
500		LOWER	ARBUCKLE GROUP ☼
	CAMBRIAN	UPPER	TIMBERED HILLS
	PRECAMBRIAN		GRANITE

Figure 3. Generalized stratigraphic column with hydrocarbon-producing formations in the Anadarko basin, Oklahoma.

HYDROCARBON - PRODUCING UNITS
ARDMORE-MARIETTA BASINS

Ma	SYSTEM	SERIES	PRODUCING UNIT
300	PERMIAN	LOWER	PONTOTOC ●
	PENN.	VIRGILIAN	CISCO ●
		MISSOURIAN	HOXBAR ●
		DESMOINESIAN	DEESE ● ☼
		ATOKAN	UPPER DORNICK HILLS ●
		MORROWAN	LOWER DORNICK HILLS ● ☼
			"SPRINGER" ● ☼
350	MISS.	CHESTERIAN	
		MERAMECIAN	
		OSAGEAN	CANEY / SYCAMORE ● ☼
		KINDERHOOKIAN	
400	DEVONIAN	UPPER	WOODFORD SHALE ●
		MIDDLE	
		LOWER	HUNTON GROUP ● ☼
	SILURIAN	UPPER	
		LOWER	
450	ORDOVICIAN	UPPER	SYLVAN SHALE
			VIOLA GROUP ● ☼
		MIDDLE	SIMPSON GROUP ● ☼
500		LOWER	ARBUCKLE GROUP ●
	CAMBRIAN	UPPER	TIMBERED HILLS GROUP
	PRECAMBRIAN		GRANITE

Figure 4. Generalized stratigraphic column with hydrocarbon-producing formations in the Ardmore and Marietta basins, south-central Oklahoma.

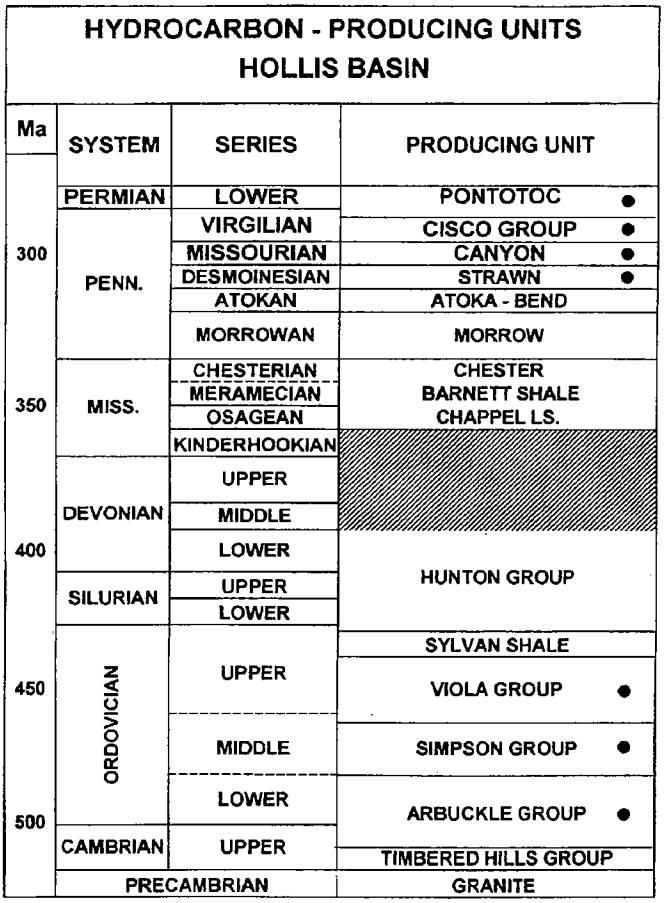

Figure 5. Generalized stratigraphic column with hydrocarbon-producing formations in the Hollis basin, southwestern Oklahoma.

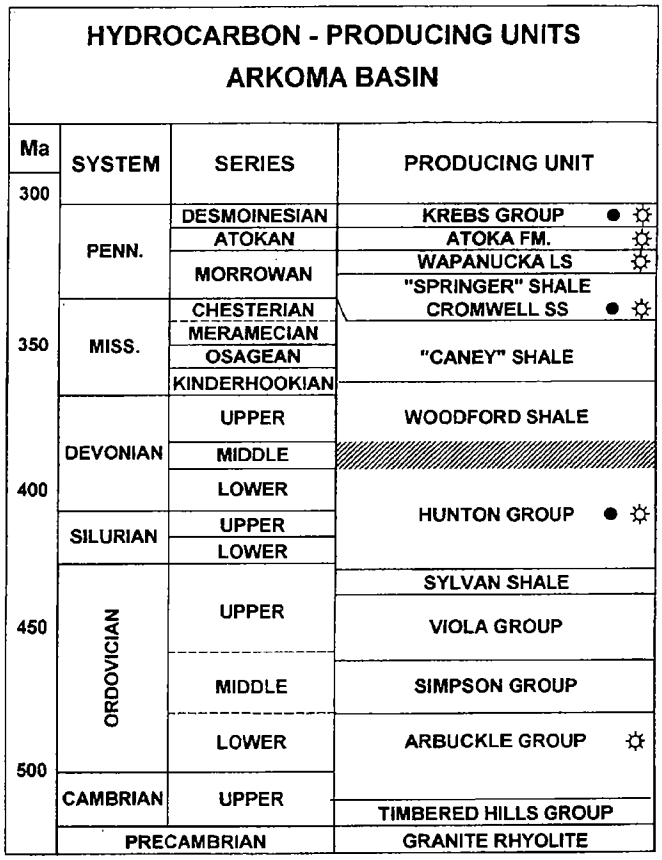

Figure 6. Generalized stratigraphic column with hydrocarbon-producing formations in the Arkoma basin, Oklahoma.

The Ouachita basin of southeastern Oklahoma and adjacent Arkansas, Texas, and Louisiana is the most complex, having been thrusted northward at least 40 mi, partly onto the southern part of the Arkoma basin, during the Early Pennsylvanian. The present architecture of the former Ouachita basin is the allochthonous Ouachita uplift. The frontal, imbricately thrusted structural zone produces prolific quantities of gas from Late Mississippian and Pennsylvanian reservoirs, but the rest of the province is under-explored. Minor amounts of oil (locally commercial) and gas have been produced from Ordovician, Devonian, and Carboniferous reservoirs. We interpret these as "shows" that imply the potential of this under-explored province; the Potato Hills gas field is the first unquestionably commercial venture that demonstrates the potential of the Ouachita uplift south of the frontal thrust belt.

There are at least two petroleum systems in the Ouachitas (Fig. 7): the Ordovician–Silurian (.), in which oil and gas generated in the Womble and Polk Creek shales occur in reservoirs in fractured Bigfork Chert and Blaylock Sandstone (.); and the Devonian–Carboniferous (.), in which gas generated in the Stanley Group and Arkansas Novaculite occur in reservoirs in fractured novaculite and in sandstones of the Stanley and Jackfork Groups. However, significant vertical migration of oil has occurred, such that Ordovician oils have been produced locally from shallow sandstones of the Stanley Group. It is important to note also that in the imbricately thrusted northern part of the province, gas generated in strata of the underlying Arkoma basin probably has migrated vertically to be produced from Carboniferous strata of both the Ouachita uplift and Arkoma basin (Suneson and Campbell, 1990; see also Suhm and Campbell, 2001).

REFERENCES CITED

Comer, J. B., 1992, Organic geochemistry and paleogeography of Upper Devonian formations in Oklahoma and northwestern Arkansas, *in* Johnson, K. S.; and Cardott, B. J. (eds.), Source rocks in the southern Midcontinent, 1990 symposium: Oklahoma Geological Survey Circular 93, p. 70–93.

Cooper, J. C., 1995, Geological evolution of the Criner Hills trend, Ardmore basin, Oklahoma, *in* Johnson, K. S. (ed.), Structural styles in the southern Midcontinent, 1992 symposium: Oklahoma Geological Survey Circular 97, p. 144–157.

Johnson, K. S.; Amsden, T. W.; Denison, R. E.; Dutton, S. P.; Goldstein, A. G.; Rascoe, B., Jr.; Sutherland, P. K.; and Thompson, D. M., 1989, Geology of the southern Midcontinent: Oklahoma Geological Survey Special Publication 89-2, 53 p. [Reprinted from Sloss, L. L., ed.,

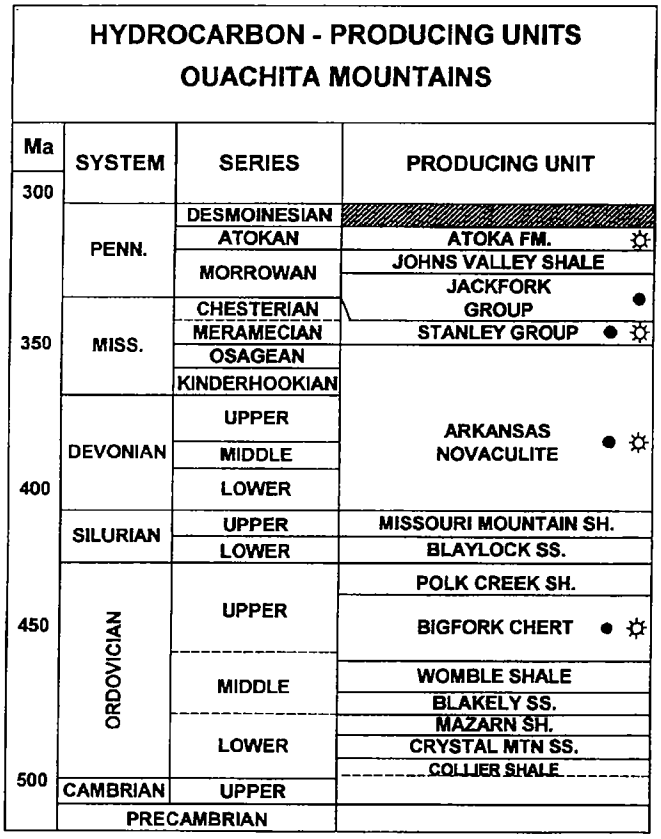

Figure 7. Generalized stratigraphic column with hydrocarbon-producing formations in the Ouachita Mountains uplift, southeastern Oklahoma.

1988, Sedimentary cover—North American craton; U.S.: Geological Society of America, Geology of North America, v. D-2, p. 307–359.]

Magoon, L. B., 1988, The petroleum system—a classification scheme for research, exploration, and resource assessment, *in* Magoon, L. B., Petroleum systems of the United States: U.S. Geological Survey Bulletin 1870, p. 2–15.

Northcutt, R. A.; and Campbell, J. A., 1996, Geologic provinces of Oklahoma, *in* Swindler, D. L.; and Williams, C. P. (compilers), Transactions of the 1995 American Association of Petroleum Geologists Mid-Continent Section meeting: Tulsa Geological Society, p. 128–134.

Suhm, R. W.; and Campbell, J. A., 2001, Pre-Atokan petroleum systems of the Arkoma and Ouachita basins, *in* Johnson, K. S.; and Merriam, D. F. (eds.), Petroleum systems of sedimentary basins in the southern Midcontinent, 2000 symposium: Oklahoma Geological Survey Circular 106 [this volume], p. 196.

Suneson, N. H.; and Campbell, J. A., 1990, Ouachitas need more exploratory drilling: Oil and Gas Journal, v. 88, no. 15, p. 65–69; no. 16, p. 85–87.

Petroleum Systems in Late Paleozoic Elevator Basins of New Mexico

Ronald F. Broadhead
New Mexico Bureau of Mines and Mineral Resources
Socorro, New Mexico

The Tucumcari, Estancia, Vaughn, and Carrizozo basins are located in northeast and central New Mexico (Fig. 1). These basins began to form during the Early to Middle Pennsylvanian. Tectonic development continued through the Early Permian. They were formed along the flanks of the late Paleozoic Sierra Grande and Pedernal uplifts in a strike-slip setting.

These basins were dominated by shallow-shelf deposition. Along the boundaries with adjoining uplifts, these basins have component elevator basins (Fig. 1), long, narrow, and structurally deep troughs bounded by high-angle faults (Figs. 2, 3). Most are elongate parallel to the axes of the adjoining uplifts. Bounding faults have vertical offsets that can exceed 5,000 ft. Basin width ranges from 2 to 10 mi.

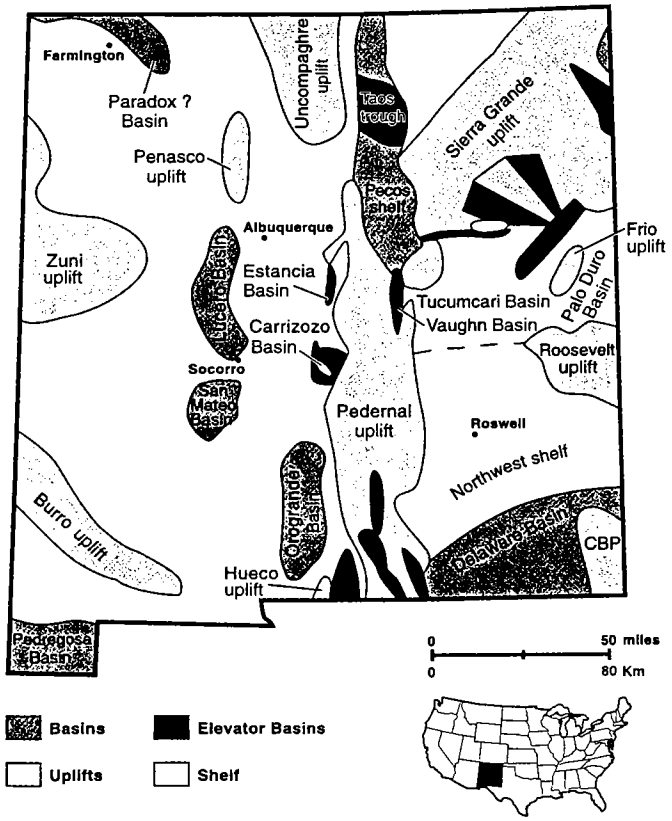

Figure 1. Pennsylvanian uplifts, deep basins, shelf areas, and elevator basins in New Mexico.

Early to Middle Pennsylvanian strata in the elevator basins are gray to black shales and sandstones. The shales are mature petroleum source rocks. Total organic carbon (TOC) can exceed 9% in black shales. Kerogens range from gas-prone woody types to oil-prone amorphous types. Greater depth of burial in the elevator basins as compared to the adjoining uplifts and shelf areas has resulted in increased levels of thermal maturation within the basins. Hydrocarbons generated within the basins have migrated upward along the bounding faults and into reservoirs on adjacent shelves as well as also being trapped in sandstones within the elevator basins.

Source rock type and reservoir type within the elevator basin petroleum system are dependent upon two variables. One variable concerns the orientation of the basin relative to the bordering late Paleozoic uplift, and the other variable concerns the relationship between the rate of subsidence in the elevator basin to the rate of sedimentary accretion in the elevator basin. In all cases, sandstones dominate the reservoirs in the basin. If rates of subsidence exceeded rates of deposition, then the source rocks within the elevator basins would be dominated by oil-prone kerogens, and reservoirs on the adjoining shelf would include marine carbonates that may be dolomitized. If the basin were parallel to the adjoining uplift, then it would separate that uplift from a broad area of shelf deposition, and fringing reefs might be deposited along the shelf side of the basin. If rates of deposition exceeded rates of subsidence, then kerogens within the elevator basin would be dominated by gas-prone kerogens, and source rocks would include coals. Reservoirs on the adjoining shelf are dominated by sandstones.

SUGGESTED READING

Broadhead, R. F., 2001a, New Mexico elevator basins 1—Petroleum systems studied: Oil and Gas Journal, v. 99, no. 2, p. 32–38.

_____ 2001b, New Mexico elevator basins 2—Petroleum systems described in Estancia, Carrizozo, Vaughn basins: Oil and Gas Journal, v. 99, no. 3, p. 31–35.

_____ 2001c, New Mexico elevator basins 3—Elevator basin models; implications for exploration: Oil and Gas Journal, v. 99, no. 4, p. 30–36.

Broadhead, R. F., 2001, Petroleum systems in late Paleozoic elevator basins of New Mexico, *in* Johnson, K. S.; and Merriam, D. F. (eds.), Petroleum systems of sedimentary basins in the southern Midcontinent, 2000 symposium: Oklahoma Geological Survey Circular 106, p. 7–8.

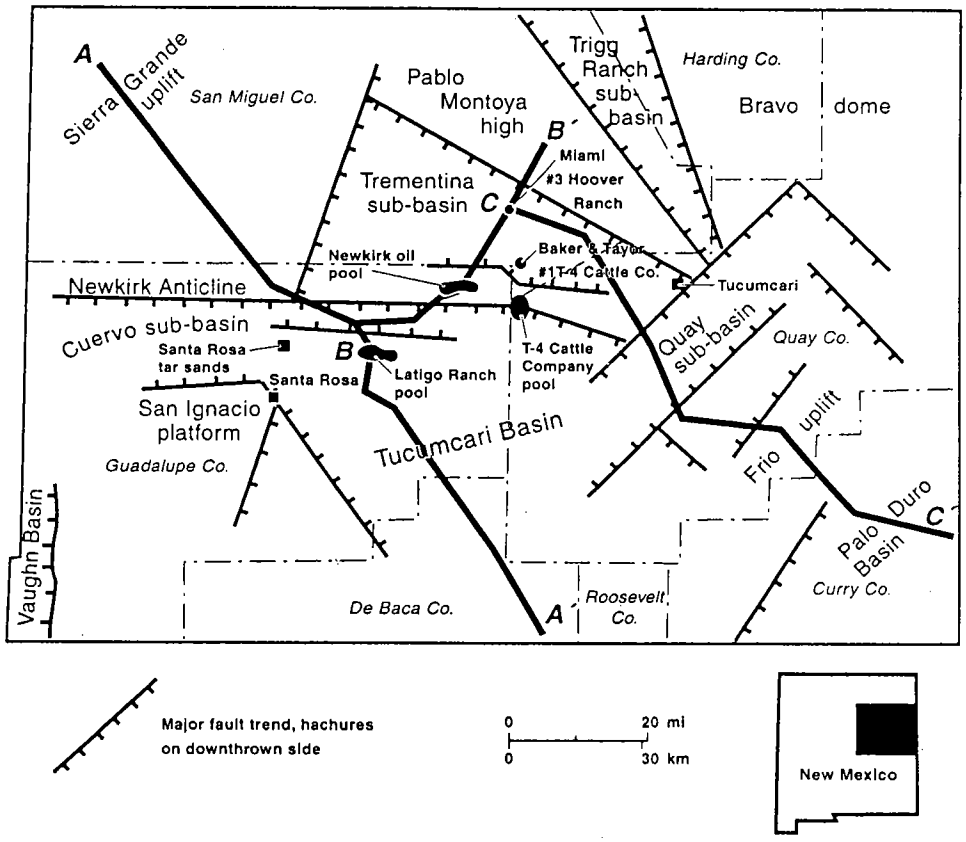

Figure 2. Map of Tucumcari basin area, showing major tectonic elements, known oil and gas pools, and line of cross section B–B´ shown in Figure 3.

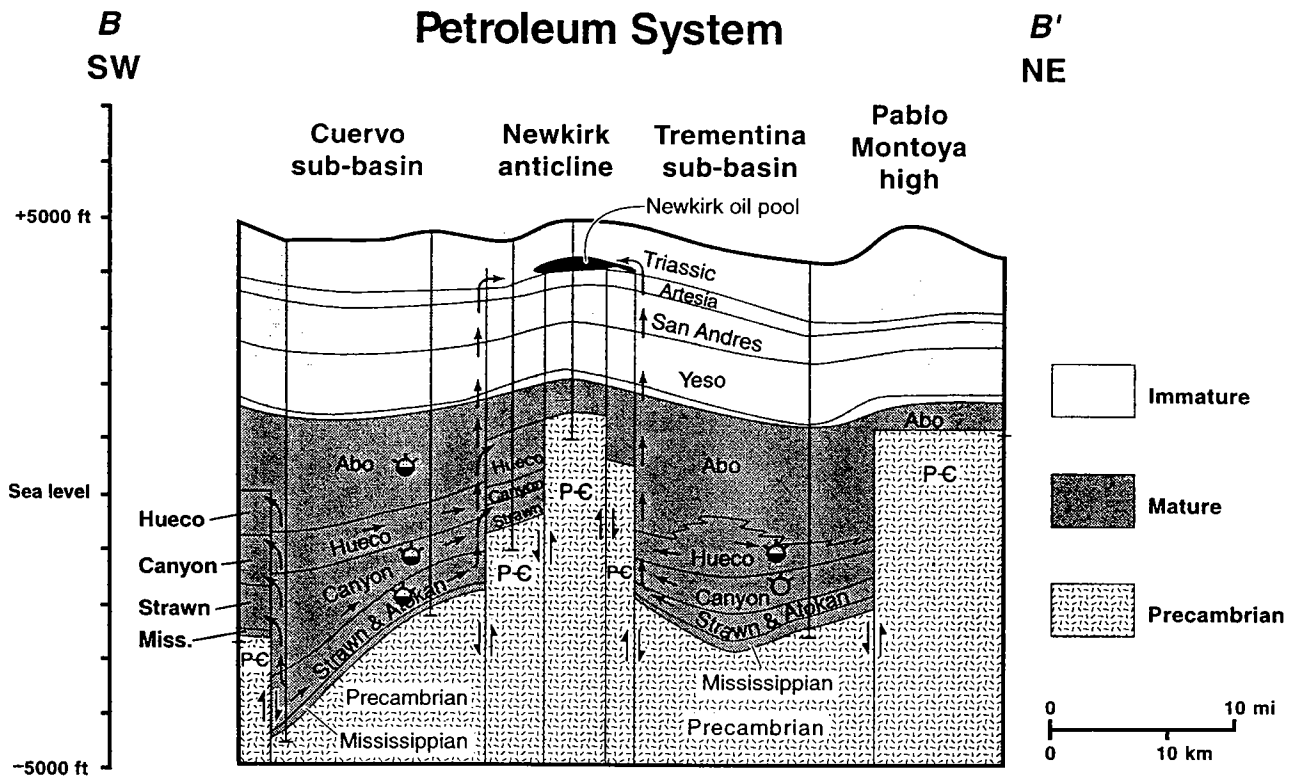

Figure 3. Southwest-northeast cross section through Tucumcari basin showing petroleum system in Pennsylvanian and Lower Permian strata of Trementina and Cuervo subbasins and the Newkirk anticline. See Figure 2 for location of cross section.

Significance of Accurate Reservoir Nomenclature and Its Impact on Identifying Petroleum Systems in the Anadarko Basin

Paul W. Smith, Walter J. Hendrickson, and Ronald J. Woods
Geological Data Services[1]
Addison, Texas

INTRODUCTION

A project recently completed by the authors examined the accuracy of reservoir nomenclature reported to State agencies for the Anadarko basin and shelf area of Oklahoma and Texas. An extensive network of cross sections was created with which more than 45,000 producing wells were examined. The perforated interval was examined on the logs and correlated with the cross sections, whereby a correct and consistent reservoir designation was determined. The regulating agencies of Oklahoma and Texas have not allocated the manpower to undertake such a project or maintain accuracy in nomenclature on such a broad scale. As a result nearly 40% of the State-reported producing formations were either too vague, missing, or simply incorrect.

A database (*Reservoir ID*) was created using a consistent and definitive nomenclature system. Subsequent production maps were constructed that demonstrate plays, trends, and reservoir distributions that were heretofore unavailable. Comparisons using the consistent Geological Data Services (GDS) reservoir nomenclature versus the State-reported nomenclature indicated dramatic differences. With the GDS nomenclature, the production potential of various reservoirs can be examined and realistic expectations of wells can be developed. Using the State-reported data with its included errors caused models to fail and expectations to be unfounded. Specifics of some of our results are included in Smith and others (2001).

STUDY AREA

Figure 1 presents a map of the Anadarko basin and shelf area of Oklahoma and Texas. The study area, as indicated on this figure, encompasses the vast majority of the Anadarko basin and adjacent shelf area.

[1]The work for this paper was completed by the Reservoir Geology Division of IHS Energy Group. Subsequent to presentation and prior to publication of this paper, the Reservoir Geology Division of IHS Energy Group was purchased by Geological Data Services (GDS; Addison, Texas), including the *Reservoir ID* database, all maps, cross sections, well/reservoir database, and expertise. The authors are currently consultants to GDS.

METHODOLOGY

The producing formation(s) in a well is (are) originally defined by way of the completion report filed with the Oklahoma Corporation Commission or the Texas Railroad Commission, in which both the perforated interval(s) and the producing formation(s) are listed. It is a requirement that the producing formation be called as fully and correctly as possible, but there are no exacting standards in his process, nor are there any mechanisms in place to insure that the producing formation has been correctly and fully defined. As a result, the nomenclature in the basin and shelf area is at times most erratic and less than precise. During a recent effort, geologists of GDS began to standardize reservoir nomenclature, and the authors generated more than 15,000 mi of geologic cross sections to demonstrate the stratigraphic sequences and relationships throughout the Anadarko basin and shelf area. Figure 2 presents the generalized stratigraphic section used in this study to designate reservoir and formation names. Figure 3 is a base map of the approximate study area indicating the network of nearly 3,000 mi of "drafted and published" cross sections that are only a small part of the total used in this project. To insure nomenclatural consistency and accuracy, the electric logs of more than 45,000 wells were reviewed for this study. Regarding the perforated interval (as reported to the appropriate State regulatory agency and indicated by completion cards), a comparison was made between the formation—as indicated by GDS regional cross sections—and the operator-defined producing formation. Where a difference between the two was found, the nomenclature indicated by the regional cross sections was used.

RESULTS

Almost 40% of the producing formations, as originally defined on completion cards, were either too vague, too broad, or incorrect, and consequently were reassigned a reservoir name to conform to the cross sections. Those reservoir names that required the highest number of corrections were the Chester and Mississippian, Springer Group, Morrow Group, Cherokee Group, and "Granite Wash."

It was also noted during the course of the study that

Smith, P. W.; Hendrickson, W. J.; and Woods, R. J., 2001, Significance of accurate reservoir nomenclature and its impact on identifying petroleum systems in the Anadarko basin, *in* Johnson, K. S.; and Merriam, D. F. (eds.), Petroleum systems of sedimentary basins in the southern Midcontinent, 2000 symposium: Oklahoma Geological Survey Circular 106, p. 9–13.

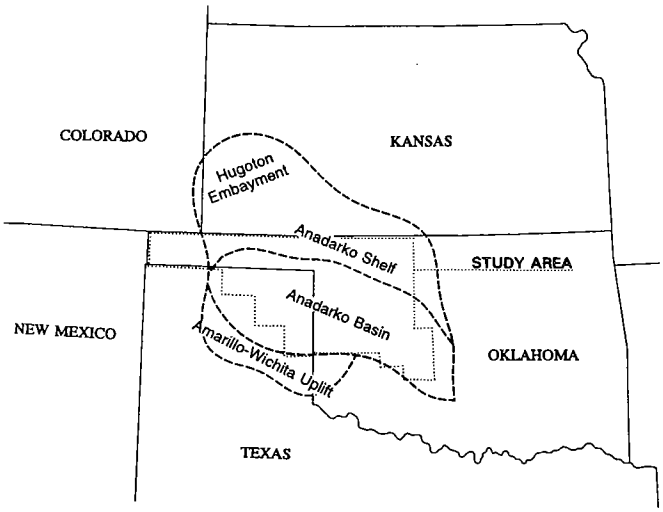

Figure 1. Map showing location of study area in Anadarko basin in western Oklahoma, the Texas Panhandle, and southwestern Kansas.

certain reservoirs tended to be correctly named. These included the Tonkawa, Oswego, Cleveland, Hunton, Viola, and Arbuckle.

Another observation that was made during the study was that about 15% of the perforated intervals required correction because (1) reporting or typographical errors were made or (2) the perforated interval was simply absent from the production records.

SPECIFIC EXAMPLES

Morrow Group

The Morrow Group suffered from poor definition and recognition of its various members. During the study, the Morrow Group was subdivided into the Upper Morrow, Lower Morrow, and Primrose members. The Upper Morrow was misidentified as Atoka for wells in a number of areas. This misidentification was corrected in the *Reservoir ID* database that was constructed for this study. Also, there was seldom any differentiation in the lower portion of the Morrow Group as reported on completion cards. To lend increased definition to these sandstones, the lower portion of the Morrow Group (below the Squawbelly marker) was subdivided into what is now identified as Lower Morrow with the lowermost portion identified as Primrose.

Additionally, there were substantial instances of Springer sandstones being misidentified as Morrow. These corrections were also made in the database.

The nomenclature inconsistency observed for the Morrow Group was very similar to that observed for the whole population. That is to say that State-reported single-zone Morrow completions would only represent approximately 58% of the actual number of single-zone Morrowan completions that are presently indicated in the GDS *Reservoir ID* database. Because commercial production databases rely upon State-reported data, all commercially available databases contain the same vague and at times erroneous data identifying the producing formation. Obviously, this condition would prevent accurate representation of any one of the Morrow members in regard to reservoir characteristics or reserve characteristics. Additionally, approximately 10% of the State-reported Morrow Group completions were not actually Morrowan. Production maps using the State-reported nomenclature would likely mask production trends and hide gaps in production that would be noted with more consistent and higher-definition nomenclature.

After the reallocation was completed and the definitive and consistent nomenclature assigned, the cumulative production values as calculated from the *Reservoir ID* database were provided (Table 1). It becomes obvious that the various reservoirs have differing production capabilities. One cannot use the term "Morrowan" since the overall population would misrepresent the production characteristics of the three subdivisions.

"Washes"

Correct identification of the "washes" suffered even more than the members of the Morrow Group from poor definition and recognition of its subdivisions. Correlation problems have long existed between the Pennsylvanian marine clastics of the northeastern half of the Anadarko basin and shelf and the Pennsylvanian terrigenous washes of the extreme southwestern portion of the Anadarko basin. These correlation problems have created nomenclature problems resulting in thousands of feet of washes commonly referred to on completion reports and production records as "granite wash" or "Atoka Wash," when much greater accuracy and specificity are both needed and possible. Analysis indicated that commonly the reservoir rocks were neither granite wash (being chert or carbonate washes) nor Atokan in age (being either younger or older).

It was possible to subdivide the washes and assign more accurate and definitive nomenclature with the regional correlations indicated by the cross sections. Certain markers proved to be regionally persistent from the marine clastics into the terrigenous washes, making the subdivision of thousands of feet of washes possible. Those of greatest importance were the top of the Marmaton, the Cherokee Marker, the Pink "Limestone" interval, the top of the Atoka, and the top of the Morrow. Once these and other subdivisions were made, production was allocated on a much more definitive basis.

Although the State-reported number of granite-wash completions totaled 1,985, the study conducted by GDS identified a total of 2,583 completions in wash reservoirs, of which 2,260 were single wash reservoir completions. In identifying wash completions from the State-reported data, it would be necessary to realize that various reservoir names have been given to wash reservoirs. It would be especially important to know that "Desmoinesian" or "Pennsylvanian" in the State-reported data could likely represent a wash completion. Yet, they could also represent a Prue, Skinner, or Red Fork completion. Even with knowledge of all the various reservoir names in the State-reported data, only

SYS.	SERIES	GROUP	UNIT	SANDSTONE	CARBONATE	EQUIVALENT
PENNSYLVANIAN	VIRGILIAN	Shawnee/Cisco	Topeka Ls Pawhuska Ls Hoover Ss Elgin Sd Oread Ls Heebner Sh Endicott Ss	Hoover Endicott	Pawhuska Oread Ls	
		Douglas/Cisco	Lovell Ls Haskell Ls Tonkawa Ss	 Tonkawa	Douglas Group	
	MISSOURIAN	Lansing/Hoxbar	Avant Ls Cottage Grove Ss	Cottage Grove	Lansing Group	
		Kansas City/Hoxbar	Dewey Ls Hogshooter Ls Layton Ss Checkerboard Ls Cleveland Ss	 Layton Cleveland Culp	Kansas City Group Melton	 Marchand Upper Marchand Lower
	DES MOINESIAN	Marmaton	Big Lime Oswego		Big Lime Oswego	Marmaton Wash
		Cherokee	Cherokee Marker Prue Ss Verdigris Ls Skinner Ss Pink Ls Red Fork Ss Inola Ls Mona	Prue Skinner Red Fork Cherokee Wash Middle Cherokee Wash Lower/ Mona	Verdigris Inola	Prue Wash Skinner Wash Red Fork Wash Bartlesville, Tussy
	ATOKAN	Atoka	Atoka 13 Finger Ls	Atoka	Atoka 13 Finger	
	MORROWAN	Morrow	Morrow Primrose	Upper Morrow Lower Morrow Primrose		
MISSISSIPPIAN	SPRINGERAN	Springer	Cunningham Britt Boatwright	Cunningham Britt Boatwright	Britt Boatwright	
	CHESTERIAN	Chester	Chester Ls		Chester	
		Manning	Manning Ls		Manning	
	MERAMECIAN	Meramec	Meramec Chat Meramec Ls		Meramec Chat Meramec	
	OSAGEAN	Osage	Osage Ls			
	KINDERHOOKIAN	Kinderhook	Kinderhook Sh			
SIL./DEV.	CHATTANOOGIAN		Woodford Sh Misener Ss	Misener		
	ULSTERIAN	Hunton	Hunton Group		Hunton (Frisco) Hunton (Bois d'Arc) Hunton (Haragan) Hunton (Henryhouse) Hunton (Chimney Hill)	
	NIAGARAN ALEXANDRIAN					
ORDOVICIAN	CINCINNATIAN	Sylvan	Sylvan Sh Maquoketa		Maquoketa	
	CHAMPLANIAN	Viola	Viola Group		Viola (Fernvale) Viola (Trenton)	
		Simpson	Simpson Dense Bromide Ss Tulip Creek Ss McLish Ss Oil Creek Ss Joins	 Bromide Tulip Creek McLish Oil Creek Joins		
	CANADIAN	Arbuckle	Arbuckle Group		Arbuckle	
CAMB.	CROIXAN					

Figure 2. Generalized stratigraphic section for Anadarko basin in western Oklahoma. Sys. = system; Camb. = Cambrian; Sil./Dev. = Silurian–Devonian.

TABLE 1. — Reallocation of Reservoir Names, Well Count, and Average Cumulative Gas and Oil Production from Morrow Group within Anadarko Basin (for *Reservoir ID* Database)

Reservoir name	Well count	Avg. cum. gas[a]	Avg. cum. oil[b]
"Single Zone Morrowan"	9,668	1,787,651	38,133
Subdivisions of the Morrow Group:			
MORROW UPPER	4,123	2,302,464	70,442
MORROW LOWER	4,473	1,370,050	13,485
PRIMROSE	1,072	1,550,109	16,717

[a]in MCF = 1,000 cubic feet
[b]in barrels of oil

TABLE 2. — Petroleum Production from Reallocated "Washes" in Anadarko Basin with Well Count and Average Gas and Oil Production (from *Reservoir ID* Database)

Reservoir	Count	Avg. gas[a]	Avg. oil[b]
Average "Wash" completion		**1,150,526**	**23,881**
Wolfcamp Wash	276	1,567,314	19,861
Tonkawa Wash	45	494,505	81,348
Cottage Grove Wash	34	572,659	18,898
Layton Wash	47	1,216,073	68,553
Cleveland Wash	51	1,012,085	73,534
Marmaton Wash	420	1,045,858	34,216
Prue Wash	417	1,199,836	19,394
Skinner Wash	213	512,671	12,602
Red Fork Wash	158	1,160,803	13,637
Cherokee Middle Wash	68	3,241,442	8,707
Cherokee Lower Wash	43	2,061,468	8,607
Atoka Wash	32	384,800	2,401

[a]in MCF = 1,000 cubic feet
[b]in barrels of oil

77% of the wash completions would be identified, and those would suffer from poor definition as to their stratigraphic position. With the lack of definition inherent in the State-reported reservoir nomenclature, no accurate and certainly no quick comparisons of production characteristics could be performed. The GDS study has indicated that consistent and definitive reservoir nomenclature is possible and highly beneficial in the "wash" reservoirs.

Table 2 is a list of the "wash" reservoirs that were identified through the GDS study and entered into the *Reservoir ID* database. Using the average "wash" completion as a guideline for predicting production performance would be within 10% of being accurate for the Marmaton, Prue, and Red Fork Washes. Other reservoirs could suffer an error from overstating by 400% to understating by 250%.

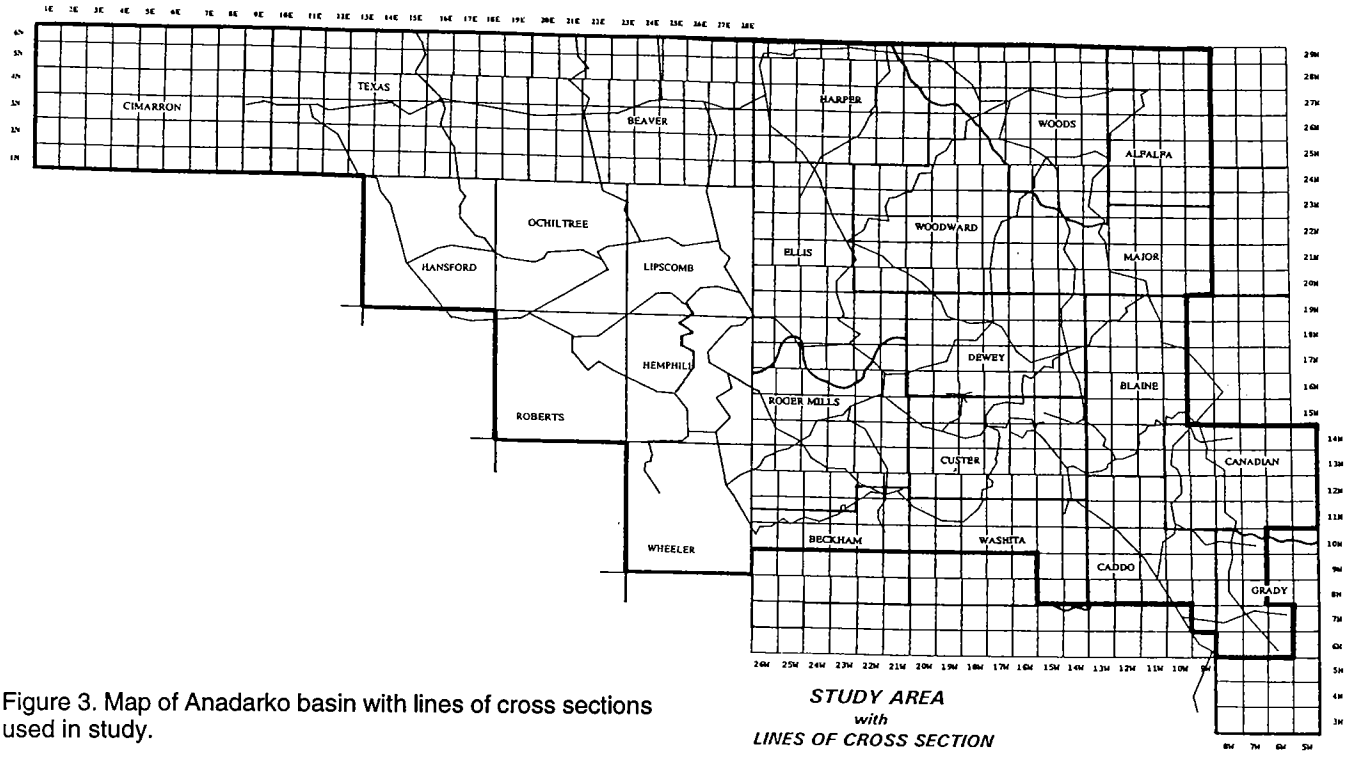

Figure 3. Map of Anadarko basin with lines of cross sections used in study.

Springer Group

It became apparent during the study that a substantial percentage of the Springer reservoirs as reported to the State were in fact Morrowan. Additionally, there was exceedingly poor definition to the Springer Group in that the reservoirs commonly were not defined past the point of being called "Springer" or even "Morrow/Springer." As with the "washes," greater definition is both possible and highly desirable. For the GDS study and in the resultant *Reservoir ID* database, the Springer Group has been divided into its members, which are, in ascending order, Cunningham Sandstone, Britt Sandstone or Carbonate, and Boatwright Sandstone or Carbonate (Fig. 2).

Cherokee Group

The Cherokee Group has very poor definition in the State-reported data and is also commonly in error. The poor definition came from reservoirs being defined as "Des Moinesian" or "Cherokee." Where individual member names were used, they were commonly used incorrectly. The study by GDS divided the Cherokee Group into the Prue, Skinner, Red Fork, and Mona (Bartlesville) members (Fig. 2) and indicated those member names in the *Reservoir ID* database along with whether those members were sandstones or washes.

CONCLUSIONS

Accurate reservoir nomenclature is something that affects every aspect of the oil business as well as the geologic scientific effort. As has been indicated by the study by GDS, accurate reservoir definition is both possible and desirable. Accurate reservoir definition provides insight into geologic plays that would otherwise be masked and/or overlooked. With better definition of reservoirs, more accurate "pre-drill" predictions can be made as to reservoir characteristics and reserve potential. Accurate reservoir definition also makes possible (with a higher degree of confidence) the comparison of production results and histories with related reservoirs.

REFERENCE CITED

Smith, P. W.; Hendrickson, W. J.; and Woods, R. J., 2001, Comparison of production and reservoir characteristics in "granite wash" fields in the Anadarko basin, *in* Johnson, K. S.; and Merriam, D. F. (eds.), Petroleum systems of sedimentary basins in the southern Midcontinent, 2000 symposium: Oklahoma Geological Survey Circular 106 [this volume], p. 19–27.

Gravity-Tide Tectonics and Sedimentary Basins

P. Jan Cannon
Planetary Data
Tecumseh, Oklahoma

ABSTRACT.—The Earth has a mobile crust that has been downwarped, uplifted, and faulted. The tectonic systems that create sedimentary basins have to be strong driving forces that also account for any associated structures.

Modern remote sensing data indicate that fractures and faults are zones of weakness propagated through 4 to 5 km of overlying sediments by the stresses of daily gravity tides. Twice each day, the Moon squeezes the Earth with a tidal bulge. Differential movement across the face or plane of a major fracture causes fatigue of the materials above the fracture. Zones of fatigue appear at the present surface as subtle physical discontinuities and minor chemical differences. These can be detected and enhanced with modern remote sensing techniques that are sensitive to these minor physical and chemical differences.

In relation to geologic history, a million years is a small amount of time. However, in a million years the different sides of a fracture have been moved past each other 730 million times—almost three-fourths of a billion times—by the gravity tides. In three million years, there would have been more than two billion episodes of differential movement. Geologic evidence indicates that the tidal cycle in the Ordovician and Cambrian was more frequent than the current one, creating at least three tidal pulses a day. The Ordovician ended more than 430 million years ago.

The effects of gravity tides are adequately demonstrated on some of the other planets and their moons. Io, the inner moon of Jupiter, is covered with volcanoes from pole to pole. The differential effects of gravity-tide stresses between Jupiter and the three other large moons, Europa, Ganymede, and Callisto, distort the mass of Io every few hours, releasing enough heat to generate volcanoes on this low-density satellite, which is about the same size as the Moon.

The Earth's tectonic features can be adequately explained with gravity-tide forces. Convection cells cannot be used, convincingly, to explain the tectonic features on the Earth or other planetary bodies. Gravity tides are a real, documented force, whereas there is no evidence that global size convection cells exist inside the mantles of planetary bodies. Plumes of rising superheated mantle do exist on planetary bodies and can be delineated with seismic data on the Earth. However, their existence does not support the presence of convection cells. In fact, such plumes cannot coexist with an active convection cell system.

Remote-sensing data have given us an unprecedented view of the solar system, a view that stresses the importance of impact cratering and gravity tides as major geologic processes. Several examples of planetary bodies indicate that the major tectonic processes in the solar system are gravity-tide driven.

EXAMPLES FROM JUPITER'S MOONS

The effects of gravity tides are adequately demonstrated on some of the other planets and their moons. Io, the inner moon of Jupiter, is covered with volcanoes from pole to pole. The differential effects of gravity-tide stresses between Jupiter and the three other large moons, Europa, Ganymede, and Callisto, distort the mass of Io every few hours, releasing enough heat to generate volcanoes on this low-density satellite, which is about the same size as the Moon.

The next moon out from Jupiter is Europa. It does not exhibit any active volcanoes but does have a geologically young surface that is evidenced by surface structures and physiography. It is riven with huge fractures and crevasses. The lack of impact craters of any size is a positive indicator of a geologically youthful surface.

Cannon, P. J., 2001, Gravity-tide tectonics and sedimentary basins, *in* Johnson, K. S.; and Merriam, D. F. (eds.), Petroleum systems of sedimentary basins in the southern Midcontinent, 2000 symposium: Oklahoma Geological Survey Circular 106, p. 15–18.

Ganymede, the third moon out from Jupiter, has a surface exhibiting a few large fractures and a great increase in impact cratering. This mix of features indicates a surface older than Io's or Europa's. Ganymede's surface has undergone only minor tectonic stress.

Impact craters are the most common landform in the solar system. The older the planetary surface is, the greater the degree of impact cratering. Any tectonically inactive planetary surface exhibits a degree of impact cratering directly related to its age (Hartmann, 1970). Chapman (1977) refers to impact craters as planetary chronometers.

Tectonically active planets such as Io and the Earth show very few impact craters because of crustal movement and the effects of active volcanism. The Moon, which has been tectonically dead for more than three billion years, shows an intensely impact cratered surface. Throughout the solar system this relationship between the degree of visible impact cratering and the intensity of global tectonics is absolute.

Based on the surface features of the three inner moons of Jupiter, it is easy to predict the surface of its fourth moon, Callisto. It has a densely cratered surface and shows none of the tectonic features found on the three inner moons. Callisto is just a little larger than the Moon but just as heavily cratered. The surface features indicate that the global tectonics of the Moon are very similar to those of Callisto. Predictably, Jupiter's moons, out beyond the four inner moons, show surfaces densely covered only with impact craters.

EXAMPLES FROM OTHER MOONS

Further evidence of the influence of gravity-tide–driven tectonics is seen on the moons of the other planets. The moons of Saturn, Uranus, and Neptune show a similar range of features. It is important to note that the rings of Saturn are located close to the planet in a gravity-tide zone just a little more intense than that which affects Io. The strings, consisting of ice and rock debris that makes the rings, show irrefutably the effects of gravity tides. Lumps or bulges of material regularly follow the tidal nodes around the rings.

The four small moons beyond Saturn's rings, Mimas, Enceladus, Tethys, and Dione, are all closer to Saturn than Io is to Jupiter and are less than one half the size of Io. These four moons all show a range in tectonics and impact cratering similar to that of Europa and Ganymede. If it were not for the fact that Saturn is the planet with the lowest density in the solar system and its mass is less than one-third that of Jupiter, these inner moons would be, in part, similar to Io. The next moon out from Saturn (Rhea) looks similar to Callisto and the Moon.

THE INNER PLANETS

The inner planets of the solar system show the same tidal-driven–tectonic effects as the moons of the big outer planets. Mercury's rotational period is 59 Earth days long and its year is 88 Earth days long. There are two mercurial years to exactly three mercurial days. This is referred to as spin-orbit coupling and is due to the strong tidal pull on the planet by the Sun. Any heat generated by the 59-day tidal bulge is dissipated during the long slow rotation. Indeed, the surface of Mercury is densely cratered like the surfaces of Callisto and the Moon. All surface features on Mercury indicate a tectonically dead planet.

Venus and Mars have similar surface features and, like Mercury, they have no true moons. Deimos and Phobos, the so-called moons of Mars, are just rocks less than 30 km in diameter and appear to be captured asteroids. They definitely do not have enough mass to generate any tidal effects on Mars.

The surfaces of Venus and Mars are covered with two distinct landforms, giant volcanoes and numerous, large impact craters. These landforms provide a key to their global tectonics. The degree of impact cratering is less than one-third of that found on Mercury and the Moon. The volcanoes on Venus and Mars are much larger than those generated on the Earth. Individual shield volcanoes on Venus are more than 1,000 km in diameter and shield/cone complexes rise more than 25 km above the surrounding plains of Mars.

The impact craters indicate a planetary surface that is geologically old—at least 2 billion years old. These are not as old as the planetary surfaces of Mercury, the Moon, or Callisto, but are much older than the surfaces of Io, Europa, and the Earth. This age is supported by the fact that these volcanoes had to sit in one place for a very long time on an immobile crust in order to build their gigantic cones and shields.

Venus and Mars have no large satellites that can generate large and rapid tidal distortions. Venus rotates only once every 243 Earth days, a period longer than its year of 224.7 Earth days. It, like Mercury, rotates so slowly that any tidal effects generated by the Sun are dissipated.

The diameter of Mars is only about half that of Venus and the Earth. The highest known volcanoes in the solar system rise over the plains of Mars. It must have an extremely thick crust in order to support such volcanic features. We do not see island arcs, fold belts, or any other evidence of global tectonics on Mars. There is no evidence that the volcanoes on Mars or Venus are active.

Because the volcanoes of Mars and Venus are stationary, they must have sat over a plume of hot mantle generated by radiogenic heat. The volcanoes on both planets lie along major fracture systems that have probably originated from gigantic impact features that occurred very early in the geologic history of the two planets.

On the Earth, the majority of volcanoes lie in island arcs that are associated with the fold belts and trenches generated by an active global tectonic system. The extremely few and relatively small impact craters are positive indications of a surface kept youthful, geologically speaking, by global tectonics.

On Venus, there are no island arcs and no fold belts. However, there are immense volcanic features and great numbers of large impact craters. These are indications of a nearly immobile crust and the lack of a global tectonic system such as that which exists within

the Earth. Some astronomers have misinterpreted large fracture zones on Venus that are associated with impact craters and volcanoes as fold belts. This is unfortunate because such misinformation has a great influence on the not geologically astute public. The problem exists because they have not been properly trained in the geologic interpretation of various types of imagery and have weak educational backgrounds in global tectonics, structural geology, and geomorphology.

The Earth and Venus are nearly identical in size and density. If convection cells were the force running the global tectonics of the Earth, and if these were a naturally occurring process dependent upon the size and mass of a planet, then the Earth and Venus would exhibit nearly identical surfaces. So why don't they show nearly identical global tectonic systems?

The major difference between the Earth and Venus is that the Earth's diameter is distorted almost twice a day by a very significant tidal bulge. A distortion of rock (20 to 30 cm in some areas) is generated by its moon and its rapid rate of rotation. This is a situation not too dissimilar to that existing on Io and Europa.

TERRESTRIAL TECTONICS

On the Earth, plates of crust, dragged over hot spots or magma plumes, give rise to islands such as the Hawaiian Islands. This feat cannot be achieved with convection cells. We can account for this phenomenon, if the crustal plates are being pulled over such hot spots by gravity tides.

If convection cells were a real process within the Earth, the amount of heat loss would be greatest at the poles because the diameter of the Earth is less through the poles than across the equator. However, this is not the case. The geothermal gradient rapidly dips into the Earth at the poles. We can account for this if the major tectonic processes within the Earth are driven by gravity tides.

The distortional effects of gravity tides are greatest at the equator, becoming less and less as you approach the poles. Gravity-tide tectonics explain the greater heat loss at the equator, the rotation of crustal plates, subduction zones, and the fact that plates or portions of plates are being dragged over other plates.

The whole premise behind convection cells is that hotter, less-dense material rises in cooler, denser material. If true, then, how is it that when convection cells get to a subduction zone they are expected to run in reverse? It goes against the laws of physics for convection cells to pull less-dense material down into denser material. Drag by gravity tides can do this. Gravity acts in concert over an entire plate. The Earth's rate of rotation generates a periodic tidal pulse that acts like the regular tap of a gigantic hammer. A similar effect occurs in the oceans. The waters of the Pacific and Atlantic oceans literally slosh with a gravity-driven periodicity (Sanchez, 1991). Gravity generates a planet-wide bulge affecting the whole face of the planet and the interior rocks.

Gravity tides are not simple ripples that race across a planetary surface. Gravity tides can selectively drag portions of the mantle faster than parts of the crust, creating basins as the crust sags into the depleted areas.

Convection-cell tectonics run on the premise that the Earth's crust is being moved in conveyor belt fashion, always with the mantle moving faster than the crust. Such movement would be in keeping with compressional tectonics with the major part of the crustal materials piled up at the subduction zones. There would exist no mechanism for tensional tectonics except over the rising limbs of two adjacent convection cells.

Tensional tectonics do exist on the Earth in areas that are distant from the spreading centers. Such centers are assumed to lie over the rising limbs of two adjacent convection cells. Also, tensional tectonics exists within continental plates far from any spreading center. However, differential drag on parts of the crust by gravity tides would create tensional and pull-apart effects within a crustal plate. Differential drag can be created by gravity tides because gravity is a mass-to-mass force.

Large slabs of crustal rock have been transported over other crustal rocks in such areas as the Appalachian and Ouachita Mountains. Such slabs of crustal rocks cannot be moved in a bulldozer fashion with convection cells or any other mechanism, because the slabs would just crumple at the bulldozer's blade. Such slabs (as a body) would stay intact when pulled over other portions of the crust with gravitational forces, because the individual parts of such a slab are each pulled in concert by gravity tides.

The adjacent limbs of two convection cells are not coupled. A mechanism that causes coupling between two such adjacent limbs does not exist. How, then, can we account for the parallel magnetic anomalies that exist on either side of a spreading zone like the Mid-Atlantic Ridge? We can do that easily with gravity-tide tectonics. The spreading rocks are like two wet sheets of paper stuck together. When you hold the top edge of one sheet stationary and pull the top edge of the other sheet away in a perpendicular direction the sheets will separate at the wet faces like the rocks at a spreading center. As the moving sheet travels away from the stationary sheet, the spreading center will move in the direction of the moving sheet. This type of movement provides a coupling mechanism that does not exist between convection cells.

If terrestrial convection cells were rising at the spreading centers, then such centers would be lines of continuous volcanic activity. This is not the case. In fact, lines of volcanoes line the subduction zones. If convection cells were acting at these areas, then, slabs of cooler rock should be sinking at these zones. It is difficult to conceive how friction from sinking cool rocks could be generating enough heat to create volcanoes but less heat than that necessary to drive global-size convection cells. It seems more plausible that oceanic plates are being forced beneath other plates at the subduction zones by the effects of gravity tides. Such forcing of rocks under other rocks could conceivably generate volcanoes but not the differential sinking of cool, denser rocks past slightly less-dense ones.

THE EARTH-MOON SYSTEM

A critical point to understand is that the Earth-Moon system is really a double planet system revolving around a common center of mass. This common center of mass is about 2,000 km below the surface of the Earth (Fig. 1). The common center of mass surges through the Earth's mantle each day.

The Moon is gravity-locked to the Earth, always keeping the same face toward the Earth. In relation to the Earth, the Moon does not rotate. If the Moon did rotate once every 10 days or faster, it would be covered with active volcanoes from pole to pole, like Io. As the solar system formed some 5 billion years ago, all planetary masses would have contained huge amounts of angular momentum. Because of this, every rock and rock/ice body would have been rapidly rotating. Four and a half billion years ago, the Moon and Mercury may have been rotating rapidly, and that would account for their ancient volcanic histories.

SUMMARY AND CONCLUSIONS

The Earth's tectonic features can be adequately explained with gravity-tide forces. Convection cells cannot be used, convincingly, to explain the tectonic features on the Earth or other planetary bodies. Gravity tides are a real, documented force, whereas no evidence exists that global-size convection cells are present inside the mantles of planetary bodies. Plumes of rising superheated mantle do exist on planetary bodies and can be delineated with seismic data on the Earth. However, their existence does not support the presence of convection cells. In fact, such plumes cannot coexist with an active convection-cell system.

Remote-sensing data have given us an unprecedented view of the solar system. This view stresses the importance of impact cratering and gravity tides as major geologic processes. Several examples of planetary bodies indicate that the major tectonic processes in the solar system are gravity-tide driven.

Of the planetary surfaces that we have investigated with remote-sensing data, only the Earth and Io have young active volcanoes. The volcanoes on Mars and Venus do not appear to be active and are extremely old constructs.

It is interesting to note that no one disagrees about the effects of gravity-tide tectonics on the four inner moons of Jupiter. However, suggest that gravity is a real force driving the tectonics of the Earth, and the howls of disbelief begin.

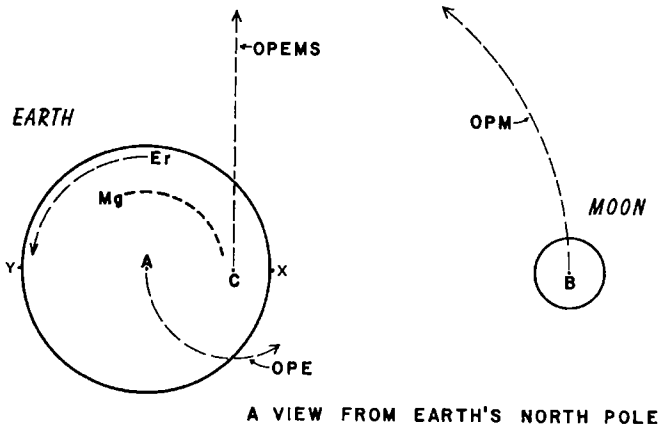

Figure 1. A diagrammatic view of the Earth-Moon system from the Earth's north pole. The diameters of the Earth and the Moon are to scale but the distance between them is compressed in order to facilitate comparisons. The high-tide nodes are always between C and B and on the Earth's surface opposite of C along the line A–C–B (the antipodal point). Point C always lies between A and B, whereas the Earth's mantle is rotated through point C. The average time between successive high tides is 12 hours and 25.5 minutes. *Explanation of symbols:* A = center of the Earth's mass; B = center of the Moon's mass; C = common center of mass about which the Earth and the Moon revolve (tidal forces are generated about this point, not from point A); Er = direction of the Earth's rotation as viewed from the north pole; Mg = zone within the Earth's mantle of the maximum value for the acceleration of gravity (g) (a common misconception is that the maximum value for g is situated at the point A); OPEMS = orbital path of the Earth-Moon system about the Sun; OPE = orbital path of Earth about the common center of mass (C); OPM = orbital path of the Moon about the common center of mass (C); X = high-tide point on the Earth's surface facing the Moon; Y = antipodal high-tide point on the Earth's surface.

REFERENCES CITED

Chapman, C. R., 1977, The inner planets: Charles Scribner and Sons, New York, p. 12–25.

Hartmann, W. K., 1970, Lunar cratering chronology: Icarus, v. 13, p. 299–301.

Sanchez, B. V., 1991, Proudman functions and their application to tidal estimation in the world ocean, *in* Parker, B. B. (ed.), Tidal hydrodynamics: John Wiley and Sons, New York, 234 p.

Comparison of Production and Reservoir Characteristics in "Granite-Wash" Fields in the Anadarko Basin

Paul W. Smith, Walter J. Hendrickson, and Ronald J. Woods
Geological Data Services[1]
Addison, Texas

INTRODUCTION

A project recently completed by the authors examined reservoir nomenclature, reservoir characteristics, and production histories of wells completed within various "granite-wash" reservoirs within the Anadarko basin of Oklahoma and Texas (Hendrickson and others, 2001; Smith and others, 2001). The initial step was to determine a consistent nomenclatural system by which the various reservoirs could be distinguished. This portion of the study was accomplished by using a substantial network of detailed cross sections and covered the Anadarko basin and shelf area of Oklahoma and Texas. A second step, which, for the purposes of this paper, involved only the Texas Panhandle, included detailed reservoir evaluation. Data collected included (but are not limited to) thickness, porosity, water-saturation, and pressure information on a well-by-well basis. A database (*Reservoir ID*) was created using a consistent and definitive nomenclatural system linked to the reservoir characteristics and production histories of individual wells. Because the reservoir nomenclature reported to the States was erratic, numerous development opportunities were identified (see Hendrickson and others, 2001; Smith and others, 2001). The results of well-level evaluations using a database of consistent well-reservoir data suggest that most wells do not drain the drill-pattern spacing used. Thickness appears to have the most pronounced influence on ultimate recovery. Pressure depletion does not appear to have a significant influence until wells are drilled on a spacing pattern less than 80 acres, or 40 acres for some reservoirs. These observations have been confirmed by recent wells and recompletions identified by using this methodology.

[1]The work for this paper was completed by the Reservoir Geology Division of IHS Energy Group. Subsequent to presentation and prior to publication of this paper, the Reservoir Geology Division of IHS Energy Group was purchased by Geological Data Services (GDS; Addison, Texas), including the *Reservoir ID* database, all maps, cross sections, well/reservoir database, and expertise. The authors are currently consultants to GDS.

STUDY AREA

Figure 1 presents a map of the Anadarko basin and shelf area of Oklahoma and Texas. The study area, as indicated on this figure, encompasses the vast majority of the Anadarko basin and shelf area. The first step of the study, which dealt with reservoir nomenclature, covered the entire indicated study area. The second step of the study, which dealt with the analysis of individual reservoirs and their production histories, covered only the Texas Panhandle counties.

METHODOLOGY

During a recent effort at Geological Data Services (GDS) to standardize reservoir nomenclature, the authors generated more than 15,000 mi of geologic cross sections to demonstrate the stratigraphic sequences and relationships throughout the Anadarko basin and shelf area. Figure 2 is a base map of the approximate study area indicating the network of nearly 3,000 mi of "published" cross sections, which are a small part of the total used in this project. To insure nomenclatural consistency and accuracy, the electric logs of more than 45,000 wells were reviewed for the study. Regarding the perforated interval (as indicated by the completion card and/or Form 1002A), a comparison was made between formation names as indicated by GDS regional cross sections and the operator-defined producing formation. Where there was a difference between the two, the nomenclature indicated by the regional cross sections was used. Figure 3 presents the stratigraphic section used in this study to designate reservoir and formation names. Specific to this study, through these detailed correlations the producing granite wash zones were assigned a definitive and consistent nomenclature. This initial part of the study covered the entire study area. For the Texas Panhandle counties, once the nomenclature was established, producing zones were subjected to extensive log analysis that was entered into a database. Additionally, "behind-pipe" potential was identified and characterized. Finally, using the definitive and consistent reservoir nomenclature, the results were evaluated.

Smith, P.W.; Hendrickson, W. J.; and Woods, R. J., 2001, Comparison of production and reservoir characteristics in "granite-wash" fields in the Anadarko basin, *in* Johnson, K. S.; and Merriam, D. F. (eds.), Petroleum systems of sedimentary basins in the southern Midcontinent, 2000 symposium: Oklahoma Geological Survey Circular 106, p. 19–27.

TABLE 1. — Competions Reported by State Records versus Completions from *Reservoir ID* Database

State reported	*Reservoir ID*	
1,985 completions	2,260	with 1 "wash" zone completed
	245	with 2 "wash" zones completed
	70	with 3 "wash" zones completed
	8	with 4 "wash" zones completed
1,985 total wells indicated	2,583	total "wash" wells indicated

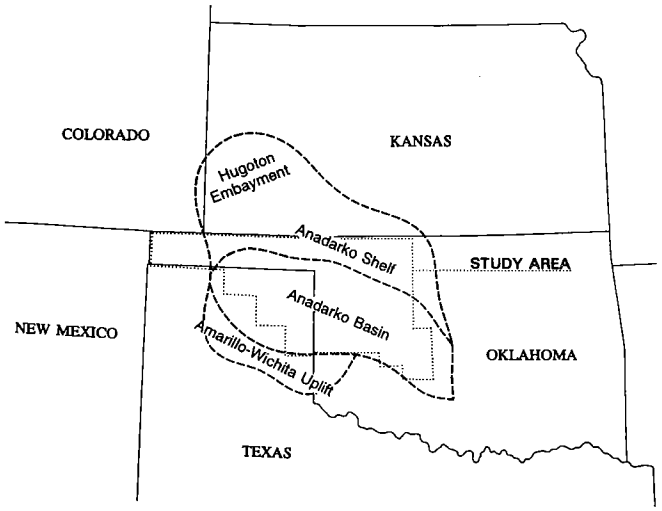

Figure 1. Map of Anadarko basin and shelf area of Oklahoma and Texas, showing study area (delineated by dotted line).

TABLE 2. — Tabulation of Average Gas and Oil Production from "Wash" Reservoirs in Anadarko Basin

Reservoir	Count	Avg. gas (MMCF)	Avg. oil (MBO)
Cherokee Wash Middle	68	3,241	9
Cherokee Wash Lower	43	2,061	9
Wolfcamp Wash	276	1,567	20
Layton Wash	47	1,216	68
Prue Wash	417	1,200	19
Red Fork Wash	158	1,161	14
Average Wash completion		**1,150**	**24**
Marmaton Wash	420	1,046	34
Cleveland Wash	51	1,012	74
Granite Wash	144	726	10
Cottage Grove Wash	34	573	19
Skinner Wash	213	513	13
Tonkawa Wash	45	495	81
Atoka Wash	32	385	2

RESULTS

Table 1 is a comparison of the number of wells producing from what has been reported to State agencies as "wash" completions and the number of wells as identified in the GDS *Reservoir ID* database. These figures represent wells located over the entire study area of Oklahoma and Texas.

Once the allocation had been completed and the

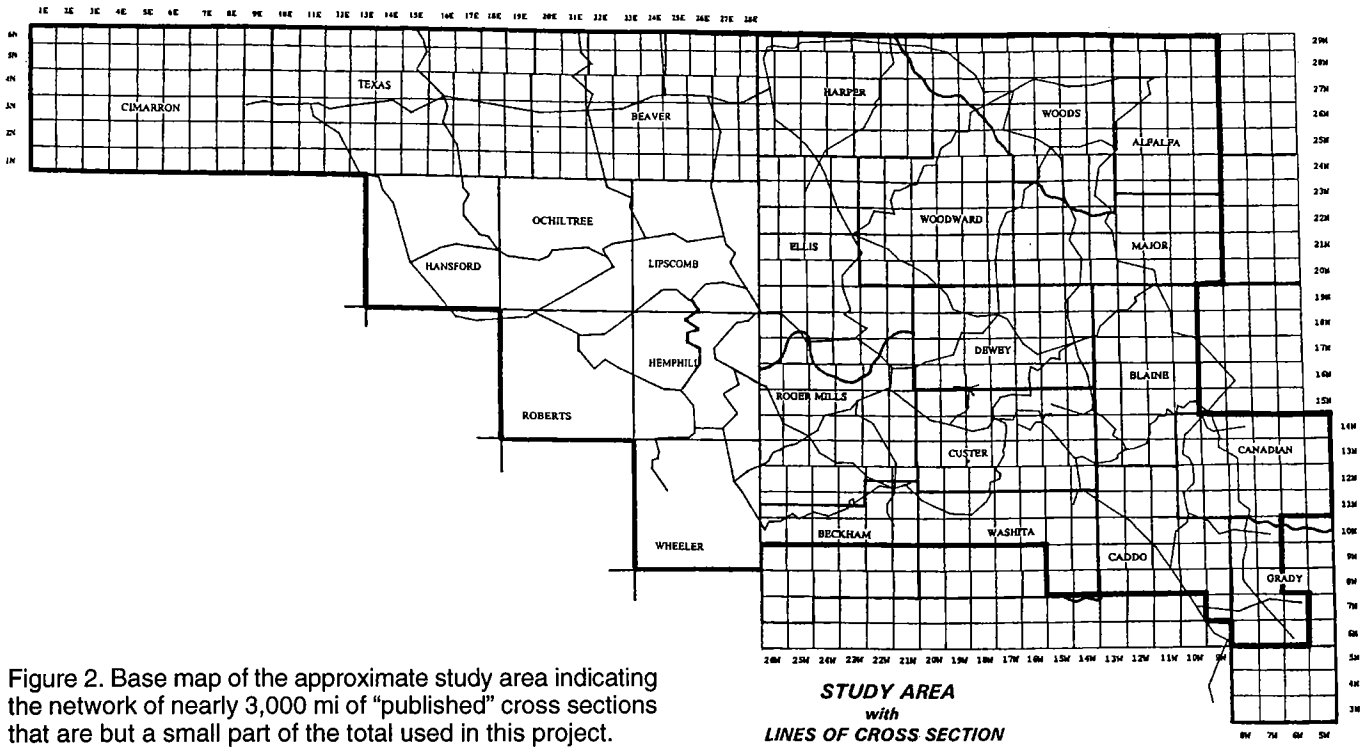

Figure 2. Base map of the approximate study area indicating the network of nearly 3,000 mi of "published" cross sections that are but a small part of the total used in this project.

SYS.	SERIES	GROUP	UNIT	SANDSTONE	CARBONATE	EQUIVALENT
PENNSYLVANIAN	VIRGILIAN	Shawnee/Cisco	Topeka Ls Pawhuska Ls Hoover Ss Elgin Sd Oread Ls Heebner Sh Endicott Ss	Hoover Endicott	Pawhuska Oread Ls	
		Douglas/Cisco	Lovell Ls Haskell Ls Tonkawa Ss	Tonkawa	Douglas Group	
	MISSOURIAN	Lansing/Hoxbar	Avant Ls Cottage Grove Ss	Cottage Grove	Lansing Group	
		Kansas City/Hoxbar	Dewey Ls Hogshooter Ls Layton Ss Checkerboard Ls Cleveland Ss	Layton Cleveland Culp	Kansas City Group Melton	Marchand Upper Marchand Lower
	DES MOINESIAN	Marmaton	Big Lime Oswego		Big Lime Oswego	Marmaton Wash
		Cherokee	Cherokee Marker Prue Ss Verdigris Ls Skinner Ss Pink Ls Red Fork Ss Inola Ls Mona	Prue Skinner Red Fork Cherokee Wash Middle Cherokee Wash Lower/ Mona	Verdigris Inola	Prue Wash Skinner Wash Red Fork Wash Bartlesville, Tussy
	ATOKAN	Atoka	Atoka 13 Finger Ls	Atoka	Atoka 13 Finger	
	MORROWAN	Morrow	Morrow Primrose	Upper Morrow Lower Morrow Primrose		
	SPRINGERAN	Springer	Cunningham Britt Boatwright	Cunningham Britt Boatwright	Britt Boatwright	
MISSISSIPPIAN	CHESTERIAN	Chester	Chester Ls		Chester	
		Manning	Manning Ls		Manning	
	MERAMECIAN	Meramec	Meramec Chat Meramec Ls		Meramec Chat Meramec	
	OSAGEAN	Osage	Osage Ls			
	KINDERHOOKIAN	Kinderhook	Kinderhook Sh			
SIL./DEV.	CHATTANOOGIAN		Woodford Sh Misener Ss	Misener		
	ULSTERIAN	Hunton	Hunton Group		Hunton (Frisco) Hunton (Bois d'Arc) Hunton (Haragan) Hunton (Henryhouse) Hunton (Chimney Hill)	
	NIAGARAN ALEXANDRIAN					
ORDOVICIAN	CINCINNATIAN	Sylvan	Sylvan Sh Maquoketa		Maquoketa	
	CHAMPLANIAN	Viola	Viola Group		Viola (Fernvale) Viola (Trenton)	
		Simpson	Simpson Dense Bromide Ss Tulip Creek Ss McLish Ss Oil Creek Ss Joins	Bromide Tulip Creek McLish Oil Creek Joins		
	CANADIAN	Arbuckle	Arbuckle Group		Arbuckle	
CAMB.	CROIXAN					

Figure 3. Generalized stratigraphic section for Anadarko basin in western Oklahoma used in this study to designate reservoir and formation names. Sys. = system; Camb. = Cambrian; Sil./Dev. = Silurian–Devonian.

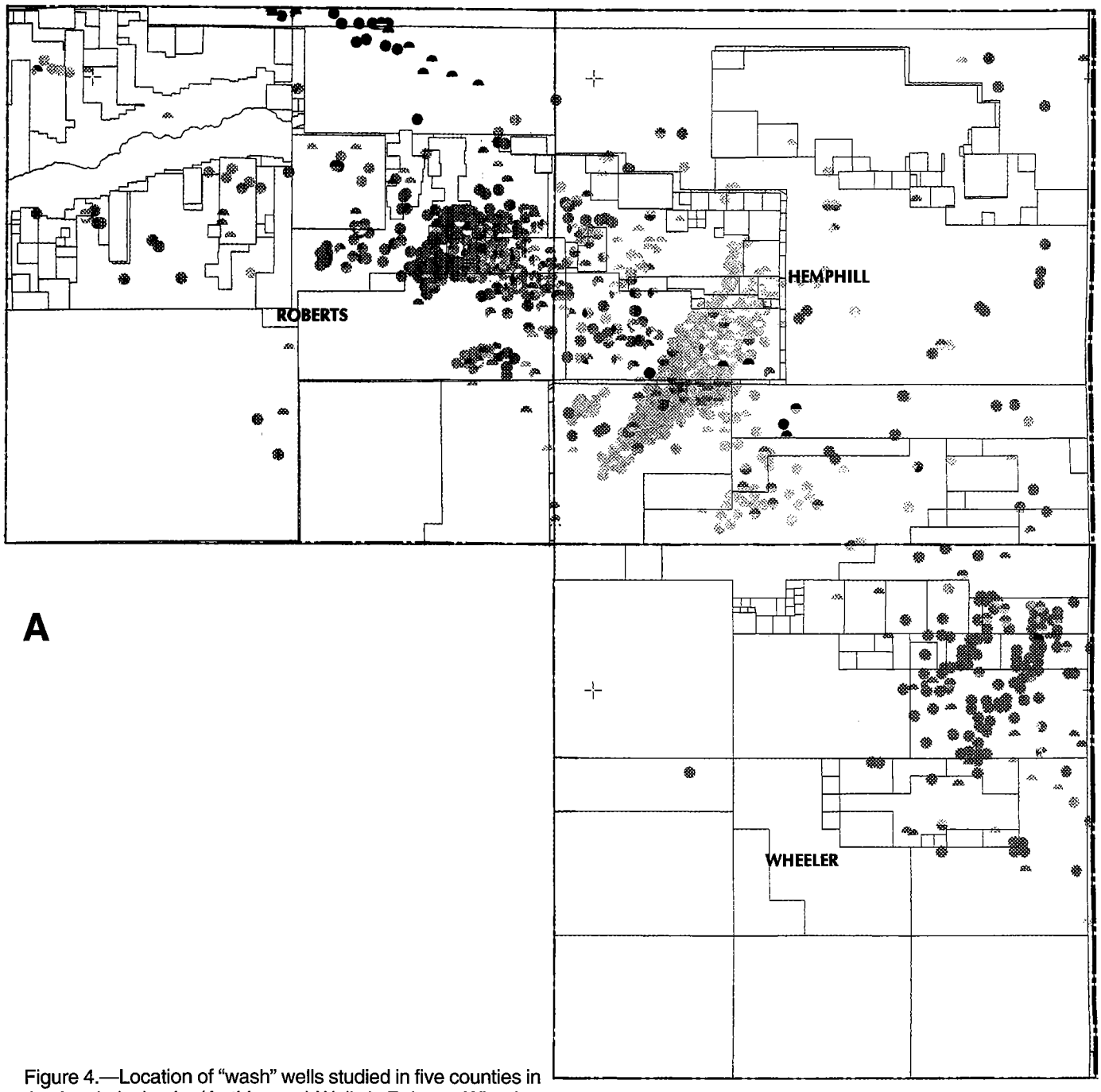

A

Figure 4.—Location of "wash" wells studied in five counties in the Anadarko basin. (A, *this page*) Wells in Roberts, Wheeler, and Hemphill Counties, Texas. (B, *facing page*) Wells studied from Becham and Washita Counties, Oklahoma. *Explanation of symbols:* Producing wells are shown by colored circles; explanation of formation of production shown by key on right side of Figure 4B; half circles represent partial production commingled or from other zones.

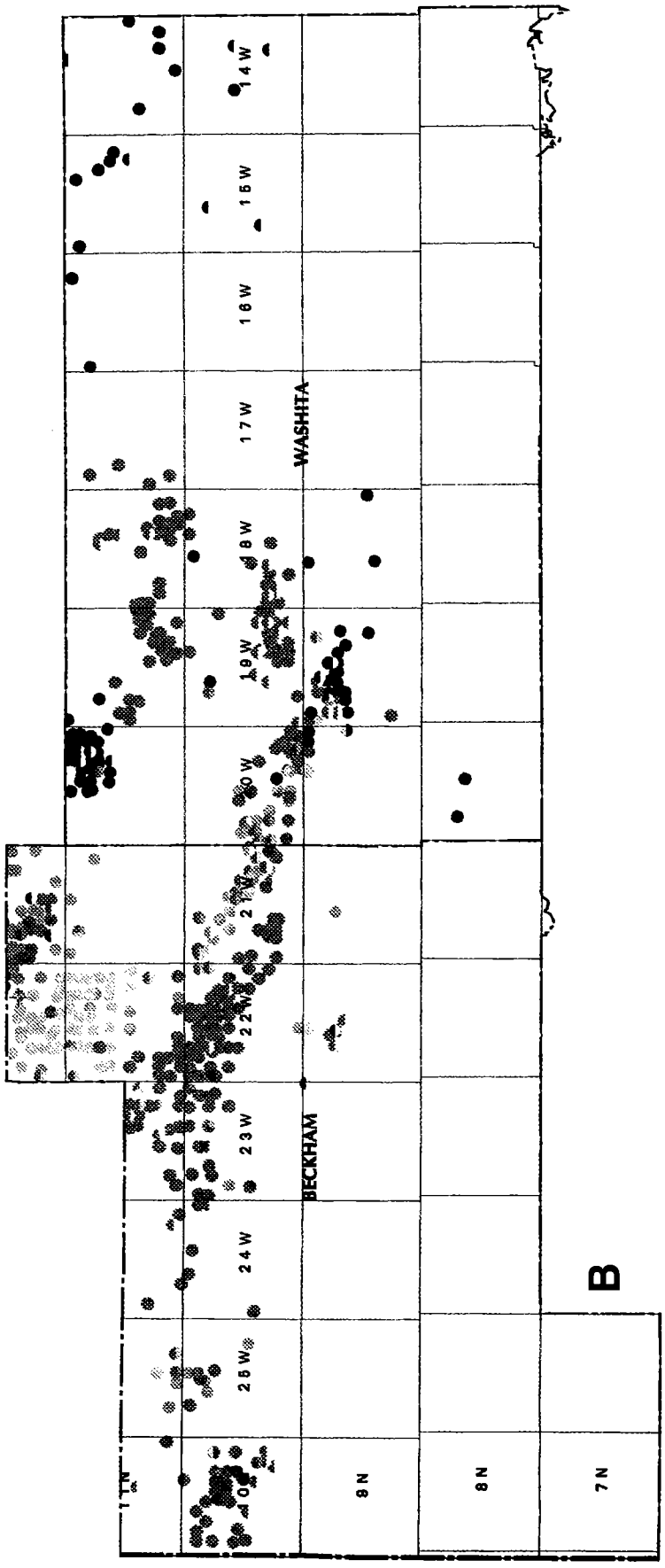

- Pennsylvanian
- Des Moinesian
- Deese
- Marmaton
- Marmaton Wash
- Big Lime
- Glover (includes Kistler)
- Oswego
- Charlson
- Cherokee
- Cherokee Carbonate
- Cherokee Wash Lower
- Cherokee Wash Middle
- Prue
- Prue Wash
- Verdigris
- Skinner (includes Hart, Pooler, Sames)
- Skinner Carbonate
- Skinner Wash
- Pink
- Red Fork
- Red Fork Wash
- Inola
- Mona (Bartlesville)
- Commingled or recompleted in other zones

producing reservoir had been assigned to conform to the GDS stratigraphic chart and cross sections, then a valid analysis of their productive capacity could be made. Table 2 is a compilation of the various "wash" zones identified in the *Reservoir ID* database. The listing was constructed using only single-zone completions and is presented in order of their productive capacity for gas, starting with the highest producer, the Cherokee Middle Wash. These figures also represent wells located over the entire study area of Oklahoma and Texas.

The second step of the study involved reservoir and production analysis of "wash" wells located in five counties, those being Roberts, Wheeler, and Hemphill Counties of Texas (Fig. 4A), and Becham and Washita Counties of Oklahoma (Fig. 4B). Because the Texas portion was completed at the time this paper was presented, only reservoir characteristics in "wash" wells in Texas are presented herein.

As shown in Figure 4, a wide geographic distribution of the Middle Pennsylvanian washes exists. These washes were sourced from the Amarillo uplift. It appears that the distribution system moved throughout time (note locations of various group washes). Also evident is the change in "wash" composition. Early washes (Morrowan) are typically chert. Atokan washes grade from cherts to carbonate. Lower and Middle Cherokee washes are typically carbonate washes. Red Fork washes are commonly carbonate washes but can also consist of granitic material. Compositions of the washes above the Red Fork section (Skinner equivalent and younger) were controlled by local drainage areas. Some of these areas were fed granitic material, and others were sourced from weathering carbonates of the Amarillo uplift.

Within the three-county area of the Texas Panhandle, four washes had completion populations of sufficient size to generate statistically valid evaluation. These washes include the Marmaton Wash, Prue Wash, Skinner Wash, and Red Fork Wash. Logs were analyzed for a host of characteristics. The figures and data that follow indicate the results of only a portion of the data collected.

Figure 5 is a graph indicating the ultimate gas recovery (in billion cubic feet, BCF) that is expected from these aforementioned reservoirs within the Texas Panhandle. Indications are that the Prue Wash is the best of the reservoirs with an average well expected to make >1.6 BCF. Figure 6 represents various measures of thickness for these reservoirs and partially explains why the Prue Wash is the best reservoir—it is, simply, the thickest wash by all measurements. Perforated thickness is just that, the number of feet perforated. Saturated thickness is the number of feet judged to be potentially hydrocarbon bearing whether or not it was perforated. Therefore, saturated thickness will always be equal to or greater than perforated thickness. In regard to the saturated thickness, two additional thicknesses were recorded. These are (1) the number of feet (thickness) that showed porosity +7%, and (2) the number of feet (thickness) that showed +4% porosity.

Figure 7 is a plot of various porosity measurements

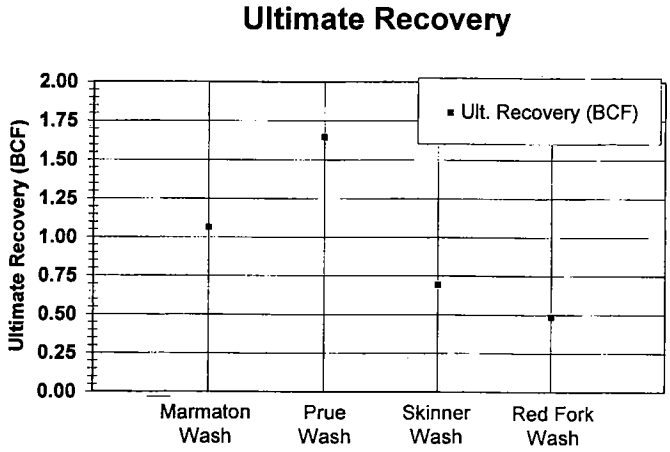

Figure 5. Plot of ultimate recovery (in billion cubic feet, BCF) versus reservoir for "washes" in the Texas Panhandle region of the Anadarko basin.

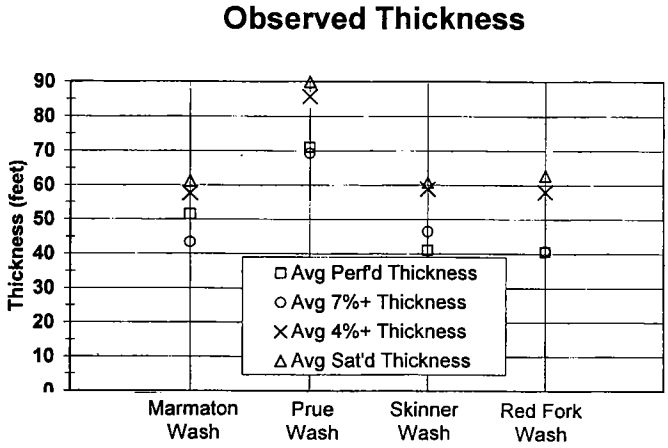

Figure 6. Plot of various parameters of thickness (in feet) versus reservoir for "washes" in the Texas Panhandle region of the Anadarko basin.

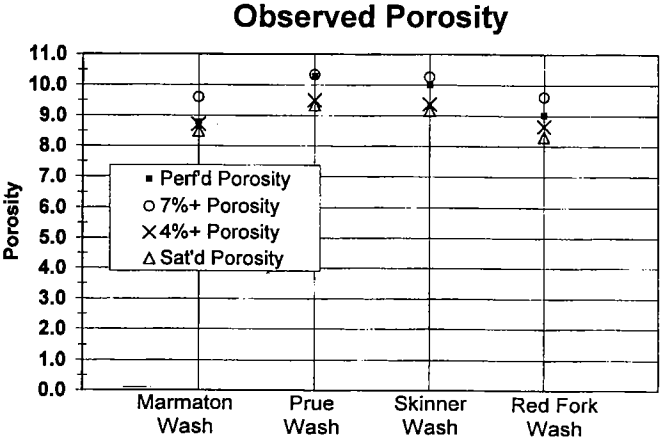

Figure 7. Plot of various parameters of observed porosity (in %) versus reservoir for "washes" in the Texas Panhandle region of the Anadarko basin. Perf'd = perforated; Sat'd = saturated.

(in %) of the wash reservoirs, and again indicates the Prue Wash to be the best of the reservoirs. Water-saturation data for all the reservoirs indicated essentially the same saturations, that being from a low of 28% in the Skinner Wash to a high of 31% in the Marmaton Wash.

An additional part of the analysis of these reservoirs involved the impact of spacing and drainage. Obvious questions to be considered were:

- Are the wells draining the drill pattern spacing?
- Do the infill completions suffer from dramatic pressure loss?
- At what point is significant pressure depletion observed?
- Are the ultimate recoveries impacted by infill wells and, if so, by how much?

To address these questions, a series of graphs were prepared and are presented.

Figure 8 is a plot of the observed spacing (in acres) versus the initial-pressure gradient (in psi/ft) and indicates little difference in the pressure gradient until the wells are drilled on well spacing smaller than 160 acres. The largest population of completions was in the Prue Wash, and the data suggest that significant pressure loss is not observed until 40-acre well spacing is drilled. Figure 9 compares ultimate recovery (in BCF) to spacing (in acres) and generally demonstrates little difference in the recoveries relative to spacing. The one anomaly observed is that the Prue Wash at 80-acre spacing indicates greatly increased recovery; however, further analysis showed that this anomaly was due to a single, notably higher quality field that was drilled on 80-acre spacing. Therefore, the increased recovery was a function of increased reservoir quality and not of spacing size. Although pressure depletion was shown in the Skinner and Red Fork Wash completions, it shows little (if any) impact on ultimate recoveries. Basically, if a well was successful on 160 acres, 80-acre offsets were typically drilled. As expected, pressures do decline below with well spacing below 80 acres, but the population of wells drilled on 40 acres is small enough to allow aberrations to appear (Skinner Wash pressure gradients; Skinner Wash and Red Fork Wash ultimate recoveries).

Using the values derived from log analysis, calculations were made to determine the area of drainage based on the cumulative production on a well-by-well basis. Ultimate recovery for the purposes of this analysis was based on two methods. On all reservoirs, production decline was used to determine ultimate recovery values. For reservoirs with adequate pressure data, pressure-gradient decline (P/Z, in psi/ft) was a second method used in determining ultimate recovery.

Figure 10 is a comparison of the calculated drainage area (in acres) versus the drill-pattern spacing (in acres). Perforated thickness and porosity as well as saturated thickness and porosity values were used with production-decline data for all wells. Additionally, with pressure-decline data, three thickness/porosity relationships were used. These are saturated thickness and porosity as well as thickness and average porosity of

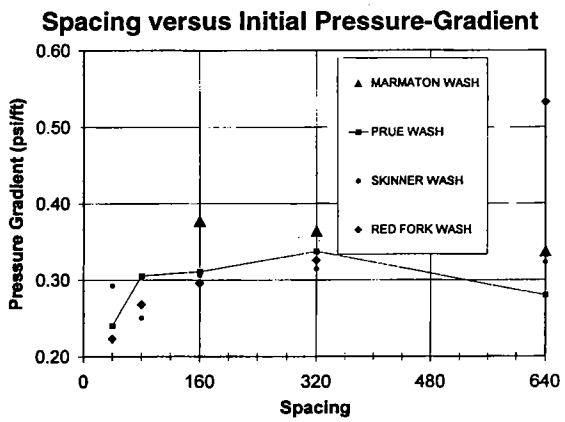

Figure 8. Plot of initial-pressure gradient (in psi/ft) versus well spacing (in acres) for various "washes" in the Texas Panhandle region of the Anadarko basin.

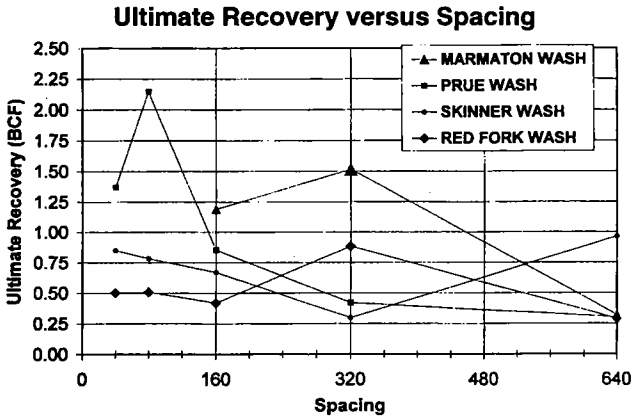

Figure 9. Plot of ultimate recovery (in billion cubic feet, BCF) versus well spacing (in acres) for "washes" in the Texas Panhandle region of the Anadarko basin.

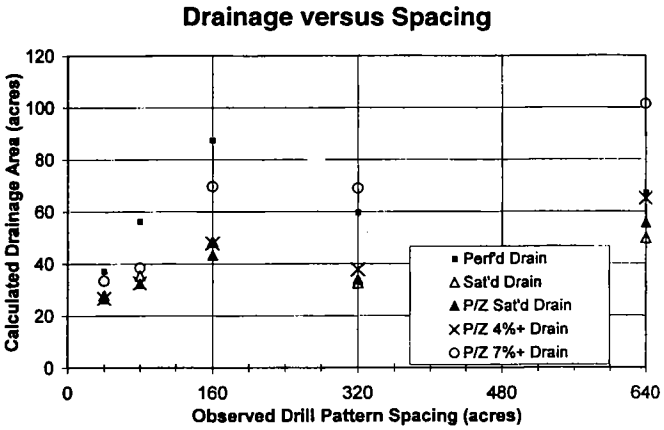

Figure 10. Plot of drainage area (in acres) versus observed drill-pattern spacing (in acres) for various "washes" in the Texas Panhandle region of the Anadarko basin. Perf'd = perforated; Sat'd = saturated; P/Z = pressure gradient (in psi/ft).

only the portion of the reservoir that exceeded the 7% or 4% porosity cut-off criteria. The results indicate that the drainage area is typically less than 80 acres. Wells drilled on 80 acres commonly drain about the same area as those on 40 acres. Perforated drainage is an unreliable marker of depletion.

This analysis suggests that substantial undrained reserves could exist in leases drilled with well spacings of greater than 80 acres, because it appeared that the wells were draining only 40 to 80 acres. To address this potential, a reserve value for each well reservoir was calculated using the thickness and average porosity of the reservoir that was in excess of 7% (7% cutoff) and using the well spacing that was indicated for that well, that being 40, 80, 160, 320, or 640 acres. From this value was subtracted the calculated ultimate recovery for each reservoir. The remainder became the undrained reserves and is plotted on Figure 11. Wells drilled on 40-acre drill patterns do not tend to leave much behind; other patterns do.

A sum of the potential undrained reserves was made and is presented in Figure 12. For the wells that have been drilled on 640-acre well spacing, the total potential undrained reserves are indicated for each of the four washes subject to this study. On a well-by-well basis, a great deal of undrained reserves is believed to be present in areas where the wells were drilled with 640-acre well spacing. However, the total potential undrained reserves do not appear notably larger than those indicated for 160- and 320-acre spacing. This situation is created because far fewer "wash" wells were drilled on 640-acre well spacing than the greater number drilled on 320-acre spacing or the even greater number drilled on 160-acre spacing. Obviously, the total potential undrained reserves is a function of the number of wells drilled on a given well spacing as well as the amount of potential undrained reserves per well. Generally, little potential undrained reserves are calculated for "wash" wells drilled on well spacing of 40 acres in that these areas are drained. The 80-acre drill patterns suggest the same scenario except for the Prue and Skinner Washes. The large value for the Prue Wash for 80-acre well spacing is due to Hemphill field, which has been drilled largely on 80-acre well spacings. Calculations indicate that these wells are not draining 80-acre well-spacing units and that 40-acre spacing would be more effective. Note that, on the 40-acre well spacing, essentially no potential undrained reserves are present.

The reservoir analysis conducted as part of this study, part of which has been presented herein, has provided answers to the questions previously posed.

- Are the wells draining the drill pattern spacing? Answer: *Typically no.*
- Do the infill completions suffer from dramatic pressure loss? Answer: *Typically no.*
- At what point is significant pressure depletion observed? Answer: *At 40-acre infill drilling, a 20–30% loss in initial pressure generally can be observed.*
- Are the ultimate recoveries impacted by infill wells? Answer: *Typically no effect; indications are that most "wash" wells do not drain their well-spacing units and that considerable horizontal reserves remain undrained.*

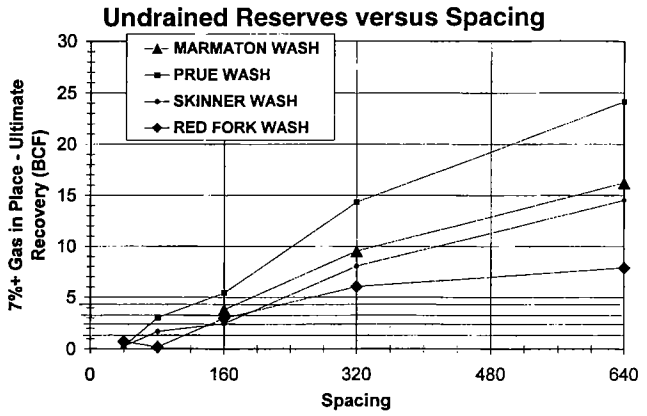

Figure 11. Plot of 7%+ ultimate recovery (in billion cubic feet, BCF) of gas-in-place (undrained reserves) versus well spacing (in acres) for "washes" in the Texas Panhandle region of the Anadarko basin.

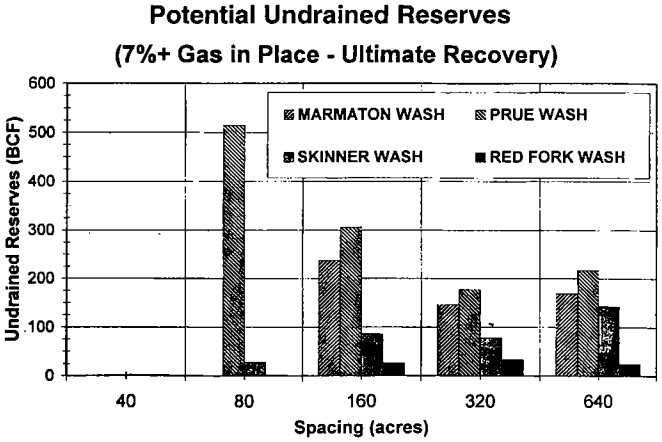

Figure 12. Plot of 7%+ undrained reserves (in billion cubic feet, BCF) of gas-in-place versus well spacing (in acres) for "washes" in the Texas Panhandle region of the Anadarko basin.

Additionally, there should be substantial "behind-pipe" (vertical) potential in these areas. Poor reservoir nomenclature has led to confusion as to which zones have been produced, and, consequently, numerous zones were left unperforated when correlative zones in nearby wells with nearly identical characteristics were perforated and produced.

Other observations that were made over the course of the study included:

- Perforated porosity and a +7% porosity cut-off are reasonable standards.
- Perforated thickness and number of feet with +7% are reasonable standards.
- The cut-off data make a good standard by which nonperforated intervals can be evaluated.

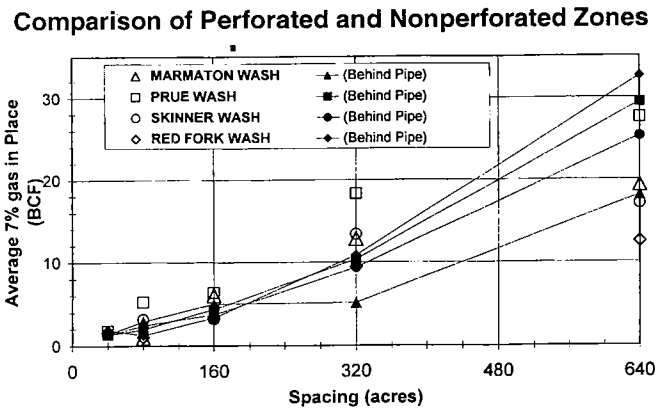

Figure 13. Comparison of perforated and nonperforated zones; plot of average 7% gas-in-place (in billion cubic feet, BCF) versus well spacing (in acres) for "washes" in the Texas Panhandle region of the Anadarko basin.

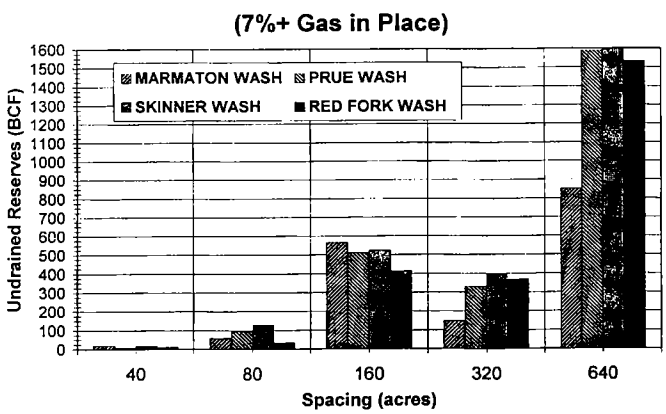

Figure 14. Illustration of potential "behind-pipe" reserves; plot of undrained reserves (in billion cubic feet, BCF) versus well spacing (in acres) for "washes" in the Texas Panhandle region of the Anadarko basin.

- Zones judged to have "behind-pipe" potential had identical water-saturation values.

Figure 13 is a comparison of the perforated zones versus the "behind-pipe" zones. This figure indicates that the quality of the "behind-pipe" zones (based on the average of the gas in place in porosity +7%) is closely analogous to the perforated and producing zones. Figure 14 summarizes the total potential "behind-pipe" reserves by zone and by the apparent well spacing.

CONCLUSIONS

A number of conclusions have been made as a result of this study in the Anadarko basin. These are summarized below:

- Concise and consistent nomenclature is critical to the oil industry and scientific efforts.
- Detailed reservoir characterization can help identify opportunities.
- Standards for thickness, porosity, and water saturation can and should be determined.
- Well spacing can be optimized with the proper data.
- Production with reduced initial pressure can be predicted and modeled.
- Considerable potential, both horizontal and vertical, remains within known "wash" fields.
- Other "wash" reservoirs not subject to this study suffer from similar correlation and nomenclature problems and likewise contain significant potential.

These results are part of an ongoing effort and demonstrate the potential of this type of work. Validation of this approach has been demonstrated by a new well flowing in excess of 3,000 MCFGPD (thousand cubic feet of gas per day) in an old area and an up-hole recompletion that flowed 200 BOPD (barrels of oil per day). Both these opportunities were identified through this study.

REFERENCES CITED

Hendrickson, W. J.; Smith, P. W.; and Woods, R. J., 2001, Regional correlation of mountain-front "washes" and relationship to marine sediments of Anadarko basin and shelf, *in* Johnson, K. J. (ed.), Pennsylvanian–Permian in the Midcontinent, 1998 symposium: Oklahoma Geological Survey Circular 105, p. 71–80.

Smith, P. W.; Hendrickson, W. J.; and Woods, R. J., 2001, Significance of accurate reservoir nomenclature and its impact on identifying petroleum systems in the Anadarko basin, *in* Johnson, K. S.; and Merriam, D. F. (eds.), Petroleum systems of sedimentary basins in the southern Midcontinent, 2000 symposium: Oklahoma Geological Survey Circular 106 [this volume], p. 9–13.

Petrophysical and Petrographic Reservoir Evaluation of Gunsight Limestone, Schleicher County, Texas

Mohamed A. Eissa
Tanta University
Tanta, Egypt, and
University of Oklahoma
Norman, Oklahoma

James M. Forgotson, Jr., and Huaibo Liu
University of Oklahoma
Norman, Oklahoma

ABSTRACT.—The wells analyzed in this study are located in West Texas on the western part of the Eastern shelf between the Bend arch on the east and the Midland basin on the west.

Drill cuttings from approximately 800-ft intervals indicating the Gunsight Limestone (base of the Cisco, Virgilian) in the Judkins #B-1 and Judkins #1 wells were examined to determine lithofacies assemblages, sedimentary environments, and types of reservoir porosity. Thin sections made from 28 samples provided petrographic information to aid in these interpretations. Four limestone lithofacies were recognized in thin sections of the Gunsight Limestone: (1) ooid grainstone, (2) bio-bafflestone, (3) skeletal packstone, and (4) wacke/mudstone. Poorly developed ooids and fine-grained skeletal material in the grainstones suggest deposition in a medium-energy environment. *In situ* and connected skeletons in the bafflestone suggest that it may have formed the core of organic-mud mounds. Calcareous green algae in the packstones indicate a shallow-water environment. The wacke/mudstone in the cuttings may have come from low-energy shelf limestone above the Gunsight.

Two types of dolomite occur within the Gunsight interval: (1) very fine to fine-crystalline dolomite with varied porosity formed from dolomitization of grainstone, bafflestone, and packstone; and (2) dolomicrite with no porosity formed by dolomitization of mudstone. The upper part of the Gunsight contains fine- to medium-grained sandy limestone. The shale above the Gunsight contains marine shell fragments that indicate a shelf environment. Shale and chert below the Gunsight indicate a deeper-water environment.

Five types of porosity were identified in thin sections: (1) intercrystal porosity in dolomites and calcites—the most important for reservoir development; (2) interparticle porosity in sandstones; (3) intraparticle porosity in skeletons; (4) moldic porosity in limestone; and (5) microfractures.

Cuttings with porosity from the Judkins #B-1 well showed light-yellow to light-brown fluorescence under ultraviolet light, and the presence of hydrocarbons was confirmed by chromatographic analysis. This interval was not tested either during drilling or completion of the well. A recompletion attempted many years later was unsuccessful because of inadequate cement bond. The Judkins Trust #3 well, drilled 500 ft away to test the Gunsight, had no shows in this interval.

All available well logs for six wells within the area were digitized and analyzed for lithology, porosity, and water saturation. Two of the eight wells studied had porosity logs. Comparison of water-saturation values determined by the Archie method with water-saturation values based on the resistivity-ratio method indicated that the latter required an adjustment of 35 water-saturation (S_w) units. This value was used as a correction to S_w computed from the resistivity logs. Corrected S_w values indicated that, for the two wells 500 ft apart and with a structural difference of 11 ft, the Judkins #B-1 well had a movable-oil interval of 42 ft with a S_w of 25%; the same interval in the Judkins Trust #3 well had calculated S_w values of 100%. Although these two wells have nearly identical gamma-ray log patterns, they are in separate reservoirs. Adjusted S_w values indicated that the Gunsight would probably be oil productive in the Judkins #1-C well, located ~3 mi southwest from these two wells.

Eissa, M. A.; Forgotson, J. M., Jr.; and Liu, Huaibo, 2001, Petrophysical and petrographic reservoir evaluation of Gunsight Limestone, Schleicher County, Texas, *in* Johnson, K. S.; and Merriam, D. F. (eds.), Petroleum systems of sedimentary basins in the southern Midcontinent, 2000 symposium: Oklahoma Geological Survey Circular 106, p. 29–54.

PURPOSE

The main objectives of study were: (1) to evaluate the Gunsight Limestone (base of the Cisco, Virgilian age), (2) to use well logs to determine the petrophysical properties of the Gunsight Limestone, (3) to compare the petrophysical parameters in two closely spaced wells to evaluate the presence of oil shows in one well and not the other, and (4) to use drill cuttings to determine lithofacies assemblages, sedimentary environments, and types of reservoir porosity.

GEOLOGIC SETTING

The paleogeography of the Permian basin was established by Pennsylvanian tectonism that deformed the Precambrian basement and lower Paleozoic sedimentary rocks. During the Permian, the region divided into two basins, the relatively deep Delaware basin on the west and the relatively shallow Midland basin on the east, which were separated by the north-northwest–trending Central basin platform (Fig. 1) (Galley, 1958; Ward and others, 1986). Continued subsidence of the West Texas region characterized both the Canyon and Cisco epochs. Deepening of Delaware and Midland basins by continuing downwarping produced profound effects upon regional sedimentation. A variety of Late Pennsylvanian reefs that varied in shape and configuration from ridge-like, round, chain-like, or clustered along with groups of composite reefs grew on the Eastern shelf (Wright, 1979).

AREA OF STUDY AND DATA

This study includes five wells drilled on the western part of the Eastern shelf between the Bend arch on the east and the Midland basin on the west, Schleicher County, Texas. Figure 2 shows the location map of the area of study. Well-log data were available for these five wells and cutting samples were available for two of them. Table 1 shows the available log data for these wells.

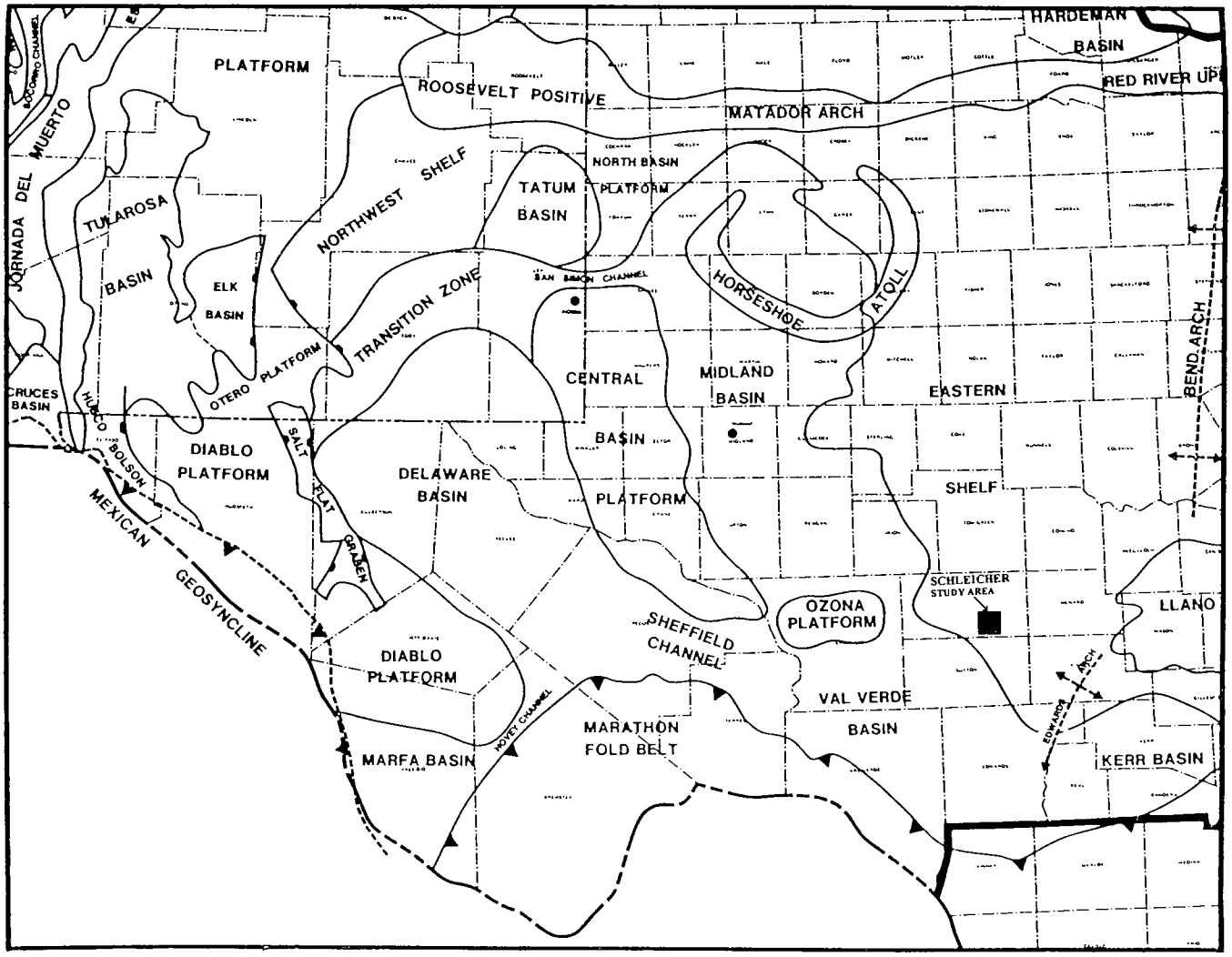

Figure 1. Regional structural features in West Texas and southeastern New Mexico, showing the study area (black box) in Schleicher County, Texas.

TABLE 1. — Available Well-Log Data

Well name	Location	KB (ft)	Drilling date	Available logs
1-Judkins Trust #3	1,422′ FSL & 1,016′ FEL, Sec. 30, Blk. A, A-981, BS&F/L.A. Helms Survey	2,232	6/17/1997	SP, GR, ILD, ILM,SFL,Cali, PhiD, PhiN, Micronormal (2″) & Micoinverse (1″*1″), mudlog
2-Judkins #B-1[a]	660′ FEL & 1,980′ FSL, Sec. 30, Blk. A, BS&F Survey	2,247	4/20/1956 Re-entered Nov. 1996	SP, Normal AM-16″, Lateral AO 18″-8″, CPN (PhiN), GR, Long & short spacing cps
3-Judkins #1[a]	660′ FS & EL, Sec. 43, Blk. A, BS&F Survey	2,311	4/4/1959	SP, Mcali, Micoinverse 1″*1″, Micronormal 2″, Induction 16″ normal, conductivity
4- Judkins #1.C.R	1,980′ FNL & 660′ FEL, Sec. 46, Blk. A, AB, MRR Co. Survey	2,352	9/12/1978	SP, GR, Induction 16″ normal, conductivity
5- Judkins #1-C	330′ FSL & 330′ FWL of East 369.7 Lse, Sec. 48, Blk. A, John H. Gibson Survey	2,350	10/11/1951	SP, Normal Am-16″, Lateral AO-15″

[a]Wells that have cutting samples.

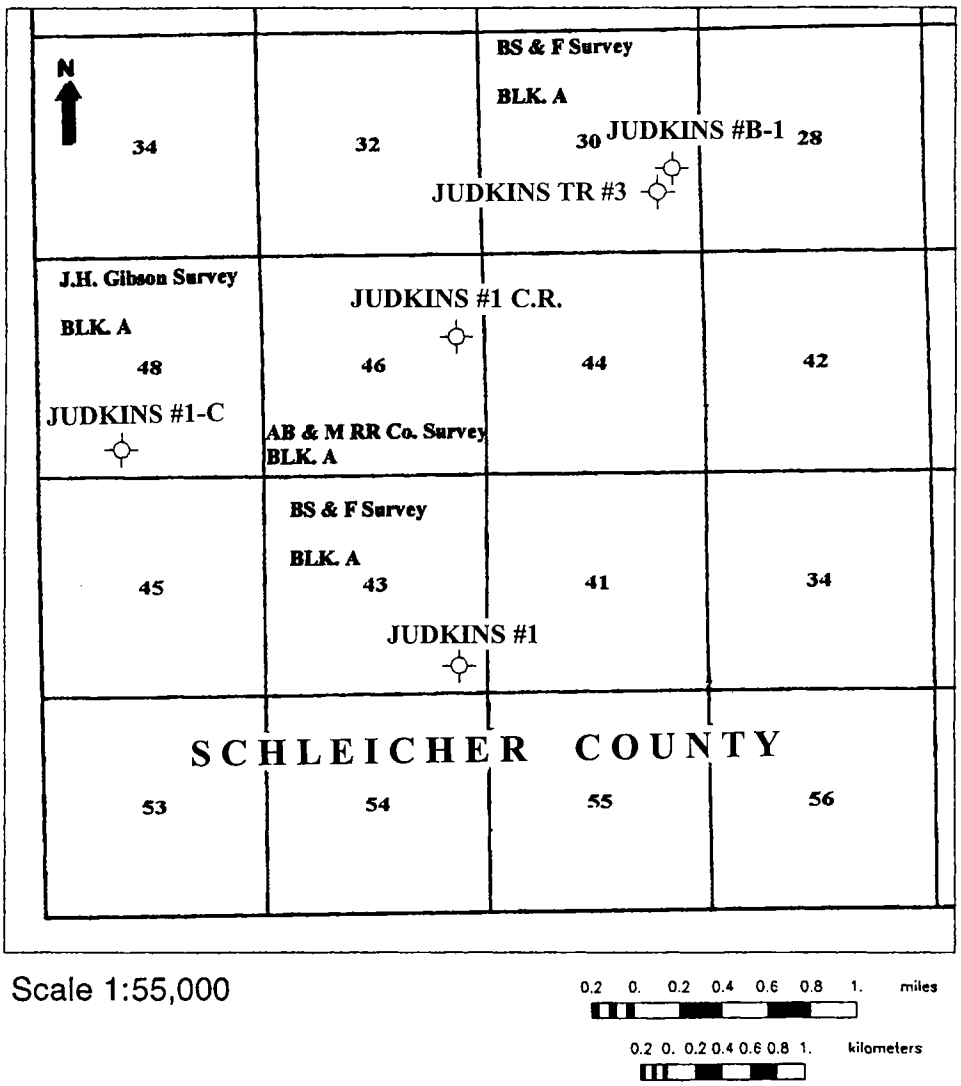

Figure 2. Detailed location map of the study area in part of Schleicher County, Texas. Exact locations are specified in Table 1.

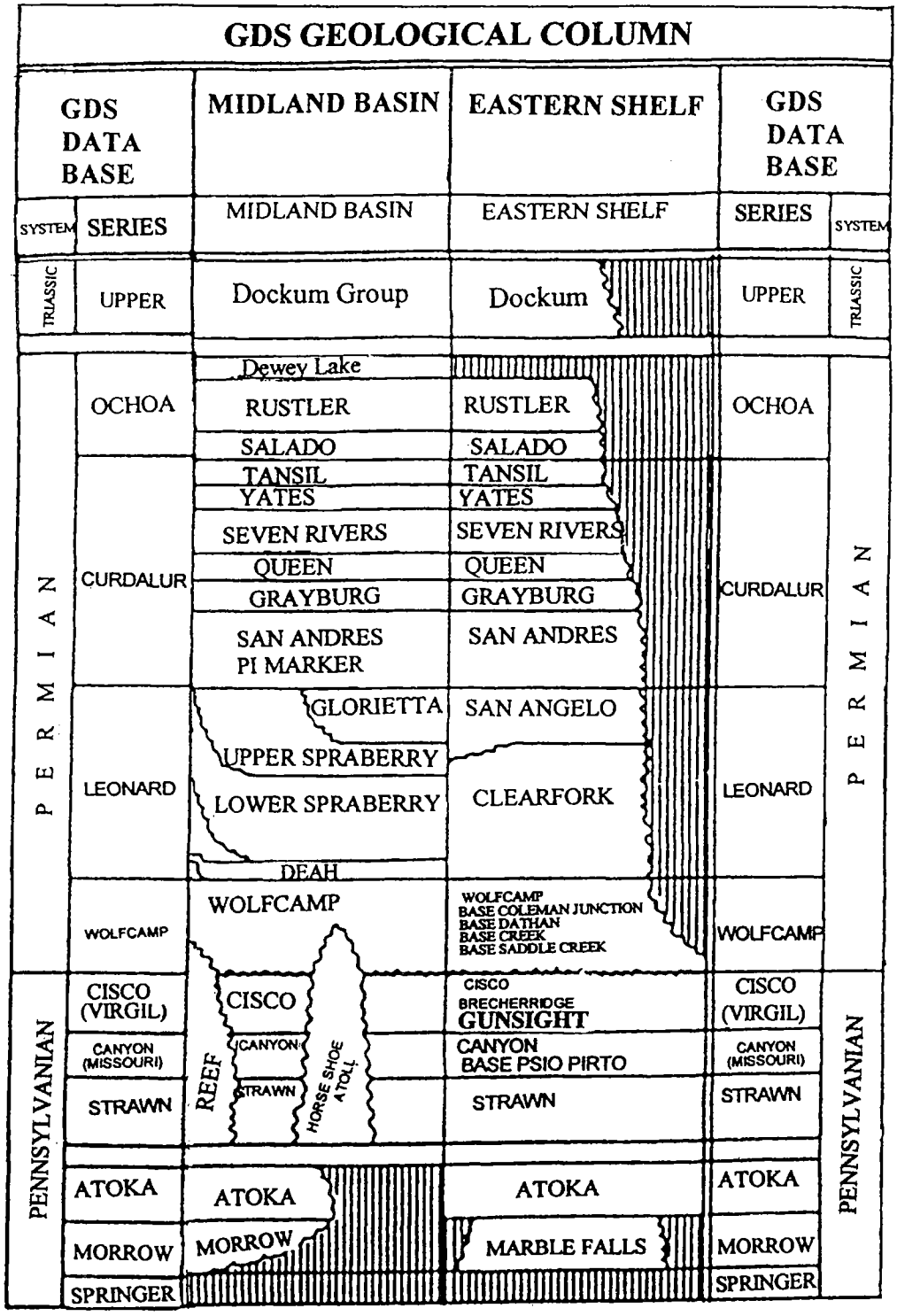

Figure 3. Stratigraphic column of the Eastern shelf and Midland basin, West Texas. Figure copyrighted (1990) by Geological Data Services, Inc., Dallas, Texas.

PLAYS IN PENNSYLVANIAN CARBONATES

Pennsylvanian reservoirs in the Midland basin and on the Eastern shelf occur in rocks assigned to the Atokan, Desmoinesian (Strawn), Missourian (Canyon), and Virgilian Series (Fig. 3). The most productive depositional-facies–controlled stratigraphic traps and combination stratigraphic-structural traps in these rocks are reefs. Relatively high-frequency eustatic variations on platform and slope-to-basin deposition exerted fundamental controls on the styles of stratigraphic traps and reservoir occurrence in Pennsylva-

TABLE 2. — Resistivity Correction for the Gunsight Limestone in the Judkins #B-1 Well

Zone	Depth (ft)	RLat18′8″	RLat18′8″/Rm	RLat18′8″Cor.	RSN16″	RSN16″/Rm	RSN16″Cor.
A[a]	2,792–2,800	450	95	304	200	75	240
B[a]	2,800–2,810	300	65	208	200	75	240
C[a]	2,810–2,816	200	45	144	200	75	240
D[a]	2,816–2,828	280	48	153	180	65	208
E[a]	2,828–2,846	600	125	400	220	85	272
F[a]	2,846–2,856	150	35	112	200	75	240

Rm @ FT = 3.2 ohm-m. Hole size 8¾ in.
[a]A water-free zone according to critical BVW method.

nian and Permian carbonates. Accessory productive facies include grainstone shoals (bioclastic and oolitic) and sponge biostromes and/or bioherms associated locally with *Shamovella* (*Tubiphytes*). These facies define fields that have reservoirs made up of shelf and shelf-margin reefs and grainstone shoals and foreshelf (offshore) atolls (Mazzullo, 1997).

PETROPHYSICAL EVALUATION

The following procedure was used for petrophysical calculation. (1) The well-log curves were digitized, using the digi-rule system. (2) The digitized curves were converted from RAT to LAS format. (3) These digitized curves were converted from LAS format to LBS format, using QLA2 Schlumberger software. (4) The raw data were corrected, using the software and log-interpretation chart books. (5) A model was built to calculate the petrophysical parameters. (6) Finally the resistivity of formation water (R_w) was calculated, using a SP log.

Data Correction

Resistivity Correction

The Tornado Chart (Schlumberger, 1989) was used to correct resistivity for invasion in Judkins Trust #3 well. Simplified resistivity departure curves Chart B-2 (Schlumberger, 1990) that correct for the influence of borehole on the 16-in. normal and for the hole and average invasion on the 18-ft, 8-in. lateral were applied in the Judkins #B-1 and #1-C wells. The Gunsight Limestone was divided into different resistivity intervals for correction purpose (see Tables 2–5). The Schlumberger Recor-8 Chart (Schlumberger, 1989) to correct the 16-in. normal recorded with the induction log was applied in Judkins #1 and Judkins #1-CR wells (see Tables 3, 4).

TABLE 3. — Resistivity Correction for the Gunsight Limestone in the Judkins #1 Well

Zone	Depth (ft)	RILD	RSN16″	RSN16″/Rm	RSN16″Cor.
A	2,835–2,870	20	140	59	137.5
B	2,870–2,882	25	60	20	50
C	2,882–2,896	9	12	4.5	11.25
D	2,896–2,906	50	90	31	77.5
E	2,906–2,912	20	30	9.8	24.5
F	2,912–2,916	70	90	31	77.5
G	2,916–2,924	30	40	13	32.5
H	2,924–2,934	30	80	27	67.5

Rm @ FT = 2.5 ohm-m. Hole size 7⅞ in.
Rm @ FT = 1.3 ohm-m. Hole size 7⅞ in.

TABLE 4. — Resistivity Correction for the Gunsight Limestone in the Judkins #1-CR Well

Zone	Depth (ft)	RILD	RSN16″	RSN16″/Rm	RSN16″Cor.
A	2,889–2,914	30	70	50	65
B	2,914–2,920	35	65	48	62.5
C	2,920–2,946	27	55	38	49.4
D	2,946–2,952	29	30	18	23.4

Rm @ FT = 1.55 ohm-m. Hole size 7⅞ in.

Porosity Correction

Porosity correction for lithology and shale effects was applied to the two wells that have porosity logs (Judkins Trust #3 and Judkins #B-1).

TABLE 5. — Resistivity Correction for the Gunsight Limestone in the Judkins #1-C Well

Zone	Depth (ft)	RLat18′8″	RLat18′8″/Rm	RLat18′8″Cor.	RSN16″	RSN16″/Rm	RSN16″Cor.
A[a]	3,031–3,042	270	110	187	50	26	44.2
B[a]	3,042– 3,060	250	95	161.5	100	60	102
C[a]	3,060–3,070	350	130	221	100	60	102
D[a]	3,070–3,076	550	200	340	100	60	102
E	3,076–3,086	40	20	34	85	49	83.3
F	3,086–3,094	2.5	—	2.5	95	55	93.5

Rm @ FT =1.7 ohm-m. Hole size 7⅞ in.
[a]A water-free zone according to critical BVW method.

TABLE 6. — Formation-Water Resistivity for the Gunsight Limestone Using SP Log

Well name	TD	BHT	ST	FT	Rmf@ST	Rmf@FT	SSp	Rmf/Rwe	Rwe	Rw@ FT
1-Judkins TR #3	2,890′	109	70	109	2.8	1.8	–100	23	0.078	0.09
2-Judkins B-1	6,013′	133	55	108	5.9	3.2	–100	23	0.139	0.14
3-Judkins-1	4,034′	118	67	106	3.9	2.7	–90	17	0.15	0.15
4-Judkins-1CR	4,936′	125	96	110	1.16	1.08	–70	9.5	0.112	0.11
5-Judkins #1-C	6,015′	147	68	114	2.8	1.7	–85	14	0.14	0.12

Formation-Water–Resistivity Determination

Formation-water resistivity (R_w) was calculated for the Gunsight Limestone using the SP log (Charts A-2, A-6, A-10, and A-12 of Schlumberger, 1990) (see Table 6).

Water-Saturation Determination in Uninvaded and Invaded Zones

Archie's Equation

Water saturation (S_w) is determined most commonly from the logging measurement of resistivity and knowledge of porosity, water resistivities, and shale volume. The interpretation procedures can be divided into two separate procedures—one for clean reservoirs and the other for shaly reservoirs. In clean reservoirs, the Archie equation (1942) is the primary method for water-saturation estimation. This fundamental relationship is expressed by the following equation:

$$S_w^n = \frac{a \times R_w}{\phi^m \times R_t}, \quad (1)$$

where, R_w = resistivity of formation water; R_t = formation resistivity in uninvaded zones; ϕ = porosity; n = saturation exponent (the most typically used value for n is 2.0); and a and m are constants determined from local experience. The most commonly used values for these constants are (for sandstone) $a = 0.81$ and $m = 2.0$ or $a = 0.62$ and $m = 2.15$ (Winsauer and others, 1952), and (for limestone) $a = 1$ and $m = 2.0$ (Carothers, 1968).

The same equation is valid for the calculation of water saturation in an invaded zone, S_{xo}, when you replace R_w and R_t by R_{mf} and R_{xo}, respectively, where R_{mf} is the resistance of mud filtrate and R_{xo} is the formation resistivity in invaded zones. The following is the Archie equation for S_{xo} calculation.

$$S_{xo}^n = \frac{a \times R_{mf}}{\phi^m \times R_{xo}} \quad (2)$$

From Resistivity Logs

If a porosity log is not available, both porosity and water saturation can be calculated from resistivity logs. When both R_{xo} and R_t are known, water saturation may be expressed by two Archie formulas, Eq. 1 and 2. Dividing the first equation by the second and substituting the empirical value $S_{xo} = (S_w)^{1/5}$ permits derivation of the following equation:

$$S_w = \left(\frac{1}{8}\right) \times \left(\frac{R_{xo}/R_t}{R_{mf}/R_w}\right)^5 \quad (3)$$

Where no porosity tool is available, an estimation of porosity in clean, water-bearing formations may be made from resistivity-log readings using the formation-factor porosity relationship, F-ϕ (Schlumberger, 1972).

$$F = S_{xo}^2 \left(R_{xo}/R_{mf}\right) \quad (4)$$

The porosity is calculated using the following equation of F-ϕ relationship:

$$F = \frac{a}{\phi^m} \quad (5)$$

The Bulk-Volume–Water Method

Bulk-volume water (BVW) is defined as the water-filled porosity.

$$BVW = S_w\phi, \text{ or } BVW^2 = S_w{}^2\phi^2, \quad (6)$$

but

$$S_w{}^2 = \frac{R_w}{\phi^2 R_t}, \quad (7)$$

so

$$BVW^2 = \left(\frac{R_w}{\phi^2 R_t}\right)\phi^2 \quad (8)$$

and

$$BVW = \sqrt{\left(\frac{R_w}{R_t}\right)} \quad (9)$$

The bulk-volume water in the invaded zone is calculated using the following formula.

$$BVW_{xo} = \sqrt{\left(\frac{R_{mf}}{R_{xo}}\right)} \quad (10)$$

Bulk-Volume–Water Ratio Method

The most appropriate way to determine whether a zone will produce water is to compare the flushed-zone water saturation with the water saturation in the uninvaded zone by determining the S_w/S_{xo} ratio.

$$\frac{S_w}{S_{xo}} = \frac{BVW}{BVW_{xo}} \quad (11)$$

If S_w/S_{xo} is equal to 1, the zone will produce water regardless of what the apparent water saturation is. If the ratio S_w/S_{xo} is less than 1, it indicates the zone contains producible hydrocarbons.

Critical Bulk-Volume Water

Critical bulk-volume water (BVW_c) is the maximum amount of water that a formation will hold without producing any water. It is a constant value in a homogenous reservoir. For examples, the Hunton Formation (limestone and dolomite) generally will have BVW_c ranging from 0.03 to 0.035. Clean Morrow or Springer sandstones generally have values around 0.048 to 0.052. Critical values of R_t can be calculated from BVW_c because $R_t = R_w / BVW^2$. Thus, the minimum R_t needed for a zone not to make water is determined.

TABLE 7.—Critical Bulk-Volume Water and Minimum Values for Resistivity in Uninvaded Zones Required for Hydrocarbon Production from Representative Lithologies

Lithology	Critical Bulk-Volume Water (BVW_c)	Minimum R_t Needed
Silty sandstone	0.07	200 R_w
Clean sandstone	0.05	400 R_w
Carbonate	0.035	800 R_w

R_t = resistivity in uninvaded zones; R_w = resistivity of formation water

An example is shown in Table 7. Once water-free zones are identified, look for porosity (ϕ) and decide if production is likely. If ϕ for sandstones is 8–10% or greater, production will be likely. If ϕ for carbonates is 5–8% or greater, production will be likely.

Hydrocarbon-Saturation Determination

Water saturation is used to calculate the hydrocarbon saturation (S_h) as follows:

$$S_h = 1 - S_w \quad (12)$$

Hydrocarbons can be differentiated into residual (S_{hr}), and movable (S_{hm}) saturations using the following equations:

$$S_{hr} = 1 - S_{xo} \quad (13)$$

$$S_{hm} = 1 - S_{hr} \quad (14)$$

APPLICATION

The water resistivity (R_w) used is 0.12 ohm-m at formation temperature. For water-saturation calculation, the Archie, ratio, BVW, and BVW_c methods were applied.

Judkins Trust #3 Well

Because the Judkins Trust #3 well has a good set of data from 2,786 to 2,856 ft, many applications were made for this study. A crossplot of DPHI (density from porosity) versus NPHI (density from neutron logs) shows that this formation consists mainly of limestone with some amount of dolomite and sandstone (Fig. 4). The environmental-correction model of Schlumberger

QLA2 was applied for resistivity and gamma-ray correction. Porosity also was corrected for lithology and shale effects. Different methods of S_w calculation were applied.

Figure 5 shows the Schlumberger QLA2-analysis log. This figure reflects that S_w is about 100%, using the Archie equation. The average porosity value is about 8%. The lithology is a limestone except the interval from depth 2,810 to 2,840 ft, which contains about 50% dolomite.

For the same well, S_w was calculated using different resistivity methods. The ratio method (Fig. 6) indicates about 35% of oil, whereas the Archie equation shows 0%. This difference is used to adjust the S_w calculated by the ratio method for those wells that did not have porosity logs.

Judkins #B-1 Well

The Archie formula has been applied for S_w calculation in the Judkins #B-1 well (2,797–2,872 ft). Figure 7 indicates that the Gunsight Limestone has high oil saturation in this well. The hydrocarbon saturation ranges from 70% to 80%. A small amount of residual hydrocarbon in the upper part of the formation is indicated. The lithology is limestone except the interval from 2,810 ft to 2,850 ft, which has 50% dolomite, as indicated by cutting analysis. The average porosity value is 10%. According to the critical BVW method, minimum R_t needed for the Gunsight Limestone to be water free is 96 ohm-m. Thus, that interval from 2,792 ft to 2,856 ft is water free (zones A, B, C, D, E, and F in Table 2).

Judkins #1 Well

The ratio method has been applied to calculate water saturation in the Judkins #1 well (2,835–2,933 ft). Figure 8 shows that S_w ranges from 48% to 58% in the upper, clean permeable interval from 2,835 ft to 2,570 ft. This interval shows good permeability indicated by the positive separation of micronormal- and

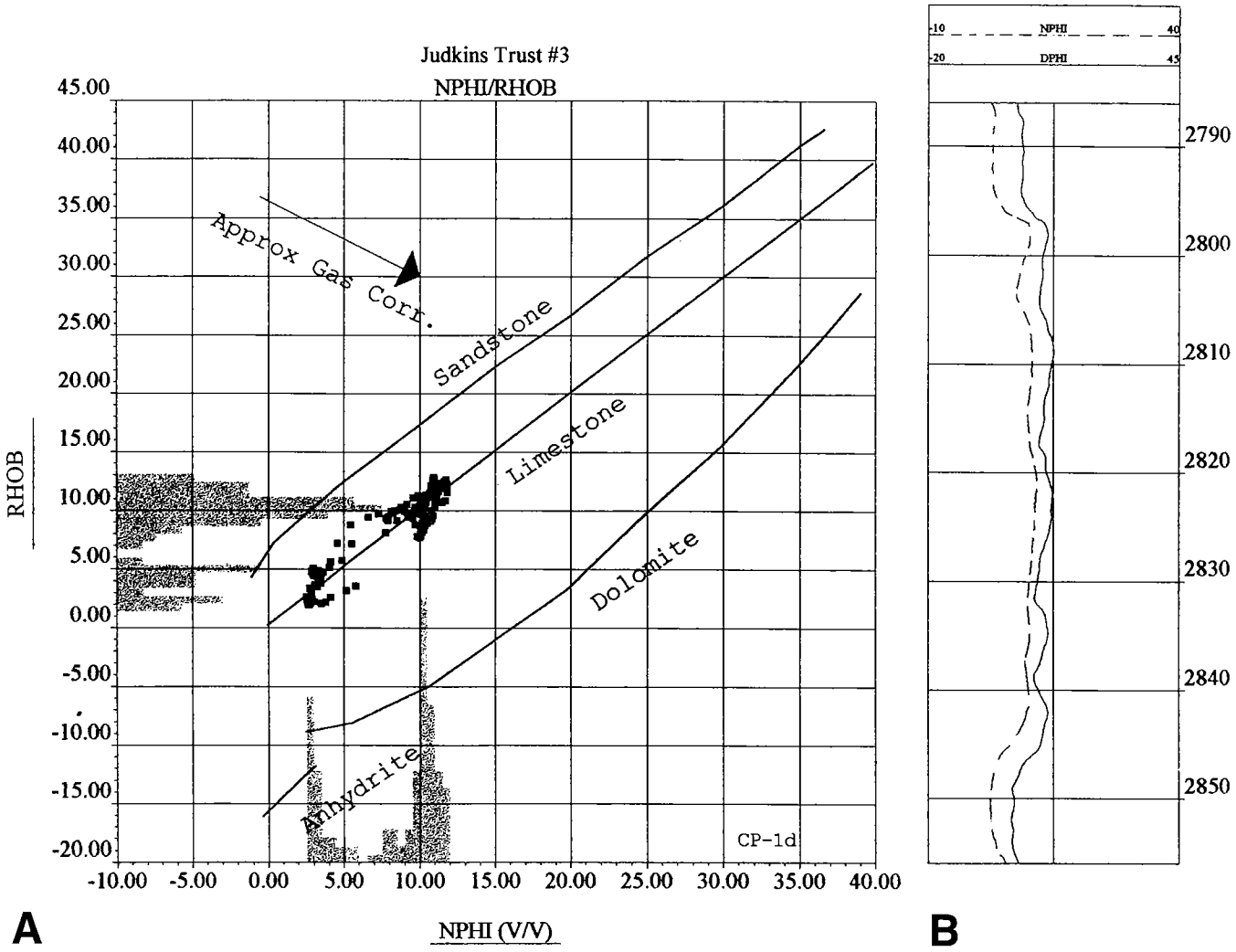

Figure 4. Density data for Gunsight Limestone in Judkins Trust #3 well, Schleicher County, Texas. (A) Cross-plot of density estimated from porosity (DPHI) versus density derived from neutron logs (NPHI). (B) Part of downhole log from which cross-plot data were derived. Depth in feet.

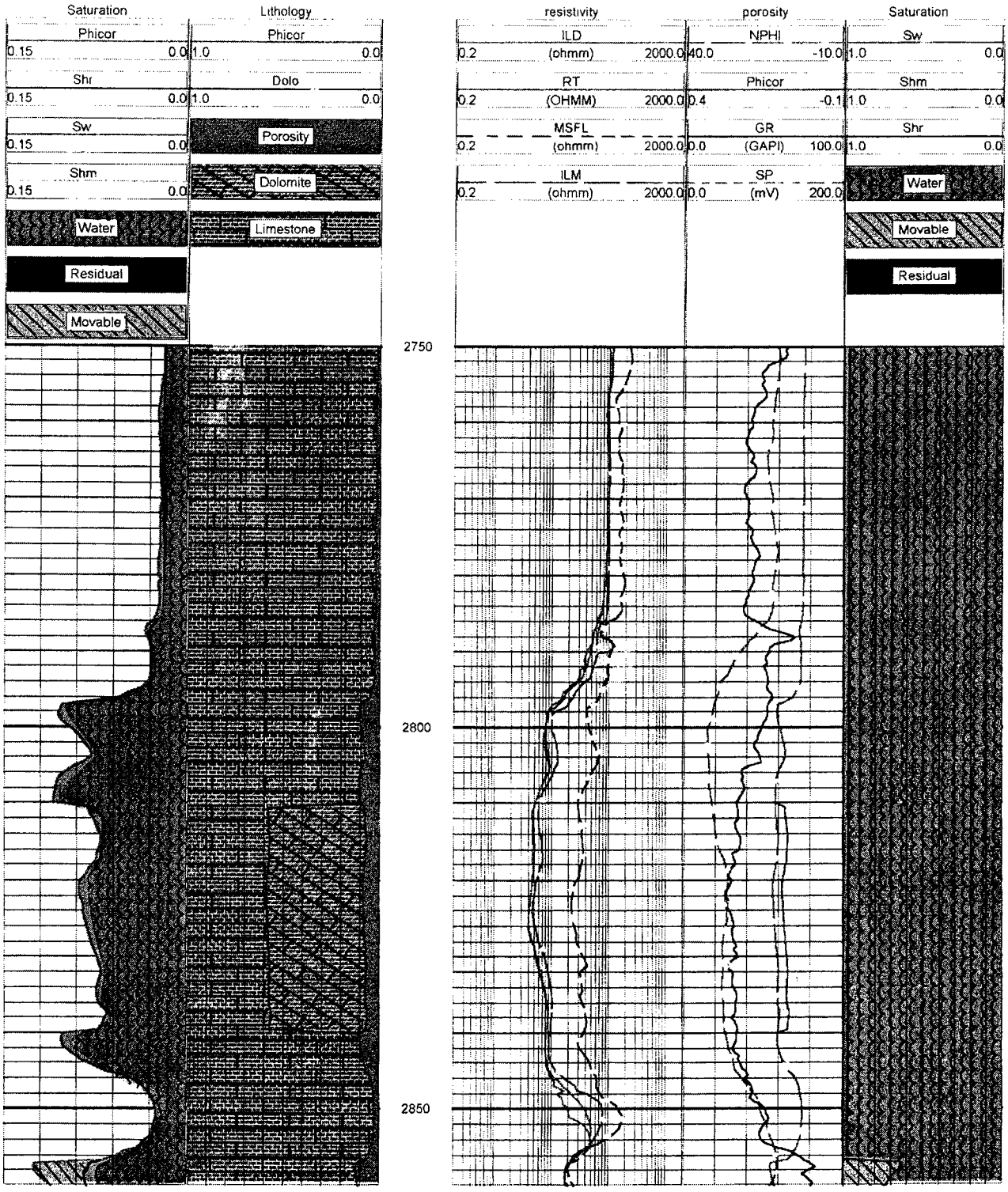

Figure 5. Schlumberger QLA2 analysis for Gunsight Limestone in Judkins Trust #3 well, Schleicher County, Texas, using porosity (in %) and resistivity (in ohm-m) for water-saturation (S_w) calculation (Archie's equation). Depth in feet below Kelley bushing.

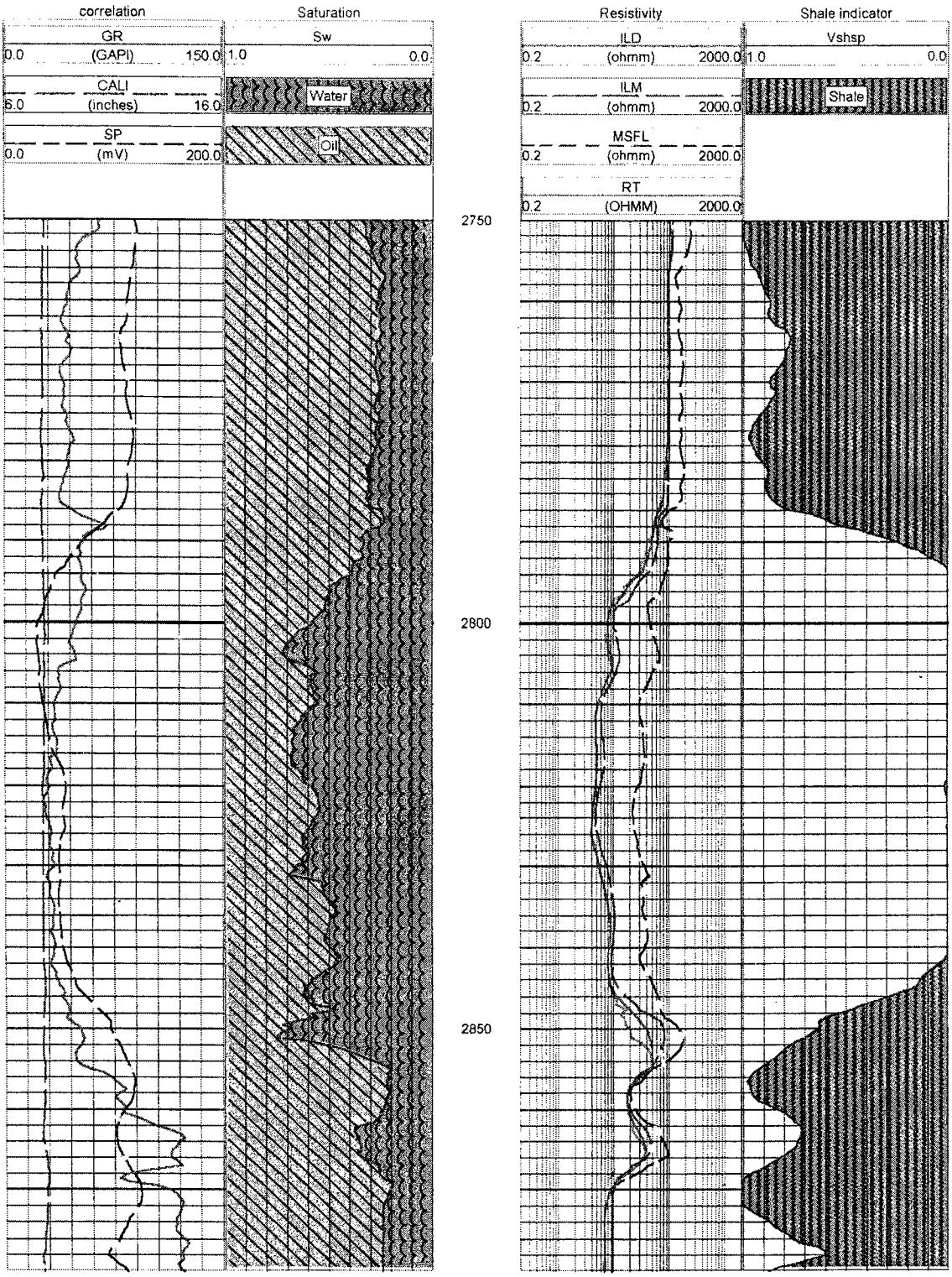

Figure 6. Schlumberger QLA2 analysis for Gunsight Limestone in Judkins Trust #3 well using resistivity (in ohm-m) only for water-saturation (S_w) calculation (ratio method). Depth in feet below Kelley bushing.

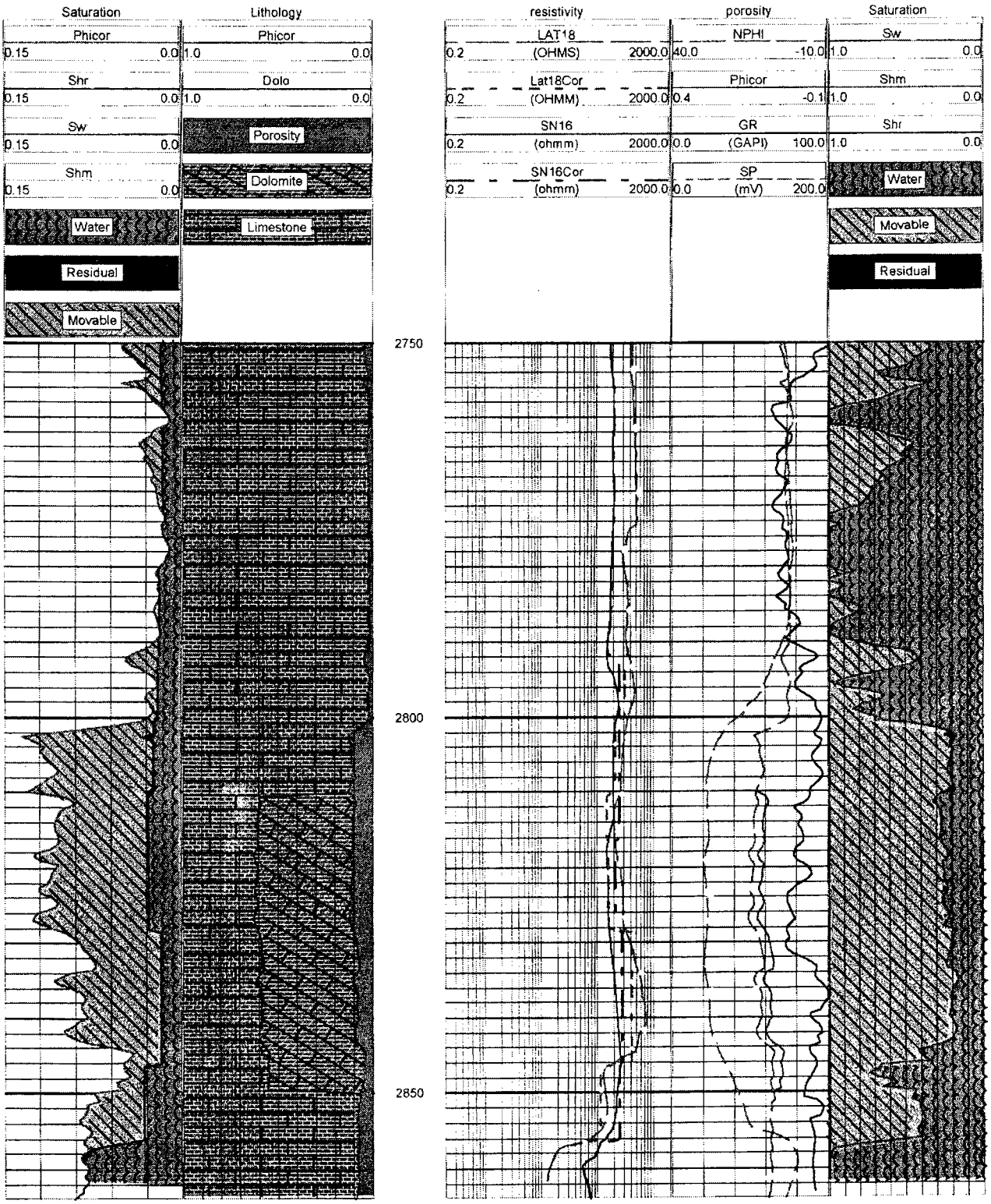

Figure 7. Schlumberger QLA2 analysis for Gunsight Limestone in Judkins #B-1 well (Archie's equation). Depth in feet below Kelley bushing.

microinverse-resistivity curves. Hydrocarbon saturation ranges from 42% to 52% according to this method of calculation. After applying the correction factor of 35% it ranges from 7% to 17%. According to the critical BVW method, this formation is interpreted to be water productive.

Judkins #1-CR Well

Figure 9 shows that hydrocarbon saturation ranges from 55% to 60% in the Judkins #1-CR well (2,889–2,977 ft) using the ratio method to calculate S_w. After applying the 35% correction factor, the hydrocarbon saturation ranges from 15% to 20% within the formation. Porosity calculation from resistivity shows an average value of about 13%.

Judkins #1-C Well

Calculations of S_w in the Judkins #1-C well (3,031–3,094 ft) by the ratio method ranges from 8% to 13% (Fig. 10). After applying the correction factor of 35%, the oil saturation ranges from 52% to 57%, which indicates oil production. The average porosity value calculated from resistivity tools is about 14%. The critical BVW method shows that the interval from 3,031 ft to 3,076 ft should produce oil with no water (Zones A, B, C, and D in Table 5).

CROSS SECTIONS AND MAPS

Two structural cross sections and three maps were constructed for the area of study. The first cross section is oriented southwest to northeast and includes the Judkins #B-1, Judkins Trust #3, Judkins #1CR, and Judkins #1-C wells (Fig. 11). This cross section shows that the Gunsight Limestone is dipping to the west and that its thickness is increasing to the northeast. Figure 12 is another cross section through the Judkins #B-1, Judkins Trust #3, Judkins #1CR, and Judkins #1 wells. It does not show much difference in the structural position, but it shows a big increase in the thickness to the south.

Figures 13 and 14 are the structure maps on the top and base of the Gunsight Limestone. These two figures reflect that the formation is dipping to the west and that the top and the base have the same structure. The isopach map (Fig. 15) shows that the thickness increases to the southeast.

PETROGRAPHIC EVALUATION

Drill cuttings from two wells, the Judkins #B-1 and Judkins #1, were examined to obtain a better understanding of the lithofacies assemblage, sedimentary environments, and reservoir porosity. Approximately 800-ft intervals from each of these wells were studied and 28 samples were chosen to make thin sections. Cuttings that exhibited UV fluorescence were collected from the Judkins #B-1 well to test the stain observed on thin sections for hydrocarbons. Photographs of thin sections were taken to document lithology and porosity.

Lithofacies

The Gunsight Limestone and its adjacent rock units include five main rock types: limestone, dolostone, sandstone, chert, and shale (Figs. 16–20).

Limestone

Four kinds of limestone lithofacies that are significant for interpretation of the sedimentary environments were recognized in the thin sections. They are: (1) ooid-grainstone, (2) bio-bafflestone, (3) bioclast-packstone, and (4) wacke/mudstone (Figs. 16–18).

The ooids in the grainstone are poorly developed (Fig. 20A), suggesting a medium-energy deposit. Other grainstones consisting of fine bioclasts also suggest a medium-energy depositional environment. The bafflestone characterized by *in situ* organisms (Fig. 16A) and connected organisms (Fig. 16C) may have formed the core of organic-mud mounds. The packstone with calcareous green algae indicates a shallow-water depositional environment. These three lithofacies make up the major part of the Gunsight Limestone carbonate buildup.

Two very important types of cement are present in the limestone cuttings—calcite cement and blocky-calcite cement. The limestone cuttings with equant-calcite cement have high porosity (Figs. 16D, 19D, 20A, B). The blocky-calcite cement (Fig. 17B) occurs in partially filled cavities and fractures.

Dolostone

Two kinds of dolomite are present in the Gunsight Limestone—very finely to finely crystallized dolomite and dolomicrite. The relict textures in some dolostone cuttings and partially dolomitized limestone show that the very finely to finely crystalline dolostone formed from dolomitization of grainstone, bafflestone, and packstone. These dolostones have variable porosity. The dolomicrites were formed by dolomitization of mudstone and have no porosity. Figure 17A, B, and D show some dolostones with less-developed porosity.

Sandstone and Chert

A few sandstone (Fig. 17C) cuttings and sandy-limestone cuttings occur in the upper part of the Gunsight Limestone. They are generally fine to medium grained and calcite cemented. Some similar sandstone and siltstone (Fig. 17D) are also found in the cuttings of shelf shale and limestone above the Gunsight Limestone. These sands may have been transported from the shoreline by fluvial, eolian, and storm (tempestite) processes and deposited in a shallow-shelf environment.

The sandstone below the Gunsight Limestone is associated with chert in the Judkins #B-1 well. These sands are fine to coarse grained, very loose (Fig. 20D) to partially cemented by overgrowth quartz or dolomite (Fig. 18A). Some sands occur as separate grains (Fig. 20B), indicating very porous sandstone beds. In the Judkins #1 well, the amount of this sandstone

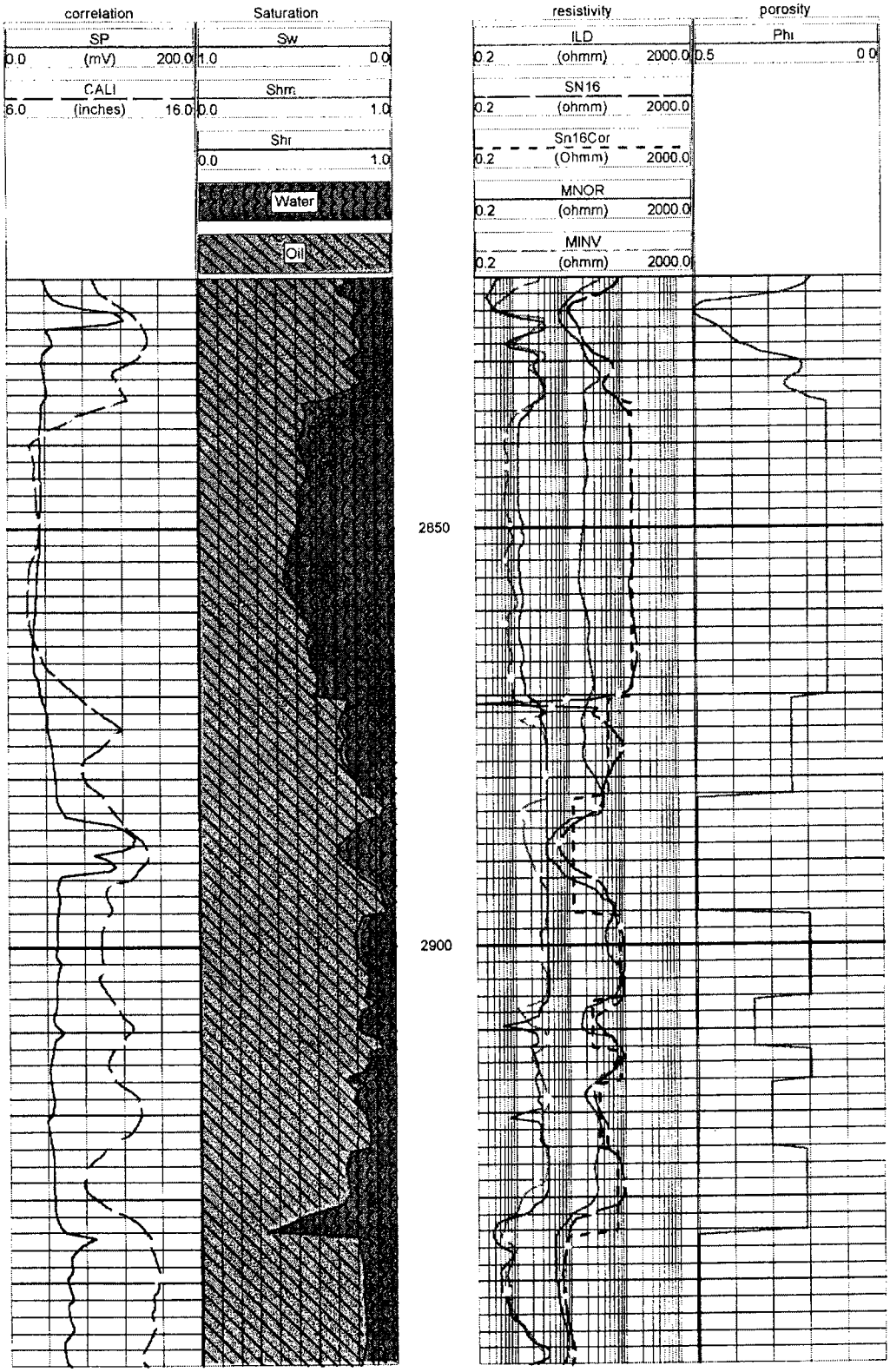

Figure 8. Schlumberger QLA2 analysis for Gunsight Limestone in Judkins #1 well (ratio method). Depth in feet below Kelley bushing.

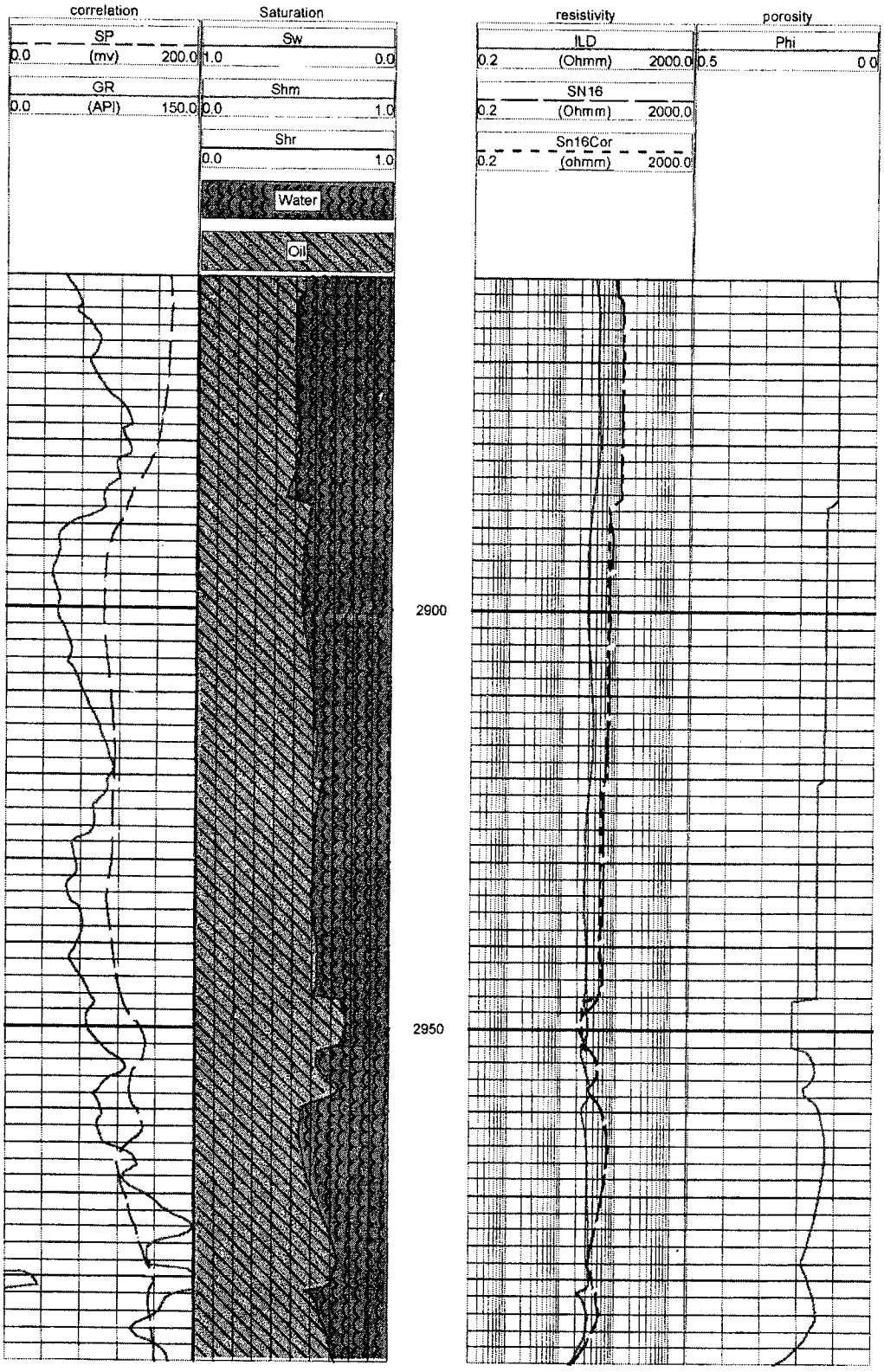

Figure 9. Schlumberger QLA2 analysis for Gunsight Limestone in Judkins #1-CR well (ratio method). Depth in feet below Kelley bushing.

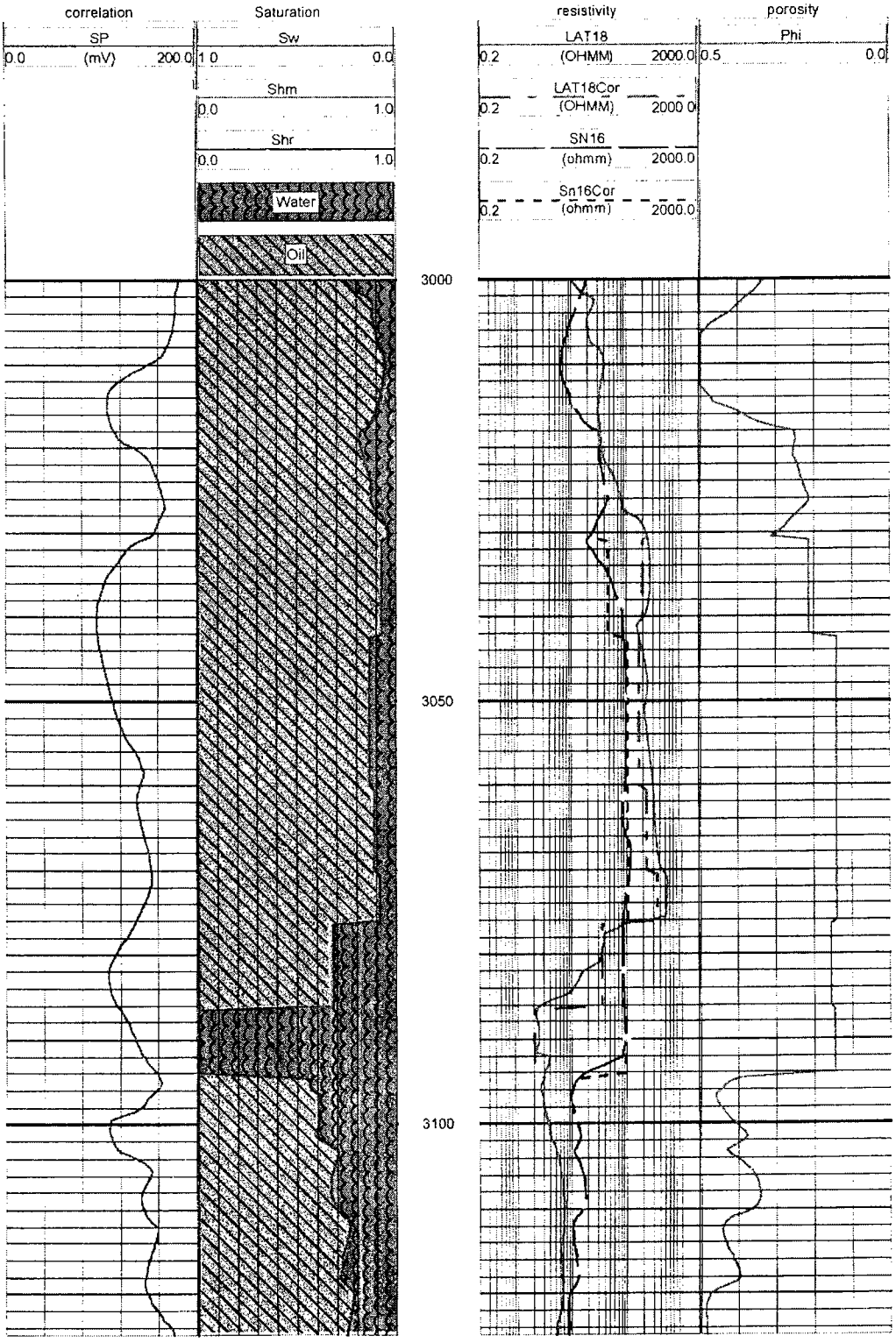

Figure 10. Schlumberger QLA2 analysis for Gunsight Limestone in Judkins #1-C well (ratio method). Depth in feet below Kelley bushing.

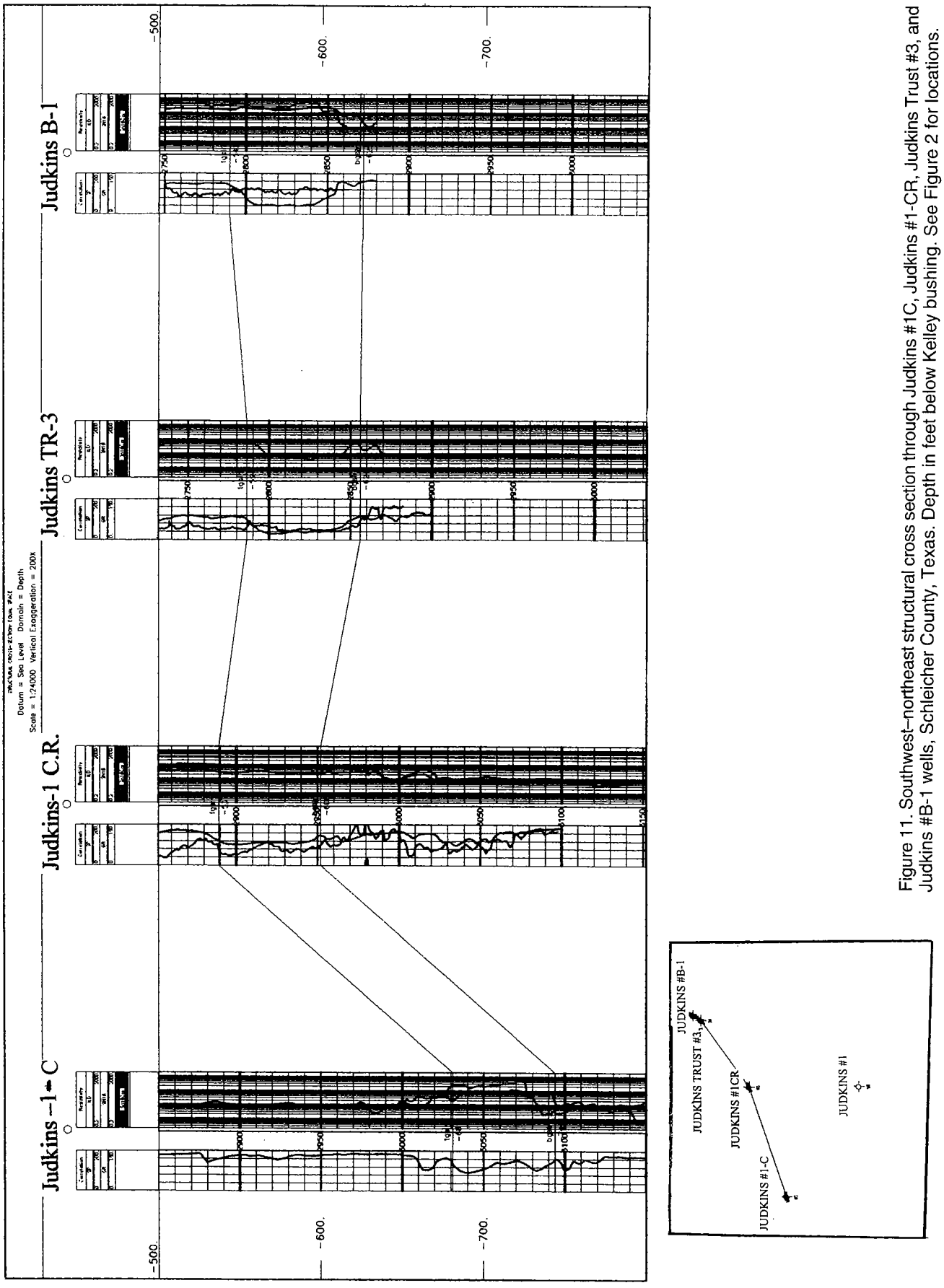

Figure 11. Southwest–northeast structural cross section through Judkins #1C, Judkins #1-CR, Judkins Trust #3, and Judkins #B-1 wells, Schleicher County, Texas. Depth in feet below Kelley bushing. See Figure 2 for locations.

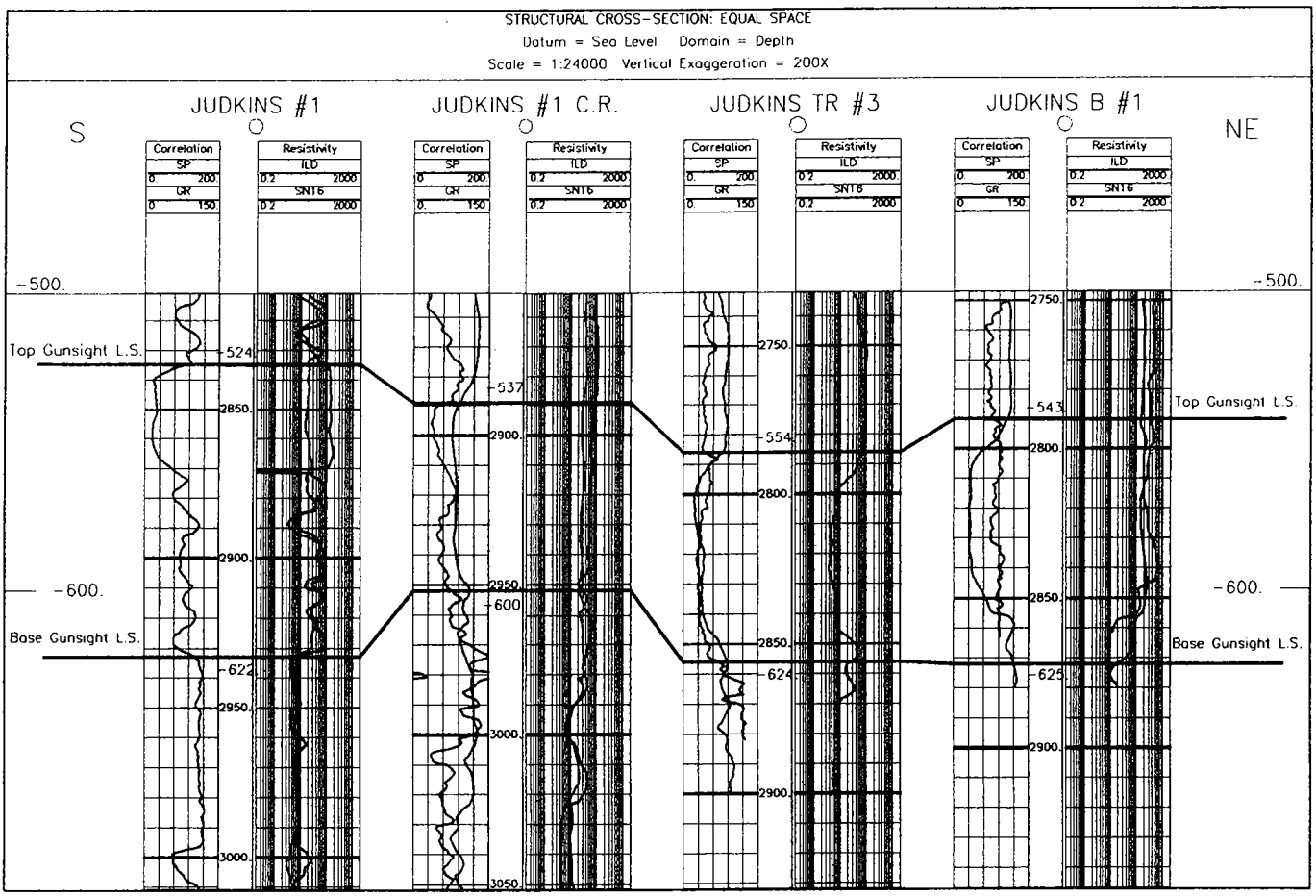

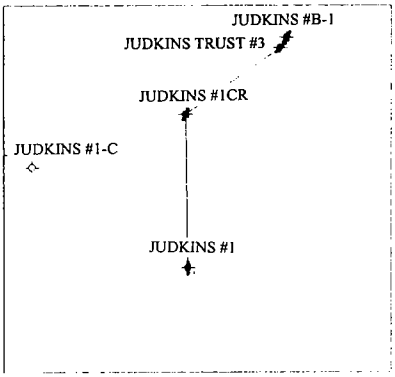

Figure 12. Structural cross section from southwest to northeast passing through Judkins #1, Judkins #1CR, Judkins Trust #3, and Judkins #B-1 wells. Depth in feet below Kelley bushing. See Figure 2 for locations of wells.

decreases, and it becomes very fine to fine grained and tight (Fig. 18C). The associated chert is dark colored (Fig. 18B) and contains radiolaria (Fig. 18D), indicating a deep-water depositional environment. This sandstone might have formed as a turbidity deposit.

Shale

The shale above the Gunsight Limestone contains marine fossils, such as crinoid, ostracode, and some shell fragments, suggesting a shelf environment. The shale below the chert bed, however, is not fossiliferous, indicating a deeper-water environment.

Sedimentary Environment

The lithology column for the Judkins #B-1 well (Fig. 21) shows two sequences of upward-shallowing facies. The lower sequence grades upward from basin shale to basin-margin chert and turbidite, to platform-slope shale and limestone, and to platform limestone at the top. The upper sequence grades upward from shelf shale and limestone to platform limestone. A similar sequence can be seen in the Judkins #1 well (Fig. 22). Based on this interpretation, the reconstructed sedimentary model for the Gunsight Limestone and the underlying sandstone is shown in Figure 23.

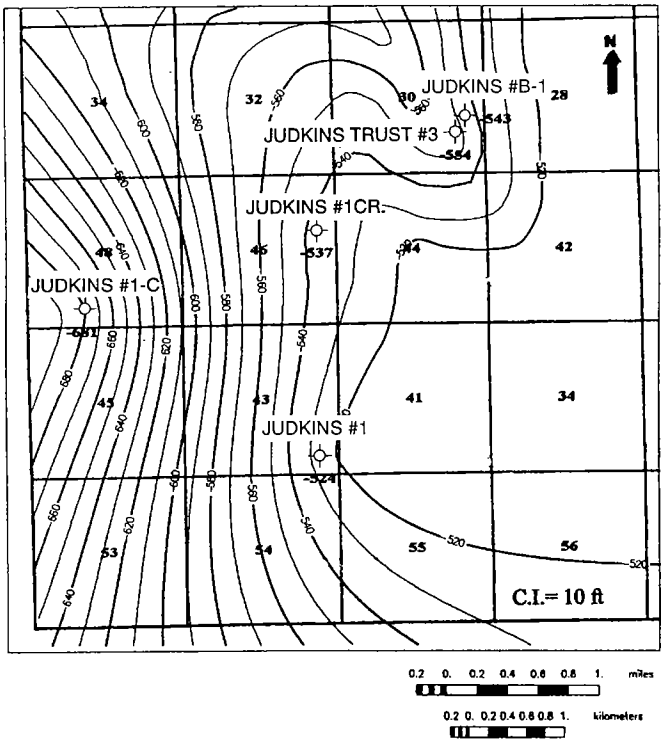

Figure 13. Structure map (in feet below sea level) for the top of Gunsight Limestone in study area, Schleicher County, Texas.

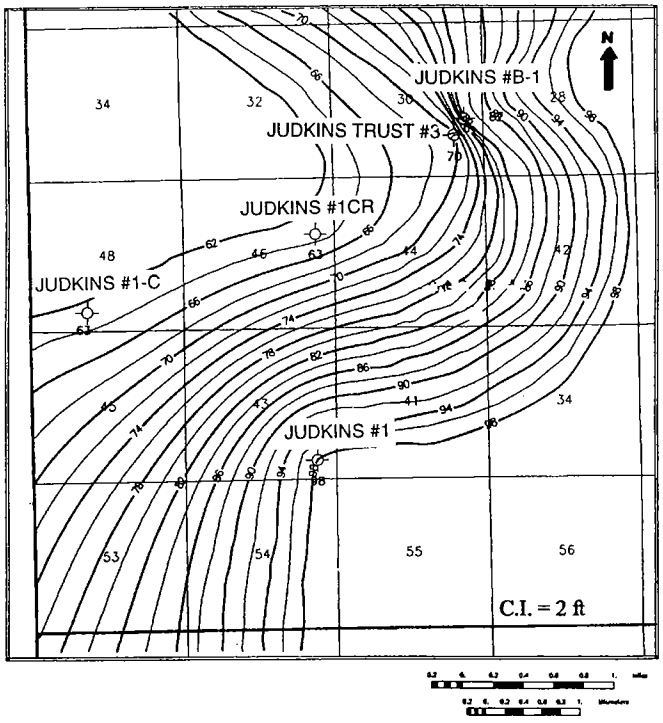

Figure 15. Thickness map (in feet) for the Gunsight Limestone in study area, Schleicher County, Texas.

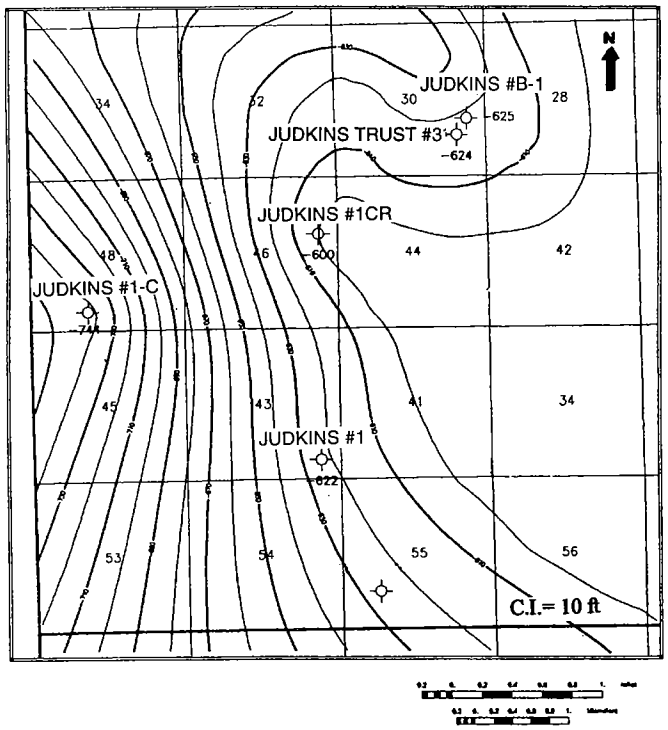

Figure 14. Structure map (in feet below sea level) for the base of Gunsight Limestone in study area, Schleicher County, Texas.

Reservoir Porosity and Hydrocarbon Shows

Five types of porosity were recognized from the thin sections: (1) intercrystal porosity in dolomites and calcites, (2) intergranular porosity in sandstone, (3) intraparticle porosity in bioclasts, (4) moldic porosity in limestone, and (5) micro-fractures (Figs. 16B, 19, 20).

The intercrystal porosity is the most important for controlling the quality of carbonate reservoirs and the intergranular porosity for sandstone reservoirs. Because the Gunsight Limestone is only partially dolomitized, not all the dolostone has porosity. The intercrystal porosity in the limestone largely determines the reservoir quality.

Ultraviolet-Fluorescent Cuttings

Seventy-seven samples of cuttings that showed light-yellow to light-brown fluorescence under ultraviolet light were chosen to analyze the hydrocarbon components and the lithology. The high peak at nc15 on Figure 24 may be contamination. The other lower peaks indicate that the observed staining is caused by hydrocarbons.

Of these 77 fluorescent cuttings, dolostone makes up 29% and limestone makes up 71% (Table 8). Only 47% of the cuttings have porosity. The estimated average porosity is less than 10%.

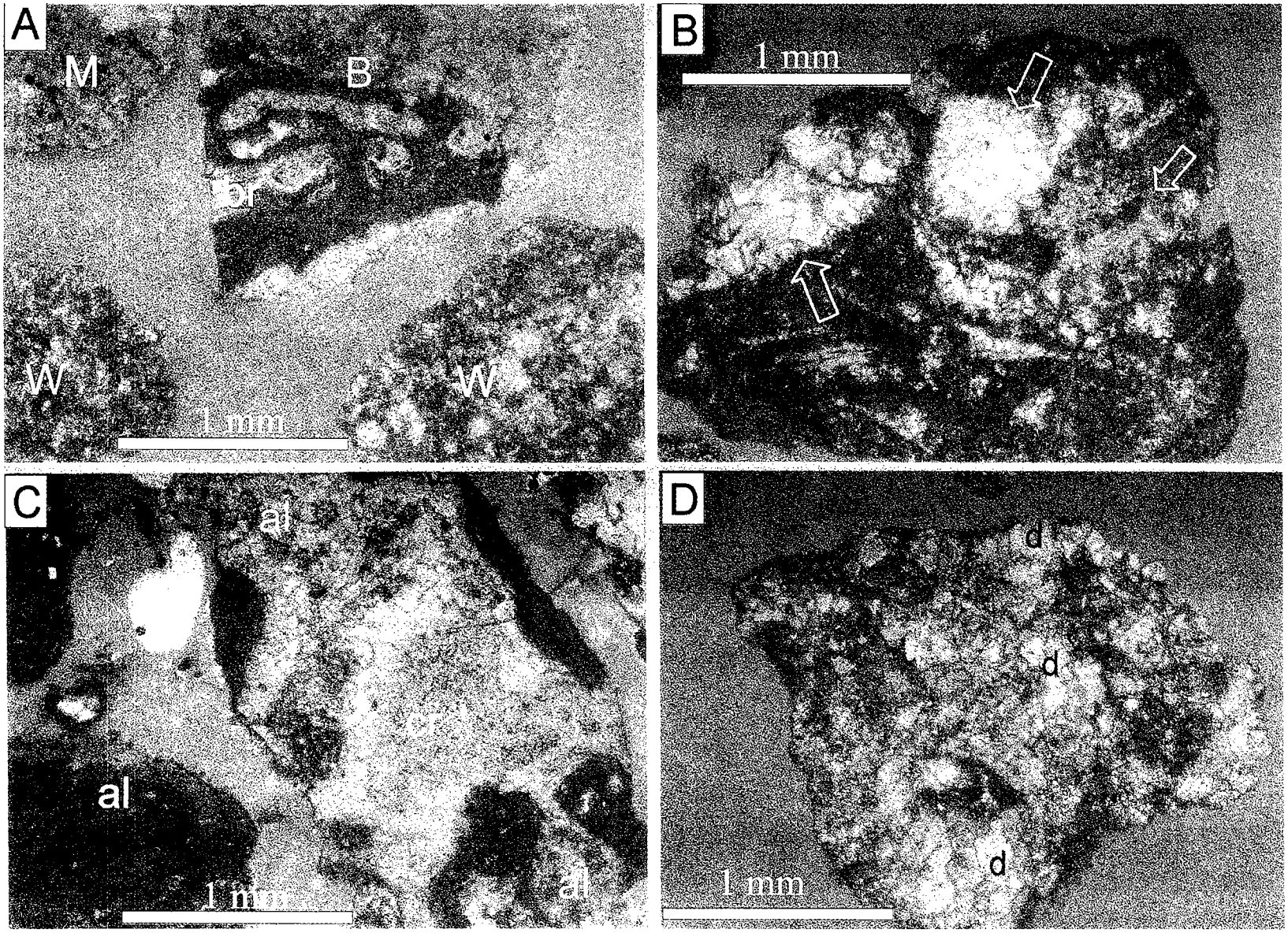

Figure 16. Ultraviolet-fluorescent photomicrographs of rock types from cuttings from Gunsight Limestone; Judkins #B-1 well, Schleicher County, Texas. (A) Limestone, showing bafflestone [B], with *in situ* bryozoa [br], wackestone [W], and mudstone [M]; 2,860–2,870 ft depth. (B) Limestone, showing packstone with calcareous green algae [arrows] and other fossil fragments; 2,820–2,870 ft depth. (C) Limestone, showing slightly dolomitized bafflestone; fragment of calcareous algae [al] at lower left; note connection between crinoid [cr] and algae [al]; 2,860–2,870 ft depth. (D) Limestone showing partially dolomitized limestone consisting of equant calcispar and dolomite [d] with intercrystal porosity; 2,820–2,860 ft depth.

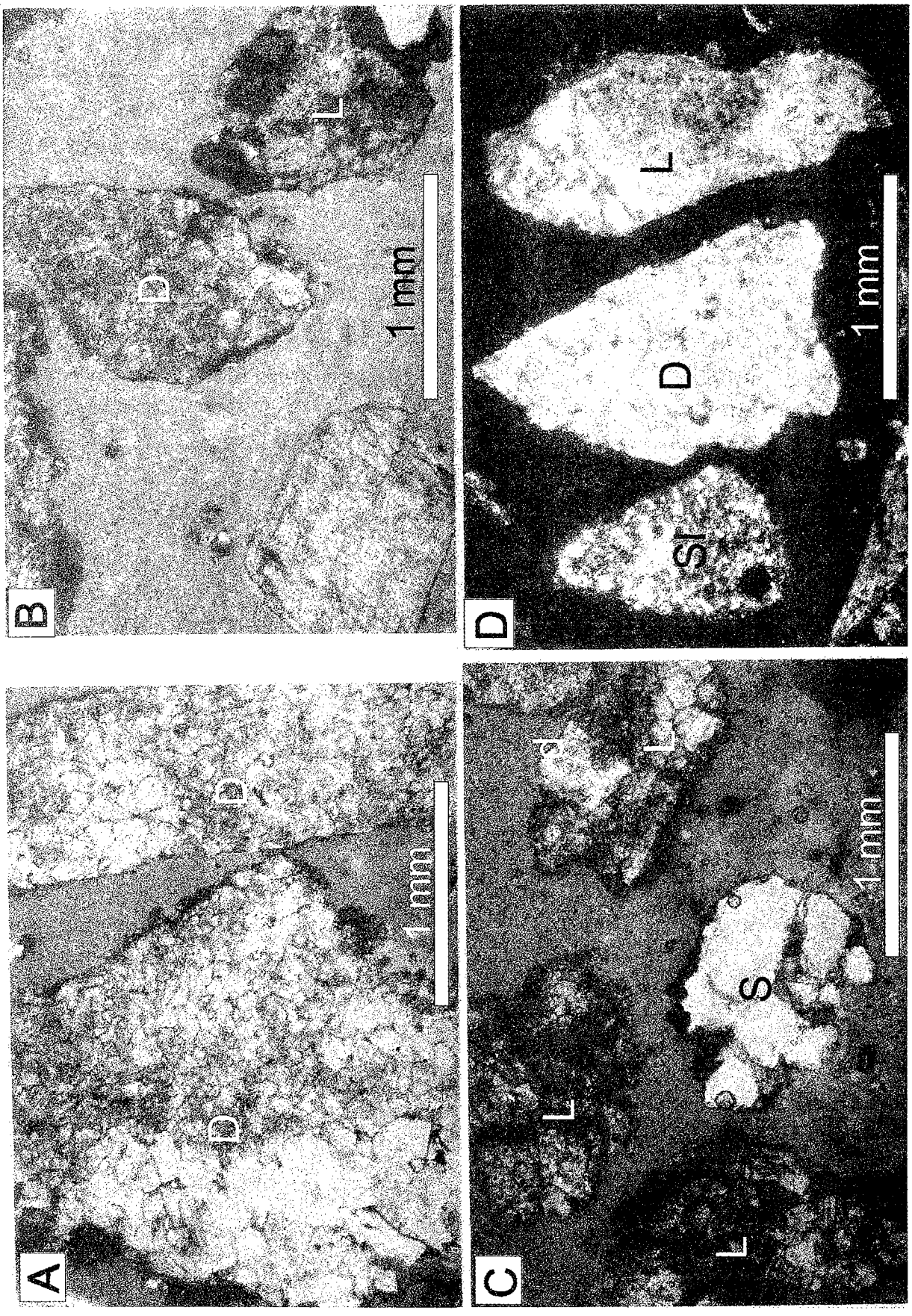

Figure 17. Ultraviolet-fluorescent photomicrographs of rock types from cuttings from within Gunsight Limestone; Judkins #B-1 well, Schleicher County, Texas. (A) Dolostone [D] with no porosity; 2,860–2,870 ft depth. (B) Dolostone [D], lime-grainstone [L], and blocky-calcite cement; 2,850–2,860 ft depth. (C) Sandstone [S], limestone [L], and dolomitized limestone [d, L] at right; 2,810–2,820 ft depth. (D) Siltstone [Sl], dolostone [D], and packstone [L]; 2,850–2,860 ft depth.

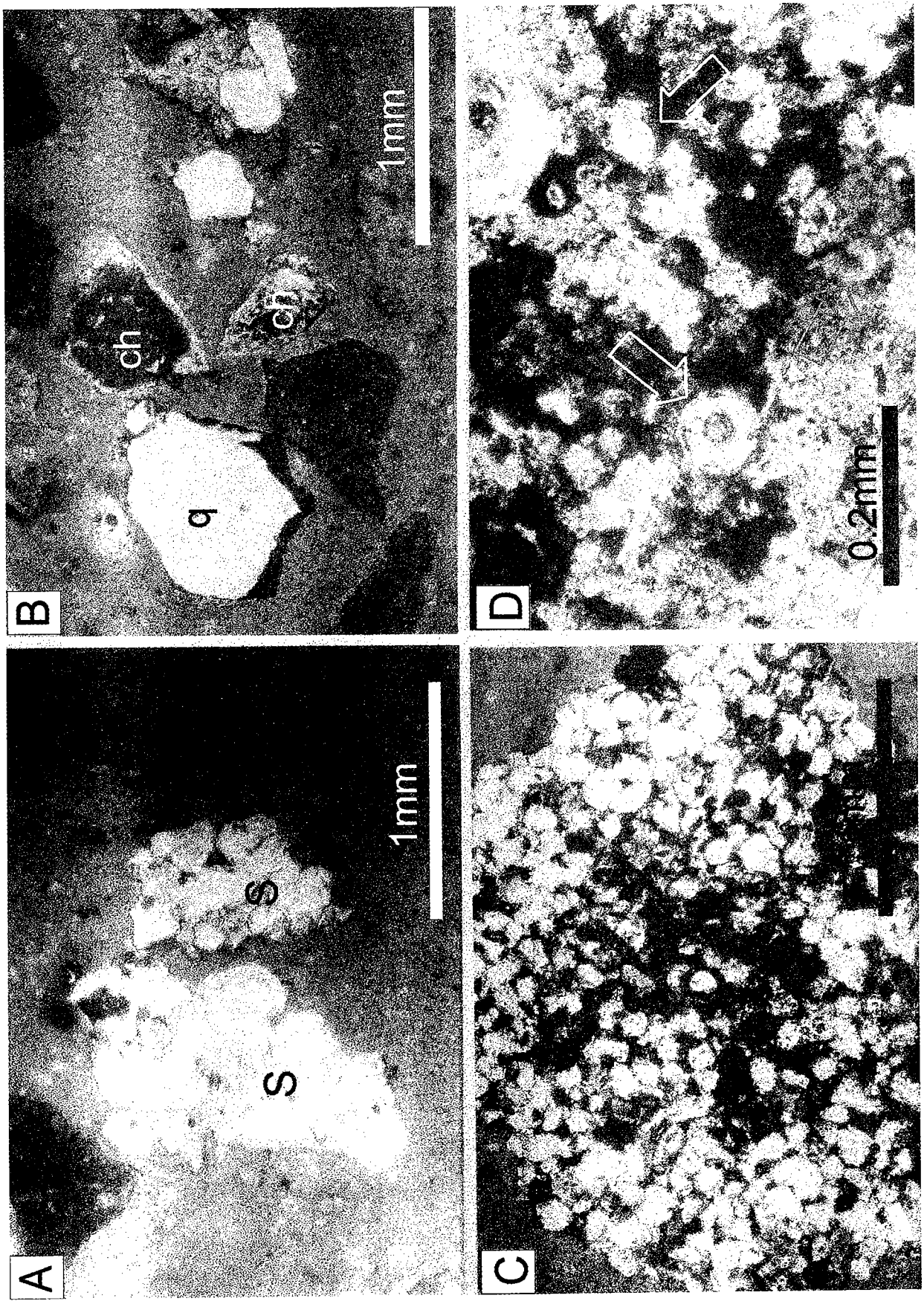

Figure 18. Ultraviolet-fluorescent photomicrographs of sandstone and chert from cuttings from below Gunsight Limestone; Judkins #B-1 well, Schleicher County, Texas. (A) Fine-grained sandstone [S] with dolomite (right) and overgrowth-quartz (left) cement; 2,950–2,960 ft depth. (B) Separated coarse-grained quartz sand [q] and chert [ch]; 2,950–2,960 ft depth. (C) Very fine grained sandstone; 3,030–3,040 ft depth. (D) Radiolaria (arrows) in chert; 2,950–2,960 ft depth.

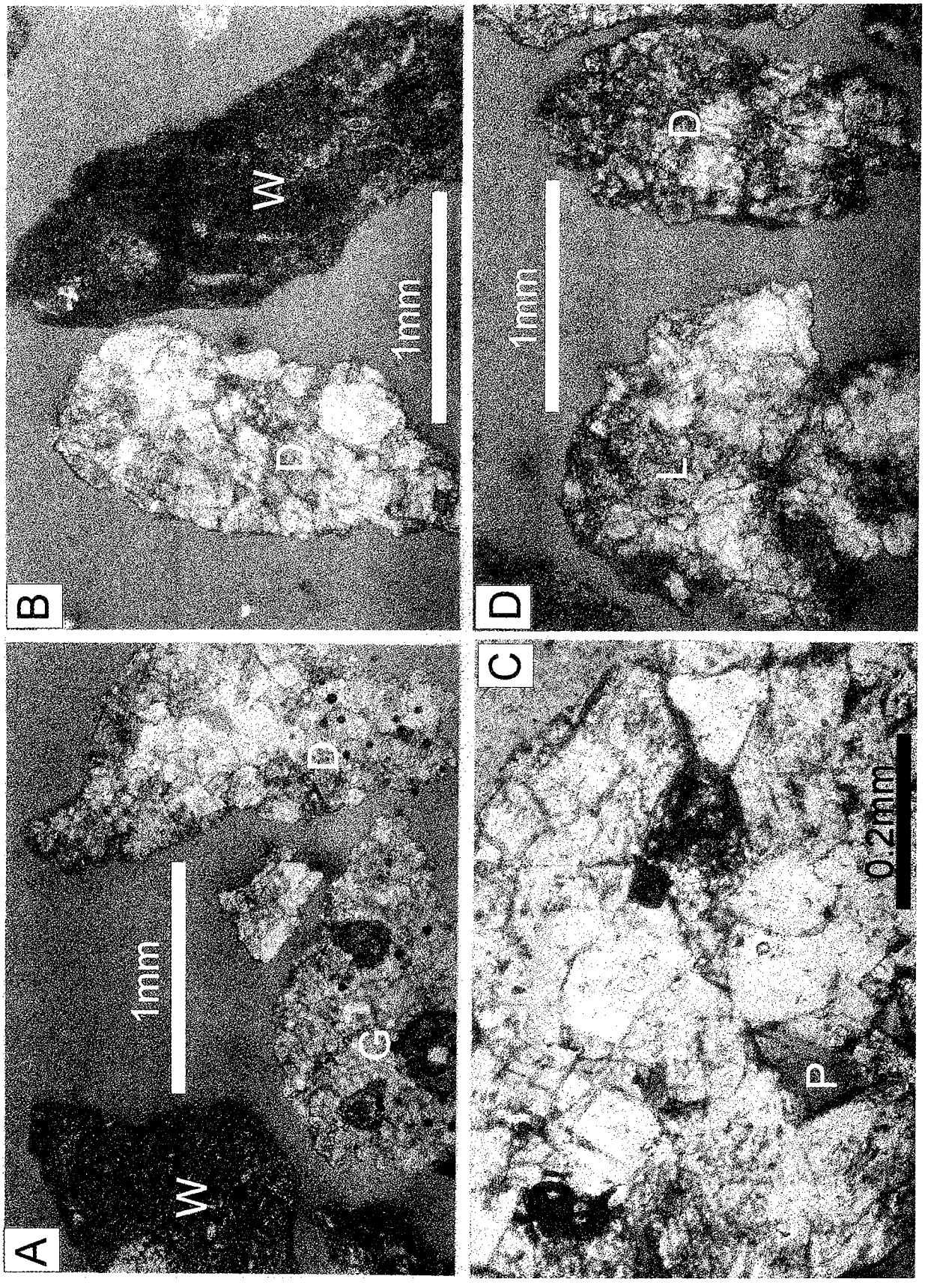

Figure 19. Ultraviolet-fluorescent photomicrographs of porosity types from cuttings from within Gunsight Limestone; Judkins #B-1 well, Schleicher County, Texas. (A, B) Dolostone [D] with intercrystal porosity, lime-grainstone [G], and wackestone [W]; 2,820–2,860 ft depth. (C) Dolostone with intercrystal porosity [P]; 2,810–2,820 ft depth. (D) Intergranular porosity in dolostone [D] and fracture and relict porosity in limestone [L]; 2,820–2,860 ft depth.

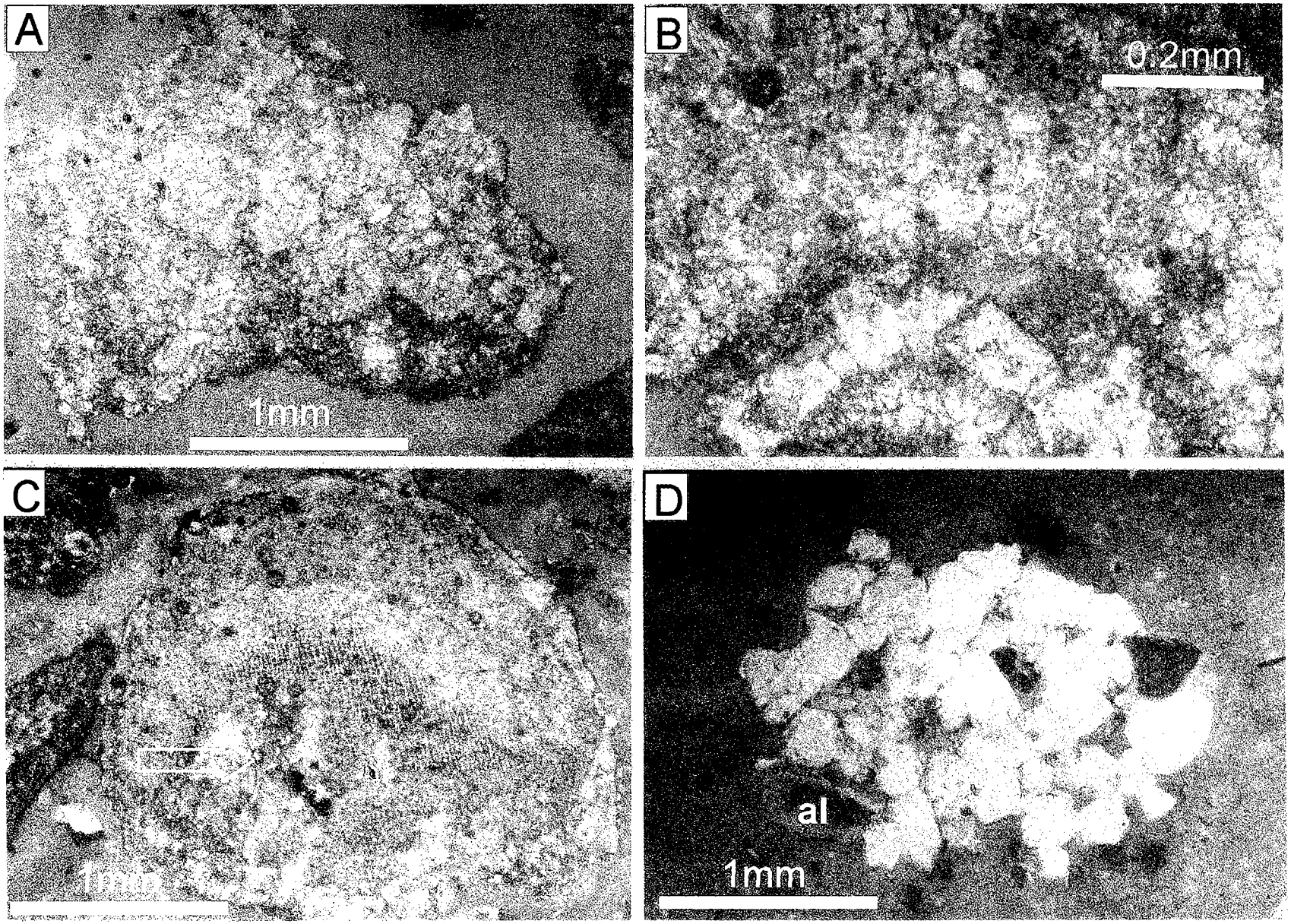

Figure 20. Ultraviolet-fluorescent photomicrographs of porosity types from cuttings from above, from within, and from the sandstone below the Gunsight Limestone; Judkins #B-1 well, Schleicher County, Texas. (A) Intercrystal porosity in limestone consisting of equant calcispar; 2,820–2,860 ft depth. (B) Moldic porosity in limestone; 2,860–2,860 ft depth. (C) Intergranular porosity in crinoid fragments; 2,760–2,770 ft depth (above Gunsight Limestone). (D) Sandstone with well-preserved intergranular porosity [al]; 2,950–2,960 ft depth.

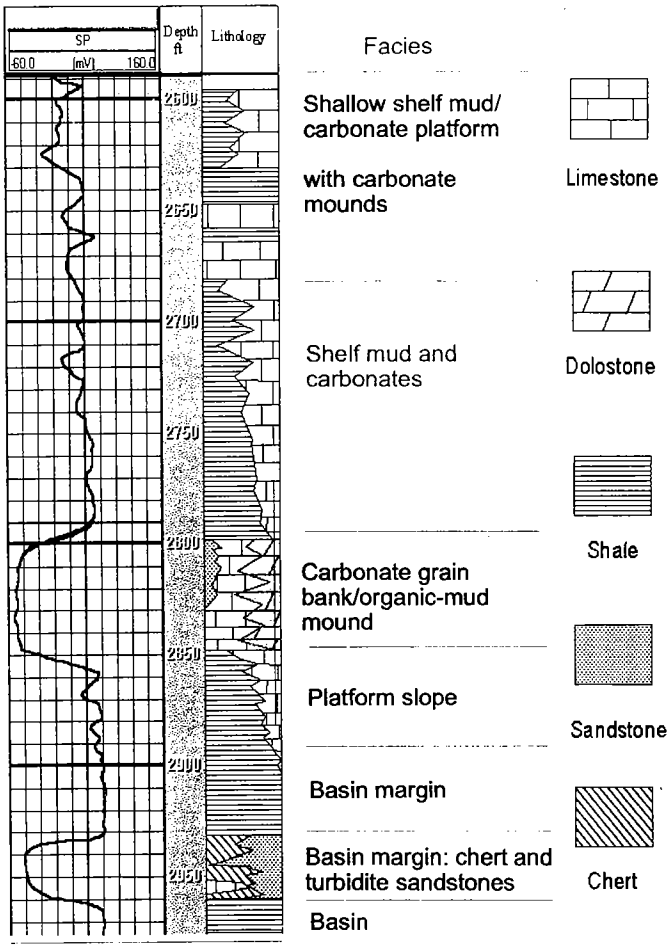

Figure 21. Lithology and sedimentary facies of Gunsight Limestone and its adjacent rocks in Judkins #B-1 well, Schleicher County, Texas. Depths in feet below Kelley bushing.

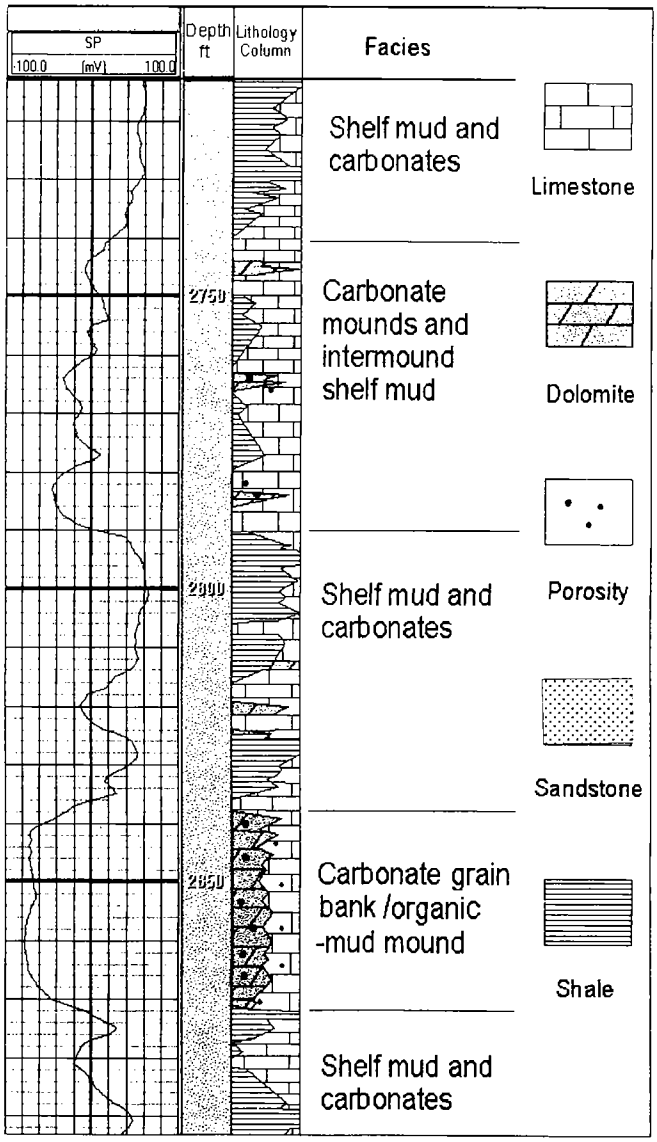

Figure 22. Lithology and sedimentary facies of Gunsight Limestone and adjacent rocks in Judkins #1 well, Schleicher County, Texas. Depths in feet below Kelley bushing.

CONCLUSIONS

The analysis of the two wells 500 ft apart—Judkins Trust #3 and Judkins #B-1—shows that the Gunsight Limestone in Judkins Trust #3 is saturated with water and the Judkins #B-1 has 70% to 80% oil saturation. This is a good indication of two separate limestone reservoirs oriented northwest–southeast. Log analysis of the Gunsight Limestone in the Judkins #1-C well indicates that it should produce oil. Oil saturation calculated by methods depending just on resistivity tools is overly optimistic by about 35%.

Ooid grainstone, bio-bafflestone, skeletal packstone, and wacke/mudstone are the Gunsight Limestone lithofacies that were identified by cutting samples from wells in the study area. Very finely to finely crystalline dolomite with varied porosity and dolomicrite with no porosity were found within the Gunsight interval. Intercrystal porosity, interparticle porosity, intraparticle porosity, moldic porosity, and microfracture porosity were recognized in the lithofacies of the Gunsight Limestone. Reservoir quality depends largely on the intercrystal porosity.

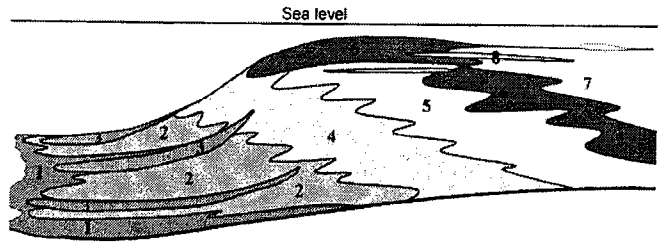

Figure 23. Sedimentary model of the Gunsight Limestone and adjacent rock unit in area of Judkins #B-1 well. (1) Basin shale, (2) basin-margin chert and shale, (3) turbidite sands, (4) platform-slope limestone and shale, (5) organic-mud mound, (6) carbonate-grain bank, (7) shelf shale and limestone, (8) tempestite sands.

TABLE 8. — Lithology and Porosity of Fluorescence Cuttings

Dolostone				Limestone							
Fine grained		Dolomicrite		Equant calcite		Grainstone		Packstone		Wackestone	
With pore[a]	No pore	With pore	No pore	With pore[a]	No pore	With pore	No pore	With pore[b]	No pore	With pore[b]	No pore
16			6	14	1		17	3	11	3	6
21%			8%	18%	1%		22%	4%	14%	4%	8%
29%				71%							

[a]Intercrystal porosity.
[b]Fracture.

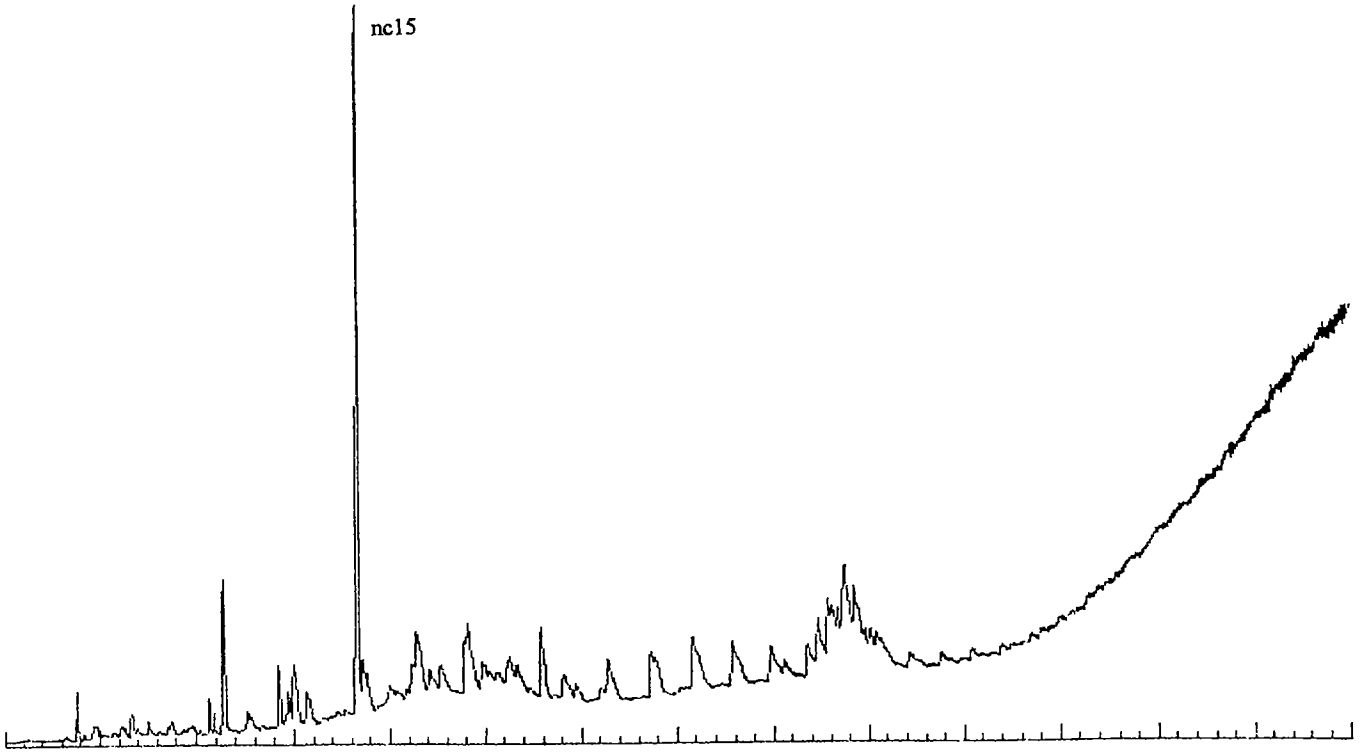

Figure 24. GC chromatograph of ultra-violet–fluorescent cutting from Judkins #B-1 well, Schleicher County, Texas. See text for explanation.

Cuttings with porosity from the Judkins #B-1 well showed light-yellow to light-brown fluorescence under ultraviolet light, and the presence of hydrocarbons was confirmed by chromatographic analysis. This interval was not tested either during drilling or completion of the well. A recompletion attempted many years later was unsuccessful because of inadequate cement bond. The Judkins Trust #3 drilled 500 ft away to test the Gunsight had no shows in this interval.

ACKNOWLEDGMENTS

The authors would like to thank James K. Anderson, the president of James K. Anderson, Inc., Exploration and Production, for providing the data and financial support.

REFERENCES CITED

Archie, G. E., 1942, The electrical resistivity log as an aid in determining some reservoir characteristics: Transactions of the American Institute of Mining and Metallurgical Engineers, v. 146, p. 54–62.

Carothers, J. E., 1968, A statistical study of the formation factor relationship: The Log Analyst, v. 9, no. 5, p. 13–20.

Dickson, J. A. D.; and Saller, A. H., 1995, Identification of subaerial exposure surfaces and porosity preservation in Pennsylvanian and Lower Permian shelf limestones, eastern Central Basin Platform, Texas, *in* Budd, D. A.; Saller, A. H.; and Harris, P. M. (eds.), Unconformities and porosity in carbonate strata: American Association of Petroleum Geologists Memoir 63, p. 239–257.

Heckel, P. H., 1986, Sea-level curve for Pennsylvanian

eustatic marine transgressive-regressive depositional cycles along Midcontinent outcrop belt, North America: Geology, v. 14, p. 330–334.

Mazzullo, S. J., 1997, Stratigraphic exploration plays in Ordovician to Lower Permian strata in the Midland basin and on the Eastern shelf, *in* DeMis, W. D. (ed.), Permian basin oil and gas fields: turning ideas into production: West Texas Geological Society Publication 97-102, p. 1–38.

Reid, A. M.; Reid, S. A. T.; and Mosely, M. A. 1991, Late Strawn and Early Canyon highstand and lowstand shelf edges and reefs on the Eastern shelf with examples from Schleicher and Tom Green Counties, Texas, *in* Candelaria, M. (ed.), Permian basin plays, tomorrow's technology today: West Texas Geological Society Publication 91-89, p. 118–119.

Reid, A. M.; Mosely, M. A.; and Tomlinson Reid, S. A., 1992, Shelf edges reefs, and associated stratigraphic traps on the Eastern shelf, *in* Mruk, D. H.; and Curran, B. C. (eds.), Permian basin exploration and production strategies: applications of sequence stratigraphic and reservoir characterization concepts: West Texas Geological Society Publication 92-91, p. 61–63.

Rollyn, W. F., 1986, Prospecting with old e-logs: Schlumberger Education Services, Houston, Texas, p. 161.

Saller, A. H.; Dickson, J. A. D.; and Boyd, S. A., 1994, Cycle stratigraphy and porosity in Pennsylvanian and Lower Permian shelf limestones, eastern Central Basin Platform, Texas: American Association of Petroleum Geologists Bulletin, v. 78, p. 1820–1842.

Shlumberger, 1989, Schlumberger log interpretation charts: Schlumberger Educational Services, Houston, Texas, p. 151.

_____ 1990, Schlumberger historical charts: Schlumberger Educational Services, Houston, Texas, p. 88.

Waite, L. E., 1993, Upper Pennsylvanian seismic sequences and facies of the eastern and southern Horseshoe Atoll, Midland basin, West Texas, *in* Loucks, R. G.; and Sarg, J. F. (eds.), Carbonate sequence stratigraphy: American Association of Petroleum Geologists Memoir 57, p. 213–240.

Walker, D. A.; Jensen, J. M.; Zodey, S. P.; and Reid, S. T., 1990, Pennsylvanian cycle stratigraphy and carbonate facies control of reservoir development in the Salt Creek field, Kent County, Texas, *in* Flis, J.; and Price, R. C. (eds.), Permian basin oil and gas fields: innovative ideas in exploration and development: West Texas Geological Society Publication 90-87, p. 107–112.

Ward, R. F.; Kendall, C. G. St. C.; and Harris, P. M., 1986, Upper Permian (Guadalupian) facies and their association with hydrocarbon—Permian basin, West Texas and New Mexico: American Association of Petroleum Geologists Bulletin, v. 70, p. 239–262.

Winsauer, W. O.; Shearin, H. M., Jr.; Masson, P. H.; and William, M., 1952, Resisitivity of brine-saturated sands in relation to pore geometry: American Association of Petroleum Geologists Bulletin, v. 36, p. 253–277.

Wright, W. F., 1979, Petroleum geology of the Permian basin: West Texas Geological Society Publication 79-71, p. 98.

Hydrocarbon System Related to a Pennsylvanian Pull-Apart Graben, North-Central Texas*

Brian S. Brister
New Mexico Bureau of Mines and Mineral Resources
Socorro, New Mexico

William C. Stephens and Gregg A. Norman
Gunn Oil Company
Wichita Falls, Texas

ABSTRACT.—Natural-gas fields in Cottle and King Counties, Texas, mark the extent of a hydrocarbon system related to the Gunn graben, an elongate 180 km^2 pull-apart basin in southeastern Cottle County. The graben results from left-step overstepping of left-lateral fault zones and is a component of the Red River–Matador structural trend of the greater Ancestral Rocky Mountains. Arkosic detritus originating from the Amarillo–Wichita uplift was transported southward, over the region containing the graben, toward the Knox–Baylor trough. Episodic graben subsidence accommodated a portion of this sediment load as syntectonic, cyclically stacked Bend Group (Atokan, lower Pennsylvanian) fluvial-deltaic to marine deposits. Organic facies within the graben fill are predominantly terrestrially derived as determined from macroscopic evidence, kerogen microscopy and Rock-Eval pyrolysis. Measured total organic carbon (TOC) in shale, exceeding 4% on average, is adequate for potential hydrocarbon generation. Lopatin-method basin modeling, vitrinite-reflectance (Ro) measurements, and Ro-calibrated pyrolysis-derived maturity measures demonstrate that the Bend Group organic facies in the graben have approached peak gas-generating maturation levels. Generated gas migrated within and outside of the basin following nonsealing faults and channelized fluvial pathways into several reservoir rock types. Producing fields represent a variety of structural and/or stratigraphic traps.

INTRODUCTION

Twenty-four natural gas fields, representing more than 50 years of exploration and development activity, are clustered in southeastern Cottle and northeastern King Counties, Texas (Fig. 1; Table 1). These fields, predominantly producing from the Pennsylvanian (Atokan) Bend conglomerate (Fig. 2), are located within a region otherwise typified by oil production. The nearest significant nonassociated gas production from the Bend conglomerate is 200 km to the east-southeast at Boonsville field of the Fort Worth basin (Gardner, 1960). More than 113 billion cubic feet of gas equivalent (Bcfe) have been produced from the Cottle/King fields through December 1999, with ultimate recovery from all existing wells projected to exceed 150 Bcfe. Two new fields were discovered in the past decade as a result of a successful effort to relate the known fields to a gas-generative basin, here termed Gunn graben. The purpose of this paper is to demonstrate application of petroleum system concepts to natural-gas exploration and to present an example of a relatively small, but productive, pull-apart graben. The hydrocarbon system described here could be considered a model for undiscovered, undeveloped, and underdeveloped systems of similar size and origin within the late Paleozoic greater Ancestral Rocky Mountains foreland region.

TECTONIC SETTING

Figure 3 is a composite of regional tectonic elements that evolved throughout the Pennsylvanian in the southern Midcontinent region. The Gunn graben is located at the juncture of the Red River uplift/arch (Thompson, 1988; Ewing, 1991) and the Matador uplift/

*Portions of this paper reprinted, with modification, from Brister, B. S.; Stephens, W. C.; and Norman, G. A., 2002, Structure, stratigraphy, and hydrocarbon system of a Pennsylvanian pull-apart basin in north-central Texas: American Association of Petroleum Geologists Bulletin, v. 86, no. 2 (February). Reprinted by permission of AAPG.

Brister, B. S.; Stephens, W. C.; and Norman, G. A., 2001, Hydrocarbon system related to a Pennsylvanian pull-apart graben, north-central Texas, *in* Johnson, K. S.; and Merriam, D. F. (eds.), Petroleum systems of sedimentary basins in the southern Midcontinent, 2000 symposium: Oklahoma Geological Survey Circular 106, p. 55–70.

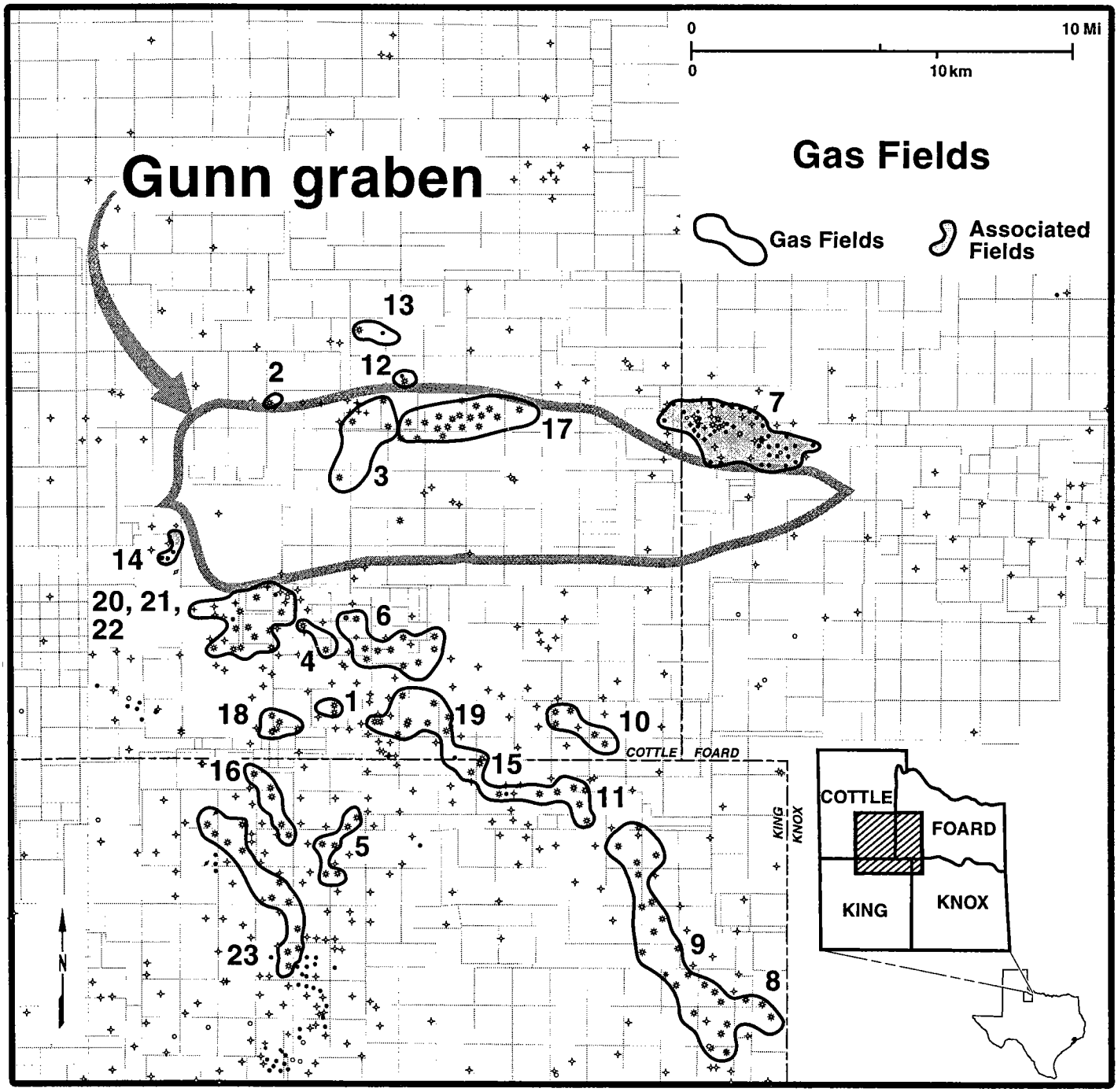

Figure 1. Map of gas-producing fields of Cottle and King Counties, Texas, that mark the extent of the hydrocarbon system related to the Gunn graben. Inset map shows location within Texas. Numbered fields are explained in Table 1.

arch (Hills, 1963, 1985; Budnik, 1989; Ewing, 1991). These features constitute a narrow, elongate structural trend that extends more than 500 km from Montague County in north-central Texas to Roosevelt County in east-central New Mexico. The trend is marked by a series of basement-cored pop-up horsts, many of which trap oil accumulations, separated by poorly documented depressions. This trend is a component of the late Paleozoic Ancestral Rocky Mountains (Kluth and Coney, 1981; Kluth, 1986; Budnik, 1986; Ye and others, 1996) formed by foreland deformation inboard of the Ouachita–Marathon overthrust belt (Walper, 1977; Kluth and Coney, 1981; Kluth, 1986).

The structurally complex zone located where the Red River and Matador features overlap and terminate is referred to here as the Red River–Matador tectonic zone (Fig. 4). Structures within this zone are interpreted from a proprietary collection of seismic and sub-

TABLE 1. — Production Statistics for Fields Shown in Figure 1

No.	Gas fields	Producing formation	County	Disc. date	Status	Cum. MCFE to 12/31/99	MCFE 1999	BBL/MMCF cond. yield, '99
1	Armstrong	Bend conglomerate	Cottle	1982	Inactive	1,231,810	NA	NA
2	Boyles	Bend conglomerate	Cottle	1989	Active	1,176,739	98,636	16.7
3	Broken Bone	Bend conglomerate	Cottle	1990	Active	3,332,712	67,661	18.8
4	Chalk, N	Bend conglomerate	Cottle	1985	Active	796,021	26,472	3.0
5	Final Blow	Bend conglomerate	King	1992	Inactive	98,590	NA	NA
6	Independent	Bend conglomerate	Cottle	1981	Active	7,694,331	54,943	0.3
7	Johnson	lower Cisco sandstone	Foard	1951	Inactive	unknown[b]	NA	NA
8	Juniper	lower Strawn limestone	King	1950	Active	4,149,211	95,939	0.4
9	Juniper	Bend conglomerate	King	1959	Active	11,076,938	2,056,349	4.6
10	Juniper, N	Bend conglomerate	Cottle	1966	Inactive	672,190	NA	NA
11	Masterson Ranch	Bend conglomerate	King	1990	Active	37,642	10,922	0
12	Moon Camp	Bend conglomerate	Cottle	1995	Inactive	63,445	NA	NA
13	Moon Camp	Palo Pinto (Canyon ls.)	Cottle	1988	Active	2,232,150	330,937	7.6
14	Paducah (oil)[a]	Cambrian sandstone	Cottle	1986	Active	2,858,149	66,816	63.6
15	Providence	Bend conglomerate	Cottle	1974	Active	22,846,592	304,842	5.2
16	Prudence	Bend conglomerate	King	1975	Active	11,654,667	353,513	2.7
17	Rhombochasm	Bend conglomerate	Cottle	1994	Active	13,381,435	4,261,093	8.9
18	Stescott	Bend conglomerate	Cottle	1976	Active	14,830,294	17,548	12.7
19	Thomas	Bend conglomerate	Cottle	1982	Active	2,822,978	43,509	4.1
20	Tippen, S	Bend conglomerate	Cottle	1978	Active	4,286,424	17,012	0
21	Tippen, SE	Bend conglomerate	Cottle	1989	Inactive	24,404	NA	NA
22	TIPPEN, SW	Bend conglomerate	Cottle	1967	Inactive	1,421,600	NA	NA
23	TOM "B"	Bend conglomerate	King	1979	Active	6,840,856	78,550	0
					TOTAL	**113,529,178**		

NOTE: Volumes in thousand standard cubic feet of gas include condensate converted to gas equivalent (Railroad Commission of Texas data).

[a]Paducah oil field: cumulative and 1999 values include only casinghead gas (not oil).

[b]Johnson gas field: a pipeline was constructed and significant volume of gas was produced and transported, but data unavailable.

surface data. This zone is significantly more deformed than the immediately adjacent areas to the north and south. Deformation was most intense during deposition of the Bend Group (Atokan), which is consistent with super-regional observations of Ham and Wilson (1967). Locally, post-Atokan tectonic activity continued until as late as Early Permian, but primarily as minor continued motion of established fault zones.

Orientation and distribution of structures along the length of the Red River–Matador trend reflect left-lateral strike slip (Budnik, 1986). The overlapping left step from the Red River to the Matador feature created complex lesser-order en echelon pop-up horsts and pull-apart grabens, the orientations of which are consistent with left-lateral strike-slip. Evidence for strike and oblique-slip (wrench) motion within the zone, interpreted from seismic and subsurface data, include: (1) presence of en echelon, laterally extensive, basement-offsetting faults; (2) faults bounding basement-involved structural blocks that tend to be high-angle normal or reverse with the two types coexisting locally; (3) along-strike change in amount of vertical displacement of faults and reversal in dip of some fault planes; (4) splaying of fault tips, apparent braiding of faults, or multiple parallel faults in narrow fault zones; (5) presence of flower structures; and (6) existence of localized, thick, rapidly deposited syntectonic Atokan sediments in graben blocks adjacent to horst blocks with coeval unconformities. Literature supporting these observations as typical of wrench-fault conditions includes papers by Moody and Hill (1956), Wilcox and others (1973), Reading (1980), Christie-Blick

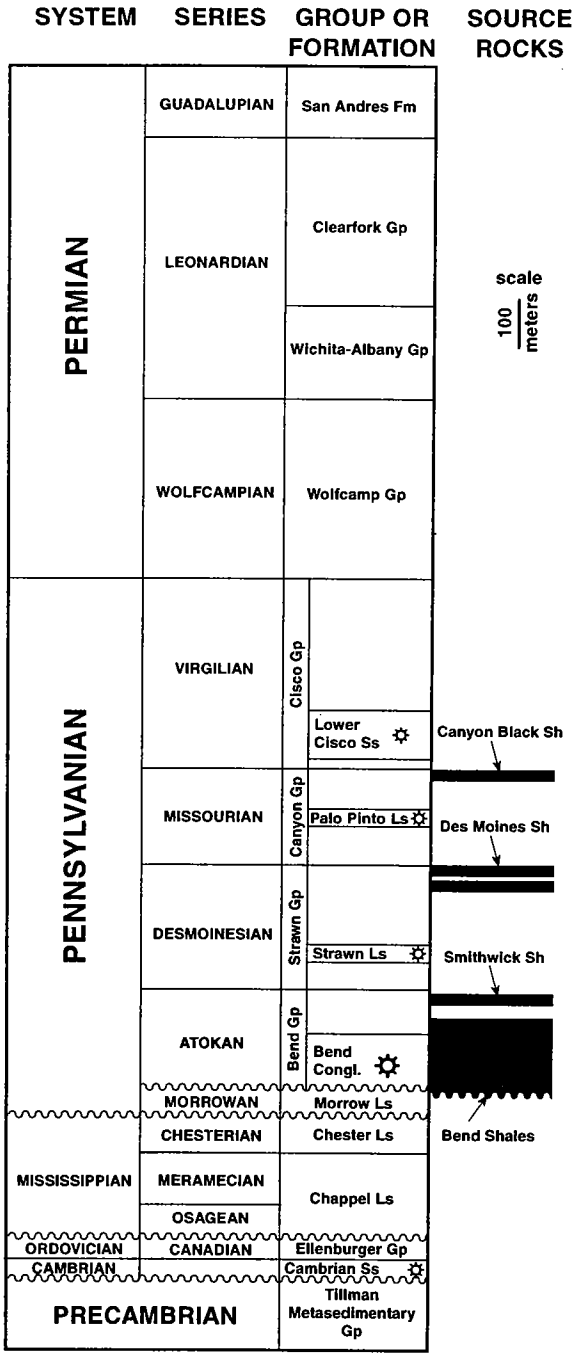

Figure 2. Stratigraphic column for Gunn graben area. Known gas reservoirs denoted by gas well symbols. Abbreviations: Congl = conglomerate, Fm = Formation, Gp = Group, Ls = limestone, Ss = sandstone, Sh = shale.

and Biddle (1985), Sylvester (1988), and Harding (1990).

Pennsylvanian and older rocks do not crop out in the region of this study. Therefore, no direct kinematic evidence is available that would quantify the amount of lateral offset for the Red River–Matador tectonic zone or for component faults. Subjective palinspastic reconstruction suggests strike-slip displacement on the order of kilometers for some of the more significant individual faults with cumulative displacement of the tectonic zone perhaps an order of magnitude higher. For comparison, displacements in the range of 12–26 km have been inferred for oblique left-slip/reverse-slip faults on the northern margin of the Wichita uplift in Oklahoma (McConnell, 1989). Pre-Atokan sedimentary units are relatively consistent in thickness and lithofacies distributions regionally and were flat lying at the time of initiation of deformation; thus, no sedimentary-related tectonic piercing lines are known.

The Red River/Matador trend reactivated a major Precambrian terrain boundary, possibly marking the southern edge of the Middle Proterozoic Oklahoma aulacogen (Ham and others, 1964; Denison and others, 1984). Precambrian penetrations south of the Red River–Matador tectonic zone in King County have yielded granitic plutonic rock, whereas several penetrations within the zone in Cottle and Foard Counties have yielded greenschist-facies metamorphosed sedimentary rocks, possibly part of the Tillman metasedimentary group of Ham and others (1964). Therefore, Precambrian units do not correlate across the zone due to the coincidence of Paleozoic deformation and the Precambrian terrain boundary.

GRABEN STRUCTURE

The Gunn graben is an elongate, rhomb-shaped depression bounded on all sides by fault zones with maximum structural relief on the base of the Pennsylvanian exceeding 2.7 km from the graben floor to the top of the adjacent Johnson horst block (Fig. 4). Within the basin-bounding fault zones, the graben is approximately 24 km long (west to east) and 7.5 km wide (north to south), resulting in a 3.2 to 1 length-to-width ratio and covering an area of 180 km^2. A central westward-plunging axial syncline extends through the length of the basin.

North-south seismic lines crossing the basin axis demonstrate that the basin axis is narrow, deep, and asymmetric. Closely spaced faults appear to merge with depth into narrow, subvertical principal displacement zones at basement level. Fault planes at the Pennsylvanian level are high angle with most demonstrating a normal sense of throw, although both normal and reverse faults coexist along the northern margin. Some faults demonstrate along-strike changes in sense of throw and fault-plane geometry. There is significant internal fault complexity partitioning the basin into structural subdomains, and, on a smaller scale, compartmentalizing potential sandstone reservoir units.

The structural characteristics of the Gunn graben suggest that it is a "rhombochasm" (Crowell, 1974) formed through left-step overstepping of left-lateral strike-slip fault zones in the Red River–Matador tectonic zone. Literature illustrating how such basins are created include Rodgers (1980), Mann and others (1983), and Aydin and Nur (1985). Sand box models of pull-apart basins by Dooley and McClay (1997) bear striking resemblance to the graben.

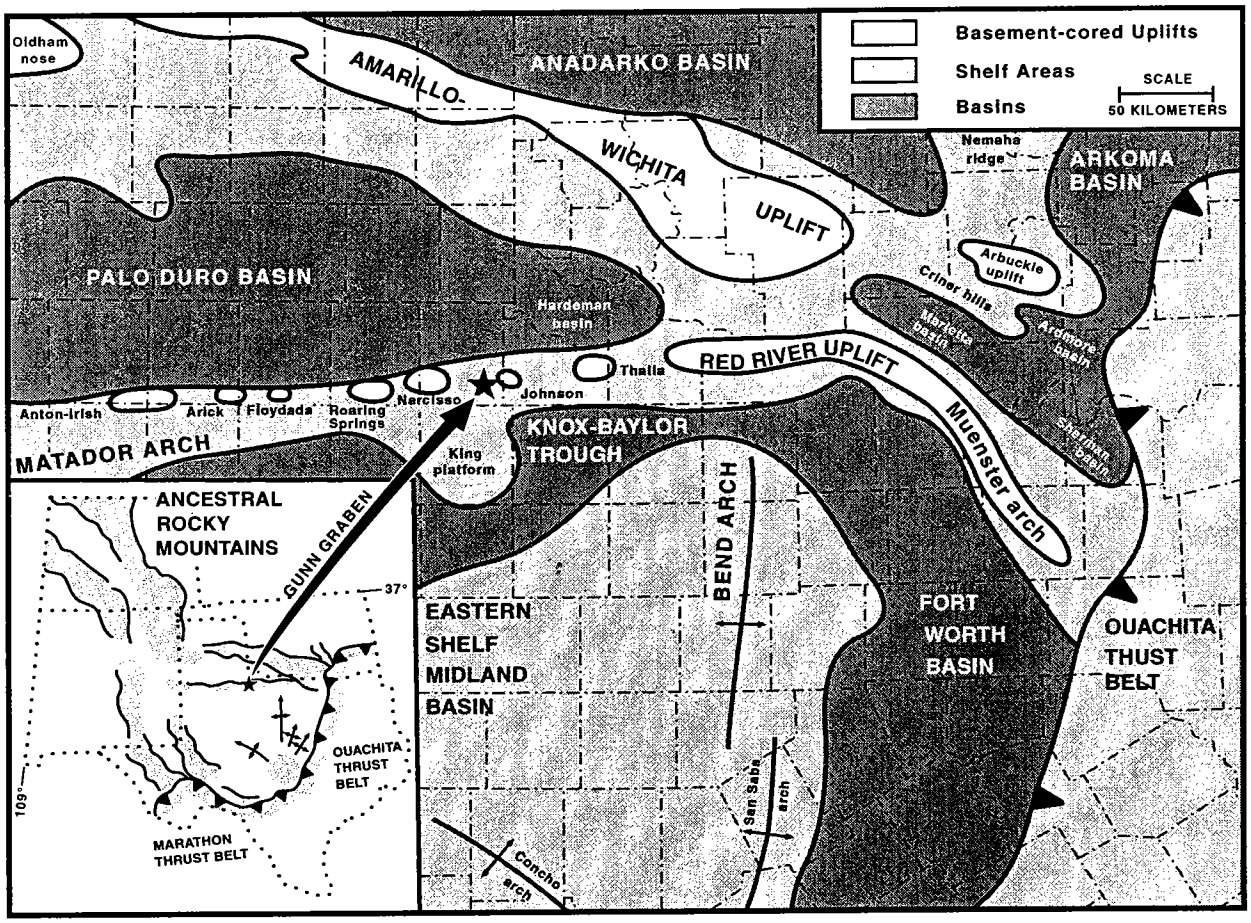

Figure 3. Regional Pennsylvanian paleotectonic elements (modified from Ewing, 1991). Inset map shows position of Gunn graben within Ancestral Rocky Mountains region (modified from Ye and others, 1996).

SYNTECTONIC DEPOSITION

Figure 5 is a cross-basin–correlation cross section that demonstrates thickening of the Bend Group within the graben relative to the graben exterior. Figure 6 includes maps of the distribution of Bend conglomerate (lower Bend Group) and sandstone lithofacies for the region and an isopach map of the entire Bend Group in the graben area. The Bend Group is less than 125 m thick over much of the region. South of the Gunn graben, in the vicinity of the Cottle–King County line, the Bend thins in places to less than 25 m in gross thickness. Maximum thickness of the Bend within the Gunn graben exceeds 1.3 km.

Atokan stratigraphy preserved within the graben is unique in that it represents a depositional record largely absent regionally due to nondeposition. During the major Atokan period of subsidence, the Gunn graben was forming within a larger piedmont region between the Amarillo–Wichita mountain chain to the north and the Knox–Baylor marine trough (Gunn, 1979) to the south (Fig. 3). Except over localized grabens and horsts, the basal Bend surface was marked by net transport of arkosic sediments rather than net erosion or deposition. Eventual sedimentation upon the surface was not synchronous over the region but transgressed northward over time. On the basis of well control, the basal Bend surface ranges from a planar, low-angle disconformity developed on Morrowan marine carbonate and clastic units in low and neutral areas to an angular erosional unconformity developed on Mississippian through Precambrian units over basement-cored pop-up horsts. The relatively small horsts in the vicinity of the Gunn graben contributed relatively minor, primarily carbonate, detritus to the subsiding graben in contrast to other parts of the Red River–Matador trend, where significant Precambrian-derived arkosic detritus was eroded from larger-scale, more deeply eroded horsts.

There are no widespread fault-derived cataclastic breccia deposits in the graben fill, as interpreted from existing well control. This observation suggests that topographic relief across the basin margins at any given time was minimal and that sufficient sediment was being transported to the graben to quickly fill the depression as it formed. Therefore, episodic graben subsidence periodically accommodated a portion of an abundant sediment supply. Cycles in the basin fill are

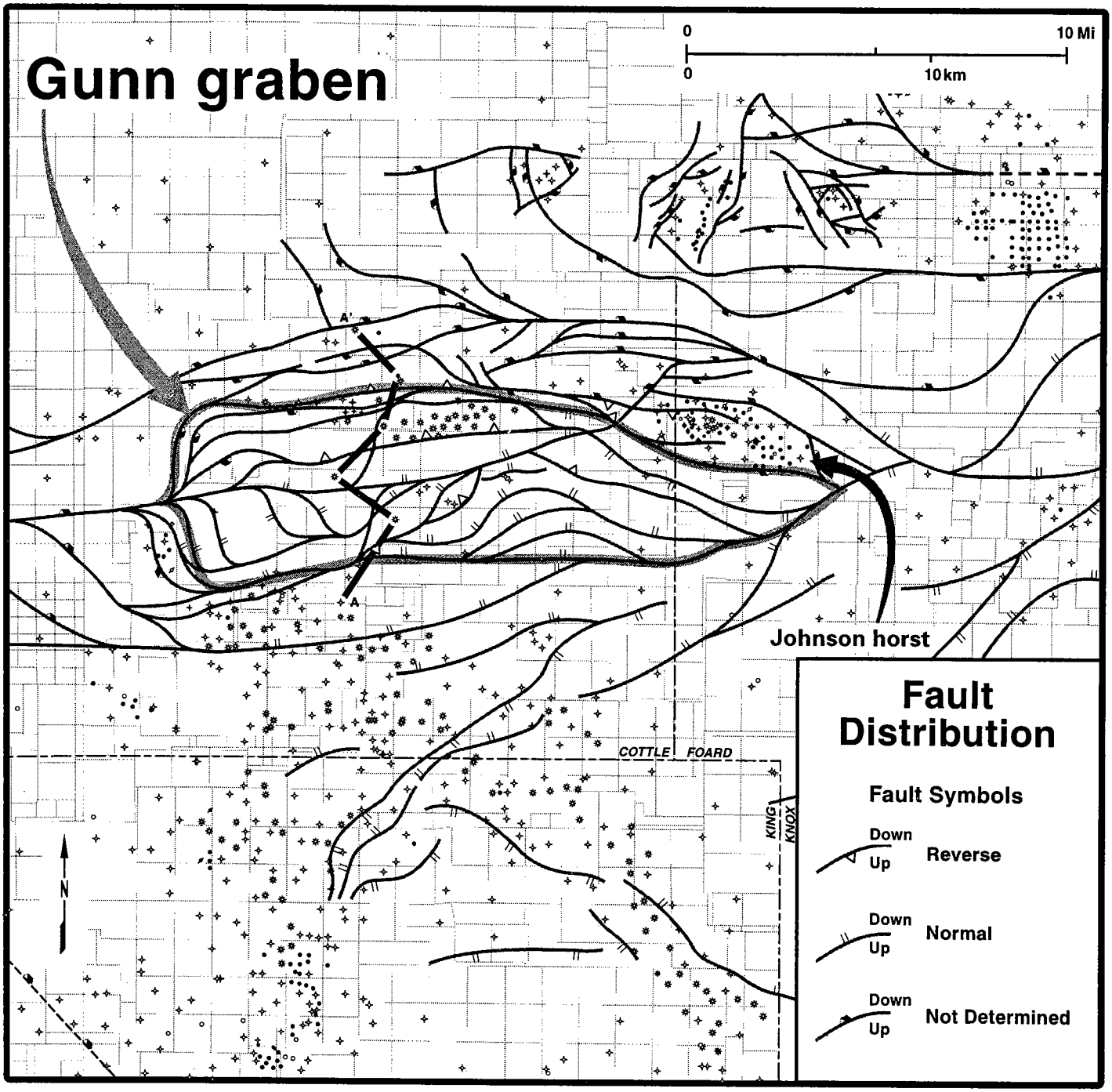

Figure 4. Fault distribution map for the Red River–Matador tectonic zone, including the Gunn graben. Line of cross-section A–A´ (Fig. 5) is depicted.

attributed to sedimentary response to local basin subsidence rather than more regional sea-level fluctuations or extra-basinal source composition or tectonic fluctuations. Cyclically stacked sheets of poorly sorted muddy units, alternating with winnowed sand-rich units, were deposited in alternating deltaic and braidplain environments, depending upon base level. Conceptually, during and immediately following a fault motion-related subsidence episode, the basin accepted all detritus until the depression was filled. Characteristic associated facies are debris-fan (pebbly mudstone), overbank (coaly mudstone), and discreet laterally limited distributary-channel (sandstone) depositional environments. During tectonically quiescent periods, and after reestablishment of a higher base level, throughgoing stream systems were reestablished, and fine materials were winnowed and carried southward toward the Knox–Baylor trough, while some coarser material dropped out of the system over the graben area. This resulted in creation of stratigraphically

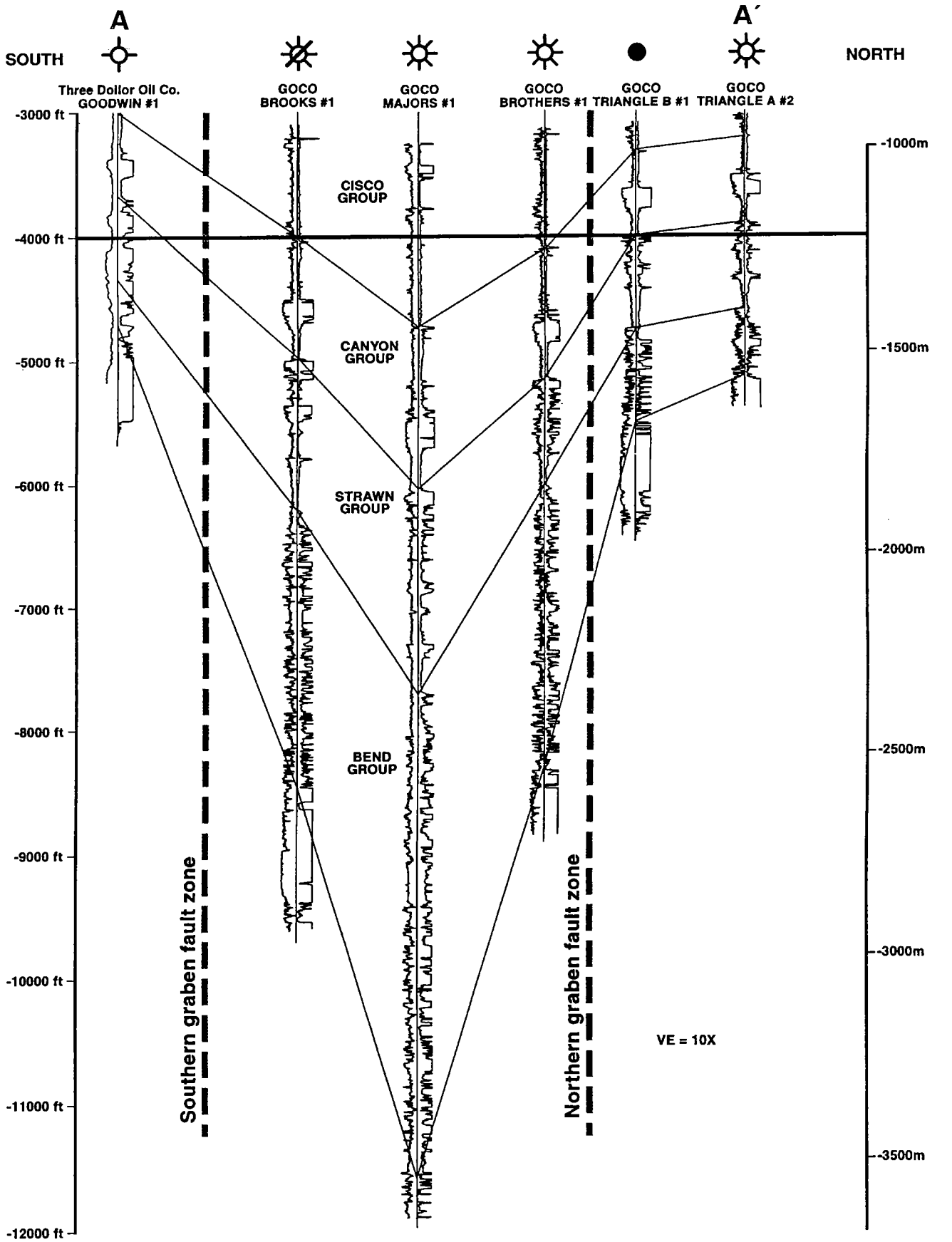

Figure 5. South–north well-log correlation cross section A–A´. Line extends outside the graben on each end and demonstrates dramatic thickening of Bend Group strata. Structural datum is 4,000 ft below sea level; 10× vertical exaggeration.

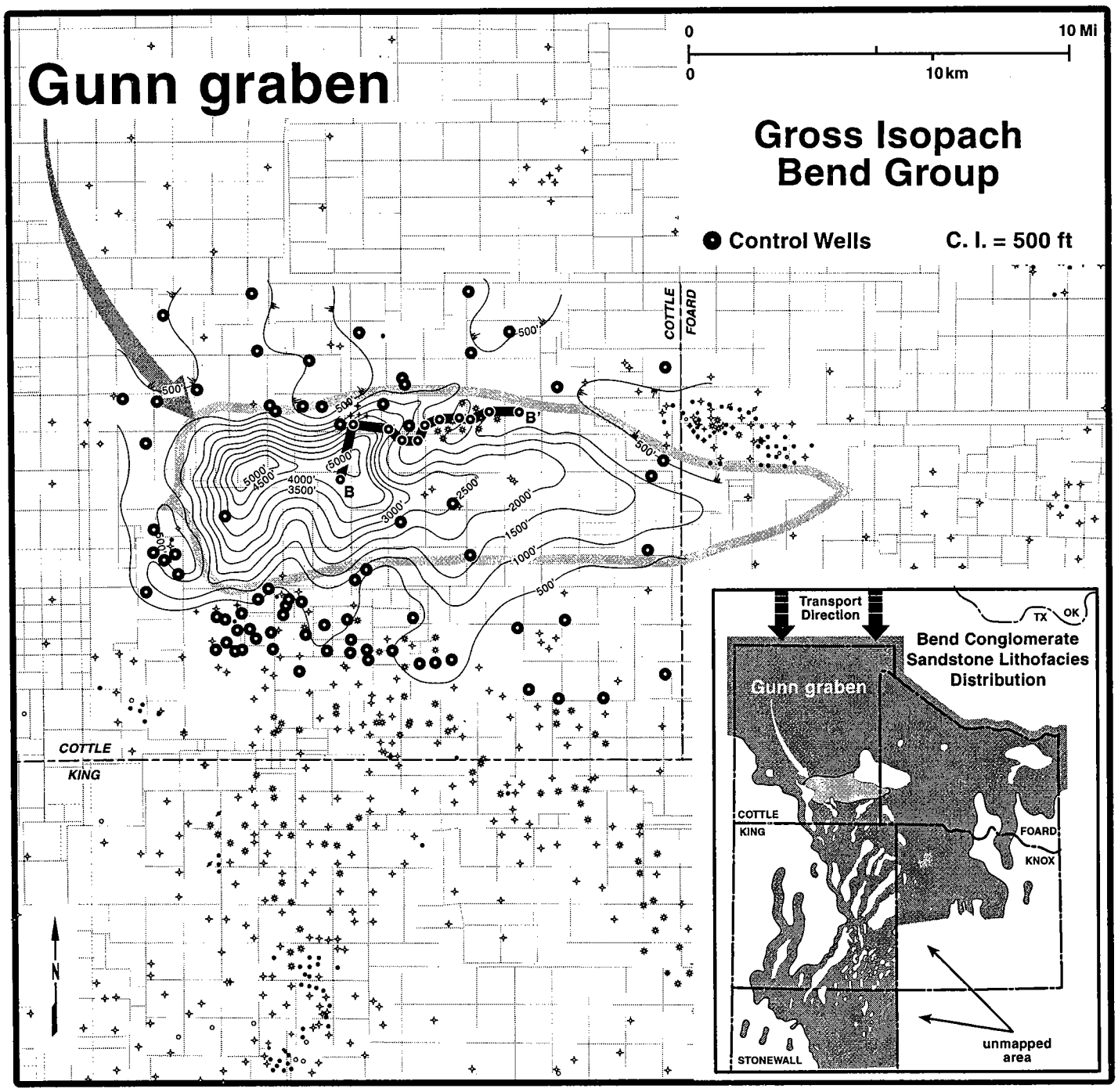

Figure 6. Isopach map of thickness (in feet) of the Bend Group in the vicinity of the Gunn graben. Note gross thickness increase in graben. Inset map shows Bend conglomerate-sandstone lithofacies distribution for a larger area, shaded where sandstone is interpreted to be present. Transport direction of sandstone is shown from the north. Line of cross-section B–B´ (Fig. 8) is depicted by heavy line.

compartmentalized, reservoir-quality, braided channels that amalgamated laterally into sheet-like deposits. Occasional reestablishment of cross-axial, through-going streams is suggested by stratigraphically complex, vertically stacked and laterally separated (possibly terraced) sand-bar development within channel systems entrenched into the pre-Bend strata in the region south of the graben (Fig. 7).

Within the Gunn graben, the Bend Group is an unconformity-bound stratigraphic sequence (Fig. 8). The basal unconformity is erosional, marked by the contact of lower Bend (Bend Conglomerate) clastic lithofacies over the shallow-marine Morrow limestone. The lower two thirds of the Bend Conglomerate is primarily nonmarine (lowstand). The beginning of regional transgression is recorded in the upper third of

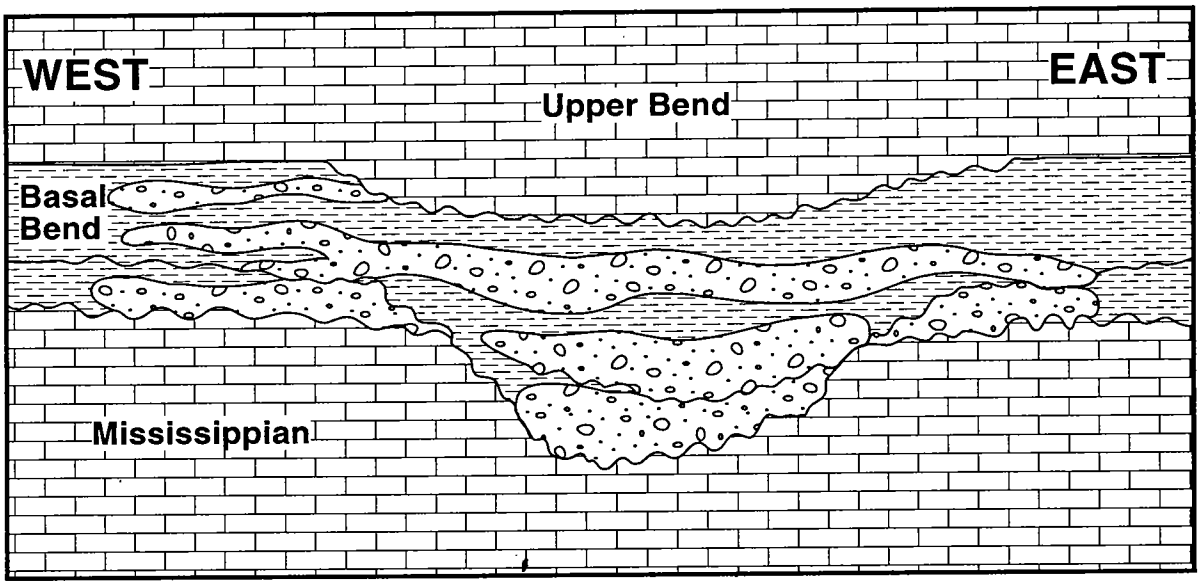

Figure 7. Schematic cross-section model for Bend Group channel systems south of the Gunn graben. This model would be typical for fields such as Providence or Tom B.

the Bend Conglomerate, which contains thin limestone units interbedded with nonmarine clastic deposits. The Bend Conglomerate can be divided into numerous parasequences by correlating radioactive organic-rich mudstone beds in adjacent wells. Subdivisions at all levels of detail tend to expand in thickness toward the structurally deep parts of the basin. In a regional sense, continued marine transgression and eventual subsidence of the Palo Duro basin, north of the graben, caused the regional depocenter to shift to a position nearer the Wichita–Amarillo mountain front, shutting off the source of coarse clastic supply to the graben area. Therefore, the upper Bend Group is entirely marine and composed of calcareous shale and argillaceous basinal carbonate units that correlate with basin-rimming carbonate buildups. Discrete sandstone beds in the upper Bend in a few wells are interpreted to be offshore-bar sands deposited locally along the basin rim. Transgression culminated in a maximum flooding event marked by the Smithwick Shale, a condensed organic-rich marker bed. Highstand marine shale overlies the Smithwick marker. A disconformity is interpreted between the upper Bend marine shale and overlying Strawn marine shale, the contact being marked by a subtle silty-shale marker.

GRABEN-RELATED HYDROCARBON SYSTEMS

Petroleum/hydrocarbon systems encompass source rocks, the processes of generation and migration of the hydrocarbons, and the geologic elements of traps, seals, and reservoirs that are essential for a hydrocarbon accumulation to exist (Magoon and Dow, 1994). Three separate systems are known in the vicinity of the Gunn graben, each related to distinct source-quality shale units. Two systems are of relatively minor importance due to minimal petroleum generation. Canyon Group (Missourian) oil-prone black shale sourced the Canyon "reef" and Cisco sandstone oil accumulations (for example, Johnson oil field). The Strawn Group (Desmoinesian) oil-prone shale is the probable source for a number of uneconomic Strawn oil shows. The third system is the gas system charged by the Bend Group (Atokan) gas-prone shales. Molecular composition of gas from selected fields is similar throughout the Bend hydrocarbon system (Table 2), suggesting that the gas in the system was generated from a common source rock type. The Gunn graben is the hydrocarbon "kitchen" (Demaison, 1984), in which the source rocks were concentrated and then cooked. Gas then migrated to the various traps that have been discovered as producing fields in Cottle and King Counties.

SOURCE ROCKS

The muddy deposits of the Bend Group preserved in the Gunn graben are obvious candidates for the source of gas migrated to the gas fields of Cottle and King Counties. The graben filled rapidly with clastic and organic debris during tectonically induced subsidence events. Rapid burial favored preservation of organic matter from oxidation and biodegradation. Examination of Bend conglomerate well samples from the Gunn graben reveals abundant terrestrially derived woody kerogen in a variety of rock types, but particularly in dark-gray to black mudstone and pebbly mudstone units. Disseminated bituminous coal is common in well cuttings from fine-grained intervals, and a thin coal seam was found in core from the north flank of the graben. Fragments of coaly material are common accessory constituents of sidewall cores drilled from sandstone units. Nitrogen content of gas in the system (Table 2) averages 3.8% and may be derived through gas generation from coaly (humic) organic matter (Whiticar, 1994).

Kerogen microscopy of upper Bend Group samples

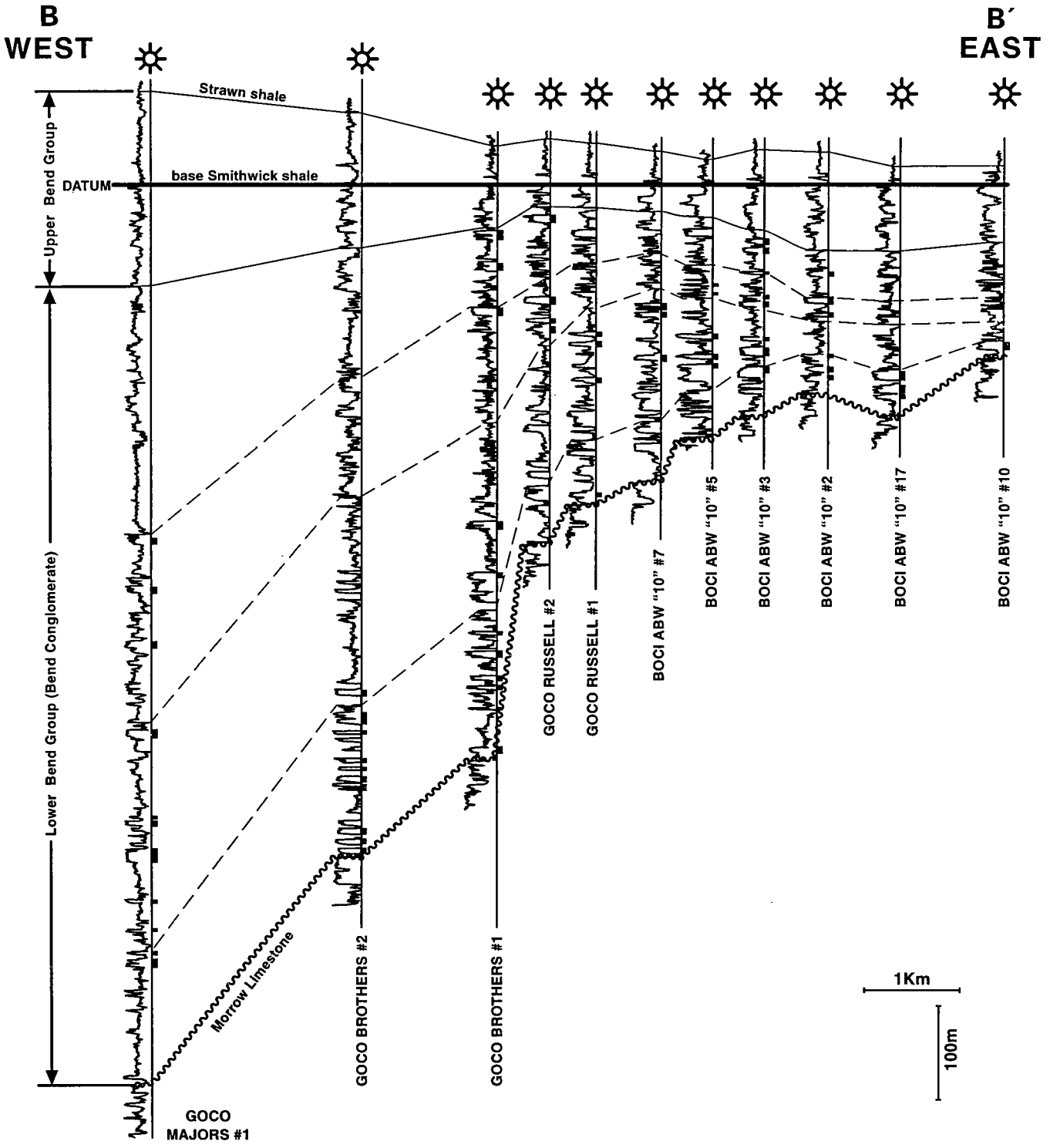

Figure 8. West–east gamma-ray log correlation cross section B–B´. Cross section is entirely within the graben. Small black bars mark reservoir-quality sand units that have been completed for gas production. Smithwick shale marker (datum) is a regional maximum-flooding surface. See Figure 6 for location. 10× vertical exaggeration.

yields primarily unstructured lipid organic matter with relatively small percentages of terrigenous vitrinite and inertinite. Lower Bend Group samples yielded abundant terrigenous organic matter, including a high percentage of vitrinite. Rock-Eval pyrolysis data (Table 3) from upper and lower Bend Group shale samples from five wells in the graben vicinity support the terrestrial (Type III) to mixed terrestrial/marine (Types II and III) origin of the Bend organic facies within the graben as plotted on a modified van Krevelen diagram (Fig. 9). The presence of gas-prone coal, which tends to give anomalously high hydrogen-index values and plots

TABLE 2. — Average Gas Compositional Analyses for Selected Bend Conglomerate Fields, Cottle and King Counties, Texas

Fig. 1 (#)	Gas fields	Methane (%)	Ethane (%)	Propane (%)	I-Butane (%)	N-Butane (%)	I-Pentane (%)	N-Pentane (%)	C6+ (%)	Nitrogen (%)	CO_2 (%)	BTU/CF	# Analyses (# Wells)
3	Broken Bone[a]	78.45	9.73	5.04	0.72	5.36	0.36	0.22	0.96	1.28	1.88	1,231.6	4
12	Moon Camp[a]	72.28	10.17	7.36	0.78	1.81	0.32	0.32	0.21	6.29	0.48	1,215.8	1
15	Providence[b]	80.27	9.87	4.43	0.67	1.07	0.47	0.13	0.17	2.63	0.20	1,194.7	3
17	Rhombochasm[a]	81.42	9.14	4.29	0.53	1.07	0.28	0.26	0.44	1.95	0.61	1,188.7	17
18	Stescott[b]	74.20	10.00	6.20	0.90	2.00	0.60	0.40	0.20	5.30	0.10	1,246.0	1
21	Tippen, SE[b]	82.20	10.00	3.80	0.40	0.90	0.30	0.10	0.10	1.70	0.30	1,176.0	1
23	TOM "B"[a]	74.98	9.86	5.24	0.62	1.19	0.23	0.19	0.15	7.42	0.12	1,145.5	2
Average 7 fields		**77.69**	**9.82**	**5.19**	**0.66**	**1.86**	**0.37**	**0.23**	**0.32**	**3.80**	**0.53**	**1,199.8**	

NOTE: Molecular composition reported in mole %.
References: [a]Operator(s). [b]Moore (1982).

TABLE 3. — Rock-Eval Pyrolysis and TOC Data for Bend Conglomerate Samples from Selected Wells

Well name	Top Bend Group (ft)	Top sampled interval (ft)	Base sampled interval (ft)	Rock type	TMAX (°C)	S1 (mg/g)	S2 (mg/g)	S3 (mg/g)	TOC (wt.%)	HI	OI	Ro measured	Ro calc from TMAX
Fields #1	9,330	9,740	9,760	shale	440	1.05	6.26	0.52	3.3	190	16	nd	0.81
		10,880	10,900	shale	448	0.21	1.4	0.3	1.98	71	15	nd	0.89
		11,250	11,270	shale	451	0.11	1.08	0.45	1.78	61	25	nd	0.91
		12,280	12,290	shale	451	0.11	0.87	0.81	2.01	43	40	nd	0.91
Majors #1	9,420	9,746	(core)	shale	448	4.59	14.57	0.42	7.40	197	6	nd	0.89
		10,670	10,710	shale	445	0.15	0.73	0.49	1.05	69	46	0.82	0.86
		11,320	11,360	shale	449	0.14	0.58	0.44	1.37	42	32	0.93	0.90
		12,230	12,240	shale	466	4.18	49.98	1.61	20.01	250	8	1.00	1.05
		12,760	12,770	shale	473	0.78	7.63	1.67	9.08	84	18	1.13	1.12
		13,530	13,550	shale	479	0.04	0.21	0.67	1.25	17	54	1.16	1.17
Brothers #1	7,660	7,750	7,800	shale	442	1.13	5.84	0.92	3.22	181	29	nd	0.83
		8,430	8,470	shale	447	0.22	0.86	0.70	4.47	58	48	nd	0.88
		9,290	9,310	shale	448	1.22	5.96	1.84	4.66	128	39	nd	0.89
		9,780	98,10	shale	450	0.19	0.76	0.92	1.27	60	72	nd	0.90
Triangle B2	6,358	6,983	(core)	coal	443	21.87	221.64	2.57	75.17	295	3	0.75	0.84
		7,007	(core)	shale	445	0.17	0.79	0.07	2.15	37	3	nd	0.86
		7,011	(core)	shale	442	0.2	0.70	0.54	1.93	36	28	nd	0.83
Triangle A2	6,304	6,770	6,790	shale	440	0.3	1.41	0.45	1.43	98	31	0.62	0.81

NOTE: Samples are from shale cuttings collected from selected wells denoted on Figure 11. Refer to Peters (1986) or Peters and Cassa (1994) for discussion of derivation of parameters. Calculated Ro (Ro calc) is based on equation derived from Ro and TMAX measurements for the Majors #1 well.

toward the Type II area of the diagram (Peters and Cassa, 1994), overrepresents the true contribution of Type II kerogen to total organic carbon (TOC) in the Bend Group.

Measured TOC from 20 shale samples collected from three deep basinal wells ranges from 1.05% to 20.01% with a mean value of 4.98%. The level of maturity determined from pyrolysis would suggest that the original organic-carbon values were at least twice the measured values and have been reduced by hydrocarbon generation and expulsion. These samples were collected from shale units with well-log characteristics of

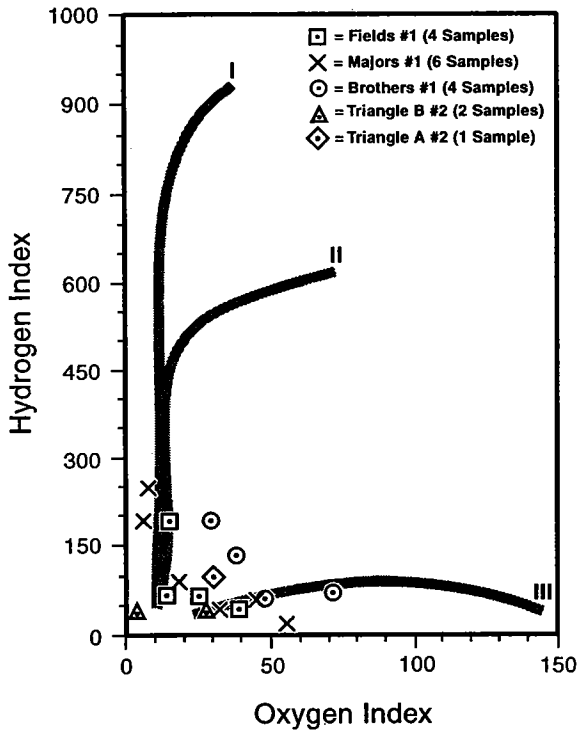

Figure 9. Plot of hydrogen index ([S_2/TOC] × 100, mg HC/g TOC) versus oxygen index ([S_3/TOC] × 100, mg CO_2/g TOC) demonstrating mixed Type II and Type III kerogen types for Bend Group organic facies (Peters, 1986). Samples are from shale cuttings collected from selected wells denoted on Figure 11. See Table 3 for values used to plot data points. TOC = total organic carbon.

high gamma-ray values, high resistivity, and low density, which are typical of organic shales (Schmoker, 1979, 1981; Passey and others, 1990; Herron, 1991). Approximately 20% of the bulk volume of the Bend Group in the Gunn graben is estimated to be similarly organic rich. Therefore, several hundred meters of source-rock-quality Bend Group shale resides in the graben.

SOURCE-ROCK MATURITY

In the late 1980s, only relatively immature source rocks were known to exist in the region (Dutton, 1980, 1986; Dutton and others, 1982; Ruppel, 1985); thus, the source of gas generated and migrated to the Cottle/King Counties gas fields was unidentified. Lopatin method time-temperature modeling (Waples, 1980) performed prior to drilling any of the deep graben wells suggested that the Bend Group in the Gunn graben should have reached thermal maturity for gas generation (Norman, 1990). Figure 10 is a typical time-temperature basin model generated for the Majors #1 well, one of the deepest in the graben. The model is relatively simple in that it demonstrates rapid basin subsidence beginning in the Pennsylvanian and ending in the Permian, with no significant tectonic activity post-Permian. The model suggests that the Bend Group of the deeper parts of the Gunn graben has achieved peak gas-generation levels (lower oil window/upper gas window). Similar models were generated for a number of wells in the vicinity. Lopatin's time temperature index (TTI) was calculated for the base of the

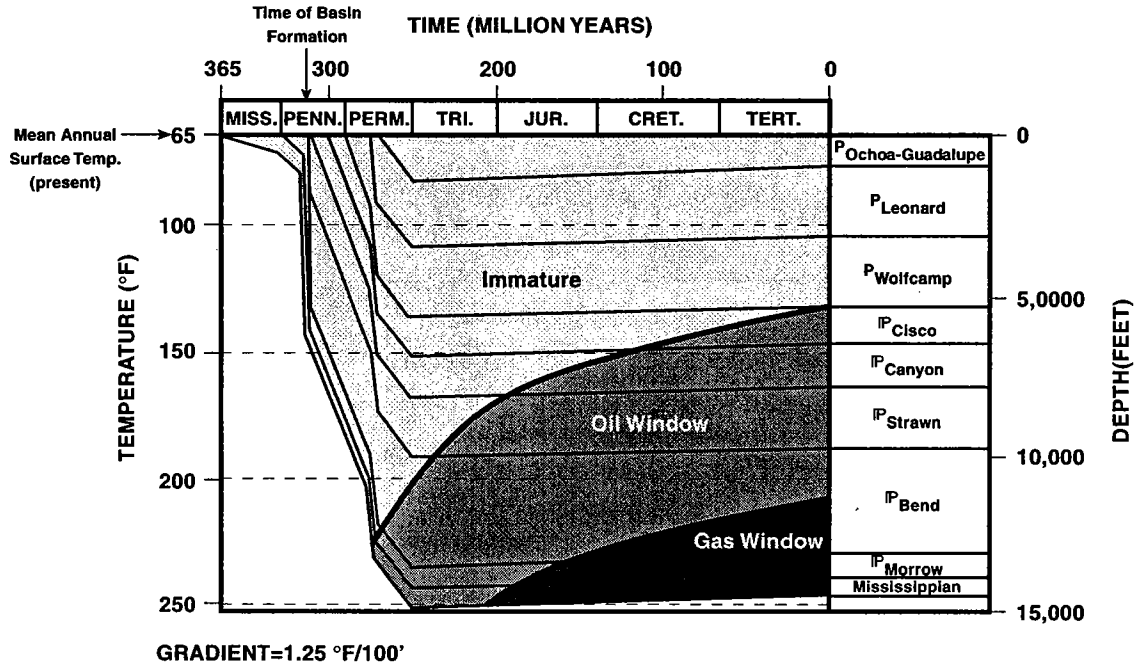

Figure 10. Burial-history chart for Majors #1 well, Cottle County, Texas (see Fig. 11 for location). Chart is an example of Lopatin's method of maturity estimation generated using basin-modeling software by Platte River Associates. Temperature in degress Fahrenheit; depth in feet. **P** = Pennsylvanian; P = Permian.

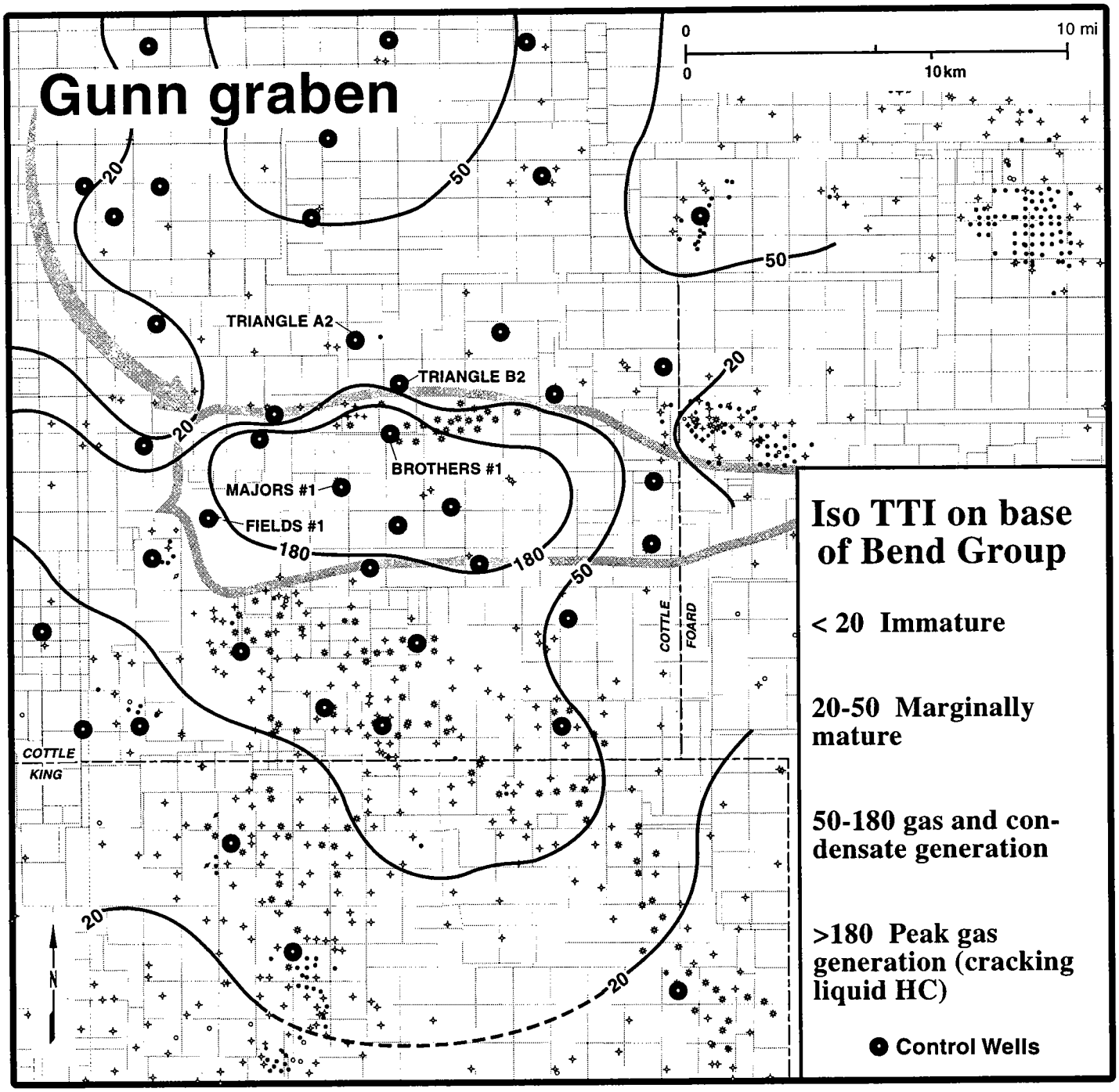

Figure 11. Isomaturity map (Lopatin's time-temperature index, TTI) demonstrating potential maturity level of the Bend Group in the vicinity of the Gunn graben.

Pennsylvanian for each model (Waples, 1980), and isomaturity was mapped over the region (Fig. 11). TTI values in the general range of 50–180 support thermal maturity sufficient for significant gas generation from Bend Group. TTI levels exceeding 180 indicate peak gas-generating potential, and this level of maturity is restricted to the Gunn graben. TTI maturity estimates indicate a slightly higher level of maturity than vitrinite reflectance values (Fig. 12). This may be attributable to errors in assumptions to build the TTI models, the limited number of Ro measurements made (used to calculate Ro), and/or lipid suppression of measured vitrinite reflectance suspected from some samples (Wallace Dow, personal communication, 1999). Despite the discrepancy, both Ro and TTI methods support significant thermal generation of hydrocarbons.

Well-based observations that support thermal maturity of the Bend rocks in the graben include gas-

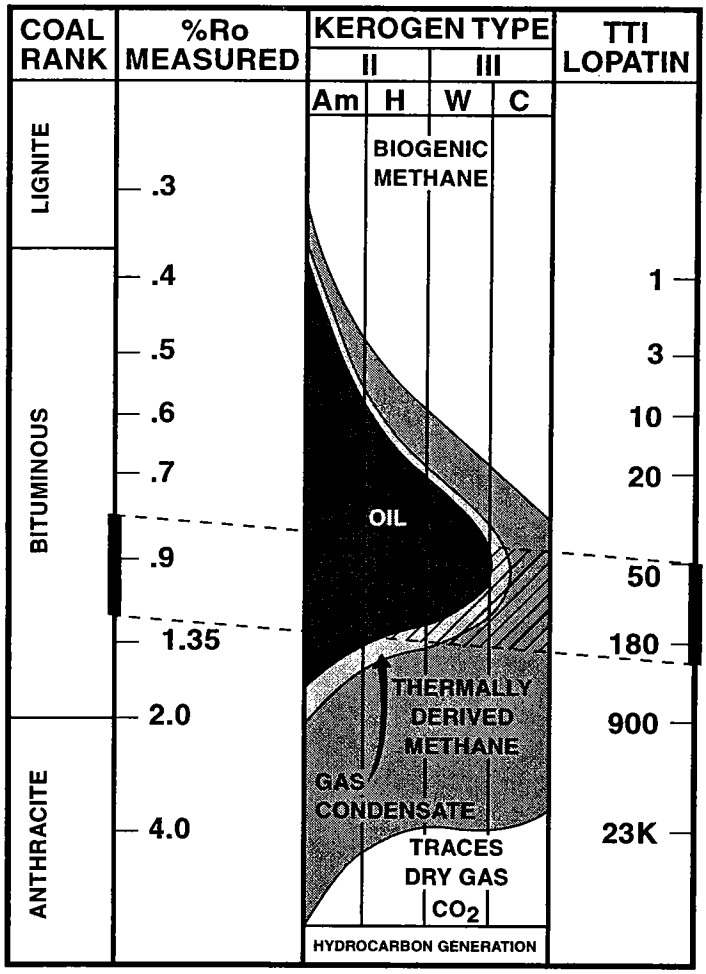

Figure 12. Diagram demonstrating level of thermal maturity of source rocks sampled in Table 3 (modified from unpublished diagram by Geochem Laboratories, Inc.). Correlation lines show range of maturity suggested by calculated time-temperature index (TTI) and vitrinite reflectance (Ro). Kerogen types: Am = amorphous, H = herbaceous, W = woody, C = coaly.

bleeding shale cuttings, indications of slight overpressure while drilling, bituminous-rank coal, and gas production from wells deep in the graben that have no other potential source. In addition, organic facies with high gamma-ray-log values show elevated resistivity-log values that can be a maturity indicator (e.g., Herron, 1991; Morel, 1999).

MIGRATION

The mature stage of drilling development in Cottle and King Counties allows inferences to be made about migration pathways within the hydrocarbon system. In the northern half of the graben, gas migrated from the source rocks to intrabasin sandstone units, where it is trapped in stratigraphically and structurally compartmented, low-permeability reservoirs. Apparently, the reverse faults common in that part of the basin were effective seals to vertical migration. In the southern part of the graben, where normal faults predominate, gas escaped vertically along "leaky" fracture zones associated with the faults, and charged porous formations at shallower depths that were connected to a channel-system migration route. Most of the gas discovered to date has been found in the basal Bend conglomerate channels south of the graben as reflected by the pattern of gas fields in Figure 1. Gas was mostly contained in the lower Pennsylvanian section due to the thick overlying Middle and Upper Pennsylvanian marine shale acting as a regional seal.

RESERVOIRS AND TRAPS

Figure 13 demonstrates the range of reservoir rock units and traps associated with the hydrocarbon system. Early discoveries were made from shallow basal Bend Group sandstone reservoirs south of the graben (Edwards, 1977, 1979), whereas significant new fields are being developed in the heart of the system within the graben (Stephens and Gunn, 1995; Brister, 1998). Bend Conglomerate sandstone reservoirs suffer from depth-related destructive diagenesis that reduces permeability and porosity by growth of authigenic clay, cementation, and compaction. However, even deep graben wells can be economic where multiple stacked reservoirs are encountered, provided appropriately designed completion methods are utilized.

Other reservoirs have contributed economic quantities of gas as well. These include Cambrian sandstone at Paducah Field, Strawn Group carbonate at Juniper Field, Canyon Group carbonate at Moon Camp Field, and Cisco Group sandstone at Johnson Field (Table 1). A combination of structure and stratigraphy provides the trapping mechanism for most fields within the system. Most of the non-Bend reservoirs and several of the Bend reservoirs are closely related to faulted graben-flank structures.

CONCLUSIONS

The Gunn graben is a complex wrench-fault–related pull-apart basin that filled with sediments as it subsided. A combination of abundant organic material, depositional environments favorable for organic material deposition, and rapid burial preserved significant quantities of source-quality organic facies. Early deep burial and relative tectonic quiescence since the Permian has allowed sufficient time and temperature for maturation of organic matter. The gas-prone organic matter has expelled gas that has migrated within and outside of the basin. The faults that formed during basin construction were variably either sealing surfaces or conduits for vertical migration. The complex regional structure and depositional facies of the Bend Group combine to create technically challenging compartmentalized reservoirs. Together, the basin, source rocks, maturation history, migration, trapping mechanisms, and reservoir rocks define a discrete hydrocarbon system. The system approach was invaluable in the discovery of recent new gas fields within the Gunn graben. The approach could similarly be applied to exploration

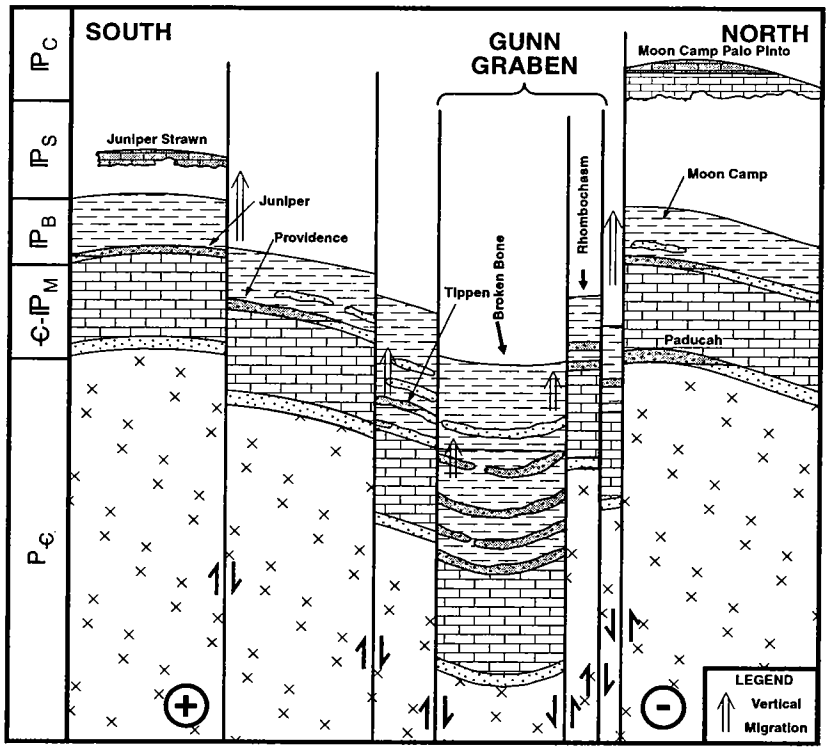

Figure 13. Schematic south–north cross section demonstrating vertical fault-related migration paths, lateral stratigraphic-related migration paths, and traps and reservoir units for selected fields. Lateral and vertical scales are arbitrary. Relative lateral motion indicators: + toward, – away. p€ = Precambrian; € = Cambrian; IP = Pennsylvanian.

elsewhere in the Ancestral Rocky Mountains and other locations where foreland wrench faulting has occurred. The conclusions of this study are based on observations of data and analyses that are low cost and readily available to large and small companies alike.

ACKNOWLEDGMENTS

The authors thank Gunn Oil Co. and Burnett Oil Co., Inc., for their support. We appreciate the many people who contributed ideas and data, particularly Robert D. Gunn, John W. Mason, Randy Ray, Pete Renick, and Don Stone. The New Mexico Bureau of Mines and Mineral Resources provided a supportive environment for research and completion of this paper, including drafting by Leo Gabaldon.

REFERENCES CITED

Aydin, A.; and Nur, A., 1985, The types and role of stepovers in strike-slip tectonics, *in* Biddle, K. T.; and Christie-Blick, N., Strike-slip deformation, basin formation, and sedimentation: Society of Economic Paleontologists and Mineralogists [SEPM] Special Publication 37, p. 35–44.

Brister, B. S., 1998, Field study: Rhombochasm (Bend conglomerate) field, Matador arch, Cottle County, TX [abstract]: American Association of Petroleum Geologists Bulletin, v. 82, p. 522–523.

Budnik, R. T., 1986, Left-lateral intraplate deformation along the Ancestral Rocky Mountains: implications for late Paleozoic plate motions: Tectonophysics, v. 132, p. 195–214.

_____ 1989, Tectonic structures of the Palo Duro basin, Texas Panhandle: University of Texas at Austin, Bureau of Economic Geology Report of Investigations 187, 43 p.

Christie-Blick, N.; and Biddle, K. T., 1985, Deformation and basin formation along strike-slip faults, *in* Biddle, K. T.; and Christie-Blick, N., Strike-slip deformation, basin formation, and sedimentation: Society of Economic Paleontologists and Mineralogists [SEPM] Special Publication 37, p. 1-34.

Crowell, J. C., 1974, Origin of late Cenozoic basins in southern California, *in* Dickinson, W. R. (ed.), Tectonics and sedimentation: Society of Economic Paleontologists and Mineralogists [SEPM] Special Publication 22, p. 190–204.

Demaison, G., 1984, The generative basin concept, *in* Demaison, G.; and Murris, R. J. (eds.), Petroleum geochemistry and basin evaluation: American Association of Petroleum Geologists Memoir 35, p. 1–14.

Denison, R. E.; Lidiak, E. G.; Bickford, M. E.; and Kisvarsanyi, E. B., 1984, Geology and geochronology of Precambrian rocks in the Central Interior region of the United States: U.S. Geological Survey Professional Paper 1241-C, p. C1–C20.

Dooley, T.; and McClay, K., 1997, Analog modeling of pull-apart basins: American Association of Petroleum Geologists Bulletin, v. 81, p. 1804–1826.

Dutton, S. P., 1980, Petroleum source rock potential and thermal maturity, Palo Duro basin, Texas: University of Texas at Austin, Bureau of Economic Geology Geological Circular 80-10, 48 p.

_____ 1986, Organic geochemistry of the Pennsylvanian and lower Permian, Palo Duro basin, Texas: University of Texas at Austin, Bureau of Economic Geology Geological Circular 86-5, 28 p.

Dutton, S. P.; Goldstein, A. G.; and Ruppel, S. C., 1982, Petroleum potential of the Palo Duro basin, Texas Panhandle: University of Texas at Austin, Bureau of Economic Geology Report of Investigations 123, 87 p.

Edwards, H. S., 1977, Atoka gas in southern Cottle and northern King Counties, Texas: American Association of Petroleum Geologists Bulletin, v. 61, no. 2, p. 294–295.

_____ 1979, Atoka gas in southern Cottle and northern King Counties, Texas [abstract]: American Association of Petroleum Geologists Bulletin, v. 63, p. 1425–1426.

Ewing, T. E., 1991, The tectonic framework of Texas, text to accompany the tectonic map of Texas: University of Texas at Austin, Bureau of Economic Geology, 36 p.

Gardner, R. A., 1960, The Boonsville (Bend conglomerate gas) field, Wise County, Texas: Abilene Geological Society, Geological Contributions 1960, p. 7–17.

Gunn, R. D., 1979, Desmoinesian depositional systems in the Knox–Baylor trough, *in* Hyne, N. J. (ed.), Pennsyl-

vanian sandstones of the Mid-continent: Tulsa Geological Society Special Publication 1, p. 221–234.

Ham, W. E.; and Wilson, J. L., 1967, Paleozoic epeirogeny and orogeny in the central United States: American Journal of Science, v. 265, p. 332–407.

Ham, W. E.; Denison, R. E.; and Merritt, C. A., 1964, Basement rocks and structural evolution of southern Oklahoma: Oklahoma Geological Survey Bulletin 95, 302 p.

Harding, T. P., 1990, Identification of wrench faults using subsurface structural data: criteria and pitfalls: American Association of Petroleum Geologists Bulletin, v. 74, p. 1590–1609.

Herron, S. L., 1991, In situ evaluation of potential source rocks by wireline logs, *in* Merrill, R. K. (ed.), Source and migration processes and evaluation techniques: American Association of Petroleum Geologists Treatise of Petroleum Geology; Handbook of Petroleum Geology, p. 127–134.

Hills, J. M., 1963, Late Paleozoic tectonics and mountain ranges, western Texas to southern Colorado: American Association of Petroleum Geologists Bulletin, v. 47, p. 1709–1725.

_____ 1985, Structural evolution of the Permian basin of West Texas and New Mexico, *in* Dickerson, P. W.; and Muehlberger, W. R., Structure and tectonics of Trans-Pecos Texas: West Texas Geological Society Publication 85-81, p. 89–99.

Kluth, C. F., 1986, Plate tectonics of the Ancestral Rocky Mountains, *in* Peterson, J. A. (ed.), Paleotectonics and sedimentation in the Rocky Mountain region, United States: American Association of Petroleum Geologists Memoir 41, p. 353–369.

Kluth, C. F.; and Coney, P. J., 1981, Plate tectonics of the Ancestral Rocky Mountains: Geology, v. 9, p. 10–15.

Magoon, L. B.; and Dow, W. G., 1994, The petroleum system, *in* Magoon, L. B.; and Dow, W. G. (eds.), The petroleum system: from source to trap: American Association of Petroleum Geologists Memoir 60, p. 3–24.

Mann, P.; Hempton, M. R.; Bradley, D. C.; and Burke, K., 1983, Development of pull-apart basins: Journal of Geology, v. 91, p. 529–554.

McConnell, D. A., 1989, Determination of offset across the northern margin of the Wichita uplift, southwest Oklahoma: Geological Society of America Bulletin, v. 101, p. 1317–1332.

Moody, J. D.; and Hill, M. J., 1956, Wrench-fault tectonics: Geological Society of America Bulletin, v. 67, p. 1207–1246.

Moore, B. J., 1982, Analyses of natural gases, 1917–80: U.S. Bureau of Mines Information Circular 8870, 1055 p.

Morel, J. A., 1999, Use resistivity as indicator of source rock maturity: Oil and Gas Journal, v. 97, no. 19, p. 72–74.

Norman, G. A., 1990, Thermal maturity of hydrocarbon source rocks within southeastern Palo Duro basin [abstract]: American Association of Petroleum Geologists Bulletin, v. 74, p. 220.

Passey, Q. R.; Creaney, S.; Kulla, J. B.; Moretti, F. J.; and Stroud, J. D., 1990, A practical model for organic richness from porosity and resistivity logs: American Association of Petroleum Geologists Bulletin, v. 74, p. 1777–1794.

Peters, K. E., 1986, Guidelines for evaluating petroleum source rocks using programmed pyrolysis: American Association of Petroleum Geologists Bulletin, v. 70, p. 318–329.

Peters, K. E.; and Cassa, M. R., 1994, Applied source rock geochemistry, *in* Magoon, L. B.; and Dow, W. G. (eds.), The petroleum system: from source to trap: American Association of Petroleum Geologists Memoir 60, p. 93–120.

Reading, H. G., 1980, Characteristics and recognition of strike-slip fault systems, *in* Ballance, P. F.; and Reading, H. G. (eds.), Sedimentation in oblique-slip mobile zones: International Association of Sedimentologists Special Publication 4, p. 7–26.

Rodgers, D. A., 1980, Analysis of pull-apart basin development produced by *en echelon* strike-slip faults, *in* Ballance, P. F.; and Reading, H. G. (eds.), Sedimentation in oblique-slip mobile zones: International Association of Sedimentologists Special Publication 4, p. 27–41.

Ruppel, S. C., 1985, Stratigraphy and petroleum potential of pre-Pennsylvanian rocks, Palo Duro basin, Texas Panhandle: University of Texas at Austin, Bureau of Economic Geology Report of Investigations 147, 81 p.

Schmoker, J. W., 1979, Determination of organic content of Appalachian Devonian shales from formation-density logs: American Association of Petroleum Geologists Bulletin, v. 63, p.1504–1537.

_____ 1981, Determination of organic-matter content of Appalachian Devonian shales from gamma-ray logs: American Association of Petroleum Geologists Bulletin, v. 65, p.1285–1298.

Stephens, W. C.; and Gunn, R. D., 1995, Early Pennsylvanian wrenching along the Red River–Matador arch: formation of a pull-apart basin, depocenter for Atokan to lower Des Moines (Bend) clastics, Cottle County, Texas [abstract]: American Association of Petroleum Geologists Bulletin, v. 79, p. 912.

Sylvester, A. G., 1988, Strike-slip faults: Geological Society of America Bulletin, v. 100, p. 1666–1703.

Thompson, D. M., 1988, Fort Worth basin, *in* Sloss, L. L. (ed.), Sedimentary cover—North American craton; U.S.: Geological Society of America, Decade of North American Geology, v. D-2, p. 346–352.

Walper, J. I., 1977, Paleozoic tectonics of the southern margin of North America: Gulf Coast Association of Geological Societies Transactions, v. 27, p. 230–241.

Waples, D. W., 1980, Time and temperature in petroleum formation: application of Lopatin's method to petroleum exploration: American Association of Petroleum Geologists Bulletin, v. 64, p. 916–926.

Whiticar, M. J., 1994, Correlation of natural gases with their sources, *in* Magoon, L. B.; and Dow, W. G. (eds.), The petroleum system: from source to trap: American Association of Petroleum Geologists Memoir 60, p. 261–283.

Wilcox, R. E.; Harding, T. P.; and Seely, D. R., 1973, Basin wrench tectonics: American Association of Petroleum Geologists Bulletin, v. 57, p. 79–96.

Ye, H.; Royden, L.; Burchfiel, C.; and Schuepbach, M., 1996, Late Paleozoic deformation of interior North America: the greater Ancestral Rocky Mountains: American Association of Petroleum Geologists Bulletin, v. 80, p. 1397–1432.

The Signal Mountain Formation—A Source Rock in Hiding

R. Nowell Donovan and Robert Critchfield
Texas Christian University
Fort Worth, Texas

ABSTRACT.—The Signal Mountain Formation is the second lowest division of the Arbuckle Group; the Cambrian–Ordovician boundary is located in the middle part of the formation. This study, which uses both outcrop and core-based information, suggests that the formation may have some potential or have acted as a source rock for hydrocarbons.

The Signal Mountain rests unconformably on the Fort Sill Formation. This unconformity records a craton-wide regression. The subsequent transgression of the Signal Mountain Formation coincided with the most rapid rate of definition of the southern Oklahoma aulacogen as a discrete element of the Cambro–Ordovician Laurentian carbonate platform. This definition led to the development of a linear deeper-water "gulf" centered on the axis of the aulacogen; evidently, subsidence rates in this gulf were great enough to challenge the potency of the Arbuckle carbonate factory.

INTRODUCTION

Quantitatively, the Arbuckle Group is the most dominant lower Paleozoic unit in southern Oklahoma. Within the confines of the southern Oklahoma aulacogen, the Arbuckle Group attains a maximum thickness of approximately 7,000 ft (~2,150 m). The Arbuckle has been divided into six limestone formations; from bottom to top, these are the Fort Sill, Signal Mountain, Mackenzie Hill, Cool Creek, Kindblade, and West Spring Creek (Fig. 1). The Cambrian–Ordovician boundary is placed within the Signal Mountain (Stitt, 1977); the top of the West Spring Creek just extends into the Whiterockian of the Middle Ordovician (Donovan, 1991). In addition to the formally recognized limestone formations, a number of laterally impersistent dolomite units have been recognized, e.g., the "Bally Dolomite" in the Slick Hills, which partially replaces parts of the upper Fort Sill Formation, and the "Saddle Mountain Dolomite" in the same area, which locally replaces much of the Kindblade and West Spring Creek Formations (Donovan and Ragland, 1986; Donovan, 1991; Johnson, 1991). The latter dolomite appears to be the surface equivalent of the "brown zone," a unit of some significance in hydrocarbon production.

Interpretation of the environment of deposition of the Arbuckle Group has focused on the carbonate-platform model. Essentially, the Arbuckle was deposited in a tropical setting on an extremely large platform characterized by oxygenated and photic conditions. Formation and, in some cases, member boundaries record a hierarchical cyclic control due to variations in sea level. Because no evidence of significant tectonism is recorded on the adjacent craton during this time, such variations were probably eustatic in origin (Donovan, 2000; McElmoyl and Donovan, 2000).

Whatever the origin of variations in sea level, it appears that water depth remained shallow regardless of cycle stage and that bottom conditions were well oxygenated, as indicated by various parameters. Thus, varieties of algal boundstone are very common, and prolific bottom-dwelling and infaunal organisms are recorded. In addition, throughout most of the Arbuckle Group, early diagenetic imprints are compatible with oxygenated groundwater. The Arbuckle environment thus is in accord with those of its stratigraphic equivalents to the north (as far as the Durness Group in northern Scotland) and to the south (at least as far as Mexico.) The Arbuckle Group can be placed in context as a major component of one of the most extensive carbonate platforms that has ever existed, marking a period when extraordinarily high global sea levels coincided with a tectonically quiescent Laurentian craton.

The one exception to this generally homogeneous setting is evidenced by the Signal Mountain Formation, a unit in which a variety of parameters suggest that the environment of deposition was deeper water than generally prevailed during deposition of the Arbuckle Group and its lateral equivalents, and that the bottom waters were, from time to time, anoxic. The purpose of this paper is to examine the implications of this interpretation for hydrocarbon production. Our work particularly builds upon two previous studies: (1) an

Donovan, R. N.; and Critchfield, Robert, 2001, The Signal Mountain Formation—a source rock in hiding, *in* Johnson, K. S.; and Merriam, D. F. (eds.), Petroleum systems of sedimentary basins in the southern Midcontinent, 2000 symposium: Oklahoma Geological Survey Circular 106, p. 71–80.

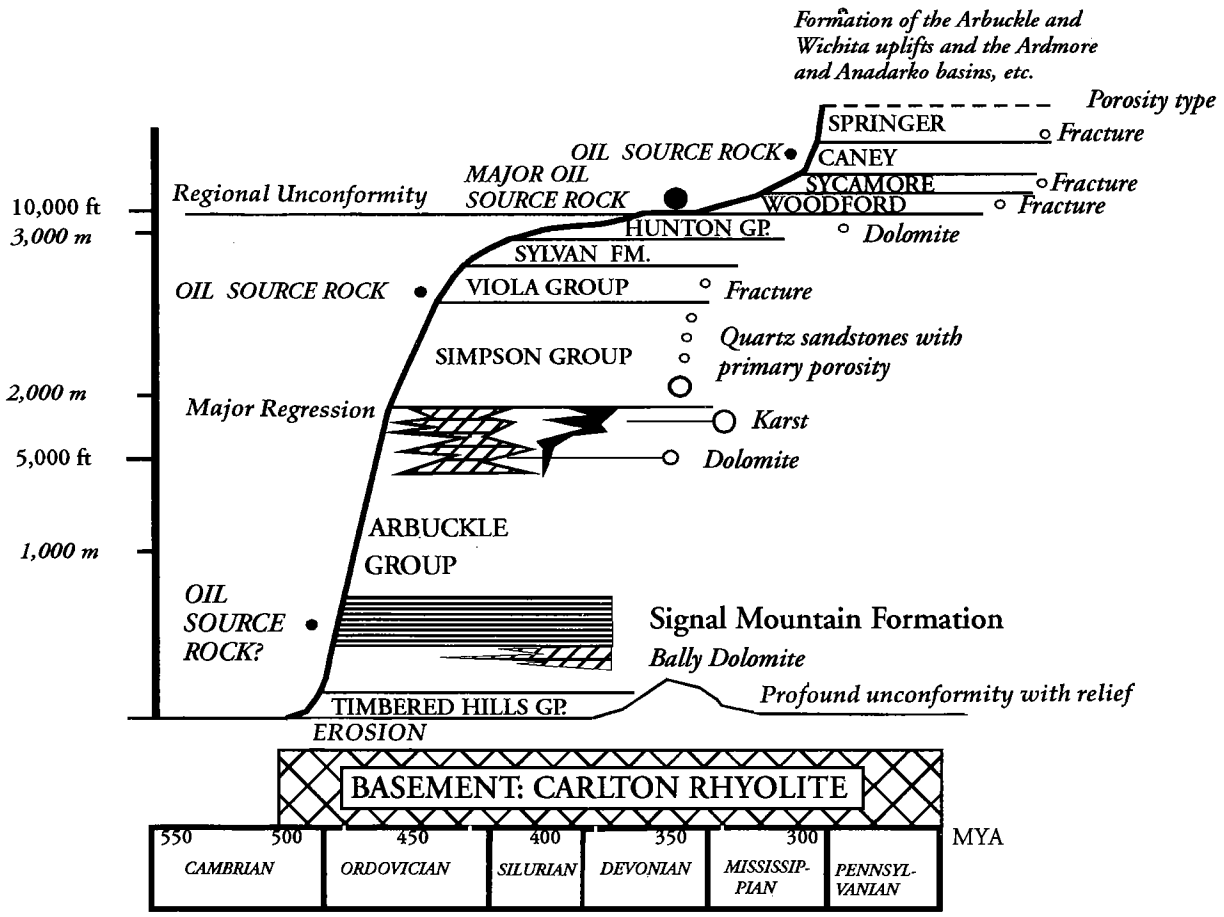

Figure 1. Lower Paleozoic stratigraphy in the southern Oklahoma aulacogen, burial-time curve illustrating position of the Signal Mountain Formation and distribution of major hydrocarbon-related parameters.

analysis of the changes that occur at the contact of the Fort Sill and Signal Mountain Formations (Hosey and Donovan, 1993, 2000), and (2) a preliminary report on a section of core from the central part of the Signal Mountain Formation (Whitehead and Donovan, 2000). A more complete report on this core forms the principal basis for this study. The Dolese Company generously made the core available. It was obtained from the company's Richard's Spur property in the southern part of the eastern Slick Hills of southwestern Oklahoma (Fig. 2). Exposures in the same area have added to the information obtained from the core. The core is approximately 400 ft (~120 m) in length; it was cut in the lower part of the Signal Mountain but did not penetrate the contact with the underlying Fort Sill Formation.

GEOLOGIC SETTING

The geometry of the exposures of the Arbuckle Group in the Slick Hills of southwestern Oklahoma is a legacy of Pennsylvanian tectonism associated with definition of the Wichita uplift and Anadarko basin (Fig. 2). The outcrops exhibit spectacular parallel folding at a variety of scales. Although the underlying basement—the Carlton Rhyolite—is a layered rock that has folded, most folds are formed by detachment from the within the Arbuckle Group. This detachment is related to numerous surfaces of bedding-plane slip and is a direct inheritance of the thinly bedded and lithologically homogeneous character of the Arbuckle Group. Because the Signal Mountain Formation is both the most thinly bedded formation in the Arbuckle Group and also the most shale-rich, it follows that the unit as a whole functions as a "sole" for deformation in the overlying formations. The intensity of this deformation is seen, on a small scale, in the core, where many clay laminae show a slickenside polish.

The Richard's Spur outcrop forms part of the eastern Slick Hills (Fig. 2), a generally homoclinal structural unit that has been inverted on the Blue Creek fault, a major back thrust with up to 8,000 ft (~2,450 m) of stratigraphic displacement. The Signal Mountain Formation can be traced in continuous outcrop for miles and can be picked up farther to the north and west in the isolated outcrops of Bally and Zodletone Mountains (Fig. 2). In the western Slick Hills, where the intensity of deformation is much greater, the Signal Mountain outcrops are concentrated to the south and west. Outcrops are much disturbed by thrusting and tight, even isoclinal folding. In some areas, the beds are overturned by as much as 45°.

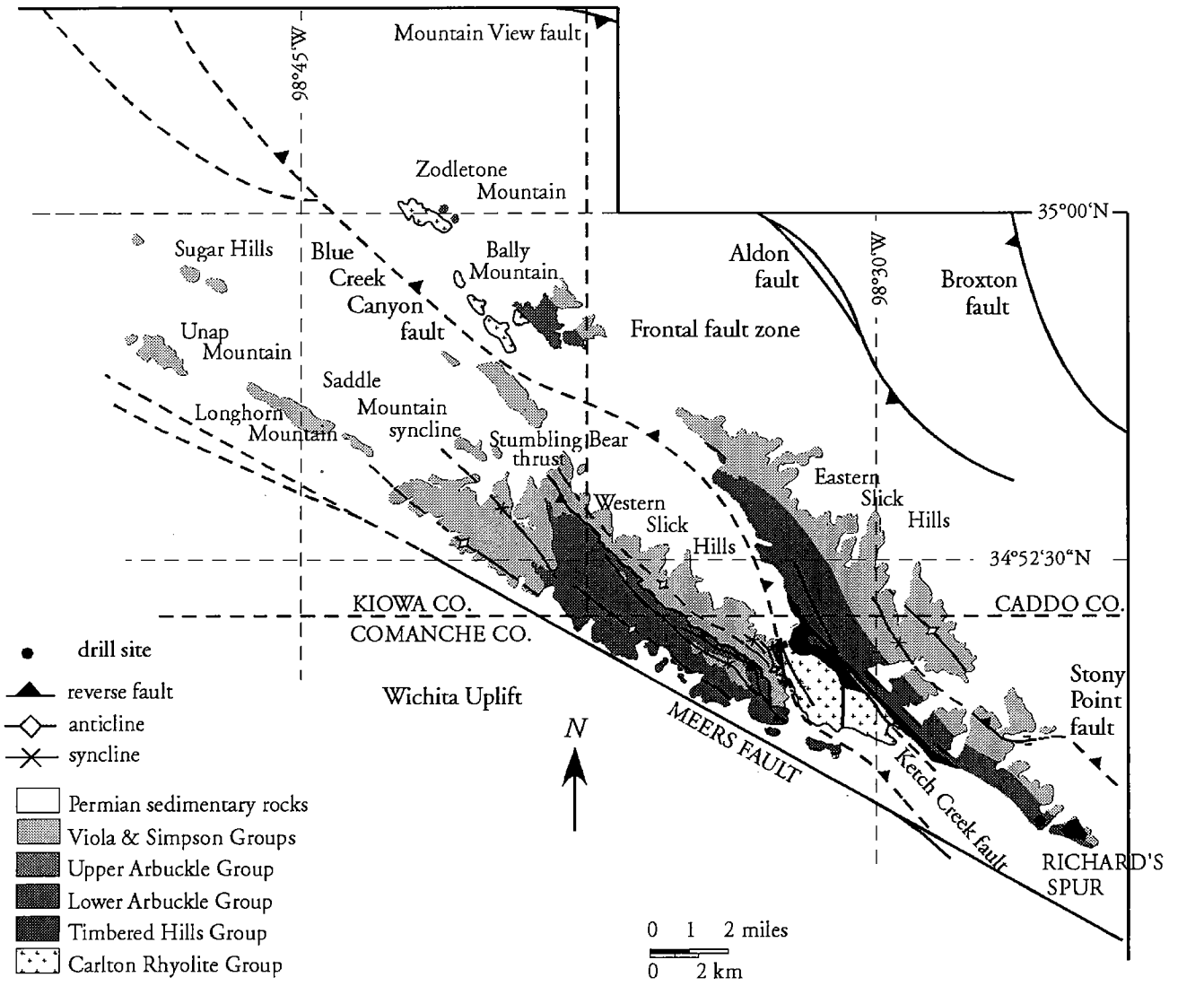

Figure 2. Geologic map of the Slick Hills region, southern Oklahoma, showing location of Richard's Spur (southeast corner of map).

DESCRIPTION OF THE SIGNAL MOUNTAIN FORMATION

Petrography

Investigation of the remainder of the Richard's Spur core extends the general findings of Whitehead and Donovan (2000). The prevailing *lietmotiv* of the Signal Mountain Formation is that it is composed of very thin (<3 cm) beds that show extraordinary variations in petrology and are juxtaposed in a very complex fashion (Ditzell, 1982).

The most commonly seen carbonate textures are gradations of mudstones, wackestones, and packstones, but grainstones also commonly occur. All four principal types of allochem—biogenic, ooids, peloids, and intraclasts—are present in various combinations, although ooids are sparse. The allochems are combined in distinctly different proportions, even in adjacent beds. Such ooids as are found tend to be "pure" and are generally grainstones. The other allochems form varieties of intrabiopelsparites and micrites. Fossils include abundant trilobites, pelmatozoans, and gastropods. Sorting is generally poor, and many of fossil fragments and intraclasts show little, if any, evidence of rounding.

Primary sedimentary structures are restricted to small-scale cross bedding, parallel lamination, and upward-fining grading. Bioturbation is commonly observed (trilobite burrows are found in some horizons) but it rarely completely destroys the primary bedding fabric. Ichnofacies include *Thalassinoides* and *Cruziana*. In some parts of the section, bioturbation is absent and primary lamination is perfectly preserved.

The Signal Mountain Formation contains much more siliciclastic detritus than is generally the case in the Arbuckle Group. Both black and, less commonly, olive-green (illitic) shales are present as numerous interbeds (generally less than a centimeter thick) with lenticular limestone. Additionally, insoluble residues of

~20% are commonly found in all the limestone textures, although less so in the grainstones (Table 1). This residue consists of silt-sized quartz in the grainstones and quartz, clay, and carbon of organic origin in the mudstone textures (Table 2). At some horizons, glauconite is abundant, particularly immediately above the base of the Signal Mountain Formation, as noted by Hosey and Donovan (2000) and also at higher levels.

TABLE 1. — Insoluble Residues in the Signal Mountain Formation Core from Richard's Spur

Lithology	Hole	Depth	Mineralogy ins.	% Insolubles
Wackestone	4	77 ft	clay	25
Bioturbated wackestone	4	129 ft	clay	24
Mudstone, black	4	157 ft, 9 in.	clay	33
Grainstone	4	165 ft, 2 in.	clay/quartz 60/40	0.07
Wackestone	2	13 ft, 4 in.	clay/quartz silt 90/10	11
Grey shale	2	33 ft, 8 in.	clay/quartz silt 90/10	92
Grey shale	2	27 ft, 9 in.	clay/quartz silt 90/10	93
Glauconitic grainstone	2	97 ft	glauconite/pyrite quartz silt	0.66
Mudstone, dark grey	2	141 ft, 2 in.	clay	33

Lithologic Associations

In an attempt to impart order to the sequence, Whitehead and Donovan (2000) recognized four principal lithologies. We have amended and expanded their descriptions, as follows:

1. Lime mudstones with variable amounts of peloids, intraclasts and fossils. All mud-supported textures are present, from sparsely fossiliferous mudstones, through wackestones to packstones. This, the most abundant lithology in the core, may or may not show signs of bioturbation.
2. Grainstones, also with variable amounts of peloids, intraclasts, and fossils. A few instances of oolitic grainstones were encountered. Hardgrounds are associated with this lithology.
3. Black to dark-gray shales, with variable amounts of quartz silt. Some of these shales are laminated and may show fining-upward grading.
4. Gray-green (illitic) shales.

Whitehead and Donovan (2000) recognized five lithologic associations in part of the core that they examined, all of which involve alternation of the four basic lithologies recognized above. Each of these lithologies occurs in sequences that are generally less than 4 ft thick:

1. Black shales alternating with lime mudstones and wackestones.
2. Black shales alternating with fossiliferous packstones and wackestones. The difference between "1" and "2" is in the proportions of allochems, particularly bioclasts.
3. Lime mudstones, wackestones, and packstones, confused by a comprehensive network of stylolites, some of which are parallel to bedding, others subvertical. This lithologic association differs from "1" and "2" in that it contains less insoluble residue, that is, shales. In addition, this lithology is more likely to be bioturbated than "1" and "2."
4. Sequences of grainstones, with bed boundaries defined by hardgrounds. This lithologic association is rarely more than a foot thick. Thin calcite veins that are normal to bedding generally cut these beds.

TABLE 2. — Total Organic Carbon Values from Selected Samples in the Richard's Spur Core

Hole	Depth	Lithology	TOC
2	83 ft, 5 in.	Black shale	0.38
2	43 ft, 5 in.	Grey shale	0.2
2	16 ft, 4 in.	Black shale	1.09
2	32 ft, 11 in.	Grey shale	0.19
2	101 ft, 11 in.	Micrite	0.16
2	113 ft, 5 in.	Grainstone	0.14
2	121 ft, 11 in.	Micrite	0.14
2	136 ft, 8 in.	Grey shale	0.26
4	83 ft, 1 in.	Black shale	0.91
4	102 ft, 5 in.	Black shale/mudstone	0.42
4	112 ft, 8 in.	Grey shale	0.47
4	112 ft, 2 in.	Grey mudstone	0.22
4	114 ft, 4 in.	Grey mudstone	0.23
4	114 ft, 4 in.	Black shale	0.52
4	120 ft	Black shale	0.75
4	138 ft	Wackestone	0.21
4	147 ft, 7 in.	Black shale/mudstone	0.2
4	150 ft	Grey mudstone	0.17
4	152 ft, 6 in.	Grey shale	0.22
2	151 ft	Black shale	0.3
4	151 ft	Black shale	1.17
4	160 ft, 5 in.	Grainstone	0.24
4	170 ft, 8 in.	Black shale	1.26
4	190 ft, 6 in.	Black shale	0.95
4	191 ft	Dolograinstone	0.24
2	98 ft, 8 in.	Grainstone	0.14
4	160 ft, 5 in.	Grainstone	0.14
4	190 ft, 6 in.	Black shale	0.85
4	190 ft, 10 in.	Grainstone	0.27
		Average	**0.43**

Data courtesy of Dan Jarvie.

5. Gray-green shales alternating with lime mudstones, wackestones, and packstones. Only one thickness of this lithology was encountered; it is the site of the greatest amount of tectonic deformation in the core.

Although three of these lithologies (1, 2, and 4) are repeated commonly in beds <1 m thick in parts of the core, the sequence does not show the clear evidence of cyclicity that characterizes much of the rest of the Arbuckle Group. The gradational nature of most association cannot be overstressed.

ORGANIC CARBON

Whitehead and Donovan (2000) recorded significant amounts of total organic carbon (TOC) in the Signal Mountain Formation. We amplify their initial observations here (Table 2). In general, data from representative lithologies show that, although insignificant amounts of organic carbon are present in the grainstones, heavily bioturbated mud-supported textures and gray-green mudstones, TOC values up to 1.26% are associated with nonbioturbated black shales and impure limestones. Such sequences may record seabed anoxia or oxygen depletion. Although the TOC values are sparse, our detailed measurements suggest that the total thickness of black shales is about 45 ft (~13.5 m) in a formation thickness of 900 ft (~280 m). Thus, about 5% of the rock volume averages ~1.0% TOC. Such source rocks may atone in thickness and areal extent for what they may lack in richness. Preliminary studies on the nature of the organic carbon suggest that it is of algal origin and thus constitutes a Type 1 kerogen.

ENVIRONMENT OF DEPOSITION

Most interpretations of the Arbuckle Group as a whole have seen the unit as part of an immense shallow-water carbonate platform that supported an abundance of life forms that lived in warm photic conditions, as mentioned in the introduction. The general hallmarks of the Arbuckle include an impressive suite of algal boundstones, an abundant bottom-dwelling fauna (principally gastropods, echinoderms, trilobites, sponges, and brachiopods), plus a very active infauna. Ooid shoals, as much as 1 m thick, are commonly seen in some formations, as are the distinctive features of evaporative tidal flats. Early diagenetic imprints include comprehensive cementation by non-ferroan calcite, abundant nodular chert, and penecontemporaneous idiotopic dolomite.

The Signal Mountain facies described above is clearly distinctively different from facies found in the rest of the Arbuckle Group (Donovan, 1991). Some specific differences include: (1) the absence of algal boundstones; (2) the paucity of ooids; (3) the preservation of carbon of organic origin in the black shale facies; (4) the incorporation of ferrous iron into carbonate cements; (5) the paucity of chert; (6) the absence of evaporite features (desiccation cracks, gypsum pseudomorphs, etc.); (7) the dominance of poorly sorted bioclastic mud-supported textures; (8) the rapid alternation of thin beds of very different character; (9) the absence of easily identifiable, shallowing-upward cyclic *motifs*; and (10) the presence of significant amounts of glauconite in parts of the section.

The Signal Mountain Formation was constructed by a large number of frequently repeated small-scale events. Following Whitehead and Donovan (2000), the principal sources of sediment for these events appear to have been: (1) an aeolian or fluvial system that supplied silt- and clay-sized siliciclastics on a regular basis; (2) a lively platform, subject to storms, colonized by a wide variety of organisms and capable of producing a great deal of lime mud; and (3) plankton.

The absence of algal boundstones, stromatolites, thrombolites, etc. suggests that the bottom may have been below the photic zone. The most commonly seen carbonate textures are gradations of poorly sorted mudstones, wackestones, and packstones. The absence or near absence of sorting in such deposits indicates that the sea bottom was generally below fair-weather wave base. Grading in mud-supported textures suggests either a storm or density-flow origin for some beds.

We agree with the suggestion of Whitehead and Donovan (2000) that the Signal Mountain Formation was deposited in a deeper water setting than was usual in the Arbuckle Group. This deeper-water setting coincided with tectonic redefinition of the southern Oklahoma aulacogen (Donovan, 2000). Various processes involving gravity- and current-controlled transport of material into a Signal Mountain "gulf" from the adjacent shallower parts of the Arbuckle platform, outwith the aulacogen, contributed to the development of an unusually disordered facies assemblage (Fig. 3). The sequence does not show the obvious evidence of cyclicity that characterizes much of the rest of the Arbuckle Group. Subtle variations in the proportion of siliciclastics and regular punctuation of the sequence by grainstones, however, may correlate with short-term regression/transgression cyclicity in the shallower parts of the platform. The hardgrounds permit the inference that regular periods of nondeposition accompanied by sustained current flow took place, perhaps as a result of contour-parallel flow. Abundant lime-mud intraclasts record reworking of a partially lithified seabed. This reworking did not necessarily occur at the depths at which the intraclasts finally were deposited. Accumulation of these mud-supported facies was interrupted by incursions of fine-grained siliciclastics deposited by gentle currents.

The various deep-water channels that serve to fragment the Bahamas Platform today may provide a partial analog for the Signal Mountain Formation "gulf," both in scale and process (Fig. 3). For example, Mullins and Neumann (1979) described the relationship between the Little Bahamas Bank and the Northwest Providence Channel. They recorded slumps, debris flows, grain flows, and surface-related mud transport. In addition, turbidity flows both normal to and parallel with the length of the Northwest Providence Channel

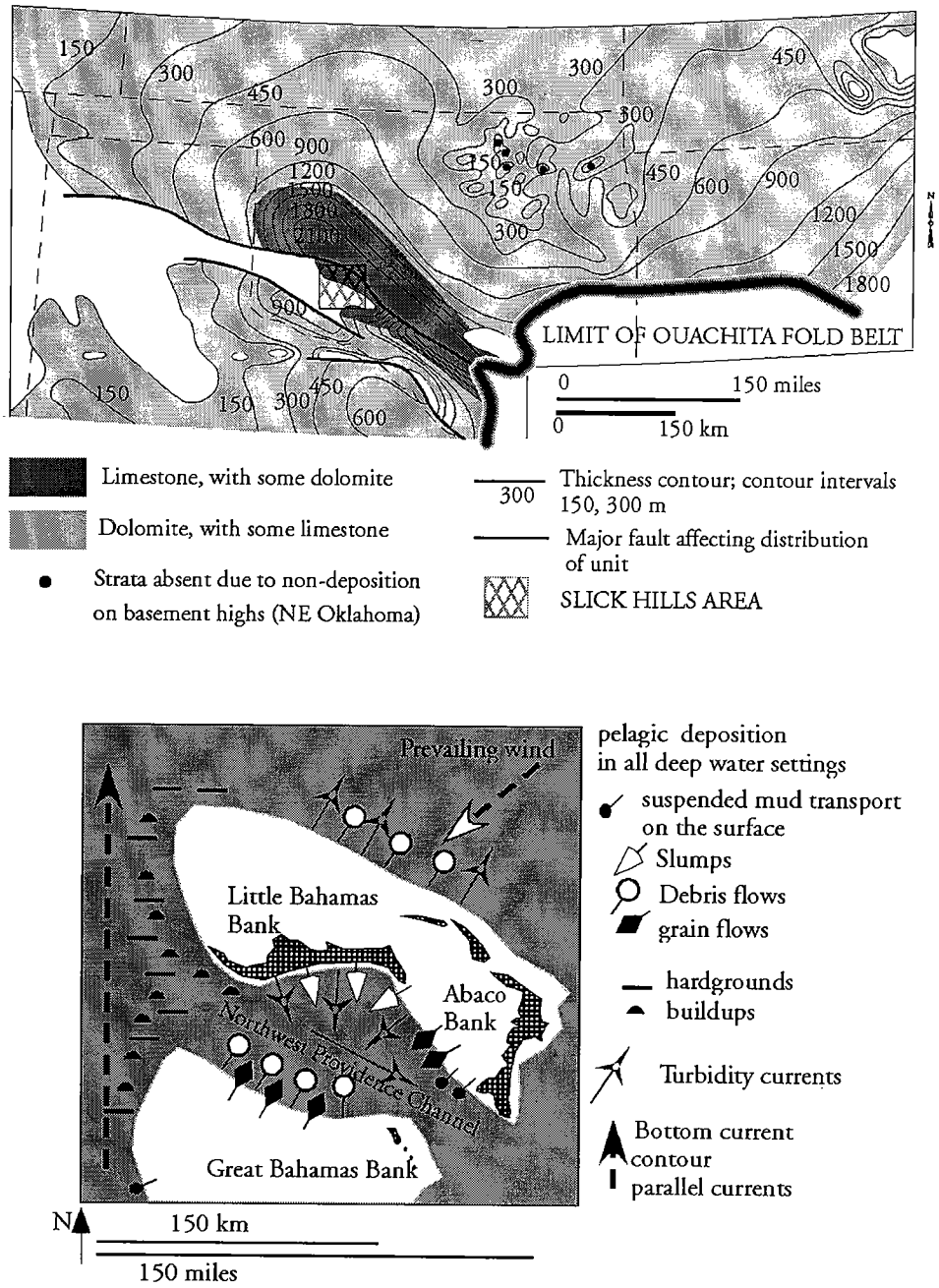

Figure 3. A comparison of the geologic setting of the southern Oklahoma aulacogen during deposition of the Arbuckle Group (derived from Johnson and others, 1989) and the northern part of the modern Bahamas Platform (derived from Mullins and Neumann, 1979). The Signal Mountain facies is centered on the "limestone" tract of the Arbuckle platform. The Bahamas diagram is twice the scale of the Oklahoma map.

occur. In other areas, a strong bottom current produces hardgrounds. The analogy cannot be taken too far, however. The tectonic setting is different, no comparable siliciclastics occur in the Bahamas, and we saw no evidence of the carbonate buildups that are recorded in some of the channels. Nevertheless, the analogy is useful in that it demonstrates a setting in which transport processes can resediment platform material into an adjacent quiet, deep-water setting, below both the photic zone and storm wave base.

DIAGENESIS OF THE SIGNAL MOUNTAIN FORMATION

Cementation

Cementation histories are complex. Hardgrounds, generally associated with grainstones, are common punctuation marks in the sequence—some are clearly erosional. Both calcite and dolomite are present as pore-filling cements: much of the calcite is ferroan and the dolomite nearly always so. In general, dolomite is

later than calcite. It is seen as fine-grained euhedral rhombs in some muddy textures and as baroque spar (partially replacive) in some grainstones. Pyrite is abundant as millimeter-scale nodules at some horizons.

Pressure-Solution and Related Diagenetic Phenomena

Pressure solution has had a dramatic impact on the Signal Mountain Formation—apparently more so than in any other formation of the Arbuckle Group. As noted by Whitehead and Donovan (2000), dissolution seams, bedding-parallel stylolites, and lenticular (wavy) bedding (Bathurst, 1987; Bucheit and Donovan, 2000) are ubiquitous and have substantially modified primary depositional features. The specific character of the pressure solution is a reflection of the percentage of siliciclastic detritus that is present in any given lithology. Thus, stylolites typically are associated with grainstones, whereas dissolution seams and wavy bedding are associated with muddy textures. The higher clay content of the latter presumably provides more sites for carbonate dissolution and thus disperses the effect. In the "cleaner" grainstones, the pressure solution is more focused. Where the percentage of shale is high, some limestone lenses were rotated and penecontemporaneously faulted; as a result of this rotation, the dip of primary lamination may vary by as much as 20° from bed to bed. Whatever the geometry of the pressure-solution phenomena, it is clear that an enormous amount of calcium carbonate has been removed from the formation. Our rough estimates of removal vary from 25% to 50%. Carbonate loss of this magnitude in a formation that is approximately 900 ft (~275 m) thick must have been an important control in the creation of accommodation space within the aulacogen.

BURIAL HISTORY OF THE SIGNAL MOUNTAIN FORMATION

Redefinition of the Southern Oklahoma Aulacogen

Late Cambrian marine sedimentation on the Laurentian craton coincided with a worldwide rise in sea level. Sections around the craton generally record an initial period of siliciclastic sedimentation that was followed by the development of enormous carbonate platform. The position and character of the Signal Mountain Formation in this setting is anomalous. In general, the Signal Mountain is restricted to the area of the southern Oklahoma aulacogen and has no lateral facies correlatives. Subsidence curves (Figs. 4, 5) indicate that the greatest rate of basin subsidence during the early Paleozoic coincided with deposition of the Signal Mountain Formation (Feinstein, 1981; Hosey and Donovan, 2000). Donovan (2000), suggesting that this increased rate of deposition marked a tectonic redefinition of the southern Oklahoma aulacogen, following weakening and failure of a lithosphere that had been thermally expanded during mid- to late Cambrian times. It was in this setting that the environmental conditions peculiar to the Signal Mountain were developed and maintained.

A further complexity is added to the story in that initiation of the aulacogen redefinition coincided with a period of craton-wide regression as a result of which rocks of the preceding transgression/regression cycle (i.e., the Fort Sill Formation) were exposed subaerially. The net result of this is that the base of the Signal Mountain Formation is both an unconformity and a major sequence boundary (Chow and James, 1987; Hosey and Donovan, 2000; McElmoyl and Donovan, 2000). Subsequent deposition of the Signal Mountain Formation marks the only time in the history of the Cambro–Ordovician Laurentian carbonate platform when long-term sedimentation rates did not exceed subsidence rates. Eventually, as the rate of subsidence slowed, sediment production exceeded the rate of development of accommodation space, and the massive algal boundstones and shallow-water sequences of the Mackenzie Hill Formation were deposited.

Pressure-Solution Effects in the Signal Mountain Formation

The onset of pressure solution presumably was coincident with increasing depth of burial. As noted, subsidence curves suggest that initial subsidence rates within the aulacogen were high and that the formation had reached a depth of 10,000 ft below the surface within 40 million years of its deposition. Subsequently, the rate of subsidence within the aulacogen greatly decreased, but the Signal Mountain remained at this general depth or slightly greater for about 140 million years, at which time, approximately 300 million years ago, a partial inversion of the aulacogen emplaced the Slick Hills at the surface. Inversion was relatively rapid. Lower Permian conglomerates directly overlie the Signal Mountain Formation at Richard's Spur.

The long residence time at depth doubtless provided a suitable environment for intense pressure solution; however, some of the details hint at greater complexity than simple burial. For example, although most of the stylolites and related phenomena are parallel to bedding, vertical stylolites appear to have partitioned groundwater-circulation patterns, as manifest by cement chemistry (Whitehead and Donovan, 2000). These vertical stylolites seem to have developed relatively early in the history of the rock, because they are cut by calcite-filled "tectonic" veins and some, but not all, bedding-parallel stylolites.

A second complexity is associated with the relationship of the calcite veins both to bedding and to bedding-parallel stylolites. The earliest veins are perpendicular to bedding and are restricted to grainstone lithologies. Some of these veins have been cut by bedding-parallel stylolites. These veins are generally filled with a single generation of drusy calcite. Later veining is more complex and took place during inversion (Ayan and others, 2000). Some veins appear to post-date bed rotation; other veins appear earlier. Cross-cutting relationships suggest that at least four generations of veining mark this period. Sequences of infill are similarly complex,

involving ferroan and nonferroan drusy calcite, euhedral dolomite, and euhedral pyrite. These veins presumably record directed-stress patterns operative during inversion. A final set of veins, which are infilled by at least one generation of fibrous calcite, utilized the existing pattern of bedding-parallel stylolites. It presumably records the lessening of confining pressure during inversion.

In summary, the section presents evidence in the form of tectonic veining (stylolites that partitioned the movement of cementing fluids, early small-scale faulting, and rotated lenticular carbonates) that suggests an early tectonic imprint. We suggest that this imprint coincided with the tectonic redefinition of the southern Oklahoma aulacogen discussed above. Bedding-parallel stylolites are a response to deep burial, although later complex vein fills record inversion.

Hydrocarbon Potential

Following relatively rapidly rapid burial during the Ordovician, the Signal Mountain Formation lay at depths of ~10,000 ft (~3,000 m) during the Late Ordovician, Silurian, and Devonian Periods. Given conventional geothermal gradients, the lowermost part of the Signal Mountain Formation entered the oil window during mid-Ordovician time, ca. 470 million years ago. This is significantly earlier than other source rocks in the southern Oklahoma area. We note that the impressive amounts of pressure solution in the section suggest that significant fluid movement took place within the formation during a long period of deep burial.

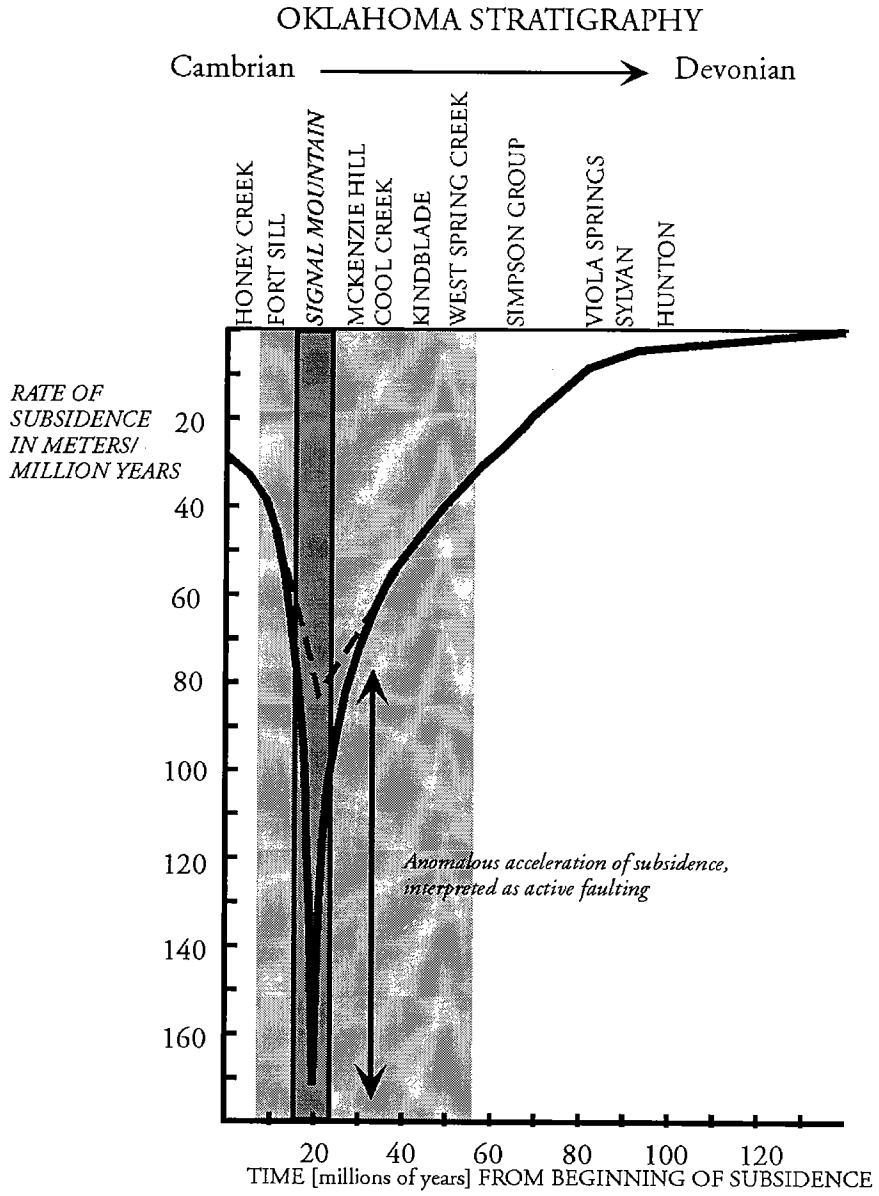

Figure 4. Subsidence rates for the southern Oklahoma aulacogen. The acceleration of subsidence during Signal Mountain deposition is anomalously high and records local tectonic adjustment of the aulacogen. Data from Feinstein (1981), modified from Hosey and Donovan (2000).

Subsequently, the Signal Mountain Formation was caught up in the late Paleozoic redefinition of southern Oklahoma, as a result of which it either became part of the sedimentary basement of various rapidly subsiding basins (Ardmore, Anadarko, Marietta, and others) or was inverted in complementary uplifts (Wichita, Arbuckle, Criner). Source-rock capacity at this time was either destroyed or became latent.

CONCLUSIONS

The Signal Mountain Formation, the second oldest formation in the Cambro–Ordovician Arbuckle Group of Oklahoma, displays facies that are distinctly different from those seen in other formations of the Arbuckle. Typical lithologies are burrow-mottled intrapelbiomicrites, poorly sorted biosparites, wackestones, mudstones, and intraformational conglomerates. Individual beds are from 1 to 5 cm thick, show little systematic ordering, and were deposited in marine, aphotic, below-wave-base settings; density and turbidity flows contributed to the sediments. The environment of deposition was a deeper water setting that developed during tectonic redefinition of the southern Oklahoma aulacogen. The Signal Mountain carries a distinct tectonic imprint that relates to rapid subsidence.

During tectonic redefinition, subsidence rates exceeded sedimentation rates. This situation created accommodation space and generated sea-floor anoxia.

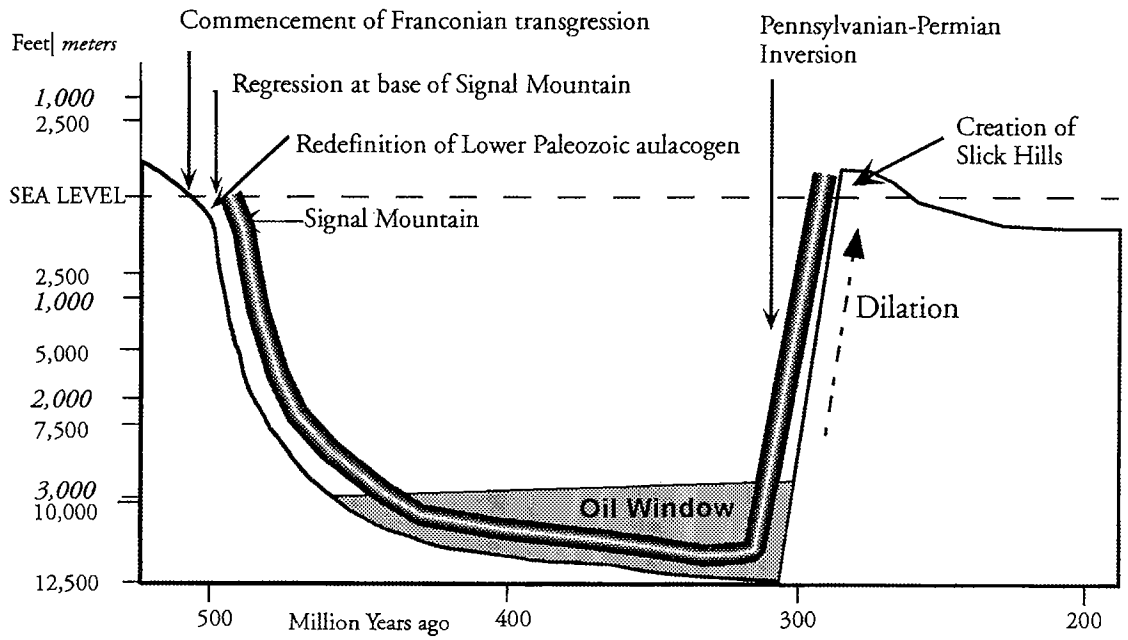

Figure 5. Burial-time curve illustrating tectono-stratigraphic history of the Signal Mountain Formation. Note the length of residence time for the formation within the oil window. Based in part on Whitehead and Donovan (2000).

Rocks deposited under these conditions lack bioturbation, and are fine-grained, laminated pelbiomicrites and thin (<2 in. [5 cm]) black shales. The presence of an anoxic environment is further supported by the preservation of organic matter. These beds yield the highest TOC values, ~1%. Preliminary work on hydrogen and oxygen indices confirms type 1 kerogen (i.e., organic matter of algal origin). We conclude that the Signal Mountain Formation may have generated commercial quantities of hydrocarbons. The burial history of this formation suggests that it entered the oil window ca. 470 million years ago. This is significantly earlier than other source rocks in the southern Oklahoma area, thus encouraging exploration of older parts of the stratigraphic section.

ACKNOWLEDGMENTS

Our principal thanks are to the Dolese Company for making the core available for our study. We additionally would like to recognize Jim Allen, Dolese's manager, and Ken Johnson of the Oklahoma Geological Survey for their interest in promoting this work. We are grateful to Dan Jarvie of Humble Geochemical Services for generously providing TOC data; a more comprehensive study of the organic matter is currently under way. Jim Pancake helped in the lab. The senior author acknowledges the assistance of the Moncrief family of Fort Worth.

REFERENCES CITED

Ayan, D.; Bucheit, A. K.; Kulow, M. J.; and Donovan, R. N., 2000, Preliminary cyclic stratigraphy of the Upper Arbuckle Group in the Richard's Spur Quarry, Slick Hills, Oklahoma, *in* Johnson, K. S. (ed.), Platform carbonates in the southern Midcontinent, 1996 symposium: Oklahoma Geological Survey Circular 101, p. 97–102

Bathurst, R. G. C., 1987, Diagenetically enhanced bedding in argillaceous platform limestones: stratified cementation and selective compaction: Sedimentology, v. 34, p. 749–778.

Bucheit, A. K.; and Donovan, R. N., 2000, Initiation of a carbonate platform: a comparison between the Lower Jurassic Broadford Limestone, Isle of Skye, Scotland, and the Cambrian Honey Creek Limestone, Slick Hills, Oklahoma, *in* Johnson, K. S. (ed.), Platform carbonates in the southern Midcontinent, 1996 symposium: Oklahoma Geological Survey Circular 101, p. 57–64.

Chow, N.; and James, N. P., 1987, Cambrian grand cycles: a northern Appalachian perspective: Geological Society of America Bulletin, v. 98, p. 418–429.

Ditzell, C. L., 1982, Sedimentary geology of the Cambro–Ordovician Signal Mountain Formation as exposed in the Wichita Mountains of southwestern Oklahoma: Oklahoma State University unpublished M.S. thesis, 165 p.

Donovan, R. N., 1991, The Arbuckle Group—an aide de memoire, *in* Johnson, K. S. (ed.), Arbuckle Group core workshop and field trip: Oklahoma Geological Survey Special Publication 91-3, p. 199–208.

_____ 2000, Initiation of the Arbuckle platform—view from the Slick Hills, Oklahoma, *in* Johnson, K. S. (ed.), Platform carbonates in the southern Midcontinent, 1996 symposium: Oklahoma Geological Survey Circular 101, p. 47–56.

Donovan, R. N.; and Ragland, D. A., 1986, Paleozoic stratigraphy of the Slick Hills, southwestern Oklahoma, *in* Donovan, R. N. (ed.), The Slick Hills of southwestern Oklahoma—fragments of an aulacogen?: Oklahoma Geological Survey Guidebook, 24, p. 13–16.

Feinstein, S., 1981, Subsidence and thermal history of southern Oklahoma aulacogen: implications for petroleum exploration: American Association of Petroleum Geologists Bulletin, v. 65, p. 2521–2533.

Hosey, R.; and Donovan, R. N., 1993, The geological significance of the boundary between the Fort Sill and Signal Mountain Formations in the lower Arbuckle Group (Cambrian) [abstract]: Geological Society of America Abstracts with Programs, v. 25, no. 1, p. 14–15.

Hosey, R. M.; and Donovan, R. N., 2000, Boundary between the Fort Sill and Signal Mountain Formations in the Lower Arbuckle Group, Slick Hills: candidate for a grand cycle boundary, *in* Johnson, K. S. (ed.), Platform carbonates in the southern Midcontinent, 1996 symposium: Oklahoma Geological Survey Circular 101, p. 79–88.

Johnson, K. S., 1991, Geologic setting of the Arbuckle Group in Oklahoma, *in* Johnson, K. S. (ed.), Arbuckle Group core workshop and field trip: Oklahoma Geological Survey Special Publication 91-3, p. 3–7.

Johnson, K. S.; Amsden, T. W.; Denison, R. E.; Dutton, S. P.; Golstein, A. G.; Rascoe, B.; Sutherland, P. K.; and Thompson, D. M., 1989, Geology of the southern Midcontinent: Oklahoma Geological Survey Special Publication 89-2, 53 p.

McElmoyl, C.; and Donovan, R. N., 2000, An unconformity in the lower part of the Cambrian Honey Creek Limestone, Slick Hills, Oklahoma: candidate for a grand cycle boundary, *in* Johnson, K. S. (ed.), Platform carbonates in the southern Midcontinent, 1996 symposium: Oklahoma Geological Survey Circular 101, p. 65–78.

Mullins, H. T.; and Neumann, A. C., 1979, Deep carbonate bank margin structure and sedimentation in the northern Bahamas, *in* Doyle, L.; and Pilkey, D. H., Geology of continental slopes: Society of Economic Paleontologists and Mineralogists Special Publication 27, p. 165–192.

Stitt, J. H., 1977, Late Cambrian and earliest Ordovician trilobites, Wichita Mountains area, Oklahoma: Oklahoma Geological Survey Bulletin 124, 79 p.

Whitehead, R. E.; and Donovan, R. N., 2000, Four hundred feet of core from the Cambrian Signal Mountain Formation, Slick Hills, Oklahoma, *in* Johnson, K. S. (ed.), Platform carbonates in the southern Midcontinent, 1996 symposium: Oklahoma Geological Survey Circular 101, p. 89–95.

Eastern Continuation of the Wilburton Triangle Zone in the Red Oak Gas-Field Area, Frontal Ouachitas–Arkoma Basin Transition Zone, Southeastern Oklahoma

İbrahim Çemen, Justin Evans, and Ata Sagnak
Oklahoma State University
Stillwater, Oklahoma

ABSTRACT.—The frontal Ouachitas–Arkoma basin transition zone of southeastern Oklahoma contains many gas fields, which produce mainly from the Spiro and Red Oak sandstone reservoirs of the Pennsylvanian Atoka Formation. Recently, Çemen and others (2001) proposed the presence of a triangle zone in the Wilburton gas-field area. This triangle zone, named here as the Wilburton triangle zone, is flanked by the Choctaw fault to the south and Carbon fault to the north and is floored by the Lower Atokan detachment (LAD) surface in the Atoka Formation.

We constructed balanced structural cross sections to delineate the structural geometry of the transition zone in the Red Oak gas-field area. The cross sections are based on the available wireline logs, seismic profiles, and surface geologic maps. Our study suggests that the Wilburton triangle zone continues in the subsurface eastward in the Red Oak gas-field area, where it is also flanked by the south-dipping Choctaw fault to the south and the north-dipping Carbon fault to the north and is floored by the LAD. East of the Wilburton gas field, the Carbon fault is not present at the surface. Although the details of the subsurface geometry between the Wilburton and Red Oak gas-field areas remain to be determined, we suggest that the Carbon fault makes a lateral ramp to the east because it can be observed in the seismic lines as a blind backthrust in the Red Oak gas-field area. When restored to their position at the time of the Spiro deposition by using the "key-bed" restoration method, the cross sections indicate >60% shortening both in the Wilburton and Red Oak gas-field areas.

Southwest of Wilburton, the Choctaw fault forms a splay, which is named here as the Northern Choctaw fault. The Spiro sandstone is well exposed on the hanging wall of the Main Choctaw fault. The absence of the Spiro sandstone in the fault wedge between the Main Choctaw and Northern Choctaw faults indicates that the Northern Choctaw fault is younger than the Main Choctaw fault. This suggests break-forward thrusting between the two faults and implies that the imbricate thrusts on the hanging wall of the Main Choctaw fault were also developed by a break-forward sequence of thrusting.

INTRODUCTION

The Ouachita Mountains and Arkoma basin are tectonic features extending through southeastern Oklahoma and west-central Arkansas. The mountains were formed during the Early and Middle Pennsylvanian Ouachita orogeny. Based on the structural style and stratigraphy, the Ouachita Mountains in Oklahoma are divided into three distinct assemblages, namely the frontal belt, central belt, and Broken Bow uplift (Fig. 1). The Arkoma basin is a foreland basin of the Ouachitas. It is bounded by the Ozark uplift to the north and by the Arbuckle Mountains to the southwest (Fig. 1), and grades onto the Cherokee platform to the northwest (Johnson, 1988). The frontal belt is bounded by the Choctaw fault to the north and the Windingstair fault to the south. The belt consists of imbricately thrusted, tilted, and tightly folded, shallow-water Morrowan strata to the south and basinal rocks to the north (Wickham, 1978). The Atokan turbidites overlie the Morrowan strata throughout the frontal belt.

As in all compressional mountains, such as the Canadian Rockies, the Alps, and the Himalayas, deformation in the Ouachita Mountains grades from the strongly deformed frontal belt into mildly deformed foreland within an area usually referred to as the

Çemen, Ibrahim; Evans, Justin; and Sagnak, Ata, 2001, Eastern continuation of the Wilburton triangle zone in the Red Oak gas-field area, frontal Ouachitas–Arkoma basin transition zone, southeastern Oklahoma, *in* Johnson, K. S.; and Merriam, D. F. (eds.), Petroleum systems of sedimentary basins in the southern Midcontinent, 2000 symposium: Oklahoma Geological Survey Circular 106, p. 81–95.

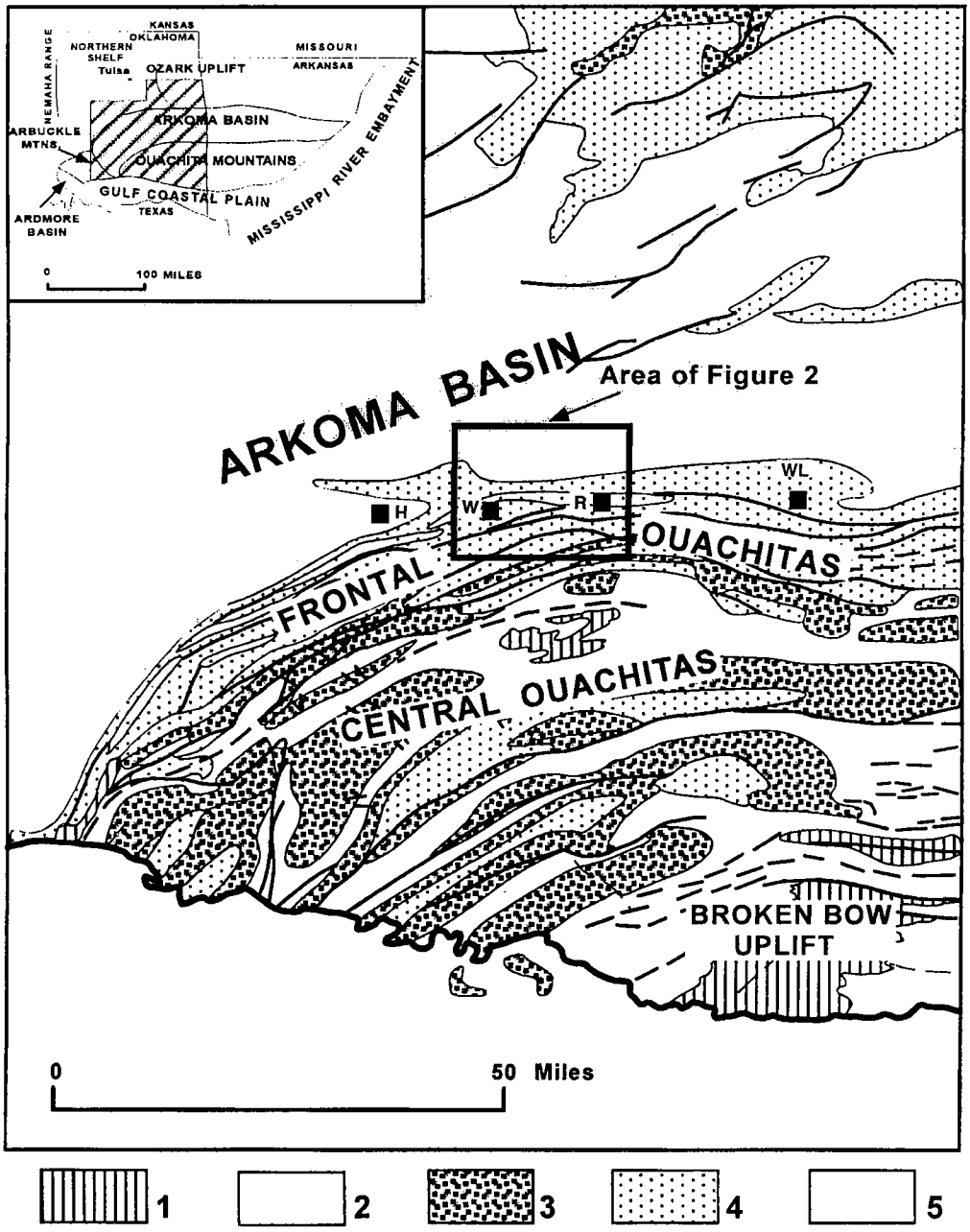

Figure 1. Simplified geologic map of the Ouachita Mountains in southeastern Oklahoma (modified from Arbenz, 1989). The insert on the top left shows major geologic provinces of eastern Oklahoma and western Arkansas (modified from Johnson, 1988). *Explanations:* (1) Early and middle Paleozoic (Cambrian through Early Mississippian); (2) Middle and Late Mississippian (Stanley Group of Ouachita facies); (3) Morrowan (Jackfork Group and Johns Valley Formations of Ouachita facies); (4) Atokan (Spiro/Wapanucka and Atoka Formations of the frontal Ouachita and Arkoma basin); (5) Desmoinesian (Hartshorne, McAlester, Savanna, and Boggy Formations of the Krebs Group of the Arkoma basin). *Abbreviations:* H = Hartshorne; W = Wilburton; WL = Wister Lake.

transition zone. The Choctaw fault is the leading edge thrust of the frontal Ouachitas and is the structural boundary between the Ouachita Mountains and the Arkoma basin in Oklahoma. Therefore, the Choctaw fault and associated structures define the transition zone in the Ouachita Mountains.

The geometry of thrust faulting in the frontal Ouachitas–Arkoma basin transition zone has been controversial. Suneson (1995) summarized several structural interpretations dealing with this geometry. These interpretations are mostly restricted to the westernmost part of the transition zone in southeastern Oklahoma; only one study in the eastern part between Wilburton and the Wister Lake area (Fig. 1) has been published. Several of the studies in the western part proposed the presence of a triangle zone with a back-

thrust (Hardie, 1988; Milliken, 1988; Camp and Ratliff, 1989; Perry and Suneson, 1990; Reeves and others, 1990; Wilkerson and Wellman, 1993; Valderrama and others, 1994). However, there is no agreement on the geometric detail and areal extent of the triangle zone. Some workers have suggested that all the thrust faults in the transition zone are south-dipping (Bertagne and Leising, 1989; Tilford, 1990), and therefore there is no triangle zone. Also controversial is the presence and detailed geometry of the duplex structure proposed by some studies (Roberts, 1992; Wilkerson and Wellman, 1993; Al-Shaieb and others, 1995; Çemen and others, 1995, 1997; Valderrama and others, 1995).

From 1992 to 1995, the sedimentology of the Spiro sandstone and the structural geology of the Wilburton gas-field area were studied by a group in the School of Geology of the Oklahoma State University with a grant from the Oklahoma Center for Advancement in Science and Technology (OCAST). The structural group in the OCAST project constructed many balanced structural cross sections and concluded that a well-developed triangle zone exists in the Wilburton gas-field area (Çemen and others, 1994, 1995, 1997; Al-Shaieb and others, 1995; Sagnak, 1996). This triangle is named here as the Wilburton triangle zone.

The Wilburton triangle zone is flanked by the south-dipping Choctaw fault to the south and the north-dipping Carbon fault to the north and is floored by the lower Atokan detachment (LAD; Figs. 2, 3). Below the triangle zone is a well-developed duplex structure, which was formed by hinterland dipping imbricate thrust faults splaying from a floor thrust and joining to the LAD in the Atoka Formation. The LAD continues in the Atoka Formation northward and displaces the Red Oak sandstone before reaching a shallower depth and forming the Carbon fault as a north-dipping back-thrust below the San Bois syncline (Figs. 2, 3). When restored to their position at the time of the Spiro deposition by using the "key-bed" restoration method, the cross sections indicate about 60% shortening in the Wilburton area.

After the OCAST project, the structural group constructed balanced structural cross sections in the Red Oak gas-field area within the Baker Mountain and Panola 7½′ quadrangles to determine the eastern continuation of the Wilburton triangle zone. The cross sections were constructed by using available wire-line well-log data, well-completion cards, interpretations of seismic profiles donated by Amoco and Exxon, and updated surface geologic maps by Suneson and Ferguson (1989), Hemish and others (1990a,b), and Suneson (1996). The e-logs were used to locate the stratigraphic positions of the Spiro, Red Oak, Panola, and Cecil sandstones and the Hartshorne Formation. These rock-stratigraphic units were used extensively in construction of the balanced structural cross sections.

The main purpose of this paper is to discuss the eastern continuation of the Wilburton triangle zone in the Red Oak gas field and surrounding areas through the discussion of several balanced structural cross sections. The Spiro, Cecil, Panola, and Red Oak sandstones of the Pennsylvanian Atoka Formation were used as the main markers in the cross sections. Therefore, we will first briefly discuss the Pennsylvanian stratigraphy of the area. In the structure section, we will (1) briefly discuss the structural geometry of thrusting in the Wilburton gas-field area mostly by using the data presented in detail by Çemen and others (2001), (2) discuss in detail the structural features of the Red Oak gas-field area, and (3) elaborate on the extension of the structural features of the Wilburton gas field into the Red Oak gas-field area.

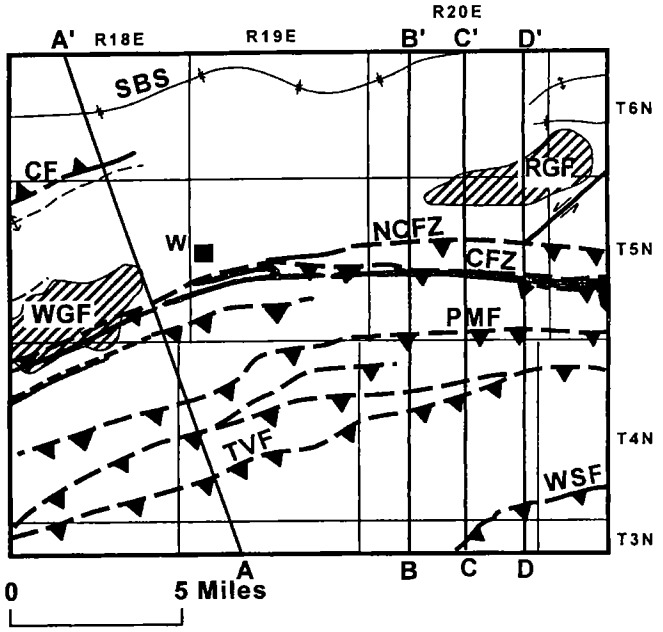

Figure 2. Simplified map of the area between the Wilburton and Red Oak gas fields showing major structural features, outcrops of the Spiro sandstone (dotted pattern), and lines of cross sections. *Abbreviations:* CF = Carbon; CFZ = Choctaw fault zone; NCFZ = Northern Choctaw fault zone; PMF = Pine Mountain fault; RGF = Red Oak gas field; SBS = San Bois syncline; TVF = Ti Valley fault; W = Wilburton; WGF = Wilburton gas field.

STRATIGRAPHY

The area between the Wilburton and Red Oak gas fields contains mostly the exposures of Pennsylvanian rocks (Fig. 1). Pre-Pennsylvanian rocks are encountered only in the subsurface. The Pennsylvanian is represented by rocks of the Atokan and Desmoinesian Series. The various pre-Pennsylvanian rock units of the Arkoma basin and Ouachita Mountains are shown, in a generalized form, in the columnar section of Figure 4. Detailed descriptions of these formations are contained in papers by Ham (1978), Johnson (1988), and Sutherland (1988). Two predominantly shale units of the pre-Pennsylvanian rocks of the Arkoma basin are structurally very important because they host two important detachment surfaces. They are (1) the Upper Devonian to Lower Mississippian (Kinderhookian) Woodford Shale, which unconformably overlies the Hunton Group; and (2) the Lower and middle Mississippian Springer Shale (Fig. 4). Springer is the informal name

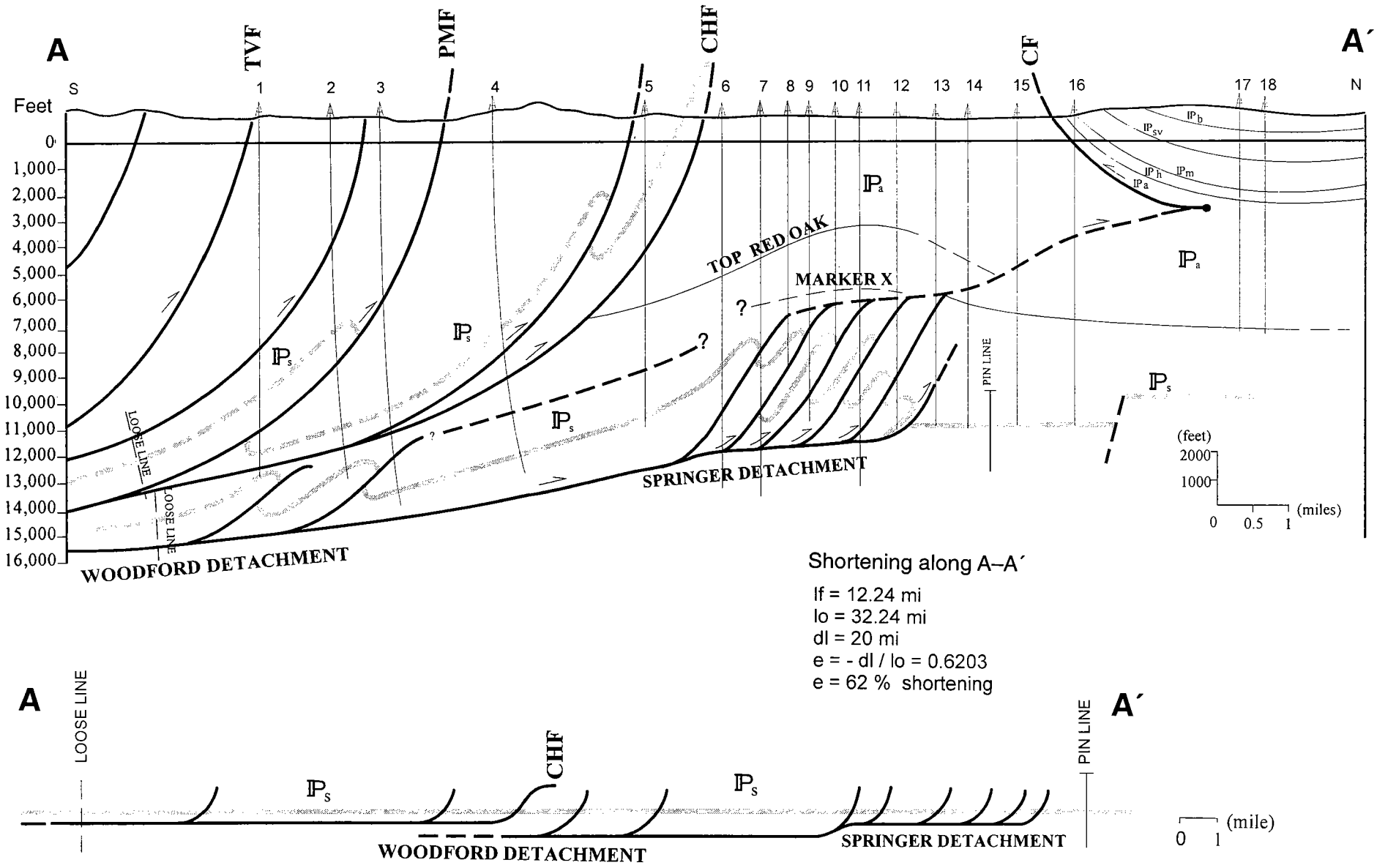

Figure 3. Cross section A–A′ and its restoration. The cross section shows the presence of the Wilburton triangle zone, duplex structure, and other structural features in the Wilburton area. Line of cross section is located on Figure 2. The restored cross section suggests 62.03% shortening along the original length of the Spiro sandstone due to Pennsylvanian thrusting in the area. *Abbreviations:* CF = Carbon fault; CHF = Choctaw fault; LAD = Lower Atokan detachment; PMF = Pine Mountain fault; IPa = Atoka Formation; IPh = Hartshorne Formation; IPm = McAlester Formation; IPs = Spiro sandstone; IPsv = Savanna Formation; TVF = Ti Valley fault.

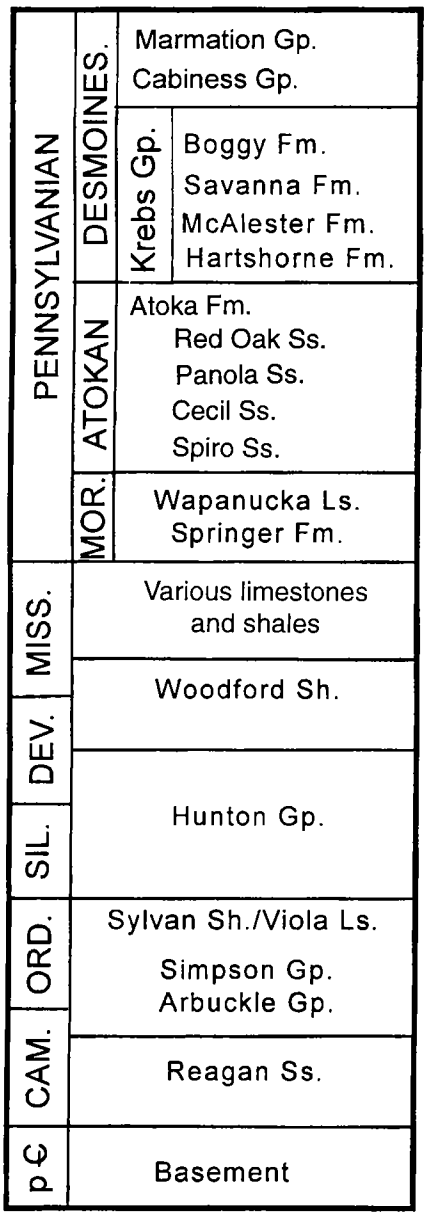

Figure 4. General stratigraphy of Oklahoma portion of the Arkoma basin (modified from Houseknecht and McGilvery, 1990). *Abbreviations:* CAM = Cambrian; DEV = Devonian; MISS = Mississippian; MOR = Morrowan; ORD = Ordovician; SIL = Silurian; p€ = Precambrian.

for the shale unit in the Caney Formation. The lowermost occurrence of siderite or clay-ironstone beds within the Lower and middle Mississippian sequence marks the boundary between the Caney and the informal Springer shale unit, which is Late Mississippian (Chesterian) in age, based on spores and pollen (Ham, 1978).

Pennsylvanian (Morrowan) strata unconformably overlie Mississippian rocks (Fig. 4). Morrowan strata in the Arkoma basin are shelf-like sediments, even though they contain large amounts of sandstone. Time-equivalent units within the Ouachita frontal belt are the Jackfork Group and the Johns Valley Formation, which are deep-marine flysch sediments (Johnson, 1988). Within the Arkoma basin, Morrowan rocks are the Cromwell sandstone, Union Valley Limestone, and the Wapanucka Formation. The Cromwell sandstone and Union Valley Limestone were deposited during a series of transgressions and regressions and consist of several discontinuous limestones and sandstones separated by shales (Sutherland, 1988). The Wapanucka Formation conformably overlies the Union Valley Limestone. The Wapanucka consists of shale and limestone and is exposed together with the Spiro sandstone on the hanging wall of the Choctaw fault. Because the combined thickness of the Wapanucka and Spiro is only about 100 ft, the two units are shown as the Spiro in the simplified map of the area between the Wilburton and Red Oak gas fields (Fig. 2). This simplification is also kept in subsurface identification of the marker beds. In the cross sections (Figs. 3, 5–7), the Wapanucka-Spiro package is shown as the Spiro marker.

The Atoka Formation of the Atokan Series was deposited unconformably on the Wapanucka Formation and is generally divided into lower, middle, and upper Atokan (Fig. 4). The division is based on the effects of syndepositional normal faults on the amount of sediments that accumulated in the basin (Johnson, 1988). The Atoka Formation is by far the thickest formation in the Arkoma basin, ranging from several hundreds of feet to about 20,000 ft (Johnson, 1988). It is roughly 70% shale. Most sandstone units are not continuous, being the result of fluvial and deltaic processes across the sometimes-exposed shelf (Sutherland, 1988).

The lower Atokan is represented by the Spiro sandstone and an overlying persistent shale. Biostratigraphic evidence suggests that the boundary between Morrowan and Atokan ages lies within the first 20–40 ft of persistent shale beds (Houseknecht and McGilvery, 1990). The Spiro sandstone was deposited in a broad delta complex with distal channels, tidal channels, and shallow water with interfingered marine sandstone bars and carbonates (Houseknecht and Kacena, 1983). Detrital constituents of the Spiro were derived from the north and northeast. A regional unconformity between the Atokan and Morrowan is present in the northern margin of the basin. However, in the southern section of the basin, the pre-Atokan unconformity is absent.

The middle Atokan section consists of the Shay, Cecil, Panola, Red Oak, and Fanshawe sandstones within a thick shale sequence. The Cecil, Panola, and Red Oak sandstones (Fig. 4) are used as markers during the cross section constructions because they are easily identifiable and are continuous in the area. The Red Oak sandstone is a major sandstone in this interval and is well observed in the well logs in the area. Vedros and Fisher (1979) interpreted the Red Oak sandstone as being deposited in a submarine-fan environment. Sediments were derived from the eastern uplift of the Ouachita orogenic belt (Houseknecht and McGilvery, 1990).

The predominant lithologies in the upper Atokan are shallow-shelf and deltaic rocks (Sutherland, 1988).

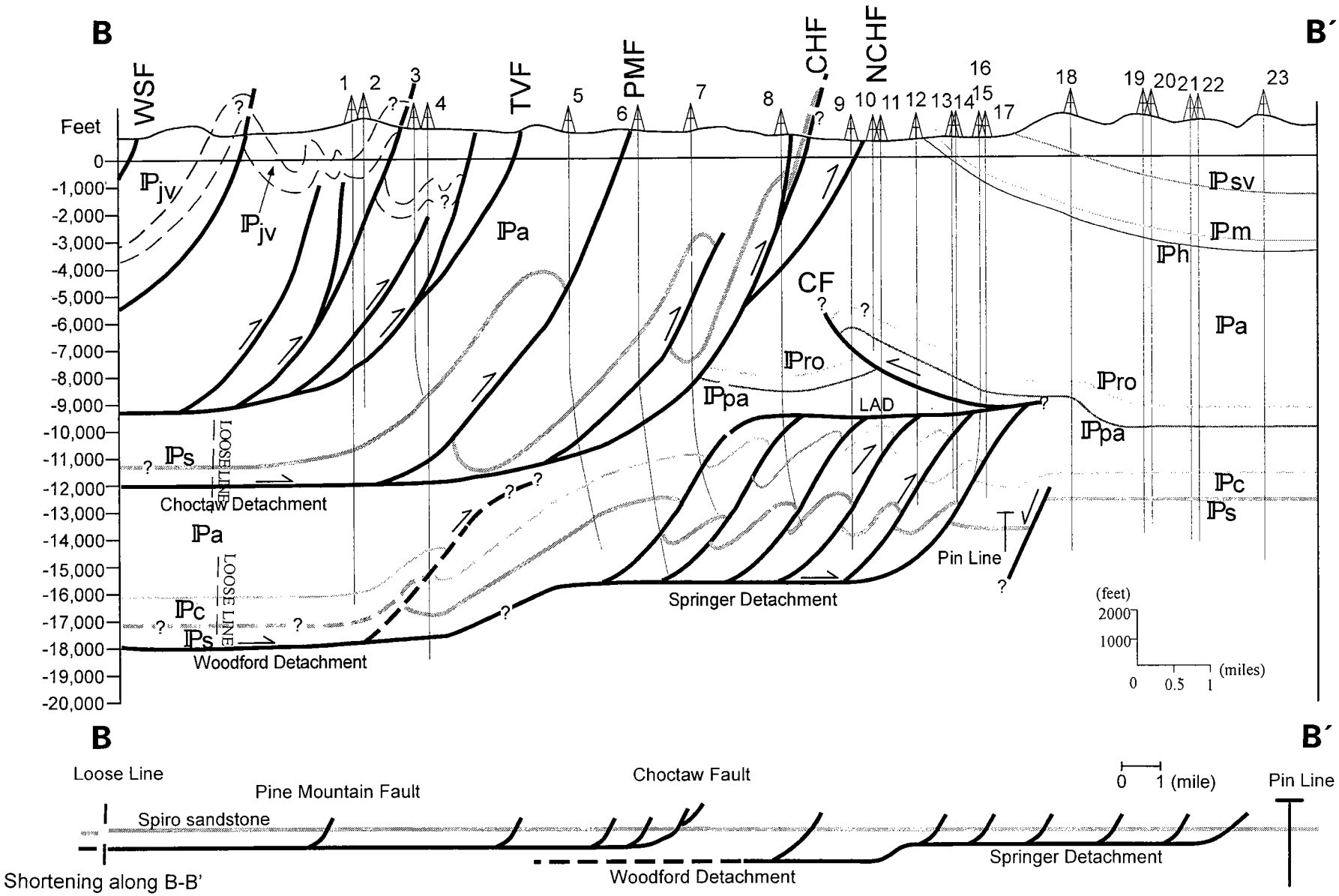

Lf = 31.625 in = 11.9 mi
Lo = 84.5 in = 31.5 mi
dL = Lf - Lo = -20.02
e = -dL / Lo = 0.625
e = 62.5 % shortening

Figure 5. Cross section B–B′ and its restoration. The cross section shows the eastern continuation of the Wilburton Triangle zone and other structural features in Red Oak gas-field area. Line of cross section is located on Figure 2. The restored cross section suggests 62.6% shortening along the original length of the Spiro sandstone due to Pennsylvanian thrusting in the area. *Abbreviations:* CF = Carbon fault; CHF = Choctaw fault; NCHF = Northern Choctaw fault; LAD = Lower Atokan detachment; PMF = Pine Mountain fault; IPc = Cecil sandstone; IPro = Red Oak sandstone; IPh = Hartshorne sandstone; IPjv = Johns Valley Formation; IPm = McAlester Formation; IPpa = Panola sandstone; IPs = Spiro sandstone; IPsv = Savanna Formation; TVF = Ti Valley fault; WSF = Winding Stairs fault.

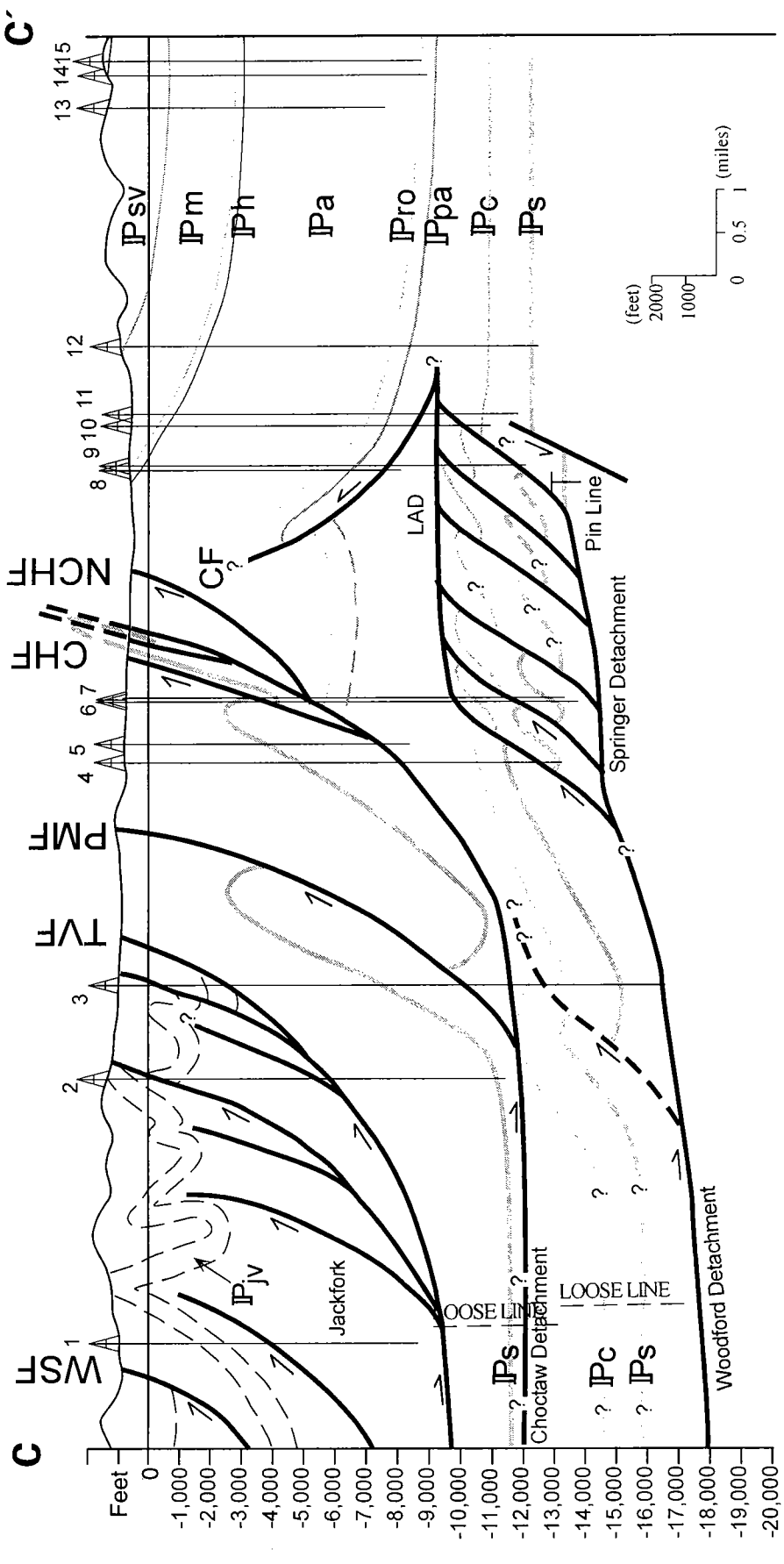

Figure 6. Cross section C–C′ showing the structural features of the Red Oak gas-field area. Line of cross section is located on Figure 2. *Abbreviations:* CF = Carbon fault; CHF = Choctaw fault; NCHF = Northern Choctaw fault; LAD = Lower Atokan detachment; PMF = Pine Mountain fault; IPc = Cecil sandstone; IPro = Red Oak sandstone; IPh = Hartshorne Formation; IPjv = Johns Valley Formation; IPm = McAlester Formation; IPpa = Panola sandstone; IPs = Spiro sandstone; IPsv = Savanna Formation; TVF = Ti Valley fault; WSF = Winding Stairs fault.

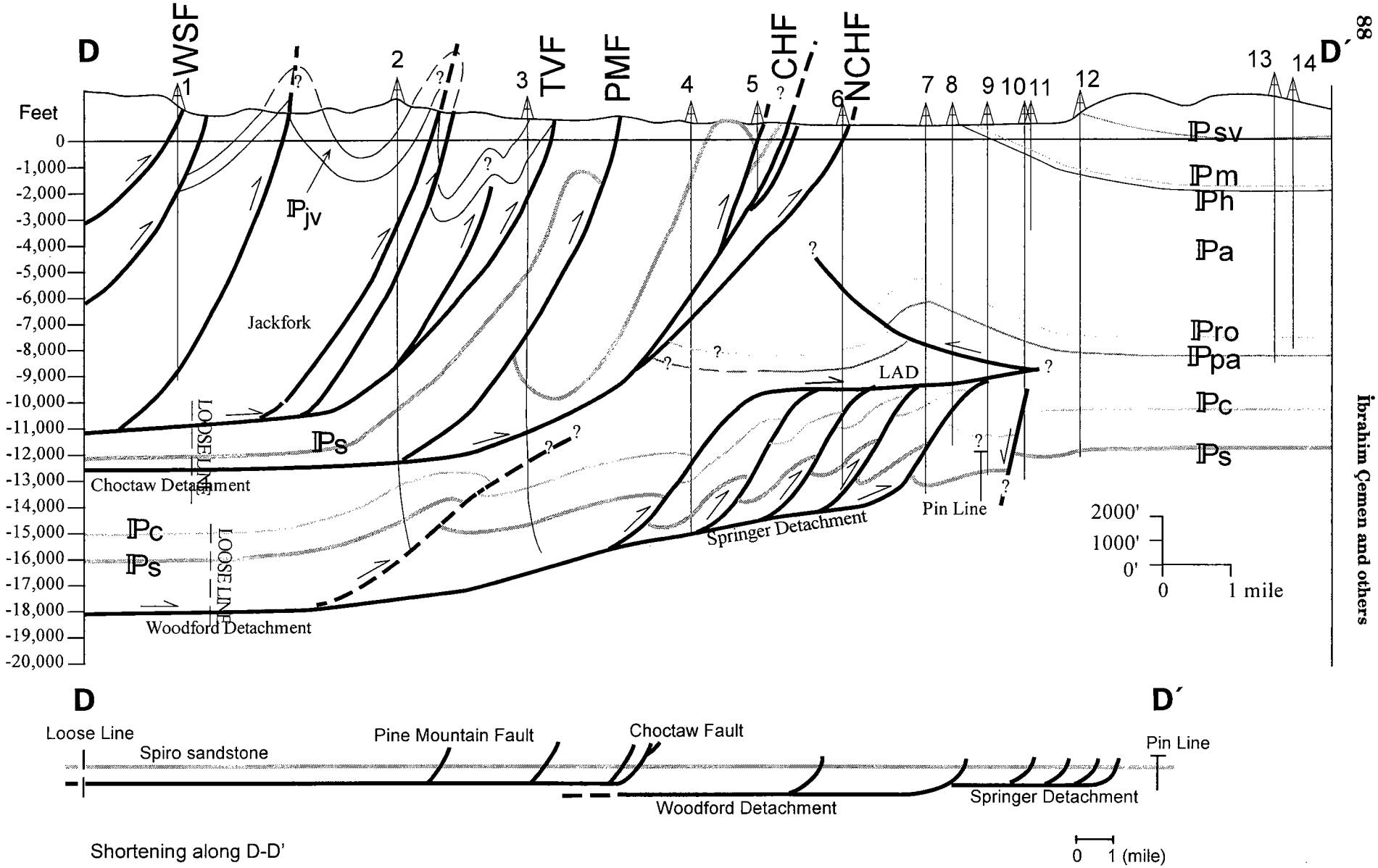

Shortening along D-D'

Lf = 11.3 mi
Lo = 30.9 mi
dL = Lf - Lo = -19.6
e = - dL / Lo = 0.634
e = 63.4 % shortening

Figure 7. Cross section D–D′ showing the structural features in the eastern part of the Red Oak gas-field area. Line of cross section is located on Figure 2. The restored cross section suggests 63.4% shortening along the original length of the Spiro sandstone due to Pennsylvanian thrusting in the area. *Abbreviations:* CF = Carbon fault; CHF = Choctaw fault; NCHF = Northern Choctaw fault; LAD = Lower Atokan detachment; PMF = Pine Mountain fault; Pc = Cecil sandstone; Pro = Red Oak sandstone; Ph = Hartshorne Formation; Pjv = Johns Valley Formation; Pm = McAlester Formation; Ppa = Panola sandstone; Ps = Spiro sandstone; Psv = Savanna Formation; TVF = Ti Valley fault; WSF = Winding Stairs fault.

Upper Atokan strata are not cut by the normal faults that controlled sedimentation patterns within the middle Atokan. The lower shales could have compacted and absorbed the displacement along the faults, rendering the upper Atokan unfaulted (Sutherland, 1988). A cessation of normal faulting due to decreased bending of the loaded lower plate also could have left the upper Atokan unfaulted.

The Desmoinesian Series within the Arkoma basin consists of the Krebs, Cabaniss, and Marmation Groups (Fig. 4). Within the study area only the Krebs Group crops out. The Krebs Group is composed of the Hartshorne, McAlester, Savanna, and Boggy Formations. The Hartshorne Formation gradationally overlies the Atoka Formation. Sutherland (1988) interpreted the Hartshorne Formation as being deposited in high constructive, tidally influenced deltaic systems. The overlying McAlester to Boggy sequence consists of fluvial/deltaic sediments deposited during a series of transgressions and regressions (Sutherland, 1988).

STRUCTURAL GEOLOGY

The area between the Wilburton and Red Oak gas fields contains well-developed south-dipping thrust faults. Hanging-wall anticlines and footwall synclines are also well developed between the thrust faults. The northernmost south-dipping thrust of the frontal Ouachitas is the Choctaw fault, which is the structural boundary between the Ouachita Mountains and the Arkoma basin in Oklahoma (Figs. 1, 2).

Southwest of the town of Wilburton, the Choctaw thrust forms a northward splay (Suneson and others, 1989). From here eastward, we refer to the northernmost fault as the Northern Choctaw fault, and to the one to the south of it as the Main Choctaw fault (Fig. 2). The Lower Atokan Spiro sandstone is well exposed at the surface on the hanging wall of the Main Choctaw fault (Fig. 2). It is not exposed, however, on the hanging wall of the Northern Choctaw fault. Moreover, the subsurface data indicate that the fault-wedge block between the Main and Northern Choctaw faults contains no Spiro (Figs. 5–7), whereas the Spiro sandstone is present in the footwall of the Choctaw fault zone. The absence of the Spiro sandstone on the hanging wall of the Northern Choctaw fault both on the surface and in the subsurface suggests that the Main Choctaw fault was formed after the deposition of the Spiro sandstone and that the Northern Choctaw fault was formed after the Main Choctaw fault. This relationship, in turn, indicates a break-forward sequence of thrusting between the Northern and Main branches of the Choctaw fault zone. If so, we suggest that the imbricate thrust faults that are well developed on the hanging wall of the Main Choctaw fault may also have developed by a break-forward sequence of thrusting (Fig. 2). Some of these imbricate thrusts extend the entire length of the frontal Ouachitas. If our interpretation is correct, these thrusts would be getting older southward. In other words, within the area of Figure 2, the oldest thrust would be the Winding Stairs fault, and the thrusting would be getting younger northward. The Ti Valley fault would be younger than the Winding Stairs thrusts and older than the Pine Mountain fault.

Wilburton Gas-Field Area

The presence of a well-developed triangle zone in the Wilburton area has been proposed by Çemen and others (1994, 1997) and Al-Shaieb and others (1995) based on eight balanced structural cross sections constructed during the OCAST project. The geometry of this triangle zone, named here as the Wilburton triangle zone, is similar to the triangle zones in the transition zones of other compressional fold-thrust belts such as the southern Cordilleran foreland in Canada (Dahlstorm, 1970; Jones, 1982, 1994; Price, 1986; Sanderson and Spratt, 1992) and in the Himalayan foreland in Pakistan (Jadoon and Frish, 1997). The structural features of the Wilburton gas-field area are discussed in detail by Çemen and others (2001). Therefore, we will briefly mention the results of their study below.

The cross section A–A′ (Fig. 3) is the easternmost cross section of Çemen and others (2001) and shows the Wilburton triangle zone between the Arkoma basin and frontal Ouachitas fold-thrust belt in the Wilburton gas-field area. The triangle zone is floored by the LAD and flanked by the Choctaw fault to the south and the Carbon fault to the north. Below the triangle zone is a well-developed duplex structure, which was formed by hinterland-dipping imbricate thrust faults splaying from a floor thrust and joining to the LAD in the Atoka Formation. The LAD continues northward and displaces the Red Oak sandstone before reaching a shallower depth and forming the Carbon fault as a north-dipping backthrust below the San Bois syncline.

Red Oak Gas-Field Area

To the east of the line of the cross section A–A′ (Fig. 2), the Carbon fault disappears on the surface. Therefore the geometry of the eastern continuation of the Wilburton triangle zone was a problem in the mid-1990s. To determine this geometry, we constructed several balanced structural cross sections in the Baker Mountain and Panola 7½′ quadrangles of Oklahoma.

We will describe in this section the structural features of the Red Oak gas field and surrounding areas based on three updated versions of the cross sections originally constructed by Evans (1997). We used concentric folding in our cross sections (Figs. 5–7). We attempted to construct the cross sections using a kink-band style of folding and the ramp-flat thrust model first developed by Suppe (1983) and successfully used by Woodward (1985), Mitra (1986, 1988), and Namson and Davis (1988). We could not use this model, however, because of the presence of competent sandstones scattered in about 15,000-ft–thick incompetent shale units of the Atoka Formation in the frontal Ouachitas and Arkoma basin (Ramsay, 1992; Çemen and others, 2001).

Cross sections B–B′ through D–D′ (Figs. 5–7) are constructed perpendicular to the tectonic transport

direction. Therefore, they show displacements along the thrust faults when appropriate piercing points are located in the hanging wall and footwall of the thrust faults. The Atoka shale is the dominant rock unit both at the surface and in the subsurface. It contains many recognizable prominent component sandstones. Therefore, the prominent sandstone units such as Spiro, Cecil, Panola, and Red Oak sandstone, are used to define the subsurface structural geometry because of their recognizable well-log signature in all cross sections (Figs. 5–7). The Wapanucka Formation and the Spiro sandstone are not identified individually, but the entire thickness is referred to as the Spiro and is assumed to have uniform thickness. Like the Spiro sandstone, the Cecil, Panola, and Red Oak sandstones are identified in the logs at their tops, and their thicknesses are considered to be constant throughout the study area. Other units identified in the cross sections include the Hartshorne Sandstone and the McAlester, Savanna, and Boggy Formations.

Choctaw Fault Zone and Associated Structures

The hanging-wall block of the Choctaw fault zone contains several south-dipping thrusts, including the Pine Mountain fault. These thrusts are interpreted as joining the Choctaw fault zone where it begins to "flatten out" to the south. They form a leading imbricate fan structure with the Choctaw fault zone as the leading thrust. Perry and Suneson (1990) suggested about 6 mi of shortening along the Choctaw fault.

Available seismic data used to construct the cross sections in the Red Oak Oil gas-field area suggest that the Choctaw and Pine Mountain faults lose their dips and become listric at depth. The cross sections (Figs. 5–7) show these faults connected to a detachment surface. Wells on the hanging wall of the Choctaw fault penetrate the Spiro sandstone at two to three places (Figs. 3, 5–7). Cross section B–B′ (Fig. 5) contains two indications of horizontal Spiro sandstone. The first is just below the Ti Valley fault at around –11,000 ft and the second is at approximately –17,000 ft. The horizontal nature of the two Spiro units indicates that a detachment surface must be present between them. Because the Choctaw fault is the leading-edge thrust, the detachment is named here the Choctaw detachment. The Choctaw and Pine Mountain faults are branches from this detachment (Figs. 5–7). Çemen and others (2001) proposed that the Choctaw detachment was a branch off the Woodford detachment. This splay must have occurred to the south of the area of the cross sections B–B′, C–C′, and D–D′ (Figs. 5–7).

The geometry of the footwall block of the Choctaw thrust is different from that of the hanging-wall block. The footwall block of the Choctaw fault displays two detachment surfaces, a duplex structure, and a triangle zone.

Basal Detachments and Duplex Structure

The two basal detachments in the footwall block of the Choctaw fault are the Woodford and Springer detachments. The Woodford detachment is named for the Woodford Shale, which is the "host" for the fault (Hardie, 1988). It is a gently southward-sloping detachment that is about 18,000 ft below sea level. In the eastern part of the area of Figure 2 along cross section A–A′ (see Fig. 3), the Woodford detachment acts as a floor thrust for the Gale-Buckeye thrusts (Wilkerson and Wellman, 1993). The Gale-Buckey thrusts must have joined together in the area between the cross sections A–A′ and B–B′ (Fig. 2) because we could find only one possible thrust fault along the cross sections B–B′, C–C′, and D–D′ (Figs. 5–7) based on our interpretation of available seismic and well data.

Northward along the Woodford detachment, the décollement rises to the level of the "Springer" Shale (Figs. 5–7) and is called the Springer detachment, which is approximately 16,000 ft below sea level. This ramp may have been caused by a normal fault in the pre-Pennsylvanian rocks of the Arkoma basin. The Springer detachment propagates northward into the basin and loses its separation under the San Bois syncline, which marks a change from the strongly folded and faulted rocks to mildly folded rocks of the Arkoma basin.

The placement and recognition of these detachments were based on available data. The Springer and Woodford Shales are at depths such that only a few well logs encountered them. Where no data were available, the detachments were placed by interpolation. The vertical distance between the base of the Spiro sandstone and the top of the Springer or Woodford Shales was recorded from logs of nearby wells and extrapolated in the cross sections to approximate the depth to detachments.

Above the Springer detachment in the northern part of the T. 5 N. and R. 20 E. along the cross sections B–B′, C–C′, and D–D′ (Figs. 5–7), the Spiro and Cecil sandstones are repeated in many wells that were drilled in the area. This suggests the presence of small thrust faults that displace the sandstones. This geometry could be interpreted in two ways: (1) the sandstones are displaced by blind thrust faults that die out in the shaly part of the Atoka Formation above the Cecil sandstone, or (2) a roof thrust above the Cecil sandstone separates the imbricately thrusted section below from the folded section above. Çemen and others (2001) provided evidence for the second interpretation in the Wilburton gas-field area. The available seismic lines in the Red Oak gas-field area, donated by Amoco, suggest the presence of a backthrust below the southern limb of San Bois syncline. The backthrust dies out into the Atoka Formation where a zero-displacement point exists (Figs. 5–7) that should be connecting to a very low angle detachment surface in the manner proposed by Jones and others (1982) in the foothills of the southern Canadian Rockies. We follow the interpretation of Çemen and others (2001) and call this the Lower Atokan detachment, which acts as a roof thrust for the small-scale thrust faults that are splayed from the Springer detachment surface (floor thrust). This geometry defines a duplex structure as it is defined by Boyer and Elliott (1982), and it has been well recognized in

many parts of the world (Woodward, 1985; Mitra, 1986, 1988).

The placement of horses within the duplex structure is inferred along the cross sections (Figs. 5–7) based on the depths of the Spiro and Cecil sandstones in the well logs that were used to construct the cross sections (see Appendix). The thrust faults separating the horses are shown as hinterland-dipping thrusts in conjunction with the break-forward sequence of thrusting that has been established in the hanging wall of the Choctaw thrust fault.

The LAD is somewhat arbitrarily located above the Cecil sandstone. The seismic profiles do not provide a well-developed velocity contrast, and the well logs do not suggest a characteristic log signature for the roof thrust. The absence of supporting evidence for the roof thrust most probably arises because the LAD is propagating within the shales of the Atoka Formation (Çemen and others, 2001). The LAD is approximately 12,000 ft below sea level. It has a gradual ramp to the north of the leading thrust of the duplex structure and becomes a backthrust above the Cecil sandstone (Figs. 5–7).

Wilburton Triangle Zone

The Wilburton triangle zone is formed by the south-dipping Choctaw fault to the south and the north-dipping Carbon fault to the north (Fig. 3). The LAD floors the zone. Just to the east of the line of the cross section A–A′ (Fig. 2), the Carbon fault disappears on the surface. The seismic lines in the Red Oak gas field suggest the presence of a blind backthrust in the subsurface in the position of the Carbon fault. Therefore, we have shown this fault as the Carbon fault along cross sections B–B′, C–C′, and D–D′ (Figs. 5–7). Although its subsurface geometry in R. 19 E., T. 5 N., between the lines of cross sections A–A′ and B–B′, remains to be determined, the Carbon fault might be making a lateral ramp to the east and may become a blind backthrust. Therefore, the north-dipping blind thrust that we see in the available seismic line in the Red Oak gas-field area should be the subsurface continuation of the Carbon fault (Figs. 5–7). This geometry shortens the north-south width of the triangle zone by about 50% (Figs. 2, 3, 5–7).

This study suggests that the Wilburton triangle zone (Çemen and others, 2001) continues into the Red Oak gas-field area. The triangle zone is flanked by the south-dipping Choctaw fault to the south and the north-dipping Carbon fault to the north. The LAD was propagated under the San Bois syncline until it became hindered and could not propagate farther. The LAD floors the triangle zone. When this happened, the detachment reached the zero-displacement point and a backthrust formed. This backthrust should be the subsurface equivalent to the Carbon fault that can be mapped at the surface in the Wilburton area. The presence of the backthrust is evidenced by relatively flat-lying Spiro and Cecil units and increasingly steeply dipping Panola and Red Oak sandstones above them along the cross sections (Figs. 5–7), which indicate a flat-lying Cecil sandstone below an upraised northward-dipping section of Red Oak and Panola sandstones. This north-dipping backthrust together with the south-dipping Choctaw fault zone form a triangle zone that is similar in some aspects to the ones proposed by Arbenz (1989) and Camp and Ratliff (1989) and is something of a hybrid between the two. Whether the Carbon fault intersects the Choctaw fault in the subsurface is unknown. Lack of well control in the proposed intersection zone makes it impossible to place the intersection. Likewise, the exact location of the zero-displacement point along the LAD-backthrust zone is difficult to determine with accuracy.

The triangle zone in the Wilburton area and the one in the Red Oak area are geometrically different because the Choctaw fault and the backthrust are much closer together in the Red Oak gas-field area than they are in the Wilburton area. This difference could be caused by a change in aspect of either fault. The duplex structure in the Red Oak area also shows some geometric differences from the one in the Wilburton area. Çemen and others (2001) reported the presence of five horses in the duplex structure in the Wilburton area (Fig. 3). We determined five horses in the duplex structure along cross sections B–B′ and C–C′ (Figs. 5, 6). Two of the small thrust faults must have joined together laterally between cross sections C–C′ and D–D′. Therefore, we could only identify four horses along the cross section D–D′.

Structural cross sections constructed by Mehdi (1998) suggest that the triangle zone also continues to the east in R. 21 E., T. 5 N., where the duplex structure is also present below the triangle zone. However, the number of horses within the duplex structure lessens down to three in that area.

Restored Cross Sections and Amount of Shortening

The balanced structural cross sections constructed in the Red Oak gas-field area (Figs. 5–7) are restored using the key-bed restoration method to calculate the amount of shortening for the Spiro sandstone. The Spiro sandstone is the only competent rock unit that is found in the footwall and hanging wall of the Choctaw fault zone. Consequently, we could restore the cross sections only by using the Spiro Sandstone as the key bed.

The pin lines for the restored cross sections are located to the north of the leading thrust of the duplex structure, where the Spiro sandstone is not affected by shortening in the frontal zone. The loose lines are located to the south, where there is no piercing point for the thrusted Spiro sandstone.

Although the geometry of the triangle zone changes substantially from the Wilburton area eastward to the Red Oak gas-field area, the amount of shortening seem to remain similar. We have found 62.2% shortening along the line of cross section B–B′ (Fig. 5) and 63.4% shortening along the line of cross section C–C′ (Fig. 6). In the Wilburton gas-field area, Çemen and others (2001) reported about 60% shortening for the Spiro

sandstone. Figure 3 is the easternmost cross section published by them and shows 62% shortening.

Normal and Strike-Slip Faults

The area between the Wilburton and Red Oak gas fields also contains down-to-the-south normal faults present in the northern part of the cross sections to the north of the leading imbricate thrust of the duplex structure (Figs. 3, 5–7). These faults are delineated based on the seismic and well-log data and have a general trend of east-west to east-northeast, paralleling the trend of the basin. Koinm and Dickey (1967) reported an abrupt increase in the thickness of the middle and lower Atokan along the normal faults and revealed that these faults were formed as growth faults. They also pointed out the presence of the turbidite-facies rocks present in the lower and middle Atoka as another line of evidence for active growth faults during the Atokan sedimentation. Therefore, these normal faults are interpreted as remnant structures from the breakdown of the continental shelf during the Pennsylvanian and as older than the thrust faults in the Ouachitas.

The cross sections (Figs. 3, 5–7) suggest that the normal faults displace the Spiro sandstone, but their displacement does not reach into the middle Atokan units such as the Cecil. Also, their extent into the pre-Atokan units could not be determined because of the absence of subsurface data below the Spiro sandstone. In the absence of enough well control, the normal faults and the Spiro sandstone are mostly inferred from the adjacent cross sections. The seismic profiles suggest the presence of normal faults below the basal detachment surfaces. Ferguson and Suneson (1988) proposed that these faults acted as barriers to the thrust faults to form a tectonic ramp from one incompetent unit to another such as the one from the Woodford Shale to the Springer Shale.

Strike-slip faults are shown on the geologic map by Hemish and others (1990a). These faults have right-lateral movement and can be classified as tear faults. The tear faults are oriented in two directions. Faults in the footwall of the Choctaw fault are oriented in a northeast-southwest direction. Faults in the hanging wall of the Choctaw fault are oriented with a southeast-northwest trend. These trends suggest a conjugate shear-fracture origin for these strike-slip faults.

CONCLUSIONS

Structural geometry and strain partitioning along the frontal Ouachita–Arkoma basin transition zone have been controversial during the 1980s and 1990s. Çemen and others (2001) proposed the presence of a triangle zone in the Wilburton gas-field area, where deformation is partitioned from the strongly faulted and folded frontal Ouachitas to the mildly folded Arkoma basin. This triangle zone, named here as the Wilburton triangle zone, is similar to the triangle zones that are delineated in transition zones in the southern Cordilleran foreland in Canada (Dahlstorm, 1970; Jones, 1982, 1994; Price, 1986; Sanderson and Spratt, 1992) and in the Himalayan foreland in Pakistan (Jadoon and Frish, 1997). This interpretation requires a zero-displacement point along the transition zone, where deformation changes from fold-thrust style in the frontal belt to folding in the foreland.

The Wilburton triangle zone is flanked by the south-dipping Choctaw fault to the south and the north-dipping Carbon fault to the north and is floored by the LAD (Fig. 3). The surface trace of the Carbon fault disappears to the east of the Wilburton area. The north-dipping Choctaw fault and associated structures are the dominant structural features in the Red Oak gas-field area on the surface. However, available seismic-reflection profiles indicate a north-dipping fault to the north of the Choctaw fault. This fault is interpreted here as the eastern continuation of the Carbon fault (Figs. 5–7). Therefore, we suggest that, in the Red Oak gas-field area, the Carbon fault is in the subsurface to the north of the Choctaw fault zone as a blind backthrust. Therefore, the Red Oak gas-field area contains the eastern continuation of the Wilburton triangle. Although the details of the subsurface geometry between the lines of cross sections A–A′ and B–B′ (Fig. 2) remain to be determined, it seems the Carbon fault makes a lateral ramp to the east so that it can be observed in the seismic lines as a blind backthrust. The triangle zone continues eastward as far east as the eastern end of the Red Oak gas field, where (1) it is still flanked by the Choctaw fault to the south and the Carbon fault to the north and is floored by the LAD, and (2) its north-south length shortens by about 50% with respect to its north-south length in the Wilburton gas-field area (Figs. 2, 3, 5–7).

The duplex structure that is well developed in the Wilburton area is also present in the Red Oak gas-field area. We determined five horses in the duplex structure in the western end of the Red Oak gas-field area (Fig. 5). However, we could determine only four horses in the eastern end of the Red Oak gas-field area (Fig. 7). Two of the small thrust faults that define a horse must have joined together laterally between the cross sections C–C′ (Fig. 6) and D–D′ (Fig. 7).

When restored to their position at the time of the Spiro deposition by using the key-bed restoration method, the cross sections indicate over 60% shortening both in the Wilburton and Red Oak gas-field areas (Figs. 3, 5, 7), although some geometric changes have been delineated between the two areas.

The hanging wall of the Choctaw fault, the leading edge thrust of the Ouachita fold-and-thrust belt, contains several south-dipping imbricate thrust faults. A northward splay branches from the Choctaw thrust just southwest of the Wilburton (Suneson and Ferguson, 1989). In the Red Oak area, we name the northernmost fault as the Northern Choctaw fault and the one to the south of it as the Main Choctaw fault (Fig. 2). The hanging wall of the Main Choctaw fault contains the Spiro sandstone, whereas the sandstone is absent on the hanging wall of the Northern Choctaw fault. Moreover, the fault wedge block between the Main and Northern Choctaw faults contains no Spiro (Figs. 5–7). This geometry suggests that the Main Choctaw fault

was formed after the deposition of the Spiro sandstone and that the Northern Choctaw fault was formed after the Main Choctaw fault. This relationship indicates a break-forward sequence of thrusting between the Northern and Main Branches of the Choctaw fault similar to the mechanism first proposed by Boyer and Elliot (1982). If this interpretation is correct, we suggest the imbricate thrust faults well developed on the hanging wall of the Main Choctaw fault may also have developed by a break-forward sequence of thrusting (Fig. 2).

ACKNOWLEDGMENTS

We thank Neil Suneson, Leroy Hemish, James Puckette, and Peter D'onfro for helpful discussions during the various stages of this investigation. This study was supported by a grant from Oklahoma State University Energy Center (UCER).

REFERENCES CITED

Al-Shaieb, Z.; Çemen, I.; and Cleaves, A., 1995, Overthrusted natural gas reservoirs in the Arkoma basin: Final Report, OCAST Project No. AR2-025:4391, 153 p.

Arbenz, J. K., 1989, The Ouachita system, *in* Bally, A. W.; and Palmer, A. R. (eds.), The geology of North America—an overview: Geological Society of America, The Geology of North America, v. A, p. 371–396.

Bertagne, A. J.; and Leising, T. C., 1989, Seismic exploration of Ouachita frontal fairway, southeastern Oklahoma: Oil and Gas Journal, v. 87, no. 4, p. 88–90.

Boyer, S. E.; and Elliot, D., 1982, Thrust systems: American Association of Petroleum Geologists Bulletin, v. 66, p. 1196–1230.

Camp, W. K.; and Ratliff, R. A., 1989, Balanced cross section through Wilburton gas field, Latimer County, Oklahoma: implications for Ouachita deformation and Arbuckle (Cambro–Ordovician) exploration in Arkoma basin [abstract]: American Association of Petroleum Geologists Bulletin, v. 73, p. 1044.

Çemen, I.; Al-Shaieb, Z.; Feller, R.; and Akthar, S., 1994, Preliminary interpretation of a seismic profile and the Spiro reservoir pressure data in the vicinity of the Wilburton gas field, *in* Suneson, N. H.; and Hemish, L. A. (eds.), Geology and resources of the eastern Ouachita Mountains frontal belt and southeastern Arkoma basin, Oklahoma: Oklahoma Geological Survey Guidebook 29, p. 249–251.

Çemen, I.; Al-Shaieb, Z.; Hess, F.; Akthar, S.; and Feller R., 1995, Geometry of thrusting in Wilburton gas field and surrounding areas, Arkoma basin, Oklahoma: implications for gas exploration in the Spiro sandstone reservoirs [abstract]: American Association of Petroleum Geologists Bulletin, v. 79, p. 1401.

Çemen, I.; Al-Shaieb, Z.; Sagnak, A.; Feller, R.; and Akthar, S., 1997, Triangle zone geometry of the frontal Ouachitas in the Wilburton area, Arkoma basin, Oklahoma: implications for fault sealing in the Wilburton gas field [abstract]: American Association of Petroleum Geologists, Annual Convention Official Program, v. 6, p. A-19.

Çemen, I.; Sagnak, A.; and Akthar, S., 2001, Geometry of the triangle zone and duplex structure in the Wilburton gas field area of the Arkoma basin, southeastern Oklahoma, *in* Johnson, K. S. (ed.), Pennsylvanian and Permian geology and petroleum in the southern Midcontinent, 1998 symposium: Oklahoma Geological Survey Circular 104, p. 87–98.

Dahlstrom, C. D. A. , 1970, Structural geology in the eastern margin of the Canadian Rocky Mountains: Bulletin of Canadian Petroleum Geology, v. 18, p. 332–406.

Evans, J., 1997, Structural geometry of thrust faulting in the Baker Mountain and Panola quadrangles, southeastern Oklahoma: Oklahoma State University unpublished M.S. thesis, 99 p.

Ferguson, C. A.; and Suneson, N. H., 1988, Tectonic implications of early Pennsylvanian paleocurrents from flysch in the Ouachita Mountains frontal belt, southeast Oklahoma, *in* Johnson, K. S. (ed.), Shelf-to-basin geology and resources of Pennsylvanian strata in the Arkoma basin and frontal Ouachita Mountains of Oklahoma: Oklahoma Geological Survey Guidebook 25, p. 49–61.

Ham, W. E., 1978, Regional geology of the Arbuckle Mountains, Oklahoma: Oklahoma Geological Survey Special Publication 73-3, 61 p.

Hardie, W., 1988, Structural styles of the frontal thrust belt of the Ouachita Mountains, southern Pittsburg County, Oklahoma: Oklahoma Geology Notes, v. 48, p. 232–246.

Hemish, L. A.; Suneson, N. H.; and Ferguson, C. A., 1990a, Geologic map of the Panola quadrangle, Latimer County, Oklahoma: Oklahoma Geological Survey Open-File Report 1-90, scale 1:24,000.

_____ 1990b, Geologic map of the Wilburton quadrangle, Latimer County, Oklahoma: Oklahoma Geological Survey Open-File Report 2-90, scale 1:24,000.

Houseknecht, D. W.; and Kacena, J. A., 1983, Tectonic-sedimentary evolution of the Arkoma basin: Society of Economic Paleontologists and Mineralogists, Mid-Continent Section, v. 1, 119 p.

Houseknecht, D. W.; and McGilvery, T. A., 1990, Red Oak field, *in* Beaumont, E. A.; and Foster, N. H. (eds.), Structural traps II; traps associated with tectonic faulting: American Association of Petroleum Geologists, Treatise of Petroleum Geology, Atlas of Oil and Gas Fields, p. 201–225.

Jadoon, I. A. K.; and Frisch, W., 1997, Hinterland-vergent tectonic wedge below the Riwat Thrust, Himalayan foreland, Pakistan: implications for hydrocarbon exploration: American Association of Petroleum Geologists Bulletin, v. 81, p. 438–448.

Johnson, K. S., 1988, General geologic framework of the field-trip area, *in* Johnson, K. S. (ed.), Shelf-to-basin geology and resources of Pennsylvanian strata in the Arkoma basin and frontal Ouachita Mountains of Oklahoma: Oklahoma Geological Survey Guidebook 25, p. 1–5.

Jones, P. B., 1982, Oil and gas beneath east dipping thrust faults in the Alberta foothills, *in* Powers, K. (ed.), Geologic studies of the Cordilleran thrust belt: Rocky Mountain Association of Geologists Guidebook, v. 1, p. 61–74.

Jones, P. B., 1994, Triangle zone geometry and terminology [abstract]: Western Canadian and international expertise, exploration update; a joint convention of CSEG and CSPG, Calgary, Alberta, p. 69–70.

Koinm, D. N.; and Dickey, P. A., 1967, Growth faulting in the McAlester basin of Oklahoma: American Association of Petroleum Geologists Bulletin, v. 51, p. 710–718.

Mehdi, S., 1998 Geometry and structural evolution of the thrust faults in the Talihina and Red Oak 7.5 minute quadrangles, Latimer County, Oklahoma: Oklahoma State University unpublished M.S. thesis, 93 p.

Millikan, J. V., 1988, Late Paleozoic and early Mesozoic geologic evolution of the Arklatex area: Rice University, Houston unpublished M.S. thesis, 259 p.

Mitra, S., 1986, Duplex structures and imbricate thrust systems; geometry, structural position and hydrocarbon potential: American Association of Petroleum Geologists Bulletin, v. 70, p. 1087–1112.

Mitra, S., 1988, Three dimensional geometry and kinematic evolution of the Pine Mountain thrust system, southern Appalachians: Geological Society of America Bulletin, v. 100, p. 72–95.

Namson, J. S.; and Davis, T. L., 1988, Structural transect of the western Transverse Ranges, California: implications for lithospheric kinematics and seismic risk evaluation: Geology, v. 16, p. 675–679.

Price, R. A., 1986, The southeastern Canadian Cordillera; thrust faulting, tectonic wedging and delamination of the lithosphere: Journal of Structural Geology, v. 8, p. 239–254.

Perry, W. J., Jr.; and Suneson, N. H., 1990, Preliminary interpretation of a seismic profile across the Ouachita frontal zone near Hartshorne, Oklahoma, *in* Suneson, N. H.; Campbell, J. A.; and Tilford, M. J. (eds.), Geology and resources of the frontal belt of the western Ouachita Mountains, Oklahoma: Oklahoma Geological Survey Special Publication 90-1, p. 145–148.

Ramsay, J. G., 1992, Some geometric problems of ramp-flat thrust models, *in* McClay, K. R. (ed.), Thrust tectonics: Chapman and Hall, London, p. 191–200.

Reeves, D. L.; Schreiner, W. P.; and Sheffield, T. M., 1990, Stop 6—New State Mountain (Amoco 1-5 Rosso Unit), *in* Suneson, N. H.; Campbell, J. A.; and Tilford, M. J. (eds.), Geology and resources of the frontal belt of the western Ouachita Mountains, Oklahoma: Oklahoma Geological Survey Special Publication 90-1, p. 37–40.

Roberts, M. T., 1992, Shelf-to-basin transect, eastern Oklahoma: Shreveport Geological Society Guidebook, p. 137–160.

Sagnak, A., 1996, Geometry of the Late Paleozoic thrust system in the Wilburton area: Oklahoma State University unpublished M.S. thesis, 101 p.

Sanderson, D. A.; and Spratt, A. D., 1992, Triangle zone and displacement transfer structures in the eastern front ranges, southern Canadian Rocky Mountains: American Association of Petroleum Geologists Bulletin, v. 76, p. 828–839.

Suneson, N. H., 1988, The geology of the Ti Valley fault in the Oklahoma Ouachita Mountains, *in* Johnson, K. S. (ed.), Shelf-to-basin geology and resources of Pennsylvanian strata in the Arkoma basin and frontal Ouachita Mountains of Oklahoma: Oklahoma Geological Survey Guidebook 25, p. 33–47.

_____ 1995, Structural interpretations of the Arkoma basin–Ouachita Mountains transition zone, southeastern Oklahoma; a review, *in* Johnson, K. S. (ed.), Structural styles in the southern Midcontinent, 1992 symposium: Oklahoma Geological Survey Circular 97, p. 259–263.

_____ 1996, Geologic map of the Hartshorne quadrangle, Latimer and Pittsburg Counties, Oklahoma: Oklahoma Geological Survey Open-File Report 1-96, scale 1:24,000.

Suneson, N. H.; and Ferguson, C. A., 1989, Geologic map of the Baker Mountain quadrangle, Latimer County, Oklahoma: Oklahoma Geological Survey Open-File Report 3-89, scale 1:24,000.

Suppe, J., 1983, Geometry and kinematics of fault-bend folding: American Journal of Science, v. 283, p. 648–721.

Sutherland, P. K., 1988, Late Mississippian and Pennsylvanian depositional history in the Arkoma basin area, Oklahoma and Arkansas: Geological Society of America Bulletin, v. 100, p. 1787–1802.

Tilford, M. J., 1990, Geological review of the Ouachita Mountains thrust belt play, western Arkoma basin, Oklahoma, *in* Suneson, N. H.; Campbell, J. A.; and Tilford, M. J. (eds.), Geology and resources of the frontal belt of the western Ouachita Mountains, Oklahoma: Oklahoma Geological Survey Special Publication 90-1, p. 169–196.

Valderrama, M. H.; Nielsen, K. C.; McMechan G. A.; and Hunter, H., 1994, Three-dimensional seismic interpretation of the triangle zone of the frontal Ouachita Mountains and Arkoma basin, Pittsburg County, Oklahoma, *in* Suneson, N. H.; and Hemish, L. A. (eds.), Geology and resources of the eastern Ouachita Mountains frontal belt and southeastern Arkoma basin, Oklahoma: Oklahoma Geological Survey Guidebook 29, p. 225–241.

Vedros, S. G.; and Visher, G. S., 1979, The Red Oak sandstone: a hydrocarbon-producing submarine fan deposit, *in* Stanley D. J.; and Kelling, G. (eds.), Sedimentation in submarine canyons, fans and trenches: Dowden, Hutchinson and Rose, Stroudsburg, Pennsylvania, p. 292–308.

Wickham, J. W., 1978, The Ouachita foldbelt: a Paleozoic continental margin, *in* Wickham, J.; and Denison, R. (eds.), Field guide to the structural style of the Arbuckle region: Geological Society of America, South-Central Section, Guidebook for field trip no. 3, p. 47–64.

Wilkerson, M. S.; and Wellman P. C., 1993, Three dimensional geometry and kinematics of the Gale-Buckeye thrust system, Ouachita fold and thrust belt, Latimer and Pittsburg Counties, Oklahoma: American Association of Petroleum Geologists Bulletin, v. 77, p. 1082–1100.

Woodward, N. B., 1985, Valley and ridge thrust belt: balanced cross sections, Pennsylvania to Alabama, Appalachian Basin Industrial Associates: University of Tennessee, Studies in Geology, v. 12, 64 p.

APPENDIX: Wells Used in Cross Sections

(Numbers to the right of the well names correspond to the numbers along the cross sections.)

Cross Section A–A′ (D–D′ of Cemen and others, 2001)

1) Anadarko
Robe "A" # 1-25
25-4N-18E

2) Bta
9001 JV-P Amason #1
24-4N-18E

3) Arco
Dollins No. 1-13
13-4N-18E

4) Bta
1-9001 JV-P Mabry
11-4N-18E

5) Coquina
Watts No. 1
34-5N-18E

6) Arco
E.V. Enis No.2
27-5N-18E

7) Arco
R.F. Mc. Alester # 3
22-5N-18E

8) Ambassador
Mc. Alester #2
22-5N-18E

9) Arco
Paschall # 3
21-5N-18E

10) Ambassador
Kilpatrick Unit # 1
16-5N-18E

11) Ambassador
Kilpatrick 2-16
16-5N-18E

12) Jmc Exp.
Toppins State # 2
9-5N-18E

13) Ambassador
Toppins State Unit # 1
9-5N-18E

14) Ambassador
Woods Unit No. 1
4-5N-18E

15) Ambassador
Sawyer Unit # 1
5-5N-18E

16) Sinclair
Mitchell Unit # 1
32-6N-18E

17) Harper Oil
Key # 1
20-6N-18E

18) Ferguson
Key No. 1
20-6N-18E

Cross Section B–B′

1. H&H Star Energy
Bear Suck Knob #1-20 "A"
20-T4N-R20E

2. H&H Star Energy
Bear Suck Knob #1-20
20-T4N-R20E

3. Amoco Production
Green Bay #1-17
17-T4N-R20E

4. Scana Exploration
Green Bay #2-17
17-T4N-R20E

5. H&H Star Energy
Lucky Strike #1-5
5-T4N-R20E

6. Anadarko Petroleum
H&H Cattle Co. #1-31
31-T5N-R20E

7. Anson Corp.
Clear Creek #1-29
29-T5N-R20E

8. Anson Corp
Buzzard Gap #1-19
19-T5N-R20E

9. Humble Oil Co.
Shay #1
17-T5N-R20E

10. Edwin L. Cox
Shay #1
17-T5N-R20E

11. Unit Drilling & Exp.
Harding #1
18-T5N-R20E

12. Williford Energy
Butzer #1-7
7-T5N-R20E

13. Williford Energy
Wiginton #1-7
7-T5N-R20E

14. Unit Drilling
Dear #1
8-T5N-R20E

15. Unit Drilling
Cox #1
8-T5N-R20E

16. Donald C. Slawson
McKee #1-5
5-T5N-R20E

17. Mec Inc
Lively #2
6-T5N-R20E

18. Leede Oil & Gas Inc
Wilburton Mountain #1
31-T6N-R20E

19. Santa Fe Minerals
Pierce #1-30
30-T6N-R20E

20. Tenneco Oil Co.
Pierce #1-29
29-T6N-R20E

21. Tenneco Oil Co.
Swart #1-20
20-T6N-R20E

22. Tenneco Oil Co.
Cecil #1-19
19-T6N-R20E

23. Leben Drilling
Jankowsky #1-18
18-T6N-R20E

Cross Section C–C′

1. H&H Star Energy
Green Bay #1-34
34-T4N-R20E

2. H&H Star Energy
Dipping Vat #1-15
15-T4N-R20E

3. Anson Corp.
Golden #1-10
10-T4N-R20E

4. Anson Corp.
Turney #1-28
28-T5N-R20E

5. Anson Corp.
Blakely #1-28
28-T5N-R20E

6. Anson Corp.
Cox #1-28
28-T5N-R20E

7. Amoco Production
Bauman Jack No. 1
27-T5N-R20E

8. Unit Drilling Co.
Go Lightly #1
9-T5N-R20E

9. Austin Production
Colvard Lm #1
10-T5N-R20E

10. Mustang Production
Cash-Mitchell
3-T5N-R20E

11. Unit Drilling Co.
Hawthorne #1
4-T5N-R20E

12. Mustang Production
Parks #1-33
33-T6N-R20E

13. Texas Oil & Gas Corp.
Parsons #1 "A"
16-T6N-R20E

14. Shell Oil Co.
Parsons #1-16
16-T6N-R20E

15. Dyco Petroleum Corp.
Parsons #A-1
16-T6N-R20E

Cross Section D–D′

1. H&H Star Energy
Middle Mountain #1-36
36-T4N-R20E

2. H&H Star Energy
Devil's Hollow #1-13
13-T4N-R20E

3. Mobil Oil
Long Creek #1-1
1-T4N-R20E

4. Anson Corp.
Long Creek #1-25
25-T5N-R20E

5. Anson Corp.
Boykin #1-24
24-T5N-R20E

6. Anson Corp.
Colley #1-13
13-T5N-R20E

7. Mustang Production
Robinson #1-11
11-T5N-R20E

8. Donald C. Slawson
Abbott #1-12
12-T5N-R20E

9. Donald C. Slawson
Foster #1-1
1-T5N-R20E

10. Kaiser-Francis Oil
Miranda #1
1-T5N-R20E

11. Gulf Oil Co.
Booth #1-1
1-T5N-R20E

12. Mustang Production Co.
Austin #1-36
36-T6N-R20E

13. Midwest Oil Co.
Garrett #1
14-T6N-R20E

14. Barrett Resources
Garrett #3
14-T6N-R20E

A Statistical Method for Correcting Log-Derived Temperatures*

Douglas W. Waples
Consultant
Evergreen, Colorado

Mahadir Ramly
Petronas Carigali Sdn Bhd
Kuala Lumpur, Malaysia

ABSTRACT.—Statistical analysis of subsurface temperatures in the Malay basin has been carried out in order to (1) determine appropriate correction methods and correction factors for temperatures obtained from wireline logs, and (2) investigate the confidence levels associated with those corrections. DST temperatures were taken as "ground truth" for these corrections. For individual log-derived temperatures the correction factor f_S, which is applied to the difference between the measured temperature and the surface temperature, is given by

$$f_S = [-0.1462\text{Ln}(\text{TSC}) + 1.699]/(0.572 \bullet Z^{0.075})$$

where TSC is the time since end of mud circulation in hours and Z is the depth in meters. For temperatures that have already been corrected by extrapolation using Horner plots, f_{HP} is given by

$$f_{HP} = -0.132\text{Ln}(\text{TSC}) + 1.52$$

where TSC is the maximum time since circulation stopped (hours) in the HP set.

Uncertainties in f_S decrease markedly as TSC and depth increase. Uncertainties in f_{HP} decrease as maximum TSC and the number of consistent temperature measurements at a given depth increase.

Although these correction factors were developed using data from a single basin, our experience suggests that they can be used with reasonable confidence in many or most other geological provinces. Additional local calibrations would help test and refine this hypothesis.

INTRODUCTION

Measured down-hole temperatures provide valuable data for estimating present-day temperature profiles in wells, which, in turn, are of great importance in maturity modeling. Unfortunately, estimates of present-day temperatures are often based on log-derived temperatures, which are notoriously unreliable and must always be corrected upward. Methods of correcting log-derived temperatures have been the subject of much research and controversy. This paper uses statistical analysis of the observed differences between log-derived temperatures and drill-stem-test (DST) temperatures to provide improved ways of correcting log-derived temperatures, and of estimating the uncertainties inherent in those corrections.

LOG-DERIVED TEMPERATURE DATA

Log-derived temperature data are normally divided into two groups: those that can be corrected using Horner plots (HPs), which estimate the true formation temperature by extrapolating to infinite time the trend of increasing measured down-hole temperatures with increasing time since the end of mud circulation, and those that cannot. Those that cannot be corrected using Horner plots have historically been corrected by a variety of other methods, all of which are generally considered to be much less reliable than the HP method. Horner plots, in contrast, are widely believed to give

*First published in Petroleum Geoscience, v. 7, 2001, p. 231–240, copyright European Association of Geoscientists and Engineers and the Geological Society of London. Slightly modified and reprinted with permission.

Waples, D. W.; and Ramly, Mahadir, 2001, A statistical method for correcting log-derived temperatures, *in* Johnson, K. S.; and Merriam, D. F. (eds.), Petroleum systems of sedimentary basins in the southern Midcontinent, 2000 symposium: Oklahoma Geological Survey Circular 106, p. 97–110.

very good estimates of true formation temperatures. Both types of data are described in the following two sections.

Single Bottom-Hole Temperature Data

The term "single bottom-hole temperature" (SBHT) as used here refers to a single temperature measured during a logging run. The depth at which the measurement was taken is assumed to be known from the recorded depth of the logging tool. The time since the end of circulation (TSC) is also often known with some reasonable degree of accuracy. In many cases, however, TSC is rounded off, is unknown, or is demonstrably incorrect. In this study each SBHT value was treated independently—that is, they were not combined with or influenced in any way by any other down-hole temperature data.

The most common error in SBHT data is systematic. Because the mud system is not in thermal equilibrium with the surrounding rocks, measured temperatures, which are measured in the mud, are always too low (e.g., Hermanrud, 1988). The time required for thermal re-equilibration of the mud depends on a number of factors, including hole size, initial temperature difference between formation and mud, circulation time, and properties of the drilling mud (Bullard, 1947; Schoeppel and Gilarranz, 1966; Funnell and others, 1996). At a given depth, the amount of error seems to depend largely upon TSC, but no simple and consistent relationship between TSC and the amount of correction has been reported.

It is common to estimate the corrected temperature T_c by simply multiplying the measured temperature T_m by a correction factor f:

$$T_c = f \bullet T_m \quad (1)$$

Although f in equation (1) is often taken to be 1.1 (10% correction), numerous workers have noted that the required correction is generally significantly greater (e.g.,Tanaka and Sato, 1977; Sekiguchi, 1984; Takherist and Hamdi, 1995; Förster and Merriam, 1999; Waples and Ramly, 1995).

A less popular but much more logical option is to apply the correction only to the increase in temperature between the surface and the point at which temperature is measured down-hole. Using this method the corrected temperature T_c is given by

$$T_c = T_s + f \bullet (T_m - T_s) \quad (2)$$

where T_s is the surface temperature. Oxburgh and Andrews-Speed (1981) chose f = 1.15, which yields similar results to a 10% correction using equation (1).

Some workers consider depth to be a good indicator of the amount of required correction. Most studies have found that the absolute amount of correction required is small at shallow depths, reaches a maximum at moderate depths, and then decreases again at great depths (e.g., Speece and others, 1985; Lucazeau and Ben Dhia, 1989; Förster and others, 1997). Gallardo and Blackwell (1999), however, found that greater absolute corrections were required at greater depths in the Anadarko basin.

Although these correction methods have met with some success, they are not highly accurate. Average anticipated uncertainties in temperatures derived by correcting SBHT data on the Norwegian continental shelf are about ±20°C (Christian Hermanrud, personal communication, 1993). Corrections to SBHT data can be expected only to shift the average values upward and to make our estimates better on the average; they cannot remove all our uncertainties.

Horner Plots

If multiple logging runs are made at the same depth, then multiple BHT measurements from a single depth made at different TSCs will usually be available. Although each individual measurement is no better than the SBHT measurements discussed above, the existence of multiple measurements made at the same depth offers us an alternative method of correcting for thermal disequilibrium of the mud, provided the TSC is available for each logging run.

The correction method utilizing multiple BHT data from a single depth relies on Horner plots, a technique originally designed to predict pressure decline (Horner, 1951) using an equation that extrapolates to infinite time:

$$T_c = T_m + A \bullet \log[\Delta t/(t + \Delta t)] \quad (3)$$

where T_c is the "true" formation temperature after full equilibration (that is, at infinite time after circulation ends), T_m is the measured temperature, t is the time of circulation, and Δt is TSC.

As a simplification of Bullard's (1947) line-source model, Horner plots are applied empirically to the problem of temperature correction, without definitive theoretical support (Dowdle and Cobb, 1975; Beck and Balling, 1988; Funnell and others, 1996; see Hermanrud and others, 1990, for a brief historical review). According to Funnell and others (1996), Bullard's (1947) theory dictates that for Horner plots to be valid, temperature measurements cannot be used unless TSC (Δt) exceeds a certain minimum value. This minimum allowable TSC, which varies with hole size, can be calculated as

$$\Delta t >> r^2/4s \quad (4)$$

where r is the borehole radius (in meters) and s is the thermal diffusivity of the mud and rock system (typically about 5×10^{-7} m^2/sec). Using this value for diffusivity, any Δt values used in Horner plots would have to be much longer than 6.9 hours for a 17.5-in. hole, 3.4 hours for a 12.25-in. hole, and 1.6 hours for a 8.5-in. hole. Because these criteria would eliminate all or most short TSC measurements, rigorous enforcement would obviously change the application of Horner plots substantially.

Other factors that affect the confidence in a particular Horner plot are the number of temperature measurements (more is better), the actual TSC values (long is good, and long and short together is good), accurate

recording of time and temperature data without rounding (rounding of short TSC can introduce large errors in the extrapolated temperature), and verification of data from the log headers themselves (human errors are common).

Time of circulation [t in equation (3)] is seldom recorded on logs, but, in most cases, even large errors will not strongly affect results of a HP calculation. Inspection of drilling records is generally necessary if one wishes to obtain t. Lacking further information, it is common to use about 2 hours as a realistic estimate of t.

Although Horner plots have a good reputation, they are, as noted above, highly variable in quality. Moreover, because HP temperatures are derived by extrapolation rather than by direct measurement, they can sometimes be susceptible to much worse errors than SBHT data, especially where TSC is short for all runs. Problems can also arise if the circulation history is not simple, because the HP method is based on the assumption that mud is circulated once for a relatively short period prior to the temperature measurement. If the circulation time is long, or if circulation is started and stopped several times, the method is no longer valid.

In actual practice, Horner plots have been shown to underestimate true formation temperatures, even where the data are of good quality (Dowdle and Cobb, 1975; Beck and Balling, 1988; Hermanrud, 1988). Temperature profiles derived from multiple Horner plots on the Norwegian continental shelf are, on the average, about 7°C too low (Hermanrud, 1988), and, when only a single HP-derived temperature was available, the average error jumped to about 24°C.

METHODOLOGY

In the present study, we have developed an empirical method to correct log-derived temperatures using temperature data from 40 wells in the Malay basin, an extensional offshore basin southeast of the Gulf of Thailand that developed during the Oligocene. The wells, which are distributed throughout the basin, were drilled over a period of about 25 years. The maximum depth penetrated in the wells was about 3,800 m, and the bulk of the temperature data came from between 1,000 and 2,500 m. Each well contained two or more internally consistent DST measurements that permitted establishment of the present-day DST-temperature profile with a good level of confidence. Five other candidate wells were rejected because they had only a single DST measurement or because multiple DST data were not internally consistent.

DST temperatures were taken from well completion reports. All log-derived temperatures and times since circulation were verified by us from log headers. Single BHT data (which include all the data used in making Horner plots as well as log-derived temperatures that could not be used for Horner plots) were available from all 40 wells. Horner plots were available for 31 of the 40 wells.

The intrinsic uncertainty associated with DST measurements was assumed to be about 2°C (Hermanrud, 1988; Hermanrud and others, 1990), although this rather modest estimate of DST errors may be too optimistic (see Hermanrud, 1988). We assumed that the highest measured DST temperatures at any depth gave the best estimate of true formation temperature at that level, because erroneous DST measurements tend to be too low rather than too high. For example, poor fluid flow out of the tested formation and adiabatic expansion of gas can both result in anomalously low DST temperatures. In each well, we discarded all DST values that were more than about 5% lower than the trend of highest DST values in that well. As noted above, we also required that the temperature profile be confirmed by at least two DST temperatures. In most cases, the confirmation came from within the same well, but in two cases it came from another well in the same field. As a result of this quality control, we believe that the DST-temperature profiles in all wells used in this study are known reasonably accurately.

The surface temperature at the sea floor was taken to be 24°C at all well locations. Water depth varies only slightly (from about 55 m to 75 m) across the study area. The mean annual air temperature in the area is about 27°C. The conclusions of this study are insensitive to any possible errors in the estimate of sea-floor temperature, which are certainly small.

We next calculated the steady-state heat flows required to fit each of the individual uncorrected SBHT temperatures, each temperature extrapolated using Horner plots, and the trend of DST temperatures within each well using BasinMod® software (Platte River Associates, Boulder, Colorado, U.S.A.). BasinMod's steady-state thermal calculation considers only basal heat flow and thermal conductivity. It ignores heat loss or gain as a result of sedimentation or erosion, radiogenic contributions, convection, and other sources and sinks for heat. The geothermal gradient across each rock unit is thus directly proportional to the heat flow, which is constant from top to bottom in each well.

Thermal conductivities of the sandstones, shales, and siltstones that dominate the Malay basin were reasonably well known from a previous large study (Wan Ismail Wan Yusoff, 1984). In any case, uncertainties about conductivities will not affect the results of this study, because by taking ratios of heat flows required to fit DST data to heat flows required to fit log temperatures, we are canceling out the effects of uncertainties in both heat flow and conductivity. We could equally well have calculated temperatures using geothermal gradients instead of steady-state heat flows, and thus completely circumvented the conductivity issue. However, by using the heat flow/conductivity method the temperature profiles generally show a slight upward convexity that would be difficult to reproduce using geothermal gradients.

Next, we calculated the ratio of the steady-state heat flow required to fit the DST data, divided by the steady-state heat flow required to fit each SBHT or HP temperature. This ratio gives the correction factor f in equation (2) required to move the SBHT or HP temperature over to the DST temperature profile.

Finally, the results were analyzed statistically. In this way we identified the physical factors controlling the amount of required correction, established standard correction factors for SBHT and HP data, and estimated the confidence level of those corrections.

In this study, we did not address the question of whether the DST temperatures themselves accurately reflect true formation temperatures. Strictly speaking, therefore, the correction factors we derived are simply designed to make log-derived temperatures statistically equivalent to DST temperatures.

RESULTS

Single Bottom-Hole Temperature Data

Temperature profiles derived from uncorrected single bottom-hole temperatures (SBHTs) are much lower than those derived from DSTs (Fig. 1). Although the required correction factors vary widely from one data point to the next, the average correction factor f in equation (2) required to move SBHT data in our study to the DST trends is 1.42, much larger than the factor of 1.15 proposed by Oxburgh and Andrews-Speed (1981).

The uncertainty of this average correction factor is also very large. The standard deviation (σ) in the population of correction factors for all data points is 0.20. Thus, if we do not know the TSC, and if we want to be highly confident (95% certain = 2σ) that we have captured the true temperature within our uncertainty limits, we can only say that the correction factor f lies somewhere between 1.02 and 1.82, with a best estimate of 1.42. These uncertainty limits are obviously much larger than we can tolerate for any geologic application. Thus, if we must use an average correction factor for SBHT data, the temperature data will usually be of little or no practical value.

As Figure 2 shows, however, the amount of correction depends rather strongly on TSC. SBHT measurements made at short TSCs require, on the average, larger corrections than do those made at longer times. If we consider the correction factor (f_S) to be only a function of TSC (in hours), then the equation of the best-fit curve through the data in Figure 2 is

$$f_S = -0.1462\text{Ln}(\text{TSC}) + 1.699 \quad (5)$$

We can test this equation by applying it to each SBHT value and comparing the calculated results with those derived from the DST measurements. Figure 3 plots the ratio of the steady-state heat flow required to fit the DST data divided by the heat flow required to fit the SBHT data corrected according to equation (5). The accuracy of the temperature predictions has been sig-

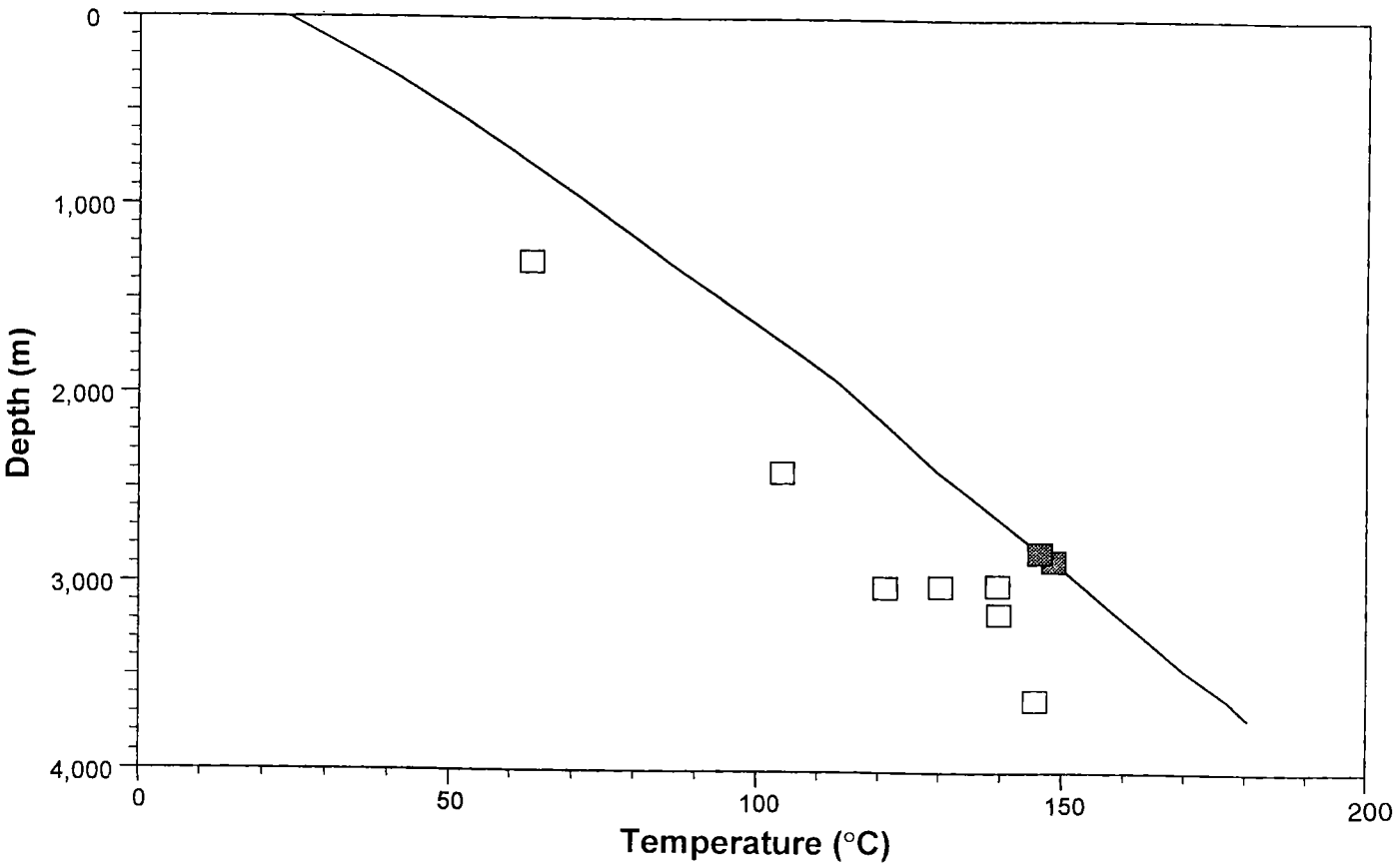

Figure 1. Plot of measured (uncorrected) temperatures with depth in Well A. Solid squares represent drill-stem-test (DST) temperatures; open squares are from logging runs. Line represents calculated present-day–temperature profile to fit DST data. Trends of uncorrected temperatures from logging runs are consistently lower than trends established using DST data.

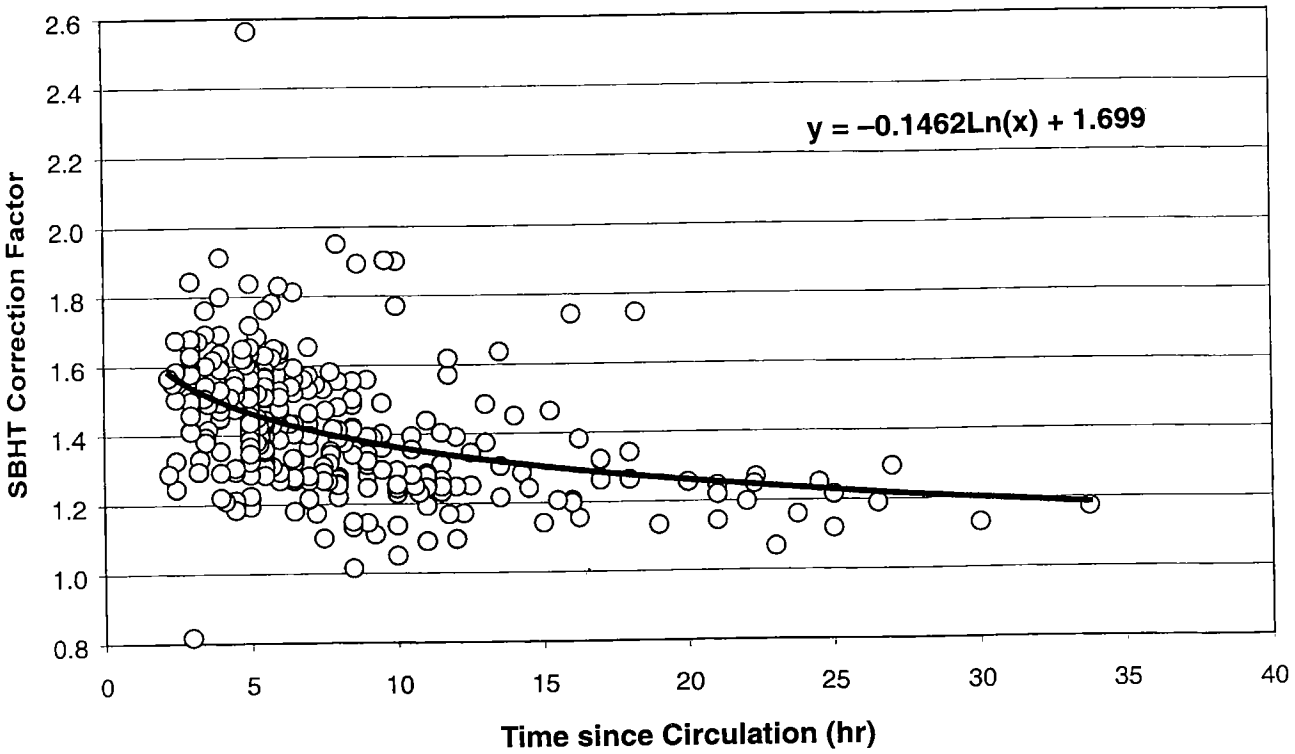

Figure 2. Correction factor f_S [see equation (2)] for individual wireline temperatures (single borehole temperature, SBHT) plotted versus time (in hours) since circulation when each temperature was measured. The line and equation represent the statistical best fit to the data.

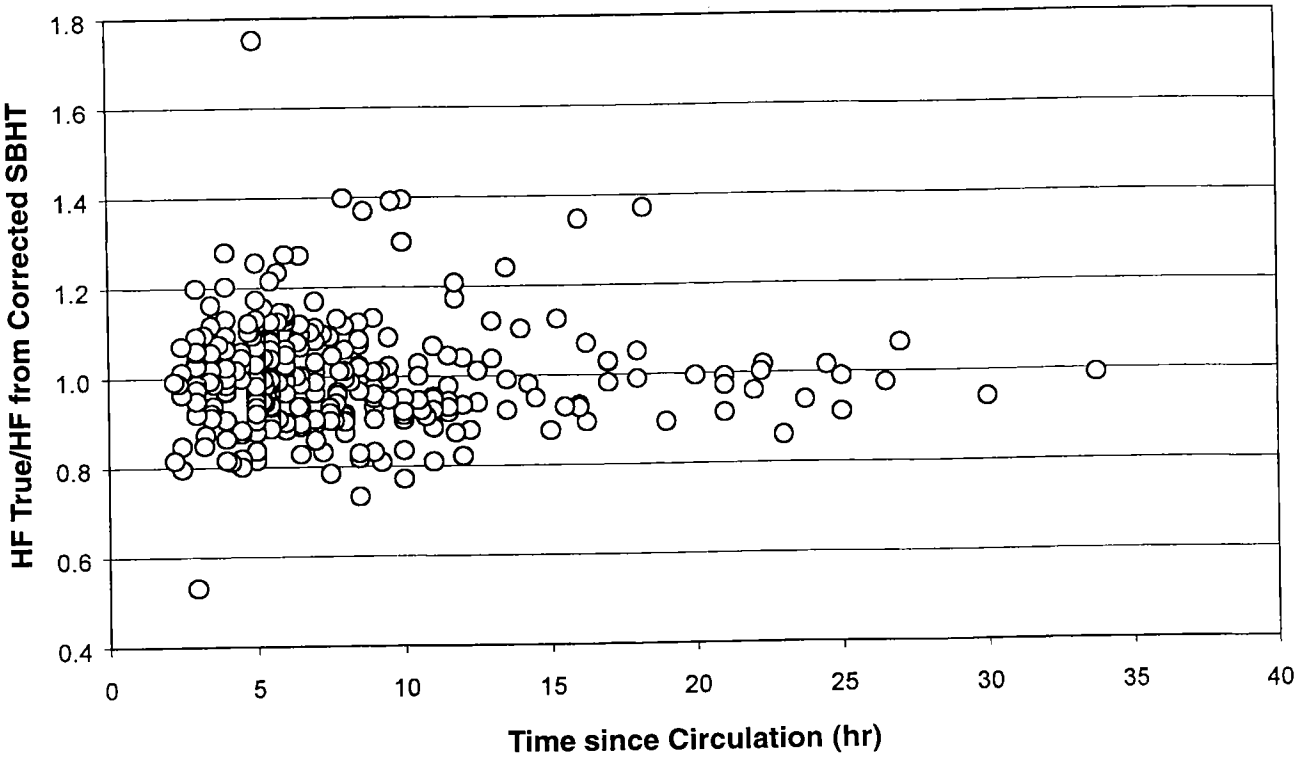

Figure 3. Error factor [ratio of steady-state heat flow required to fit drill-stem-test (DST) data to steady-state heat flow required to fit single bottom-hole ttemperature (SBHT) data corrected according to equation (5)] plotted versus time (in hours) since circulation. A value of 1.0 represents perfect agreement between the "true" temperature interpolated from the trend of DST measurements and the corrected value of a temperature measured during a logging run.

nificantly improved by including TSC (compare Fig. 3 with Fig. 2). However, although equation (5) yields corrected temperatures that are, on the average, equivalent to DST temperatures, there is still considerable potential error in any individual correction.

As noted in the Introduction, a number of workers have proposed that temperature corrections should be based partly or entirely on depth. Thus far, we have taken depth into account indirectly, because there is some correlation between TSC and depth. However, it is worth examining whether the correction factor also depends on depth. One could argue plausibly that systematic variations in hole size, mud density or viscosity, circulation times, porosity, or lithology (among other possible factors) might create a depth dependence independent of any implied by the inevitable increase in average TSC with increasing depth.

Figure 4 shows the ratio of the heat flow required to fit the DST temperatures to the heat flow calculated to fit SBHT data corrected using equation (5) for a relatively homogeneous subset of the data used to construct Figure 3 (all TSCs were between 10 and 12 hours). The correction factor from equation (5) is somewhat too small at shallow depth and too large at greater depth. The same trend is seen for all other sets of data representing narrow ranges of TSC, as well as for the entire data set (Fig. 5). The amount of correction required thus depends on depth as well as on TSC.

The data in Figure 5 suggest that, when temperatures are measured at depths shallower than about 2,000 m, the correction factor needs to be increased slightly as a function of depth, and when they are measured below 2,000 m, it needs to be decreased. Empirical adjustment of equation (5) following these guidelines yields a new equation for the correction factor f_S:

$$f_S = (-0.1462\mathrm{Ln}(\mathrm{TSC}) + 1.699)/(0.572 \bullet Z^{0.075}) \quad (6)$$

where Z is the depth (m) at which the BHT temperature is measured. Figure 6 shows that when we use equation (6) the accuracy of the correction is now independent of depth.

Table 1 shows the correction factor (f_S) calculated using equation (6) for four different depths and a range of TSC. Correction factors interpolated within the range of depths and TSC in the calibration data set vary from 1.66 for TSC = 2 hours at a depth of 1,000 m to about 1.12 for TSC = 35 hours at a depth of 3,500 m. There were no data in our database to test predictions of equation (6) at longer TSC or greater depth.

We can estimate the uncertainty in our SBHT corrections by comparing the heat flows (or geothermal gradients) required to fit the raw SBHT data with those required to fit the DST data. Standard deviations in the ratio of these two heat flows were then calculated for groups of measurements with similar TSCs. As Figure 7 shows, there is an empirical relationship between standard deviation σ and TSC for SBHT data. The equation for the regression line for SBHT data of unknown quality (data belonging to Groups 2 and 3 as defined in the next section) is

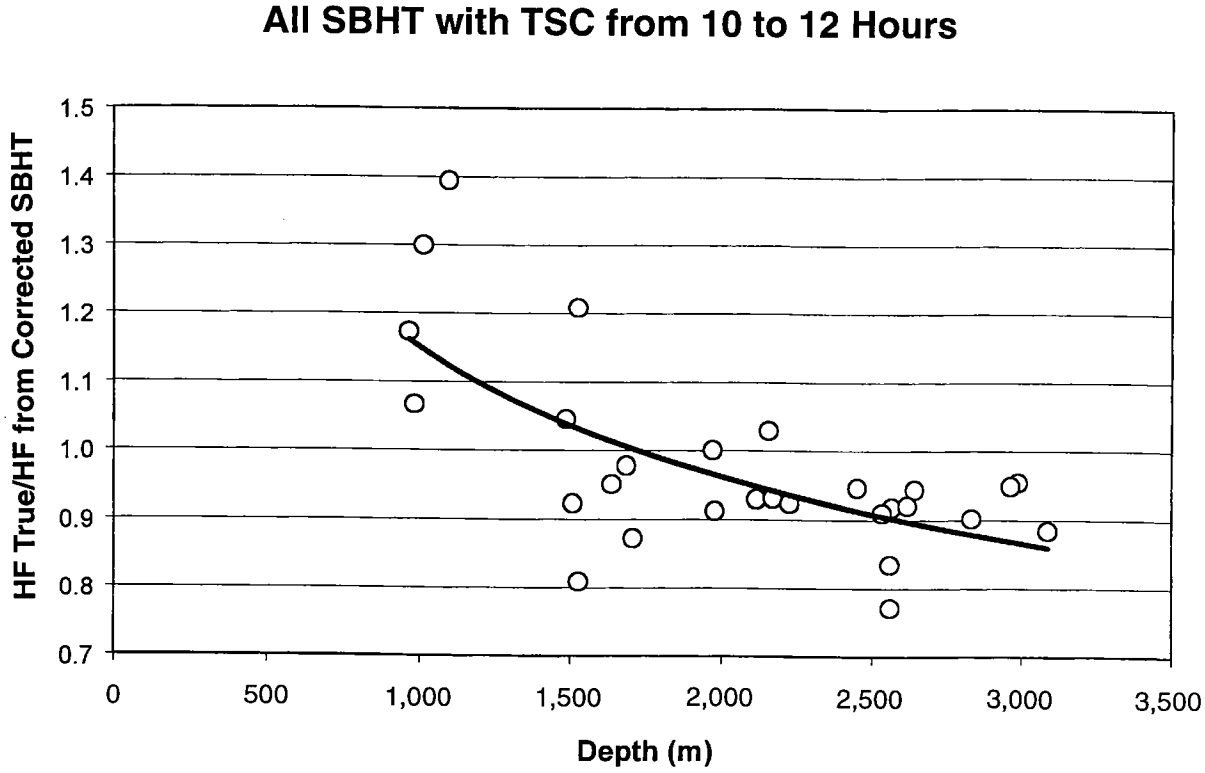

Figure 4. Ratio of steady-state heat flow (HF) required to fit drill-stem-test (DST) data to steady-state heat flow required to fit single bottom-hole temperature (SBHT) data corrected using equation (5), plotted versus depth for all SBHT data with time since end of circulation (TSC) between 10 and 12 hours. The accuracy of the correction is obviously dependent on depth.

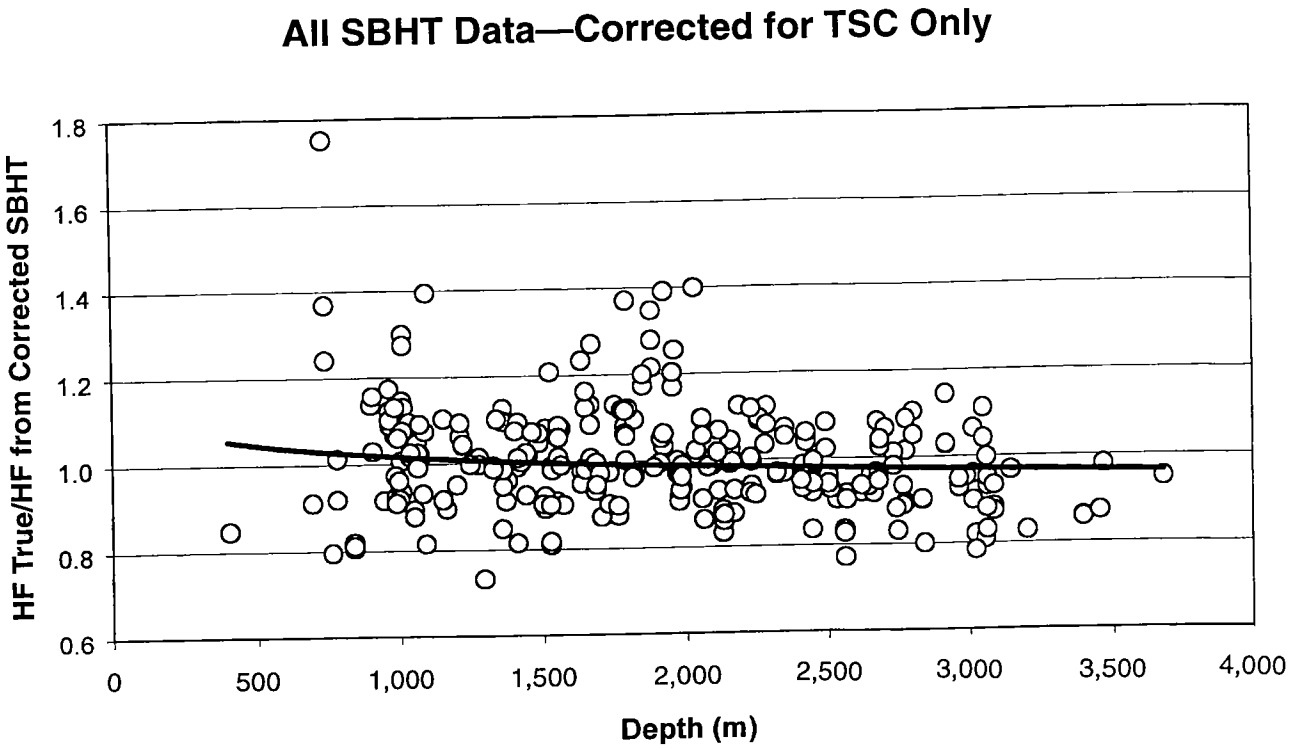

Figure 5. Same plot as for Figure 4, except that it includes all single bottom-hole temperature (SBHT) data. The trend is the same as that observed in Figure 4, confirming that the correction applied using only time since end of circulation (TSC) is too small at shallow depths and too large at depths greater than 2,000 m. The line represents the best least-squares fit to the data using a power function.

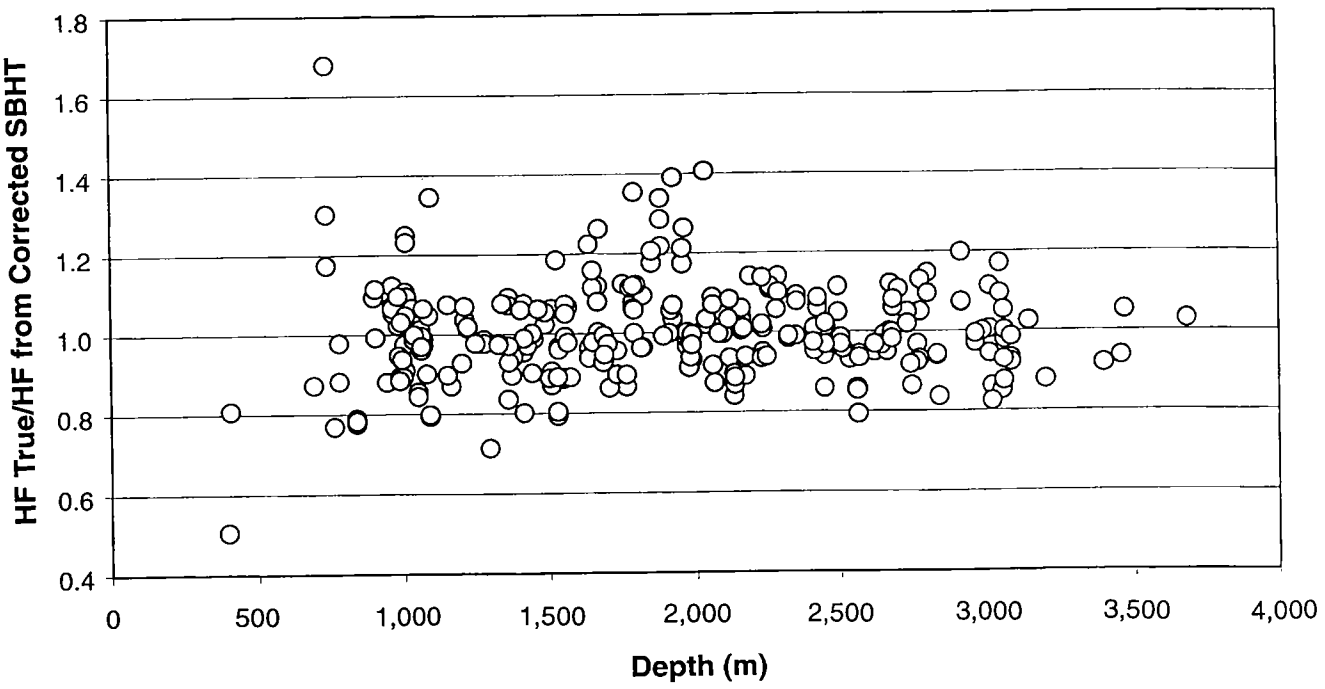

Figure 6. Ratio of steady-state heat flow required to fit drill-stem-test (DST) data to steady-state heat flow required to fit single bottom-hole temperature (SBHT) data corrected for both time since end of circulation (TSC) and depth according to equation (6), plotted versus depth for all data. The error in the correction is now independent of depth.

TABLE 1. — Correction Factors for Single Bottom-Hole Temperature (SBHT) Data as Function of Time Since Circulation (TSC) and Depth and Horner-Plot- (HP-) Extrapolated Temperatures as Function of Maximum TSC

	Correction Factor					Standard Deviation[a]			
	SBHT				HP	SBHT		HP	
TSC (hours)	Depth = 1,000 m	Depth = 2,000 m	Depth = 3,000 m	Depth = 3,500 m	All depths	All depths, uncertain data quality[b]	All depths, best data[c]	All depths, three temps.[d]	All depths, two temps.[e]
2	1.66	1.58	1.53	1.51	NC	0.13	0.09	NC	NC
3	1.60	1.52	1.48	1.46	NC	0.13	0.08	NC	NC
4	1.56	1.48	1.44	1.42	1.33	0.13	0.08	0.10	0.16
5	1.52	1.45	1.40	1.39	1.30	0.12	0.08	0.08	0.15
6	1.50	1.42	1.38	1.36	1.28	0.12	0.08	0.08	0.14
8	1.45	1.38	1.34	1.32	1.24	0.11	0.07	0.08	0.13
10	1.42	1.35	1.31	1.29	1.21	0.10	0.07	0.08	0.11
12	1.39	1.32	1.28	1.27	1.19	0.10	0.06	0.08	0.11
15	1.36	1.29	1.25	1.24	1.16	0.09	0.06	0.07	0.10
20	1.31	1.25	1.21	1.20	1.12	0.08	0.05	0.07	0.09
25	1.28	1.21	1.18	1.16	1.09	0.06	0.04	0.07	0.08
30	1.25	1.19	1.15	1.14	1.07	0.05	0.04	0.06	0.08
35	1.23	1.17	1.13	1.12	1.05	0.05	0.03	0.06	0.07
40	1.21	1.15	1.11	1.10	1.03	0.04	0.03	0.06	0.07
50	1.17	1.11	1.08	1.07	1.00	0.03	0.02	0.05	0.06

NOTES: NC = not calculated; it is not realistic to have a HP with such a short maximum TSC.
[a]Values of standard deviation corrections to SBHT data that are confirmed by other SBHT data are about two-thirds that shown on table.
[b]All data.
[c]Only data confirmed correct by HP tests.
[d]HP data using three temperatures.
[e]HP data using two temperatures.

$$\sigma = 0.1421\exp[-0.0317(TSC)] \quad (7)$$

When TSC is short, the standard deviation calculated using equation (7) is moderately large (Table 1). As TSC gets longer, however, the uncertainty diminishes considerably. However, when the SBHT data are known to be internally consistent (Group 1 of the HP data, as defined in the next section), σ is significantly lower. Equation (7) can thus be modified to

$$\sigma = 0.0915\exp[-0.0317(TSC)] \quad (8)$$

whenever we are confident that the SBHT temperatures and TSCs are correct. These standard deviations are also compiled in Table 1.

Figure 8 shows an example of how correcting SBHT data using equation (6) brings the corrected temperatures into better agreement with measured DST temperatures.

HP-Extrapolated Temperatures

Data sets used in constructing Horner plots were divided into three groups. Horner plots in Group 1 are internally consistent and of maximum reliability: all contain three measured temperatures, and all three points fall on or very close to the HP regression line. (No Horner plots in this study had more t temperatures.)

In contrast, Group 3 HP data sets had only two temperatures available. Because there is no way to determine whether these two measurements are internally consistent, the individual data points and the Horner plots derived from these are considered to be less reliable than those of Group 1.

Group 2 HP data sets all have three temperatures, but the temperatures do not all fall precisely on the HP line (Fig. 9). The measured temperatures (or TSC values) are therefore internally inconsistent. Three measured temperatures are valuable for Horner plots only if the three data points are internally consistent. If they are inconsistent, the entire data set must be viewed with caution.

The extrapolated temperatures obtained from inconsistent Horner plots (Group 2) were deleted from our database. Internally inconsistent HP data should be rejected routinely in any evaluation of subsurface temperature. However, the raw temperature data can still be used as SBHT data, as in this study.

All HP extrapolations in this study were computed using an assumed circulation time [t in equation (3)] of 2 hours. An average correction factor of 1.20 was established using all HP data from Groups 1 and 3. Although an average correction factor for Horner plots is of limited value, it could be applied as a correction to subsurface temperatures that are described as having been

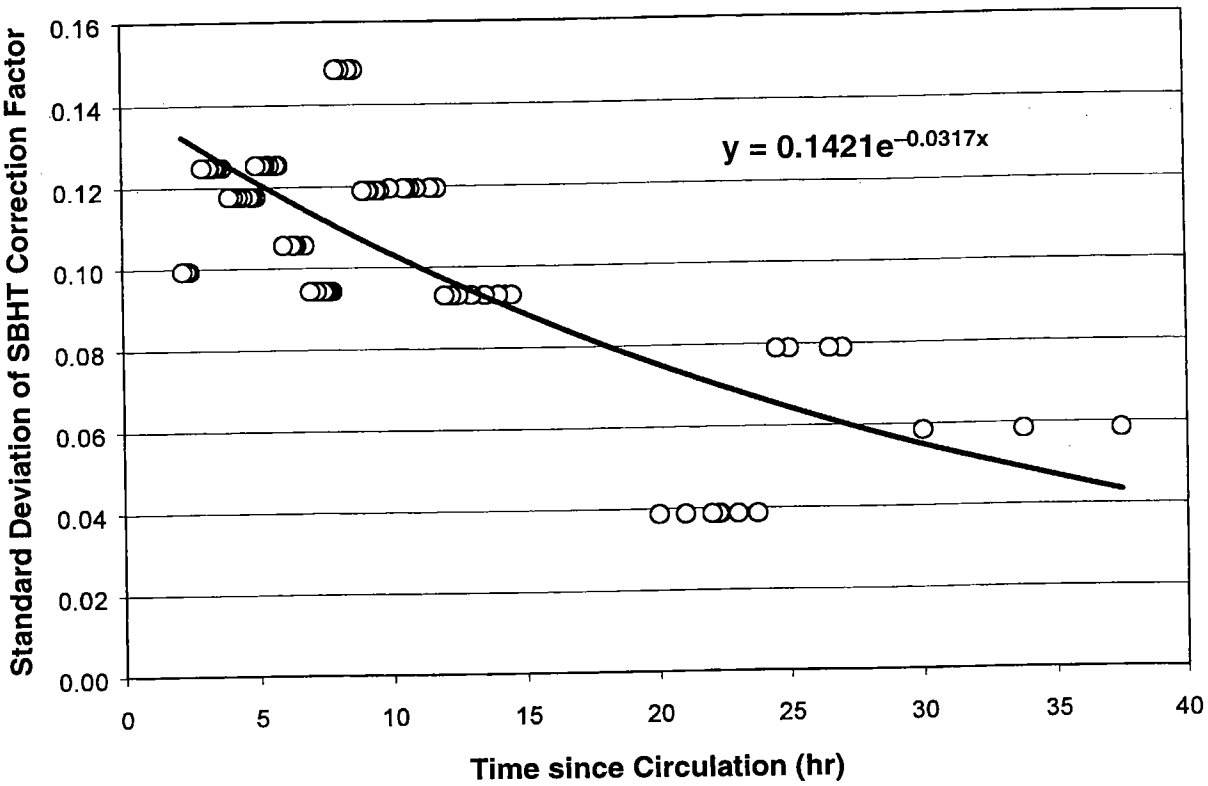

Figure 7. Standard deviations for homogeneous groups of single bottom-hole temperature (SBHT) data plotted versus time since circulation. The regression line, which represents the statistical best fit to the data, permits estimation of uncertainty in the correction factor if time since end of circulation (TSC) is known.

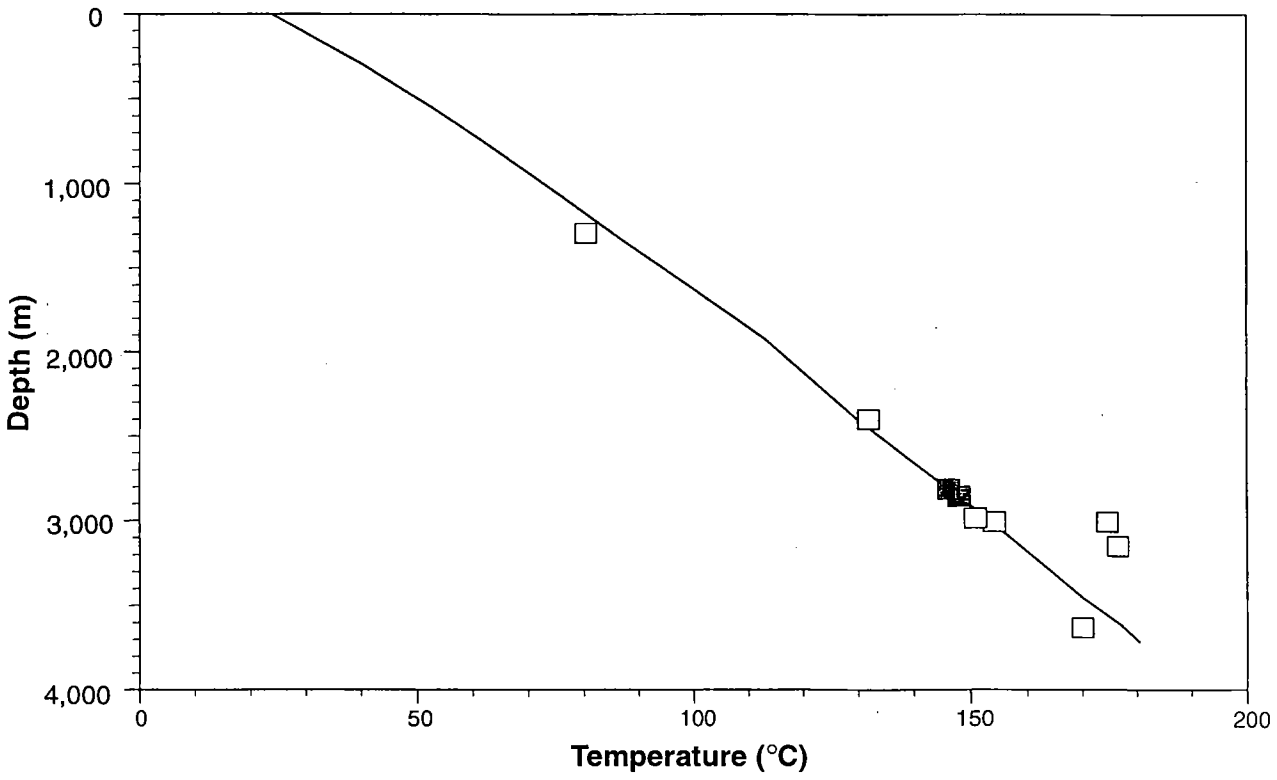

Figure 8. Corrected temperature data for Well A plotted versus depth. Compare with uncorrected temperatures in Figure 1. Solid squares represent drill-stem-test (DST) temperatures (uncorrected); open squares are corrected temperatures from logging runs. The line represents calculated present-day temperature profile to fit DST data.

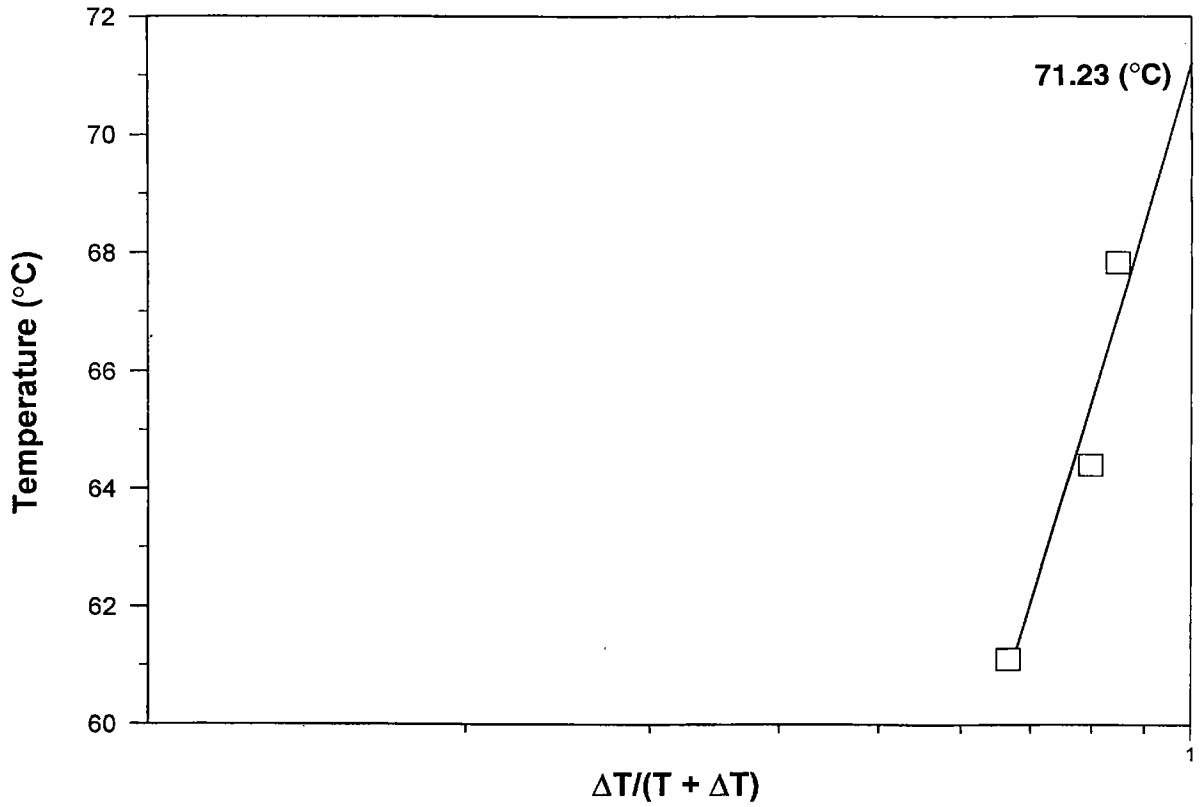

Figure 9. Horner plot from Well B [see equation (3)]. The three data points are inconsistent (Group 2) because they do not fall along a straight line.

derived from Horner plots, but where the HP data themselves are not available. However, it is generally more informative to characterize HP data according to the maximum TSC used in constructing the Horner plot. Figure 10 shows that the correction factors required for extrapolated HP temperatures decrease for both sets of HP data as the maximum TSC in the Horner plot increases. A logarithmic regression line was found to fit the best HP data (Group 1). [A very similar equation would also fit the data from Horner plots with only two temperatures (Group 3).] The magnitude of the correction factor, therefore, does not depend on the number of measured temperatures used in making a Horner plot:

$$f_{HP} = -0.1293\text{Ln(TSC)} + 1.5081 \quad (9)$$

Correction factors for Horner plots are highest when maximum TSC is short and decrease substantially as maximum TSC increases (Table 1; Fig. 10). The correction factors for HP data calculated using equation (9) are, as expected, smaller than those calculated for SBHT data using equation (6) (Table 1).

Although the magnitude of the correction factor is the same for all Horner plots, the uncertainty in the correction depends strongly on the number of measured temperatures used in constructing the Horner plot. Horner plots constructed from three temperatures have lower standard deviations than do those constructed from two temperatures (Fig. 11; Table 1):

$$\sigma_{(3\ \text{temperatures})} = 0.1275 \bullet \text{TSC}^{(-0.2055)} \quad (10)$$

$$\sigma_{(2\ \text{temperatures})} = 0.2803 \bullet \text{TSC}^{(-0.3872)} \quad (11)$$

Standard deviations in correction factors are slightly greater for corrections made to Horner plots than those made to SBHT data of equivalent quality (compare HP data with three temperatures with the best SBHT data, or compare HP data with two temperatures with SBHT data of uncertain quality in Table 1). This result is probably a consequence of some poor Horner plots (bad temperature or TSC data, or very short TSC), in which the extrapolated value is quite wrong. SBHT data, which are not subject to potentially large errors that can result from extrapolation of poor data, are slightly more consistent, even though the amount of correction required for SBHT data is greater.

In contrast to the findings for SBHT data, the data in this study do not indicate a need for an additional correction to HP temperatures based on depth. The accuracy of our HP correction is thus independent of depth (Fig. 12).

The rather large uncertainties in the correction factors for many SBHT and HP data (especially when TSC is short and depth is shallow) indicate that subsurface-temperature profiles cannot be established with good confidence using only wireline temperatures from a single depth. However, if measurements at several depths are available, if at least some are taken at

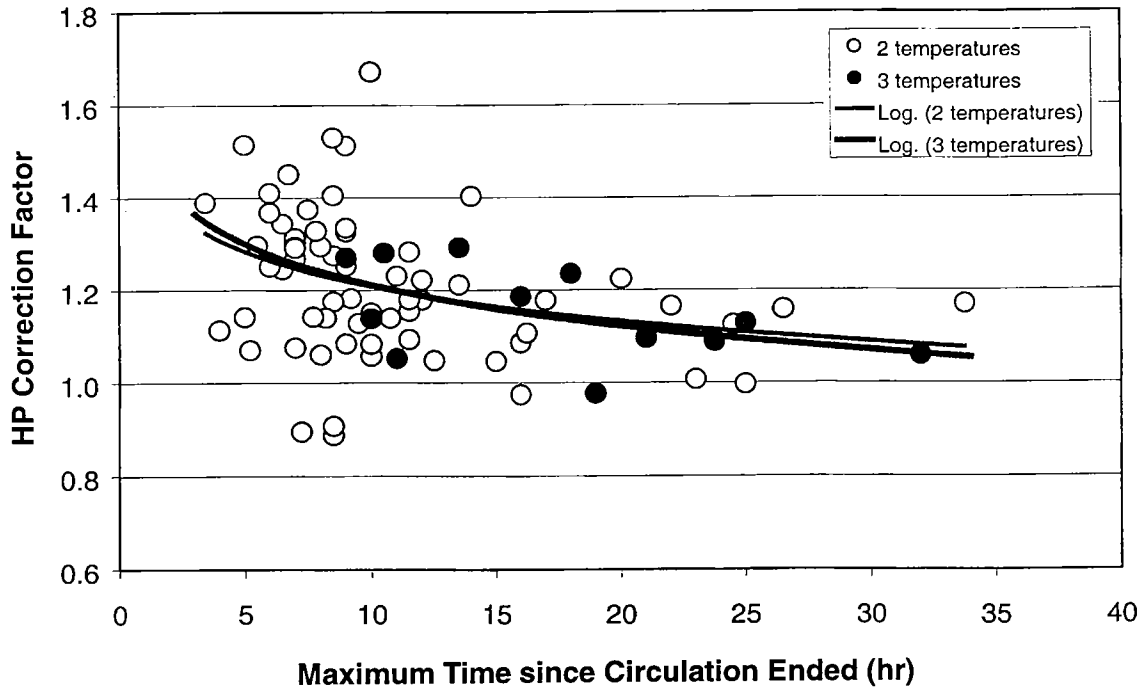

Figure 10. Plot of correction factors applied to temperatures obtained by Horner-plot (HP) extrapolation versus maximum time since end of circulation (TSC) used in the HP calculation for all data in Groups 1 and 3 (three temperatures and two temperatures, respectively). The required correction factor decreases as maximum TSC increases for both data sets. Logarithmic regression lines represents best fit to the two data sets. The great similarity of the regression lines shows that the correction factor for HP temperatures is independent of the number of temperatures used in constructing the Horner plot.

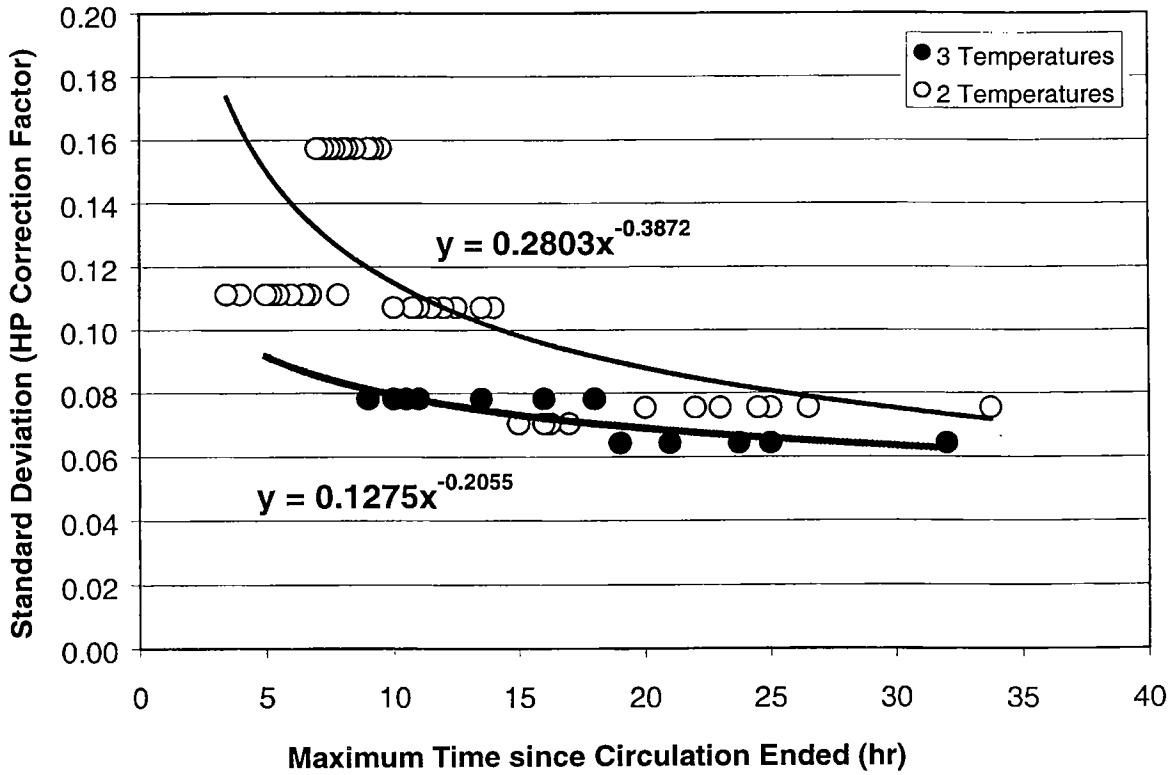

Figure 11. Standard deviations for homogeneous groups of Horner-plot (HP) data (Groups 1 and 3: three and two temperatures, respectively) plotted versus maximum time since end of circulation (TSC). Regression lines, which represent statistical best fits to each data set, permit estimation of uncertainty in the correction factor if maximum TSC is known. Uncertainty is much lower when using Horner plots of three temperatures.

reasonably long times after circulation stops, and if those data are handled properly, a subsurface-temperature profile can sometimes be constrained much more tightly than it can by using a single data point.

This point is illustrated in Figure 13, which shows that the range of possible heat flows and temperature profiles that can simultaneously fit a set of temperature data is narrower than the range of allowed values for any one of the individual measurements. In this example, if we were to use only the deepest temperature measurement to constrain the geothermal gradient, we would be 95% confident that the "true" temperature at 3,630 m is between 148°C and 192°C. However, if we use all eight SBHT values with their appropriate 2σ limits, the range of possible temperatures is much narrower (169°C to 187°C).

CONCLUSIONS

The amount of upward correction required for measured wireline-log temperatures and extrapolated temperatures derived from Horner plots depends on the time between cessation of circulation (TSC) and arrival of the logging tool on the bottom. For wireline temperatures the correction also depends to a small degree on the depth at which the measurement was taken. Empirical equations have been developed in this study for correcting wireline temperatures if TSC and depth are known, and for correcting temperatures extrapolated using Horner plots if the maximum TSC is known. Application of these correction methods will, on the average, make a set of log-derived temperatures equivalent to DST temperatures from the same well.

These corrections, however, are only approximate for any given measurement. Uncertainties in the corrections are quite high when TSC is short, but decrease substantially as TSC increases. Uncertainties are greatly reduced for both wireline temperatures and temperatures extrapolated from Horner plots if the accuracy of the recorded temperature and TSC can be independently confirmed. Uncertainties for HP temperatures are slightly higher than for wireline temperatures, probably because of the intrinsic potential for large errors when extrapolations are used. We recommend using 2σ (95% confidence) to indicate the range of possible corrected temperatures. Although these corrections represent a substantial improvement over existing methods, DST and production test temperatures are still extremely valuable in estimating subsurface temperature profiles.

These ideas and correction factors are considerably more pessimistic than the conventional wisdom, which often states that single BHTs require only a modest upward correction, and that neither TSC nor depth need be explicitly considered. Conventional wisdom also asserts, incorrectly, that Horner plots provide adequate and accurate corrections. However, our ideas are in fundamental agreement with those expressed by most specialists who have studied temperature corrections in detail. In the future, much more attention should be paid to properly correcting log-derived temperatures in general and to recognizing and avoiding major errors in the application of Horner plots.

Our study included data from a single Tertiary extensional basin with high geothermal gradients. Application of the conclusions of this study to other basins is still largely speculative. However, in preliminary tests of the model in several other totally unrelated basins of different ages, tectonic styles, and depths (as much as 8 km) in different parts of the world, application of these correction factors yielded results that were highly encouraging and in excellent agreement with available DST data. We are therefore optimistic that these correction factors, while perhaps not fully universal, will prove useful for many or most other areas. Additional local calibration tests would be welcome. Moreover, it would be desirable in future investigations to include data for TSC greater than 35 hours, depths greater than 3,500 m, and data for Horner plots constructed from four or more temperatures.

ACKNOWLEDGMENT

We thank Petronas Carigali Sdn Bhd for support of this work and for permission to publish this study.

REFERENCES CITED

Beck, A. E.; and Balling, N., 1988, Section 3.—Determination of virgin rock temperatures, *in* Haenel, R.; Rybach, L.; and Stegena, L. (eds.), Handbook of terrestrial heat-flow density determination: Kluwer, Amsterdam, p. 59–85.

Bullard, E. C., 1947, The time necessary for a borehole to attain temperature equilibrium: Monthly Notes of the Royal Astronomical Society, v. 5, p. 127–130.

Dowdle, W. L.; and Cobb, W. M., 1975, Static formation temperature from well logs—an empirical method: Journal of Petroleum Technology, v. 27, p. 1326–1330.

Förster, A.; and Merriam, D. F., 1999, Problems and potential of industrial temperature data from a cratonic basin environment, *in* Förster, A.; and Merriam, D. F. (eds.), Geothermics in basin analysis: Kluwer/Plenum, New York, p. 35–59.

Förster, A.; Merriam, D. F.; and Davis, J. C., 1997, Spatial analysis of temperature (BHT/DST) data and consequences for heat-flow determination in sedimentary basins: Geologische Rundschau, v. 86, p. 252–261.

Funnell, R.; Chapman, D.; Allis, R.; and Armstrong, P., 1996, Thermal state of the Taranaki basin, New Zealand: Journal of Geophysical Research, v. 101, p. 25197–25215.

Gallardo, J.; and Blackwell, D. D., 1999, Thermal structure of the Anadarko basin: American Association of Petroleum Geologists Bulletin, v. 83, p. 333–361.

Hermanrud, C., 1988, Determination of formation temperature from downhole measurements: University of South Carolina unpublished Ph.D. thesis.

Hermanrud, C.; Cao, S.; and Lerche, I., 1990, Estimates of virgin rock temperature derived from BHT measurements: bias and error: Geophysics, v. 55, p. 924–931.

Horner, D. R., 1951, Pressure build-up in wells, *in* Proceedings of the Third World Petroleum Congress, The Hague, Section II: E. J. Brill, Leiden, Netherlands, p. 503–521.

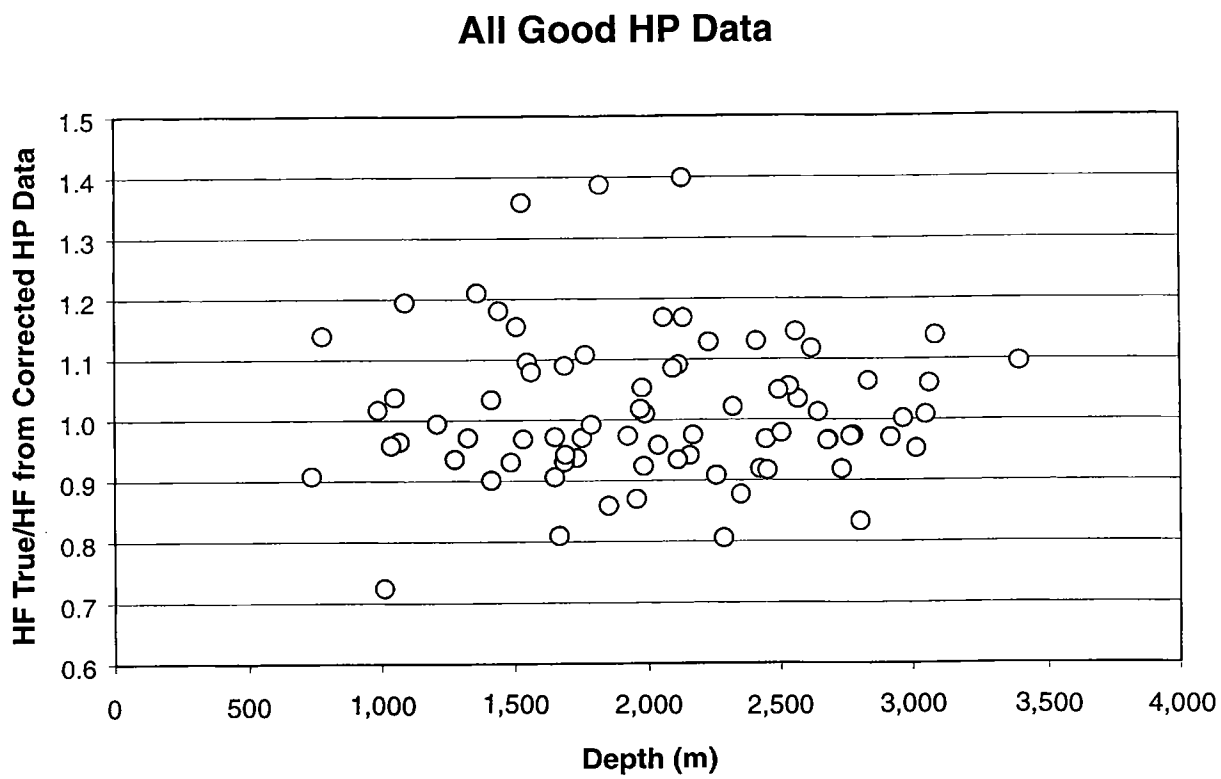

Figure 12. Ratio of steady-state heat flow required to fit drill-stem-test (DST) data to steady-state heat flow required to fit good Horner-plot (HP) data corrected according to equation (9), plotted versus depth for all data. The error in the correction is now independent of depth.

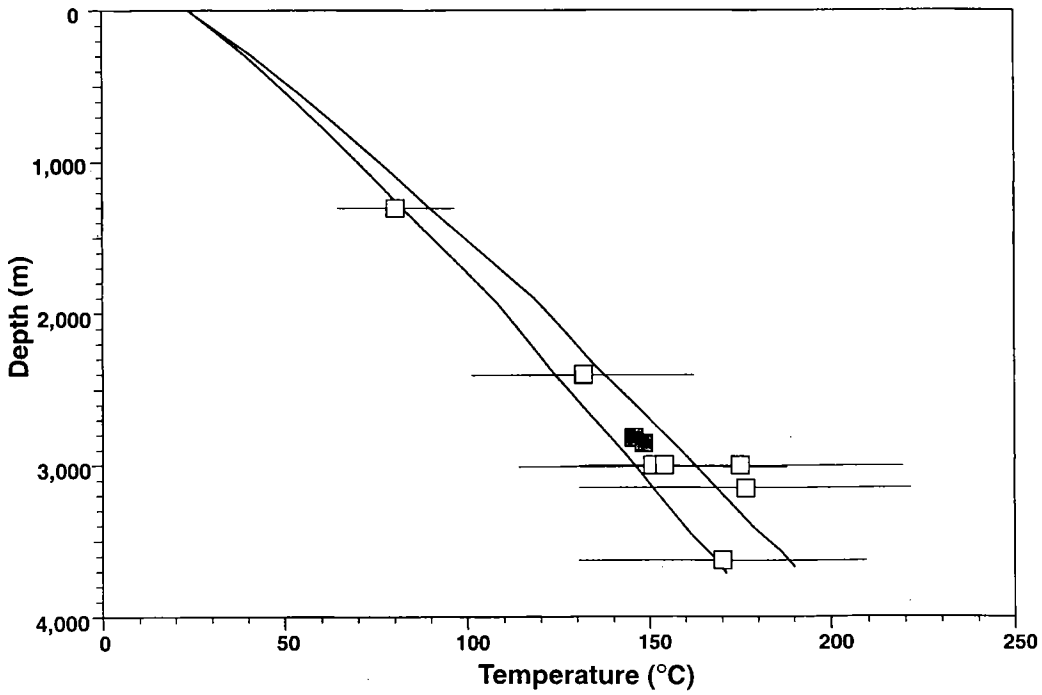

Figure 13. Temperature plotted with depth for Well A. All temperatures are corrected by the methods established in this paper. Solid squares represent uncorrected drill-stem-test (DST) temperatures; open squares represent best estimates of corrected log-derived temperatures. Error bars show 2σ (95% confidence limits) for each corrected temperature. The two solid lines represent minimum and maximum temperature profiles that fit all corrected temperatures within the 95% confidence limits. As discussed in the text, the allowed range of temperatures is narrower when more temperature data are used. In this case the DST temperatures fall in the middle of the allowed range of temperatures.

Lucazeau, F.; and Ben Dhia, H., 1989, Preliminary heat-flow density data from Tunisia and the Pelagian Sea: Canadian Journal of Earth Science, v. 26, p. 993–1000.

Oxburgh, E. R.; and Andrews-Speed, C. P., 1981, Temperature, thermal gradients and heat flow in the southwestern North Sea, *in* Illing, L. V.; and Hobson, G. D. (eds.), Petroleum geology of the Continental Shelf of northwest Europe: Heyden, London, p. 141–151.

Schoeppel, B. J.; and Gilarranz, S., 1966, Uses of well log temperatures to evaluate regional geothermal gradients: Journal of Petroleum Technology, v. 18, p. 667–673.

Sekiguchi, K., 1984, A method for determining terrestrial heat flow in oil basinal areas, *in* Cermák, V.; Rybach, L.; and Chapman, D. S. (eds.), Terrestrial heat flow studies and the structure of the lithosphere: Tectonophysics, v. 103, p. 67–79.

Speece, M. A.; Bowen, T. D.; Folcik, J. L.; and Pollack, H. N., 1985, Analysis of temperatures in sedimentary basins: the Michigan basin: Geophysics, v. 50, p. 1318–1334.

Takherist, D.; and Hamdi, L., 1995, Thermal anomaly at In Salah: possible consequences for petroleum potential, *in* Well conference evaluation, Algerie 1995: Schlumberger, p. II-7-1–II-7-19.

Tanaka, T.; and Sato, K., 1977, Estimation of subsurface temperature in oil and gas producing area, northeast Japan [in Japanese]: Journal of the Japanese Association of Petroleum Technology, v. 42, p. 229–237.

Wan Ismail Wan Yusoff, 1984, Heat flow study in the Malay basin, *in* Combined proceedings of the joint ASCOPE/CCOP workshops on heat flow 1 and 2: ASCOPE/TP, v. 5, CCOP/TP, v. 15, p. 77–87.

Waples, D. W.; and Mahadir, Ramly, 1995, A simple statistical method for correcting and standardizing heat flows and subsurface temperatures derived from log and test data: Bulletin of the Geological Society of Malaysia, Special Publication 37, p. 253–267.

Exploration Strategy for the Salina Basin in Kansas Based on Organic Geochemical Data and Maturation Modeling

K. David Newell
Kansas Geological Survey
Lawrence, Kansas

Joseph R. Hatch
U.S. Geological Survey
Denver, Colorado

ABSTRACT.—The Salina basin, which underlies north-central Kansas, has petroleum production only at its extreme southern end. The lack of commercial accumulations of hydrocarbons in the Salina basin proper is thought to be the result of being situated in a migration "shadow zone." In this scenario, oil that migrated northward out of the Anadarko basin in Oklahoma encountered the arch at the southern end of the Salina basin and then was diverted onto the Central Kansas and Nemaha uplifts. However, research into the maturation and geochemistry of organic matter and oils in Kansas indicates that some of the oil produced from the southern Salina basin is likely to be generated locally from organic-rich shale in the Middle Ordovician Simpson Group. This type of oil is geochemically distinct and apparently unique to Ordovician source rocks worldwide, having characteristics attributed to a type of fossil blue-green algae known as *Gloeocapsomorpha prisca*.

The Forest City basin lies east of the Salina basin, and *G. prisca* oils also occur in several Paleozoic pay zones along its axis. Both basins have a common geologic history and similar stratigraphy. The axes of both basins are presently at approximately the same depth. Thermal maturation modeling and Rock-Eval™ organic-matter–maturation data indicate that the lower Paleozoic rocks in the axes of both basins are in early stages of oil generation.

The Devonian–Mississippian Chattanooga Shale and Pennsylvanian shales contain sufficient organic matter for generation of petroleum, but they are higher in the stratigraphic section and thus are not as thermally mature as the Simpson Group. The Upper Ordovician Maquoketa Shale is almost as thermally mature as the Simpson Group, but available organic analyses indicate it is not a viable source rock.

Prospective structural trends in the Paleozoic section of the axis of the Salina basin are anticipated to be associated with reactivation of fault zones along the western margin of the underlying Precambrian Central North American rift system. This tectonic boundary trends north-northeast–south-southwest and passes under the axis of the Salina basin in Lincoln and Mitchell Counties. Major anticlines plunging into the basin also may have local closures in lower Paleozoic strata that may serve as structural traps. To increase the odds of success in an exploration program in the Salina basin, wildcat wells should be drilled at least through the Simpson Group and where thermal maturation is likely greatest.

INTRODUCTION

The Salina basin, which underlies much of north-central Kansas, has petroleum production only at its extreme southern end (Fig. 1A,B). Most of this production seems contiguous with production in the Sedgwick basin immediately to the south. These oil and gas fields generally have been accepted to be the result of long-distance oil migration out of the deep Anadarko basin in Oklahoma (Rich, 1931, 1933; Price, 1980). Concomitantly, the lack of commercial accumulations of petroleum in the main part of the Salina basin is thought to be the result of this northward-migrating oil being shunted updip onto the Central Kansas uplift and Nemaha uplifts (Fig. 1A,B). This diversion of the northward-migrating oil occurs where it encounters the

Newell, K. D.; and Hatch, J. R., 2001, Exploration strategy for the Salina basin in Kansas based on organic geochemical data and maturation modeling, *in* Johnson, K. S.; and Merriam, D. F. (eds.), Petroleum systems of sedimentary basins in the southern Midcontinent, 2000 symposium: Oklahoma Geological Survey Circular 106, p. 111–120.

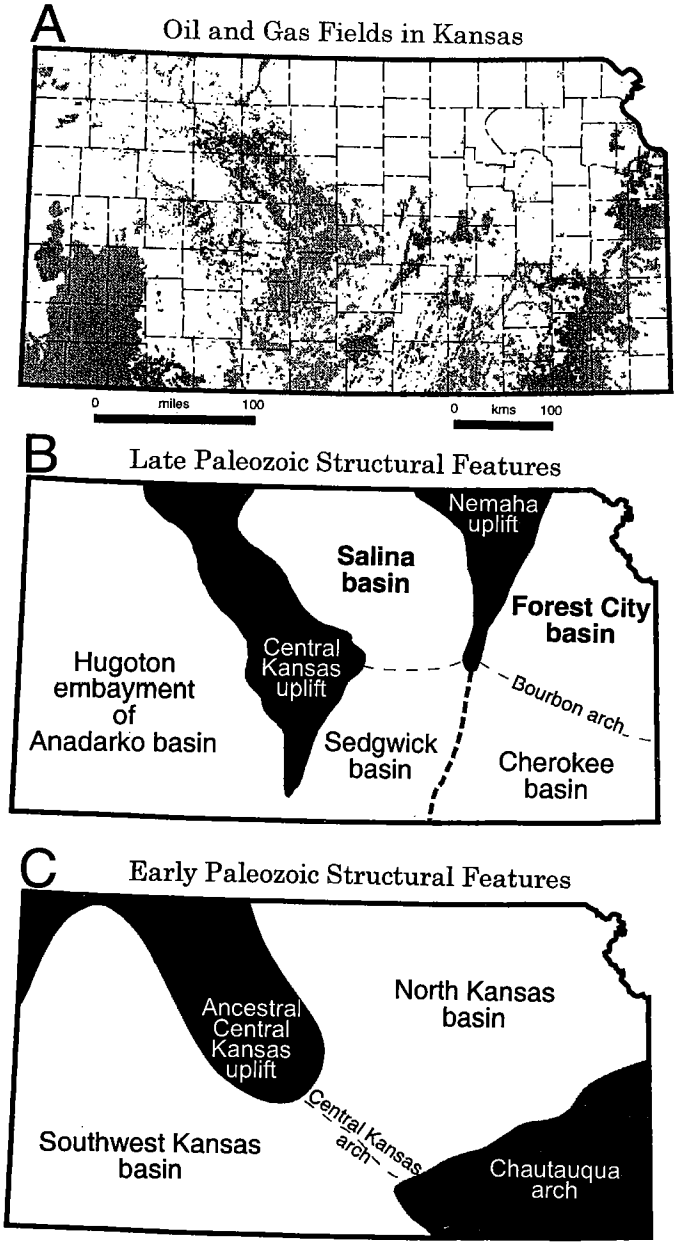

Figure 1. (A) Oil and gas fields in Kansas. Production trends extend from the Sedgwick basin northward into the Salina basin. (B) Late Paleozoic structural features of Kansas (from Merriam, 1963). A low, unnamed arch separates the Sedgwick basin from the Salina basin. (C) Early Paleozoic structural features of Kansas (from Merriam, 1963). The region encompassing the Forest City and Salina basins were once part of a larger, nearly circular cratonic basin called the North Kansas basin.

broad and ill-defined arch between the Salina basin and Sedgwick basin. In effect, this situates the Salina basin in a migrational "shadow zone."

HABITAT OF OIL IN THE SALINA AND FOREST CITY BASINS

If all the oil in the southern end of the Salina basin were the product of long-distance migration out of the deep Anadarko basin, it may be expected that this oil would be homogenized along each migration conduit, having been well mixed along its long updip journey. Although a significant amount of oil could have accumulated in Kansas by the process of long-distance migration, our research indicates that some of the oil produced in the southern Salina basin has a geochemical signature that is distinct from most of the other oils produced in Kansas (Fig. 2). Furthermore, this class of oil can be correlated precisely with extracts from shale from the Middle Ordovician Simpson Group (Hatch and others, 1987; Newell and others, 1987; Jacobson and others, 1988; Hatch and Newell, 1999). This type of oil is differentiated easily from other oils by gas chromatography (Fig. 2). It has a relative abundance of *n*-alkanes with carbon numbers less than 20, a predominance of odd-numbered *n*-alkanes between C_{10} and C_{20}, and relatively small amounts of branched and cyclic alkanes (Hatch and Newell, 1999). These unique geochemical characteristics are attributed to a type of fossil blue-green algae known as *Gloeocapsomorpha prisca* (Fowler, 1992; Reed and others, 1986; Longman and Palmer, 1987; Jacobson and others, 1988). Various Ordovician oils in several cratonic basins display these distinctive geochemical characteristics (Hatch and others, 1987; Longman and Palmer, 1987; Jacobson and others, 1988).

Oils produced from the axis of the Forest City basin seem to be uniformly *G. prisca* oil, with the exception of a relatively uncommon type of oil that occurs only in the Pennsylvanian Kansas City Group at the Davis Ranch field (see Hatch and Newell, 1999). The pay zones in the axis of the Forest City basin include Devonian–Silurian dolomites, Mississippian limestones, and sandstones immediately above the basal Pennsylvanian unconformity, so evidently the *G. prisca* oil leaked from deeper Ordovician source rocks. Oil fields along the flank of the Forest City basin (along the Kansas-Missouri state line) that are contiguous with production trends in the Cherokee basin to the south (Fig. 1B) do not produce *G. prisca* oils. Instead, they contain a relatively abundant type of oil that has been generated by Devonian source rocks (Hatch and others, 1989). This oil is similar to that in Figure 2B.

Because of their common geologic histories, the stratigraphy of the Salina basin and Forest City basin are similar, and this similarity encourages the idea that the axis of the Salina basin may hold oil fields similar to those in the axis of the Forest City basin. Subsidence of both basins was initiated during the Middle to Late Ordovician, when they were combined as a single large basin named the North Kansas basin (Merriam, 1963) (Fig. 1C). In the Late Mississippian–Early Pennsylvanian the south-southwest–plunging Nemaha uplift bisected the North Kansas basin (Fig. 1C) into the present two basins. By the Late Pennsylvanian, however, the Nemaha uplift was covered, and stratigraphic units were again contiguous across northern Kansas (Merriam, 1963). The axes of both basins at Ordovician level are presently at approximately the same depth (Fig. 3). By geologic analogy with the Forest City basin, *G. prisca* oil may be more extensive in

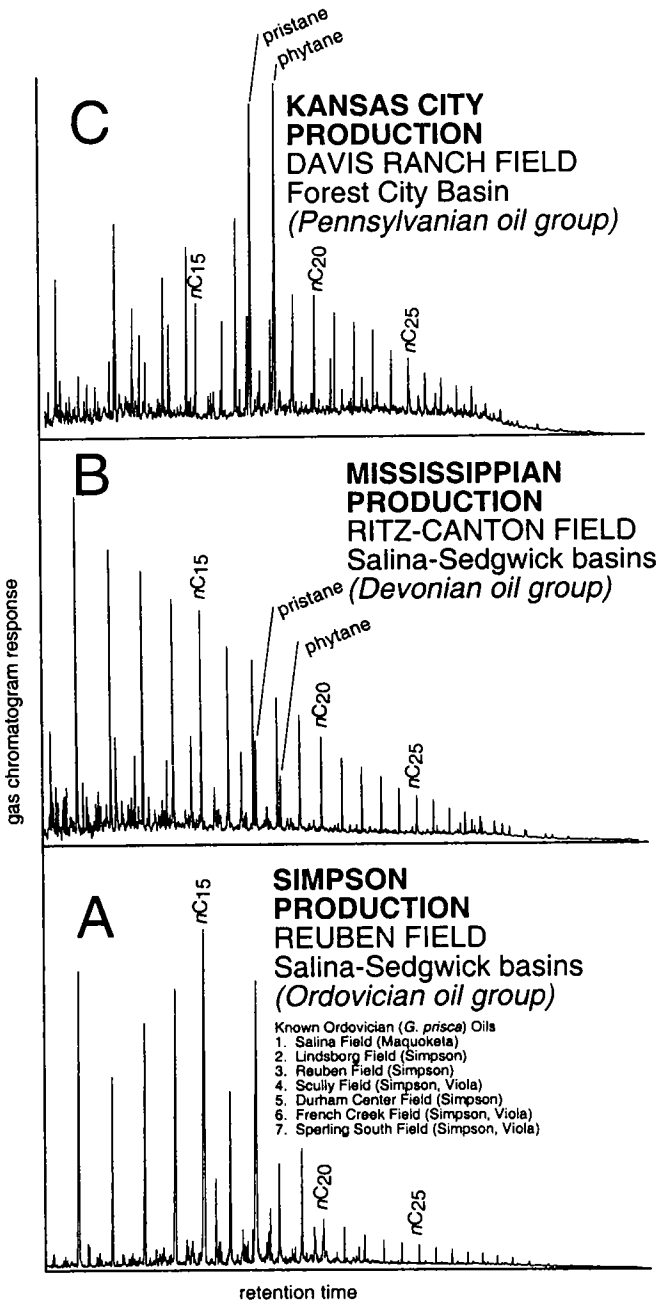

Figure 2. Gas chromatograms of oils collected in northeastern Kansas (see text for discussion). (A) *Gloeocaposomorpha prisca* oils collected to date in the Salina basin are listed adjacent to the gas chromatogram for this type of oil. A list of these categories of oils in the Forest City basin is given in Hatch and Newell (1999). (B) A more common oil is that associated with oils found above the Chattanooga Shale. This type of oil is common in the Cherokee basin and along the eastern flank of the Forest City basin (Hatch and others, 1989; Hatch and Newell, 1999). (C) This is an unusual and uncommon type of oil that occurs in Pennsylvanian strata in eastern Kansas in only isolated localities (Hatch and Newell, 1999).

the Salina basin than just the isolated occurrences at its southern end.

SOURCE ROCKS AND MATURATION

Rock-Eval™ organic-matter maturation data gathered from both the Salina basin and Forest City basin (Appendix 1, Fig. 4) indicate that lower Paleozoic rocks in both basins are in early stages of oil generation about the –2,000-ft level (i.e., the approximate depth corresponding to where T_{max} measurements exceed 435°C). The data in the Appendix are after Hatch and Newell (1999) and Newell and Hatch (2000). API gravities of *G. prisca* oils in both basins also increase with depth (Fig. 4). *G. prisca* oils in the Salina basin even appear to have slightly higher API gravities than those in the Forest City basin at similar depth (Fig. 4). Maturation models in Newell and others (1987) and Newell (1997a) agree with the early stage of oil generation of the Ordovician source rocks, as indicated by the geochemical analyses.

Analyses of organic matter in the Salina basin (see Newell and Hatch, 2000) show that the Simpson Group contains some shales that have sufficient organic matter for petroleum generation (Fig. 5). Presumably, it is these shales that produce the *G. prisca* oils that occur in the southern end of the Salina basin and in those fields along the axis of the Forest City basin. Other stratigraphic units in the Salina basin also may contain adequate amounts of organic matter necessary for generation of petroleum, but they are higher in the stratigraphic section and thus are not as thermally mature as the rocks of the Simpson Group. The Upper Ordovician Maquoketa Shale is almost as thermally mature as the Simpson Group, but available organic analyses indicate it is not a viable source rock (Fig. 5). The Devonian–Mississippian Chattanooga Shale can be as thick as 250 ft in the southern end of the Salina basin. It may be a viable source rock at this vicinity, but it thins rapidly and changes from gray to reddish-brown shale northward (Lambert, 1992) and is completely absent at the Kansas-Nebraska state line. It is thus not a likely potential source rock for the axis of the Salina basin. Pennsylvanian shales can be rich in organic matter (i.e., >10 wt % total organic carbon), but they generally are immature with respect to hydrocarbon generation all over northern Kansas (Figs. 4, 5).

EXPLORATION GUIDELINES FOR THE SALINA BASIN

To increase the odds of success in an exploration program in the Salina basin, wildcat wells should be drilled at least through the Simpson Group and where thermal maturation is likely greatest. Deeper source-rock zones may be present in the Cambrian–Ordovician Arbuckle Group and the underlying Cambrian Reagan Sandstone, but limited sampling has yet to detect such beds. Because of its relatively deep burial, the axis of the basin has the greatest chance for the thermal maturation necessary for petroleum generation. Conversely, the broad, relatively shallow eastern flank of

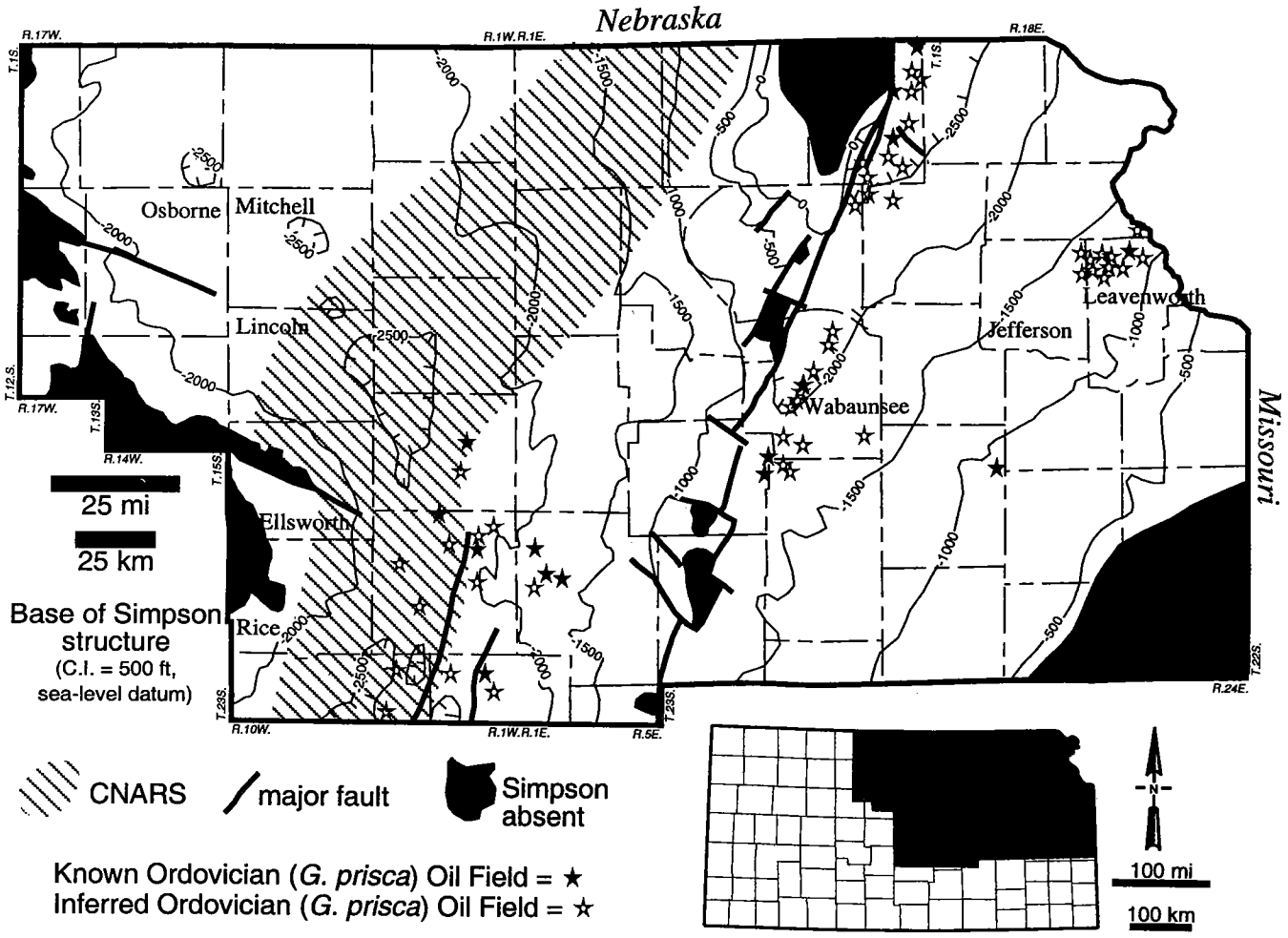

Figure 3. Structure at the base of the Simpson Group in northeastern Kansas, taken from Merriam and Smith, 1961; Merriam, 1963). Confirmed and inferred *Gloeocaposomorpha prisca* oil fields (from Hatch and Newell, 1999; Newell and Hatch, 2000) are shown. Both the axis of the Salina basin and the axis of the Forest City basin are presently at approximately the same depth. Approximate boundary of the Precambrian Central North American rift system (CNARS) is shown. Structures associated with reactivation of the marginal faults of this tectonic entity and anticlines that plunge into the axis of the Salina basin, such as those present in Osborne and Ellsworth Counties, may have closures that could be prospective for oil at the Simpson level. C.I. = contour interval.

the basin is likely too thermally immature for petroleum locally generated from the Simpson Group.

The western margin of the Precambrian Central North American rift system underlies several Paleozoic structural trends in the western part of Rice and Ellsworth Counties (Fig. 3), and some of these trends contain oil and gas fields (Fig. 1). Prospective structural trends in the Paleozoic section of the Salina basin axis are anticipated to be associated with reactivation of fault zones along the western margin of the underlying Central North American rift system (Fig. 3). This tectonic boundary trends north-northeast–south-southwest and passes under the axis of the Salina basin in Lincoln and Mitchell Counties (Fig. 3). Major anticlines plunging into the basin also may have local closures that may serve as structural traps for locally generated petroleum. The east-southeast–plunging Ellsworth-Kanopolis anticline in Ellsworth County and a similarly oriented, unnamed anticline farther north in Osborne County are two prominent examples, but other more subtle structures of this type may exist. Generally, the axis of the Salina basin is sparsely drilled with less than two tests per township. If an exploration program can define lower Paleozoic structural closures in this region, these structures may represent the best chance for future petroleum discoveries.

ACKNOWLEDGMENTS

We thank Lawrence Brady and Daniel Merriam for reviewing this manuscript.

REFERENCES CITED

Fowler, M. G., 1992, The influence of *Gloeocapsomorpha prisca* on the organic geochemistry of oils and organic-rich rocks of Late Ordovician age from Canada, *in*

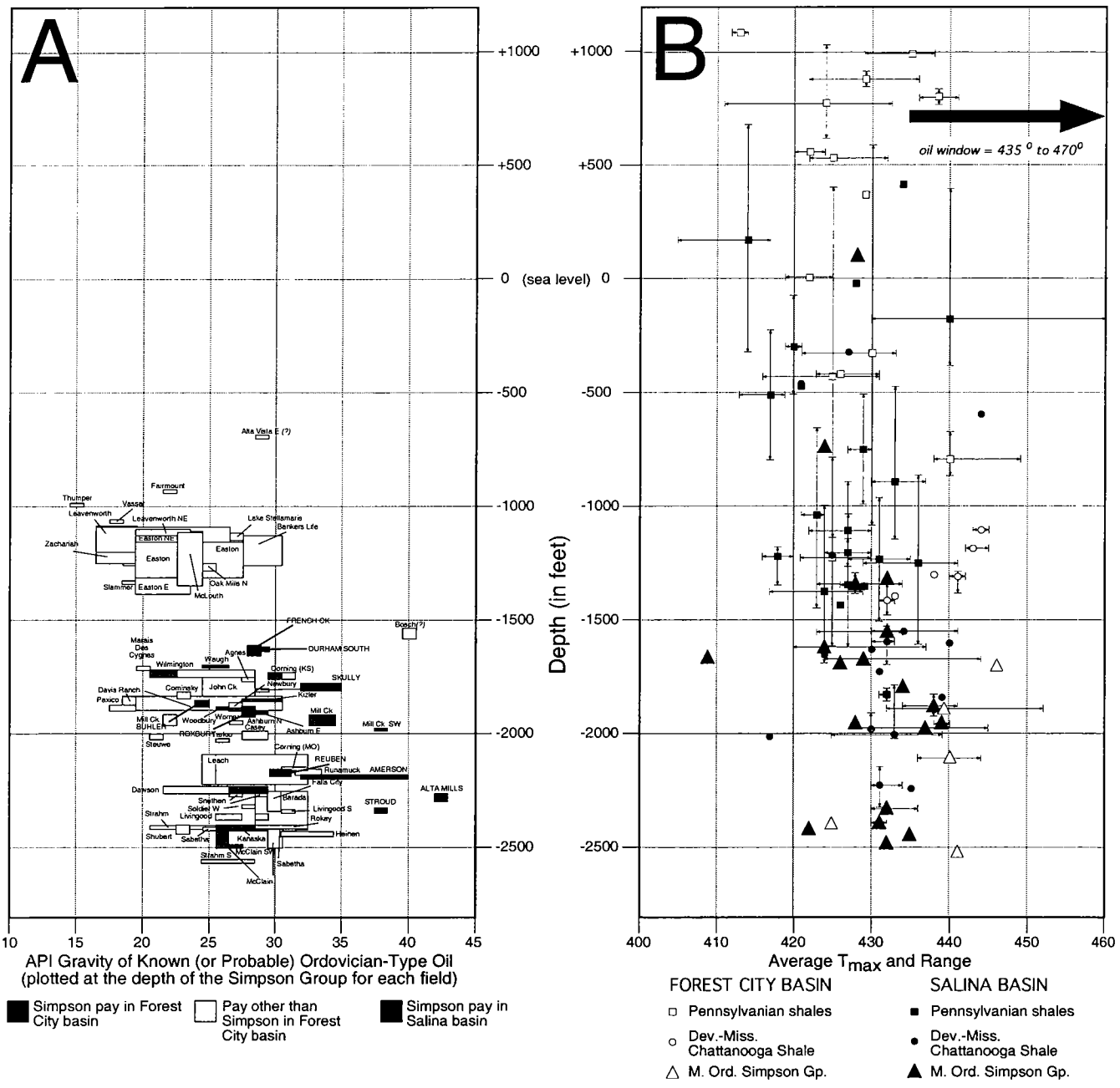

Figure 4. Depth relationships of oil API gravity (*Gloeocaposomorpha prisca* oils only) and Rock-Eval™ T_{max} maturation data from the Forest City and Salina basins. (A) The cross plot of API gravity of the *G. prisca* oils versus depth (from Newell, 1997b). The API gravities increase with depth for both basins. The API gravity seems slightly higher in the Salina basin than the Forest City basin at identical depths. Although there is considerable scatter in (B), the T_{max} versus depth cross plot, the two basins also seem to have similar maturation profiles. No maturation data at Simpson level are available for the group of fields on the eastern flank of the Forest City basin. [These are the fields in which the Simpson Group is at –1,000 ft to –1,400 ft (sea-level datum).] If these fields have maturation profiles similar to the rest of northeastern Kansas, the Simpson Group may be capable of producing commercial amounts of petroleum even if it registers T_{max} values less than 435°C. This value usually is considered the minimum T_{max} for the beginning of the oil window (Peters, 1986). T_{max} data are summarized in the Appendix.

Schidlowski, M.; and others (eds.), Early organic evolution: implications for mineral and energy resources: Springer-Verlag, Berlin, p. 336–356.

Hatch, J. R.; and Newell, K. D., 1999, Geochemistry of oils and hydrocarbon source rocks from the Forest City basin, northeastern Kansas, northwestern Missouri, southwestern Iowa and southeastern Nebraska: Kansas Geological Survey Technical Series 13, 32 p.

Hatch, J. R.; Jacobson, S. R.; Witzke, B. J.; Risatti, J. B.; Anders, D. E.; Watney, W. L.; Newell, K. D.; and Vuletich, A. K., 1987, Possible late Middle Ordovician organic carbon isotope excursion; evidence from

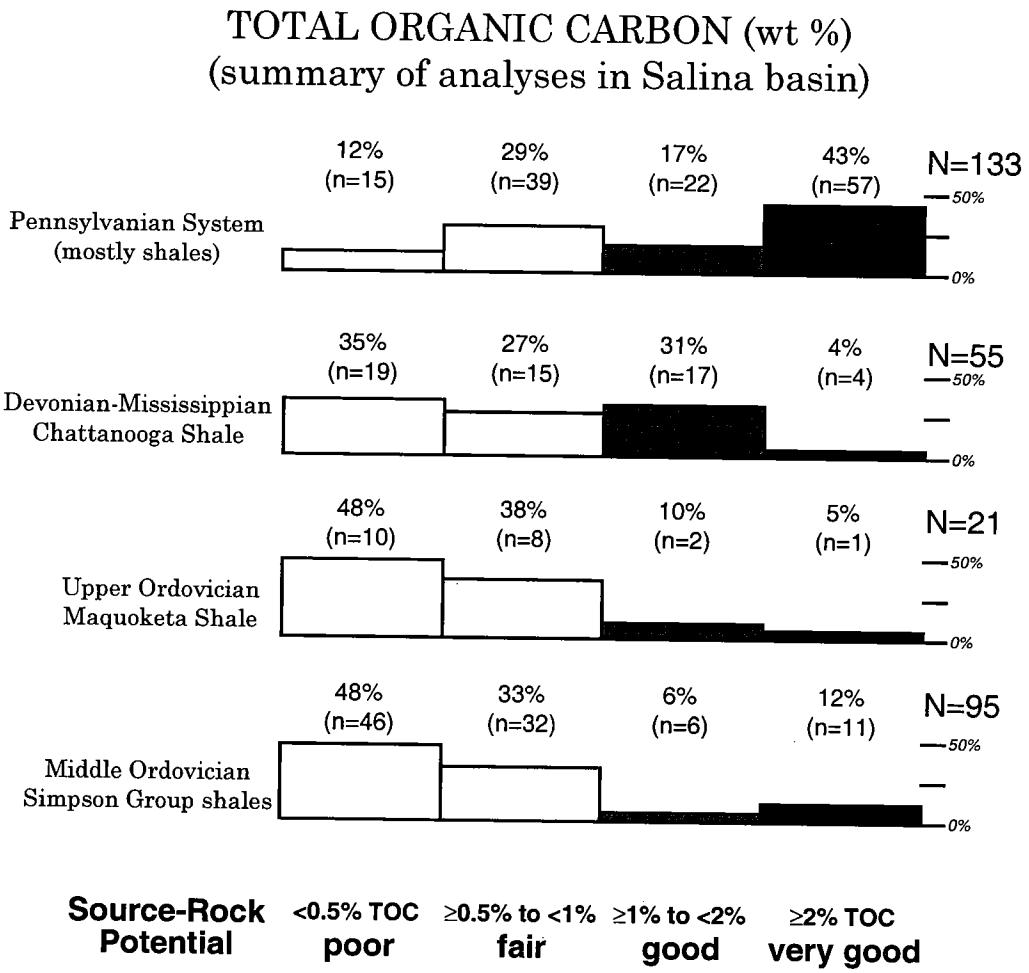

Figure 5. Summary of total-organic-carbon (TOC) analyses from well cores and cuttings from the Salina basin. Although Pennsylvanian shales generally are richest in organic matter, they generally are thermally immature with respect to petroleum generation. The Simpson Group displays marginal maturity, but correlation of produced oils to extracts from the Simpson Group indicates that the Simpson Group nevertheless has generated oil. The Maquoketa Shale seems to be too poor in organic matter for petroleum generation. The Chattanooga Shale and Maquoketa Shale are less mature than the Simpson Group. The Chattanooga Shale may have generated some oil where it is rich in organic matter; however, more detailed studies are necessary to prove (or disprove) its viability as a petroleum source rock. N and n = sample size.

Ordovician oils and hydrocarbon source rocks, Midcontinent and east-central United States: American Association of Petroleum Geologists Bulletin, v. 71, p. 1342–1354.

Hatch, J. R.; King, J. D.; and Daws, T. A., 1989, Geochemistry of Cherokee Group oils of southeastern Kansas and northeastern Oklahoma: Kansas Geological Survey Subsurface Geology Series 11, 20 p.

Jacobson, S. R.; Hatch, J. R.; Teerman, S. C.; and Askin, R. A., 1988, Middle Ordovician organic matter assemblages and their effect on Ordovician-derived oils: American Association of Petroleum Geologists Bulletin, v. 72, p. 1090–1100.

Lambert, M. W., 1992, Internal stratigraphy of the Chattanooga Shale in Kansas and Oklahoma, *in* Johnson, K. S.; and Cardott, B. J. (eds.), Source rocks in the southern Midcontinent, 1990 symposium: Oklahoma Geological Survey Circular 93, p. 94–105.

Longman, M. W.; and Palmer, S. E., 1987, Organic geochemistry of Midcontinent Middle and Late Ordovician oils: American Association of Petroleum Geologists Bulletin, v. 71, p. 938–950.

Merriam, D. F., 1963, The geologic history of Kansas: Kansas Geological Survey Bulletin 162, 317 p.

Merriam, D. F.; and Smith, Polly, 1961, Preliminary regional structural contour map on top of Arbuckle rocks (Cambrian–Ordovician) in Kansas: Kansas Geological Survey Oil and Gas Investigations 25, map, scale 1:633,600.

Newell, K. D., 1997a, Comparison of maturation data and fluid-inclusion homogenization temperatures to simple thermal models; implications for thermal history and fluid flow in the Mid-continent: Kansas Geological Survey Bulletin 240, p. 13–27; www.kgs.ukans.edu/Current/1997/Newell/newell1.html.

_____ 1997b, Oil-gravity and depth data for oil fields in the Forest City basin of northeastern Kansas, southeastern Nebraska, and northwestern Missouri:

Kansas Geological Survey Open-File Report 1997-15, 14 p.

Newell, K. D.; and Hatch, J. R., 2000, A petroleum system for the Salina basin in Kansas based on organic geochemistry and geologic analog: Natural Resources Research, v. 9, p. 169–200.

Newell, K. D.; Watney, W. L.; Stephens, B. P.; and Hatch, J. R., 1987, Hydrocarbon potential in Forest City basin: The Oil and Gas Journal, v. 85, no. 42, p. 58–62.

Peters, K. E., 1986, Guidelines for evaluating petroleum source rock using programmed pyrolysis: American Association of Petroleum Geologists Bulletin, v. 70, p. 318–329.

Price, L., 1980, Shelf and shallow basin oil as related to hot-deep origin of petroleum: Journal of Petroleum Geology, v. 3, no. 1, p. 91–116.

Reed, J. D.; Illich, H. A.; and Horsfield, B., 1986, Biochemical evolutionary significance of Ordovician oils and their sources: Organic Geochemistry, v. 10, no. 1–3, p. 347–358.

Rich, J. L., 1931, Function of carrier beds in long-distance migration of oil: American Association of Petroleum Geologists Bulletin, v. 15, p. 911–924.

_____ 1933, Distribution of oil pools in Kansas in relation to pre-Mississippian structure and areal geology: American Association of Petroleum Geologists Bulletin, v. 17, p. 793–815.

APPENDIX: Summary of Rock-Eval™ Analyses, Salina Basin and Forest City Basin, Kansas

Number of Analyses	Well, Location Age / Group / Formation	Elevation Shallowest	 Deepest	 Average	Tmax Values Lowest	 Highest	 Average
CORE SAMPLES							
	Damac #1 Allen, SW¼ sec. 7, T. 17 S., R. 3 W. (SALINA BASIN), 1,360′ datum						
4	Devonian–Mississippian / Chattanooga Shale	–1,994	–2,008	–1,999	424	439	433
	Champlin #1 Kottman, NE¼SW¼ sec. 19, T. 19 S., R. 8 W. (SALINA BASIN), 1,714′ datum						
6	Ordovician / Simpson Group	–1,165	–1,672	–1,669	426	444	429
	Sutton #3 Bell, NE¼NW¼ sec. 33, T. 19 S., R. 8 W. (SALINA BASIN), 1,614′ datum						
1	Devonian–Mississippian / Chattanooga Shale	–1,649	–1,649	–1,649	424	424	424
	NNG #35-9 Pulliam, N½S½N½ sec. 35, T. 19 S., R. 8 W. (SALINA BASIN), 1,726′ datum						
10	Ordovician / Simpson Group	–1,550	–1,550		430	430	
	NNG #1 Madsen, NE¼SE¼ sec. 35, T. 19 S., R. 8 W. (SALINA BASIN), 1,725′ datum						
3	Ordovician / Simpson Group	–1,542	–1,549		423	434	
	Average Simpson depth and Tmax for Bell, Pulliam, and Madsen wells		–1,546			432	
	NNG #1 Caldwell, NE¼NE¼ sec. 2, T. 20 S., R. 8 W. (SALINA BASIN), 1,720′ datum						
15	Ordovician / Simpson Group	–1,580	–1,627	–1,613	420	437	424
	Champlin #8 Speck, NE¼ sec. 7, T. 20 S., R. 8 W. (SALINA BASIN), 1,671′ datum						
1	Ordovician / Simpson Group	–1,775	–1,775	–1,775	434	434	434
	Derby #4 Arnold, NW¼SW¼ sec. 16, T. 21 S., R. 1 W. (SALINA BASIN), 1,482′ datum						
1	Devonian–Mississippian / Chattanooga Shale	–1,835	–1,835	–1,835	439	439	439
	Shell #4 Koehn, SW¼NE¼NE¼ sec. 16, T. 21 S., R. 3 W. (SALINA BASIN), 1,450′ datum						
2	Ordovician / Simpson Group	–1,957	–1,959	–1,958	438	440	439
	Mabee-Shell #1 Friessen, NW¼SW¼SE¼ sec. 33, T. 21 S., R. 3 W. (SALINA BASIN), 1,465′ datum						
1	Devonian–Mississippian / Chattanooga Shale	–2,011	–2,011	–2,011	417	417	417
	Shell #1 A.C. Gordon, W½W½NE¼ sec. 21, T. 21 S., R. 10 W. (SALINA BASIN), 1,727′ datum						
1	Ordovician / Simpson Group	–1,689	–1,689	–1,689	426	426	426
	Tomlinson #1 Boese, N½NW¼NW¼ sec. 24, T. 22 S., R. 2 W. (SALINA BASIN), 1,474′ datum						
2	Ordovician / Simpson Group	–1,958	–1,988	–1,973	428	445	437
	Derby #1 Wood, NE¼NE¼ sec. 36, T. 22 S., R. 5 W. (SALINA BASIN), 1,531′ datum						
1	Devonian–Mississippian / Chattanooga Shale	–2,239	–2,239	–2,239	435	435	435
1	Ordovician / Maquoketa Shale	–2,354	–2,354	–2,354	434	434	434
	Derby #1 Rainbow, NW¼NW¼SE¼ sec. 33, T. 22 S., R. 7 W. (SALINA BASIN), 1,600′ datum						
3	Ordovician / Simpson Group	–2,318	–2,332	–2,325	430	436	432
	Kansas Geological Survey Vermillion Core, SE¼NE¼NW¼ sec. 3, T. 4 S., R. 12 E. (SALINA BASIN), 1,210′ datum						
1	Ordovician / Simpson Group	105	105	105	428	428	428
	Texaco #1 Poersch, SW¼SW¼ sec. 31, T. 5 S., R. 5 E. (SALINA BASIN), 1,411′ datum						
5	Ordovician / Simpson Group	–1,293	–1,387	–1,339	423	434	428
	Kansas Geological Survey #1A Edmonds, SE¼NW¼SW¼ sec. 35, T. 9 S., R. 22 E. (FOREST CITY BASIN), 941′ datum						
4	Pennsylvanian	538	540	539	422	432	425
	Carter #2-A Davis, SW¼NE¼SW¼ sec. 33, T. 13 S., R. 10 E. (FOREST CITY BASIN), 1,428′ datum						
10	Pennsylvanian	–435	–436	–435	423	431	426
4	Devonian–Mississippian / Chattanooga Shale	–1,550	–1,552	–1,551	430	441	434
10	Ordovician / Simpson Group	–1,871	–1,898	–1,890	432	452	439
	Shell #1 Farr, NW¼SE¼SW¼ sec. 7, T. 20 S., R. 12 E. (FOREST CITY BASIN), 1,135′ datum						
1	Devonian–Mississippian / Chattanooga Shale	–1,240	–1,240		442	442	
	Shell #1 Friday, NE¼SW¼SW¼ sec. 9, T. 20 S., R. 12 E. (FOREST CITY BASIN), 1,187′ datum						
1	Devonian–Mississippian / Chattanooga Shale	–1,379	–1,379		440	440	
	Average Chattanooga depth and Tmax for Farr and Friday wells		–1,309			441	

(continued on next page)

Number of Analyses	Well, Location Age / Group / Formation	Elevation Shallowest	Deepest	Average	Tmax Values Lowest	Highest	Average
	Marathon #50 J.W. Martindell, SW¼ sec. 31, T. 23 S., R. 10 E. (FOREST CITY BASIN), 1,423′ datum						
5	Pennsylvanian	–673	–792	–866	440	449	445
	ERDA #1 Stauffer, NE¼ sec. 20, T. 23 S., R. 12 E. (FOREST CITY BASIN), 1,136′ datum						
5	Devonian–Mississippian / Chattanooga Shale	–1,099	–1,109	–1,104	442	445	443
	ERDA #1 Bock, SW¼NE¼NE¼ sec. 15, T. 23 S., R. 12 E. (FOREST CITY BASIN), 1,065′ datum						
6	Devonian–Mississippian / Chattanooga Shale	–1,099	–1,109	–1,104	443	445	444
	Kansas Geological Survey #5A Woodward, NE¼SE¼SW¼SE¼ sec. 12, T. 25 S., R. 21 E., 1,045′ datum (estimated)						
6	Pennsylvanian	995	948	993	429	439	435
	Big J Production #1 Harper-Sibberson, SE¼NE¼NW¼ sec. 20, T. 1 N., R. 16 E. (FOREST CITY BASIN—Nebraska), 895′ datum						
1	Devonian–Mississippian / Chattanooga Shale	–1,301	–1,301	–1,301	438	438	438
	Missouri Geological Survey core USAF MC 121, SW¼ sec. 1, T. 40 N., R. 32 W. (FOREST CITY BASIN—Missouri), 851′ datum						
3	Pennsylvanian	789	747	773	436	441	439
	Core WM-9, NE¼SE¼ sec. 9, T. 53 N., R. 36 W. (FOREST CITY BASIN—Missouri), 770′ datum (estimated)						
1	Pennsylvanian	367	367	367	429	429	429
	Core WM-10, SE¼SE¼ sec. 4, T. 59 N., R. 34 W. (FOREST CITY BASIN—Missouri), 1,000′ datum (estimated)						
2	Pennsylvanian	584	578	581	420	424	422
	Iowa Geological Survey Bedford Core, SE¼ sec. 4, T. 67 N., R. 34 W. (FOREST CITY BASIN—Iowa) 1,110′ datum (estimated)						
7	Pennsylvanian	562	1008	754	411	433	423
	Iowa Geological Survey Riverton Core, SE¼SE¼SW¼ sec. 20, T. 67 N., R. 41 W. (FOREST CITY BASIN—Iowa) 1,140′ datum (estimated)						
4	Pennsylvanian	3	1	2	419	433	422
	Iowa Geological Survey Core CP37, NE¼SE¼NE¼ sec. 2, T. 72 N., R. 26 W. (FOREST CITY BASIN—Iowa) 1,130′ datum						
4	Pennsylvanian	865	824	854	422	436	429
	Iowa Geological Survey Jefferson Quarry Core, SE¼NW¼ sec. 17, T. 77 N., R. 31 W. (FOREST CITY BASIN—Iowa) 1,180′ datum (estimated)						
2	Pennsylvanian	1,095	1,094	1,095	412	414	413
CUTTINGS SAMPLES							
	Mallard Drlg. #1 Broeckelman, N½NE¼NE¼ sec. 15, T. 1 S., R. 10 W. (SALINA BASIN), 1,922′ datum						
8	Pennsylvanian	–783	–1,613	–1,226	421	430	425
1	Ordovician / Simpson Group	–2,223	–2,223	–2,223	439	439	439
	Pemsco #1 Schou, NE¼SE¼NE¼ sec. 23, T. 4 S., R. 2 W. (SALINA BASIN), 1,488′ datum						
1	Devonian–Mississippian / Chattanooga Shale	–1,227	–1,227	–1,227	425	425	425
1	Ordovician / Simpson Group	–1,947	–1,947	–1,947	428	428	428
	Wakefield #1 Nelson, SE¼SW¼SW¼ sec. 6, T. 9 S., R. 3 W. (SALINA BASIN), 1,397′ datum						
3	Pennsylvanian	–653	–1,448	–1,041	421	424	423
	Kosarek #1 Lessor, SW¼SE¼SE¼ sec. 11, T. 11 S., R. 9 W. (SALINA BASIN), 1,491′ datum						
2	Pennsylvanian	–1,064	–1,634	–1,349	426	427	427
2	Ordovician / Simpson Group	–2,372	–2,407	–2,390	430	432	431
	Kosarek #1 Nielson, NE¼NE¼ sec. 16, T. 11 S., R. 9 W. (SALINA BASIN), 1,491′ datum						
1	Pennsylvanian	–1,434	–1,434	–1,434	426	426	426
1	Devonian–Mississippian / Chattanooga Shale	–1,729	–1,729	–1,729	431	431	431
	Sunflower #1 Wohler, NW¼NE¼NE¼ sec. 2, T. 11 S., R. 10 W. (SALINA BASIN), 1,507′ datum						
6	Pennsylvanian	–998	–1,688	–1,378	417	432	424
1	Ordovician / Simpson Group	–2,481	–2,481	–2,481	432	432	432
	Shields #2 Strecker, W½SE¼NE¼ sec. 31, T. 11 S., R. 12 W. (SALINA BASIN), 1,739′ datum						
2	Pennsylvanian	–1,143	–1,268	–1,206	424	430	427
	Ogle #1 Stanley, SE¼SW¼ sec. 15, T. 12 S., R. 3 W. (SALINA BASIN), 1,287′ datum						
3	Pennsylvanian	–1,078	–1,348	–1,221	416	420	418
1	Devonian–Mississippian / Chattanooga Shale	–1,978	–1,978	–1,978	430	430	430
1	Ordovician / Simpson Group	–2,391	–2,391	–2,391	425	425	425

(continued on next page)

Number of Analyses	Well, Location Age / Group / Formation	Elevation Shallowest	Deepest	Average	Tmax Values Lowest	Highest	Average
	Range #1 Winslow, N½S½ sec. 5, T. 14 S., R. 2 W. (SALINA BASIN), 1,213′ datum						
11	Pennsylvanian	–892	–1,357	–1,106	423	430	427
4	Devonian–Mississippian / Chattanooga Shale	–1,522	–1,692	–1,591	430	433	432
	Brandt #10 Dunsford, SW¼ sec. 23, T. 19 S., R. 2 W. (SALINA BASIN), 1,550′ datum						
2	Pennsylvanian	–1,348	–1,365	–1,356	428	429	429
4	Ordovician / Simpson Group	–1,825	–1,920	–1,878	434	441	439
	Holl #1-23 IHDE, NE¼NE¼SE¼ sec. 23, T. 19 S., R. 6 W. (SALINA BASIN), 1,582′ datum						
2	Pennsylvanian	–963	–1503	–1,233	427	435	431
	Walker #1 Baerg, SE¼NW¼ sec. 25, T. 20 S., R. 4 W. (SALINA BASIN), 1,472′ datum						
4	Pennsylvanian	–863	–1,503	–1,251	429	441	436
	Walker #1-08 Goertzen, SE¼NW¼SW¼ sec. 8, T. 22 S., R. 4 W. (SALINA BASIN), 1,535′ datum						
2	Pennsylvanian	–1,805	–1,855	–1,830	431	432	432
4	Devonian–Mississippian / Chattanooga Shale	–2,145	–2,330	–2,226	430	434	431
1	Ordovician / Simpson Group	–2,445	–2,445	–2,445	435	435	435
	Dallas Group #1-83 Rift, NE¼SE¼NW¼ sec. 8, T. 1 S., R. 1 E. (SALINA BASIN), 1,604′ datum						
3	Pennsylvanian	–236	–796	–513	413	419	417
1	Ordovician / Simpson Group	–1,561	–1,561	–1,561	409	409	409
	Roxy Resources #1-14 Schneider, NW¼SE¼SW¼ sec. 14, T. 1 S., R. 14 E. (FOREST CITY BASIN), 1,204′ datum						
10	Pennsylvanian	399	–1,131	–430	416	431	425
2	Devonian–Mississippian / Chattanooga Shale	–1,341	–1,481	–1,411	431	433	432
1	Ordovician / Simpson Group	–2,506	–2,506	–2,506	441	441	441
	Producers Eng. et al. #1-4 Finn, S½S½NE¼ sec. 4, T. 4 S., R. 7 E. (SALINA BASIN), 1,362′ datum						
1	Ordovician / Simpson Group	–738	–738	–738	424	424	424
	Mid Gulf #1 Caudle Farm, NE¼NE¼NW¼ sec. 28, T. 4 S., R. 20 E. (FOREST CITY BASIN), 1,025′ datum						
6	Pennsylvanian	575	–1,090	–325	426	434	429
1	Ordovician / Simpson Group	–1,703	–1,703	–1,703	446	446	446
	Texaco #1 Poersch, SW¼SW¼ sec. 31, T. 5 S., R. 5 E. (SALINA BASIN), 1,411′ datum						
4	Pennsylvanian	676	–327	169	405	421	414
1	Devonian–Mississippian / Chattanooga Shale	–459	–459	–459	421	421	421
	Pendleton #1 Steinlage, SE¼NE¼ sec. 27, T. 5 S., R. 12 E. (SALINA BASIN), 1,290′ datum						
1	Pennsylvanian	408	408	408	434	434	434
1	Devonian–Mississippian / Chattanooga Shale	–318	–318	–318	427	427	427
1	Ordovician / Simpson Group	–1,315	–1,315	–1,315	432	432	432
	Pendleton #1 Hermesch, NW¼SE¼SE¼ sec. 9, T. 5 S., R. 13 E. (FOREST CITY BASIN), 1,342′ datum						
1	Devonian–Mississippian / Chattanooga Shale	–1,393	–1,393	–1,393	433	433	433
1	Ordovician / Simpson Group	–2,418	–2,418	–2,418	422	422	422
	Wakefield #1 Bergin, N½SE¼NW¼ sec. 36, T. 7 S., R. 2 E. (SALINA BASIN), 1,213′ datum						
4	Pennsylvanian	–302	–652	–472	409	433	421
	Heller #1 Stice, NW¼ sec. 11, T. 14 S., R. 8 E. (SALINA BASIN), 1,481′ datum						
10	Pennsylvanian	296	–394	–176	430	460	440
1	Devonian–Mississippian / Chattanooga Shale	–594	–594	–594	444	444	444
	Discovery #1 Rindt, NE¼NE¼NW¼ sec. 23, T. 16 S., R. 5 E. (SALINA BASIN), 1,479′ datum						
2	Pennsylvanian	–76	–506	–291	419	421	420
	Range Oil #1-A Gutsch, SE¼NE¼NW¼ sec. 14, T. 17 S., R. 5 E. (SALINA BASIN), 1,442′ datum						
1	Pennsylvanian	–20	–20	–20	428	428	428
	Diamond-Shamrock #1-9 Skully 181, SE¼SE¼ sec. 9, T. 18 S., R. 1 E. (SALINA BASIN), 1,439′ datum						
6	Pennsylvanian	–471	–1,146	–891	430	434	433
1	Devonian–Mississippian / Chattanooga Shale	–1,596	–1,596	–1,596	440	440	440
3	Ordovician / Simpson Group	–1,829	–1,836	–1,821	443	451	447
	Walker #1-15 Unruh, NW¼SW¼SE¼ sec. 15, T. 20 S., R. 1 E. (SALINA BASIN), 1,485′ datum						
2	Pennsylvanian	–509	–994	–752	427	430	429
1	Devonian–Mississippian / Chattanooga Shale	–1,630	–1,630	–1,630	430	430	430
	Stone #1 McCartney, SE¼SE¼SE¼ sec. 5, T. 64 N., R. 39 W. (FOREST CITY BASIN—Missouri), 1,039′ datum						
5	Ordovician / Simspon Group	–2,087	–2,134	–2,107	437	442	440

Compartmentalization of the Overpressured Interval in the Anadarko Basin

Zuhair Al-Shaieb and Jim Puckette
Oklahoma State University
Stillwater, Oklahoma

Phebe Deyhim
Anadarko Petroleum
Houston, Texas

Amy Close
Oklahoma State University
Stillwater, Oklahoma

ABSTRACT.—Reservoir pressures within the lithologic column in the Anadarko basin are a tiered system. The overpressured zone termed the *megacompartment complex* (MCC) is overlain and underlain by normally pressured intervals. Compartments are classified in three different groups or levels. The basin-wide MCC is termed Level 1 compartment. Within the MCC, reservoirs that form fields or districts generally have similar pressure values. These fields or districts are termed Level 2 compartments. Detailed analyses of initial pressure, fluid types, and decline curves indicate that Level 1 and 2 compartments contain many smaller and isolated (sealed) compartments termed Level 3 type. The seals occur mainly in clay- or sand-rich rocks and may exhibit diagenetic banding patterns.

Banding patterns in clay-rich rocks seem to form independently of sedimentary textures or result from the enhancement or modification of sedimentary features. Diagenetic bands in sandstones typically consist of silica- and carbonate-cemented layers that are separated by clay-coated porous layers. Stylolites and other pressure-solution features such as penetrating grain boundaries suggest a mechanism for the source of silica cements. The integration of tectonic history, stratigraphic relationships, facies distribution, thermal history, and diagenetic patterns of seal zones suggests that seals and compartments evolved primarily during the Pennsylvanian orogenic episode. This occurred during the rapid subsidence phase of the orogeny during a period of approximately 30 million years.

INTRODUCTION

Basin compartmentalization, a concept introduced by Bradley (1975) and Powley (1987), is an important concept in the exploration and production of hydrocarbons in deep sedimentary basins. A compartment consists of a porous internal volume and a surrounding low-permeability seal. Compartmentalization occurs beyond a certain depth because of the interplay of a number of geologic processes, particularly subsidence and sedimentation rates, lithologies, and diagenetic modifications. These compartments within abnormally pressured zones exhibit distinctly different pressure as contrasted to their immediate surroundings. They are recognized most easily on pressure-depth profiles by their departure from the normal hydrostatic gradient.

The Anadarko basin provides an excellent example to study geometric configuration and sealing processes of abnormally overpressured compartments. Integrated pore-pressure and subsurface geologic data indicate the presence of an overpressured and completely sealed compartment of a basin-wide scale; the term *megacompartment complex* (MCC) was thus introduced by (Al-Shaieb and others, 1990; Al-Shaieb, 1991) to describe this feature (Fig. 1). The MCC encompasses sections in the Devonian, Mississippian, and Pennsylvanian Systems. It consists of a network of totally isolated, smaller nested compartments.

Isolation of the MCC has been maintained for a considerably long geologic time (early Missourian to present) by means of encasement by top, basal, and lateral seals (Al-Shaieb and others, 1990, 1994a).

Al-Shaieb, Zuhair; Puckette, Jim; Deyhim, Phebe; and Close, Amy, 2001, Compartmentalization of the overpressured interval in the Anadarko basin, *in* Johnson, K. S.; and Merriam, D. F. (eds.), Petroleum systems of sedimentary basins in the southern Midcontinent, 2000 symposium: Oklahoma Geological Survey Circular 106, p. 121–131.

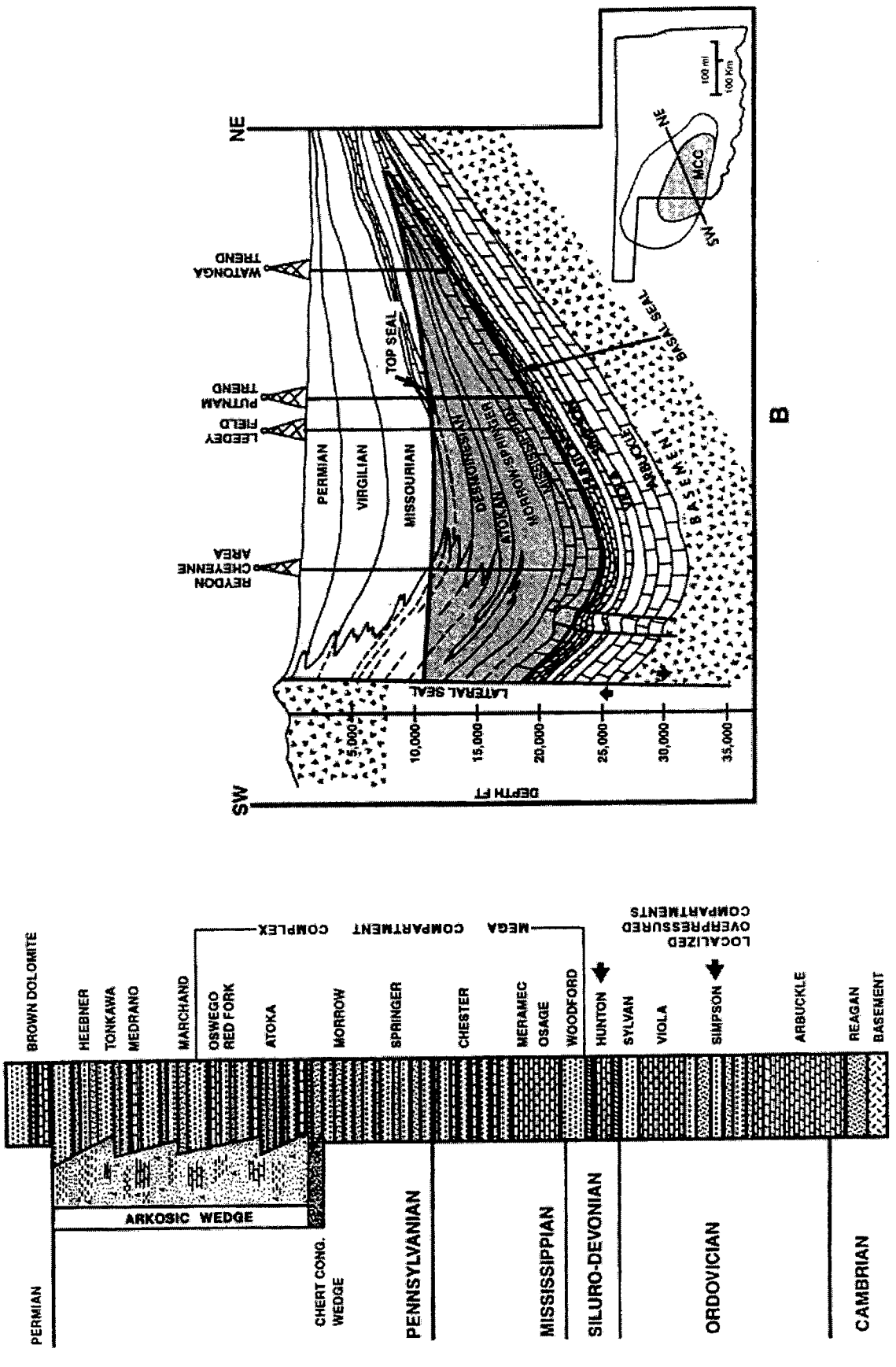

Figure 1. (A) Generalized stratigraphic column of the Anadarko basin showing the intervals contained within the megacompartment complex (MCC); also the stratigraphic position of two localized overpressured compartments (arrows) outside the MCC (after Evans, 1979). (B) Generalized cross section of the Anadarko basin showing the spatial position of the MCC within the basin. Geopressures within the MCC are maintained by top, lateral, and basal seals.

Compartments nested within the MCC are isolated from each other by an intricately complex framework of seals. Seal rocks display unique diagenetic banding structures that formed as a result of the mechano-chemical processes of compaction, dissolution, and precipitation.

LEVELS OF COMPARTMENTALIZATION

Three distinct levels of compartmentalization were recognized (Al-Shaieb and others, 1994b). Level I is a regional feature that transects stratigraphic boundaries and includes most of the overpressured rocks in the basin. Level II is a field- or district-sized feature with relatively uniform pressure gradients that occurs within a stratigraphic interval. Level III compartments are the smallest in size and consist of single, small field- to reservoir-size compartments within a particular stratigraphic unit. The size and geometry of these compartments are linked strongly to their depositional setting and facies.

Level I Compartments

The first level of compartmentalization is a basin-wide overpressured volume termed the megacompartment complex. The MCC in the Anadarko basin is an elongate body of overpressured rocks approximately 240 km (150 mi) long and 113 m (70 mi) wide that has a maximum thickness of about 4,880 m (16,000 ft) (Fig. 1). Pressure data indicate that the top of the MCC is located between 2,290 m (7,500 ft) and 3,050 m (10,000 ft) below the surface. The top is shallower in the proximity of the Nemaha Ridge in central Oklahoma and dips gently westward toward the basin axis, where it occurs about 3,050 m (10,000 ft) deep in western Oklahoma. The MCC contains strata from the Upper Pennsylvanian at 2,290 m (7,500 ft) to the Woodford Shale at 3,050 m (10,000 ft). All reservoirs within this complex are overpressured (Fig. 1).

Level II Compartments

Level II compartments typically are restricted to a specific stratigraphic horizon. Pressure measurements within each horizon are relatively uniform and predictable across a trend. Examples, such as the Morrowan Watonga and Chert Conglomerate trends, may be identified by their distinct pressure regimes. They also are delineated by use of pressure gradients and potentiometric-surface maps. Figure 2 is a three-dimensional Morrowan potentiometric diagram showing the Watonga trend as a "ridge-like" feature along the eastern edge of the basin, whereas peaks of the Chert Conglomerate potentiometric values are identified as the "castle-like" feature in the southwestern corner of the basin. The individual peaks within these Level II compartments represent the third compartmentalization level.

Level III Compartments

The Level III compartments are single, small field- or reservoir-size subdivisions generally nested within Level II. The geometry is related closely to the depositional facies of the associated reservoirs. Examples of this type include the Southwest Leedey Red Fork Sandstone reservoir (Al-Shaieb and others, 1990), the "Old Woman" channel-fill reservoir in the North Geary area of the Watonga trend, and individual reservoirs within the Upper Morrowan Chert Conglomerate (Reydon-Cheyenne fields in western Oklahoma). Their distinct pressure gradients, fluid types (gas/oil and water ratios), and pressure-decline curves that indicate isolation from nearby reservoirs, identify these Level III compartments.

Figure 3 is a schematic diagram that depicts the relationship between the three levels of compartmentalization in the Anadarko basin. Figure 4 is a pressure-depth profile that graphically portrays the relationship among Level I, II, and III compartments.

BANDING FEATURES WITHIN MEGACOMPARTMENT COMPLEX

Many seal rocks display unique diagenetic banding that formed as a result of the interplay of stress-induced mineral reactions, pore-fluid interactions, mass transport, and precipitation. This banding is observed in rocks that were buried deep enough to enter the "seal window." In the Anadarko basin, the seal window occurs between 1,829 and 3,000 m (6,000–9,843 ft). Rocks from shallower intervals clearly lack banding features. The origin of such features has been simulated using reaction-transport models developed by Dewers and Ortoleva (1988, 1990).

Banding in Sandstones

Silica-cement bands (Fig. 5) occur in sandstones and consist of zones of enhanced quartz overgrowths alternating with bands of preserved interparticle porosity. The silica seemingly was derived from pressure solution of quartz grains in the adjacent band. Porous regions generally contain thicker clay coatings on grains, suggesting clay-inhibition of quartz cementation in these areas. Silica bands may occur relatively early in the diagenetic history of the rocks—at depths of 2,000 m (~6,500 ft) and temperatures at ~65°C—and reflect the mechano-chemical processes associated with burial compaction, dissolution, and precipitation as described by Ortoleva and others (1993).

The alternation of permeable and cemented sandstones within the diagenetically banded pressure seal in the Ordovician Simpson Group in Oklahoma is a manifestation of these processes. The compositionally homogeneous First Bromide Sandstone Member contains silica bands that seemingly were generated by local dissolution and precipitation. Sandstones with thin nonpervasive clay-grain coating had undergone compaction and became a likely silica source. Adjacent intervals received imported silica and evolved into silica-cemented bands. In contrast, clay coatings inhibited silica precipitation and preserved primary porosity.

A second type of banding observed in sandstones consists of carbonate that postdated the silica bands. Carbonate-cementation bands may consist of calcite or

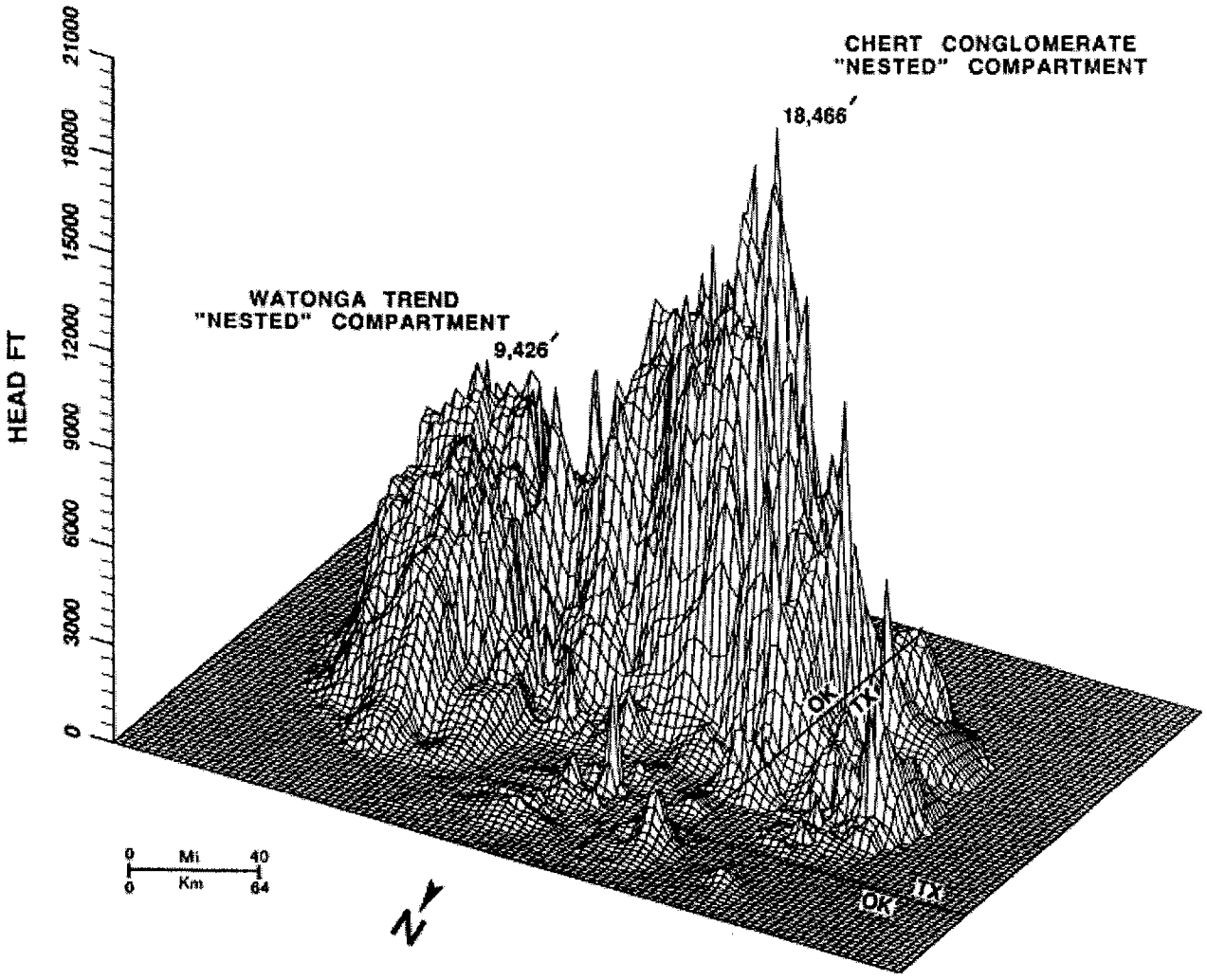

Figure 2. Three-dimensional diagram of potentiometric surface values of Morrowan Series that constitute the middle and part of the lower portion of the megacompartment complex (MCC). All peaks represent overpressured Morrowan rocks within the MCC. The plane of zero feet coincides with the surface elevation of the Anadarko basin.

dolomite that alternate with porous bands of silica-cemented sandstones (Fig. 6). Carbonate bands occur on scales similar to those observed for silica bands. They may form a collection of millimeter-scale bands within a thin (4-in.; 10-cm) interval or consist of thicker (2–4-in., 5–10-cm) bands.

In the Bromide sandstone interval, the earliest diagenetic calcite cements seemly were derived from compactional dissolution of carbonates within or adjacent to the sandstones. Potential sources include limestone beds and fossil-rich zones within the sandstone and perhaps from the overlying Bromide and Viola carbonates.

In the Simpson sandstone seal, $\delta^{13}C$ and $\delta^{18}O$ values of several carbonate cements range from –5 to –9 and from –7 to –11, respectively. These isotopic compositions indicate that the carbon was derived partially from an organic source, whereas the oxygen-isotope ratios indicate relatively higher-temperature fluids. On the other hand, the $\delta^{13}C$ values of most carbonate cements [0–4 PDB (Pedee belemnite isotopic standard)] suggest a marine source for the carbon. A crossplot of carbon- and oxygen-isotopic compositions is shown in Figure 7.

Fluid inclusions within the silica and carbonate cements in the Ordovician Simpson Group sandstone seal interval were examined to determine the timing, temperature, and nature of fluids that resulted in generation of diagenetic cements. A burial-history curve, modified after Schmoker (1986), was constructed for the southeastern part of the Anadarko basin. The homogenization temperatures (T_h) of fluid inclusions from various cement phases (Fig. 8) were plotted on the curve (Fig. 9) to depict the timing relationships of cementation phases during burial history.

Relationships of Cementation Phases

Inclusion homogenization temperatures (T_h) of four cementation episodes (labeled Q-1, C-1, C-2, and Q-2) are shown in Figure 8. The first episode consists of two-

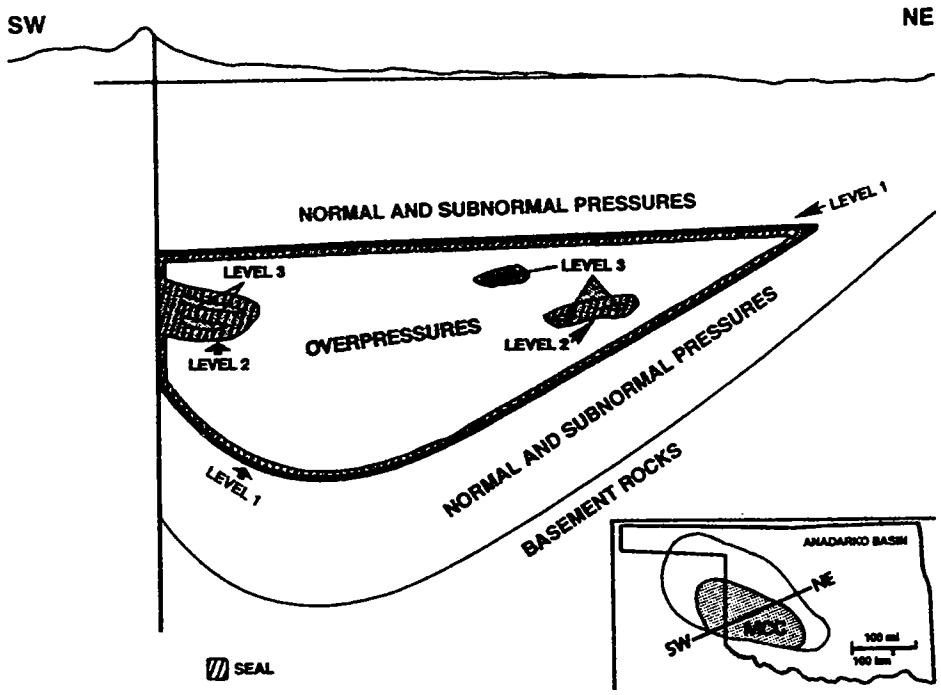

Figure 3. Schematic diagram illustrating the spatial relationship of the three levels of compartmentation in the Anadarko basin. Inset map shows the areal extent of the megacompartment complex (MCC) within the basin.

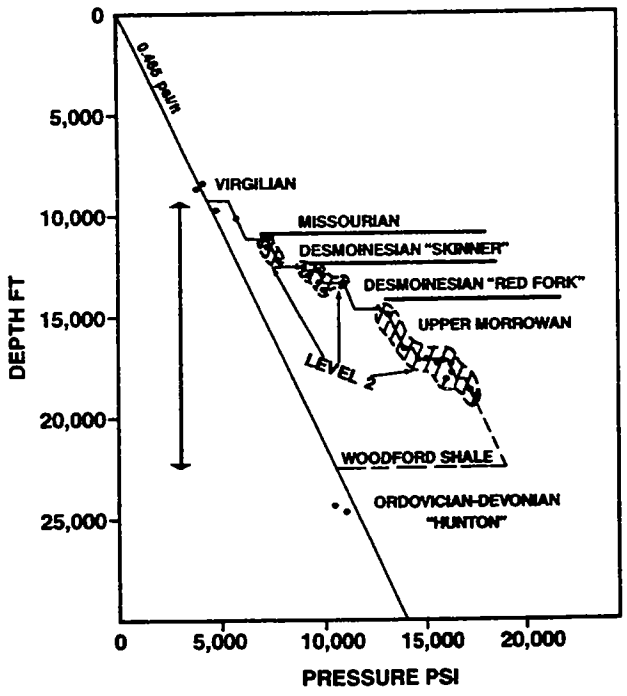

Figure 4. Graphic representation on a pressure-depth profile illustrating the relationship among Levels 1, 2, and 3. Note Level 2 compartments essentially are clusters of isolated Level 3 compartments. The pressure-depth profile was constructed in the Reydon-Cheyenne area in western Oklahoma.

phase aqueous-fluid inclusions from silica cement (Q-1) with T_h values ranging from 70°C to 100°C. The second episode consists of two-phase aqueous-fluid inclusions from calcite cement (C-1) with T_h values concentrated between 80°C and 110°C. The third episode consists of petroleum-bearing and aqueous inclusions from second calcite (C-2) cement. The T_h values for the hydrocarbon-bearing inclusions range from 95°C to 140°C. The fourth episode is later silica (Q-2) cement that contains hydrocarbon inclusions. The T_h values of the second silica cement range from 110°C to 120°C. The genesis of petroleum-free, higher-temperature calcite (C-1) inclusions (T_h >120°C) may be related to hot, basinal fluids. The relationship of the cement stratigraphy, therefore, is highly important in the interpretation of seal evolution.

Banding in Clay-Rich Rocks

Shales and siltstones of seal intervals contain distinct diagenetic bands. Comparative analyses of cores and outcrops of shales and siltstones reveal that this banding is noticeably absent in rocks that were never buried deeply enough to become overpressured. In the Pennsylvanian Pink Limestone/Red Fork Sandstone interval, diagenetic bands seemingly developed independently of any depositional facies. On the other hand, banding in the Devonian Woodford Shale generally occurs as an enhancement or modification of existing sedimentary features.

The Pink Limestone/Red Fork Sandstone seal interval consists of calcareous black shales and thinly laminated siltstones and shales. The frequency of

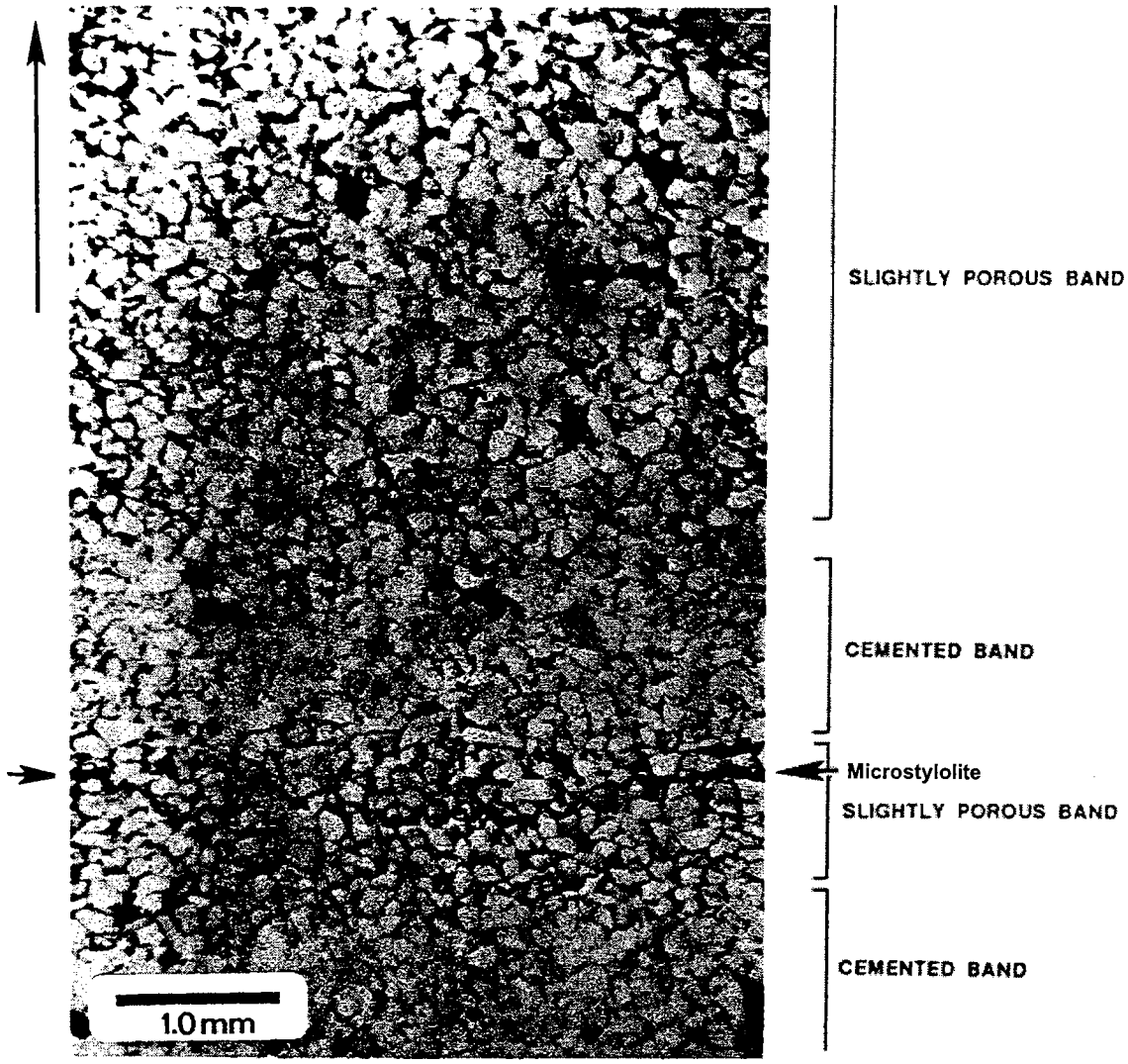

Figure 5. Alternating porous and silica-cemented bands in the Springer Lower Cunningham sandstone. The microstyolite is manifestation of pressure solution. Silica liberated by dissolution was apparently precipitated as adjacent cemented bands. Gulf, Miller No. 1, Caddo County, Oklahoma. Depth 5,022 m (16,475 ft).

diagenetic bands and lateral extent of the banded interval suggest that this is an effective seal for the underlying overpressured Red Fork reservoirs (Al-Shaieb and others, 1994c). The core data indicate that the seal interval consists of at least 6 m (20 ft) of black shale that contains repetitive diagenetic bands. These bands have specific morphologic characteristics. One group has sharp boundaries between the band and the surrounding shale (Fig. 10). These bands generally are characterized by: (1) uniform thickness and flat shape, or (2) irregular thickness and hummocky or concretionary appearance. The bands are typically chlorite rich. They generally range from 3 to 10 cm (1.25–4 in.) in thickness and are separated by finely laminated, illitic black shale. Some of the bands are cross-cut by fractures that are calcite cemented.

Mercury injection tests indicate that the chlorite bands have much lower porosity and smaller pore throats than the surrounding shales (Powers, 1991). Band porosity is approximately 0.6% contrasted to 6.6% for the host shale. Most pore throat radii in the bands are less than 0.004 microns whereas those in the shale are between 0.011 and 0.004 microns (Powers, 1991). These measurements suggest that repetitive bands restrict fluid flow much more effectively than unaltered shale and are critical to seal competence.

CONCLUSIONS

Integrated pore pressure and potentiometric and geologic data in the Anadarko basin demonstrate the existence of a basin-wide, completely sealed, overpressured compartment, termed a megacompartment complex. Top, basal, and lateral seals enclose the megacompartment complex, and the interior of the complex is subdivided into myriad smaller compartments with distinct pressure gradients. Three levels of compartmentalization were recognized: (1) The top seal is

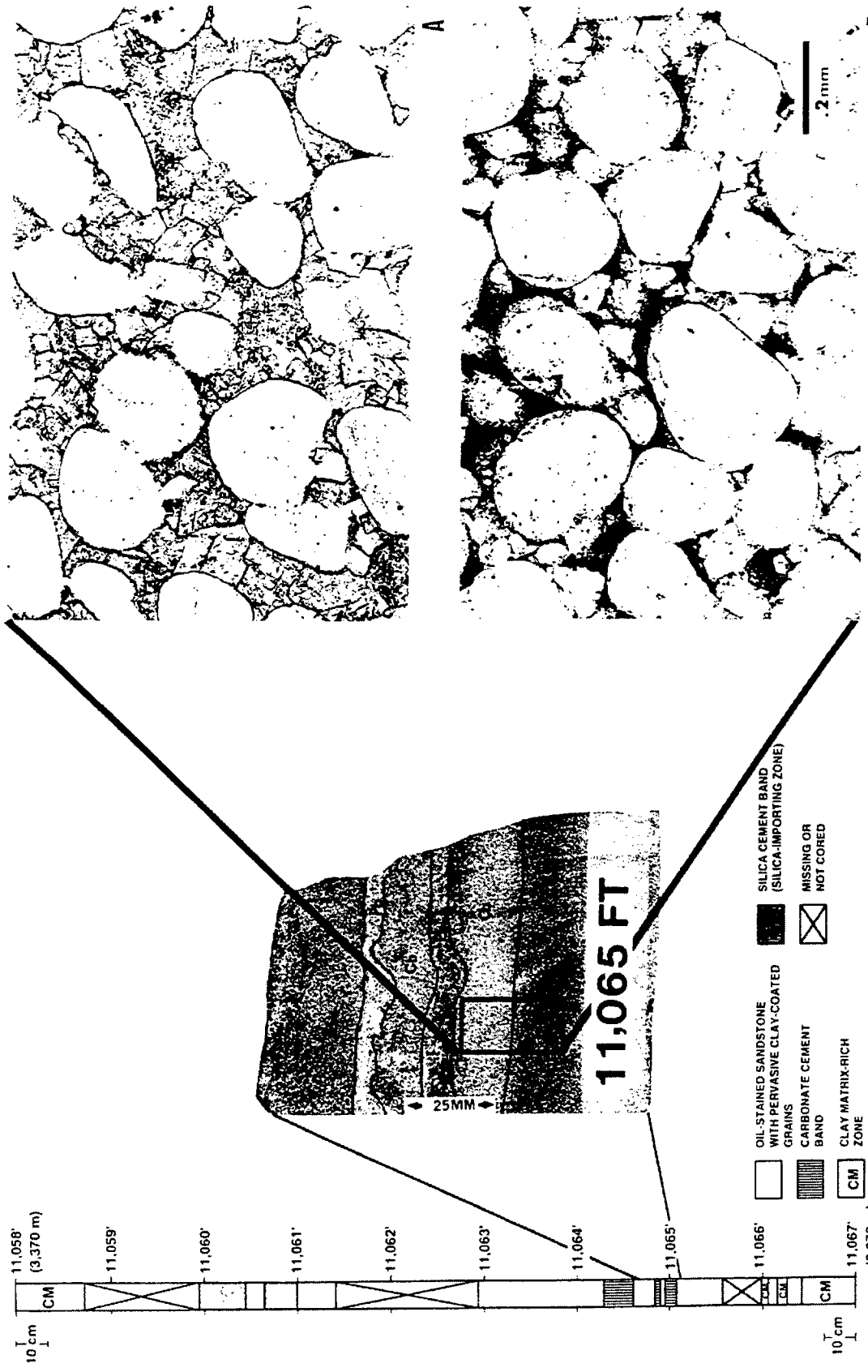

Figure 6. Calcite-cemented bands (Cb) alternating with porous bands (Pb). Photomicrographs: (A) carbonate band, (B) porous band. Gulf, Weaver No. 1. Depth 3,372 m (11,065 ft).

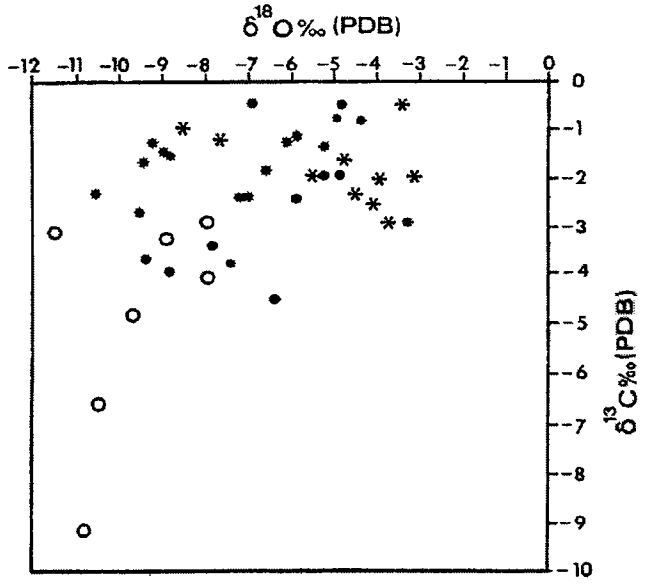

Figure 7. Cross-plot of carbon and oxygen isotope composition for carbonate cements in the Simpson sandstone seal interval. Data are from Al-Shaieb and others (1992), Mitcheltree (1991), and Pitman and Burrus (1989). *Abbreviations:* m = calcite, Weaver Unit No 1; S = dolomite, Weaver Unit No. 1; I = calcite, Costello No. 1 and No. 1 Mazur; R = dolomite/ankerite, Costello No. 1 and No. 1 Mazur.

located between 8,500- and 10,000-ft depths and exhibits distinct banding. (2) The basal seal is basically the Woodford Shale and possibly the Caney Shale. (3) Lateral seals are either associated with fault zones or formed by convergence of the top and lateral seals.

ACKNOWLEDGMENTS

The authors gratefully acknowledge the Gas Research Institute for funding this research through Contract No. 5089–261805. Fluid-inclusion analyses were performed under the supervision of David I. Norman at New Mexico Tech, to whom we express our gratitude. We would also like to thank the American Association of Petroleum Geologists for permission to reprint material from "Compartmentalization of the Overpressured Interval in the Anadarko Basin." We also would like to thank Jingyao Gong and an anonymous reviewer for their constructive editorial comments.

REFERENCES CITED

Al-Shaieb, Z., 1991, Compartmentation, fluid pressure important in Anadarko exploration: Oil and Gas Journal, v. 89, no. 27, p. 52–56.

Al-Shaieb, Z.; Puckette, J.; Ely, P.; and Abdalla, A., 1990, Annual Report prepared for the Gas Research Institute, Chicago, Illinois.

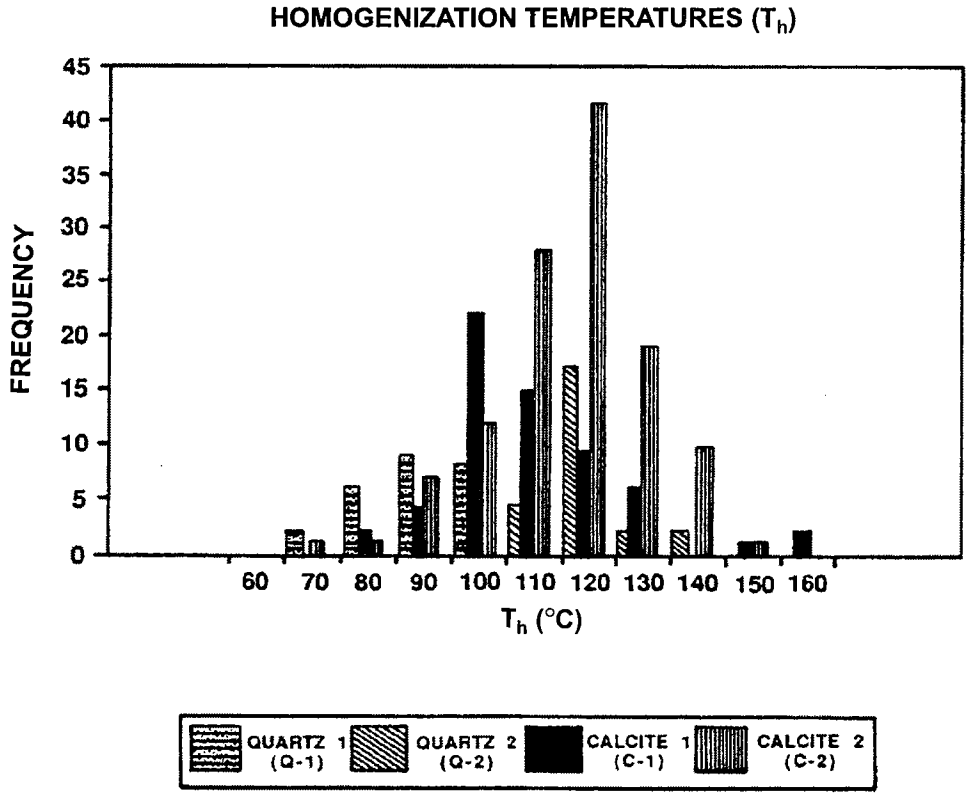

Figure 8. Homogenization temperatures (T_h) of various cement episodes within the Simpson sandstone seal, Gulf, Weaver No. 1.

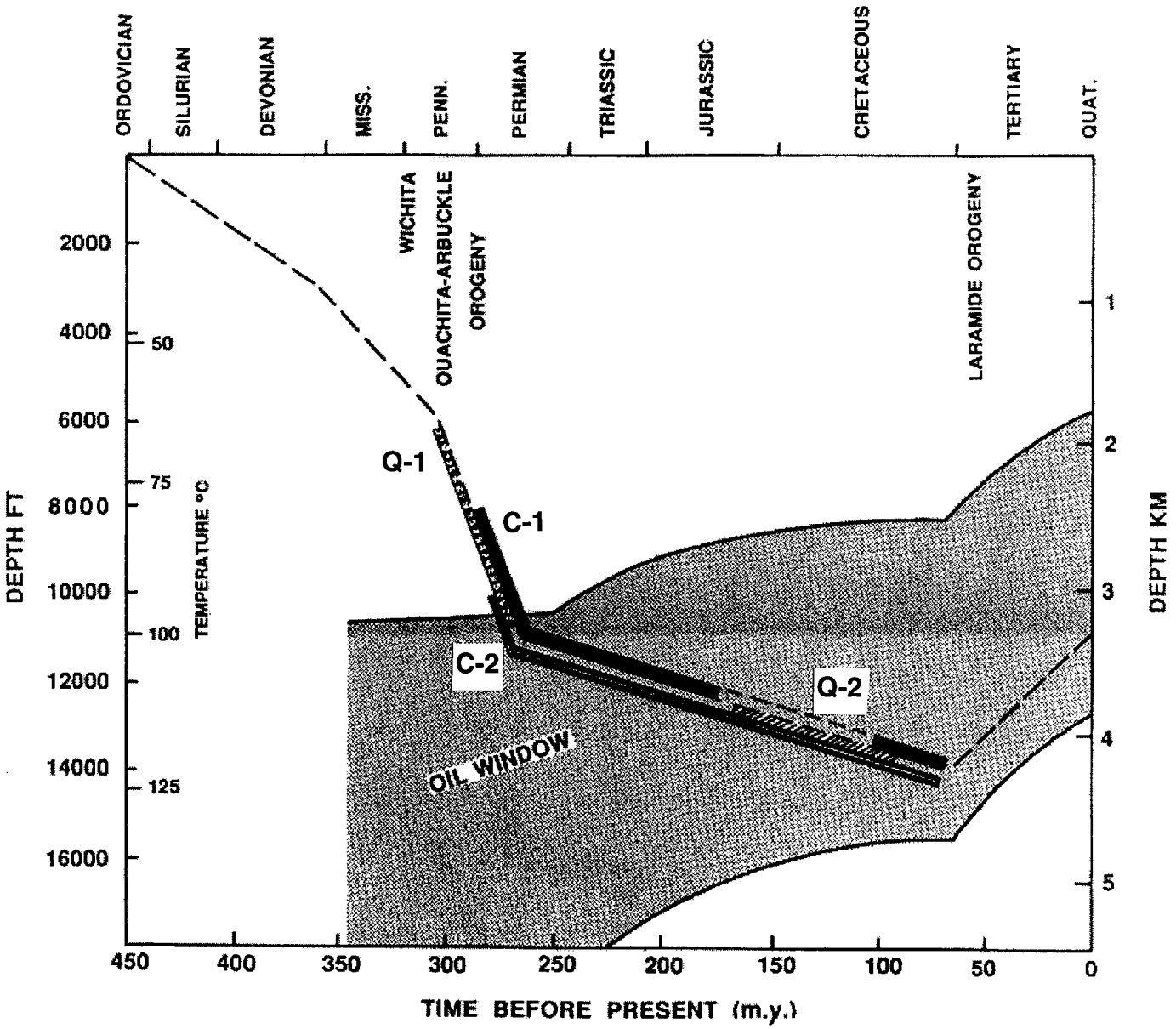

Figure 9. Timing of top-seal-cementation phases in relation to burial history of Simpson interval, Gulf, Weaver No. 1 well.

Al-Shaieb, Z.; Ely, P.; and Abdalla, A., 1992, Isotopic composition of carbonate cements, Gulf Weaver Core: Unpublished report, Oklahoma State University, Stillwater.

Al-Shaieb, Z.; Puckette, J.; Abdalla, A.; and Ely, P. B., 1994a, Megacompartment complex in the Anadarko basin: a completely sealed overpressured phenomenon: American Association of Petroleum Geologists Memoir 61, p. 55–62.

_____ 1994b, Three levels of compartmentation within the overpressured interval of the Anadarko basin: American Association of Petroleum Geologists Memoir 61, p. 70–73.

_____ 1994c, The banded character of pressure seals: American Association of Petroleum Geologists Memoir 61, p. 352–363.

Bradley, J. S., 1975, Abnormal formation pressure: American Association of Petroleum Geologists Bulletin, v. 59, p. 957–973.

Dewers, T.; and Ortoleva, P., 1988, The role of geochemical self-organization in the migration and trapping of hydrocarbons: Applied Geochemistry, v. 3, p. 287–316.

_____ 1990, A coupled reaction/transport/mechanical model for intergranular pressure solution, styolites, and differential compaction and cementation in clean sandstones: Geochimica et Cosmochimica Acta, v. 54, pt. 2, p. 1609–1625.

Evans, J. L., 1979, Major structural and stratigraphic features of the Anadarko basin, *in* Hyne, N. J. (ed.), Pennsylvanian sandstones of the Midcontinent: Tulsa Geological Society Special Publication 1, p. 97–113.

Mitcheltree, D. B., 1991, Diagenetic pressure seal analysis

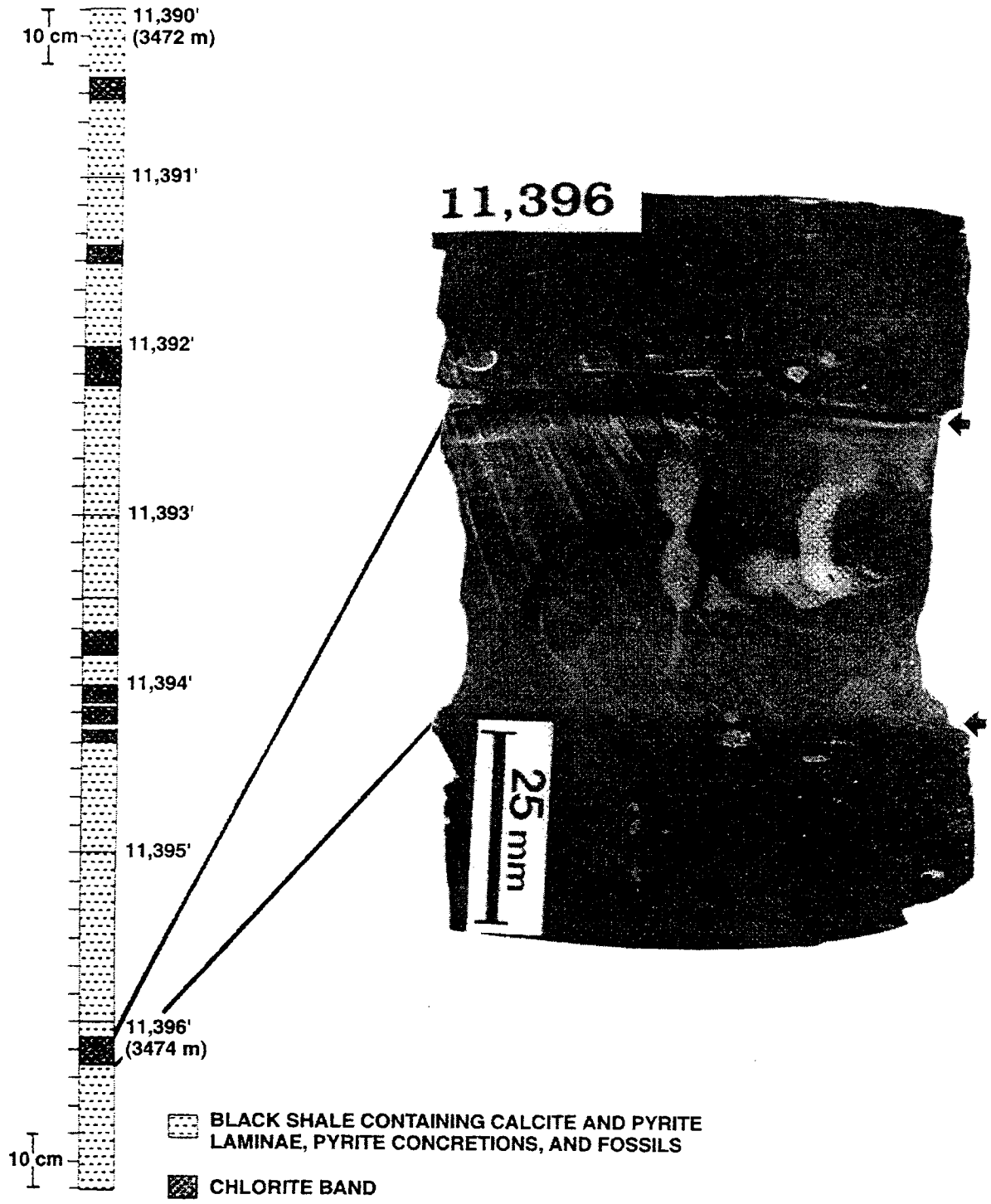

Figure 10. Diagenetic band exhibiting sharp boundaries (arrows) with shale host rock. Fractures are calcite cemented. Schematic diagram indicates location of described feature within the seal zone. Woods, Switzer No. 1, Roger Mills County, Oklahoma. Depth 3,474 m (11,396 ft).

using fluid inclusions and stable isotopes, the Simpson Group (Middle Ordovician), Anadarko basin, Oklahoma: New Mexico Institute of Mining and Technology, Socorro, unpublished M.S. thesis, 107 p.

Ortoleva, P.; Dewers, T.; and Sauer, B., 1993, Modeling diagenetic bedding, stylolites, concretions, and other mesoscopic mechano-chemical structures, *in* Rezak, R.; and Lavoie, D. (eds.), Carbonate microfabrics: Springer-Verlag, New York, p. 291–300.

Pitman, J. K.; and Burrus, R. C., 1989, Diagenesis of hydrocarbon-bearing rocks in the Middle Ordovician Simpson Group, southeastern Anadarko basin, Okla-

homa, *in* Johnson, K. S. (ed.), Anadarko basin symposium, 1988: Oklahoma Geological Survey Circular 90, p. 134–142.

Powers, G. R., 1991, A petrographic study of lithologies forming the top seal in the Anadarko basin: University of Tulsa unpublished M.S. project report, 46 p.

Powley, D. E., 1987, Abnormal pressure seals: Gas sands workshop, Gas Research Institute, Chicago, Illinois.

Schmoker, J. W., 1986, Oil generation in the Anadarko basin: Oklahoma Geological Survey Special Publication 86-3, 40 p.

Overpressures in the Anadarko Basin, Southwestern Oklahoma: Static or Dynamic?*

Youngmin Lee[1] and David Deming
University of Oklahoma
Norman, Oklahoma

ABSTRACT.—Fluid-pressure and temperature data were collected along a north–south linear trend through the Anadarko basin in southwest Oklahoma. Subsurface temperature was estimated from corrected bottom-hole temperature data; the average thermal gradient was 21°C/km. Fluid pressures were estimated from mud weights and well-head shut-in pressures. Fluid pressures above hydrostatic start at a depth of about 2.5 km. On a normalized scale where hydrostatic pressure = 0 and lithostatic pressure = 1, estimates of fluid pressures were found to range from 0.4 to 0.8 over a depth range of 4 to 7 km.

Evaluation of stratigraphic data and paleothermal indicators constrains the Anadarko basin to have undergone from 1 to 3 km of Mesozoic and/or Cenozoic sedimentation followed by subsequent erosion, which started about 50 Ma. Analysis of vitrinite reflectance and apatite fission-track data suggests that the average thermal gradient in the Anadarko basin has been in the range of 21° to 25°C/km over the last 50 Ma. Geologic data indicate unambiguously that the Anadarko basin has cooled over the last tens of millions of years.

Using scale analyses and a simple numerical model, we evaluated two end-member hypotheses (compaction-disequilibrium and hydrocarbon-generation) as possible causes of overpressuring in the Anadarko basin. If compaction disequilibrium is the primary cause of present-day overpressures in the Anadarko basin, the Anadarko basin is required to have an average permeability of 10^{-23} m^2 or lower. If geopressures in the Anadarko basin result from hydrocarbon generation, average basin permeabilities can be as high as 10^{-21} m^2. Scaling these average permeabilities down to thicknesses of 100 m or less implies permeabilities lower than 10^{-25} m^2 are required in the most optimistic scenario. The lowest permeabilities ever measured on sedimentary rocks are in the neighborhood of 10^{-22} to 10^{-23} m^2. Thus, it is not possible to reconcile the existence of overpressures in the Anadarko basin with classic hydrodynamic theories that maintain that aquicludes do not exist. Either some unknown process is generating excess fluid pressures or the Anadarko basin contains pressure seals.

Geopressure models that invoke compaction disequilibrium and are commonly applied to Cenozoic basins undergoing rapid sedimentation (e.g., Gulf Coast basin of southeastern United States) do not appear to apply to the Anadarko basin. The Anadarko basin belongs to a group of cratonic basins that are tectonically quiescent and are characterized by the association of abnormal pressures with natural gas.

INTRODUCTION

Fluid pressures above hydrostatic are common in sedimentary basins throughout the world (Fertl, 1976; Hunt, 1990; Bigelow, 1994; Osborne and Swarbrick, 1997) and are commonly referred to as "geopressures" or "overpressures." Abnormally high fluid pressures in sedimentary basins can potentially be caused by a number of different geologic mechanisms. These include the rapid accumulation of low-permeability sediments, hydrocarbon generation, diagenic dehydration, and aquathermal pressuring (Bethke, 1986; Shi and Wang, 1986; Spencer, 1987; Luo and Vasseur, 1992; Bredehoeft and others, 1994; Audet, 1995; Gordon and Fleming, 1998). The degree to which overpressuring develops depends upon competition between the geologic pressuring-mechanism and pressure dissipation

*This paper is preprinted with permission and with slight modifications from Lee, Youngmin; and Deming, David, 2002, Overpressures in the Anadarko basin, southwestern Oklahoma: static or dynamic: American Association of Petroleum Geologists Bulletin, v. 86.

[1] Present address: Dept. of Geology and Geophysics, Louisiana State University, Baton Rouge.

Lee, Youngmin; and Deming, David, 2001, Overpressure in the Anadarko basin, southwestern Oklahoma: static or dynamic?, *in* Johnson, K. S.; and Merriam, D. F. (eds.), Petroleum systems of sedimentary basins in the southern Midcontinent, 2000 symposium: Oklahoma Geological Survey Circular 106, p. 133–150.

as determined by the hydraulic diffusivity of rocks within a basin (Bredehoeft and Hanshaw, 1968; Neuzil, 1995; Osborne and Swarbrick, 1997).

As discussed by Bredehoeft and others (1994), there are two distinct schools of thought on the creation and maintenance of anomalous fluid pressures in the Earth. The static school (Bradley, 1975; Bradley and Powley, 1994) believed that abnormal pressures are maintained by pressure seals (Hunt, 1990; Ortoleva, 1994). A pressure seal was defined by Hunt (1990, p. 2) as:

> A zone of rocks capable of hydraulic sealing, that is, preventing the flow of oil, gas, and water. The term does not refer to capillary seals . . . the term refers to seals that prevent essentially all pore fluid movement over substantial intervals of geologic time.

The above quote clearly shows that the original intention was to apply the term to rock units that essentially behave as if they have zero permeability over substantial periods of geologic time (about 10^7–10^8 years). However, in the literature in recent years one more commonly finds the term "pressure seal," loosely defined to be any low-permeability unit that is capable of confining abnormal fluid pressures over any time period. This is better defined as an aquitard. In this paper, we prefer to follow Hunt's (1990) original intention and reserve the term "pressure seal" to designate a layer that has zero or near-zero permeability.

In contrast to the static paradigm, the dynamic school embraces the classical hydrogeologic tenet that "there are no totally impermeable geologic materials" (Bredehoeft and others, 1982, p. 297). Although exceptions can be made for unusual materials such as permafrost and salt, the dynamic view is that pressure seals do not exist and are certainly not common in sedimentary basins. In the dynamic paradigm, abnormal formation pressures arise from transient disturbances related to an ongoing geologic process such as rapid sedimentation (Bethke, 1986), time-dependent compaction (Dewers and Ortoleva, 1994), clay dehydration (Audet, 1995; Gordon and Fleming, 1998), or hydrocarbon generation (Spencer, 1987; Bredehoeft and others, 1994). The existence of abnormal fluid pressures implies as a corollary the parallel existence of a geologic process that is actively creating a pressure gradient.

The existence of overpressures in young, rapidly subsiding basins, such as the Gulf Coast basin of the southeast United States or the South Caspian basin of the former Union of Soviet Socialist Republics (Bredehoeft and others, 1988), presents no problems for the dynamic school. Overpressures in these settings are readily explainable as transient compaction disequilibrium related to high sedimentation rates and a predominance of low-permeability shales (Bredehoeft and Hanshaw, 1968; Sharp and Domenico, 1976; Bethke, 1986; Mello and others, 1994). For example, Bethke (1986, p. 6538) showed that anomalous formation pressures in the Gulf Coast basin could be maintained at sedimentation rates of 100–10,000 m/Ma if average shale permeabilities were in the range of 10^{-18} to 10^{-20} m^2. These values are consistent with laboratory measurements of shale permeabilities from the Gulf Coast (Neglia, 1979) as well as estimated Plio–Pleistocene sedimentation rates.

What is not well understood at the present time is how overpressures can exist in older basins that have not undergone active subsidence for tens or hundreds of millions of years. The Anadarko basin in southwestern Oklahoma is known to have areas of extensive overpressuring (Fig. 1) (Hunt, 1990; Al-Shaieb and others, 1992; Al-Shaieb and others, 1994a,b), yet the Anadarko basin has not experienced significant sedimentation for more than 200 million years, and has undergone uplift and erosion for about the last 40 to 50 million years (Gilbert, 1992; Carter and others, 1998; Corrigan and others, 1998; Lee and Deming, 2002, in press).

It is in areas such as the Anadarko basin that the divergence of static and dynamic school hypotheses indicates how little we understand concerning the origin and maintenance of abnormal pressures in older sedimentary basins. The fundamental questions are: what is the cause of the overpressuring, and how is it maintained? In this paper, we approach this problem from the perspective of testing two end-member hypotheses. We first consider as a static hypothesis what average permeability will allow overpressuring in the Anadarko to be explained as a remnant of Paleozoic compaction disequilibrium. Alternatively, we then consider under what circumstances hydrocarbon generation can explain overpressuring.

GEOLOGIC SETTING

The Anadarko basin (Fig. 1), bounded by the Wichita-Amarillo uplift on the south, the Nemaha uplift on the east, and the Cimarron arch on the west, is the deepest sedimentary basin on the North American craton. Total sediment thickness in the deep Anadarko basin exceeds 12 km and consists of sandstones, limestones, and shales of Cambrian to Permian age (Johnson, 1989) (Fig. 2). The Anadarko basin is a prolific producer of both petroleum, and, more important, natural gas. Cumulative hydrocarbon production as of 1985 was >5 million barrels of oil and 2.3 trillion cubic meters of natural gas (Davis and Northcutt, 1989). The Anadarko basin contains ~50 major fields and hundreds of minor ones; production is from both stratigraphic and structural traps. Identified source rocks in the Anadarko basin and surrounding areas mainly consist of Ordovician (Simpson Group shales), Devonian–Mississippian (Woodford Shale), and Pennsylvanian (thick, dark shales) (Johnson and Cardott, 1992). Summaries of the geologic history, stratigraphy, and tectonic setting of the Anadarko basin are given by Gilbert (1992) and in the volume edited by Johnson (1989).

FLUID-PRESSURE DATA

The Anadarko basin is reported in the geologic literature to have areas of overpressuring (Jorgensen, 1989; Hunt, 1990; Al-Shaieb and others, 1992, 1994a, b). Al-Shaieb and others (1992, 1994a,b) stated

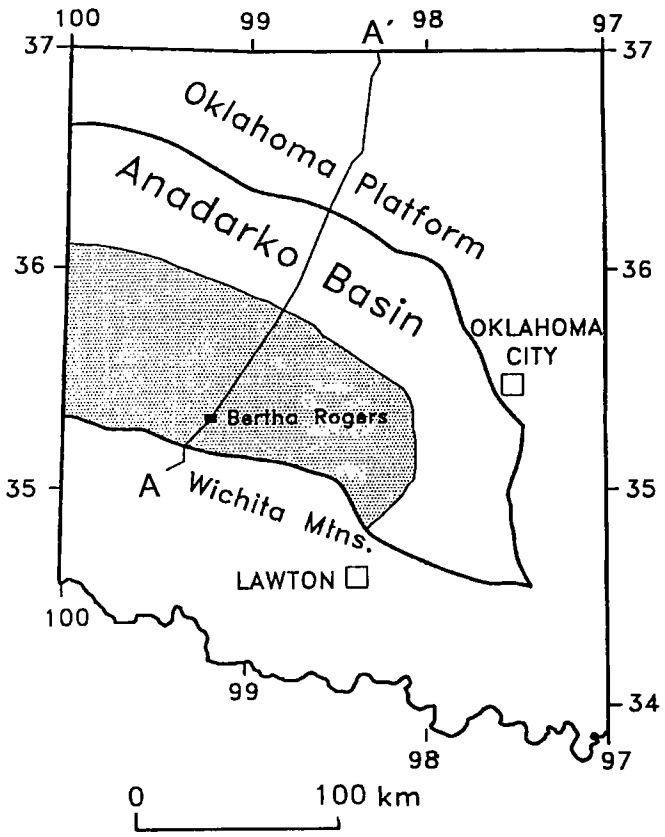

Figure 1. Location of the Anadarko basin and cross section A–A′ in western Oklahoma (after Johnson, 1989). Stippled area represents overpressure zone.

that fluid pressures exceeding hydrostatic generally start at about 2.3 to 3.0 km depth, but return to near-hydrostatic below the Woodford Shale. The three-dimensional overpressured zone was identified by Al-Shaieb and others (1992, 1994a,b) in map view as oval in shape, extending about 267 km along a northwest-southeast trend, and about 100 km from southwest to northeast. Within this three-dimensional volume, high fluid-pressures are not ubiquitous. Rather, they are evidently confined to distinct zones termed compartments. Al-Shaieb and others (1992, 1994a,b) termed the entire volume occupied by pressurized compartments a "megacompartment complex."

To present our data and modeling results, we use a dimensionless normalized pressure (P_n) defined as

$$P_n = \frac{P - P_{hydro}}{P_{lith} - P_{hydro}} \quad (1)$$

where P is fluid pressure, P_{hydro} is hydrostatic pressure (9.8 MPa/km), and P_{lith} is lithostatic pressure (22.5 MPa/km). P_n ranges from 0 for hydrostatic pressure to 1 for lithostatic pressure.

We estimated fluid pressures in the Anadarko basin from two types of data—drilling-mud weights reported on well log headers and well-head shut-in pressures. Due to the size and complexity of the Anadarko basin, we chose to concentrate our data collection and analysis along a southwest–northeast line perpendicular to the strike of the basin structure (Figs. 1, 2).

Mud-weight data (Fig. 3A) were collected from the

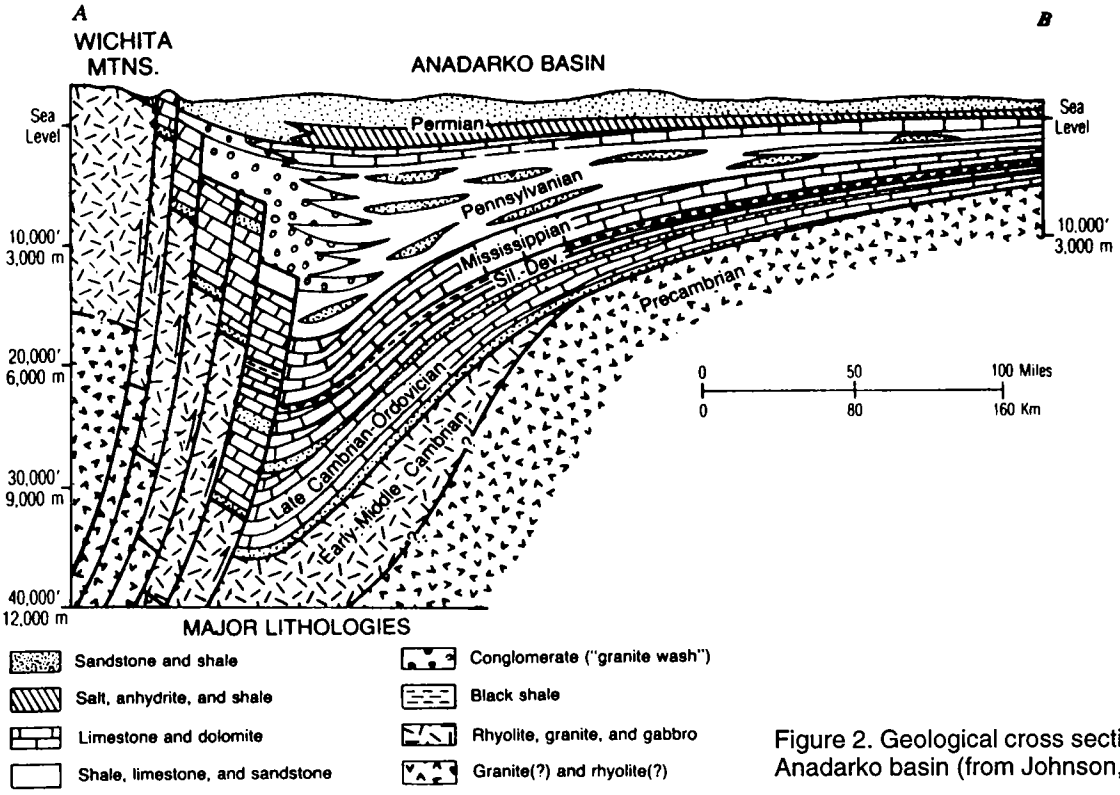

Figure 2. Geological cross section (A–A′) through the Anadarko basin (from Johnson, 1989).

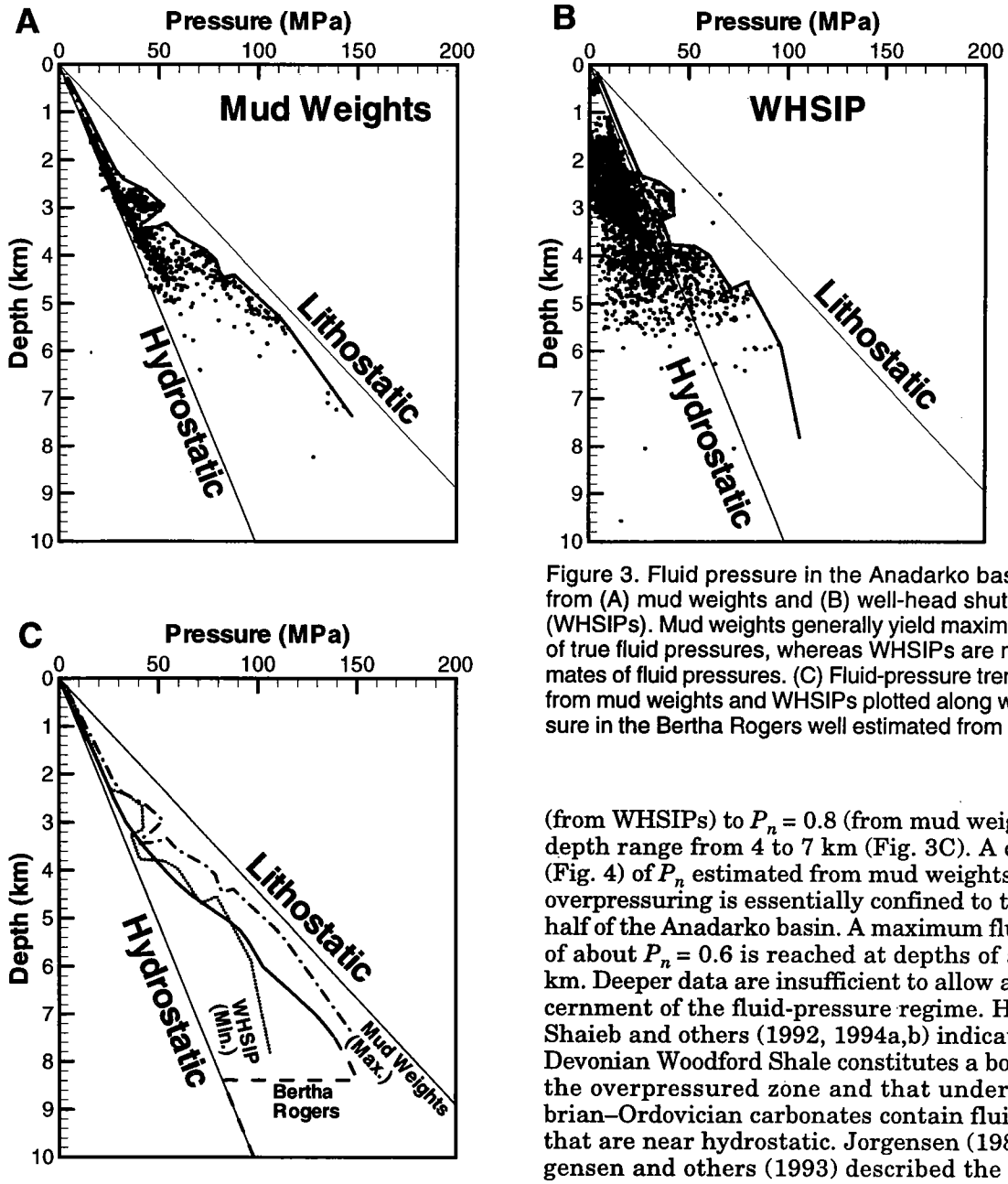

Figure 3. Fluid pressure in the Anadarko basin estimated from (A) mud weights and (B) well-head shut-in pressures (WHSIPs). Mud weights generally yield maximum estimates of true fluid pressures, whereas WHSIPs are minimum estimates of fluid pressures. (C) Fluid-pressure trends estimated from mud weights and WHSIPs plotted along with fluid pressure in the Bertha Rogers well estimated from mud weights.

Oklahoma Geologic Survey well-log library. The ability to estimate *in situ* pressures from drilling-mud weights has limitations. However, the method has been successfully applied in the Gulf Coast basin by Hanor and Sassen (1990). Mud weights represent an upper limit on formation pressure, as the weight of the mud column in the borehole must be greater than formation pressure to avoid the possibility of a blowout. We also estimated fluid pressures from well-head shut-in pressure (WHSIP) data donated by Dwight's Energy Data (Fig. 3B). WHSIPs represent minimum estimates of true formation pressures, because reservoir pressures may be drawn down by production. Comparing the two data types (Fig. 3C) allows us to estimate the limits of probable resolution.

Normalized fluid pressure ranges from $P_n = 0.4$ (from WHSIPs) to $P_n = 0.8$ (from mud weights) for the depth range from 4 to 7 km (Fig. 3C). A contour plot (Fig. 4) of P_n estimated from mud weights shows that overpressuring is essentially confined to the southern half of the Anadarko basin. A maximum fluid pressure of about $P_n = 0.6$ is reached at depths of about 5 to 6 km. Deeper data are insufficient to allow accurate discernment of the fluid-pressure regime. However, Al-Shaieb and others (1992, 1994a,b) indicated that the Devonian Woodford Shale constitutes a bottom seal to the overpressured zone and that underlying Cambrian–Ordovician carbonates contain fluid pressures that are near hydrostatic. Jorgensen (1989) and Jorgensen and others (1993) described the Cambrian–Ordovician carbonates of the central United States as constituting part of the Western Interior Plains aquifer system. However, Jorgensen and others (1993) also said that in "deep basins" the permeability is "greatly reduced" and cited a permeability range of 10^{-12} to 10^{-18} m^2. Although a minimum permeability of 10^{-18} m^2 would be too low to qualify as an aquifer, it is also too high to effectively retain abnormal formation pressures over geologic time (Deming, 1994). It thus seems likely that the geopressured zone in the Anadarko basin does not extend into the basal Cambrian–Ordovician carbonates.

MATHEMATICAL MODELING

General Approach and Philosophy

Mathematical models should be used adjunctively to understand the physics of geologic processes. Most geo-

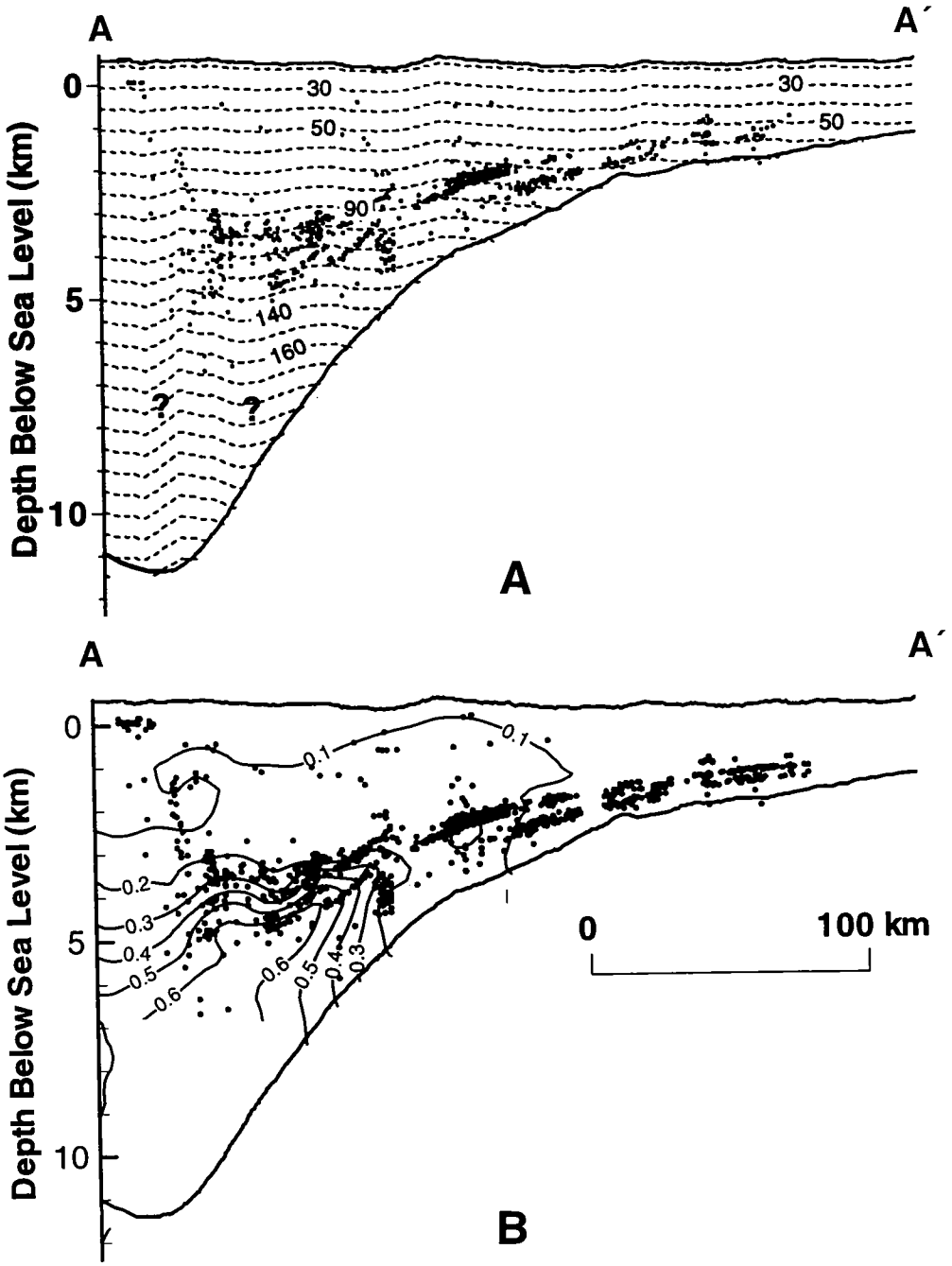

Figure 4. (A) Estimated temperature (degrees Celsius) along the cross section A–A′ through the Anadarko basin and the Oklahoma platform. Dashed lines show estimated temperature, dots show location of bottom-hole–temperature measurements. (B) Fluid pressure estimated along cross section A–A′. Contour lines represent normalized pressure (P_n) estimated from mud weight, and dots show location of mud-weight measurements.

logic settings, including sedimentary basins, are far too complex to reproduce accurately in modern digital computers. As the degree of model complexity grows, so does the problem of obtaining meaningful constraints and results. We therefore favor simple models, because these provide the most insight into the physics of complex geologic problems.

The simplest approach that can be taken with diffusion problems is to conduct a scale analysis that explores the relationship between characteristic times and lengths for different values of a key physical property such as hydraulic diffusivity. For example, Deming (1994) used this approach to demonstrate that in order for geologic units thinner than 100 m to effectively confine anomalous fluid pressures for more than a million years, their permeability would have to be lower than 10^{-23} m^2.

In this study, we found it useful to construct a

TABLE 1. — Model Parameters

Parameter	Value
Specific storage	1×10^{-6}/m
Permeability	variable
Surface temperature	17.5°C
Thermal gradient at present	21°C/km
Thermal gradient at 250 Ma	21–25°C/km
Water viscosity	2.121×10^{-4} kg/m-s
Matrix density	2,650 kg/m^3
Water density	1,000 kg/m^3
Kerogen density	1,150 kg/m^3
Oil density	850 kg/m^3
Gas density	0.718 kg/m^3

simple numerical model for evaluating alternative hypotheses concerning the generation of overpressures in the Anadarko basin. Our approach was to identify one variable, permeability, as the largest unknown, and to pose the following question: For what value or values of permeability is this hypothesis viable? In this approach, other variables (Table 1) were generally held fixed. The justification for this approach was that permeability was unknown by several orders of magnitude, whereas variables such as fluid viscosity were well known to vary within a predictable range.

In keeping with our philosophy of employing the simplest methods available, we used a one-dimensional model with uniform permeability. However, we included a realistic representation of source rocks in this model, because we had reasonably good constraints on depths, kerogen types, and total organic carbon (see below). In contrast, permeability data were essentially missing.

Numerical Model

A generalized description of fluid flow in one dimension is

$$\frac{\partial}{\partial z}\left(K\frac{\partial h}{\partial z}\right)=S_s\frac{\partial h}{\partial t}+\Gamma \qquad (2)$$

where K is hydraulic conductivity, h is hydraulic head, S_s is specific storage, t is time, and Γ is a geologic forcing term (Neuzil, 1995, p.748). Fluid pressure (P) can be estimated from hydraulic head (h) as

$$P=\rho g(h-z) \qquad (3)$$

where ρ is fluid density, g is gravitational acceleration, and z is elevation. In this study, where we dealt with fluid pressures of the order of 10–100 MPa, we assumed that atmospheric pressure on the surface (~0.1 MPa) was negligible.

In general, two different methods can be used for evaluating pressures due to hydrocarbon generation: single and multiphase modeling. Multiphase modeling (e.g., Luo and Vasseur, 1996) is more rigorous than single-phase modeling because the hydraulic properties of three different phases (water, oil, and gas) can be treated separately. However, single-phase modeling can provide feasible results for the distribution of fluid pressures, even though it cannot provide the details of oil migration, hydrocarbon saturation, and capillary pressure (Bredehoeft and others, 1994). Therefore, we used single-phase modeling as the simplest approach that would provide insight into the physics of pressure generation and dissipation in this setting.

Our numerical code was tested against an analytical solution to equation (2) for a homogeneous domain with similar spatial and temporal scales. Carlslaw and Jaeger (1959, p. 131) provide an analytical solution to equation (2) for the case where the forcing function Γ is equal to $A_0\exp(-\beta t)$, where A_0 and β are constants and t is time. In comparison with the analytical solution, the numerical solution provided a maximum relative error of 0.7%.

In nature, when fluid pressures exceed lithostatic values, hydraulic fracturing occurs and overpressures are dissipated. Fracturing can be simulated in a numerical model by increasing local permeability until the local pressure returns to lithostatic or below (e.g., Bredehoeft and others, 1994; Mello and Karner, 1996). An alternative method of dealing with this problem is to simply create a local negative source term. In other words, fluid pressures that exceed lithostatic are numerically set back to lithostatic. This procedure mimics the hydraulic fracturing and pressure dissipation that must occur in nature. In this study, we chose the latter approach as the simplest. Most of our critical simulations dealt with studying the circumstances under which the present-day observed maximum fluid pressure (P_n = ~0.6) could be produced and therefore did not result in lithostatic pressures.

Hydrocarbon Generation

Overpressures in sedimentary basins can potentially be generated from a number of different geologic processes. These include aquathermal pressuring, active flow, diagenetic alteration, tectonic stresses, and clay dehydration (Bethke, 1986; Shi and Wang, 1986; Spencer, 1987; Luo and Vasseur, 1992; Bredehoeft and others, 1994; Audet, 1995; Gordon and Fleming, 1998). Recent reviews by Osborne and Swarbrick (1997) and Neuzil (1995) indicate, however, that hydrocarbon generation may be one of the most potentially effective mechanisms for generating high fluid pressures in sedimentary basins. Due to the large change in volume, the conversion of solid kerogen or liquid oil to gas is an especially potent mechanism (Barker, 1990). The Anadarko basin is a prolific producer of natural gas. It therefore follows that gas generation may be a viable hypothesis for explaining the origin of high fluid pressures in this setting.

Our treatment assumes that oil and gas in the

TABLE 2. — Kinetic Parameters for Hydrocarbon Generations
(Quigley and others, 1987)

	A (1/s)	E (kJ/mol)	σ (kJ/mol)[a]
Kerogen type II	1.58×10^{13}	208	5
Kerogen type III	1.83×10^{18}	279	13

[a]Standard deviation.

Anadarko basin were generated from the thermal maturation of organic-rich source rocks. The biogenic theory of the origin of oil and gas is well accepted, although abiogenic theories are resurgent (Gold, 1993, 1999).

Modeling of the hydrocarbon generation process must take into account not only the increase in volume that takes place due to gas and/or oil generation, but also the porosity increase due to kerogen/oil consumption (Bredehoeft and others, 1994; Luo and Vasseur, 1996). Oil or gas generation can be estimated from a first-order kinetic model,

$$\frac{dV_k}{dt} = -kV_k \tag{4}$$

where V_k is volume of kerogen per volume of rock. The kinetic-rate constant for oil or gas generation from kerogen (k), is given by Arrhenius equation as

$$k = A\exp(-E/RT) \tag{5}$$

where A is the Arrhenius constant (Table 2), E is the activation energy (Table 2), R (8.314 J/mole-K) is the universal gas constant, and T is temperature in °K. There are no experimental constraints on appropriate values for either the Arrhenius constant (A) or activation energy (E) for Anadarko-basin source rocks. Therefore, we used generic values (Table 2) for kerogen types II and III as given by Quigley and others (1987). We assumed that kerogen type II is converted to oil even though a part of kerogen type II is converted to gas (Mackenzie and Quigley, 1988), whereas kerogen type III is converted to gas. For oil or gas generation from kerogen, or porosity increase due to kerogen consumption, the geologic forcing term of equation (2) was derived by the conservation of mass as

$$\Gamma = -\left(\frac{\rho_k}{\rho_p} - 1\right)kV_k \tag{6}$$

where r_k is kerogen density (1,150 kg/m^3), ρ_p is petroleum density (oil density = 850 kg/m^3; gas density = 0.718 kg/m^3), V_k is volume of kerogen per volume of rock that can be estimated from kerogen density, rock density, and TOC, and k is the rate constant for petroleum generation (oil or gas) from kerogen. V_k can be estimated from equations (5) and (6) as

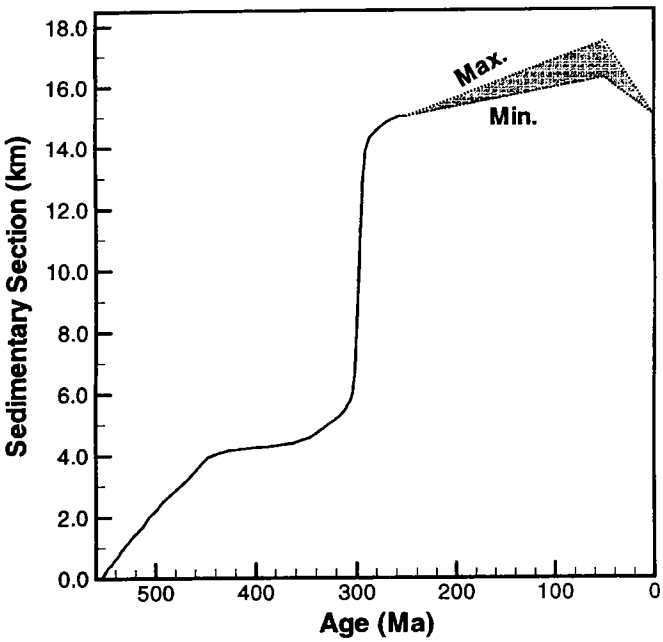

Figure 5. Burial history of the Anadarko basin (after Gilbert, 1992). Maximum and minimum burial histories from 250 to 0 Ma were estimated from stratigraphic relationships and paleothermal indicators as discussed in the text.

$$V_k = V_k^o \exp(-kt) \tag{7}$$

where V_k^o is the initial volume of kerogen per volume of rock and t is time.

MODEL CONSTRAINTS

Burial History

The history of Paleozoic sedimentation in the Anadarko basin (Fig. 5) is relatively well known, because most of the sediments deposited during this era are retained today (Johnson, 1989; Gilbert, 1992). However, the post-Paleozoic burial history of the Anadarko basin is more controversial and less well constrained because most Mesozoic and Cenozoic strata have been eroded.

There is geologic evidence for sedimentary deposition in the Anadarko basin during the Mesozoic. Extension of the Cretaceous seaway across the Anadarko basin during the last great inundation of the Western Interior of the United States implies that sedimentary strata were deposited in a marine environment during the Cretaceous (Garner and Turcotte, 1984; Johnson, 1989). Remnants of Triassic, Jurassic, Cretaceous, and Tertiary sedimentary strata (about 200–500 m) are found today in the western parts of Anadarko basin and the Oklahoma Panhandle (Johnson, 1989; Johnson and Cardott, 1992). The Denver and Raton basins, which are located between the Rocky Mountains and the Anadarko basin, probably had the same Cretaceous sediment provenance as the Anadarko basin, and these basins contain preserved Cretaceous sedimentary strata with thicknesses that range from 560 to 2,890 m (Baars and others, 1988).

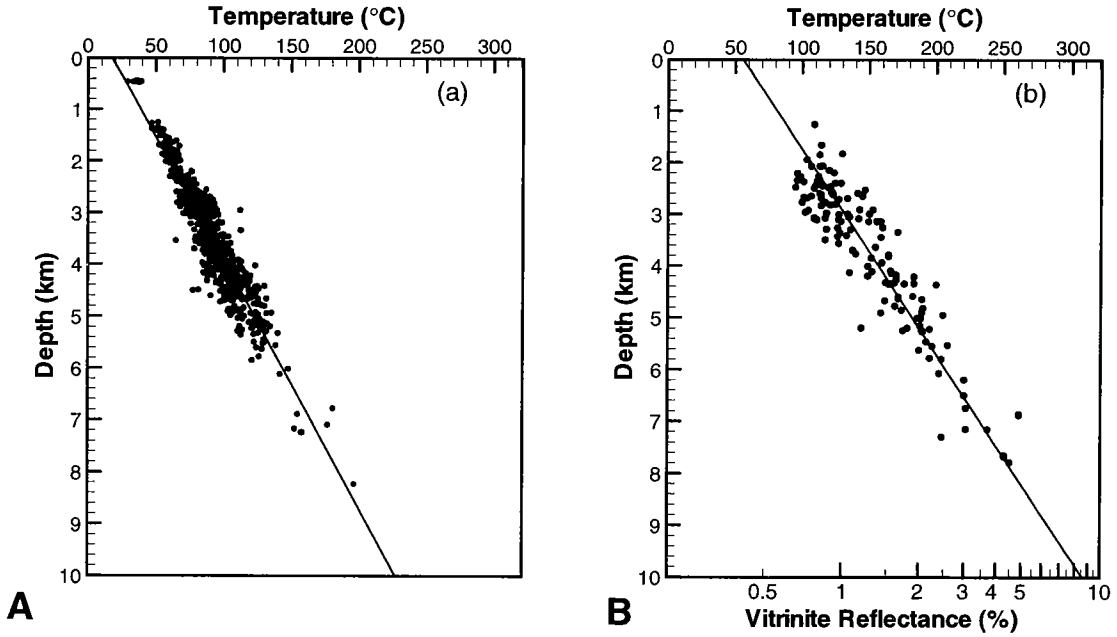

Figure 6. (A) Corrected bottom-hole temperature data from wells lying along cross section A–A′. Average thermal gradient is 21°C/km. (B) Vitrinite-reflectance data from the Anadarko basin and equivalent maximum temperature. Average paleothermal gradient is 24°C/km.

The primary tectonic activity in the vicinity of the Anadarko basin since the Late Cretaceous has been erosion. The amount and timing of erosion in the Anadarko basin and surrounding areas is not known with precision. Neither are regional variations in erosion amounts or timing well known. However, analysis of apatite–fission-track (AFT) and vitrinite-reflectance (R_o) data allow us to place some approximate constraints on the total amount and timing of Cenozoic erosion.

AFT data can be used to estimate both the amount and timing of erosion. Carter and others (1998) interpreted AFT data from both the Wichita Mountains and eastern deep parts of the Anadarko basin as representing total erosion of ~1.5 km that started about 40–50 Ma. Corrigan and others (1998) interpreted AFT data from uplifts along the Ouachita trend as indicating total erosion of ~1.0 km in an epeirogenically uplifted southern midcontinent during the last ~40 Ma (Corrigan and others, 1998).

Vitrinite-reflectance (R_o) data can be used to estimate total erosion by extrapolating semi-log plots of R_o versus depth to presumed surface values of R_o = 0.2 (Fig. 6B). Three previous researchers (Schmoker, 1986; Cardott, 1989; Pawlewicz, 1989) used vitrinite-reflectance data to estimate the total amount of post-Paleozoic erosion in southwest Oklahoma to be in the range of 630 m to 2.5 km. Lee and Deming (2002, in press) reviewed vitrinite-reflectance data collected by previous workers, and concluded that varying erosion estimates could have been affected by regional variations and suppression of vitrinite reflectance in the Woodford Shale (Buchardt and Lewan, 1990). After excluding data from outside the Anadarko basin (e.g., the Ouachita Mountains and the Oklahoma platform) and correcting for suppression of reflectance in the Woodford Shale, Lee and Deming (2002, in press) interpreted vitrinite-reflectance data from the Anadarko basin as indicating from 1.8 to 2.5 km of total Cenozoic erosion (Fig. 6B).

Although there is some variance in the estimates of post-Paleozoic erosion made by different methods, all of the estimates fall in the range of 1.0 to 3.0 km (Fig. 5). AFT data indicate erosional cooling started about 40–50 Ma. We thus conclude that existing data allow us to reasonably conclude that maximum sediment thicknesses in the Anadarko basin were reached in the Late Cretaceous or Tertiary and have been followed by 1–3 km of subsequent erosion.

Present-Day Temperature

We estimated subsurface temperature in the Anadarko basin from 856 corrected bottom-hole temperatures (BHTs) collected from log headers of 589 oil and gas wells located along cross section A–A′ (Fig. 1) through the Anadarko basin and Oklahoma platform (Fig. 6A). The temperature data were corrected using a Horner plot and average depth-time correction (Deming, 1989). The methodology we used is identical to that employed by Lee and others (1996) and discussed in several other papers (Deming, 1989; Deming and others, 1990; Lee and others, 1994; Lee and Deming, 2002, in press). We believe our estimates of subsurface temperature (Fig. 4B) have an average accuracy of ±5°C (see discussion in Lee and others, 1996). There are a few direct temperature measurements in the Anadarko basin (e.g., Carter and others, 1998). However, the oil and gas wells used for temperature measurements by Car-

ter and others (1998) are not close enough to our cross section A–A′ (Fig. 1) to allow meaningful comparisons.

Based on corrected BHT data, the average geothermal gradient in the deep, southern part of the Anadarko basin in the south is 21°C/km, whereas the average geothermal gradient in the northern part of the Anadarko basin and the Oklahoma platform is 23°C/km (Fig. 6A). There is little regional variation in the thermal state from south to north (see discussion by Lee and Deming, 2002, in press) (Fig. 4A). A simple least-squares regression on all temperature data yielded an average thermal gradient of 21°C/km.

Thermal History

If vitrinite-reflectance data are available over a significant depth interval, paleothermal gradients can be estimated from an empirical relationship between maximum temperature and vitrinite reflectance (Barker and Pawlewicz, 1994) as

$$T = \frac{\ln R_o + 1.68}{0.0124} \tag{8}$$

Using vitrinite-reflectance data previously reported by other researchers (Schmoker, 1986; Cardott, 1989; Pawlewicz, 1989), Lee and Deming (2002, in press) both corrected for reported suppression of reflectance in the Woodford Shale (Buchardt and Lewan, 1990) and excluded data from outlying areas. After corrections, existing data yielded estimates of the paleothermal gradient that ranged from 22°C/km to 25°C/km. When all data are lumped together, a regression yields an estimated paleothermal gradient of 24°C/km (Fig. 6B).

Because vitrinite reflectance is believed to have an exponential dependence upon temperature (Sweeney and Burnham, 1990), the reflectance of vitrinite recovered from the Anadarko basin was probably determined at the time of maximum burial. If we assume that remnants of Triassic, Jurassic, Cretaceous, and Tertiary sedimentary strata found today in the western parts of Anadarko basin and the Oklahoma Panhandle (Johnson and Cardott, 1992; Johnson, 1989) indicate more-or-less continuous Mesozoic sedimentation, maximum burial was probably reached between the end of the Cretaceous (65 Ma) and early Tertiary (40–50 Ma) when AFT data (Carter and others, 1998) indicate uplift and cooling began. In the absence of any evidence that the Anadarko basin has experienced significant tectonothermal events for the last several hundred million years (e.g., the youngest volcanic rocks are more than 500 million years old; McConnell and Gilbert, 1990), we concluded that the paleothermal state recorded by vitrinite-reflectance data was probably established at the time of maximum burial, ca. 40–50 Ma.

We recognize that there are limitations inherent in the analysis of vitrinite-reflectance data. Vitrinite can be reworked, reflectance may depend upon lithology, and determinations on the same samples from different laboratories may vary by as much as 0.4%. Oxidation can affect vitrinite reflectance, resulting in estimates that are too high by 0.1–0.3%. Samples obtained from drill chips may not represent the actual depth of record, but may be contaminated by vitrinite introduced by borehole caving at more shallow levels (Heroux and others, 1979; Barker and Pawlewicz, 1986; Robert, 1988; Feazel and Aram, 1990). These limitations and possible sources of error are all serious and should be taken into account in the interpretation of vitrinite-reflectance data. However, undoubtedly, a strong causal relationship exits between vitrinite reflectance and temperature. Despite all of the problems, vitrinite is one of the best paleothermal indicators available. Lacking better constraints, we used the best indicator available to us.

We also recognize that more sophisticated methods of relating vitrinite reflectance to time and temperature exist (e.g., Sweeney and Burnham, 1990). However, in the absence of better constraints on timing, we chose to utilize a simple method that recognizes the strong relationship between R_o and maximum temperature. Under different circumstances (e.g., forward modeling) it might have been appropriate to model the possible influence of time on maturation profiles.

Geochemical Constraints

Primary source rocks in the Anadarko basin (Table 3) are Ordovician Simpson Group shales, the Devonian–Mississippian Woodford Shale, and certain thick, dark shales of Pennsylvanian age (Johnson and Cardott, 1992). We estimated dominant kerogen types and total organic carbon (TOC) content for these source rocks from published analyses of samples obtained from the Anadarko basin (Table 3). The depth and thickness of source rocks were constrained by analysis of samples from the Bertha Rogers well (Table 3) in the south-central part of the Anadarko basin (Fig. 1). The Bertha Rogers well is noteworthy as the deepest petroleum well in the world (9.59 km). Core samples from the Bertha Rogers well have been subjected to intensive geologic and geochemical studies (e.g., Price and others, 1981; Kareem, 1992). In our modeling, we assumed that initial TOC prior to the initiation of hydrocarbon generation was equal to maximum present-day values and 50% of initial TOC was inert.

Permeability

Average reservoir permeabilities in the Anadarko basin are in the neighborhood of 10^{-13} to 10^{-15} m^2 (Harrison and Routh, 1981; Bebout and others, 1993). In the context of our problem of understanding the origin and evolution of overpressures, these numbers imply little to nothing. In a discussion of Midcontinent hydrogeology, Jorgensen and others (1993) stated that "most oil and gas reservoirs are anomalous subsurface zones." The critical permeabilities are those of the nonreservoir units, the aquitards. Generally speaking, these data do not exist.

We arranged for a limited number of permeability measurements on two geologic units identified by Al-Shaieb and others (1992) as pressure seals. We submitted two samples from each of four sites, taking care to submit samples that exhibited diagenetic banding or

TABLE 3. — Source Rock Data of the Anadarko Basin
(Kareem, 1992)

	Formation	Formation top (m)	Formation bottom (m)	Thickness (m)	Rock type	Kerogen type	TOC (%)[a]
Pennsylvanian	Virgilian	1,341	2,592	1,251	Shale	II, III[b]	1–25
Pennsylvanian	Atoka	3,920	5,335	1,415	Shale (70%) Limestone (30%)	III	1–25
Pennsylvanian	Morrowan	5,335	6,565	1,230	Shale	III	0.5–3.4
Pennsylvanian	Springer	6,565	7,134	569	Shale	III	0.5–3.4
Devonian	Woodford	8,388	8,465	77	Shale	II[b], III	1–14
Ordovician	Sylvan	8,802	8,855	53	Shale	II	1–9
Ordovician	Simpson	9,072	9,521	449	Shale	I, II[b]	1–9

[a] From Johnson and Cardott (1992)
[b] Dominant kerogen

otherwise appeared to suggest low permeability. The results were inconclusive. One of the supposed seal layers (the Simpson sandstone) had permeability too high ($\sim 10^{-17}$ m^2) to allow it to function as a pressure seal. However, measurements on the Devonian Woodford Shale (Fig. 7) yielded permeabilities that are among the lowest ever measured ($\sim 10^{-22}$ to 10^{-24} m^2). We also measured two samples of a Pennsylvanian shale that yielded very low permeabilities (Fig. 7).

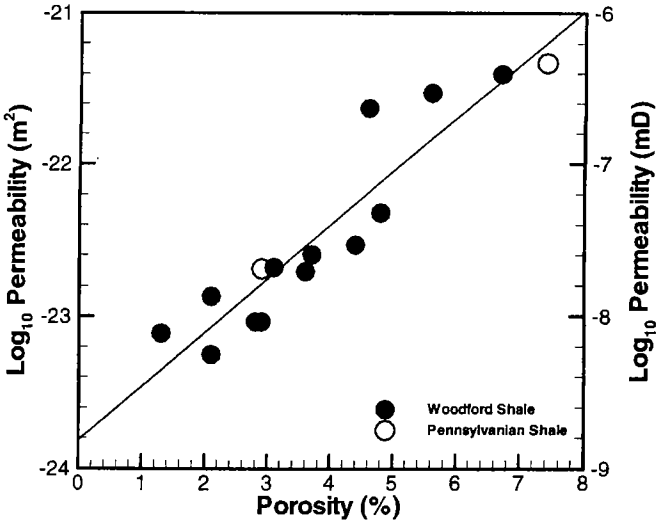

Figure 7. Porosity versus $\log_{10}$ permeability for Woodford Shale and Upper Pennsylvanian shale samples.

HYPOTHESIS TESTING

Compaction Disequilibrium

As discussed earlier, we conceptualize two end-member hypotheses for the cause of overpressuring in the Anadarko basin. The first of these is compaction disequilibrium, wherein high fluid pressures were originally developed during rapid Paleozoic sedimentation (see Fig. 5) about 250–300 Ma and have been sustained for several hundred million years by pressure seals. Compaction disequilibrium is "an important, if not the prime, source of overpressures in many basins" (Kooi, 1997). However, Kooi (1997) concluded that it was difficult to explain high fluid pressures in pre-Cenozoic sedimentary basins with this mechanism.

Extremely low rock permeabilities are necessary if compaction disequilibrium is to be successfully invoked as a mechanism to explain overpressuring in the Anadarko basin. The simplest way to demonstrate this is with a scale analysis (Deming, 1994). It is well known (Carslaw and Jaeger, 1959; Bredehoeft and Hanshaw, 1968; Neuzil, 1986; Bethke, 1988; Deming, 1994) that, for diffusion problems, the characteristic time (t) for a hydraulic disturbance to diffuse through a layer of thickness z is

$$t = \frac{z\alpha\mu}{4k} \tag{9}$$

where t is time, z is thickness, α is compressibility (Pa^{-1}), μ is fluid viscosity (kg/m-s), and k is permeability (m^2). If we take α to be the dynamic viscosity of pure water at 95°C ($\sim 3.0 \times 10^{-4}$ kg/m-s) (Touloukian and others, 1970) and shale compressibility (α) to be 10^{-9} Pa^{-1}, then equation 9 reduces to

$$t = \left(\frac{z^2}{k}\right) \times 2.4 \times 10^{-27} \tag{10}$$

where k is the permeability (in m^2) of a layer of thickness z (in m) necessary to confine anomalous pressures for a time t (in Ma). If overpressures in the Anadarko basin are due to compaction disequilibrium resulting from Paleozoic sedimentation (Fig. 5), then they have

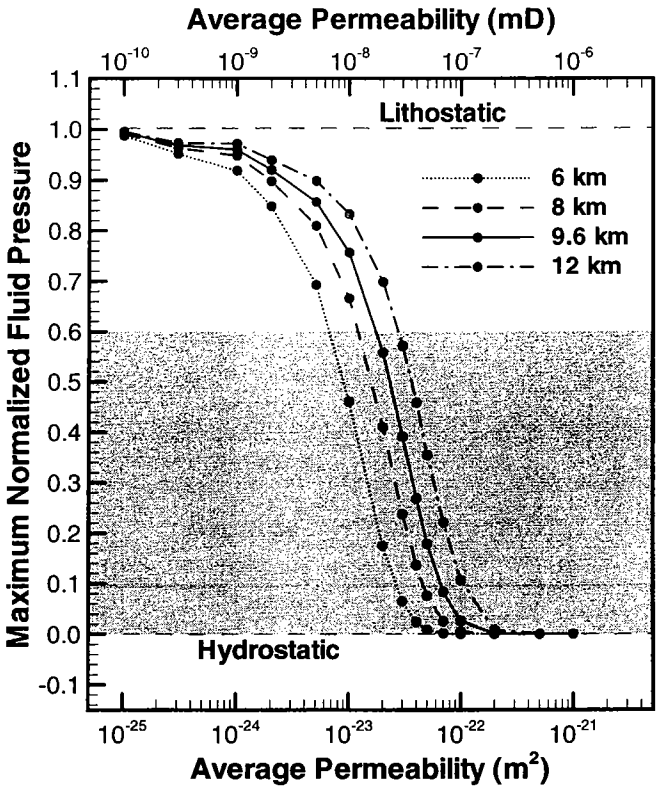

Figure 8. Maximum normalized pressure (P_n) in MPa at present day as calculated by a homogeneous numerical model to test a compaction-disequilibrium hypothesis. Shaded area corresponds to present-day observed fluid pressures in the Anadarko basin. Modeling results show that average basin permeabilities in the neighborhood of 10^{-23} m^2 are required to explain present-day overpressures as resulting from Paleozoic compaction disequilibrium.

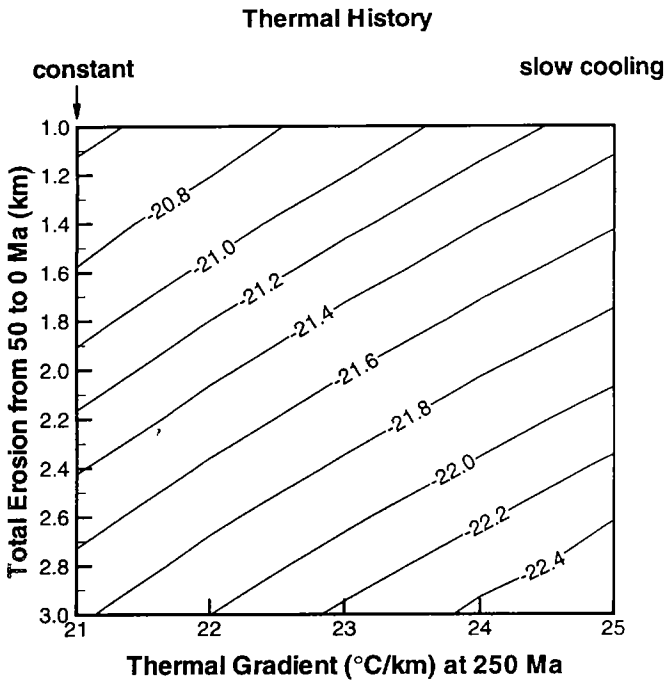

Figure 9. Log_{10} of average basin permeability required to reproduce observed present-day overpressures (P_n = 0.6 at depth of maximum pressure) as calculated by a homogeneous numerical model for different thermal and burial histories. In these simulations, overpressuring is induced by hydrocarbon generation. In general, lower permeabilities (10^{-23} m^2) are required for hotter thermal histories (lower-right corner). Colder-thermal histories (upper-left corner) allow overpressuring to exist at higher average permeabilities (10^{-23} m^2).

persisted for 250 Ma. Thus, according to equation (10), a pressure seal 100 m thick would of necessity have permeability lower than about 10^{-25} m^2. If pressure seals are thinner zones of diagenic alteration, even lower permeabilities are required. Seals of 10-m and 1-m thickness would require permeabilities of 10^{-27} m^2 and 10^{-29} m^2, respectively. These numbers are so low as to essentially be equivalent to zero.

We also evaluated the compaction-disequilibrium hypothesis using a one-dimensional numerical model of pressure diffusion. The initial condition was specified as lithostatic pressure through a homogeneous section that varied in thickness from 6 to 12 km. Boundary conditions were prescribed as constant hydrostatic pressure. We then determined present-day maximum fluid pressure as a function of permeability (Fig. 8). To satisfy observed constraints, simulations had to result in a normalized fluid pressure P_n of 0.6 at the depth of maximum absolute pressure. This requirement demands an average basin permeability of the order of 10^{-23} m^2 (Fig. 8).

Hydrocarbon Generation

The second hypothesis we evaluated as a possible cause of overpressuring was hydrocarbon generation. The most critical variables in these simulations were temperature and permeability. The enormous volume change associated with gas generation has a strong overpressuring effect, and gas generation has an exponential dependence upon temperature. Our approach was therefore to determine the permeability necessary to satisfy present-day fluid pressures by varying parameters affecting the thermal state through ranges constrained by geologic data. Lacking any constraint on the pre-Cenozoic thermal state, we held the thermal gradient at a constant value ranging from 21°C/km to 25°C/km up to 50 Ma, and then linearly decreased it to the present-day average value of 21°C/km. Similarly, the burial history was varied through a "maximum" and "minimum" range of Mesozoic sedimentation and Tertiary erosion (Fig. 5). The confluence of different burial and thermal histories had the effect of combining to produce "hot" and "cold" histories (Figs. 9, 10).

We found, in general, that overpressuring can be achieved with the highest permeabilities if the thermal gradient has been constant through time with the least erosion. In other words, colder-thermal histories allow present-day hydrocarbon generation (Fig. 10). Under the "cold" end-case scenario, the thermal gradient is constant, and only 1 km of Mesozoic sedimentation and

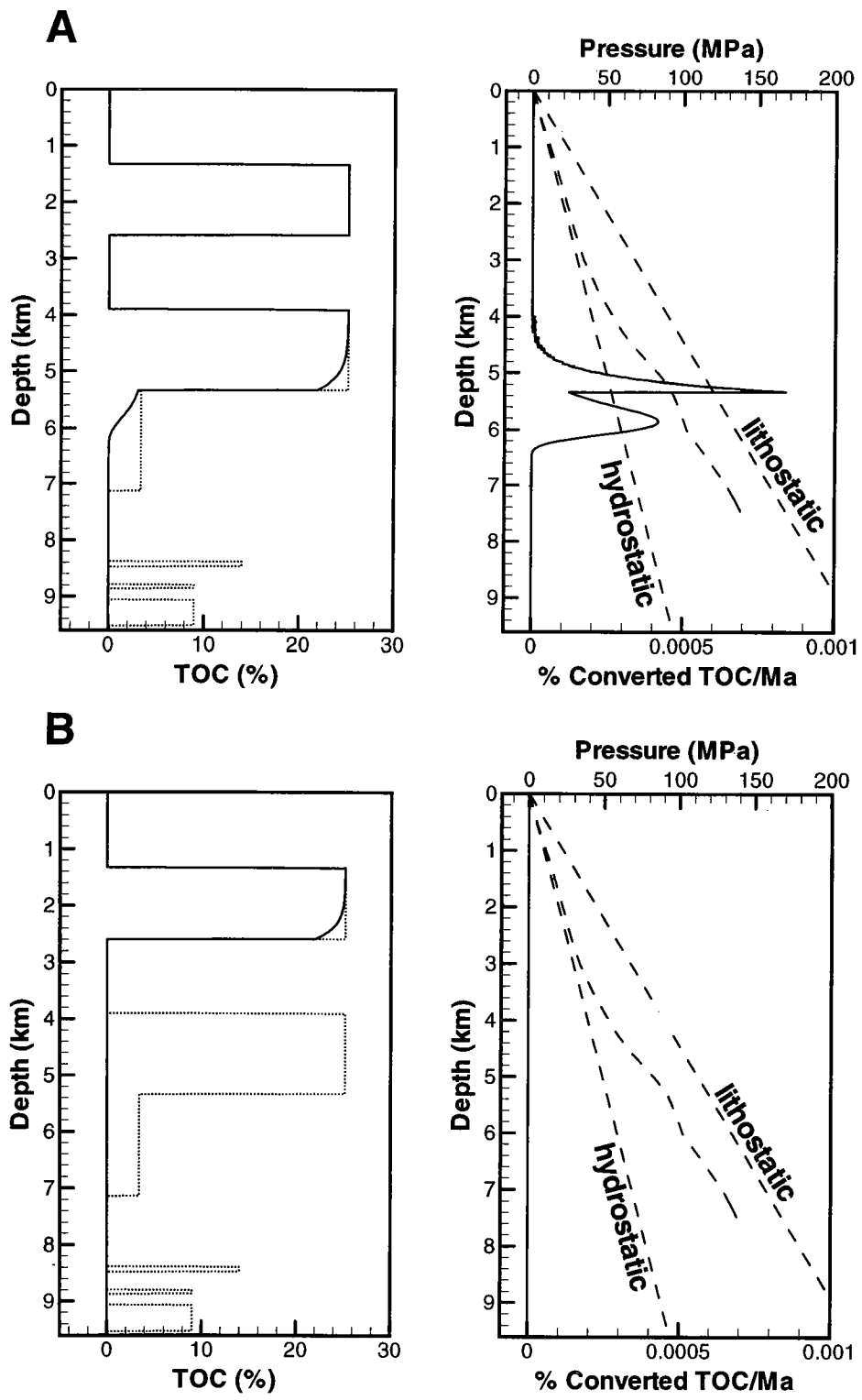

Figure 10. Distribution of total organic carbon (TOC) in source rocks, present-day hydrocarbon-generation rate, and observed present-day fluid pressures for (A) "cold" end-case burial and thermal history and (B) "hot" end-case burial and thermal history, as described in text. Solid line shows existing TOC; dotted line shows original TOC before hydrocarbon generation. In "hot" end-case scenario, Pennsylvanian source rocks are totally exhausted and there is no present day hydrocarbon generation. In "cold" end-case scenario, present-day hydrocarbon generation occurs between 4.5 and 6.5 km, near the depths at which maximum overpressures are observed.

subsequent erosion occur. In this case, an average basin permeability of about 10^{-21} m^2 is required to explain present-day overpressuring (Fig. 9), and hydrocarbon generation is ongoing for Pennsylvanian source rocks between depths of about 4.5 and 6.5 km. These depths correspond reasonably well to the depths at which maximum overpressures are observed today (Fig. 10).

In the "hot" end case, the thermal gradient cooled from 25°C/km to 21°C/km, and 3 km of Mesozoic sedimentation and Tertiary erosion occurred. If hotter conditions prevailed in the past, an average basin permeability near 10^{-23} m^2 is required to produce high fluid pressures (P_n = 0.6). In this scenario, Pennsylvanian, Devonian, and Ordovician source rocks are totally exhausted. Upper Pennsylvanian (Virgilian) source rocks remain viable but are not currently at high-enough temperatures to generate hydrocarbons. There is no present-day mechanism for overpressuring, and the very low inferred permeabilities (10^{-23} m^2) are required to preserve anomalous pressures generated tens of millions of years previous.

A comparison of the compaction-disequilibrium and hydrocarbon-generation hypotheses is shown in Figure 11. In both cases, permeability was held at a constant value of 5×10^{-22} m^2, and the thermal gradient decreased from 23°C/km to 21°C/km. For an initial condition of lithostatic pressure, high fluid pressures due to compaction disequilibrium dissipate by 200 Ma. However, for burial histories with between 1 and 3 km of sedimentation and erosion, model simulations with hydrocarbon generation can successfully reproduce present-day maximum fluid pressures (P_n = 0.6). In general, the essential difference between the two hypotheses is that average permeabilities 1 to 2 orders of magnitude lower are required if compaction disequilibrium is to

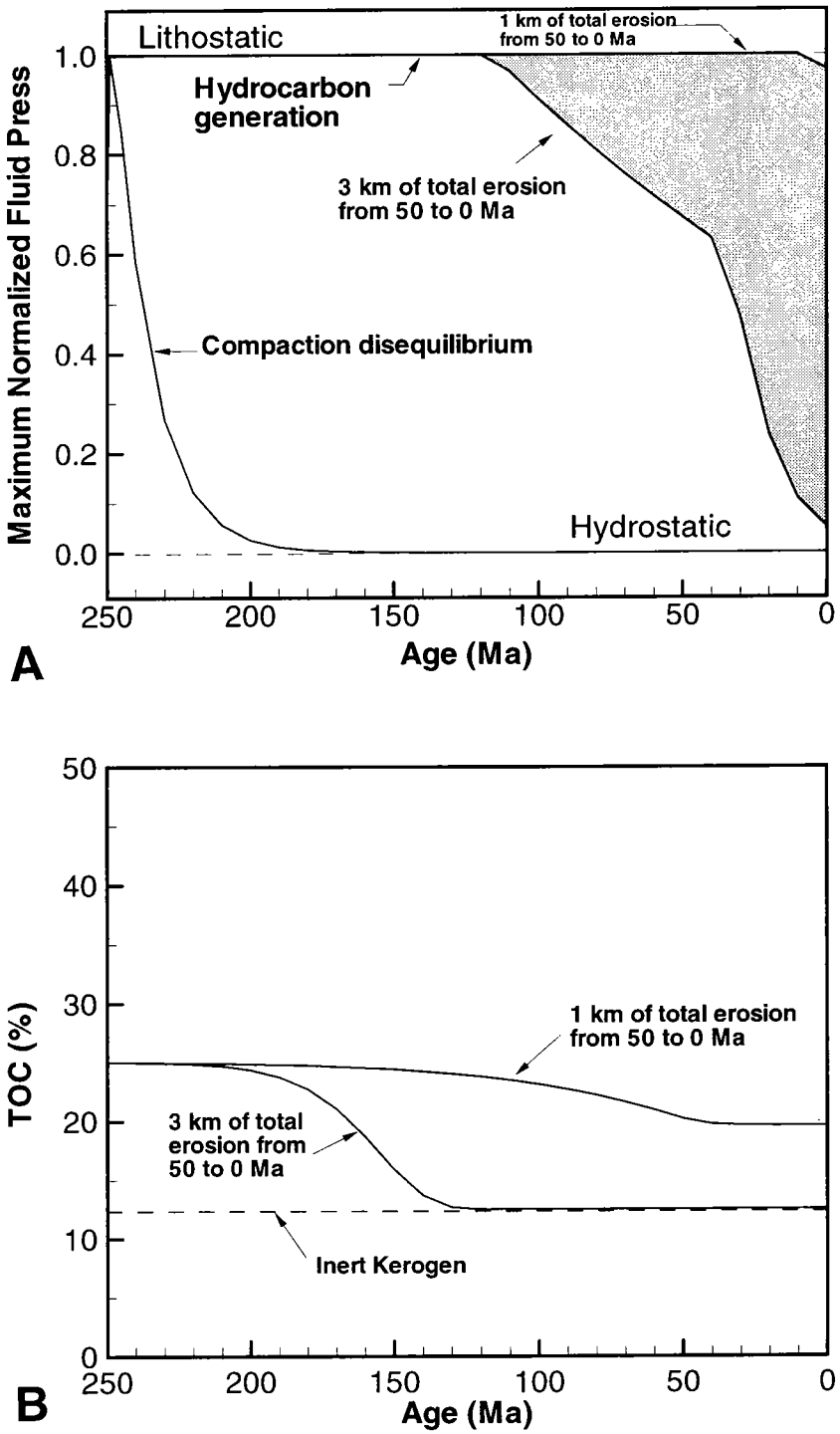

Figure 11. (A) Maximum normalized pressure (P_n) as a function of time at a fixed depth of 5.14 km as calculated by a homogeneous numerical model. Permeability is held constant at a value of 5×10^{-22} m^2. In these simulations, the thermal gradient is a constant 23°C/km from 250 to 50 Ma, then decreases linearly to 21°C/km at present day. Compaction disequilibrium is simulated by assuming lithostatic fluid pressures at 250 Ma, when rapid Paleozoic sedimentation ended. Hydrocarbon-generation scenarios show that present-day overpressures can be reproduced if total erosion was between 1 and 3 km. (B) Total organic carbon (TOC) as a function of time as calculated by a kinetic model for a source rock in the Pennsylvanian Atoka formation at 5.14 km depth. Hotter thermal histories with 3 km of sedimentation and erosion result in reactive source-rock exhaustion by about 130 Ma and make it substantially more difficult to ascribe present-day overpressuring.

be invoked as a cause of present-day overpressuring.

Sensitivity Analyses and Uncertainties

Different approaches have been taken in the use of numerical models to represent and study geologic processes. Some modelers use one preferred set of values for model parameters and do not explore the consequences of uncertainties. This approach is useful for the purpose of demonstrating the feasibility of a proposed process but cannot be used to establish causality unless the difficult question of uncertainty is investigated.

An ideal application of numerical modeling would rely upon physical parameters constrained by precise and exhaustive physical and chemical measurements. The uncertainties introduced by variations in model parameters could then be explored through a series of sensitivity analyses. In practice, this ideal is rarely approached. Geologic problems are generally complex and depend upon a wide range of physical and chemical variables that are commonly poorly constrained.

Our approach in this study is intermediate. We have reasonably good constraints on the thermal history and some source-rock characteristics. Recognizing that the most critical variable, permeability, is essentially unconstrained, we have defined the problem by casting our results in terms of the permeability values necessary to validate hypotheses. Sensitivity analyses are implicit in our variation of thermal and burial histories. We recognize that the values we used for variables such as specific storage, matrix and fluid densities, etc., are not constant, but rather are variables that are dependent upon factors such as lithology, temperature, and pressure. However, in most cases, the uncertainties inherent in these variables are considerably less than an order of magnitude. As the number of variables becomes very large, an exhaustive set of sensitivity analyses would lead to incoherent ambiguity. Pragmatically, we interpret the effect of these uncertainties as implying that the permeabilities inferred from our scale analyses and numerical modeling have implicit uncertainties of an order of magnitude. For example, if mean activation energies (E) are varied by plus-or-minus one standard deviation (Table 2), inferred permeabilities change by a factor of 2 to 3.

DISCUSSION

Permeability Structure

Our primary results can be summarized in terms of the maximum average permeabilities required to lead to overpressuring in the Anadarko basin. If overpressures originate from compaction disequilibrium, the average basin permeability must be lower than 10^{-23} m^2. If overpressures originate from hydrocarbon (mostly gas) generation, the average basin permeability can be as high as 10^{-21} m^2 depending upon the basin's thermal history. For a given thermal and burial history, the uncertainty inherent in these numbers is about a factor of 10.

The results of our modeling must be interpreted with an understanding of the importance of physical scaling. A basin consisting of interlayered and mixed units of highly contrasting permeability will respond differently than a thick, homogeneous layer (Bethke, 1988). Although our simple, one-dimensional model provides insight into the physics of pressure generation and dissipation, the assumed homogeneous permeability structure is unrealistic. The permeability of sedimentary rocks in the Anadarko basin likely varies from maximum values near 10^{-12} m^2 for certain hydrocarbon reservoirs and other rocks, to values as low as 10^{-23} m^2 for the Woodford Shale (Fig. 7).

The nominal thickness (9.6 km) used in most of our model simulations makes it easier to confine high fluid pressures with higher permeabilities. However, in nature low-permeability confining layers must constitute some fraction of the entire sedimentary section. Therefore, the permeabilities of the confining layers in the Anadarko basin must be substantially lower than the average values deduced from our modeling exercises. The permeabilities of these confining layers can be estimated by noting that for diffusion problems the ratio of thickness squared (z^2) to permeability (k) must be constant [equation (10)]. If confining rocks constitute 10% of the sedimentary section in the Anadarko basin (~1 km thickness), application of equation (10) implies that permeabilities of 10^{-25} m^2 or lower are necessary to validate the compaction-disequilibrium hypothesis. Even a scenario with energetic gas generation necessitates permeabilities in the range of 10^{-23} to 10^{-25} m^2. More realistically, if confining layers have thicknesses in the neighborhood of 100 m or less, permeabilities in the range of 10^{-25} to 10^{-23} m^2 are necessary to explain the occurrence of present day overpressures. These permeabilities are uncomfortably low. Neuzil (1994) reviewed permeability data for clays and shales, and found that permeability on the laboratory scale (~0.1 m) ranged from 10^{-15} to 10^{-23} m^2 for a number of argillaceous media. Laboratory measurements are generally interpreted as minimum estimates of *in situ* permeabilities as permeability tends to increase with scale. It is thus difficult to reasonably conclude that any sedimentary rock could act as a pressure seal unless it were altered diagenetically to a layer of virtually zero permeability. Furthermore, some type of active sealing mechanism would probably be necessary, as it seems unlikely that any rock layer could escape fracturing or faulting for hundreds of millions of years. Our measurements on the Woodford Shale found permeabilities as low as 10^{-23} m^2. However, the Woodford is an atypical shale; deeply buried, dense, and highly indurated. Scaling our results down to the thickness of the Woodford Shale (100 m) would imply that permeability lower than 10^{-25} m^2 would be necessary even if the Anadarko basin has undergone a minimal amount of Cenozoic cooling.

In Cenozoic basins undergoing active sedimentation (e.g., the Gulf Coast basin of the southeastern United States), overpressuring is readily attributable to the rapid accumulation of several kilometers of shale with permeability in the range of 10^{-16} to 10^{-20} m^2 (Bethke, 1986). The Anadarko basin is very much different from this setting; it contains less than 50% shale (Fig. 2) and lacks any discernible geologic process that can apparently account for pressure generation. The primary problem is that the AFT and vitrinite-reflectance data indicate unambiguously that the basin has been subject to Cenozoic erosion greater than a kilometer, with cooling of at least about 20°C. This cooling effectively dampens the most promising mechanism for overpressuring, hydrocarbon generation. As a result, we are led inexorably to conclude that our understanding of why and how the Anadarko basin is overpressured is incomplete.

Several possibilities suggest themselves. It may be that some unknown process exists that allows the Anadarko basin to remain overpressured. If such a process exists, it probably would not be one of the many mechanisms commonly discussed in the geologic literature. For example, processes such as aquathermal pressuring and clay alteration are driven by temperature just as hydrocarbon generation is. Whatever mechanism is operating must not be substantially influenced by Cenozoic cooling.

Another complication that we have not considered or described is compartmentalization. Although our level of analysis does not allow us to discern small-scale pressure compartments, Al-Shaieb and others (1992; 1994a,b) described overpressures in the Anadarko basin as being compartmentalized. Instead of one monolithic overpressured area, they described a broad area of overpressured compartments existing next to hydrostatically pressured units. Empirical evidence of compartmentalization is commonly encountered during drilling in the deep Anadarko basin (Kennedy, 1982, p. 77). It is common to encounter "kicks," which are sudden increases in pressure due to the rush of gas into a borehole that penetrates a zone of relatively high permeability. If the invaded zone were not highly permeable, the "kick" would not occur. Furthermore, if the permeable zone were not surrounded by less permeable boundaries, high pressures would not exist. Thus, a compartment is required. The presence of compartmentalization makes it difficult to ascribe pressure confinement in the Anadarko basin to a few low-permeability units such as the Woodford Shale or Permian evaporites. Rather, a multitude of relatively thin pressure seals must exist. The results of our modeling imply that these pressure seals must have permeabilities so low as

to be effectively zero. Furthermore, the seals must exist in all three dimensions. The inferred presence of these pressure seals is in contradiction to established hydrodynamic paradigms and appears to partially validate the static viewpoint. We are not predisposed to hydrodynamic theories but find it difficult to escape from a static interpretation in this case.

Gas Capillary Seals

Larry Cathles and his coworkers at Cornell recently proposed that abnormal pressures could be preserved for long periods of time in sedimentary basins through capillary seals induced by the presence of gas (Revil and others, 1998). In brief, the idea is that capillary forces prevent gas from being displaced from relatively coarse-grained rocks into relatively fine-grained lithologies. A gas capillary-seal is a layer of zero permeability to fluid phases unless fluid pressures become high enough to overcome capillary forces and displace pore gasses. Formations that consist of alternating layers of relatively coarse- and fine-grained sediment may develop several barriers, the effect of which is cumulative.

Although we are not necessarily inclined to either favor or disfavor this hypothesis, it must be conceded that it appears to have several advantages. The gas-generation hypothesis is parsimonious in that it simultaneously provides a mechanism for both generating and maintaining anomalous fluid pressures. Capillary sealing provides a mechanism for achieving zero permeabilities without contradicting established dynamic paradigms that maintain that aquicludes are sparse to nonexistent. Capillary sealing also explains how pressure compartments can be sealed in all three dimensions. Gas follows fluids along the path of least resistance until all escape routes are plugged. Finally, sealing by capillary forces can produce the type of compartmentalization apparently observed in such basins as the Anadarko. The existence of levels of pressure compartmentalization is difficult to explain unless some type of physical or chemical sealing mechanism is invoked.

More generally, it is worth noting that the presence of gas in sedimentary basins is commonly associated with anomalous pressures, both overpressures and underpressures. Subnormal pressures are associated with gas accumulations in the Western Canadian sedimentary basin in Alberta and in the San Juan basin in New Mexico (Davis, 1984; Hunt, 1990). Overpressures are found in association with gas in the Red Desert and Green River basins of Wyoming (Davis, 1984). Davis (1984, p. 189) stated that the gas-saturated sections of North American sedimentary basins were "never" normally pressured. The strong confluence of gas with anomalous subsurface pressures suggests a causal relationship between the presence of gas and reduced permeability.

Effect of Pressure on Hydrocarbon Generation

Although it is well known that hydrocarbon generation from kerogen has an exponential dependence upon temperature, the dependence on pressure has received less attention (Price and others, 1983; Domine, 1991; Price and Wenger, 1992; Domine and Enguehard, 1992; Fang and others, 1995; Jackson and others, 1995). Recent experimental work shows that increasing pressure can increase the activation energy of hydrocarbon generation, thus retarding hydrocarbon generation (Fang and others, 1995). If this effect were significant, it might explain how overpressures could be maintained in sedimentary basins for long periods of time through a negative feedback mechanism.

The effect of ambient pressure on hydrocarbon generation, however, seems to be most pronounced at moderate pressures—i.e., below 20 MPa (Ungerer, 1993). For example, an experimental result from hexane pyrolysis showed that rates of hydrocarbon generation did not change drastically between 20 and 200 MPa (Domine and Enguehard, 1992). A pressure of 20 MPa corresponds approximately to the hydrostatic fluid pressure at 2 km depth (Fig. 3). In the Anadarko basin, overpressuring begins at about 2.5 km. The range of fluid pressures encountered in the overpressured zone is about 30 to 150 MPa (Fig. 3). Thus, we tentatively conclude that high fluid pressures in the Anadarko basin have not significantly retarded hydrocarbon generation. However, the magnitude of pressure dependence is still uncertain, and more experiments for a wide range of conditions are needed (Jackson and others, 1995).

CONCLUSIONS

1. Although old and tectonically quiescent, the Anadarko basin in southwestern Oklahoma is extensively overpressured. Well-head shut-in pressures and mud weights collected in the vicinity of a north–south cross section through the basin show that overpressures are first encountered at a depth of about 2.5 km. Normalized fluid pressures P_n range from about 0.4 to 0.8, where $P_n = 0$ is hydrostatic pressure, and $P_n = 1$ is lithostatic pressure.
2. The average thermal gradient along a north-south cross section through the Anadarko basin is 21°C/km.
3. Although it is difficult to reconstruct eroded sections, the Anadarko basin appears to have experienced Mesozoic sedimentation followed by 1–3 km of Cenozoic erosion starting ca. 40–50 Ma.
4. The average thermal gradient in the Anadarko basin as estimated from vitrinite-reflectance data was 21°C/km to 25°C/km at the time of maximum burial, ca. 40–50 Ma.
5. Explaining overpressuring in the Anadarko basin as resulting from the lingering effect of Paleozoic compaction disequilibrium requires that the average permeability of the 10-km-thick basin be in the neighborhood of 10^{-23} m^2. More realistically, if pressures have been preserved through low-permeability layers whose thickness is 100 m or less, permeabilities lower than 10^{-27} m^2 are required. These inferred permeabilities are uncertain by a factor of 10.

6. Explaining overpressuring in the Anadarko basin as resulting from hydrocarbon generation requires that the average permeability of the 10-km-thick basin be in the range of 10^{-21} to 10^{-23} m^2. Lower permeabilities are required if the basin was hotter in the past, because a hotter thermal history has exhausted the generation potential of existing source rocks. More realistically, if pressures have been preserved through low-permeability layers the thickness of which is of the order of 100 m or less, permeabilities in the range of 10^{-25} to 10^{-27} m^2 or lower would be required. These inferred permeabilities are uncertain by a factor of 10, but are as low or lower than the lowest values ever recorded for sedimentary rocks.
7. Due primarily to the apparently well-constrained geologic fact that the Anadarko basin has experienced 1–3 km of uplift, erosion, and cooling over the last tens of millions of years, it is difficult to reconcile the existence of overpressuring with any known geologic mechanism. Permeabilities that are at or below the extreme end of measured values appear to be necessary. The pressure regime in the Anadarko basin is apparently compartmentalized by the existence of numerous and relatively thin layers of near-zero permeability.
8. The presence of anomalous pressures in older sedimentary basins does not appear to be analogous to compaction disequilibrium in Cenozoic basins undergoing relatively rapid sedimentation. The Anadarko appears to belong to a group of older basins in which anomalous pressures are associated with the presence of gas.
9. The presence of overpressures in the Anadarko basin appears to be better explained by static paradigms that invoke pressure seals than by classic hydrodynamic theories that rely upon the slow diffusion of pressure transients through aquitards. At the present time, the occurrence and preservation of geopressures in the Anadarko basin seem to be best explained by gas generation and gas capillary seals.

ACKNOWLEDGMENTS

Acknowledgment is made to the Donors of The Petroleum Research Fund, administered by the American Chemical Society, for the partial support of this research. Dwight's Energy Data generously donated wellhead shut-in pressure data. The authors benefited from comments by Chris Neuzil, Jeff Nunn, and Ulisses T. Mello.

REFERENCES CITED

Al-Shaieb, Z.; Puckette, J.; Ely, P.; and Tiger, V., 1992, Pressure compartments and seals in the Anadarko basin, *in* Johnson, K. S.; and Cardott, B. J. (eds.), Source rocks in the southern Midcontinent, 1990 symposium: Oklahoma Geological Survey Circular 93, p. 210–228.

Al-Shaieb, Z.; Puckette, J. O.; Abdalla, A. A.; and Ely, P. B., 1994a, Megacompartment complex in the Anadarko basin: a completely sealed overpressured phenomenon, *in* Ortoleva, P. J. (ed.), Basin compartment and seals: American Association of Petroleum Geologists Memoir 61, p. 55–68.

Al-Shaieb, Z.; Puckette, J. O.; Abdalla, A. A.; Tigert, V.; and Ortoleva, P. J., 1994b, The banded character of pressure seals, *in* Ortoleva, P. J. (ed.), Basin compartment and seals: American Association of Petroleum Geologists Memoir 61, p. 351–367.

Audet, D. M., 1995, Mathematical modeling of gravitational compaction and clay dehydration in thick sediment layers: Geophysical Journal International, v. 122, p. 283–298.

Baars, D. L.; Bartleson, B. L.; Chapin, C. E.; Curtis, B. F.; De Voto, R. H.; Everett, J. R.; Johnson, R. C.; Molenaar, C. M.; Peterson, F.; Schenk, C. J.; Love, J. D.; Merin, I. S.; Rose, P. R.; Ryder, R. T.; Waechter, N. B.; and Woodward, L. A., 1988, Basins of the Rocky Mountain region, *in* Sloss, L. L. (ed.), Sedimentary cover—North American craton: The Geology of North America, v. D-2, Geological Society America, Boulder, Colorado, p. 109–220.

Barker, C., 1990, Calculated volume and pressure changes during the thermal cracking of oil to gas in reservoirs: American Association of Petroleum Geologists Bulletin, v. 74, p. 1254–1261.

Barker, C. E.; and Pawlewicz, M. J., 1986, The correlation of vitrinite reflectance with maximum temperature in humic organic matter, *in* Buntebarth, G.; and Stegna, L. (eds.), Paleogeothermics: evaluation of geothermal conditions in the geological past: lecture notes in earth sciences: Springer-Verlag, Berlin, p. 79–93.

Barker, C. E.; and Pawlewicz, M. J., 1994, Calculation of vitrinite reflectance from thermal histories and peak temperatures: a comparison of methods, *in* Mukhopadhyay, P. K.; and Dow, W. G. (eds.), Vitrinite reflectance as a maturity parameter: applications and limitations: American Chemical Society Symposium Series 570, p. 216–229.

Bebout, D. G.; Woodward, M.; and Mendenhall, J. M., 1993, Atlas of major Midcontinent gas reservoirs: Gas Research Institute, Bureau of Economic Geology, University of Texas at Austin, 85 p.

Bethke, C. M., 1986, Inverse hydrologic analysis of the distribution and origin of Gulf Coast-type geopressured zones: Journal of Geophysical Research, v. 91, p. 6535–6545.

_____ 1988, Reply (to discussion on "A numerical model of compaction-driven groundwater flow and heat transfer and its application to the paleohydrology of intracratonic sedimentary basins"): Journal of Geophysical Research, v. 93, p. 3500–3504.

Bigelow, E. L., 1994, Global occurrences of abnormal pressures, *in* Fertl, W. H.; Chapman, R. E.; and Hotz, R. F. (eds.), Studies in abnormal pressures: developments in petroleum science 38: Elsevier, Amsterdam, p. 1–17.

Bradley, J. S., 1975, Abnormal formation pressure: American Association of Petroleum Geologists Bulletin, v. 59, p. 957–973.

Bradley, J. S.; and Powley, D. E., 1994, Pressure compartments in sedimentary basins: a review, *in* Ortoleva, P. J. (ed.), Compartment and seals: American Association of Petroleum Geologists Memoir 61, p. 3–26.

Bredehoeft, J. D.; and Hanshaw, B. B., 1968, On the maintenance of anomalous fluid pressures: I.—Thick

sedimentary sequences: Geological Society of America Bulletin, v. 79, p. 1097–1106.

Bredehoeft, J. D.; Back, W.; and Hanshaw, B. B., 1982, Regional ground-water flow concepts in the United States: historical perspective, *in* Narasimhan, T. N. (ed.), Recent trends in hydrogeology: Geological Society of American Special Paper 189, p. 297–316.

Bredehoeft, J. D.; Djevanshir, R. D.; and Belitz, K. R., 1988, Lateral fluid flow in a compacting sand-shale sequence, south Caspian basin: American Association of Petroleum Geologists Bulletin, v. 72, p. 416–424.

Bredehoeft, J. D.; Wesley, J. B.; and Fouch, T. D., 1994, Simulations of the origin of fluid pressure, fracture generation, and the movement of fluids in the Uinta basin, Utah: American Association of Petroleum Geologists Bulletin, v. 78, p. 1729–1747.

Buchardt, B.; and Lewan, M. D., 1990, Reflectance of vitrinite-like macerals as a thermal maturity index for Cambrian–Ordovician Alum shale, southern Scandinavia: American Association of Petroleum Geologists Bulletin, v. 74, p. 394–406.

Cardott, B. J., 1989, Thermal maturation of the Woodford Shale in the Anadarko basin, *in* Johnson, K. S. (ed.), Anadarko basin symposium, 1988: Oklahoma Geological Survey Circular 90, p. 32–46.

Carslaw, H. S.; and Jaeger, J. C., 1959, Conduction of heat in solids: Oxford Science Publications, Oxford, England, 510 p.

Carter, L. S.; Kelly, S. A.; Blackwell, D. D.; and Naeser, N. D., 1998, Heat flow and thermal history of the Anadarko basin, Oklahoma: American Association of Petroleum Geologists Bulletin, v. 82, p. 291–316.

Corrigan, J.; Cervany, P. F.; Donelick, R.; and Bergman, S. C., 1998, Postorogenic denudation along the late Paleozoic Ouachita trend, south-central United States of America: magnitude and timing constraints from apatite fission track data: Tectonics, v. 17, p. 587–603.

Davis, T. B., 1984, Subsurface pressure profiles in gas-saturated basins, *in* Masters, J. A. (ed.), Elmworth case study of a deep basin gas field: American Association of Petroleum Geologists Memoir 38, p. 189–203.

Davis, H. G.; and Northcutt, R. A., 1989, The greater Anadarko basin: an overview of petroleum exploration and development, *in* Johnson, K. S. (ed.), Anadarko basin symposium, 1988: Oklahoma Geological Survey Circular, 90, p. 13–24.

Deming, David, 1989, Application of bottom-hole temperature corrections in geothermal studies: Geothermics, v. 18, p. 775–786.

_____ 1994, Factors necessary to define a pressure seal: American Association of Petroleum Geologists Bulletin, v. 78, p. 1005–1009.

Deming, D.; Hanor, J. S.; and Nunn, J. A., 1990, Method of variable bias and its application to estimating subsurface temperature: Geophysical Research Letters, v. 17, p. 1949–1952.

Dewers, T.; and Ortoleva, P., 1994, Nonlinear dynamical aspects of deep basin hydrology: fluid compartment formation and episodic fluid release: American Journal of Science, v. 294, p. 713–755.

Domine, F., 1991, High pressure pyrolysis of n-hexane, 2,4-dimethylpentane and 1-phenylbutane. Is pressure an important geochemical parameter?: Organic Geochemistry, v. 17, p. 619–634.

Domine, F.; and Enguehard, F., 1992, Kinetics of hexane pyrolysis at very high pressures. 3.—Application to geochemical modeling: Organic Geochemistry, v. 18, p. 41–49.

Fang, H.; Yongchuan, S.; Sitian, L.; and Qiming, Z., 1995, Overpressure retardation of organic-matter maturation and petroleum generation: a case study from the Yinggehai and Qiongdongnan basins, South China Sea: American Association of Petroleum Geologists Bulletin, v. 79, p. 551–562.

Feazel, C. T.; and Aram, R. B., 1990, Interpretation of discontinuous vitrinite reflectance profiles: American Association of Petroleum Geologists Bulletin, v. 74, p. 91–93.

Fertl, W. H., 1976, Abnormal formation pressures: Elsevier, New York, 382 p.

Garner, D. L.; and Turcotte, D. L., 1984, The thermal and mechanical evolution of the Anadarko basin: Tectonophysics, v. 107, p. 1–24.

Gilbert, M. C., 1992, Speculations on the origin of the Anadarko basin, *in* Mason, R. (ed.), Basement tectonics: International Basement Tectonics Association Publication 7, Kluwer Academic Publications, Netherlands, p. 195–208.

Gold, T., 1993, The origin of methane in the crust of the Earth, *in* Howell, D. G. (ed.), The future of energy gases: U.S. Geological Survey Professional Paper 1570, p. 57–80.

_____ 1999, The deep hot biosphere: Copernicus, New York, 235 p.

Gordon, D. S.; and Flemings, P. B., 1998, Generation of overpressure and compaction-driven fluid flow in a Plio–Pleistocene growth-faulted basin, Eugene Island 330, offshore Louisiana: Basin Research, v. 10, p. 177–196.

Hanor, J. S.; and Sassen, R., 1990, Evidence for large-scale vertical and lateral migration of formation waters, dissolved salt, and crude oil in the Louisiana Gulf Coast, *in* Schumacher, D.; and Perkins, B. F. (eds.), Gulf Coast oils and gases: Society of Economic Paleontologists and Mineralogists, Tulsa, p. 283–296.

Harrison, W. E.; and Routh, D. L., 1981, Reservoir and fluid characteristics of selected oil fields in Oklahoma: Oklahoma Geological Survey Special Publication 81-1, 317 p.

Heroux, Y.; Chagnon, A.; and Bertrand, R., 1979, Compilation and correlation of major thermal maturation indicators: American Association of Petroleum Geologists Bulletin, v. 63, p. 2128–2144.

Hunt, J. M., 1990, Generation and migration of petroleum from abnormally pressured fluid compartments: American Association of Petroleum Geologists Bulletin, v. 72, p. 1–12.

Jackson, K. J.; Burnham, A. K.; Braun, R. L.; and Knauss, K. G., 1995, Temperature and pressure dependence of n-hexadecane cracking: Organic Geochemistry, v. 23, p. 941–953.

Johnson, K. S., 1989, Geological evolution of the Anadarko basin, *in* Johnson, K. S. (ed.), Anadarko basin symposium, 1988: Oklahoma Geological Survey Circular 90, p. 3–12.

Johnson, K. S.; and Cardott, B. J., 1992, Geologic framework and hydrocarbon source rocks of Oklahoma, *in* Johnson, K. S.; and Cardott, B. J. (eds.), Source rocks in the southern Midcontinent, 1990 symposium: Oklahoma Geological Survey Circular 93, p. 21–37.

Jorgensen, D. G., 1989, Paleohydrology of the Anadarko basin, central United States, *in* Johnson, K. S. (ed.), Anadarko basin symposium, 1988: Oklahoma Geological Survey Circular 90, p. 176–193.

Jorgensen, D. G.; Helgesen, J. O.; and Imes, J. L., 1993, Regional aquifers in Kansas, Nebraska, and part of Arkansas, Colorado, Missouri, New Mexico, Oklahoma, South Dakota, Texas, and Wyoming—geohydrologic framework: U.S. Geological Survey Professional Paper 1414-B, 72 p.

Kareem, M. R., 1992, Geological constrained modeling of the temporal and spatial evolution of hydrocarbon generation in the Anadarko basin: University of Oklahoma unpublished M.S. thesis, 191 p.

Kennedy, C. L., 1982, The deep Anadarko basin: Petroleum Information Corporation, 359 p.

Kooi, H., 1997, Insufficiency of compaction disequilibrium as the sole cause of high pore fluid pressures in pre-Cenozoic sediments: Basin Research, v. 9, p. 227–241.

Lee, Y.; and Deming, D. 1999, Heat flow and thermal history of the Anadarko basin and the western Oklahoma platform: Tectonophysics, v. 313, p. 399–410.

Lee, Y.; Chen, K. F.; and Deming, D., 1994, Subsurface temperatures in the Arkoma basin, southeastern Oklahoma, *in* Suneson, N. H.; and Hemish, L. A. (eds.), Geology and resources of the eastern Ouachita Mountains frontal belt and southeastern Arkoma basin, Oklahoma: Oklahoma Geological Survey Guidebook 29, p. 277–282.

Lee, Y.; Deming, D.; and Chen, K. F., 1996, Heat flow and heat production in the Arkoma basin and Oklahoma platform, southeastern Oklahoma: Journal of Geophysical Research, v. 101, p. 25387–25401.

Luo, X.; and Vasseur, G., 1992, Contributions of compaction and aquathermal pressuring to geopressure and the influence of environmental conditions: American Association of Petroleum Geologists Bulletin, v. 76, p. 1550–1559.

_____ 1996, Geopressuring mechanism of organic matter cracking: numerical modeling: American Association of Petroleum Geologists Bulletin, v. 80, p. 856–874.

Mackenzie, A. S.; and Quigley, T. M., 1988, Principles of geochemical prospect appraisal: American Association of Petroleum Geologists Bulletin, v. 72, p. 399–415.

McConnell, D. A.; and Gilbert, M. C., 1990, Cambrian extensional tectonics and magmatism within the southern Oklahoma aulacogen: Tectonophysics, v. 174, p. 147–157.

Mello, U. T.; and Karner, G. D., 1996, Development of sediment overpressure and its effect on thermal maturation: application to the Gulf of Mexico basin: American Association of Petroleum Geologists Bulletin, v. 80, p. 1367–1396.

Mello, U. T.; Karner, G. D.; and Anderson, R. N., 1994, A physical explanation for the positioning of the depth to the top of overpressure in shale-dominated sequences in the Gulf Coast basin, United States: Journal of Geophysical Research, v. 99, p. 2775–2789.

Neglia, S., 1979, Migration of fluids in sedimentary basins: American Association of Petroleum Geologists Bulletin, v. 63, p. 573–579.

Neuzil, C. E., 1986, Groundwater flow in low-permeability environments: Water Resources Research, v. 22, p. 1163–1195.

Neuzil, C. E., 1994, How permeable are clays and shales?: Water Resource Research, v. 30, p. 145–150.

Neuzil, C. E., 1995, Abnormal pressures as hydrodynamic phenomena: American Journal of Science, v. 295, p. 742–786.

Ortoleva, P. J. 1994, Basin compartments and seals: American Association of Petroleum Geologists Memoir 61, 447 p.

Osborne, M. J.; and Swarbrick, R. E., 1997, Mechanisms for generating overpressures in sedimentary basins: a reevaluation: American Association of Petroleum Geologists Bulletin, v. 81, p. 1023–1041.

Pawlewicz, M. J., 1989, Thermal maturation of the eastern Anadarko basin, Oklahoma: U.S. Geological Survey Bulletin 1866-C, 12 p.

Price, L. C.; and Wenger, L. M., 1992, The influence of pressure on petroleum generation and maturation as suggested by aqueous pyrolysis: Organic Geochemistry, v. 19, p. 141–159.

Price, L. C.; Clayton, J. L.; and Rumen, L. L., 1981, Organic geochemistry of the 9.6 km Bertha Rogers No. 1. well, Oklahoma: Organic Geochemistry, v. 3, p. 59–77.

Price, L. C.; Wenger, L. M.; Ging, T.; and Blount, C. W., 1983, Solubility of crude oil in methane as a function of pressure and temperature: Organic Geochemistry, v. 4, p. 201–221.

Quigley, T. M.; Mackenzie, A. S.; and Gray, J. R., 1987, Kinetic theory of petroleum generation, *in* Doligez, B. (ed.), Migration of hydrocarbons in sedimentary basins: Editions Technip, Paris, France, p. 649–665.

Revil, A.; Cathles, L. M.; Shosa, J. D.; Pezard, P. A.; and de Larouziere, F. D., 1998, Capillary sealing in sedimentary basins: a clear field example: Geophysical Research Letters, v. 25, p. 389–392.

Robert, P., 1988, Organic metamorphism and geothermal history-microscopic study of organic matter and thermal evolution of sedimentary basins: D. Reidel, Dordrecht, Holland, 311 p.

Schmoker, J. W., 1986, Oil generation in the Anadarko basin, Oklahoma and Texas: modeling using Lopatin's method: Oklahoma Geological Survey Special Publication 86-3, 40 p.

Sharp, J. M.; and Domenico, P. A., 1976, Energy transport in thick sequences of compacting sediment: Geological Society of America Bulletin, v. 87, p. 390–400.

Shi, Y.; and Wang, C.-Y., 1986, Pore pressure generation in sedimentary basins: overloading versus aquathermal: Journal of Geophysical Research, v. 91, p. 2153–2162.

Spencer, C. W., 1987, Hydrocarbon generation as a mechanism for overpressuring in Rocky Mountain region: American Association of Petroleum Geologists Bulletin, v. 71, p. 368–388.

Sweeney, J. J.; and Burnham, A. K., 1990, Evaluation of a simple model of vitrinite reflectance based on chemical kinetics: American Association of Petroleum Geologists Bulletin, v. 74, p. 1559–1570.

Touloukian, Y. S.; Liley, D. E.; and Saxena, S. L., 1970, Thermophysical properties of matter; v. 3—Thermal conductivity: nonmetallic liquids and gases: Plenum, New York, 120 p.

Ungerer, P., 1993, Modeling of petroleum generation and expulsion—an update to recent reviews, *in* Dore, A. G. (ed.), Basin modeling: advances and applications: Norwegian Petroleum Society (NPF), Special Publication, no. 3, p. 219–232.

Thermal Regime of a Large Midcontinent Oil Field (Butler County, Kansas) from High-Resolution Temperature Logs

J. R. McKenna and D. D. Blackwell
Southern Methodist University
Dallas, Texas

ABSTRACT.—Analysis of a suite of high-resolution temperature logs from six currently nonproducing wells from the East and West Shumway domes in the El Dorado oil field, a large long-term producing field in south-central Kansas, demonstrates that these logs can provide reliable, equilibrium-temperature measurements in an active petroleum setting. These high-resolution temperature logs illustrate generally conductive, equilibrium-temperature well profiles. The lower temperatures measured in two of the wells over the East Shumway Dome appear to be the result of a significant change in thermal gradient, perhaps from mass transport of hydrocarbons and/or *in situ* thermal conductivity changes related to the presence of hydrocarbons, and not inter-well lithologic variability. A preliminary analysis of high-resolution temperature logs and log-header derived borehole-temperature (BHT) data at the top of two productive zones (the Kansas City and Arbuckle Groups) within the West Shumway Dome suggests that the anomalously high BHT data present at the top of both horizons are close to the actual formation temperature, and encompass a much broader region of the dome than previously believed.

INTRODUCTION

Thermal disturbances have been observed for many years in a variety of petroleum settings (e.g., Roberts, 1980). The rapid upflow and migration of hydrocarbons, and thermal effects created by complex structures, may produce strong surficial temperature anomalies centered on oil and/or natural-gas deposits. Even in a static conductive setting, the presence of low-thermal-conductivity natural gas (0.05 Watts per meter-degree Kelvin, W/m•K), oil (0.2 W/m•K), and water (0.6 W/m•K) in the pore space may contribute to unusual thermal conditions at depth.

Thermal anomalies have been identified in both active and static hydrocarbon regimes with the aid of borehole temperature (BHT) data. However, any thermal anomalies delineated in such a manner are difficult to interpret correctly because BHT data are not equilibrium-temperature measurements and because the errors of BHT measurements are large and may be systematic. Furthermore, BHT data provide little if any insight into the mechanism responsible for the thermal disturbance (i.e., fluid migration versus a change in heat flow with depth). A better method to investigate the source and spatial extent of thermal anomalies is with high-resolution temperature logs.

Recent advances in technology, including fiberoptic (Förster and others, 1997) and computer tools (Wisian and others, 1998), as well as electric-line tools (Blackwell and Spafford, 1987), allow the routine acquisition of high-resolution (± 0.001°C) temperature logs that record temperature as a function of depth with submeter resolution (0.1 m). High-resolution temperature logs have been acquired in producing and nonproducing oil, gas, and geothermal wells and successfully used to detect upflow and to interpret small-scale lithologic variations (Blackwell and Steele, 1989; Blackwell and others, 1999). We use high-resolution temperature logs from the El Dorado oil and gas field (Fig. 1), Butler County, Kansas, to characterize a portion of the thermal regime of a large, long-term producing, Midcontinent oil field.

The El Dorado field is an old field (discovered in 1915), consisting of seven fault-bounded domes striking roughly parallel to the Nemaha ridge (azimuth 020°) in south-central Kansas (Fath, 1921; Reeves, 1929). The El Dorado field has produced steadily (~300 million bbl, cumulative) from Ordovician sands (Simpson Group), dolomites (Viola and Arbuckle Groups), Upper Pennsylvanian carbonates (the Lansing and Kansas City Groups), and Lower Permian sands (Admire Group) (Ramondetta, 1990). A significant pre-Pennsylvanian unconformity is present throughout Kansas, and is particularly prominent in the El Dorado field (Walters, 1958). This unconformity represents the contact between the younger, overlying Pennsylvanian shales of the Cherokee Group and the fractured and weakly deformed lower Paleozoic formations. Below the

McKenna, J. R.; and Blackwell, D. D., 2001, Thermal regime of a large Midcontinent oil field (Butler County, Kansas) from high-resolution temperature logs, *in* Johnson, K. S.; and Merriam, D. F. (eds.), Petroleum systems of sedimentary basins in the southern Midcontinent, 2000 symposium: Oklahoma Geological Survey Circular 106, p. 151–161.

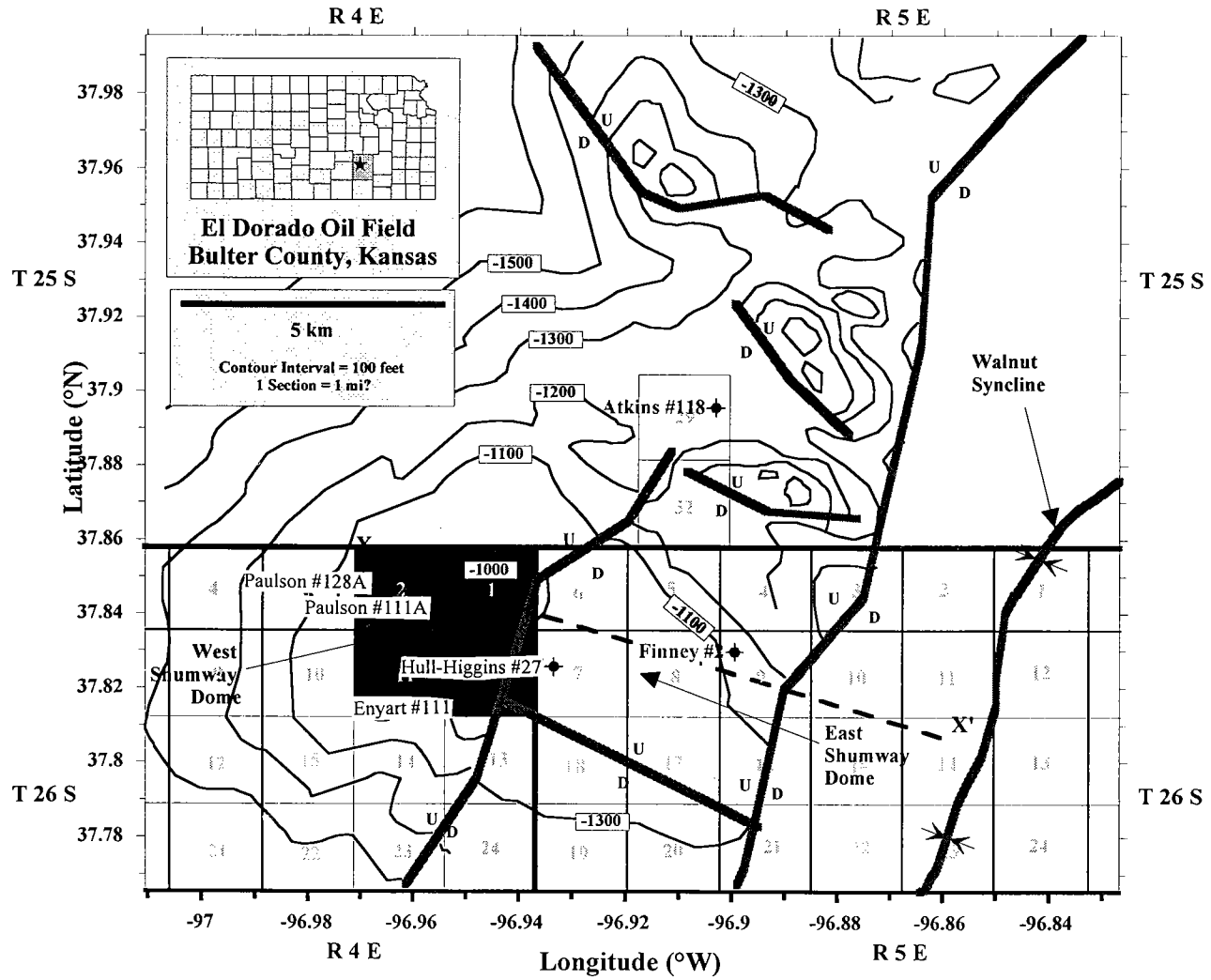

Figure 1. Location of El Dorado oil field, Kansas. The wells logged in this study appear as black dots. The stippled area represents the sections containing wells with high-resolution temperature logs and borehole-temperature data. The dashed line labeled X–X′ is the approximate location of the cross section presented in Figure 2. One section is equal to 1 mi². Structural data modified from Ramondetta (1990).

unconformity is Precambrian granitic basement (Ramondetta, 1990).

We discuss in this paper six high-resolution temperature logs acquired in nonproducing wells in and around the West and East Shumway domes along the western margin of the El Dorado field. This project is the initial phase of a study to investigate the thermal regime in Midcontinent oil fields using high-resolution temperature logs. The six logs described here were collected in a period of three days in the summer of 1999. Additional logging is planned in the future to develop a detailed data set for comparison to the log-header–derived BHT data that indicate a thermal anomaly of as much as 9°C associated with the field. The geologic features of the field and the sites of the logged wells are shown on the map in Figure 1. A schematic cross section (X–X′) through the fault-bounded West and East Shumway domes is shown in Figure 2 (the location of the cross section appears as a dashed line in Fig. 1). The approximate on-strike projected locations of five of the wells discussed in this study along with the total depth logged in each well also are shown. Because the hydrocarbon reservoirs at El Dorado are characterized by limited connectivity, isolated oil/gas pockets are present throughout much of the field (Ramondetta, 1990). These isolated hydrocarbon pockets occur as thin lenses situated above the fault contact between the West and East Shumway domes (Fig. 2). Any relief across the pre-Pennsylvanian unconformity by means of faulting or differential erosion in this region should juxtapose units with contrasting thermal conductivity (i.e., the shales and sandstones of the Cherokee Group versus carbonates of the Arbuckle Group) and thus may generate local conductive thermal anomalies.

The effect of discrete, static, fluid bodies and contrasting thermal-conductivity units to the overall thermal regime of the field is unknown at this stage of the study, because of the wide spacing of the logged wells.

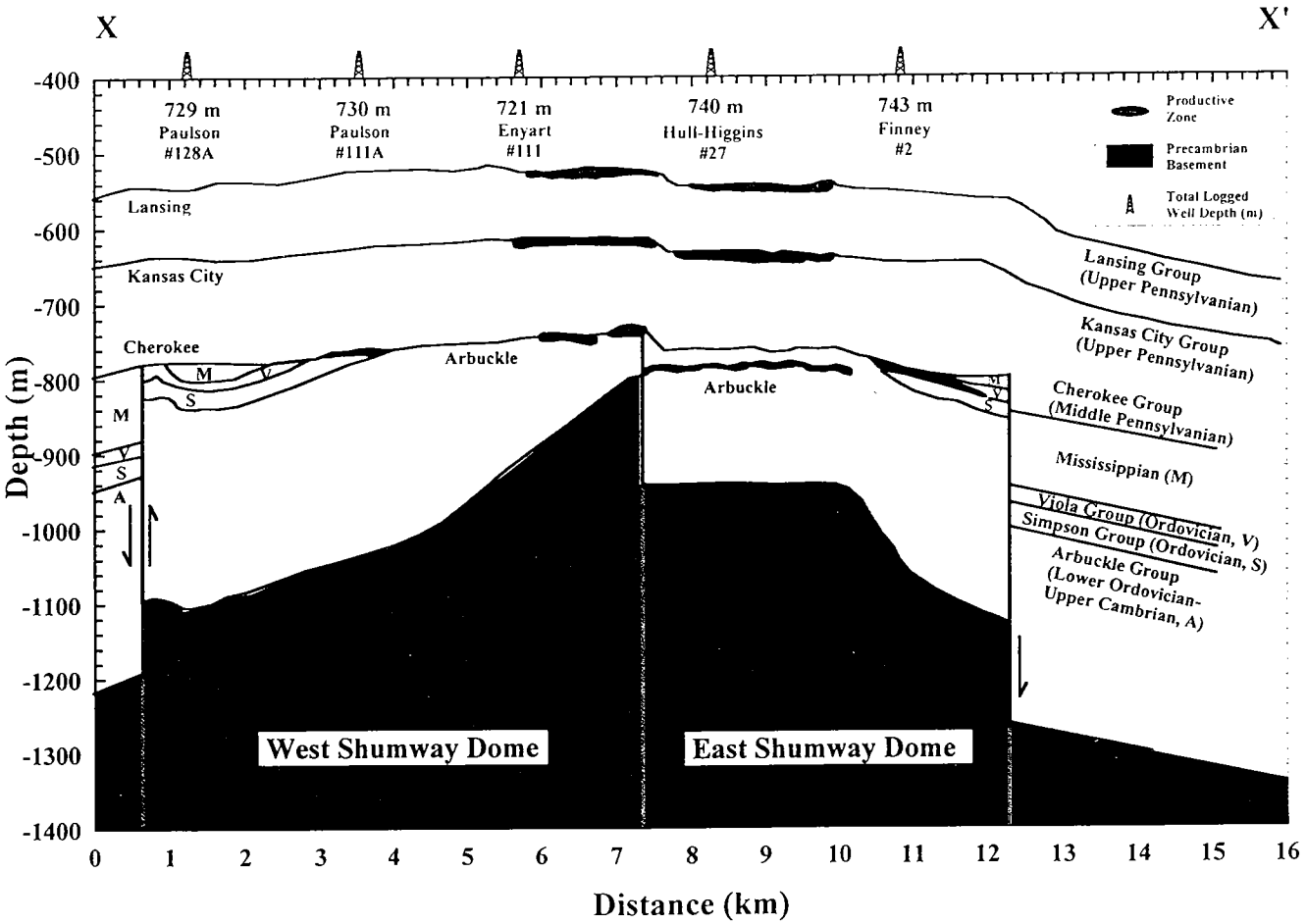

Figure 2. Schematic cross section across the West and East Shumway domes, El Dorado. Well locations are approximate. Note that the vertical exaggeration (28×) makes the slightly dipping normal faults bounding the Shumway domes appear vertical. Modified from Ramondetta (1990).

However, the thermal conditions in these individual wells will be discussed in a following section.

HIGH-RESOLUTION TEMPERATURE LOGS

The logged wells were drilled originally to target the Arbuckle Group at ~710–760 m depth but were either marginal or had watered out. Consequently, all the wells have been shut-in for some time, accumulating a column of oil in the borehole generally overlying water and allowing thermal equilibrium to be reached in the absence of fluid flow within the borehole. Generally, little pressure build-up occurred in each well owing to the paucity of natural gas throughout the field. The temperature-depth curves for all six wells that were logged are shown in Figure 3. The strong negative-temperature shift near 80 m depth in the Paulson #111A well (and between 80 and 120 m in three of the other wells) is the location of the air-fluid contact (i.e., water-table). This sort of a deflection is a general characteristic of temperature logs acquired in mostly fluid-filled wells and is due to the fact that the moving probe does not reach thermal equilibrium in the air column part of the well. All six wells were undisturbed for a period of months to years prior to logging and display generally conductive (linear by segments) temperature profiles. The temperature log of Enyart #111, however, displays some upflow in the borehole between 150 and 380 m (possibly as deep as 570 m), causing the measured temperatures to seem hotter for the disturbed depth interval than in all of the other wells. The main effect of this upflow within the well bore is that the upper part of the well is hotter than projected from the temperature information at the bottom part of the well. Additionally, because the holes are open for the last ~16 m, some minor upflow is present in a few of the logs but is restricted to the last few meters of the log. The long production time for the field does not appear to have changed the temperatures in the Arbuckle reservoir except to a very minor extent.

The temperatures and the gradient patterns for five of the six wells are nearly identical—the variation in BHT is only about 1°C. However, thermal conditions in Finney #2 seem to be significantly cooler than the other wells. The temperature log BHT in Finney #2 is about 2°C less than the average temperature log BHT in wells near the crest of the West and East Shumway Domes. Interestingly, the next lowest temperature-

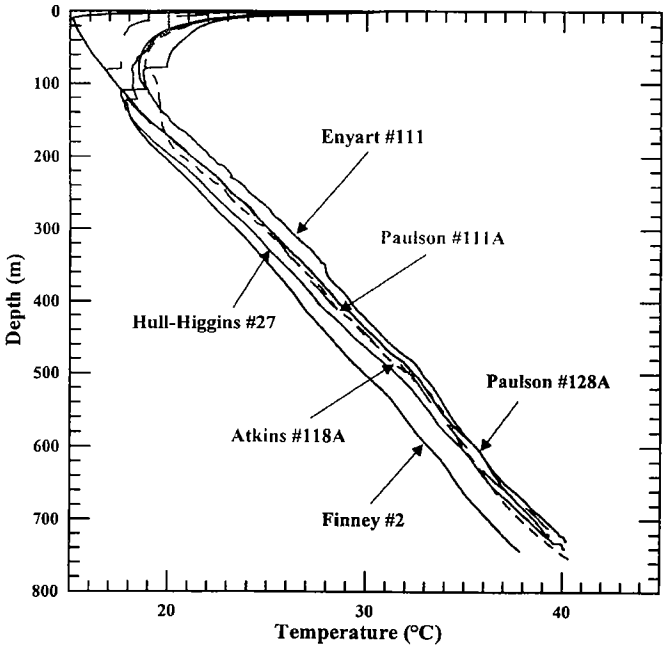

Figure 3. High-resolution temperature logs acquired in El Dorado field during the summer of 1999. All wells were logged with an electric-line temperature probe at 8 m/min. No post-processing was performed. All the logged profiles generally seem conductive with the exception of Enyart #111 well, which is disturbed in the upper part,

depth curve is that of Hull-Higgins #27, which also is situated within the East Shumway dome block.

It is instructive to compare temperature and thermal-gradient logs recorded in the Paulson #111A and Finney #2 wells (Fig. 4A), Finney #2 and Hull-Higgins #27 wells (Fig. 4B), and Paulson #111A and Hull-Higgins #27 wells (Fig. 4C) directly so that the salient features of high-resolution temperature logs are readily apparent. In Figure 4A–C, the gradient log was formed by simply calculating $\Delta T/\Delta Z$, where T is temperature, and Z is depth. All the gradient logs presented in Figure 4 have been smoothed with a 7-point (0.6 m) moving-average window for clarity.

If conditions in a well are conductive, then the product of the thermal gradient and thermal conductivity is the vertical heat-flow out of the well. This is Fourier's Law: if the heat-flow is constant with depth, any decrease/increase in thermal conductivity with depth should cause the thermal gradient to increase/decrease (e.g., Blackwell and Steele, 1989; Blackwell and others, 1999). For example, the Finney #2 gradient log (Fig. 4A) is much less noisy than the Paulson #111A gradient log, and, therefore, is able to resolve small variations in lithology. Between the top (~500 m) and bottom (~550 m) of the Lansing Group, the Finney #2 thermal gradient decreases from approximately 45°C/km to 25°C/km. Again, assuming that the heat-flow does not decrease with depth, this drop in thermal gradient implies that a corresponding increase in thermal conductivity has occurred, perhaps from a relatively low thermal conductivity shale (~1.5 W/m•K) to a higher conductivity "clean" limestone (~3 W/m•K).

Ideally, we would like to attribute the cause of the lower temperatures encountered in the Finney #2 well to systematic differences in the thermal gradient and not lithologic variability. Unfortunately, a direct comparison of the gradient logs is difficult because they differ substantially. A better comparison is available in Figure 4B, which compares the temperature measurements obtained in the Finney #2 well, which is located in the easternmost portion of the East Shumway dome (Fig. 1), with temperature measurements made in Hull-Higgins #27, which is situated over the East Shumway dome, but is close to the bounding fault between the West and East domes.

Examining the temperature-depth curves it is apparent that Finney #2 is somewhat cooler than Hull-Higgins #27. The gradient logs are both smooth and appear almost identical, with a minor (~35 m) offset present as a result of a thicker sequence of the Toronto Group in Finney #2. Nonetheless, it is clear that Hull-Higgins #27 is characterized by a systematically higher thermal gradient over the entire length of the log, despite possessing a stratigraphy similar to Finney #2. Because of this systematic variation, we interpret that the different log characteristics are not the result of normal variations in lithology nor are they a consequence of borehole disturbances. Rather, the different log characteristics are due to distinct thermal conditions in the West and East Shumway domes. This is one of the types of effects that can lead to variation in high-resolution log BHTs but cannot be uniquely determined from the BHT data alone.

Figure 4C compares the temperature measurements obtained in Paulson #111A and Hull-Higgins #27. Even though the two wells are located in different regions of the field and the Paulson #111A log is somewhat noisy, the high-resolution temperature logs yield relatively similar temperature/depth curves. The gradient logs for these two wells are similar, but the measurable differences present seem to arise from the normal variations in lithology expected in sedimentary sections.

It is unclear what the contribution of lithologic variation in each well is to the temperature data. The Upper Pennsylvanian Lansing and Kansas City Groups are massive, relatively clean limestone units. Therefore, little variation in thermal gradient would be expected. However, the unexpected offset in thermal gradient through these units in both wells requires modeling to explain whether these observations arise from (1) conductive disturbances related to the complex structure of the field or (2) hydrocarbon accumulation and migration through the producing Arbuckle Group. We plan to investigate these affects in future work.

HIGH-RESOLUTION TEMPERATURE LOGS VERSUS WELL-HEADER BHT DATA

Borehole-temperature data are generally used to evaluate thermal history and to constrain the timing of

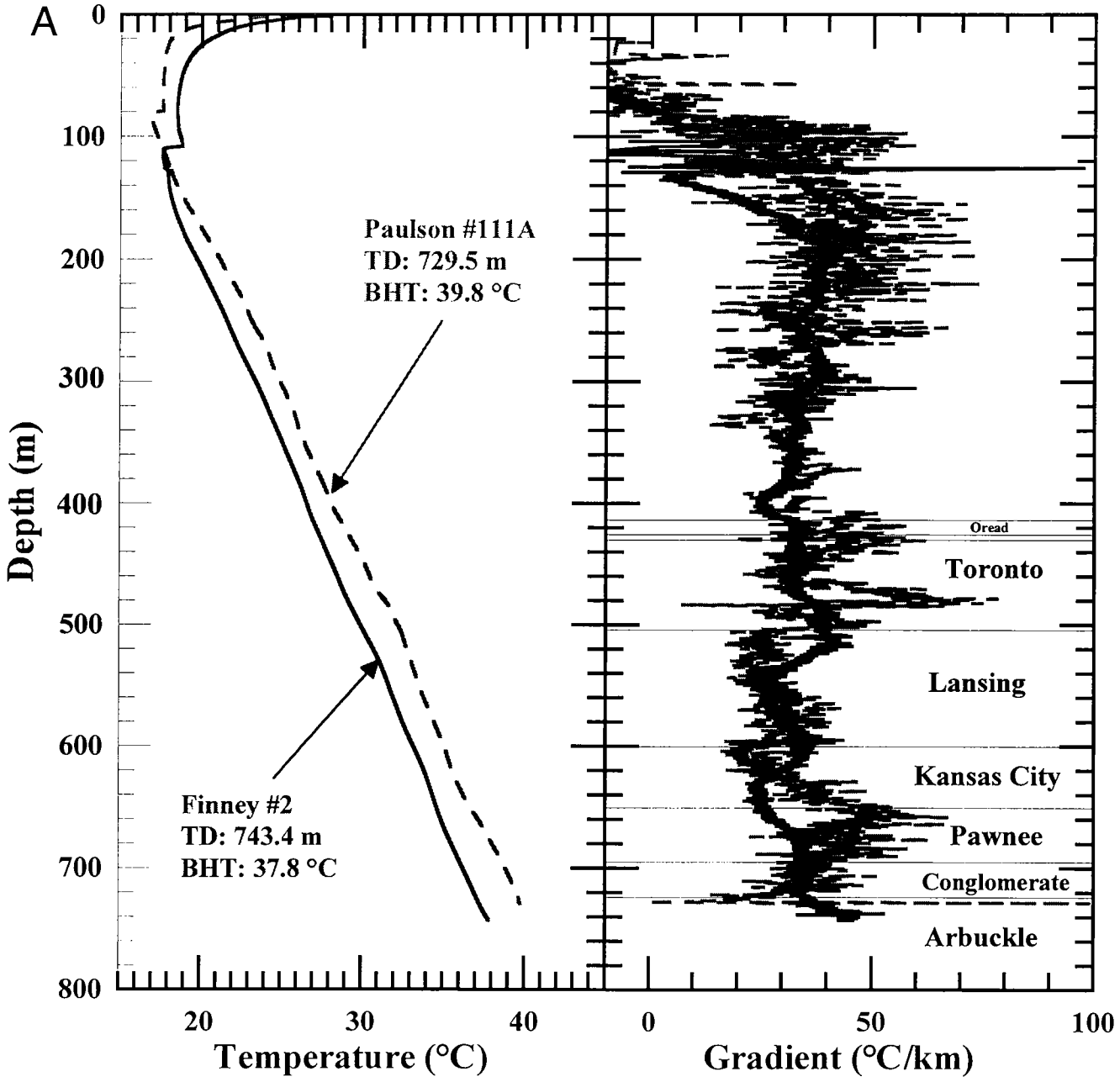

Figure 4 *(above and following pages).* (A) A comparison of high-resolution temperature measurements logged in the Paulson #111A (dashed curve) and Finney #2 (solid curve) wells, El Dorado, Kansas. Finney #2 appears cooler than Paulson #111A. Whether this is a direct result of the two wells being in the East and West Shumway domes, respectively, is unknown. The gradient logs appear different, partially because the Paulson #111 log is noisy, rendering it difficult to assess any lithologic contribution to the observed temperature differences. (B) Comparison of high-resolution temperature measurements in the Hull-Higgins #27 (dashed curve) and Finney #2 (solid curve) wells, El Dorado, Kansas. Both gradient logs are quiet, and seem to be well correlated, as expected, because both wells are situated over the East Shumway dome. The Hull-Higgins #27 gradient log is systematically higher for the entire length of the log, suggesting that the lower temperature in Finney #2 is due to a real heat-flow difference and not a convective disturbance from past production or upflow. (C) A comparison of high-resolution temperature measurements logged in the Paulson #111A (dashed curve) and Hull-Higgins #27 (solid curve) wells, El Dorado, Kansas. The gradient logs appear similar even though Paulson #111A is located over the West Shumway dome, whereas Hull-Higgins #27 is located close to the contact between the East and West domes. The differences in temperatures, however, are probably the result of lithologic variations present in the sedimentary section at the El Dorado field.

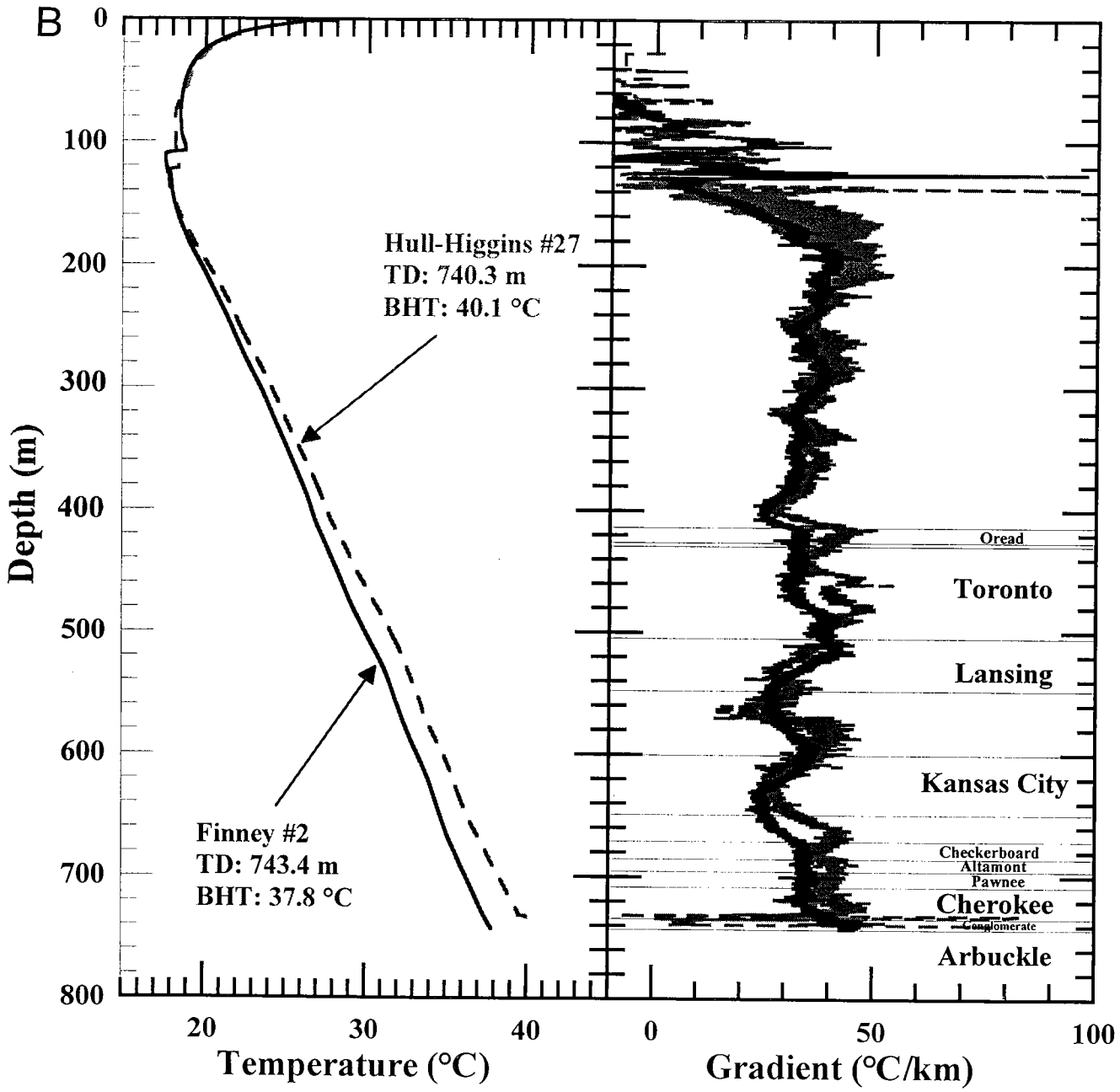

Figure 4 *(continued).*

hydrocarbon generation in key source beds in active petroleum settings. Temperature-time histories generated by utilizing BHT data can be inaccurate, however, simply because the BHT data themselves are inherently inaccurate. Before any attempt to model the thermal history of a particular source bed is made, the present-day thermal regime of the field must be accurately determined. However, because BHT data are not equilibrium-temperature measurements, they must be corrected for drilling disturbances prior to use. The correction factor generally applied is empirical and specific to a particular field or lithologic unit. Only with additional log-header information, such as the time since circulation of drilling fluid and the shut-in time of the well, can an equilibrium-temperature measurement be extrapolated and the "true" formation temperature be determined (Bullard, 1947). A better method of constraining the present-day equilibrium thermal regime in petroleum settings is with high-resolution temperature logs.

Blackwell and others (1999) discuss several limitations inherent in utilizing BHT data to understand and model the thermal structure of sedimentary basins. They argue that the relative ease and low cost of acquiring high-resolution temperature logs, coupled with their superior information content make their use preferable to BHT data in almost all instances. For example, thermal-gradient estimates obtained from log-

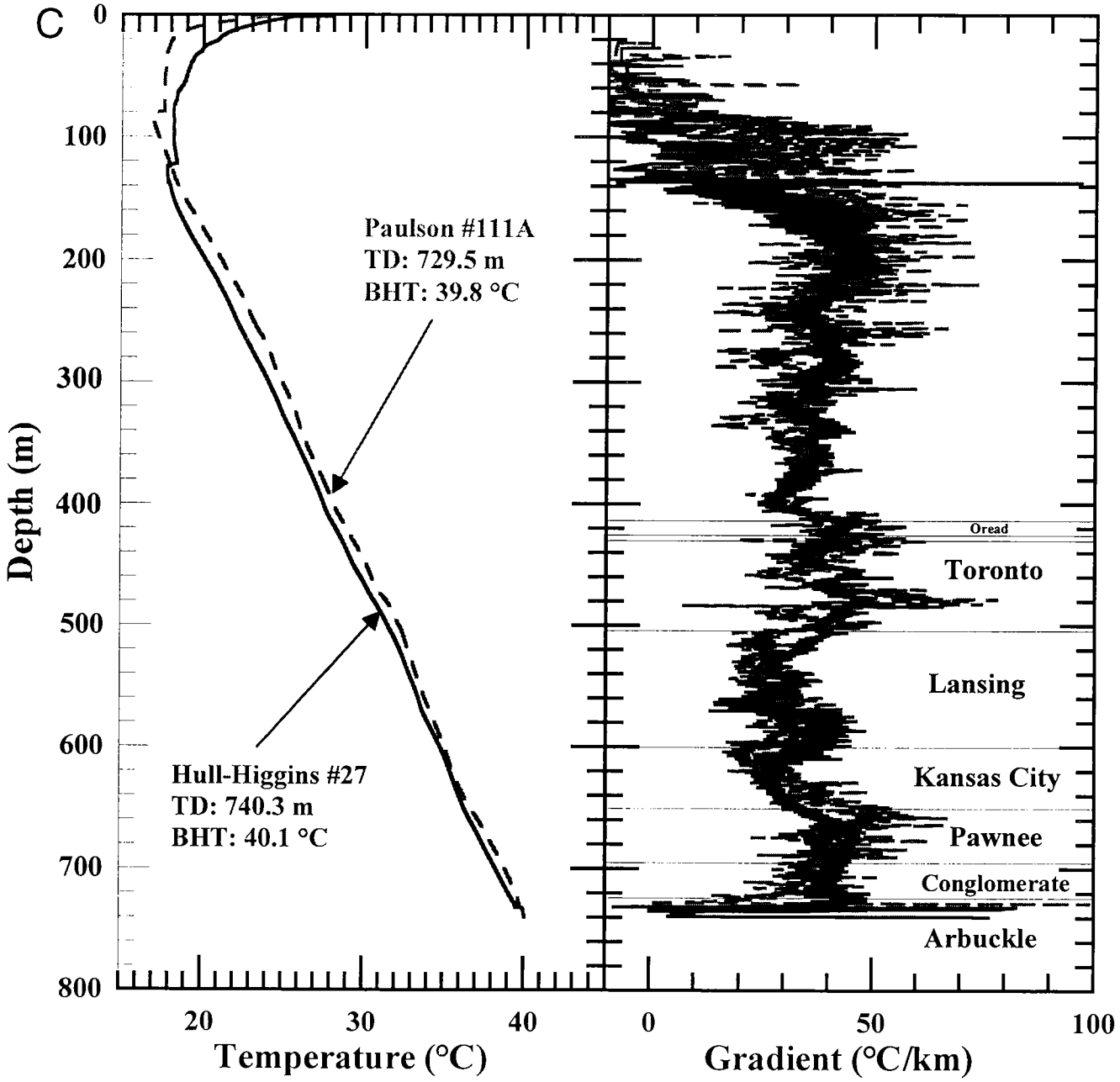

Figure 4 *(continued).*

header BHT are rarely more accurate than ±10–25%, whereas thermal-gradient information derived from high-resolution temperature logs are perhaps accurate to ±0.5°C/km at 1 m resolution. Furthermore, because BHT data tend to cluster around a few depths, they cannot provide vertical depth resolution of the thermal gradient (e.g., Jessop, 1990).

High-resolution temperature logs, unlike BHT data, can provide sufficient resolution to assess thermal-gradient fluctuations with depth and provide constraints on variations in lateral and vertical *in situ* thermal conductivity because of lithologic variations. Perhaps the most advantageous feature of high-resolution temperature logs is that appearance of the log itself (through the gradient log) affords a measure of the borehole conditions. A "noisy" gradient log suggests that nonequilibrium or even nonconductive well conditions may dominate, thereby providing a semi-qualitative indicator of the reliability of the log. BHT data cannot be similarly assessed.

To demonstrate the inaccuracies of BHT data, we present the temperature field atop two prominent horizons present in the El Dorado field—the Upper Pennsylvanian Kansas City Group (limestone) and the Upper Cambrian–Lower Ordovician Arbuckle Group (dominantly dolomite, but with some chert, shale, and sandstone). Both units have been prolific producers of hydrocarbons in Kansas and in the El Dorado field.

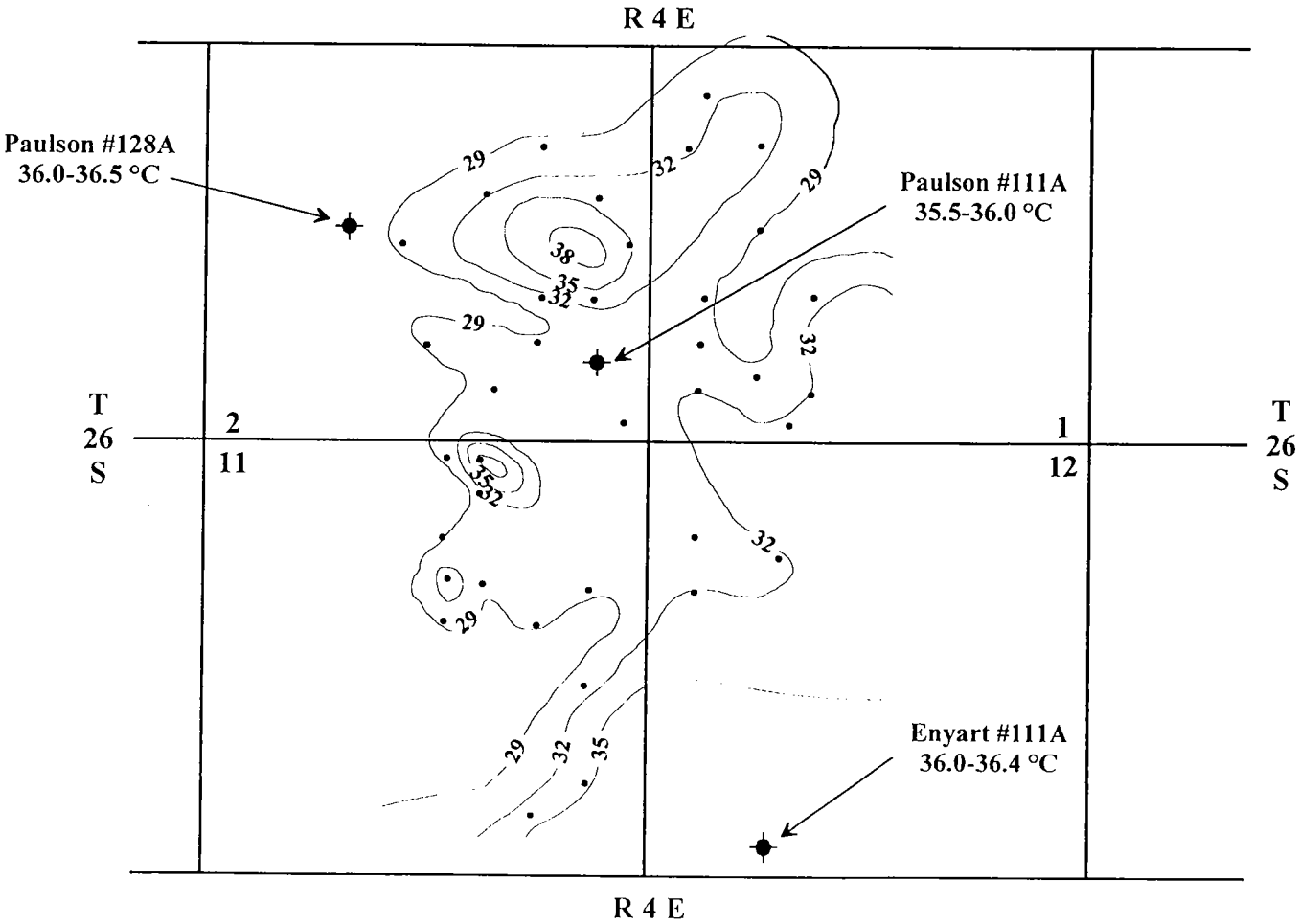

Figure 5. High-resolution temperature log and uncorrected log-header borehole-temperature (BHT) data from the top of the Kansas City Group (615–633 m), West Shumway dome, El Dorado, Kansas. The contour interval is 3°C. One section is equal to 1 mi^2. The high-resolution measurements suggest that the ~8°C BHT anomaly actually encompasses the entire dome instead of a restricted region near the dome crest. BHT data are courtesy of Dan Merriam, Kansas Geological Survey.

Accordingly, both units have been the target of numerous BHT observations (e.g., Förster and Merriam, 1999).

Shown in Figure 5 are the contoured, uncorrected well-header BHT data sampled at the depth of the Kansas City Group (615–633 m) within the West Shumway dome. Also shown are the temperature ranges from the high-resolution logs encountered in the three wells (Paulson #128A, Paulson #111A, and Enyart #111A) closest to the crest of the dome (where sections 1, 2, 11, and 12 intersect) at the same depth interval. The BHT data show a broad region of 29°C temperature centered over the dome and two smaller regions in which the temperature is in excess of 37°C. The high-resolution temperature measurements covering approximately the same area of the dome all show an average temperature of 36°C. Even though the wells are isolated from one another, the limited high-resolution data suggest that the >8°C BHT anomaly, restricted to two small areas on the dome, is in fact, not anomalous, but rather is closer to the equilibrium temperature of the Kansas City Group.

Figure 6 is similar to Figure 5, except that the contoured, uncorrected well-header BHT data here represent estimates of the temperature field at the top of the Arbuckle Group (707–838 m). Also shown is the range of temperatures encountered from 707 m to the total logged-depth in the three wells closest to the crest of the West Shumway dome. As before, the BHT data illustrate a broad region roughly corresponding to the dome of temperature of at least 32°C. In general, however, there is somewhat less complexity to the Arbuckle Group BHT-delineated thermal structure at this depth interval than that of the shallower Kansas City Group (Fig. 5). The thermal structure here varies uniformly and is seen to reach a maximum of 41°C as the crest of the dome is approached from all sides. Although the amplitude of the well-header BHT anomaly for the Arbuckle Group is about 11°C, it probably is somewhat less because the depth interval at which the BHT data are recorded span the rather large depth range of about 130 m. The high-resolution temperature measurements nearest to the dome all recorded similar observations, the mean temperature being about 39°C. Again,

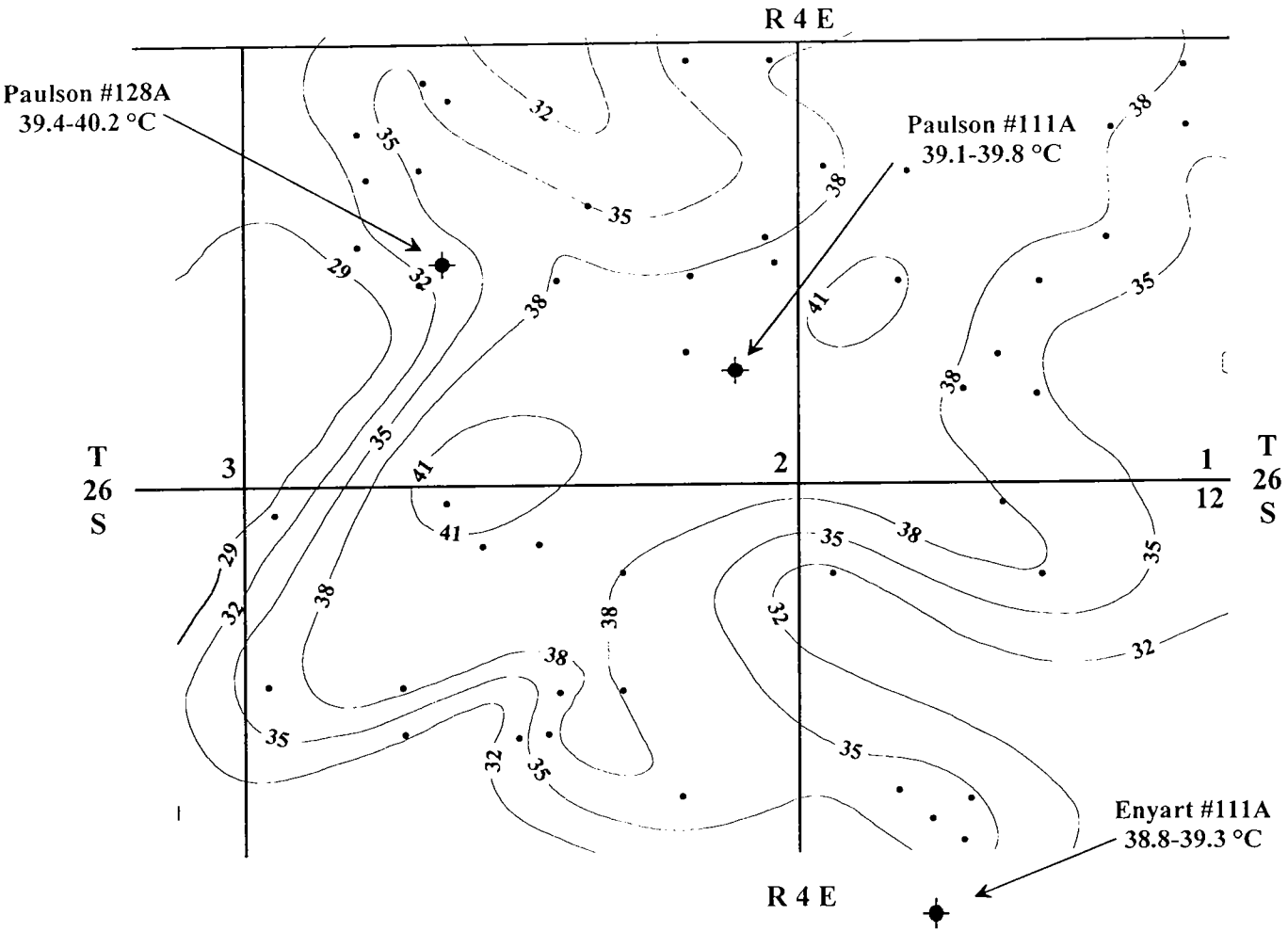

Figure 6. High-resolution temperature log and uncorrected log-header borehole-temperature (BHT) data from the top of the Arbuckle Group (707–838 m), West Shumway dome, El Dorado, Kansas. The contour interval is 3°C. One section is equal to 1 mi^2. The high-resolution temperature measurements seem to indicate a much broader and hotter region than the ~11°C anomaly delineated by BHT data. BHT data are courtesy of Dan Merriam, Kansas Geological Survey.

the results of the high-resolution temperature measurements in wells centered over the West Shumway dome suggest a broader region of high temperature at the top of the Arbuckle Group than delineated by the BHT data.

To emphasize the different interpretations of the thermal regime of the El Dorado field suggested by the log-header BHT data and by the high-resolution temperature logs, we present a composite temperature/depth plot of all available temperature measurements and uncorrected BHT data at the top of the Kansas City and Arbuckle Groups (Fig. 7). The average temperature/depth curve for the high-resolution logs was constructed by sampling the temperature of all six high-resolution logs at 250, 400, 650, and 720 m depth (triangles) and averaging these measurements (stars). The resulting mean thermal gradient for the three intervals is plotted as a solid line. The individual temperature measurements appear similar until a depth of 650 m is reached. At this depth, one well (Finney #2) appears to be significantly cooler than the other wells, suggesting that distinct thermal conditions in the deeper portion of the well prevail. Ignoring the individual well-temperature differences, it is apparent that the mean thermal gradient remains relatively constant from 200 to 650 m. After this depth is reached, the thermal gradient increases by about 4°C/km, indicating that the deepest part of the wells are maintained at a higher temperature than that of the upper portion of the well. The cause for this remains unknown.

The Kansas City and Arbuckle BHT data cannot provide further insight into thermal conditions in the El Dorado Field because they are not equilibrium-temperature measurements. However, it is interesting to compare the scatter in both types of data at the two horizons (Fig. 7). The open and vertically striped polygons represent the range (in both temperature and depth) of the high-resolution temperature measurements at the top of the Kansas City and Arbuckle Groups, respectively. When compared with the log-header BHT data for these two lithologies, it is seen that the scatter in temperature/depth space of the high-resolution logs is less. The wide scatter

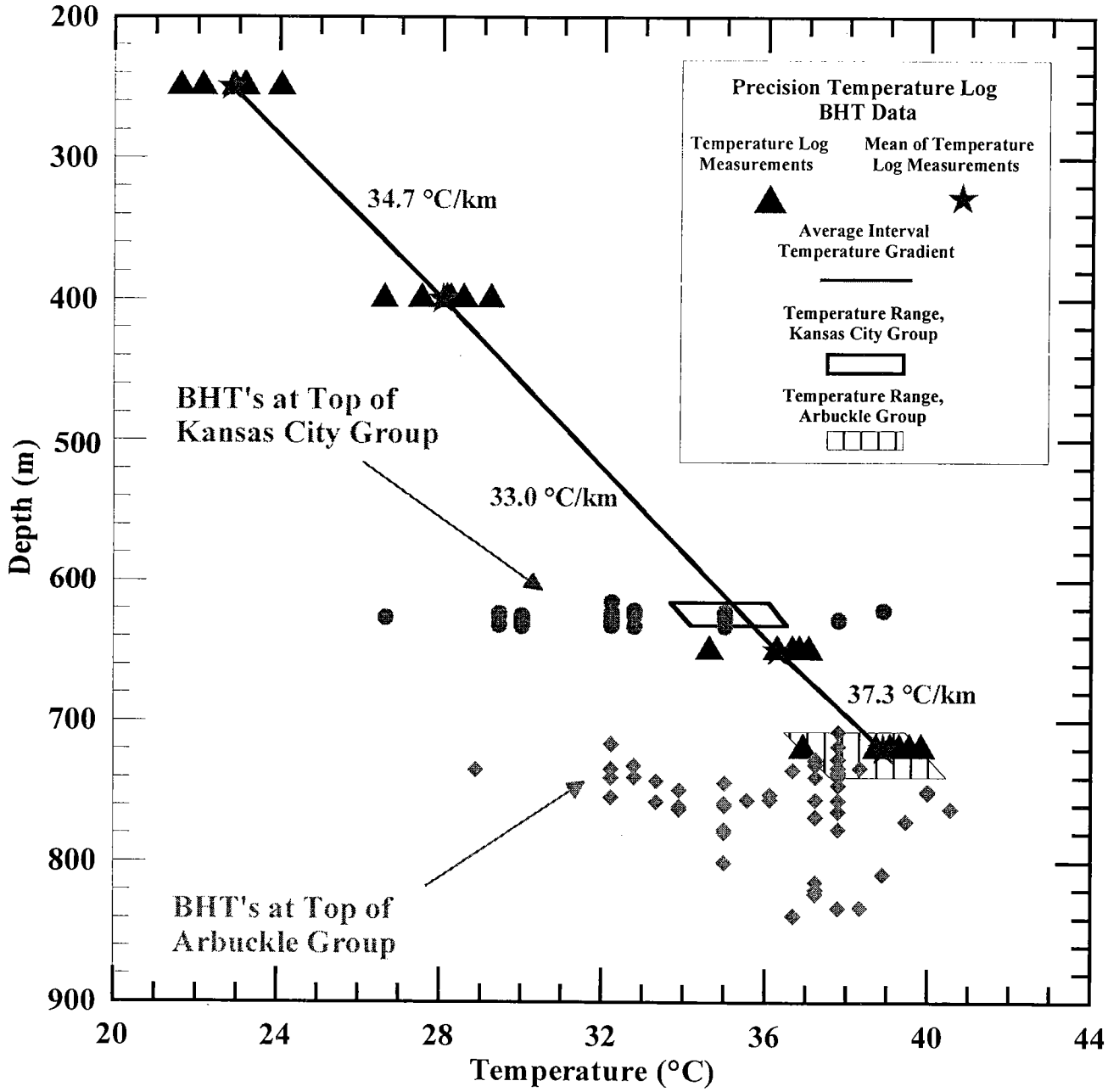

Figure 7. High-resolution temperature log and uncorrected log-header borehole-temperature (BHT) data, El Dorado oil field, Kansas. The small scatter in the high-resolution temperature measurements (triangles) at the top of two important producing horizons—the Kansas City (open polygon) and Arbuckle Groups (vertically striped polygon)—illustrates the overall consistency and reliability of the high-resolution temperature logs. The means of the log temperature at depths 250, 400, 650, and 720 m (stars) were used to calculate the mean interval thermal gradient. BHT data are courtesy of Dan Merriam, Kansas Geological Survey.

in the BHT data at these two horizons emphasizes the consistency and accuracy of the high-resolution temperature logs. The other prominent feature apparent from Figure 7 is that with few exceptions, the BHT data are colder than the high-resolution measurements. This pattern of colder than normal (as defined by the high-resolution temperature measurement as an equivalent depth) BHT data is consistent with either drilling disturbances (cooling at depth from circulating drilling mud) or production effects. Either interpretation emphasizes the nonequilibrium character of BHT data in general and these data in particular, which have not been corrected.

CONCLUSIONS

Although the results presented in this study are preliminary, a few observations are worth noting:

1. High-resolution temperature logs can provide reliable, equilibrium-temperature measurements in active petroleum settings.
2. High-resolution temperature logs acquired in the producing El Dorado oil field, Kansas, illustrate generally conductive, equilibrium-temperature well profiles.
3. The lower temperatures measured in the Finney #2 and Hull-Higgins #27 wells over the East Shumway dome appear to be the result of a significant change in thermal gradient, perhaps from mass transport of hydrocarbons and/or *in situ* thermal conductivity changes related to the presence of hydrocarbons, and not inter-well lithologic variability.
4. A preliminary analysis of high-resolution temperature logs and log-header–derived BHT data at the top of two productive zones (the Kansas City and Arbuckle Groups) within the West Shumway dome suggests that the anomalously high BHT data present at the top of both horizons are close to the actual formation temperature, and encompass a much broader region of the dome than previously believed.

One possible explanation for the apparently broad isothermal conditions atop the Arbuckle Group in that the pre-Pennsylvanian unconformity that separates the Middle Ordovician Viola (dolomite) and Simpson (sandstone) Groups and the deformed Arbuckle Group from the younger overlying shales of the Cherokee Group is a permeable pathway for fluid migration (Ramondetta, 1990).

In the future, we plan to log additional wells off-axis of the West Shumway dome and wells in the East Shumway dome in order to develop a more complete data set. These data then will be modeled to determine whether the observed temperature variations are from conductive as opposed to conductive disturbances and are therefore related to hydrocarbon accumulation and migration. A more complete comparison with the BHT data, both corrected and uncorrected, also will be carried out to evaluate the real errors of using such data. This error evaluation cannot be performed using the log-header BHTs themselves due to the lack of "true" data.

ACKNOWLEDGMENTS

The authors would like to thank Dan Merriam of the Kansas Geological Survey for locating the El Dorado wells logged in this study and for providing the BHT data. We would also like to thank Steve Darwin of Oil Hill Services for granting permission to log the El Dorado well and for providing general field assistance.

REFERENCES CITED

Blackwell, D. D.; and Spafford, R. E., 1987, Experimental methods in continental heat-flow, *in* Sammis, C. G.; and Henyey, T. L. (eds.), Geophysics, methods of experimental physics, v. 24, part B: Academic Press, San Diego, California, p. 189–226.

Blackwell, D. D.; and Steele, J. L., 1989, Heat flow and geothermal potential of Kansas, *in* Steeples, D. W. (ed.), Geophysics in Kansas: Kansas Geological Survey Bulletin 226, p. 267–291.

Blackwell, D. D.; Beardsmore, G. R.; Nishimori, R. K.; and McMullen, M. J., Jr., 1999, High-resolution temperature logs in a petroleum setting, examples and applications, *in* Förster, A.; and Merriam, D. F. (eds.), Geothermics in basin analysis: Kluwer Academic Press, New York, p. 1–33.

Bullard, E. C., 1947, The time necessary for a borehole to attain temperature equilibrium: Mon. Not. R. Astron. Soc., Geophysics Supplemental, v. 5, p. 127–130.

Fath, A. E., 1921, Geology of the Eldorado oil and gas field, Butler County, Kansas: Kansas Geological Survey Bulletin 7, 187 p.

Förster, A.; and Merriam, D. F., 1999, Problems and potential of industrial temperature data from a cratonic basin environment, *in* Förster, A.; and Merriam, D. F. (eds.), Geothermics in basin analysis: Kluwer Academic Press, New York, p. 35–59.

Förster, A.; Schrotter, J.; Merriam, D. F.; and Blackwell, D. D., 1997, Application of optical-fiber temperature logging: an example in a sedimentary environment: Geophysics, v. 62, p. 1107–1113.

Jessop, A. M., 1990, Comparsion of industrial and high resolution thermal data in a sedimentary basin: Pageoph, v. 133, p. 251–267.

Ramondetta, P. J., 1990, El Dorado: an old field with potential: Oil and Gas Journal, v. 88, p. 110–116.

Reeves, J. R., 1929, El Dorado oil field, Butler County, Kansas, *in* Structure of typical American oil fields, vol. 2: American Association of Petroleum Geologists, Tulsa, Oklahoma, p. 160–167.

Roberts, W. H. III, 1980, Design and function of oil and gas traps, *in* Roberts, W. H.; and Cordell, R. J. (eds.), Problems of petroleum migration: American Association of Petroleum Geologists, Studies in Geology 10, p. 217–240.

Waters, R. F., 1958, Differential entrapment of oil and gas in Arbuckle dolomite of central Kansas: American Association of Petroleum Geologists Bulletin, v. 42, p. 2133–2173.

Wisian, K. W.; Blackwell, D. D.; Bellani, S.; Henfling, J. A.; Normann, R. A.; Lysne, P. C.; Förster, A.; and Schritter, J., 1998, Field comparison of conventional and new technology temperature logging systems: Geothermics, v. 27, p. 131–141.

Estimation of Heat-Flow Density from Nuclear Logs and Drill-Stem Test Temperature Data

John H. Doveton
Kansas Geological Survey
Lawrence, Kansas

Andrea Förster
GeoForschungsZentrum Potsdam
Telegrafenberg, Potsdam, Germany

D. F. Merriam
Kansas Geological Survey
Lawrence, Kansas

ABSTRACT.—Heat flow is generally computed from temperature log data combined with rock thermal conductivity measured from core or cuttings samples of the stratigraphic units encountered in the well bore. These heat-flow values and associated thermal conditions are important in many aspects of basin analysis, especially in the determination of the alteration of organic matter and the generation of hydrocarbons. Heat-flow density measurements are sparse in the Midcontinent of the United States, however, and values are available from only seven boreholes in the Paleozoic in eastern and central Kansas. By contrast, tens of thousands of exploration and production wells have been logged by electric and nuclear devices. By calibrating standard geophysical logs with thermal-conductivity measurements and applying these to temperature data from drill-stem tests (DSTs), it is possible to estimate heat-flow values at locations with no recovery of core or cuttings. Although the methodology provides only an indirect estimate of heat-flow density, the much greater availability of boreholes with nuclear logs and DSTs suggests that reasonable values can be obtained in studies that use multiple wells.

INTRODUCTION

In the Midcontinent of the United States, large archives of commercial wireline logs are readily available on paper copy and are increasingly accessible over the Internet from digital databases such as that maintained by the Kansas Geological Survey (www.kgs.ukans.edu). Nuclear wireline logs supply measurements of rock mineralogy and porosity, which can be calibrated for the prediction of thermal conductivities. Temperature measurements from drill-stem tests (DSTs) and bottom-hole temperatures (BHTs) provide the necessary data for temperature gradients. Combined with the predicted thermal conductivities, heat flow may be computed at each well. Although high-precision temperature logs and laboratory measurements of subsurface thermal conductivity are preferred in heat-flow studies, they are extremely sparse contrasted to the number of petrophysical wireline logs. If reasonable estimates of heat flow based on these data can be made in the areas where dense control of oil and gas wells exists, then the larger database can be extended to the evaluation of thermal structure over large regions.

PREDICTIVE METHODOLOGY

In an earlier Kansas geothermal study, thermal conductivity and geologic descriptions were recorded for drill cuttings from four wells that were logged by a high-precision temperature device (Blackwell and Steele, 1989). These boreholes were also logged by neutron, density, sonic, and gamma-ray wireline tools, so that well-log parameters could be linked with thermal-conductivity values measured in the laboratory on samples from coincident depths. Although earlier studies have emphasized the dominant role of porosity on rock thermal conductivity (e.g., Bullard, 1954), this conclusion has been drawn for successions with moderate to high porosities. Thermal conductivities in the Paleozoic rocks of the Kansas subsurface are more influenced by the minerals forming the rock matrix because of the low porosities in the carbonates (average 6%).

Doveton and others (1997) developed a statistical

Doveton, J. H.; Förster, Andrea; and Merriam, D. F., 2001, Estimation of heat-flow density from nuclear logs and drill-stem test temperature data, *in* Johnson, K. S.; and Merriam, D. F. (eds.), Petroleum systems of sedimentary basins in the southern Midcontinent, 2000 symposium: Oklahoma Geological Survey Circular 106, p. 163–168.

predictive relationship for matrix thermal conductivity from the relationship between laboratory measurements and rock matrix descriptors derived from the well-log response. The equation took the form:

$$\lambda = 8.45 \times \rho_{maa} - 4.64 \times V_{sh} - 18.66$$

where λ is the prediction of matrix thermal conductivity; ρ_{maa} is the apparent matrix density computed from the density log and apparent porosity; and V_{sh} is the volume of shale estimated from the gamma-ray log. The equation was shown to be not only an effective predictor for carbonates but also an effective predictor for thermal-conductivity values for shale. These values show a reasonable match with subsurface estimates (Blackwell and Steele, 1989).

When used for prediction of *in situ* thermal conductivity in oil or gas wells, matrix thermal conductivities are first estimated using wireline-log data and then converted to bulk thermal conductivities by incorporation of a porosity term, also derived from the logs. An advantage of this indirect approach is that thermal conductivity is calculated as a continuous function of depth for sections of the particular rock type for which the predictive equation was derived. Cumulative thermal conductivities of subsurface successions combined with interval temperature gradients allow heat-flow density values to be estimated. Where a temperature profile is available, local intervals of anomalous heat flow in the borehole can be recognized. If a continuous temperature profile is not available, average temperature gradients can be computed in all wells through the use of end-member temperature anchor-points, provided by surface and corrected BHTs or temperatures from DSTs. Additional temperature values measured at intermediate depths in a well allow a more reliable estimation of an average temperature gradient in the well by regression analysis or even an estimate of an interval gradient for a particular section or for different formations. Generally, the more data points that are available in a well, the better will be the estimate of a temperature gradient used for heat-flow determination, given the uncertainties with single temperature data from petrophysical well logging or well testing. For problems in determining heat flow from BHTs and DST temperatures, the reader is referred to Deming (1989), Förster and others (1997), and Förster and Merriam (1999) and references therein.

KANSAS CASE STUDY

Kansas boreholes penetrate a relatively thin cover of sedimentary rocks that overlie the Precambrian crystalline basement. The succession consists of thick Cambro–Ordovician dolomites and limestones overlain by the Devonian Chattanooga Shale and a sequence of undifferentiated Mississippian carbonates. Above the Mississippian, the Pennsylvanian section consists predominately of alternating shale and limestone with some sandstone and coal, overlain by Permian rocks, which are similar in character to the Pennsylvanian sequence. Shales, limestones, cherty limestones, dolomites, and cherty dolomites dominate the sequence, whereas sandstones are less abundant. This situation is typical for the Midcontinent Paleozoic

An ideal well for predictive purposes of heat flow would be one that had a minimum of a gamma-ray, neutron, and density wireline-log suite and, in the absence of a temperature profile, a number of DSTs that had recovered formation fluid to provide temperature data to supplement corrected bottom-hole and surface temperatures. The use of temperature data from a number of DSTs within the same well at different depths allows several replicate estimates of heat-flow density to be estimated for comparison and validation. Also, estimates are generally considered more reliable in sections dominated by carbonates with little shale, because of the anisotropic and heterogeneous nature of shale thermal conductivity.

Although the well Patrick Herd #1 would not be considered as ideal, it has features that make it better than typical and worthy of a case study in the examination of the strengths and weaknesses of the indirect estimation of heat-flow density. Located in Comanche County in southern Kansas, close to the Oklahoma border, the well had six DSTs run over an interval ranging from the Pennsylvanian sequence to the Arbuckle Formation at the bottom of the hole. The depth range of the tests covers a lower Paleozoic section, the generalized lithologic composition of which is shown in Figure 1. The generalized compositions are estimated from density, neutron, and photoelectric logs, using methods described by Doveton (1994).

Many authors (e.g., Förster and others, 1997) have noted that DSTs should provide better temperature estimates than the BHTs, which represent the temperature of the drilling mud at the bottom of the well under nonequilibrium conditions. The relative abundance of temperature data provided by these DSTs, however, must be tempered by the realization that their reliability is influenced by the volume and nature of the fluid recovered. This is illustrated on Figure 2, where a time-temperature record is plotted for all six tests. The tests are conveniently paired into three different types of fluid recovery: gas (#2 and #3), mud (#4 and #5), and water (#1 and #6). The four periods of flow and shut-in causes complex temperature records to be measured by the sensor on the DST-valve assembly. The two gas tests provide excellent graphic illustrations of the cooling effect of gas expansion from the formation. The two mud tests reflect the recovery of relatively small amounts of mud-filtrate that have invaded the formation, and, thus, a slow build-up in temperature over the test periods. Both water recoveries show an initial rapid increase in temperature during the first flow period, a maximum temperature reached within the test, and a decline in temperature in the final shut-in period.

Temperature variation within the borehole can be studied based on measurements from the DSTs, the average surface temperature at the borehole location, and the adjusted BHT using the correction factor proposed by Kehle (1972). When the maximum temperature from each test is plotted against depth (Fig. 3), the points show a consistent and coherent pattern when

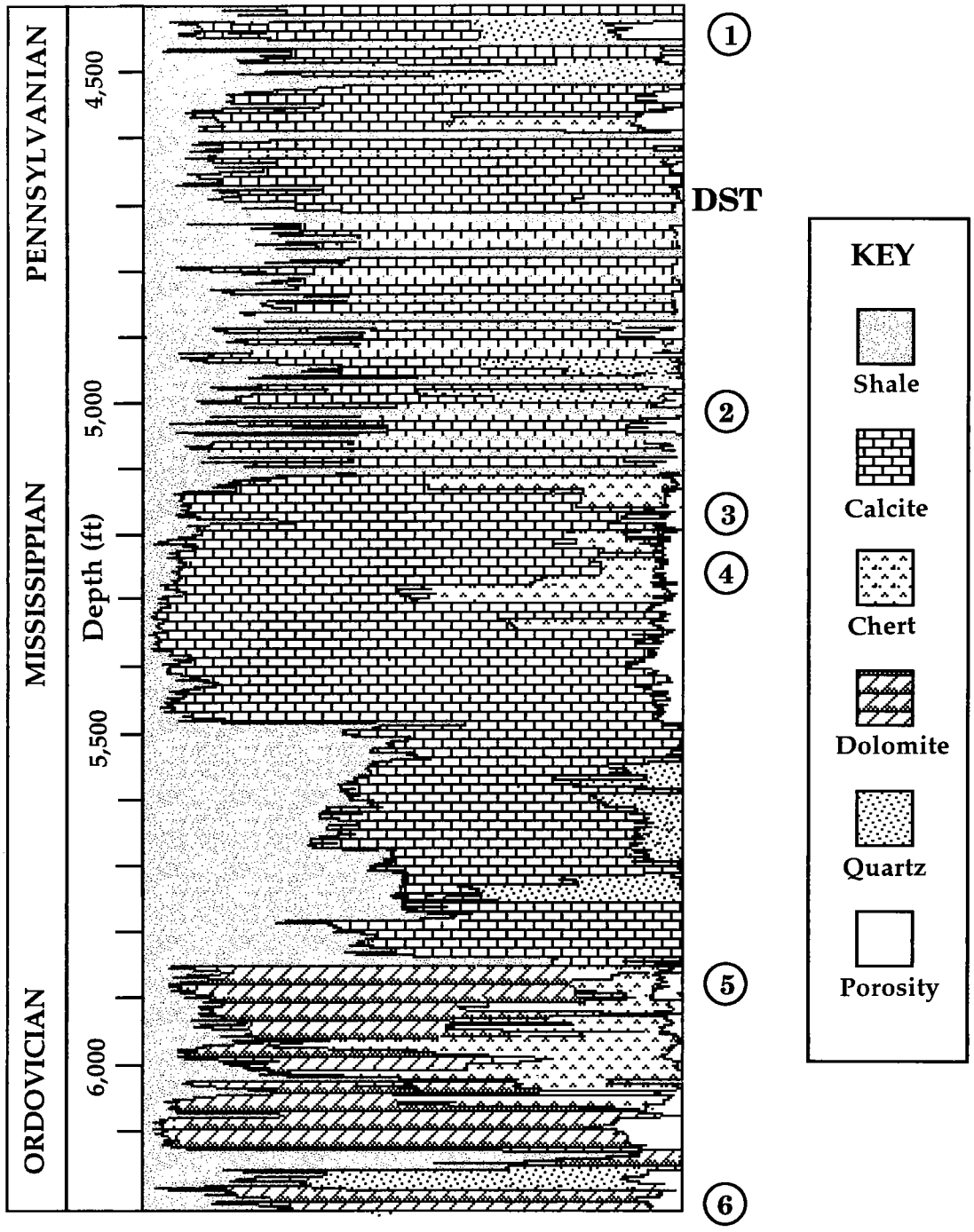

Figure 1. Compositional profile of part of the Paleozoic section estimated from nuclear wireline logs in Patrick Herd No. 1 well, NE¼NE¼NE¼ sec. 4, T. 33 S., R. 19 W., Comanche County, Kansas. Depth in feet. Circled numbers on the section locate the depths of six drill-stem tests (DSTs) in the well.

related to the temperature gradient drawn to link the average surface temperature with the corrected bottom-hole temperature recorded by the wireline log. Temperatures from the two gas tests are cooler than the mud-column gradient because of gas-expansion cooling. The two mud-recovery temperatures closely honor the mud-column gradient, presumably because the mud filtrate of invasion is in equilibrium with the mud column rather than with the formation temperature. Finally, the maximum temperatures recorded by the two water recoveries are significantly higher than the mud-column gradient and thus are interpreted to reflect formation temperatures, which are higher than the cooler mud column.

The temperatures from the two DSTs with water recoveries were used to constrain a temperature gradient for this interval and the heat flow, which is considered typical for the entire well. The use of the two DST

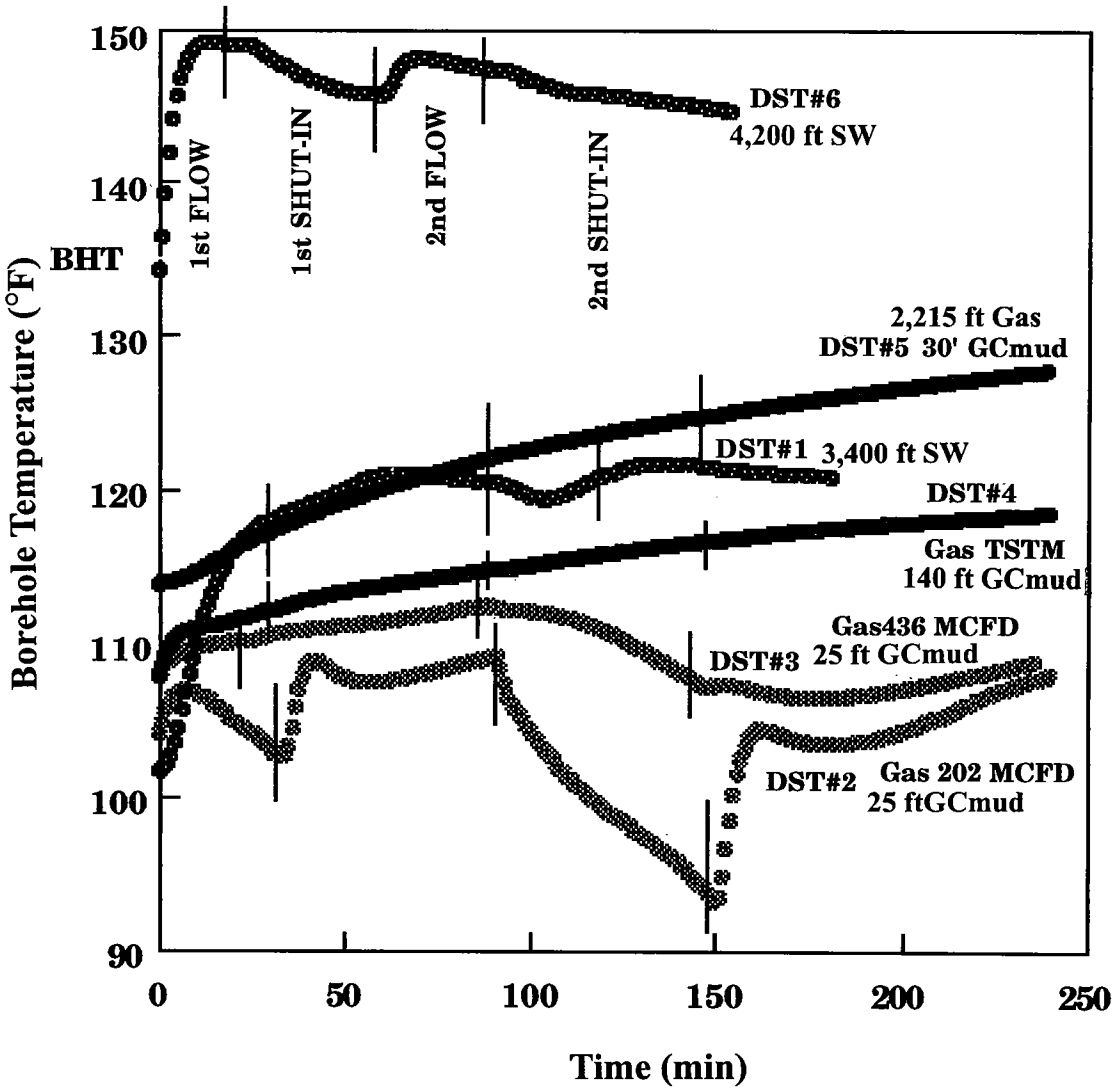

Figure 2. Records of drill-stem tests (DSTs) of temperature (in °F) versus time (in min) from the Patrick Herd No. 1 well, NE¼NE¼NE¼ sec. 4, T. 33 S., R. 19 W., Comanche County, Kansas. *Abbreviations:* Gcmud = gas-cut mud; SW = salt water; MCFD = thousand cubic feet [gas] per day.

values has the additional advantage that the interval between them has less shale and a higher proportion of carbonate rocks than higher in the section. The estimation of realistic shale thermal conductivities is difficult for indirect methods such as used in this paper or for direct measurements from core or cuttings samples, because of anisotropy and other factors (Blackwell and Steele, 1989). Therefore, the use of sections that are dominated by carbonates and bounded by good DST temperature measurements are preferable for model estimates of heat-flow density.

The digital gamma-ray, density, and neutron logs in Patrick Herd #1 were processed to obtain estimates of apparent matrix density (ρ_{maa}) and volume of shale (V_{sh}) and used to predict a profile of the matrix thermal conductivity (λ). Bulk thermal conductivities were then computed by modifying the matrix values by the thermal conductivity of the pore water, using porosities estimated from the density and neutron logs. The cumulative sum of the thermal conductivities in the section between the two DSTs combined with the temperature gradient from the DST temperature measurements enabled an estimate of the heat-flow value to be made at this location. Using these data, a simulation of a temperature log and its derivative temperature-gradient log generated is shown in Figure 4. The high-frequency fluctuations of temperature gradient in the upper part of the section reflect the interbedding of relatively thin shales in the Pennsylvanian rocks, which contrasts with the more massive carbonates at deeper levels.

The application of the temperature gradient between the two water-recovery DSTs (28.44°C per km; 1.56 °F per 100 ft) with the average bulk conductivity of the intervening section gave a heat-flow value of 75.4 mW/m^2. This value is higher than that estimated in most Kansas geothermal wells to date. It should be noted that the high value is caused primarily by

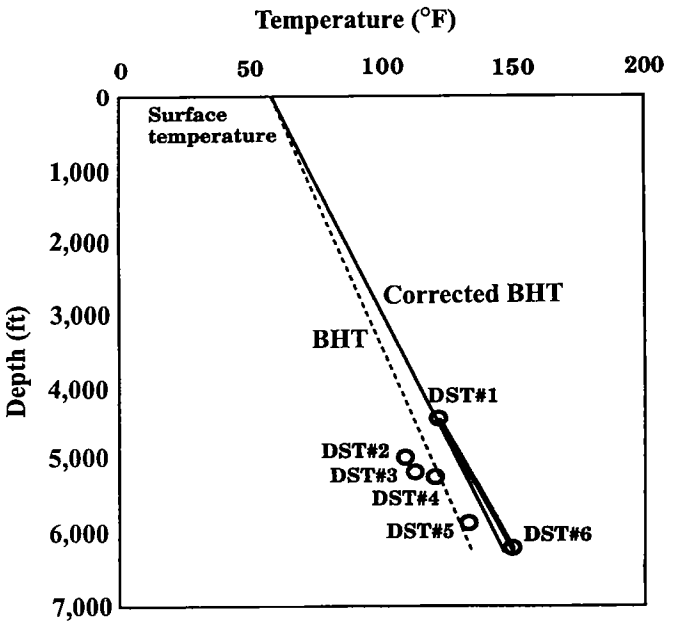

Figure 3. Depth plot of drill-stem test (DST) temperatures (in °F) versus depth (in feet) in the Patrick Herd No. 1 that links the mean annual surface temperature with the uncorrected and corrected borehole temperature recorded by the wireline-logging tool. The temperature gradient constrained by DST #1 and DST #6 is considered as a "best" value.

the high temperature gradient in this well (shown by both DST data and corrected BHT measurement), rather than intrinsic problems with the indirect estimation of thermal conductivities from the wireline logs. Difficulties in estimating the thermal conductivities of shales in the section, however, cannot be ignored as a contributing factor to uncertainties in heat-flow estimation. In future studies, the use of multiple estimates of heat-flow within individual wells from a large sample of wells will allow shale thermal conductivity to be calibrated from the well data as a by-product of the solution of robust and consistent heat-flow values.

CONCLUSIONS

If both the anomalously high temperature gradient (1.56 °F per 100 ft) and heat-flow value (75.4 mW/m^2) calculated from logs and drill-stem tests are correct, then this could be the result of either locally high heat production in the Precambrian basement or the effects of local fluid movement upward in the overlying sediments. Bodies of granitic rocks in the Precambrian basement are known from geophysical work in the Midcontinent. Ireland (1955) described the Osage-type structural features (the "Tulsa Mountains") in the subsurface of northeastern Oklahoma, and Cole (1976) showed similar features in Kansas. Later, Gay (1989) outlined "Graniteville-type" Proterozoic igneous intrusions in southeastern Kansas as interpreted from geophysical evidence. It is likely that differences exist in radiogenic-heat production of these bodies, causing areal contrasts in heat-flow generation. If these paleotopographic features or the intrusives are radioactive, they could account for the localized high heat-flow values. However, localized high heat-flow values have also been suggested to result from subsurface fluid flow through the sedimentary cover. For example, high heat-flow values in the vicinity of Tulsa, Oklahoma, are attributed to regional groundwater flow through the sedimentary cover (Cranganu and others, 1998). Förster and others (1997) noted that fluid flow may affect subsurface temperatures locally in the Cherokee basin.

The ambiguous conclusions of this paper are typical of geothermal studies in the Midcontinent (e.g., Cranganu and others, 1998) caused by the relative paucity of data, poorly understood geological mechanisms, and the struggle to distinguish systematic features from artifacts. However, this experiment shows the feasibility of heat-flow density estimation based on wireline logs and drill-stem tests from a single well. In future studies, the procedure could be applied to the large database associated with exploration and production wells. The increase in the number of estimates would mark a significant improvement in the recognition of systematic heat-flow patterns. The estimation procedures would give valuable insights into improved estimations of temperature from DSTs with different fluid-types and volumes of recovery. Finally, the expanded database would allow the heat-flow estimation procedure to be fine-tuned, particularly with respect to its weakest feature (in common with all current geothermal methods), which is the estimation of realistic thermal conductivities of shales.

REFERENCES CITED

Blackwell, D. D.; and Steele, J. L., 1989, Heat flow and geothermal potential of Kansas: Kansas Geological Survey Bulletin 226, p. 267–295.

Borel, R.; and Deming, D., 1993, Heat flow in north-central Oklahoma [abstract]: American Geophysical Union Transactions Eos, v. 74, p. 607.

Bullard, E. C., 1954, The flow of heat through the floor of the Atlantic Ocean: Proceedings of the Royal Society of London, ser. A, v. 222, p. 408–429.

Carter, L. S.; Kelley, S. A.; Blackwell, D. D.; and Naeser, N. D., 1998, Heat flow and thermal history of the Anadarko basin, Oklahoma: American Association of Petroleum Geologists Bulletin, v. 82, p. 291–318.

Cole, V. B., 1976, Configuration of the top of Precambrian rocks in Kansas: Kansas Geological Survey, Map Series M-7, scale 1:500,000.

Cranganu, C.; Lee, Y.; and Deming, D., 1998, Heat flow in Oklahoma and the south-central United States: Journal of Geophysical Research, v. 103, p. 107–127.

Deming, David, 1989, Application of bottom-hole temperature corrections in geothermal studies: Geothermics, v. 18, p. 775–786.

Doveton, J. H., 1994, Geologic log analysis using computer methods: American Association of Petroleum Geologists Computer Applications in Geology, no. 2, 169 p.

Doveton, J. H., Förster, Andrea; and Merriam, D. F., 1997, Predicting thermal conductivity from petrophysical

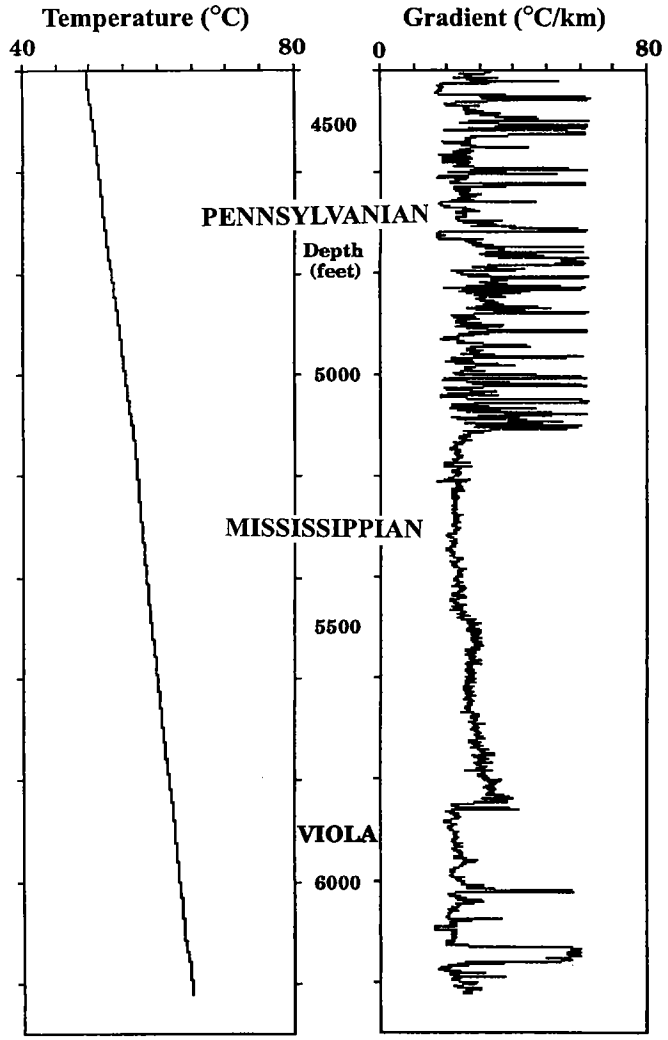

Figure 4. Model prediction of temperature (in °C) and temperature-gradient log (in °C/km) in Patrick Herd No. 1 well based on bulk thermal conductivities estimated from wireline log-responses and temperatures obtained during drill-stem tests (DSTs) with water recovery.

logs: a Midcontinent Paleozoic case study, *in* Pawlowky-Glahn, V. (ed.), Proceedings of the International Association for Mathematical Geology '97, Part 1: International Centre for Numerical Methods in Engineering, Barcelona, Spain, p. 212–217.

Förster, Andrea; and Merriam, D. F., 1999, Problems and potential of industrial temperature data from a cratonic basin environment, *in* Förster, Andrea; and Merriam, D. F. (eds.), Geothermics in basin analysis: Kluwer Academic/Plenum Publishers, New York, p. 35–59.

Förster, Andrea; Merriam, D. F.; and Davis, J. C., 1997, Spatial analysis of temperature (BHT/DST) data and consequences for heat-flow determination in sedimentary basins: Geologische Rundschau, v. 86, p. 252–261.

Gay, P. S., Jr., 1989, "Graniteville-type" Proterozoic igneous intrusions mapped in southeast Kansas: Kansas Geological Survey Bulletin 226, p. 229–243.

Gosnold, W. D., Jr., 1999, Basin-scale groundwater flow and advective heat flow: an example from the northern Great Plains, *in* Förster, Andrea; and Merriam, D. F. (eds.), Geothermics in basin analysis: Kluwer Academic/Plenum Publishers, New York, p. 99–116.

Ireland, H. A., 1955, Precambrian surface in northeastern Oklahoma and parts of adjacent states: American Association of Petroleum Geologists Bulletin, v. 39, p. 468–483.

Kehle, R. O., 1972, Geothermal survey of North America: American Association of Petroleum Geologists 1971 Annual Progress Report, 31 p.

Reservoir Characterization Using Inter-Well Seismic in a Shallow-Shelf–Carbonate Reservoir

J. H. Justice and J. C. Woerpel
Advanced Reservoir Technologies, Inc.
Carrollton, Texas

G. P. Watts and W. H. Waddell
Oxy USA
Midland, Texas

ABSTRACT.—Reservoir characterization is a topic of considerable current interest in the oil and gas industry. Reservoir characterization is an activity that attempts to combine or integrate various types of reservoir data to arrive at the most accurate and detailed model possible for the reservoir. In this study, new approaches to combining log, core, and high-resolution, inter-well seismic data are examined in order to arrive at the most detailed and accurate description possible for a specific shallow-shelf–carbonate reservoir located in the Permian basin of West Texas. By utilizing certain results from petrophysical research, the resulting reservoir characterization can include detailed maps of reservoir porosity and permeability distributions between wells. Having done this, a new method is then examined for estimating spatial statistics of porosity and permeability distributions directly from the inter-well data, to be used for three-dimensional (3-D) geostatistical extrapolation from the inter-well survey lines into the full reservoir volume. The result is a detailed 3-D reservoir description that honors all of the input data as well as the statistical characteristics of those data.

This work is part of an ongoing U.S. Department of Energy (DOE) Class II Oil Project sponsored jointly by Oxy USA and the DOE. Goals of the project include the acquisition of inter-well seismic data for the purposes of reservoir characterization and to monitor the location and movement of injected CO_2 in this pilot CO_2-injection project. The ultimate goal of all of this work is to examine and evaluate the use of CO_2 injection as a tool for improving production in marginal, shallow-shelf carbonate reservoirs.

INTRODUCTION

As world supplies of oil and gas are drawn down, and the probability of discovery of new reserves to replace these depleted resources become economically more challenging, there is increasing interest in using technology to reveal more information about existing reservoirs. These efforts to increase our understanding of the reservoir by means of the use of technology generally are categorized as reservoir description or reservoir characterization. These efforts ideally result in building detailed reservoir models that are then analyzed and studied in an effort to better manage these existing resources and to attempt to maximize production from the reservoir before abandonment.

Geostatistical procedures for reservoir modeling and simulation have gained wide acceptance and use in the past few decades. One of the greatest problems faced in building geostatistical reservoir models is the need to identify and use both hard and soft reservoir data that may be available to constrain the model and to provide statistics related to spatial and azimuth variation of model parameters.

Direct sampling of the reservoir volume is generally limited to the well bore or to outcrops. Measurements made on outcrops may or may not be reliable indicators of *in situ* reservoir properties. As an alternative, seismic data offer a potentially important means for sampling the *in situ* reservoir volume between wells. The problems associated with the use of seismic data for this purpose relate to questions of spatial resolution and to the need to relate seismic measurements to the actual reservoir properties needed for successful modeling and simulation. These properties include both porosity and permeability variations in the reservoir rock.

Coincident with the development of geostatistical reservoir-characterization techniques has been the

Justice, J. H.; Woerpel, J. C.; Watts, G. P.; and Waddell, W. H., 2001, Reservoir characterization using inter-well seismic in a shallow-shelf–carbonate reservoir, *in* Johnson, K. S.; and Merriam, D. F. (eds.), Petroleum systems of sedimentary basins in the southern Midcontinent, 2000 symposium: Oklahoma Geological Survey Circular 106, p. 169–174.

investigation and development of seismic technology for reservoir imaging and surveillance. We find increasing numbers of references in the literature to the use of three-dimensional (3-D) surface seismic, borehole seismic, and four-dimensional (time-lapse) seismic surveys for the purposes of reservoir management and monitoring. These developments have, in turn, prompted increased interest and activity in petrophysical research aimed at relating seismic measurements to reservoir properties. The goal of all of this work is to bring the power of seismic imaging to the service of engineers involved in reservoir management, development, and simulation.

Surface seismic data suffer from limited bandwidth, which typically limits spatial resolution at the reservoir level. Borehole seismic technology has been developing as a means of acquiring seismic data using existing well bores, with sources and receivers at or near reservoir level. As a result, much broader bandwidths are generally possible, with the consequence that resolution can be much higher than can be obtained with surface seismic imaging. Further, because of the unique geometries involved, borehole seismic data can be processed as either transmission data, using tomographic imaging, or as reflection data, similar to surface seismic data or vertical-seismic-profile (VSP) data. Whereas surface seismic bandwidth is normally limited to at most a few hundred Hertz (cycles per second), borehole seismic data may exhibit bandwidths of several thousand Hertz.

Surface seismic data does offer the advantage of being able to sample a full 3-D reservoir volume, whereas borehole seismic data normally sample a vertical cross section between two or more wells. The significantly increased resolution and flexibility of the latter, however, makes possible more detailed studies of the reservoir volume and can provide a powerful new means for deriving spatial statistics required for geostatistical approaches to reservoir modeling and simulation. As a result, borehole seismic imaging should be viewed as a powerful and important new tool for reservoir studies.

Borehole seismic data can be processed as reflection data (two-way travel path), in which case the measurements with which we typically work relate to acoustic impedance (product of acoustic-wave velocity and rock density), amplitude, or derived attributes or characteristics of the seismic signal (wavelet). When processed as transmission data (one-way travel path), using tomographic image reconstruction algorithms, the resulting measurement is generally acoustic-wave velocity at each "point" in the imaged region. Because acoustic waves propagate in two distinct modes, namely shear and compressional modes, we obtain a distinct finite set of measurements, such as shear- and compressional-wave velocities within the reservoir volume, from which to derive or estimate reservoir parameters of interest. It is fortunate that research in wave propagation and rock physics is providing relationships between many rock properties and these seismic measurements. When used together, we can commonly infer much about the reservoir environment from indirect seismic measurements.

Our principal objective is to use borehole seismic tomographic imaging between wells to derive measurements, or estimates, of the compressional- and shear-wave acoustic velocities of the reservoir rock as a function of spatial position in the reservoir. We then relate these to reservoir porosity using log and core data together with petrophysical relationships known as the Biot-Gassmann equations. Log and core data are used with the inter-well data to calibrate equation parameters at the well. Using this calibration, we then extrapolate into the inter-well volume (vertical cross section) using the inter-well seismic data alone. From these results, we then have enough information, obtained within the reservoir itself, to extract spatial statistics needed for geostatistical reservoir modeling and simulation in 3-D. To our knowledge, this represents the first use of high-resolution, inter-well seismic data for estimating spatial statistics needed for geostatistical reservoir modeling.

We focus on the estimation of reservoir porosity directly from the seismic data, using the procedure outlined above. We then use various cross plots (as a function of rock type) to infer permeability from the derived porosity distributions in the inter-well cross sections. Having done this, the resulting spatial maps of poros-

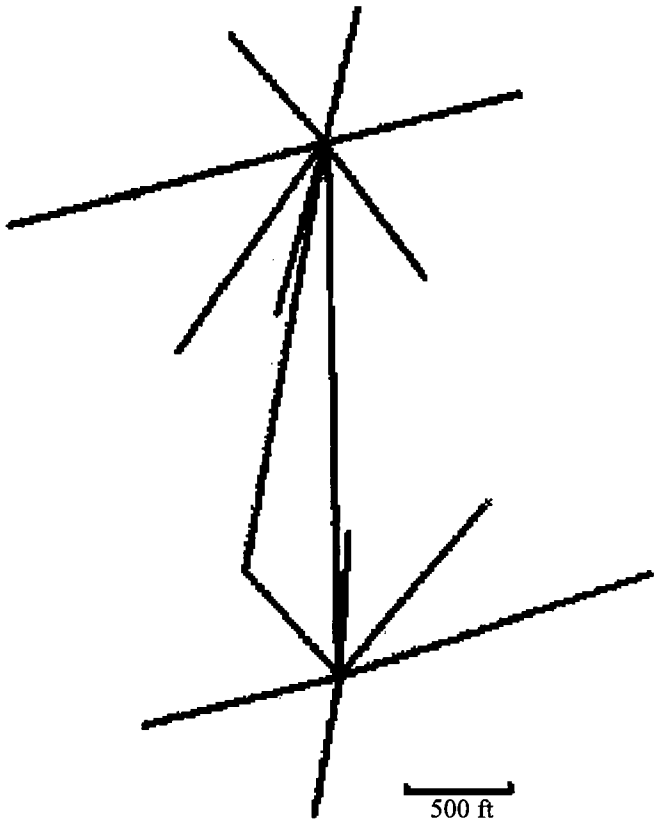

Figure 1. Layout of 15 inter-well survey lines used in this study. Lines are oriented in two patterns, north and south, with a center seismic-source well in each. Each source well is surrounded by multiple seismic-receiver wells. The radial pattern permits azimuth variation of spatial statistics to be estimated.

ity and permeability between wells can be used to extract variograms needed for full 3-D geostatistical reservoir modeling and simulation. If the inter-well survey lines are well distributed azimuthally, then azimuth variations in the statistics can be inferred. Figure 1 shows the actual layout of the wells and the inter-well survey lines used in this study. The survey lines are grouped into a north and a south pattern, each having a central seismic-source well surrounded by a number of seismic-receiver wells. Inter-well borehole seismic data are acquired between each pair of wells joined by a line in the figure.

BIOT-GASSMANN EQUATIONS

The key to relating seismic measurements to rock properties lies in the realm of rock physics (or petrophysics) research. An increasingly large body of literature, appearing over a relatively long time span, has given much insight into seismic-wave propagation as a function of the type of rock medium in which the waves propagate. In particular, it is now known that seismic-wave propagation in porous-rock media is influenced by properties of the rock matrix or rock fabric itself (rock mechanics), the characteristics of the pore space within the rock (orientation, aspect ratio, connectivity, tortuosity, etc.), and the characteristics of the pore-filling fluid (or gas), to name a few.

Fundamental research on wave propagation in porous rock media was carried out by M. Biot during the 1950s. His pioneering theoretical work has been extended and modified in a number of ways as well as supplemented and tested by laboratory investigations. Out of this work has grown an increasingly substantial collection of equations and relationships that can be called into service for the type of work reported here.

One set of equations that relate shear and compressional acoustic velocities to specific rock properties is of interest to us in this work. In particular, we wish to consider a relationship known as the Biot-Gassmann equations, given by:

$$\rho V_s^2 = G_f$$

$$\rho V_p^2 = K_f + \frac{4}{3} G_f + \frac{\left(1 - \frac{K_f}{K_s}\right)^2}{\left(1 - \Phi - \frac{K_f}{K_s}\right)\frac{1}{K_s} + \frac{\Phi}{K_p}}$$

where subscripts s and p stand for shear and compressional, respectively, when associated with a seismic velocity, V. Otherwise, subscript s refers to the solid (mineral) phase of the rock, and subscript p refers to the pore fluid. The subscript f refers to the dry frame of the porous rock. Rock density is denoted by ρ, and porosity is denoted by Φ. K stands for either the bulk modulus of the dry porous rock frame (K_f), the bulk modulus of the solid phase of the rock (K_s), or the bulk modulus of the pore filling fluid (K_p). G_f is the shear modulus of the rock frame.

Density and the various moduli of the rock or pore fluids are based on physical or mechanical properties of the rock or fluid. The Biot-Gassmann equations relate these properties to shear and compressional acoustic velocities and to a reservoir parameter of particular interest to us, porosity. Technically, for example, the density and moduli of the rock and pore fluid could be measured or estimated directly from core and fluid samples. If this were done, then the acoustic shear- and compressional-wave velocities could be obtained from the inter-well tomographic imaging computed from the seismic data. From these elements, the equations could be solved directly for an estimate of porosity at each "point" (determined by resolution) within the reservoir.

In our case, the physical measurements of the requisite rock properties were not available to us. We did know that the pore fluid is dead oil and that the basic rock type is dolomite. We also had a complete set of cores through the reservoir interval, and these cores had been subjected to analysis, including measurement of core porosity and permeability. Core analysis was further used to partition the reservoir interval into a sequence consisting of four specific rock types. Each distinct rock type is characterized by unique pore geometry and/or lithologic characteristics.

USE OF BIOT-GASSMANN EQUATIONS FOR CALIBRATION

Although we did not have direct measurements of the various moduli and densities of rock and fluid for use in the Biot-Gassmann equations, we realized that we did have sufficient information at the well bore to use these equations to infer some of the unknown moduli. In addition, we had access to published values for the bulk modulus of the dead-oil pore-filling fluid and for the bulk modulus of the solid phase of the mineral dolomite. We also had core porosity measurements at the well bore, and we had the shear- and compressional-wave velocities from the inter-well seismic processing at the well bore. Together, these provided enough information to compute the bulk modulus of the dry porous rock frame (K_f) for each rock layer at the well. The shear modulus (G_f) actually can be computed directly from the shear velocity (V_s) at each point in the inter-well cross section.

With all of the bulk moduli known or computed using the Biot-Gassmann equations at the well, as explained, these were substituted into the Biot-Gassmann equations, along with the inter-well shear and compressional velocities to derive the inter-well porosity distribution in the vertical cross section between the wells. The frame modulus for each rock layer is actually a function of pore geometry. The frame modulus itself was not held constant within each layer between wells, but the pore geometry was assumed not to vary within a layer. The spatial variation of the layer vertically and horizontally was honored between the wells, based on the tomography and inter-well VSP

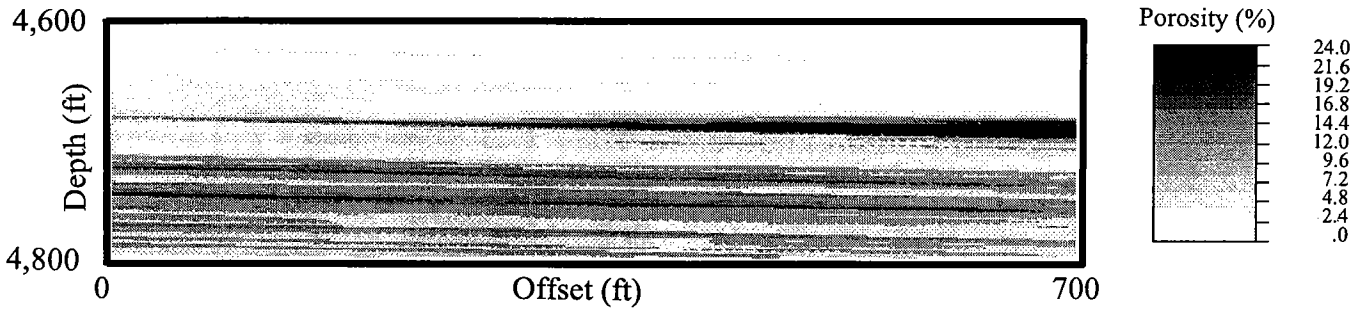

Figure 2. Inter-well porosity (in %) derived using Biot-Gassmann equations using inter-well seismic and core data. Wedge-shaped unit near center, right, with high porosity is an oolitic limestone that is known to exhibit high porosity and permeability.

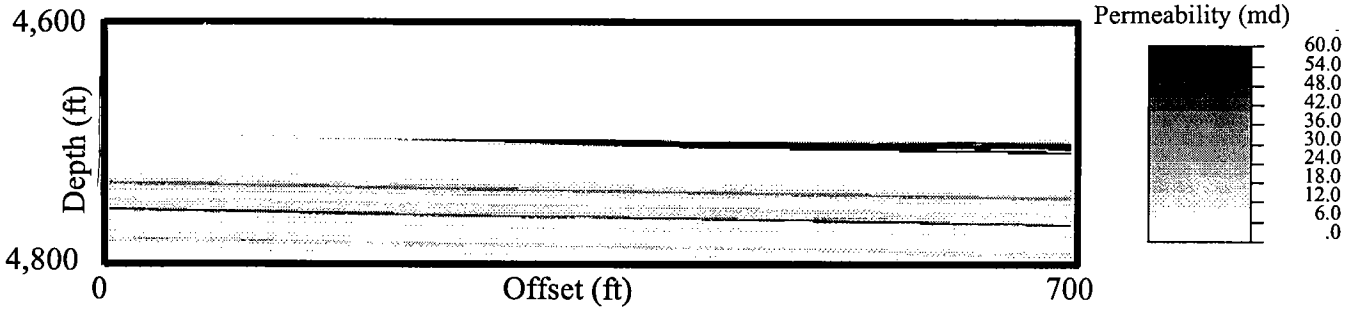

Figure 3. Inter-well permeability (in millidarcies, md) from same inter-well line as Figure 2. Vertical permeability barriers are clearly evident. High permeability of the oolitic-limestone unit is also apparent.

(reflection data). This was done to insure that the proper frame modulus was used at each point in the inter-well cross section. All of the variation in observed compressional and shear wave velocities was therefore assumed to arise from variations in porosity and not from variations in pore geometry within a layer.

The calibration described above, using core porosity, was actually carried out only at the center (seismic-source) well in each case. In fact, these were the only wells for which core data were available. By comparing the computed porosities at the other well (seismic-receiver well) using neutron porosity logs, a good fit was observed in each case, which strongly supported the approach that we had taken and gave credence to our inter-well porosity computations. The source well is located at the left side of both Figures 2 and 3. The receiver well is at the right side of these figures.

DERIVATION OF PERMEABILITY FROM POROSITY

Having computed the inter-well porosity distributions, as described, it is of interest to use this information to derive permeability distributions, if possible. There is no known analog to the Biot-Gassmann equations for computing permeability. However, we did have considerable porosity information available from our previous computations, and permeability is commonly inferred from porosity using cross plots.

It turns out that the four rock types that had been identified in the reservoir individually yielded good cross plots between porosity and permeability, based on core analysis. As a result, we identified each rock type spatially in the inter-well cross section. Using the appropriate cross plot for that rock type, we used the computed porosity to obtain an estimate of permeability at each point in the reservoir cross section.

At this point, we had obtained inter-well cross sections of porosity and permeability with useable resolution for reservoir modeling (about 1 ft vertical resolution). We then realized that two detailed data sets (porosity and permeability) were available from which spatial statistics could now be inferred for use in geostatistical 3-D reservoir modeling.

GEOSTATISTICAL 3-D RESERVOIR MODELING

We believe that this is the first time that inter-well seismic data has been used as a basis to derive the variograms and other statistics needed for geostatistical reservoir modeling. This approach offers a potentially important alternative for deriving these statistics based on data acquired in the reservoir environment under *in situ* conditions. We will not go into detail about the derivation of the spatial variograms, because this is a standard procedure once the input data are available. We simply derived statistics from the inter-well porosity and permeability maps that we had computed, as described earlier, to compute spatial variograms. Because we had a radial pattern of inter-well survey lines available, it is possible to derive

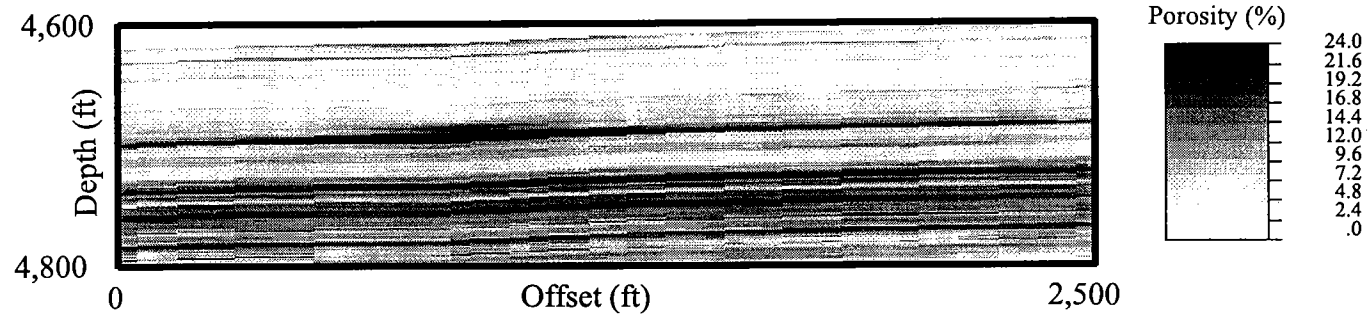

Figure 4. East–west cross section from 3-D kriged, porosity-reservoir model (porosity in %). High-porosity oolitic-limestone unit is clearly visible in the cross section. Bin size is 1 ft vertical by 50 ft lateral.

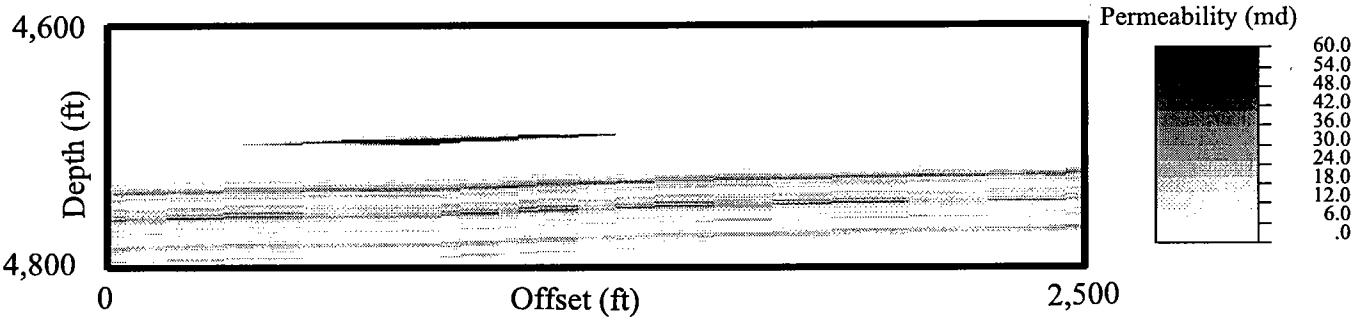

Figure 5. East–west cross section from 3-D kriged, permeability-reservoir model (permeability in millidarcies, md). Cross section is in the same location as the cross section in Figure 4. Bin size is 1 ft vertical by 50 ft lateral.

these statistics as a function of azimuth in each well pattern.

Once the requisite spatial variograms are derived, many alternatives are available for generating 3-D geostatistical reservoir models. We began by generating one model using simple kriging. Kriging is a very smooth and predictable procedure for interpolation, using the derived variograms, so it provided a reservoir model that we believed would be most useful for geologic interpretation in the full 3-D reservoir volume (cross sections, fence diagrams, etc.). A conditional simulation model is also shown in the examples using the derived variograms. This latter type of model is more representative of the kind of model that might be used for reservoir simulation.

EXAMPLES

To illustrate our results, we begin with the porosity and permeability maps derived from one of the inter-well survey lines. The resulting porosity map is shown in Figure 2, and the corresponding permeability map is shown in Figure 3. Note that a wedge-shaped zone of very high porosity and permeability can be seen in each figure, tapering from about the center to the right-hand side. This is an oolitic limestone that is known to occur in the southern part of the field and was not included in the four original rock types because it did not occur at either of the central wells that were cored. Because our assumption was that all of the rocks were dolomite, the equations possibly overshoot the actual porosity and permeability of this rock. However, it is known to have very high porosity and permeability, consistent with our computations.

It was from these inter-well porosity and permeability maps that the spatial variograms were derived that would be used for 3-D geostatistical reservoir modeling. An east–west cross section from the kriged 3-D model is shown in Figure 4. The bin size is 1 ft vertical by 50 ft lateral. The model honors the inter-well data where the inter-well survey lines intersect the cross sections of the kriged 3-D model. The corresponding permeability cross section from the kriged 3-D model is shown in Figure 5. The kriged models are smooth and provide an aid to geologic interpretation of the reservoir environment. The east–west slice was chosen to intersect the oolitic-limestone body that shows up clearly delineated in the kriged 3-D model.

Finally, an east–west cross section from a 3-D conditional-simulation model is shown in Figure 6. Bin size is again 1 ft vertical by 50 ft lateral in this model. The corresponding permeability model is shown in Figure 7. The location of the east–west slice (cross section) is the same as in Figures 4 and 5.

CONCLUSIONS

A pilot CO_2-injection project in the Permian basin of West Texas has provided the opportunity to acquire and to study the use of inter-well (borehole) seismic data, together with log and core data for the purposes of building a high-resolution reservoir description of a

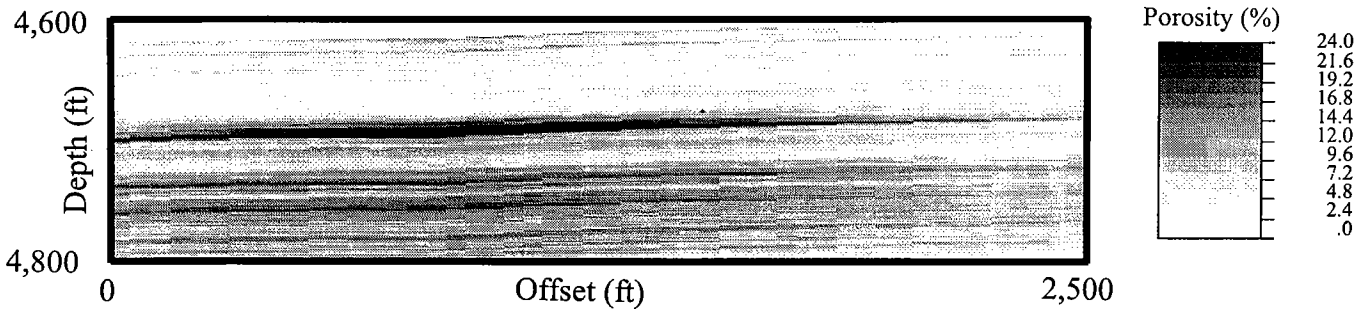

Figure 6. East–west cross section of porosity (in %) from 3-D conditional-simulation reservoir model. Cross section is in same location as cross section in Figure 4. Detailed statistical variations in this model distinguish it from the kriged model in Figure 4.

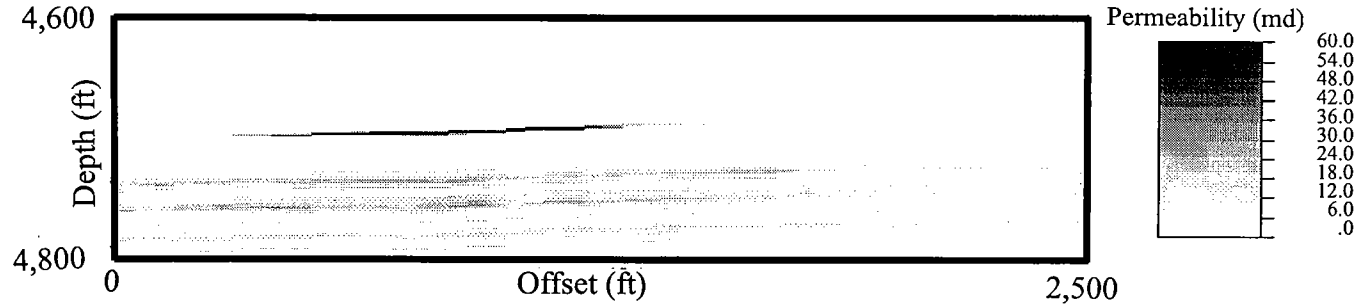

Figure 7. East–west cross section of permeability (in millidarcies, md) from 3-D conditional-simulation reservoir model. Cross section is in the same location as Figure 5. Detailed statistical variations in this model distinguish it from the kriged model in Figure 5.

shallow-shelf–carbonate reservoir. As part of this work, we have outlined a new procedure for transforming inter-well shear- and compressional-velocity (tomographic) images to obtain maps of inter-well porosity and permeability distribution using the Biot-Gassmann relations together with core and log data and cross-plots.

We have shown further that the resulting porosity and permeability maps can represent a viable basis for deriving spatial statistics, such as variograms, needed for subsequent geostatistical reservoir modeling and simulation in 3-D. Using all of the available data, we have developed a method for high-resolution reservoir characterization resulting in full 3-D models of the reservoir that honor the available data as well as the derived statistics of those data. The resulting reservoir characterization provides detailed 3-D models of both porosity and permeability distributions within the reservoir. These models can then be used to develop reservoir-management plans to include infill drilling, and can be used as the basis for detailed reservoir-simulation models to study and design future EOR programs such as the CO_2-injection program, which is currently being evaluated for this reservoir.

ACKNOWLEDGMENTS

We gratefully acknowledge the support of Oxy USA, its partners in the Welch Field, and the support of the U.S. Department of Energy (DOE), which made this study possible. This work was carried out in conjunction with Cooperative Agreement DE-FC22-93BC14990 of the DOE.

REFERENCES CITED

Bourbie, T.; Coussy, O.; and Zinszner, B., 1987, Acoustics of porous media: Gulf Publishing Co., Houston, 334 p.

Deutsch, C. V.; and Journel, A. G., 1992, GSLIB Geostatistical library and user's guide: Oxford University Press, New York, 340 p.

Guegen, I.; and Palciauskas, V., 1994, Introduction to the physics of rocks: Princeton University Press, Princeton, New Jersey, 294 p.

White, J. E., 1983, Underground sound: Elsevier Science Publishing Co., New York, 253 p.

Determination of Flow Potential from Oil Reservoirs to Aquifers through Abandoned Wells: Implications for Area-of-Review Variances for Class II Injection Wells

Robert C. Laudon, Donald L. Warner, Leonard F. Koederitz, and Shari Dunn-Norman
University of Missouri–Rolla
Rolla, Missouri

ABSTRACT.—Recent litigation in the United States alleging contamination of groundwater supplies through abandoned oil wells has prompted the groundwater industry as well as the petroleum industry to look closely at two areas where potential for contamination is recognized. The first involves areas where individual abandoned wells, by themselves, may act as conduits for contamination. The second occurs in association with injection operations in active oil fields.

A procedure involving computer generation of residual maps (head-difference maps) has been developed to address this problem. The procedure involves the following five processes: (1) gridding and contouring of the free-standing–water level for an aquifer; (2) conversion of hydrocarbon reservoir-pressure data to head-equivalent data through standard-pressure to head-gradient calculations; (3) gridding and contouring of the hydrocarbon reservoir-head equivalent; (4) subtraction of the two grids to create a residual grid; and (5) contouring of the residual grid.

Areas mapped as negative residuals outline areas where the potential for flow from the hydrocarbon reservoir to the aquifer is negative, and there is no potential for contamination of the aquifer through an abandoned well even if the well were open to both horizons (assuming the well is filled with water or a brine of the appropriate gradient). Areas mapped as positive residuals outline areas where the potential for flow is from the oil reservoir toward the aquifer and where contamination could occur in well bores that are not protected by other means. The procedure has been successfully used to identify areas of low contamination potential in several areas of North America. It has also been used to identify areas where area-of-review (AOR) variances for certain Class II injection wells have been granted.

INTRODUCTION AND BACKGROUND

It has been recognized for many years that abandoned oil and gas wells represent avenues for potential vertical migration of oil, gas, and brines from active or abandoned hydrocarbon reservoirs to shallow aquifers sometimes referred to as underground sources of drinking water. Many people in both the petroleum industry as well as the groundwater industry have indicated concern about this problem. For most abandoned oil and gas reservoirs, the reservoir pressure at abandonment is generally so low that the potential for migration through the well to an aquifer is extremely low. However, in active oilfields—particularly in oilfields where injection operations are occurring—the potential is very real.

In 1980, when the underground injection control (UIC) regulations were promulgated, all subsequent Class II injection wells (saltwater-disposal and secondary injection-recovery wells) were required to satisfy certain area-of-review (AOR) requirements. Typically, all abandoned wells within a certain radius (commonly 0.25 mi) were required to pass specific tests to ascertain that no leakage of fluids could occur through that well to underground sources of drinking water. Existing injection wells were excluded from the AOR requirements. In 1992, a Federal Advisory Committee recommended that AORs for existing wells, some 100,000 in the United States, be performed within five years of promulgation of the amended UIC regulations. The final document recognized that, under certain circumstances, individual wells, whole fields, or whole basins could be exempted from the AOR procedure through a variance program. According to the Federal Advisory Committee recommendations, a variance could be granted according to any of the following criteria:

Laudon, R. C.; Warner, D. L.; Koederitz, L. F.; and Dunn-Norman, Shari, 2001, Determination of flow potential from oil reservoirs to aquifers through abandoned wells: implications for area-of-review variances for Class II injection wells, *in* Johnson, K. S.; and Merriam, D. F. (eds.), Petroleum systems of sedimentary basins in the southern Midcontinent, 2000 symposium: Oklahoma Geological Survey Circular 106, p. 175–185.

TABLE 1. — Density (lb/ft³) and Pressure Gradient (psi/ft) for Selected Fluids

Fluid	Density	Gradient
Fresh water	62.4	0.433
Sea water	64.3	0.446
Brine	72.0	0.500

(1) the absence of an underground source of drinking water; (2) the hydrocarbon reservoir is underpressured relative to the underground source of drinking water; (3) local geologic conditions preclude upward fluid movement that could endanger an underground source of drinking water; and (4) other compelling evidence.

This paper addresses the second criterion as a means of granting an AOR variance to individual wells, whole fields, or whole basins.

FLUID FLOW IN THE SUBSURFACE

Fluids in the subsurface do not necessarily flow from areas of high pressure to areas of low pressure. They flow from areas of high head to areas of low head. Head elevations for aquifers are relatively easy to measure because they are represented by free-standing–water levels in wells that are open to the aquifers. To determine whether fluids will flow vertically from an abandoned hydrocarbon reservoir to an aquifer through an abandoned well, the head elevation for the aquifer must be compared against the potential head elevation for the hydrocarbon reservoir.

PROCEDURE TO CONVERT PRESSURE TO HEAD

The head elevation for a hydrocarbon reservoir is determined by three factors—elevation, reservoir pressure, and fluid gradient. Elevation is the vertical distance above or below some datum, generally mean sea level, where the pressure measurement is taken. Pressure is the fluid gauge pressure as measured or calculated at the subsurface point of interest. The fluid gradient is a function of the density of the fluid in the well bore, which is typically a function of the salinity of the fluid left in the hole. Example gradients are shown in Table 1.

An example follows. To determine the potential head elevation for a hydrocarbon reservoir having a reservoir pressure of 1,900 psi located at 4,000 ft below sea level in a well containing sea water:

$$H_t = H_z + H_p$$

where H_t is the total head, H_z is the elevation of the pressure measurement, and H_p is the head caused by the pressure and gradient, where H_p is the reservoir pressure divided by the fluid gradient, and the fluid gradient is a function of the salinity of the fluid in the well bore. Thus:

$$H_p = (1{,}900 \text{ psi})/(0.446 \text{ psi/ft}) = 4{,}260 \text{ ft}$$

$$H_t = -4{,}000 \text{ ft} + 4{,}260 \text{ ft} = +260 \text{ ft}$$

This calculation determines that the free-standing sea water in this well bore will rise to a head elevation of 260 ft above sea level as a result of the reservoir pressure pushing against the hydrostatic head of the sea water in the well bore.

CONCEPT OF THE RESIDUAL

A residual is simply the difference between two head elevations at any geographic location (Fig. 1). Thus, at the well bore listed above, if the free-standing–water level for an underground source of drinking water is 500 ft above sea level, then the difference between the hydrocarbon-reservoir head elevation relative to the aquifer head elevation is –240 ft. A negative residual, as defined here, means that, even if the well bore were standing open to both horizons, no potential would exist for flow from the hydrocarbon reservoir to the aquifer. In fact, flow would be from the aquifer toward the hydrocarbon reservoir, and no potential would exist for contamination of the aquifer from the hydrocarbon reservoir.

A positive residual, on the other hand, implies that a potential for flow from the reservoir to the aquifer does exist, and the potential for contamination is present, provided there are no other barriers to fluid flow, such as packers, cement plugs, or bridge plugs in the well.

The above discussion applies to one well and one geographic location and is two-dimensional. To get to three dimensions, a map must be made. The computer mapping of residuals is a multistage process that involves the following seven steps. (1) Collect, post, grid and contour the aquifer data. (2) Collect the hydrocarbon-reservoir pressure data. (3) Convert reservoir pressures to heads. (4) Post, grid, and contour the heads derived from reservoir pressures. (5) Subtract the two grids to create a residual grid. (Note that the two grids

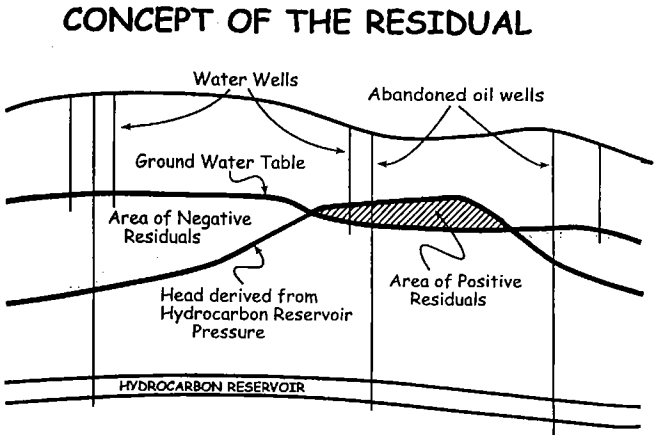

Figure 1. Illustration of the concept of the residual. Areas where the free-standing–water level for the aquifer (aquifer head) falls below heads derived from reservoir pressures define the areas of positive residuals.

must be created such that they are identical aerially in terms of size, shape, and grid spacing.) (6) Contour the residual grid. (7) Edit all of the above.

Our experience has shown that residual maps are very sensitive to bad data on either horizon. We have found that it is important to not skip the posting and contouring of each of the horizons, because this is where bad data points can commonly be identified. Usually, but not always, a bad data point on one horizon also will show up on the residual map. We have found that it is very important to check all maps at every stage because, if either of the original maps has errors or bad data, then the residual map will certainly have errors and is likely to not make sense.

We also have found that the zero line on a residual map can be very sensitive to the fluid density assumptions, particularly if the hydrocarbon reservoir is deep and the hydraulic gradient is effective over a large vertical column. Additionally, edge effects can give very erroneous residuals, especially where exponential curve-fitting gridding algorithms are used. All edge effects and areas of sparse data on any map should be examined carefully.

GRAPHICAL RESIDUAL-MAP PROCEDURE

It is possible to create residual maps without a computer. In the graphical procedure, data for both horizons are collected, posted, and contoured (but not gridded) on separate maps. The two maps are overlain, and the intersection points of all contour lines are posted with a number representing the difference between the contour lines at the intersection points on the different maps. These intersection points are then contoured as in Figure 2.

EXAMPLE FROM THE SAN JUAN BASIN, NEW MEXICO

The San Juan basin is a nearly circular basin that covers approximately 15,000 mi^2 in the Four Corners Region of New Mexico (Fig. 3). Most of the basin is located in New Mexico, although outer margins are located in Colorado, Utah, and Arizona. The basin is an asymmetric depression (Fig. 3) that formed principally during Laramide deformation (latest Cretaceous to early Tertiary). Dips on the north flank average 8°–10°, whereas dips on the south flank average <2°.

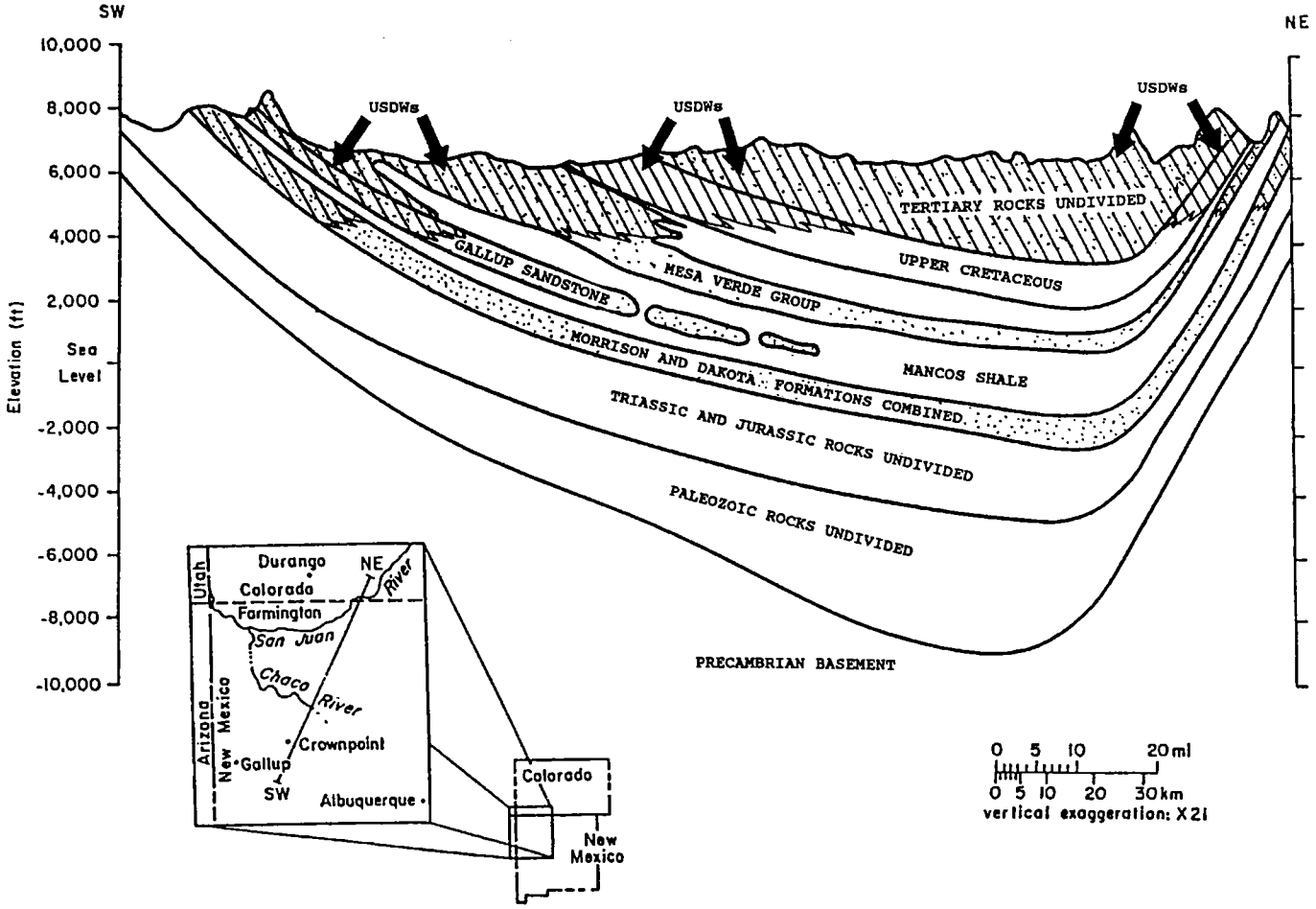

Figure 2. Schematic southwest–northeast cross section through the San Juan basin, northwestern New Mexico, showing major hydrocarbon-producing units and underground sources of drinking water. Note that all underground sources of drinking water become more saline with depth and that these units are also hydrocarbon-producing units in many cases.

GENERALIZED STRATIGRAPHY OF THE SAN JUAN BASIN, NEW MEXICO

GEOLOGIC TIME UNITS	FORMATIONS	AQUIFERS	PRODUCING HORIZONS
Quaternary	Alluvium	Q-T Aquifer	Gas
Tertiary	Santa Fe Group Galisteo Fm. Baca Fm. San Jose Fm. Animas Fm. Nacimiento Fm. Ojo Alamo Ss. McDermott Fm		
Cretaceous	Kirtland-Fruitland	Upper Cretaceous Aquifer	Gas
	Pictured Cliffs		Gas
	Lewis Shale		
	Cliff House Ss.	Mesa Verde Group	Gas
	Menefee Fm.		Oil
	Point Lookout Fm.		Gas
	Crevasse Canyon		
	Mancos-Gallup	Gallup Aquifer	Oil
	Dakota Ss.	Dakota Aquifer	Gas and Oil
Jurassic	Morrison Fm.	Morrison Aquifer	Oil
	Bluff Sandstone Summerville Fm. Todilto Fm. Entrada Fm.		
Triassic	Glen Canyon Group Wingate Ss. Chinle Fm.		
Paleozoic Undifferentiated	San Andres Fm.	San Andres Fm.	Oil and Gas
	Paradox Fm.		

Figure 3. Generalized stratigraphy of the San Juan basin, northwestern New Mexico, containing main oil- and gas-producing horizons and underground sources of drinking water. The upper six underground sources of drinking water are the most significant in this study. Q–T = Quaternary–Tertiary. (Modified from Stone and others, 1982; and Landes, 1970.)

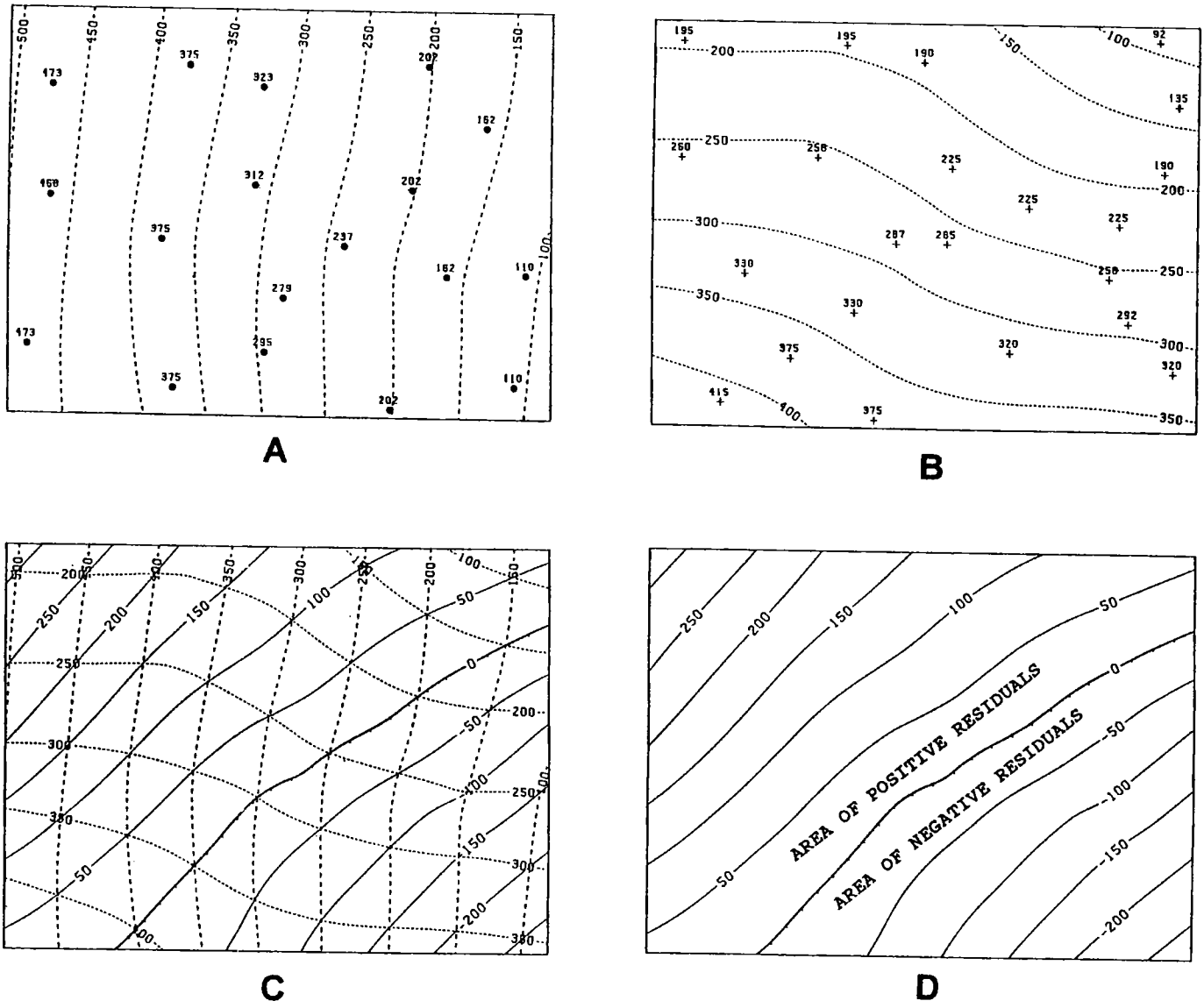

Figure 4. Hypothetical graphic procedure for creation of a residual map. (A) Data points and contour map for the first horizon. (B) Data points and contour map for the second horizon. (C) An overlay of A on B and intersection points for creation of the residual map. (D) The resulting residual map.

The basin contains seven underground sources of drinking water, and oil and gas production occurs from at least 11 different stratigraphic horizons (Fig. 4). All formations dip toward the center of the basin, and all underground sources of drinking water contain fresh water in areas where they occur within approximately 2,000 ft of the surface. All underground sources of drinking water become more saline toward the center of the basin. With the exception of the Tertiary, all underground sources of drinking water consist of an outer doughnut-shaped area of fresh water that grades into higher-salinity nonpotable water toward the central part of the basin (Fig. 3). The Tertiary underground source of drinking water contains potable water throughout the central part of the basin.

Because of the geometry of the basin, residuals were prepared using differential comparisons between each producing horizon and all overlying data for underground sources of drinking water. For example, the Mesa Verde residual map is a comparison between Mesa Verde Group petroleum-reservoir heads measured against all head data for overlying underground sources of drinking water combined (Upper Cretaceous and Tertiary). The Dakota residual compares Dakota Formation petroleum-reservoir heads measured against the combined underground sources of drinking water from the Gallup, Mesa Verde, Upper Cretaceous, and Tertiary underground sources of drinking water. For the Tertiary underground sources of drinking water, no residual maps were prepared because (1) only four reliable pressures were recorded in Tertiary reservoirs, and (2) no overlying underground sources of drinking water are present.

Example of an Underpressured Sink Zone

Figures 5, 6, and 7 show examples of computer-contoured maps from the Mesa Verde Group of the San Juan Basin. Figure 5 shows a head map for all data for underground sources of drinking water that overlie the Mesa Verde Group. Figure 6 shows a head map derived from reservoir pressures in the Mesa Verde Group, and Figure 7 shows the resulting residual map. The Mesa Verde residual map (Fig. 7) shows a negative residual through the east-central part of the basin. The Mesa Verde Group has long been noted as an underpressured geologic unit, and this residual map confirms that there is very little potential for contamination of overlying underground sources of drinking water by wells that penetrate the Mesa Verde Group.

The Mesa Verde Group is a good example of a sink or thief zone. Because it is underpressured, it protects overlying underground sources of drinking water from contamination by all underlying oil- and gas-producing horizons. For example, if an abandoned well were leaking some sort of contaminant such as hydrocarbons or a brine from the underlying Gallup Formation, it is unlikely that the contaminant would ever reach an overlying underground source of drinking water because it would be diverted into the underpressured Mesa Verde Group thief or sink zone.

Example of an Overpressured Zone

Figure 8 shows the residual map for all producing horizons below the Morrison Formation. These are mostly Paleozoic producers and many of the formations are overpressured. A strong positive residual is shown throughout the western part of the basin, and a potential for contamination from fluid flow exists throughout this area. An additional part of the study was to analyze well-construction practices throughout the basin to determine the potential for contamination through well-bore mechanics. It is interesting to note that the total potential for contamination (the combination of fluid flow and mechanics) in this positive residual area is quite low because additional precautions in the form of extra casing strings were present in all analyzed deep holes throughout this area.

DISCUSSION

Several observations about computer-generated maps have been made in creating the San Juan basin maps.

1. Edge effects should be examined very carefully. Computer-generated maps respond to mathematical algorithms that are designed to extrapolate into sparse and no-data areas. These extrapolations can result in false residuals, especially if nonlinear extrapolations are used.
2. Residual maps are very sensitive to heads derived from reservoir pressures. Small reservoir-pressure errors can result in large head errors. Reservoir pressures derived from surface shut-in pressures were considered especially unreliable.
3. Reservoir pressures vary with time from first production. Depleted or partially depleted oil or gas reservoirs almost always appear to be underpressured. Maximum reservoir pressures were used in an attempt to identify virgin reservoir pressures under the assumption that all reservoirs will eventually return to initial or near-initial pressure conditions on abandonment.
4. All data, and especially pressure data, must be edited carefully. Areas that look like strong positive or negative residuals commonly occur near bad-data points or in areas where closely spaced data points create strong gradients. Although strong positive or negative residuals may be caused by true anomalies, they should be analyzed critically to be certain that they make geologic sense.
5. Overpressured (gradients >0.45 psi/ft) oil and gas reservoirs almost always result in overlying positive residual conditions, and underpressured (gradients <0.45 psi/ft) reservoirs generally result in overlying negative residual conditions. This makes intuitive sense, because most groundwater tables are not far below the ground surface and the "average" subsurface hydraulic gradient is around 0.45 psi/ft. This generalization does not hold, however, where the groundwater table is deep in the subsurface.
6. To be done accurately, heads should be compared for conditions at the base of the aquifer. This is only important if there is a long fresh-water column in the aquifer and brine in the well.

CONCLUSIONS

The following six conclusions can be reached using the methods described in this paper.

1. Although the concept of a residual is not new, the application of determining flow potential by combining groundwater data with oilfield pressure data is, to our knowledge, new and unique.
2. The procedure has been used for recommending a variance to the area-of-review (AOR) procedure for Class II (salt-water–disposal and secondary-recovery) injection wells in selected fields in the San Juan basin and for the East Texas field.
3. A negative residual implies that (for a well filled with the appropriate fluid) there is no potential for flow from the petroleum reservoir to the underground source of drinking water, even if the well bore were standing open at both horizons.
4. A negative residual, by itself, does not automatically qualify an area for an AOR variance. To qualify for a variance, bottom-hole pressures during injection must be maintained such that positive residual conditions are not created.
5. The procedure may also identify thief or pressure sink zones that may protect aquifers from contamination by upward-flowing water from petroleum reservoirs.
6. Areas of positive residuals also identify areas where the potential for contamination through abandoned wells is greatest and additional precautions are required.

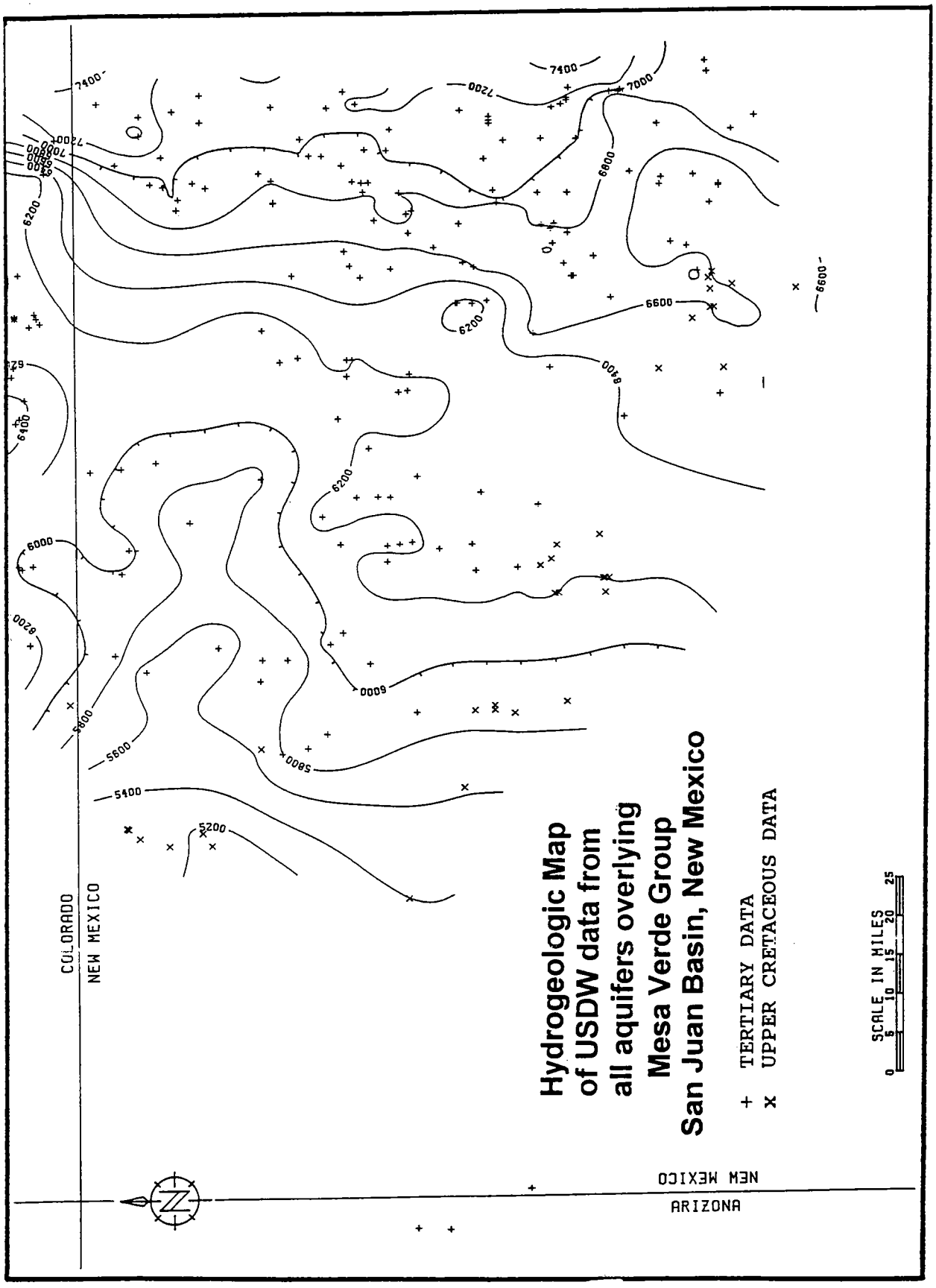

Figure 5. Hydrogeologic map of data for all underground sources of drinking water for all aquifers overlying the Mesa Verde Group, San Juan basin, New Mexico.

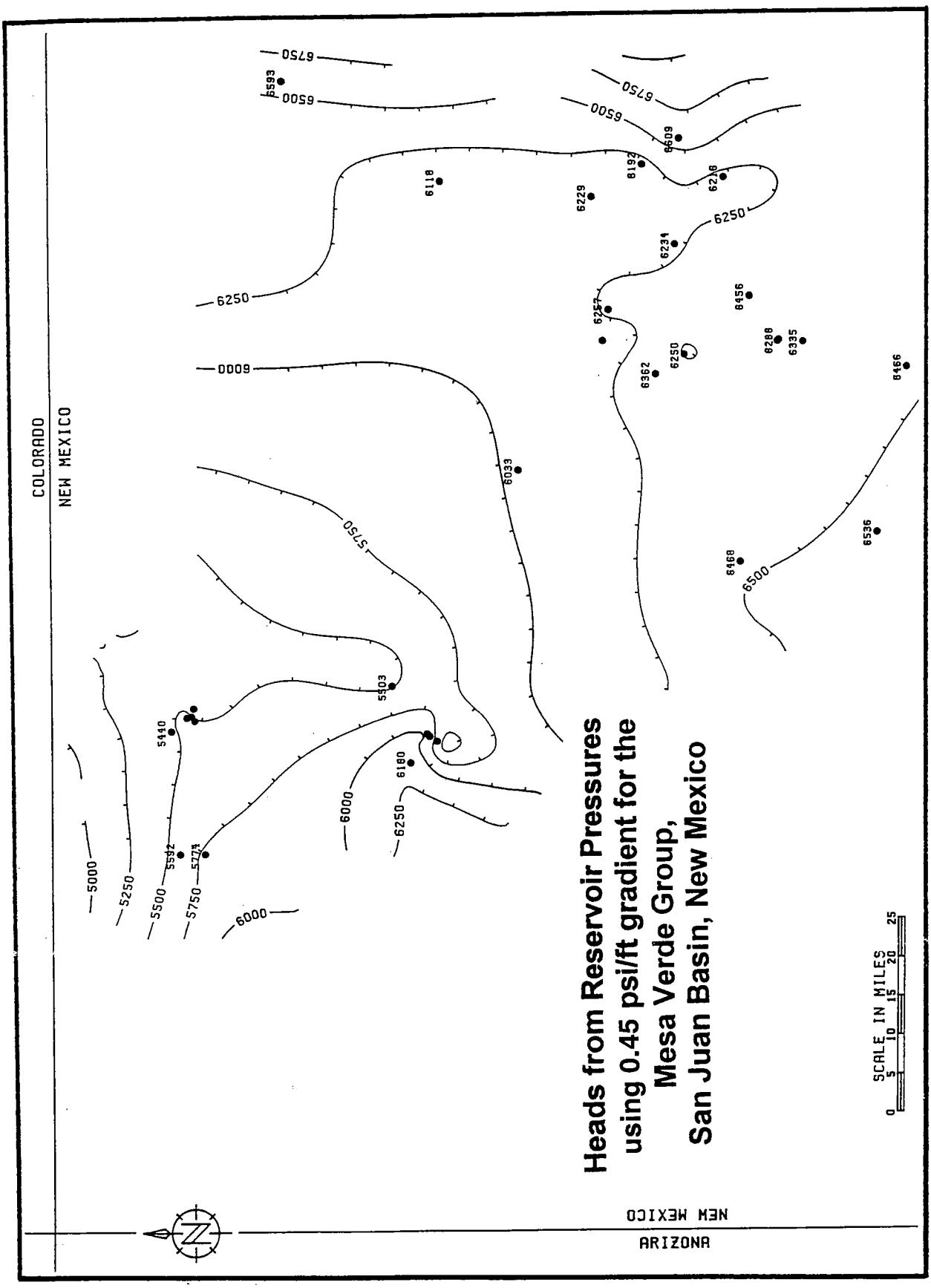

Figure 6. Contour map of heads derived from hydrocarbon reservoir pressures using a 0.45 psi/ft gradient for the Mesa Verde Group, San Juan basin, New Mexico.

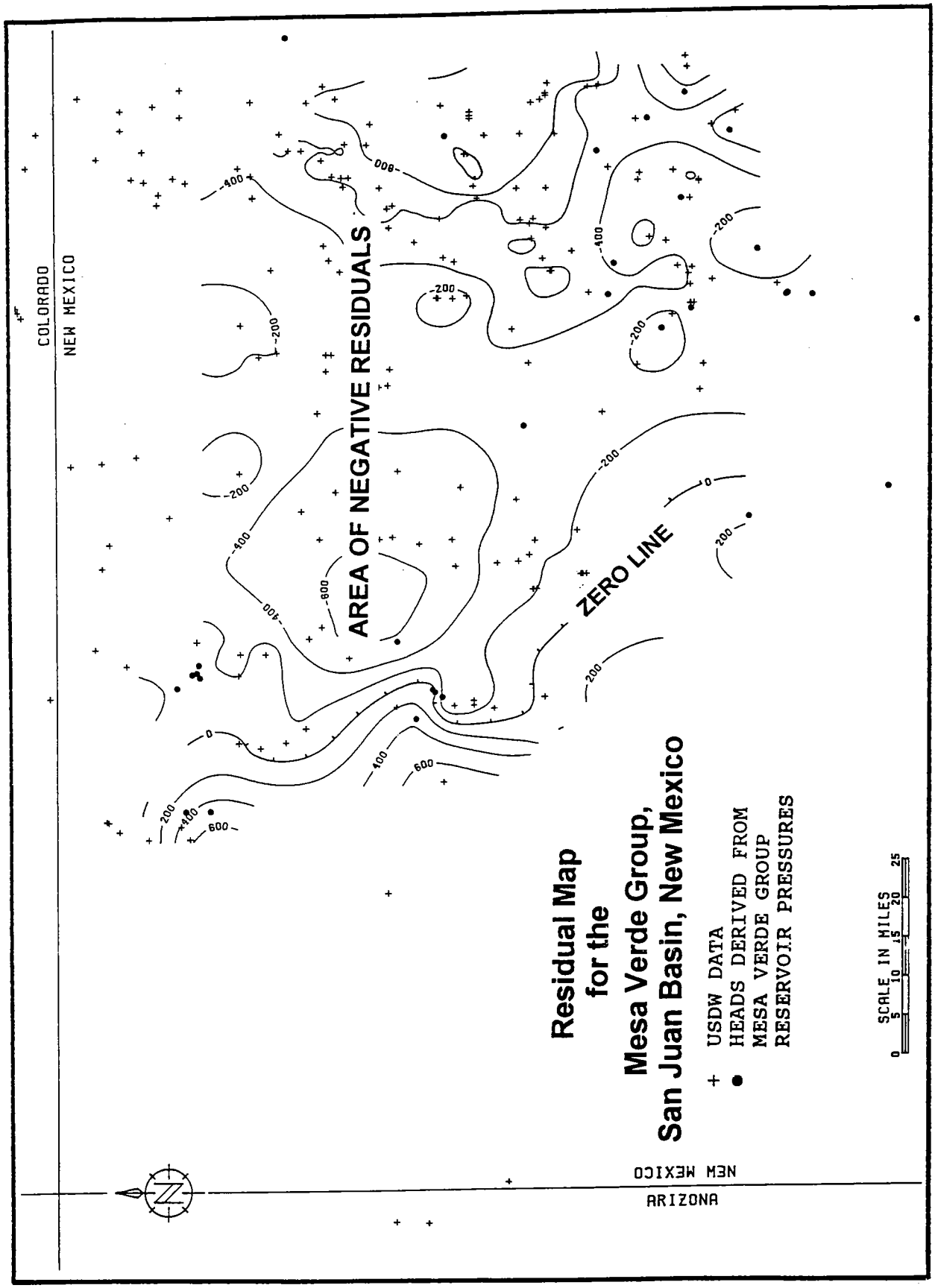

Figure 7. Residual map derived from Figures 5 and 6 for the Mesa Verde Group, San Juan basin, New Mexico, showing mostly negative residuals. USDW = underground source of drinking water.

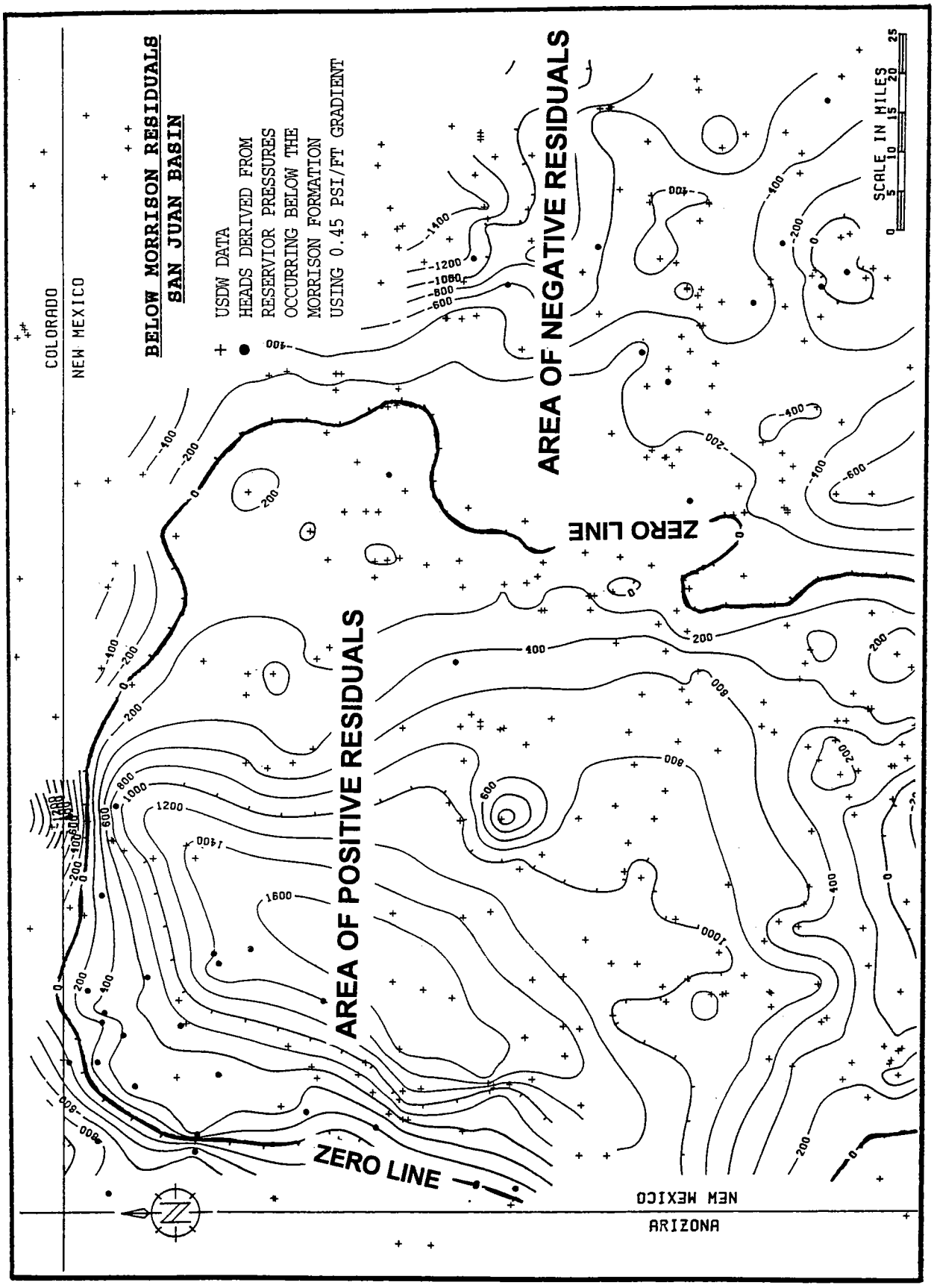

Figure 8. Residual map for underground sources of drinking water above the Morrison Formation and heads from pressures for all hydrocarbon-bearing horizons below the Morrison Formation, San Juan basin, New Mexico. Note that the majority of the residuals are positive, reflecting overpressure conditions for many Paleozoic horizons of the San Juan basin. USDW = underground source of drinking water.

REFERENCES CITED

Landes, K. K., 1970, Petroleum geology of the United States: Wiley-Interscience, New York, 571 p.

Stone, W. J.; Lyford, F. P.; Frenzel, P. F.; Mizell, N. H.; and Padgett, E. T., 1983, Hydrogeology and water resources of San Juan basin, New Mexico: New Mexico Bureau of Mines and Mineral Resources Hydrologic Report 6, 70 p.

SUGGESTED READING

Laudon, R. C.; Warner, D. L.; Koederitz, L. N.; and Dunn-Norman, S., 1994, Determination of flow potential from oil reservoirs to underground sources of drinking water in the San Juan basin, New Mexico: American Association of Petroleum Geologists, Division of Environmental Geosciences Journal, v. 1, no. 1, p. 21–31.

_____ 1998, Residual maps, a new procedure for identification of potential hydrocarbon contamination of groundwater supplies through abandoned wells, *in* Bucchianti, A.; and Potenza, R. (eds.), Proceedings of the International Association of Mathematical Geology, v. 4, p. 898–903.

Warner, D. L.; and McConnell, C. L., 1993, Assessment of environmental implications of abandoned oil and gas wells: Journal of Petroleum Technology, v. 45, no. 9, p. 874–880.

Small-Scale Inversion Feature on the Flanks of the Ardmore Basin: Structural Study of the Milroy Field

Robert E. Harmon and Bryan Tapp
University of Tulsa
Tulsa, Oklahoma

ABSTRACT.—Several models have been proposed for structures in and adjoining the Arbuckle uplift, but to date no balanced sections of these smaller features have been presented. The purpose of this study was to prepare a balanced section from comparing various structural interpretations of a cross section in the Milroy field to determine which model best imitates the regional geology. Primary emphasis is placed on the application of the line-length balance method to prepare a balanced cross section. The Milroy field is a small reservoir that runs from southeastern Stephens County into northwestern Carter County. The cross section used in this project begins in Stephens County, sec. 23, T. 2 S., R. 4 W., continues into sec. 24, T. 2 S., R. 4 W., and ends in Carter County, sec. 18, T. 2 S., R. 3 W.

Two models of the same cross section were evaluated. The original cross-section model used in this project was developed by F. P. Schweers for his paper on the Milroy field, published in 1959. Schweers interpretation of the structural features seen was to mold the cross section into a "rabbit-ear" anticline model. The "best-fit" model of the cross section is a backthrust feature into the Ardmore basin as a result of inversion in the Arbuckle Mountains.

INTRODUCTION

The Milroy field, one of many smaller fields that make up the giant Sho-Vel-Tum field, is located in Stephens and Carter Counties in southern Oklahoma about halfway between the towns of Ardmore and Duncan. Aerially, the field consists of about 2,650 acres in northeastern Stephens County and northwestern Carter County. The field covers the central-eastern part of T. 2 S., R. 4 W. in Stephens County and extends into T. 2 S., R. 3 W. in Carter County (Fig. 1). The structure of the field is an elongate, domal anticline that lies on the West Fox–Velma trend, with an axis of N 65° W. Discovered in 1917, the Milroy field is one of many fields that are found near regional, typically northwest-southeast–trending, fault structures that emanate from the Arbuckle Mountains (Schweers, 1959).

STATEMENT OF THE PROBLEM

This paper is primarily concerned with using balancing techniques to test the structural model for the Milroy field. Schweers's original cross section included 13 wells in secs. 23 and 24 of T. 2 S., R. 4 W. and sec. 18 of T. 2 S., R. 3 W. Models to be evaluated were the "rabbit-ear" anticline model of Schweers and the inversion-produced backthrust model (Fig. 2). Inversion is the deformation mechanism that occurs when basin controlling faults reverse the direction that a fault originally traveled.

BALANCED SECTIONS

Balancing a cross section is the process of taking a deformed structure back to its original geometry (Mitra, 1993). Steps used to develop the inversion-produced backthrust model were regional geology and models of backthrusts. According to Tapp (1995), positive inversion is seen in the Arbuckle region in the form of room-accommodation backthrusts formed as a result of rollover anticlines. Backthrusts could be shown as faults moving through formations where a branch off of the fault, known as a footwall shortcut, forms to relieve stress.

Mitra (1990) has shown translation of fault propagation folds along thrusts where the propagation is through the axial plane of the syncline—apparently what happened in the 13-well cross section. Mitra's drawing is done in "straight-line" form, as are the inversion-produced backthrust figures in this report, so as to assure better measurement for balancing and modeling purposes.

Two basic methods that can be used to balance cross sections are the area method and the line-length method. The area method measures areas of bed layers before and after deformation. This method is the most

Harmon, R. E.; and Tapp, Bryan, 2001, Small-scale inversion feature on the flanks of the Ardmore basin: structural study of the Milroy field, *in* Johnson, K. S.; and Merriam, D. F. (eds.), Petroleum systems of sedimentary basins in the southern Midcontinent, 2000 symposium: Oklahoma Geological Survey Circular 106, p. 187–190.

difficult method to use for inversion, because inversion commonly entails a loss of material that makes exact area measurement difficult. The line-length method measures lengths of beds using a string or rolling map measure. Distances are measured from a specific point called a "pin line." The line length method is the best choice for measuring inversion in regions where areas are unknown. Line-length balancing can be measured from pictures, as well as from the actual outcrop (Price and Cosgrove, 1990).

METHODS

Before balancing the "inversion-produced backthrust" cross section, each cross section was measured and evaluated with a rolling map measure according to bed lengths. Both cross sections had for identical bed lengths beneath the unconformity. Balancing would involve those formations beneath the unconformity or at the top of the Goddard Shale if no unconformity existed. The unconformity starts nearly halfway between wells #6 and #7, and continues on past well #13. For wells #1 through #6, balancing started with the Goddard Shale. The cross section was then drawn to extend the formations that had seen erosion. These formations included the Goddard Shale through the Hunton Formations (Fig. 3). Pin lines were located on both sides of the cross section where the formations would "flatten" horizontally. The entire cross section was then reproduced horizontally to check for accuracy in balancing. Thicknesses of beds were maintained only as far as they could be "visually" drawn to scale. The cross section was considered balanced when bed lengths in the deformed and restored (horizontal) sections were equal within 5–10% (Rowland and Duebendorfer, 1994).

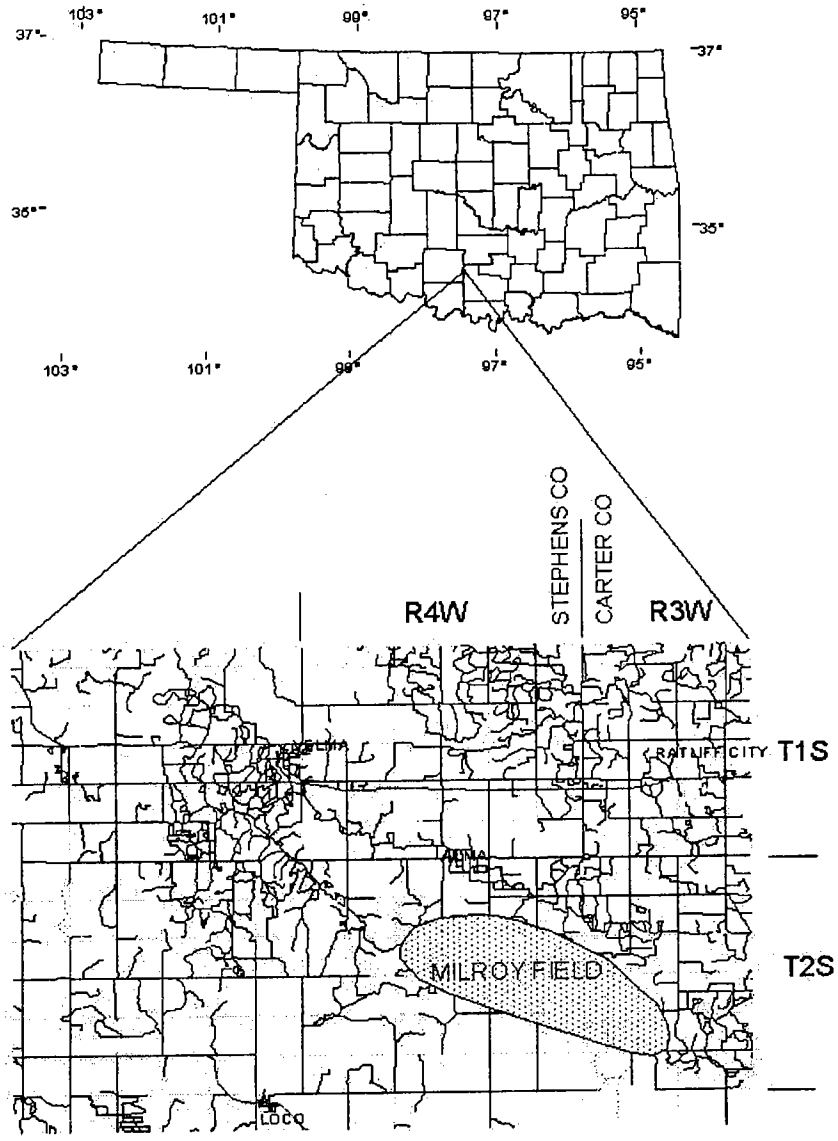

Figure 1. Location map of the Milroy field (modified from Schweers, 1959).

RESULTS

The results of comparing and balancing the two cross-section models show that the inversion-model balances and is a better geologic model for the region than is the "rabbit-ear" anticline model. A balanced model oftentimes is said to be a "not wrong but also not always right" type of model. However, because the inversion-produced backthrust model not only balanced but also incorporated the regional style of geology in its interpretation, it appears to be the best Milroy field model produced thus far.

CONCLUSIONS

The balancing data supports the following two conclusions. (1) The inversion-produced backthrust model balanced because of how the bed lengths in the deformed and restored sections were equal within 5–10%, according to the line-length method. (2) Balancing of the inversion-produced backthrust regional model places this model at or near the top of structural interpretation models for the Milroy field.

REFERENCES CITED

Mitra, S., 1990, Fault-propagation folds: geometry, kinematic evolution, and hydrocarbon traps: American Association of Petroleum Geologists, v. 74, p. 921–945.

_____ 1993, Geometry and kinematic evolution of inver-

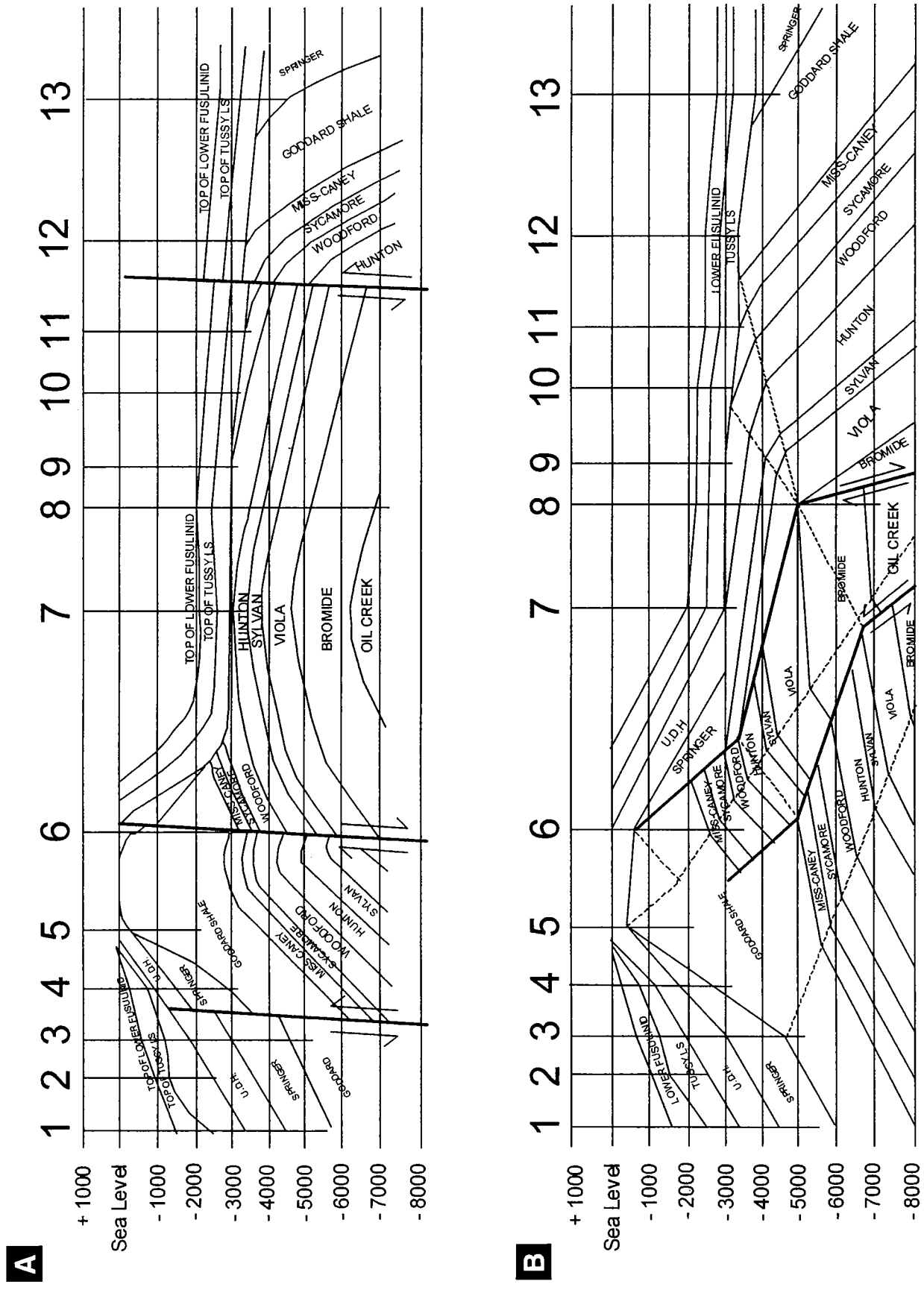

Figure 2. (A) "Rabbit-ear" anticline model (modified from Schweers, 1959). (B) Inversion-produced backthrust model.

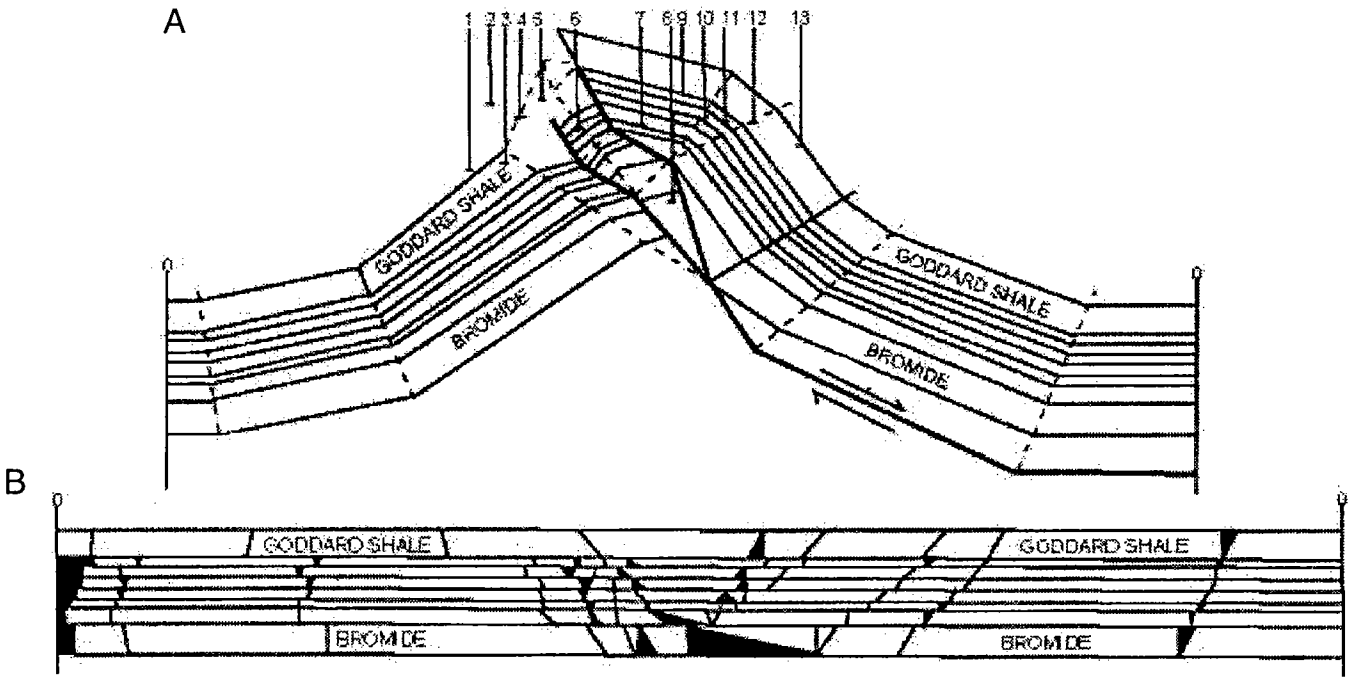

Figure 3. (A) Balanced cross section with extension of eroded beds. (B) Balanced cross section "flattened" horizontally.

sion structures: American Association of Petroleum Geologists, v. 77, p. 1159–1191.

Price, N. J.; and Cosgrove, J. W., 1990, Analysis of geological structures: Cambridge University Press, Cambridge, 502 p.

Rowland, S. M.; and Duebendorfer, E. M., 1994, Structural analysis and synthesis: a laboratory course in structural geology: Blackwell Scientific Publications, Inc., Cambridge, 279 p.

Schweers, F. P., 1959, Milroy field, Stephens and Carter Counties, Oklahoma, *in* Mayes, J. W.; Westheimer, J.; Tomlinson, C. W.; and Putman, D. M. (eds.), Petroleum geology of southern Oklahoma, v. 2: American Association of Petroleum Geologists, Tulsa, Oklahoma, p. 220–226.

Tapp, B., 1995, Inversion model for the structural style of the Arbuckle region, *in* Johnston, K. S., (ed.), Structural styles in the southern Midcontinent, 1992 symposium: Oklahoma Geological Survey Circular 97, p. 113–118.

The Arbuckle Group and Its Lateral Equivalents: The Texas–Oklahoma–Scotland Connection

Amy Callaway, R. Nowell Donovan, and Briann Zimmermann
Texas Christian University
Fort Worth, Texas

ABSTRACT.—Laurentia (also known as "Proto-North America") first became a discrete cratonic block about 570 million years ago. Initially, it was tied to Baltica but subsequently (from ca. 550 Ma) functioned as an independent player that moved northward until (by the Late Cambrian and Early Ordovician) it was centered astride the equator between latitudes 30°N and 30°S. At this time, the craton was oriented 70° clockwise from its present position.

During the Early Cambrian, a general transgression related to the opening of Iapetus and recorded by basal siliciclastics and platform carbonates inundated the "Baltic" (i.e., the eastern) end of the craton. Subsequently, beginning in the Late Cambrian (Franconian), a major transgression of similar character inundated the entire craton. Thus, by the Late Cambrian, one of the largest carbonate platforms that have ever existed linked Scotland and Texas. What is now Texas and Oklahoma were located on the western margin of this platform between latitudes 8°–10°S. This part of the craton was subject to a maritime equatorial climate. More specifically, it was on the lee side of the continent with respect to southeast trade winds. What is now northwest Scotland was located at a similar latitude but on the eastern or windward margin of the continent. Texas and northwest Scotland were located on passive continental crust. In contrast, southern Oklahoma was located astride an aulacogen and thus received about four times more sediment.

The depositional facies encountered in the three areas have much in common—e.g., mud-dominated fabrics, storm-influenced facies, abundant algal boundstones, no major buildups, penecontemporaneous dolomitization, cherts, small-scale cyclic patterns, and no significant primary porosity. The greater abundance of siliciclastic detritus at the western edge of the platform can be attributed to global wind-circulation patterns. Source-rock potential is limited to the Signal Mountain Formation in the Arbuckle Group of Oklahoma—a result of enhanced rates of subsidence within the aulacogen. All three areas show the effects of pervasive dolomitization, which appears to have been an early rather than late diagenetic event (although subject to later modification). Porosity exists in this dolomite, but it is patchy and difficult to predict.

Reservoir potential reflects four principal controls: dolomitization, karst, fracturing, and tectonic history. Karst events affected the entire platform. Most syndepositional events were low relief and related to small-scale regression. Of more significance in karst development was the major Early Ordovician regression that predated deposition of the Simpson Group and its lateral equivalents. The effects of this regression have not been detected in Scotland. By ca. 400 Ma, northwest Scotland was involved in overthrusting related to the Caledonian orogeny. This part of the platform subsequently followed an independent story line that has not involved hydrocarbon dynamics. Oklahoma tectonics involved redefinition of the aulacogen into high-relief basins and uplifts during the Pennsylvanian; this led to source rock maturation, fracturing, deeper level dolomitization, and local relief-related karst in the uplifts. Central Texas played a passive role. Karst systems here were lined by spectacular dolomite encrustations that were produced by warm brine migration. West Texas provided a basement for the development of deep Permian basins.

Callaway, Amy; Donovan, R. N.; and Zimmermann, Briann, 2001, The Arbuckle Group and its lateral equivalents: the Texas–Oklahoma–Scotland connection, *in* Johnson, K. S.; and Merriam, D. F. (eds.), Petroleum systems of sedimentary basins in the southern Midcontinent, 2000 symposium: Oklahoma Geological Survey Circular 106, p. 191.

Paleogeomorphology of the Pre-Pennsylvanian Unconformity on the Arbuckle Group (Cambrian–Lower Ordovician)

Jason R. Cansler and Timothy R. Carr[1]
Kansas Geological Survey and University of Kansas
Lawrence, Kansas

ABSTRACT.—The pre-Pennsylvanian unconformity is the most important surface controlling the distribution of oil and gas in Kansas. Understanding the paleogeomorphology of the erosional surface, the influence of Precambrian topography, and the relationship of karst landform development to preexisting structure and stratigraphy are important components for continued hydrocarbon exploration and production. The karst geomorphology of the Arbuckle Group rocks (Cambrian and Lower Ordovician) was examined at various scales, from regional mapping to core, over the southern extent of the central Kansas uplift (Barton, Ellsworth, Rice, and Stafford Counties). Structure contour and interval isopach maps were produced to reconstruct the paleotopography using abundant well information from areas where the well density in the studied counties exceeds 24 wells per km^2 (40 per mi^2). Major karst landform geometries (dolines, poljes, and blind and half-blind valleys) were identified, and landform development was related to the basement structure of the area. Arbuckle karst erosional features also show the influence of groundwater sapping processes. Scalloped-shaped escarpment edges and U-shaped stubby channels on the downdip side of local highs are indicative of slumping of Arbuckle carbonates by groundwater sapping. In contrast, updip scarp edges are relatively straight and form divides between drainage basins. Removal of slump blocks by continued weathering and fluvial processes is essential to maintain the effectiveness of groundwater sapping and consequent scarp retreat. Subsurface groundwater piracy appears to be an important process resulting in significant basin head widening. Differences in paleogeomorphic patterns can be attributed to structural and stratigraphic constraints that determine the relative effectiveness of groundwater (sapping) processes.

Constructing cross-sections and core examination refined the characterization of landforms controlled by structure, karst, and groundwater sapping. Integration of the core and well data provided the basis to delineate the stratigraphic controls on the morphology of the erosional surface and the distribution of reservoir facies. Data at a wide range of scales were used to develop a model of reservoir formation and distribution within the Arbuckle Group of Kansas, and genesis and geomorphology of large-scale, early Paleozoic karst terranes.

[1]Present address: Chevron, Bakersfield, California.

Cansler, J. R.; and Carr, T. R., 2001, Paleogeomorphology of the Pre-Pennsylvanian unconformity on the Arbuckle Group (Cambrian–Lower Ordovician), *in* Johnson, K. S.; and Merriam, D. F. (eds.), Petroleum systems of sedimentary basins in the southern Midcontinent, 2000 symposium: Oklahoma Geological Survey Circular 106, p. 192.

Thermal Maturation of the Woodford Shale in Eastern Oklahoma

Brian J. Cardott
Oklahoma Geological Survey
Norman, Oklahoma

ABSTRACT.—A petroleum system contains a mature hydrocarbon-source rock (petroleum generation and expulsion), reservoir rock (migration and accumulation), and seal rock (retention; Magoon and Dow, 1994). Lack of any of these rocks will not result in a hydrocarbon accumulation.

The study area included the Cherokee platform, Arkoma basin, and the frontal belt of the Ouachita Mountains in eastern Oklahoma. The petroleum system that was evaluated is the Woodford/Chattanooga–Paleozoic (.) system (source-reservoir [certainty (hypothetical)]; Magoon, 1992). The Woodford Shale (also known as the Chattanooga Formation in eastern Oklahoma; Upper Devonian to Lower Mississippian) is widely regarded as an important hydrocarbon source rock, containing oil-generative organic matter (type II kerogen). The Arkoma basin is known as a gas province. The exclusive occurrence of natural gas could be due to high thermal maturity or lack of oil-generative organic matter. High thermal maturity is the obvious conclusion based on the occurrence of bituminous-rank coal beds at the surface. However, the occurrence of pyrobitumen in post-mature Woodford Shale samples indicates oil-generative organic matter was originally present.

Thermal maturity of the Woodford Shale was determined by measuring the reflectance of the vitrinite maceral (derived from woody tissues) in well cuttings, core, and grab samples from 60 wells and outcrops. Mean random vitrinite reflectance (fixed stage, oil immersion; % R_o) was determined from a minimum of 20 measurements. Maximum vitrinite reflectance, important for values greater than 1%, could not be measured due to small phytoclast size. Depth to top of the Woodford Shale in wells ranged from 618 to 17,854 ft. Thickness of the Woodford Shale ranged from 17 to 314 ft.

Thermal maturation of the Woodford Shale increases from west to east and with increasing present depth in the Arkoma basin. Mean random vitrinite reflectance ranged from 0.49% to 6.36%. The oil window (main zone of oil generation) is from 0.5% to 1.3% R_o. The tentative dry gas preservation limit is 5% R_o. Therefore, the Woodford Shale in the study area is mature to postmature with respect to oil generation.

Additional estimates of thermal maturity were determined from bitumen reflectance and alginite fluorescence. Vitrinite-reflectance equivalent (VRE) was estimated from a limited number (1–17) of bitumen-reflectance values. Qualitative fluorescence of *Tasmanites* alginite indicated a narrow thermal-maturity range containing fluorescence; fluorescence is extinguished by 0.72% R_o.

REFERENCES CITED

Magoon, L. B., 1992, Identified petroleum systems within the United States—1992, *in* Magoon, L. B. (ed.), The petroleum system—status of research and methods, 1992: U.S. Geological Survey Bulletin 2007, p. 2–11.

Magoon, L. B.; and Dow, W. G., 1994, The petroleum system, *in* Magoon, L. B.; and Dow, W. G. (eds.), The petroleum system—from source to trap: American Association of Petroleum Geologists Memoir 60, p. 3–24.

Cardott, B. J., 2001, Thermal maturation of the Woodford Shale in eastern Oklahoma, *in* Johnson, K. S.; and Merriam, D. F. (eds.), Petroleum systems of sedimentary basins in the southern Midcontinent, 2000 symposium: Oklahoma Geological Survey Circular 106, p. 193.

Temperature Analysis in the Mature Hydrocarbon Province of Kansas: Utilizing a Large Database of Petrophysical Well Logs

Andrea Förster
GeoForschungsZentrum Potsdam
Potsdam, Germany

Daniel F. Merriam and W. Lynn Watney
Kansas Geological Survey
Lawrence, Kansas

ABSTRACT.—Commercially obtained bottom-hole temperatures (BHTs) were analyzed at regional scale in the large mature hydrocarbon province of Kansas, which is in the Midcontinent region of the United States, to investigate their usefulness for geothermal studies. The large Petroleum Information Well-History Control System (WHCS) database was used to access the BHTs recorded in exploration wells. BHTs were retrieved for the Mississippian (Lower Carboniferous) and the Cambro–Ordovician Arbuckle Group and were plotted and contoured to create a regional temperature pattern for each stratigraphic unit. BHTs were assumed to be at or near the top of the units. These patterns then were compared visually with other geological features, such as sediment thickness and structure.

An empirical BHT correction factor established to a depth of 1,000 m in a subarea in southeastern Kansas was applied to the large data set to correct for drilling disturbance. Because of the poor resolution of the BHT data for a given stratigraphic unit on the order of ±5°C, the corrected BHTs of the Arbuckle and Mississippian obtained 100–400 m apart from each other are practically similar over much of the area. The application of the empirical correction factor results in temperatures that approximate formation temperatures in the eastern area but deviate slightly in central and western Kansas. Despite those differences, the general BHT pattern of the two sedimentary units reflects the regional geological structure, which means that the BHTs increase to the west with increasing depth of the tops of the units..

No correlation was evident between the temperature pattern and the type of Precambrian basement rock.

Förster, Andrea; Merriam, D. F.; and Watney, W. L., 2001, Temperature analysis in the mature hydrocarbon province of Kansas: utilizing a large database of petrophysical well logs, *in* Johnson, K. S.; and Merriam, D. F. (eds.), Petroleum systems of sedimentary basins in the southern Midcontinent, 2000 symposium: Oklahoma Geological Survey Circular 106, p. 194.

Applications of Borehole-Temperature Measurements

William D. Gosnold, Jr.
University of North Dakota
Grand Forks, North Dakota

ABSTRACT.—The potential applications of borehole-temperature measurements include a large number of basic science and engineering investigations, *inter alia*, tectonics, maturation of petroleum source rocks, radioactivity, stratigraphy, structure, confined groundwater flow between basins, confined and unconfined groundwater flow within a basin, geothermal resources, permafrost conditions, underground coal gasification, and climate change. The key to unlocking this information is to understand heat flow variables, specifically thermal conductivity, temperature gradient, and the three-dimensional nature of heat conduction. This paper includes examples of temperature–depth (T–z) data with interpretations relating to all of the above applications.

Gosnold, W. D., Jr., 2001, Applications of borehole-temperature measurements, *in* Johnson, K. S.; and Merriam, D. F. (eds.), Petroleum systems of sedimentary basins in the southern Midcontinent, 2000 symposium: Oklahoma Geological Survey Circular 106, p. 195.

Pre-Atokan Petroleum Systems of the Arkoma and Ouachita Basins

Raymond W. Suhm
Consulting Geophysicist and Geologist
Oklahoma City, Oklahoma

Jock A. Campbell
Oklahoma Geological Survey
Norman, Oklahoma

ABSTRACT.—Two of the least drilled and most poorly understood hydrocarbon-bearing areas in North America are: (1) the "deep" Arkoma basin (cratonic facies) that partly underlies allochthonous thrust sheets of the Ouachita facies, and (2) the autochthonous Ouachita trough beneath its thrusted counterpart. The structural styles of these essentially unpenetrated basins consist of south-dipping strata broken by down-to-the-south fault blocks of varying widths, as well as horsts and grabens. Reservoir-quality rocks, organic-rich source beds, and structural traps appear to be present in both areas and, hence, are favorable to substantial recoverable hydrocarbon reserves.

From an interpretation of geophysical data, published reports, and independent regional studies, the southern edge of the Arkoma basin consists of a 25–30-mi-wide linear "horst block" (referred to here as Black Springs horst). The Black Springs horst extends from beneath the Paris arch in Lamar County, Texas (penetrated by the Hunt #1 Neely, Lamar County, Texas), to the Broken Bow uplift in McCurtain County, Oklahoma (penetrated by the Sohio #1-22 Weyerhaeuser), and to the Benton uplift in Benton and Montgomery Counties, Arkansas. This linear horst was locally above sea level during the Paleozoic and apparently was eroded down to the Precambrian igneous complex. Boulders of crystalline rock eroded from the horst have been emplaced locally into the Ouachita facies, establishing the long geologic life of this prominent structure.

Simultaneous with this discovery, the Ouachita trough depocenter, about 100 mi wide, received detritus from the craton to the north and from the continental block on the south (Llanoira). Detrital contributions began with clay of the Collier Shale (Arbuckle equivalent). The Collier represents the oldest formation in which a regional décollement is likely to have developed. The Collier may rest on a thick section of basinal limestone/dolomite equivalent to the Marathon Limestone in West Texas. Quartz sandstones of the Crystal Mountain and Blakely Formations (Simpson Group equivalents) were derived from the craton, whereas, the fine-grained clay of the Mazarn and Womble Shales (Ordovician) was derived from humid hilly terrain of Llanoria. Biogenic silica and silica from Llanorian volcanic sources resulted in precipitation of the Bigfork Chert (Ordovician) and Arkansas Novaculite (Devonian–Mississippian). During later episodes of the Mississippian, elevated Llanorian and eastern source areas contributed vast quantities of synorogenic detritus from the Stanley and Jackfork Formations, which were deposited in a variety of deltaic and marine environments. With the regional uplift of Llanoria, large segments of the Ouachita facies were thrust northward over the subsiding Arkoma basin. The Bigfork Chert, Arkansas Novaculite, and Stanley and Jackfork Formations are all locally productive of hydrocarbons in the allochthonous Ouachita facies.

The "deep" Arkoma basin (from the Black Springs horst to the vicinity of the Choctaw thrust) is a northeast–southwest embayment present at depths greater than 10,000 ft below the base of the Ouachita allochthon. Unlike shallow parts of the Arkoma, which experienced uplift and erosion after deposition of Simpson and Hunton, the "deep" Arkoma underwent more continuous deposition, resulting in a thicker sedimentary section. A recent interpretation of seismic data reveals that it has a structural and stratigraphic component of an interior basin similar to that of the nearby Ardmore basin rather than that of the Ouachitatrough.

Secondary solution and fracture porosities are probable in the carbonates and cherts of the Arbuckle, Simpson, Viola, Hunton, Woodford, Sycamore (Boone), Pitkin, and Wapanucka sections. Craton-derived quartz sands of the Simpson Group, however, are the most attractive reservoirs in the "deep" Arkoma. The quartz grains are likely to have porosity-preserving clay coats that contrast with the porosity-plugging cements of the South Ozark platform. Much of the clay fraction in pre-Atoka rocks of the "deep" Arkoma was derived from the erosion of Llanoria; the amount of which was dependent on rainfall and relief of Llanoria. During Mississippian and Pennsylvanian time, extremely thick sections of dark-colored mudstone with excellent sourcing capabilities as well as excellent reservoir-quality sandstones were generated and deposited in the "deep" Arkoma. Therefore, substantial hydrocarbon potential exists in the untested deep Arkoma basin facies and in the autochthonous Ouachita facies. This reinterpretation can now be used to prospect for untested hydrocarbon traps.

Suhm, R. W.; and Campbell, J. A., 2001, Pre-Atokan petroleum systems of the Arkoma and Ouachita basins, *in* Johnson, K. S.; and Merriam, D. F. (eds.), Petroleum systems of sedimentary basins in the southern Midcontinent, 2000 symposium: Oklahoma Geological Survey Circular 106, p. 196.

Improved Modeling of a Shallow-Shelf Carbonate Reservoir Using 3-D Seismic Attributes, Welch Field, Permian Basin, Texas

George P. Watts
OXY USA, Inc.
Midland, Texas

Gregory D. Hinterlong
Texaco Exploration and Production, Inc.
Midland, Texas

Archie R. Taylor
Continental Resources
Enid, Oklahoma

ABSTRACT.—OXY USA, Inc., and the U.S. Department of Energy are partners in an advanced technology demonstration project (DE-FC22-93BC14990) at the West Welch Unit in the Welch Field in Dawson County, Texas. The project requires detailed characterization of reservoir properties to create a three-dimensional (3-D) geologic model to simulate fluid flow within the reservoir under carbon dioxide (CO_2) flood. Oil production at the Welch Field is from a stratigraphic trap in a low permeability San Andres reservoir of Permian age. Post-depositional diagenesis, mostly anhydritic cementing, has created a high degree of variability in the porosity and permeability distributions across the field. The single biggest challenge for the reservoir modeling effort is defining the reservoir properties in the inter-well space. A modern 3-D seismic-data volume was contributed by OXY to assist the effort, and a method was developed to integrate the seismic data with the well data at the reservoir level. This method was successfully applied to the San Andres reservoir in the West Welch Unit.

The methodology uses statistical correlation of reservoir properties to seismic attributes to estimate reservoir properties in the seismic volume. Structure, amplitude, and phase were used to estimate the porosity at the seismic bin locations. These seismic-guided porosity values tie to the well data accurately, provide detailed variations of the reservoir in the inter-well space, and reveal extensions of the reservoir beyond the well control. Ten new wells were drilled since the seismic-guided porosity map was produced. The predicted seismic-guided porosity values tie within one porosity unit of the log-measured porosity at the new well locations. The difference is within the accuracy of the log measurement itself. The method has used seismic measurements to shape the inter-well geologic variability. A porosity-to-permeability conversion relationship was developed from the core data and applied to the seismic-guided porosity values to acquire permeability values at each seismic bin location.

Reservoir simulation runs were applied to two versions of the reservoir characterization model: (1) well data only, and (2) well data integrated with 3-D seismic data. The runs with the well data required many modifications in porosity and permeability across large areas to achieve a history match. The runs using the seismic-enhanced model required no porosity or permeability changes to establish a relatively good history match.

Watts, G. P.; Hinterlong, G. D.; and Taylor, A. R., 2001, Improved modeling of a shallow-shelf carbonate reservoir using 3-D seismic attributes, Welch Field, Permian basin, Texas, *in* Johnson, K. S.; and Merriam, D. F. (eds.), Petroleum systems of sedimentary basins in the southern Midcontinent, 2000 symposium: Oklahoma Geological Survey Circular 106, p. 197.

Sequence Stratigraphy of the Swope Formation (Missourian Series, Pennsylvanian System) in Eastern Kansas and Western Missouri

Nathan A. Wilke and Timothy R. Carr
Kansas Geological Survey
Lawrence, Kansas

ABSTRACT.—Subaerial exposure surfaces and associated features are common components of shallow-marine carbonate Paleozoic sequences in the Midcontinent. Recognition of such surfaces is economically important because the distribution of reservoir facies is closely associated with subaerial exposure. Problems in lithostratigraphic correlation at both the reservoir and regional scales are caused by the absence of distinct lithologic and petrographic evidence of subaerial exposures in these sequences. An Upper Pennsylvanian carbonate sequence—the Swope Formation of the Kansas City Group (Bronson Subgroup)—in eastern Kansas and western Missouri was investigated to understand the style of alteration associated with subaerial exposure, to derive criteria to recognize distinctive signatures in both the surface and subsurface, and to better understand the sequence stratigraphy of the carbonate sequences. Detailed field descriptions, petrographic examination, and spectral gamma-ray logs of outcrops and shallow cores were the bases of the study.

A sequence stratigraphic model for the Swope Limestone was developed to account for lithologic changes and to recognize small-scale cyclicity in outcrop and core. Radioactive anomalies were recognized at contacts of the vadose and marine-phreatic zones related to both known and previously unrecognized exposure surfaces. These exposure surfaces and their related paleo-water tables were used to map individual system tracts and sequences. The study focused on understanding the response of depositional and postdepositional processes to changes in relative sea level.

Wilke, N. A.; and Carr, T. R., 2001, Sequence stratigraphy of the Swope Formation (Missourian Series, Pennsylvanian System) in eastern Kansas and western Missouri, *in* Johnson, K. S.; and Merriam, D. F. (eds.), Petroleum systems of sedimentary basins in the southern Midcontinent, 2000 symposium: Oklahoma Geological Survey Circular 106, p. 198.